AN EXPERIMENTAL AND ANALYTICAL ASSESSMENT OF GEOMAGNETIC INTENSITY VARIATION SINCE THE DEVONIAN: LINKS WITH GLOBAL GEOLOGICAL PROCESSES

Andrew J. Biggin

A thesis submitted in partial fulfilment of the
requirements of Kingston University
for the degree of Doctor of Philosophy.

February 2001

Doctor of Philosophy

AN EXPERIMENTAL AND ANALYTICAL ASSESSMENT OF GEOMAGNETIC INTENSITY VARIATION SINCE THE DEVONIAN: LINKS WITH GLOBAL GEOLOGICAL PROCESSES

Andrew J. Biggin

Abstract

This study was broadly concerned with acquiring geomagnetic palaeointensity estimates and interpreting existing data in the wider context of the global geodynamic system.

Two-hundred and ninety-eight samples from nine suites of Mesozoic and Permian intrusions (comprising thirty-one individual rock units) from eastern Australia were subjected to rock magnetic and palaeodirectional analyses. The grain size distributions of these were generally observed to contain a significant fraction of large pseudo-single domain (PSD) and multi-domain (MD) grains. This frequently allowed a substantial part of their blocking temperature spectrum (~ 350°C) to be overprinted by a thermal event affecting this region during the mid-Cretaceous. The modified Thellier palaeointensity method was employed on samples from seven of the intrusion suites producing virtual dipole moment (VDM) estimates generally lower than the present value (8×10^{22} Am^2) and variable in quality. Mean values of VDM were obtained for the following periods: 90 Ma (< 5.9×10^{22} Am2); 127 Ma (7.9×10^{22} Am^2); 172 Ma (1.2×10^{22} Am^2); 200 – 178 Ma (6.3×10^{22} Am^2); 255 Ma (7.5×10^{22} Am^2). Despite being in good agreement with previously acquired data, few of these estimates satisfied all conventional acceptance criteria and consequently a reliability (R) factor was invoked to allow qualitative comparisons of estimates to be made.

A simulated Thellier experiment was also performed on pre-treated rock samples containing magnetic grains dominantly within the single domain (SD) range. This produced a surprising amount of variable non-ideal behaviour. In particular, a number of samples significantly overestimated the 'palaeointensity' when only a low temperature, seemingly ideal, portion of their blocking temperature spectra was used. Five proposed mechanisms of non-ideal behaviour succeeded in explaining most of this non-ideal behaviour and correcting the results of 50% of the samples. One of these, '*demagnetisation bias,*' could be developed into an extremely useful tool for correcting convex-down NRM-TRM plots produced by assemblages of MD grains and allow this widespread problem to be overcome in future palaeointensity studies.

The global dipole moment record for the period 400 – 10 Ma was subject to a detailed statistical analysis allowing it to be segmented into periods defined by the distribution of the data themselves. Additionally, a system of grouping estimates into 'rock suites' was developed to avoid over-representation of secular

variation (SV) in the record. Variation of poloidal field strength (PFS; recorded in VDM estimates) since the Devonian was shown to be largely decoupled from geomagnetic reversal frequency except during superchrons when its lower limit may have been raised. It was discovered that periods of intense true polar wander (TPW) and large igneous province (LIP) emplacement, which have previously been associated with changes in reversal frequency, may perturb the geodynamo's capacity to generate poloidal field but certainly do not control it.

An excellent time correlation between PFS and the supercontinent amalgamation-dispersion cycle since the Devonian was observed. The following model, comprising four phases, was developed to explain this. (1) Prior to the formation of Pangaea (> 350 Ma) the upper and lower mantle convected separately, the latter was hot allowing only a small heat flux across the CMB, and consequently PFS was kept low. (2) During the final assembly of Pangaea (350 – 325 Ma), there was a catastrophic avalanche of cold material through the 660 km transition into the lower mantle which increased CMB heat flux and PFS dramatically. (3) The maintenance of Pangaea through the period 325 – 180 Ma allowed both the upper and lower mantle to warm gradually, causing PFS to fall steadily. (4) In the mid-Jurassic, the continents began to disperse and the high temperature contrast between lithosphere and mantle provided the subducting slabs with sufficient momentum to penetrate the 660 km transition and gradually cool the lower mantle. PFS has risen (steadily or in small jumps) since this time as a consequence.

This model is entirely consistent with long-term trends in PFS since the Devonian, and provides a benchmark to be tested by the addition of more palaeointensity data and quantitative mantle modelling.

Acknowledgements

I have received many visitors to my 'ivory tower' over the last three and a half years. Unfortunately, neither space nor memory (addled as it is by five months of intensive thesis writing) will allow me to mention them all here. If I have left you out, sorry, but thanks anyway.

Thanks must first go to my supervisor, Dr Neil Thomas, for being an excellent teacher, boss, colleague and friend to his first research student. I am delighted to be working alongside him in the future. I am particularly grateful for his and Paula's contribution to two highly successful and disgracefully enjoyable field trips down under.

Thanks also to my two other supervisors: Dr Nick Petford, who looked down microscopes many a time on my behalf and was an excellent source of relevant literature, and Dr Tim Rolph (and family) who provided immeasurable support prior, during, and after our trips to the bush. The same must also be said for Phil and Janice Schmidt who provided a very warm welcome to this distant country.

I gratefully acknowledge the help of Prof. John Shaw, in facilitating my use of the geomagnetism lab at the University of Liverpool, and Dr Steve Openshaw and Dr Mimi Hill for their technical support there. Thanks also to my friends Louise and Brendan, for giving me a place to stay during my trips back to my student homeland.

A good deal of credit goes to other staff of my school and faculty at Kingston University. Andy Swan, Joyce Evans, and Ian Gill deserve a special mention for the time and effort they spent in helping to produce this piece of work.

Many thanks also to all my post-graduate colleagues for the friendship and support (not least in the Surrey Club) that they provided. Some of these are: Jon, Jen (you beeraging this evening?), Jo, Stella, Simon, Elaine, Des (moped turncoat), Steff, Lorraine, Dan, Nuria, and Karl.

The people who I have lived with down in London (all of them friends) deserve a mention too: Yorkie, Landers, Rutter, Kebab, Lepki, Pippa, Michael, Sarah, Paul, Seth (for three days in a muddy field) and, not forgetting, 'alchy Jim.'

Especial thanks to my 'lovely assistant' Brigid for allowing me to bore her with conversation about my work, providing ubiquitous welcome distraction, and offering to help with sorting this damned thing for binding this afternoon. I'm sure Querétaro will be even more fun than SE27.

Finally, I thank my family (Allison, Kathryn, Ellen, and Amy) for moral support while writing this thesis. I am dedicating the whole thing to my Mum and Dad in return for their love, friendship, and support through my life. Without their advice, help with money, endless cups of coffee, and delicious food over the last four months, this thesis would *never* have been written.

23 February, 2001

Table of contents

PART II

1. Introduction

This thesis is primarily concerned with variation in the absolute strength of the Earth's magnetic (geomagnetic) field over the last 400 Myr.

The geomagnetic field is generated by a system known as the geodynamo involving the motion of an iron alloy fluid within the outer core of the planet. This electrically conducting liquid is confined to the outer core by the solid silicate mantle above it and the solid iron-nickel inner core at its base.

The geomagnetic field is recorded in the magnetisation of rocks as they form through a variety of mechanisms (§ 2.1.3); the record of the field preserved in rocks since the Archaean shows unambiguously that the field has reversed its polarity many times. Currently, the geomagnetic field undergoes polarity reversal an average of 4 to 5 times every million years (Merrill *et al*., 1996).

The frequency at which the geomagnetic field reverses polarity is variable on a timescale of ~ 10^8 years; it is difficult to imagine any processes operating within the core that could cause such long timescale variation. However, the lower mantle controls the magnitude and pattern of heat flow out of the core by dictating its thermal boundary conditions. Therefore, it is widely believed that thermal convection, operating in the lower mantle, is responsible for varying flow patterns within the core and consequently geomagnetic reversal frequency on the timescales observed (e.g. McFadden and Merrill, 1984; Stacey, 1991).

Coupling between lower and upper mantle convection is expected, though plausible levels and mechanisms are currently a source of great debate. Upper mantle convection is driven primarily by plate tectonics at the surface of the Earth (Davies, 1998). Consequently, it can be reasoned that certain lithospheric processes may exhibit a causal link with long-term variations in geomagnetic field behaviour. It would then be possible to link the different layers of the Earth and the processes that

occur within them in what will be referred to here as a *global geodynamic system*. Various qualitative models have already been proposed to explain observed correlations between geomagnetic and lithospheric behaviour (e.g. Eide and Torsvik, 1996; Larson and Olson, 1991). However, this issue remains contentious.

One important constraint that has been largely ignored by the advocates of global dynamic models thus far is that of the intensity of the geomagnetic field. Geomagnetic intensity represents the effectiveness of the geodynamo in generating *poloidal field* that is measurable at the surface of the Earth and may be diagnostic of the style and / or magnitude of fluid motion in the outer core. This study aimed to evaluate geomagnetic intensity variation in the context of a global geodynamic system.

This thesis is split into two parts because of the dichotomous nature of the data that the study analyses and interprets. Those chapters comprising **part 1** are concerned with the acquisition of *primary* data, specifically palaeointensity (ancient geomagnetic field intensity) estimates. This takes the form of both providing new estimates from periods of time and palaeogeographical localities for which the data coverage is poor (chapter 4), and in gaining an empirical insight into means of assessing and ensuring the reliability of these and other data (chapter 5). **Part 2** is concerned with the analysis and interpretation of *secondary* palaeointensity data, acquired prior to this study, in the context of the global geodynamic system.

Chapter 2 firstly provides some theoretical background that is critical to understanding the practises of rock and palaeo-magnetism (§ 2.1) although the reader is directed elsewhere for a fuller description. The rest of the chapter is concerned with the experimental and analytical techniques used in chapters 4 and 5.

Chapter 3 provides a geological background of the field areas adopted by this study and of the sampled rocks themselves. It begins by briefly describing the geological history of eastern Australia before focussing upon the sedimentary basins in which

the sampled rocks were located, and finally the sampled igneous intrusions themselves. The precise locations of the sampling sites within the suites of rocks and the broad properties of the rocks extracted at these are also given in order that any follow-up studies can be planned easily.

The results of all the primary experimental studies conducted on the sampled rocks are presented and interpreted in chapter 4. This chapter represents the most time-intensive portion of the study and is consequently the most voluminous. It deals with each of the suites of intrusions separately so that the results of the different analyses performed on them can be easily cross-referenced.

The analysis described in chapter 5, additional to the original project's remit, was undertaken in an attempt to evaluate the reliability of results presented in the previous chapter and in other palaeointensity studies. The results of a palaeointensity experiment, performed on pre-treated rock samples that recorded a magnetic field of known intensity, are presented and discussed.

Chapter 6 is a review of recent multidisciplinary advances and ongoing debates concerning the primary components of the global geodynamic system. It contains information that is relevant not only to this study but also to any other studies which concern the global geodynamic system. It is split into three sections covering different aspects and components of the system, namely: geomagnetic field observations (§ 6.1), mantle processes (§ 6.2), and models and mechanisms of interaction between the lithosphere, mantle and core (§ 6.3).

Chapter 7 describes a statistical analysis of the published dipole moment (normalised palaeointensity) record for the period 400-10 Ma. This analysis is described as objective because it does not attempt to make comparisons with any variables external to the record, but instead looks to the record itself to produce patterns of variations. This was done to ensure that conclusions formed were in no

way biased through the active search for correlations with other geomagnetic and mantle variables.

Comparisons with external variables and appropriate interpretations comprise the bulk of chapter 8. A simple but presently plausible model to account for the variation observed in the dipole moment record and its quasi-correlation with plate tectonics is proposed in § 8.5.

Chapter 9 contains a general discussion regarding the study as a whole, concentrating on the most important results and matters that are relevant to more than one chapter. Chapter 10 lists the primary conclusion of the study and highlights the areas urgently requiring further research.

Appendix 1 provides a glossary of terms for reference; terms which are included in this appendix appear in italics in the text. The other appendices contain data and explanations regarded as ancillary to the normal text, each is referenced where appropriate.

2. Experimental Methods

2.1 Background

2.1.1 Introduction

This chapter will describe the experimental techniques used to obtain the results presented in chapters 4 and 5. The research presented as part 1 of this study is focussed around the collection of reliable palaeointensity estimates from ancient igneous intrusive rocks. There are several major problems associated with palaeointensity analysis, namely: the inherently time consuming nature of the method employed, its very high average failure rate, non-repeatability of experiments, and ambiguity concerning the reliability of results yielded. These difficulties necessitate a range of preliminary investigations designed to maximise the effectiveness of the analysis and assist in the interpretation of its results. § 2.2 and § 2.3 describe these ancillary studies while the preceding sections provide the necessary background.

When the studies described in this chapter are applied in combination to a suite of samples, they yield a comprehensive description of its magnetic characteristics and experimental potential. This is not only useful and necessary in assessing the likelihood of successful palaeointensity recovery, it may also provide information useful to investigations beyond the scope of this study. For example, the magnetic mineralogy of a rock is a product of its original composition and cooling history. The wide range of intrusive rock types sampled for the purpose of this study may raise awareness about the tendency of each type to be palaeomagnetically stable and therefore, its suitability for future investigation.

Various criteria have been suggested as a basis for accepting or rejecting samples for palaeointensity analysis based on information provided by the methods described in

§ 2.4 and § 2.5 and others (e.g. Senanayake and McElhinny, 1981; Thomas, 1993). These are useful because they are frequently retrospectively derived from experience of samples proving (un)suitable for palaeointensity analysis. Every rock is unique however and this study did not adhere to any rigid criteria when selecting samples for the palaeointensity analysis. Samples were rejected when preliminary results agreed with both theory and previous empirical evidence in precluding them from yielding a reliable palaeointensity estimate.

2.1.2 Sampling procedure

A geological description of the intrusions sampled for this study is given in chapter 3. In most cases, the convention of standard palaeomagnetic sampling was adhered to and an intrusion, or suite of small intrusions, was sampled in a number (ideally greater than 5) of spatially distinct sites, each comprising 4 – 10 cores within a few metres of one another. Cores were drilled using a standard petrol-driven palaeomagnetic portable drill. Prior to extraction, they were oriented in situ using a sun compass rather than a magnetic compass when possible to avoid deviation resulting from local geomagnetic field anomalies associated with the sampled body. Unoriented block samples were also taken from some sites to provide additional material for palaeointensity analysis.

The approach of sampling an intrusion at numerous sites allowed direction and intensity results to be tested for self-consistency within sites, while *secular variation* was represented through between-site dispersion of results. The cores taken were generally between 2 and 5 inches long allowing them to be divided into several palaeomagnetic samples. Whenever surface weathering was observed, samples were always preferentially taken from the deeper part of the core.

2.1.3 Origin of remanence and domain states

This section merely intends to introduce basic, pertinent aspects of the theory behind palaeomagnetism. For a more comprehensive treatment, the reader is directed towards published textbooks on the subjects (e.g. Butler, 1992; Tauxe, 1998; Dunlop and Özdemir, 1997).

Ferromagnetic material can acquire a *remanent magnetisation* (or *remanence*) when it is subjected to a magnetic field under certain conditions. These conditions define the type of remanence that is acquired (table 2.1).

The *natural remanent magnetisation* (NRM) of a single rock sample may contain several different types of remanence across its *blocking temperature spectrum*. For example, VRM usually only affects grains with low *blocking temperatures* (T_B) and a TRM is often the *characteristic remanence magnetisation* (ChRM) of an igneous rock.

Important to the understanding of this study is the concept of *partial thermoremanent magnetisation* (pTRM). This is simply a portion of TRM residing between two blocking temperatures and can be imparted in the laboratory by heating a sample to a certain temperature and cooling it to another while subjecting it to a magnetic field. Similarly, if a sample is heated to a certain temperature and cooled in zero magnetic field, the sample loses the remanence held in ferromagnetic grains with *unblocking temperatures* below the upper temperature. This technique is called thermal demagnetisation and was widely used for the purpose of this study.

Thermoremanent magnetisation (TRM): The most important type of remanence to this study, acquired when a material cools below its *Curie temperature* (T_C) in the presence of a magnetic field. The primary remanence of an igneous rock is usually a TRM.

Chemical or Crystallisation Remanent magnetisation (CRM): Remanence acquired as new ferromagnetic mineral forms or is altered in the presence of a magnetic field. Often caused by severe weathering in nature.

Isothermal remanent magnetisation (IRM): Remanence acquired when material is subject to a very strong field under normal conditions. IRM is often caused by lightening bolts in nature and is recognisable by its high intensity and random direction.

Viscous remanent magnetisation (VRM): Remanence acquired because of exposure to a weak field over a very long time.

Thermoviscous remanent magnetisation (TVRM): A combination of TRM and VRM acquired when a material is subjected to elevated temperatures for prolonged periods in the presence of a magnetic field.

Thermochemical remanent magnetisation (TCRM): Remanence acquired when a material is subjected to chemical changes at elevated temperatures.

Natural remanent magnetisation (NRM): Umbrella term for any remanence(s) acquired naturally; can comprise any of the above in isolation or combination.

Table 2.1: Types of remanence important to this study and the conditions under which they are acquired.

If a ferromagnetic grain does not exceed the *critical single domain size*, then T_{UB} is equal to T_B and the grain is *single domain* (SD). However, if the grain exceeds this size it segregates itself into numerous *magnetic domains* and becomes *multidomain* (MD). MD grains behave in a more complex manner than SD grains with T_{UB} greater than T_B. Consequently, a separate section (§ 2.6.4) will deal with TRM in these grains. They generally exhibit lower *coercivities* than SD grains and are said to be magnetically 'soft'. This effectively means that the remanence they carry is more easily removed or replaced than that carried in SD grains and that they are less palaeomagnetically stable.

In actuality, there is a continuous spectrum of behaviour between that of true SD and true MD grains. Occupying this spectrum is the (hypothetical) pseudo-single domain (PSD) grain, which is that most frequently encountered in palaeomagnetic studies of igneous rocks. PSD grains of magnetite range in size between approximately 1 μm and 10 μm (Butler, 1992) and have coercivities intermediate of those of SD and MD grains. Unsurprisingly, finer PSD grains are preferred in palaeomagnetic studies.

2.1.4 Important ferromagnetic minerals

The TiO_2-FeO_2-Fe_2O_3 ternary diagram (figure 2.1) indicates the composition of the most important ferromagnetic minerals: the iron-oxides. Lines of oxidation are parallel to the base of the diagram and the solid solution series of titanomagnetite and titanohaematite, of primary importance here, are indicated.

Titanomagnetites are commonly the most important ferromagnetic minerals in igneous rocks, they form a primary crystallisation phase and are described by the formula:

$$Fe_{3-x}\ Ti_{x}\ O_4$$

where x signifies the proportion of titanium present in the lattice, varying between 0 (magnetite) and 1 (ulvöspinel).

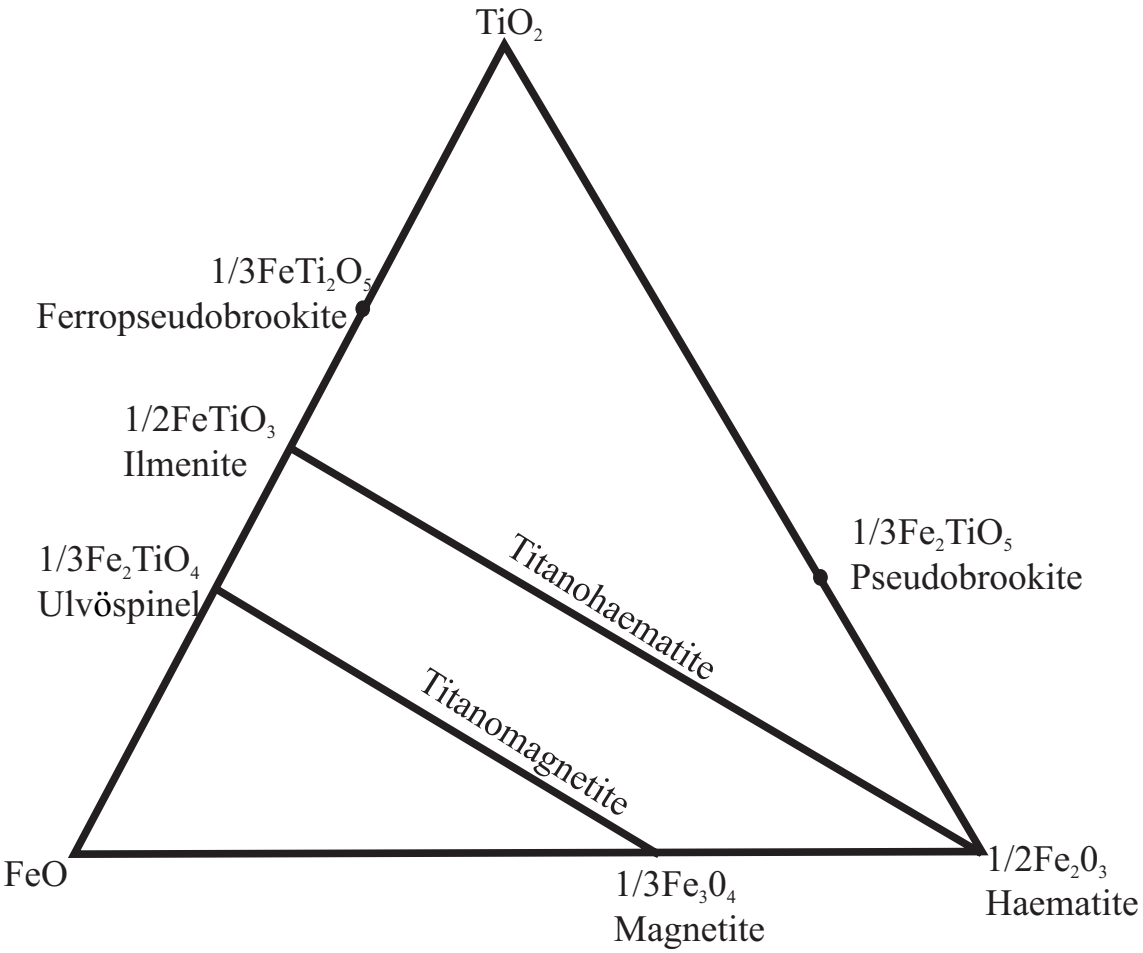

Figure 2.1: TiO_2-FeO-Fe_2O_3 ternary diagram (normalised so that lines of oxidation are horizontal), solid solution series are indicated.

Mineral	T_C (°C)	M_S (Am^2/kg)	H_C†	Critical SP size (μm)	Critical SD size (μm)
Magnetite Fe_3O_4	580	92	10's of mT	0.025	0.08
Titanomagnetite (TM60) $Fe_{2.4}Ti_{0.6}O_4$	150	24	~ 8 mT	0.08	0.2
Haematite αFe_2O_3	675	0.4	Up to 10's of T	0.025	15
Maghaemite γFe_2O_3	590 - 675*	74	Similar to magnetite		0.06
Pyrrhotite Fe_7S_8	325*	0.4 -20	Varied, generally greater than magnetite		1.6

Table 2.2: Magnetic parameters of minerals commonly found in intrusive igneous rocks. Critical SP size refers to the maximum length of a grain exhibiting *superparamagnetism*. * Maghaemite inverts to haematite at > 250°C, Pyrrhotite breaks down to magnetite at ~ 500°C. † H_C values are for guidance only as they are dramatically affected by changes in domain state. Data taken from Dunlop and Özdemir (1997) and Tauxe (1998).

Pure magnetite (Fe_3O_4) has a Curie temperature of 580°C and high *saturation magnetisation* (M_S). Increasing substitution of Ti into the lattice decreases the Curie temperature and M_S. A value of $x > 0.8$ means the titanomagnetite is *paramagnetic* at room temperature and above.

The generalised formula for titanohaematite is:

$$Fe_{2-x}Ti_xO_3$$

x varies from 0 for haematite to 1 for ilmenite. Haematite (denoted here as αFe_2O_3 to distinguish it from maghaemite) does not suffer significant loss of magnetisation

until close to T_C. It has low M_S allowing *magnetocrystalline anisotropy* to be much more effective than *shape anisotropy*, the resulting coercivity can be very high and haematite is said to be magnetically hard. The introduction of Ti into the lattice again causes T_C to fall linearly, to below room temperature by x = 0.8.

Titanomaghaemites are formed from the diffusion of ferrous Fe cations from titanomagnetite during low temperature (< 200°C) oxidation. They are chemically identical to titanohaematite (the end member maghaemite is denoted as γFe_2O_3) but retain the spinel structure of magnetite. Consequently they are sometimes referred to as cation deficient, or CD magnetite.

The saturation magnetisation is less than that of titanomagnetite but H_C is not significantly different (Opdyke and Channell, 1996). The Curie temperature of maghaemite has been inferred to be higher than that of magnetite (Özdemir and Banerjee, 1984), although it is metastable and transforms to titanohaematite when heated. The range of temperature at which (titano) maghaemite inverts to (titano) haematite appears to range from 250°C to greater than 750°C and is likely to depend on grain size and the degree of oxidation (Dunlop and Özdemir, 1997).

Pyrrhotite is usually transformed to Magnetite above 500°C. It is common in plutonic rocks but, like haematite, often goes unnoticed because of coexisting (Ti-poor titano) magnetite, which is far more magnetic.

2.1.5 Origin of ferromagnetic minerals in intrusive igneous rocks

Intrusive rocks were sampled for the purpose of this study for reasons given in § 3.1. The long cooling histories of these tend to generate a wide range of grain sizes, which often exceeds an order of magnitude (Dunlop and Özdemir, 1997) Stable components of magnetisation held in SD / PSD grains are frequently encountered within samples from intrusive rocks. These fine-grained ferromagnetic minerals are

not primary in the strictest sense but are formed by processes such as exsolution, *deuteric oxidation* (oxyexsolution), and secondary alteration.

Titanomagnetites and to a lesser extent, titanohaematites are primary phases in igneous melts crystallising at ~ 1300°C. These intermediate phases usually exsolve into Ti – rich and Ti – poor constituents upon cooling, the formation of exsolution lamellae sub-divides the crystals decreasing effective grain size. Exsolution is occasionally bypassed in quenched lavas but this is not possible in slower cooled intrusive rocks.

Fluids are retained in the bodies of cooling intrusive rocks with the result that some *deuteric oxidation* usually takes place between 900°C and 500°C (Grommé *et al*, 1969; Tucker and O'Reilly, 1980b). Wilson and Watkins (1967) and Watkins and Haggerty (1967) developed a classification system showing that as high-temperature oxidation is allowed to progress, ilmenite lamellae appear within the titanomagnetites (TM), these together with the TM oxidise towards their Ti-poor end members and eventually even the TM is replaced with haematite and rutile (TiO_2). This latter stage of oxidation is not commonly observed in intrusive rocks but the mechanism is usually effective enough to ensure that inter-grown Ti-poor magnetite dominates the magnetic mineral assemblage (Dunlop and Özdemir, 1997).

Another important source of fine-grained ferromagnetic material, particularly in plutonic rocks, is from inclusions in so-called 'magnetic silicates'. These inclusions are ubiquitous and can cause the rock to display a bi-modal blocking temperature spectrum (Evans and McElhinny, 1969). This is the composite of a soft MD magnetisation held in either the 'primary' material or in large inclusions in a particular silicate (Wu *et al*, 1974), and a hard SD-like remanence in smaller, more elongate inclusions. These inclusions can form from deuteric oxidation of the silicate at > 800°C (resulting in TRM acquisition) or from secondary alteration at lower temperatures (resulting in CRM acquisition).

Low temperature oxidation of (titano) magnetite can occur in all igneous rocks and culminates in the generation of maghaemite or even haematite. It is of particular concern to this study because a CRM is imparted to the newly formed mineral and this can render the results of a palaeointensity analysis meaningless (§ 2.5).

2.1.6 Alteration induced in the laboratory

The palaeodirectional and palaeointensity methods described in subsequent sections involve heating samples of rock in the laboratory, this commonly causes alteration to the magnetic minerals in the sample. Heating-induced alteration of magnetic grains involves changes in the physical and chemical properties of the grain. Changes in the magnetic properties of the grains (M_S, M_{RS}, H_C. etc.) need not be caused by any wholesale chemical alteration (Kosterov and Prévot, 1998) but any chemical changes that do occur are likely to have consequences for the magnetic properties. As will become evident in § 2.5, any change in these properties can be problematic for palaeointensity determination. Means by which such alteration are identified or predicted are discussed in the following sections.

Common alteration processes occurring in the laboratory are: magnetite oxidising to haematite (> 500°C), titanomagnetite oxidising to magnetite (> 300°C) and the inversion of (titano)maghaemite to (titano)haematite (> 250°C) (O'Reilly, 1984; Dunlop and Özdemir, 1997). These and other process will be discussed further when they are encountered in chapter 4.

2.2 Rock magnetic Analyses

Whole-rock magnetic analyses of samples were used in this study to ascertain the dominant magnetic minerals and their domain state. In turn, this provided information on the types of remanence carried, the susceptibility of the minerals to

laboratory-induced alteration, and therefore their potential for use in palaeointensity analysis.

The behaviour of samples during many of the analyses described in this section have been rigorously categorised by previous studies. For the most part, such categorisations receive only passing mention in this section as they often apply to only one rock type (mainly basalt flows). Instead, individual results will be interpreted in chapter 5 on the basis of generic information given in this and preceding sections.

2.2.1 Thermomagnetic analysis

The saturation magnetisation (M_S) of a grain is independent of its size and shape and so is often diagnostic of the mineral itself. However, to make use of this for whole rock samples, the mass concentration of the mineral in the sample would need to be known. The Curie temperature (T_C) is that at which thermal energy overcomes exchange coupling and M_S reduces to zero, T_C can also be diagnostic of magnetic mineralogy and does not vary for differing concentrations.

Thermomagnetic analysis measures the function $M_S(T)$ while heating a sample from room temperature to above T_C and then cooling it back down. The machine used for these experiments is called a translation balance. It operates by applying a constant strong field (600 mT) to a small (~ 0.5g) crushed sample of rock and measuring the response as a function of temperature. The intersecting tangents method of Grommé *et al* (1969) was used to overcome the paramagnetic signal and extract T_C from plots of $M_S(T)$ (figure 2.2). This method was also used in cases where a combination of ferromagnetic phases was present in a sample.

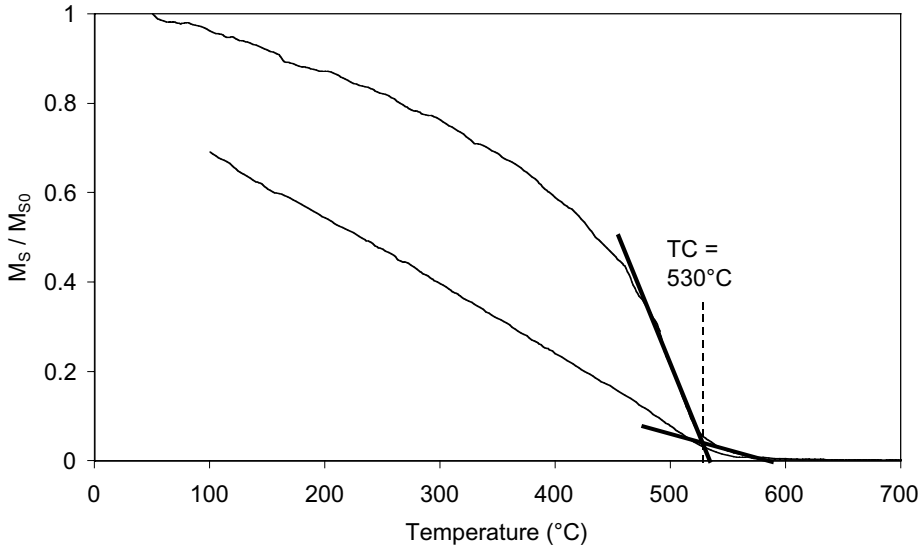

Figure 2.2: Example of the intersecting tangents method of Grommé *et al*. (1969) being used to ascertain T_C from a thermomagnetic curve.

Thermomagnetic analysis is also useful in identifying the type and extent of alteration in a heated sample. This is done by examining differences between the heating and cooling curves of the $M_S(T)$ plot. Mankinen *et al.* (1985) developed a categorisation system for $M_S(T)$ curves of basaltic lava from studying those of Steens Mountain, Oregon. Thomas (1992) added another 3 categories to these to account for behaviour observed in basalt flows from the Gardar succession, Greenland. These categories will not be reported here, as their applicability to intrusive rocks is not clear. The significance of individual $M_S(T)$ curves will be discussed as they are presented in chapter 4.

In addition to performing the complete thermomagnetic experiment described above, some samples were cycled between progressively higher temperatures and room temperature. This allowed the temperature(s) at which alteration occurred to be constrained to above that at which the cooling curves were still reversible.

2.2.2 Analysis of hysteresis properties at room temperature

2.2.2.1 Hysteresis loops

Hysteresis loops were plotted from the response of small samples to varied fields using either the vibrating sample magnetometer (VSM) or the variable field translation balance (VFTB). The shapes of the loops depend strongly on the type of anisotropy controlling the remanence of the dominant ferromagnetic grains within the sample. This in turn is a function of the domain state and mineralogy of these grains.

When samples comprise only one phase of ferromagnetic grains, hysteresis loops are relatively simple (fig. 2.3). When two or more significant phases (domain states and / or minerals) are present however, the loops become composites of different behaviour and may be more complex.

The shape of a hysteresis loop is dictated by certain parameters namely*: saturation magnetisation* (M_S), *saturation remanence* (M_{RS}), *coercivity* (H_C), *coercivity of remanence* (H_{CR}), low-field *susceptibility* (χ_{LF}) and high-field susceptibility (χ_{HF}). The last of these is a measure of the *paramagnetism* of the sample and must be used to correct the loop so that the ferromagnetic signal is isolated. Figure 2.3(a) shows how M_S, M_{RS}, and H_C, can be measured from the loop, H_{CR} can either be measured directly from a back-field IRM experiment (§ 2.2.2.2), or estimated from the loop itself. If the entire loop is shifted down by an amount equal to M_{RS}, the x – intercept of the ascending loop approximates H_{CR}. The relationship of these four parameters indicate the average domain state of the remanence carriers within a sample (Day *et al*., 1977).

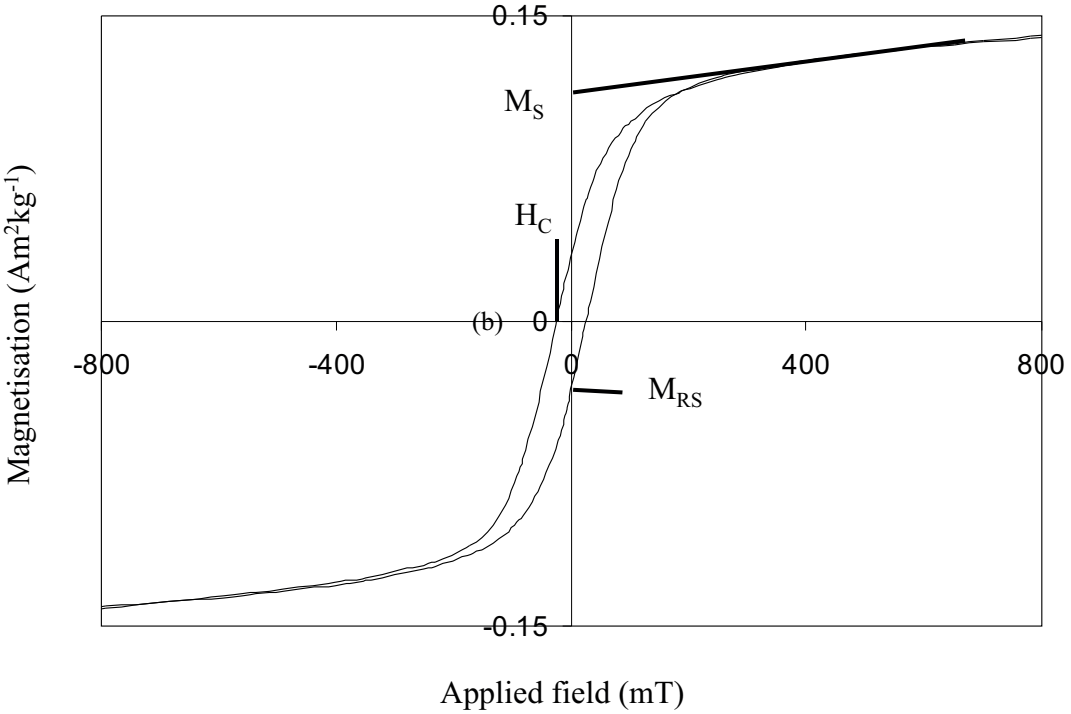

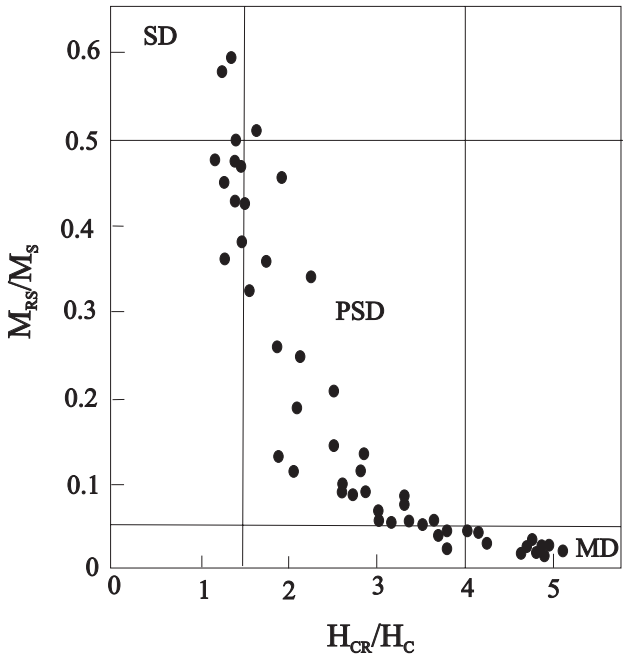

Figure 2.3:(a) Example of a hysteresis loop showing important parameters. (b)Day plot showing distribution of size fractioned titanomagnetite samples (redrawn from Day *et al*. (1977))

M_S is essentially independent of grain size whereas M_{RS} is far larger for SD than MD grains. This is because SD grains relax only by domain rotation to their easy axis whereas MD grains relax by a combination of this and the movement of unpinned domain walls.

The ratio of M_S / M_{RS} has been shown theoretically (Dunlop and Özdemir, 1997) and empirically (Day *et al*., 1977) to be between 0.5 and 1 for assemblages of only SD grains and less than 0.05 for true MD grains. Values of this ratio between 0.5 and 0.05 indicate that either PSD grains are predominant in the sample or that a mixture of SD and MD are present.

The ratio of H_{CR} / H_C is less reliable as a diagnostic indicator of domain state (Dunlop and Özdemir, 1997) but is still widely quoted. H_C is strongly dependent on the number of domains in a grain and does not exceed 10 mT for MD magnetite. H_{CR} can be very high in MD grains because of the internal demagnetising field. A value for H_{CR} / H_C of between 1 and 2 is expected for uniaxial SD grains and greater than 4 for MD grains (Dunlop and Özdemir, 1997).

These two ratios are usually plotted against one another on a Day plot and values from both natural and synthetic magnetite should be confined to a relatively narrow section of it (figure 2.3(b)).

2.2.2.2 IRM acquisition and demagnetisation

This method allows an intuitive insight into the remanence carriers within a sample, and is useful for displaying small concentrations of high coercivity material that may be overlooked by standard hysteresis analysis. The experiment is conducted on ~30g core samples by first applying increasingly large DC magnetic fields and measuring the IRM acquired by the sample in a spinner magnetometer. This is halted once saturation isothermal remanent magnetisation (SIRM, equal to M_{RS}) or the limit of the pulse magnetiser is reached; the field is then applied in the opposite direction,

increasing from small values again, until the sample is demagnetised. This experiment was also conducted using a VFTB with the advantage that only very small (~ 0.2g) samples were used, leaving more material for other analyses.

The measured IRMs after each field exposure are plotted against the strength of the applied field in a partial remanent hysteresis loop (figure 2.4). This effectively displays the coercivity spectrum within a sample, 'soft' phases such as magnetite are indicated by an early flattening of the curve whereas SIRM is seldom achieved when 'hard' phases (e.g. haematite) are present. The field required to impart half the SIRM ($H_{1/2}$), which can be diagnostic of the domain state and the coercivity of remanence (H_{CR}) can be measured directly from partial remanent hysteresis loop (figure 2.4). Samples that contain both hard and soft phases are distinctive because of inflexions in the curves.

2.2.2.3 Measurement of bulk susceptibility at room temperature

Low-field χ can be measured directly from the hysteresis loop or, more commonly, measured using a Bartington MS2 susceptibility bridge. This is advantageous in that palaeomagnetic core samples can be measured quickly without affecting their remanence. This allowed the susceptibility of samples to be monitored between heating steps during the palaeodirectional and palaeointensity analyses as a check for laboratory induced alteration.

Intuitively, χ_{LF} (denoted as just χ from here on) depends on the ratio M_S / H_C and therefore changes in both domain state and mineralogy are reflected in its variation. Such changes can rarely be used alone to diagnose the type of alteration however, additionally it must be remembered that bulk susceptibility can be dictated by ferromagnetic phases within a sample that do not necessarily contribute significantly to its remanence.

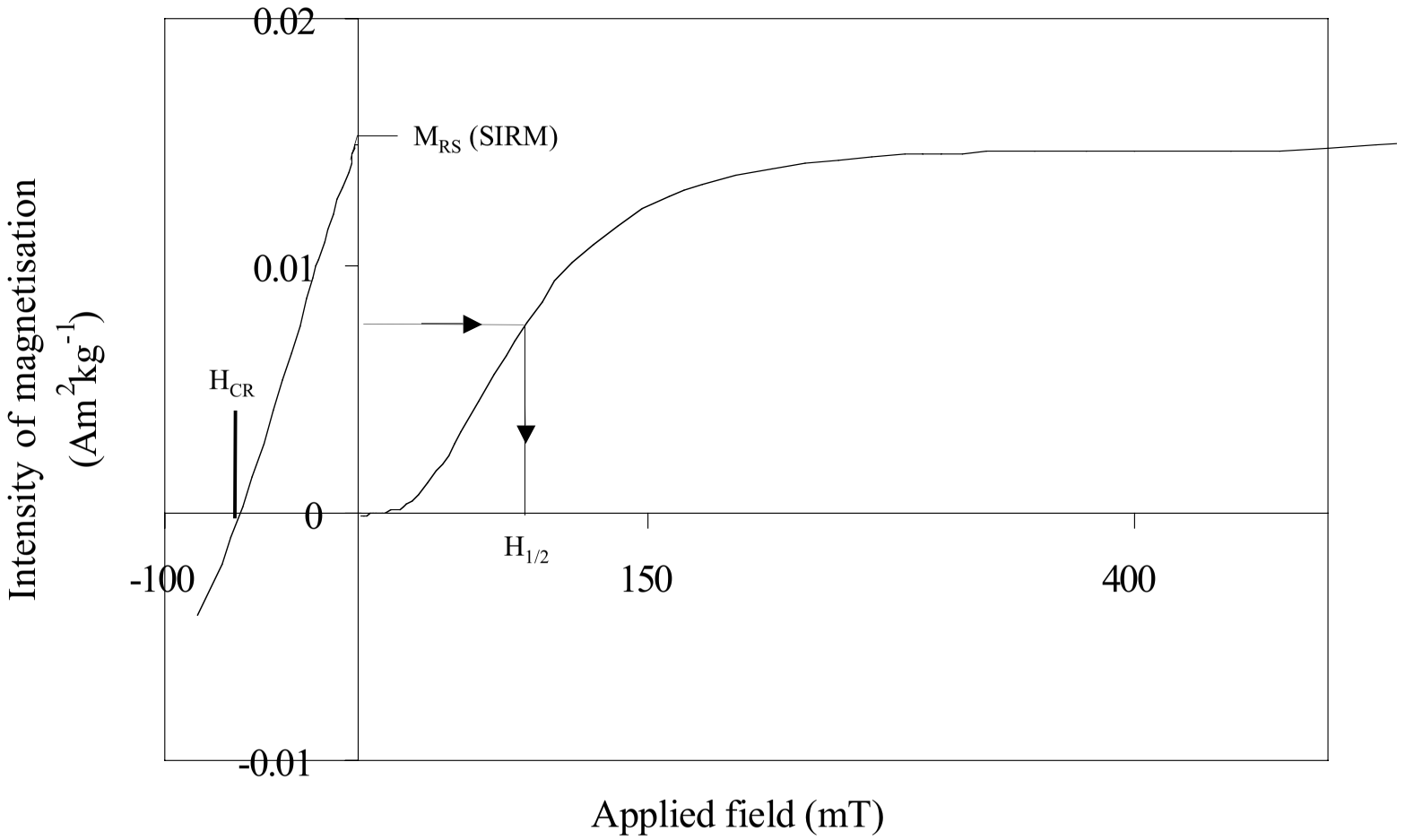

Figure 2.4: Example of a partial remanent hysteresis loop showing important parameters

An assemblage of superparamagnetic (SP) grains has a very high low-field susceptibly that will obscure the signal from any remanence carriers in a sample. The presence of SP grains can be diagnosed from their dramatically viscous behaviour by measuring bulk susceptibility at different frequencies of an applied alternating field. A significant presence of SP grains will be indicated by an increase in χ for high frequency measurements as these grains are further excited. Larger grains do not display this frequency dependence, as their relaxation times are much lower than the frequency of the applied field.

2.2.3 Low temperature susceptibility (χ_{LT}) analysis

Bulk susceptibility can be monitored quasi-continuously as a sample, previously cooled in liquid nitrogen (-196°C), warms back to room temperature. The shape of the χ–T curve produced is strongly dependent on the mineralogy and domain state (specifically type of anisotropy) of the dominant ferromagnetic phase(s) within the sample.

SD magnetite is controlled by shape anisotropy when elongation exceeds 10%, the shape of a grain and therefore its susceptibility does not change significantly down to -196°C (Levi and Merrill, 1976, 1978).

Magnetocrystalline anisotropy is strongly temperature dependent however, the isotropic point is the temperature at which the characteristic easy direction changes its orientation and the anisotropy constant K1 changes sign. In magnetite this occurs at -150°C which generates a peak in susceptibility at this temperature. In haematite, this is called the Morin transition and occurs at -10°C (Hunt *et al*., 1995), haematite grains of all sizes are expected to display this transition.

Magnetite grains larger than SD size generate a peak in susceptibility at -150°C, however it will still be present in a whole rock sample if MD (PSD) grains only comprise a small proportion of it. The relative susceptibility (RS) ratio (χ_{-196} / χ_{30},

critical value 0.5) is argued to be a good indicator of the proportion of MD to SD grains in a sample that displays a peak at the isotropic point (Thomas, 1993).

SP grains should also display some variation in susceptibility with temperature. The increase in relaxation time that accompanies a reduction in thermal energy implies that some grains will behave as SD grains at very low temperatures. Consequently, the susceptibility of a sample containing SP grains should increase steadily with increasing temperature giving RS ~ 0.1 (Radhakrishnamurty *et al*., 1977).

χ–T curves indicative of titanomagnetites and (titano)maghaemite are disputed (Senanayake and McElhinny, 1981; Radhakrishnamurty, 1985). The effect of introducing Ti appears to suppress the peak at -150°C, while SD maghaemite has been observed to behave similarly to SD magnetite (Senanayake and McElhinny, 1981).

2.2.4 The thermomagnetic criterion

Blocking and unblocking temperatures are not equal in MD grains and this causes a pTRM acquired between two temperatures to have a 'tail' that is still present after thermal demagnetisation to the higher of these temperatures (§ 2.4.4). A technique known as the thermomagnetic criterion or pTRM tail check (Shcherbakova *et al*., 2000) uses this behaviour to ascertain the domain state of the **remanence carriers** within a sample.

The method involves heating a sample to T_C and imparting a pTRM between 300°C and T_R during the cooling phase (a $pTRM_A$; § 2.4.4). Thermal demagnetisation is then performed up to 300°C and the measured remanence is expressed as a percentage of that measured prior to thermal demagnetisation. Shcherbakova *et al*. (2000) proposed that a tail greater than 15% of the pTRM indicated that MD grains were dominant below 300°C whereas a tail less than 4% indicated SD grains.

2.3 Palaeodirectional Analysis

The experimental aspect of palaeodirectional analysis consisted of using a Molspin spinner magnetometer to measure the direction of remanent magnetisation in a sample after each application of stepwise thermal demagnetisation (§ 2.1.3). Thermal demagnetisation was applied to progressively higher temperatures to eliminate *secondary magnetisations* residing in grains with lower blocking temperatures first, and was halted when the sample was observed to have no remanence remaining.

Vector components of magnetisation were identified and isolated on an orthogonal vector plot (OVP; Zijderveld, 1967; appendix 2). The acceptance criteria for any recognised vector is generally that it must display no overall curvature (which is indicative of two or more components overlapping in the blocking temperature spectrum, (see appendix 2) and that the *maximum angular deviation* (MAD) was less than 15°.

The direction (declination and inclination) of each component isolated on the OVP was corrected for the in situ orientation of the core to yield an absolute direction of magnetisation. It then becomes necessary to compare the directions of components (usually from similar parts of the blocking temperature spectrum) in different samples from the same site.

Dispersion of measured directions, due to random error in the case of intra-site directions and *secular variation* in the case of inter-site directions, is expected to be normally distributed about the mean. Fisher (1953) developed a probability density function (PDF), equivalent to a Gaussian distribution, to explain dispersion of measurements on a sphere. Two parameters: k and α_{95}, derived from this PDF, are reported with every mean direction, calculated from three or more directions, in chapter 4. k is an estimate of the precision parameter (κ) of the dispersion and extends into infinity for a set of well clustered directions. When $k > 30$ for a set of

directions, they can be confidently treated as representing moderate dispersion around a meaningful average. In chapter 4, site mean directions with $k < 10$ are usually excluded from overall mean calculations on the grounds of their questionable reliability.

The α value is analogous to the standard error of the mean in a Gaussian distribution. A probability of 0.05 was chosen for this study and the resulting value, α_{95} indicates the angular radius of a circle, centred on the mean, in which there is a 95% probability of the true mean occurring. An α_{95} value of less than 16° indicates that a mean direction is reasonably well constrained (Van der Voo, 1993).

The geomagnetic pole that would cause samples at latitude λ and longitude ϕ to acquire the average remanence direction observed is calculated to allow comparison with average remanence directions in samples from different localities. This is termed a *virtual geomagnetic pole* (VGP; see e.g. Butler, 1992 for equations). The confidence limit, previously a circle with radius α_{95}, becomes an ellipse around the VGP. This is described by the length of the semi-axis along the site-to-pole great circle (dp), and the perpendicular semi-axis (dm). These two angular lengths will be presented alongside all VGP positions in chapter 4.

The ChRMs found in this study were likely to be the primary TRMs of the igneous rocks sampled but supporting evidence was sought. The VGP produced by the mean ChRM direction was compared with well-established *palaeopoles* of a similar age to that of the intrusion. Palaeopoles relevant to this study, and the *apparent polar wander path* (APWP) they describe will be discussed in § 4.1. If the VGP of the ChRM was consistent with other palaeopoles from the time the intrusion formed, it was generally assumed that the remanence was primary. VGP's derived from the mean directions of secondary magnetisations were also compared to the APWP so that the time that they were acquired might be ascertained.

The rock magnetic analyses described in § 2.4 were another means employed to investigate the likelihood of the ChRM being a primary TRM. Results that indicated significant low temperature oxidation had affected the samples suggested that the sample was incapable of retaining a primary magnetisation.

The primary purpose of the palaeodirectional analyses was to isolate the ChRM and confirm it as a primary TRM suitable for palaeointensity analysis. The method of palaeointensity analysis described in § 2.6 involves thermal demagnetisation, therefore it is possible to fulfil these two objectives without resorting to a separate analysis. However, there were two sound reasons why, for the most part, this was not done. The first was that, given that the palaeointensity analysis is much more time consuming than straight-forward thermal demagnetisation, it was wise to focus it on the part of the blocking temperature spectrum where the TRM was known to reside. The second is that minerals can chemically alter during heating in the laboratory (§ 2.1.6). If the samples are simply being thermally demagnetised, this makes little difference. However, the palaeointensity analysis consists of remagnetisation heating steps during which a field is applied. If such alteration occurred during these, a TCRM would form which may have $T_{UB} > T_{LAB}$. Without the preliminary palaeodirectional results to indicate otherwise, this could be mistaken as a genuine ChRM component.

2.4 Palaeointensity Analysis

Many methods have been proposed to estimate the strength of the applied field at the time of remanence acquisition in a rock. However, it is the Thellier's (Thellier and Thellier, 1959) method (and its variants, see below) which is widely regarded as the most reliable (e.g. Prévot *et al*., 1990; Perrin, 1998).

Another popular method, not least because of the considerable time it saves compared to the Thellier method, is that proposed by Shaw (1974). Although this method can produce accurate palaeointensity results, it requires even more specific

(perfect) rock magnetic properties in ancient samples than the Thellier method (Thomas, 1993) and therefore the failure rate is very high. Additionally, the assumption of *anhysteretic remanent magnetisation* (ARM) equivalence with TRM, which Shaw's method relies upon, is not supported theoretically (Bailey and Dunlop, 1977) and has been shown in some cases to be empirically wrong (Kono, 1987).

For these reasons and because of the difficulty in accessing *AF demagnetisation* equipment while performing this study, only the Thellier method was employed in the palaeointensity analysis.

2.4.1 Principles of the Thellier method

Néel (1955) showed theoretically that the intensity of TRM at room temperature is linearly proportional to the intensity of the magnetic field (H) which imparted it, providing H < 120 μT (which appears to have always been the case for the geomagnetic field).

Unfortunately, the constant of proportionally is very specific to the physical properties of the material retaining the TRM and cannot be directly measured in the case of a rock sample that contain grains with a range of magnetic properties. However, it can be eliminated if a sample is subject to a measured field in the laboratory (H_{lab}) which imparts a measurable TRM (TRM_{lab}) and these parameters are combined with those occurring in nature. The palaeointensity (H_{pal}) of the ancient field can then be calculated from the equation:

$$H_{pal} = \left(\frac{TRM_{pal}}{TRM_{lab}} \right) H_{lab} \qquad \text{providing: } H_{pal} < 120\mu T,\ H_{lab} < 120\mu T$$

where TRM_{pal} is the natural, measured TRM of the sample.

This relationship obviously fails if the aforementioned 'constant' changes at any time. In real terms, this means that the grains that retain the TRMs must undergo no physical or chemical alteration either in nature, since TRM_{pal} was acquired, or in the laboratory before TRM_{lab} is measured.

The obvious approach of measuring the NRM of a sample, then giving it a TRM through its entire blocking temperature spectrum and feeding the results into the above equation would be hugely unreliable for two reasons. Firstly, very few rocks can be heated to above their Curie temperature in the laboratory without undergoing significant magnetic alteration. Secondly, most rocks naturally contain some form of magnetic overprinting, which would cause the measured 'TRM_{pal}' to deviate from its true value.

The method of Thellier and Thellier (1959) introduced double heating steps to allow the palaeointensity to be ascertained prior to the sample being heated to T_C. The sample was first heated to a certain temperature (T) beneath T_C and cooled in an applied field. The step was then repeated with the applied field equal and opposite to that in the first case. Vector calculations allowed the fraction of NRM (TRM_{pal}) with $T_{UB} < T$ lost, and that of TRM_{lab} with $T_B < T$, gained through this heating to be ascertained. Coe (1967b) later modified this procedure, performing the first heating step in zero field and the second in an applied field. In both cases, the entire process was repeated at progressively higher temperatures to T_C.

The fraction of NRM lost after each heating step when plotted against the pTRM (as a fraction of total NRM) gained will fall on a straight line if no alteration has occurred (Nagata *et al*., 1963). A loss of linearity indicates that the experiment should be halted, however the (negative) slope of the straight line prior to this can be multiplied by the laboratory field intensity to yield the intensity of the palaeofield. Hence, even though alteration has occurred below (perhaps well below) T_C, the palaeointensity can still be determined.

So far the Thellier method has been discussed assuming Néel's original model of a ferromagnetic assemblage consisting of only non-interacting SD grains. This was incorporated into Thellier and Thellier's method by requiring two laws to be obeyed by the TRM carriers in a sample. Thellier's laws are:

- **The Law of additivity.** For the simplest case of two pTRMs:

$$pTRM_{(T1,T3)} = pTRM_{(T1,T2)} + pTRM_{(T2,T3)}$$

- **The Law of independence** states that $pTRM(T_1,T_2)$ is fully removed by demagnetisation to T_1 (where $T_1 > T_2$) i.e. $T_B = T_{UB}$; pTRMs acquired over separate temperate intervals are completely independent of each other and a pTRM is not affected by any demagnetisation which occurs below the lowest temperature at which the pTRM was acquired.

Thellier's laws are only fully obeyed by SD grains, PSD and MD grains have $T_{UB} > T_B$. Nevertheless, PSD grains are regarded by many as reliable palaeointensity recorders. This topic will be further discussed in § 2.4.4.

2.4.2 Experimental and analytical procedure

Standard palaeomagnetic samples (~30g cylinders) were selected for palaeointensity analysis on the basis of positive results from rock magnetic and palaeodirectional analysis of samples from the same core.

The treatment of the samples consisted of heating them to a certain temperature, holding this temperature for sufficient time to ensure the entire sample had reached it, and cooling the sample back to room temperature in either zero or a constant laboratory field (25 or 50 μT). After each thermal treatment the total remanence (direction and intensity) of the sample was measured in a spinner magnetometer.

The nomenclature used from here on for these measurements is that of three numbers. The first two represent the first two figures of the three-figure temperature the sample was heated to, e.g. 25 represents 250°C. The final figure represents the stage of the experiment and is 0 for NRM demagnetisation and 1 for imparting of TRM. For example, 250 denotes a measurement after NRM demagnetisation up to 250°C was performed and 401 indicates that a TRM was imparted between 400°C and T_R before the remanence was measured. The only exception to this rule is the first NRM measurement made before any thermal treatment, which is denoted: 0.

The standard double heating procedure of the modified Thellier experiment at 100°C intervals would then be: 0, 100, 101, 200, 201, 300, 301,…, and so on until the Curie temperature of the samples was exceeded. The NRM measurement is then just that measured at 0, 100, 200 etc. whereas the TRM can be calculated by simple vector subtraction: 101-100, 201-200, etc. The two would be plotted on an NRM-TRM plot and the slope of the line through the low temperature, linear points (providing no secondary magnetisations were present) would be used to calculate the palaeointensity.

A non-linear NRM-TRM plot is always indicative of non-ideal conditions for palaeointensity determination, however the plot may remain linear while such conditions prevail. An example of this was provided by Prévot *et al*. (1983) who presented results from submarine basalt samples that maintained a linear plot between two temperatures, while rock magnetic measurements clearly showed that they were altering in this period.

However, such behaviour is irreversible and can be detected by the sliding pTRM checks which are used in most modern studies. In this study, pTRM checks were measured by performing another demagnetisation stage to a lower temperature than that at which a pTRM had just been imparted. For example, after stage 301, thermal demagnetisation might be performed to 200°C, followed by a measurement (denoted

202 to show that it was a pTRM check). The vector calculation 301-202 could then be compared to 201-200 to see if any variation in the pTRM capacity of the sample between T_R and 200°C had occurred since the 200 and 201 measurements were made.

In addition to the double-heating step and the sliding pTRM check, another measurement called a NRM check was performed in some of the experiments described in chapter 4. This merely involves re-doing the first demagnetisation stage to the same temperature, after the pTRM acquisition and pTRM check stages; i.e. following the 300, 301, and 202 stages of the example above, the sample would again be thermally demagnetised to 300°C and measured (stage 303). Significant differences between 300 and 303 would indicate that the NRM of the sample had been affected during stages 301, 202, or 303.

The measurements in a full Thellier experiment, with 50°C intervals and pTRM checks after every stage would be conducted in the following order: 0, 100, 101, 103, 150, 151, 102, 153, 200, 201, 152, 203,….T_C.

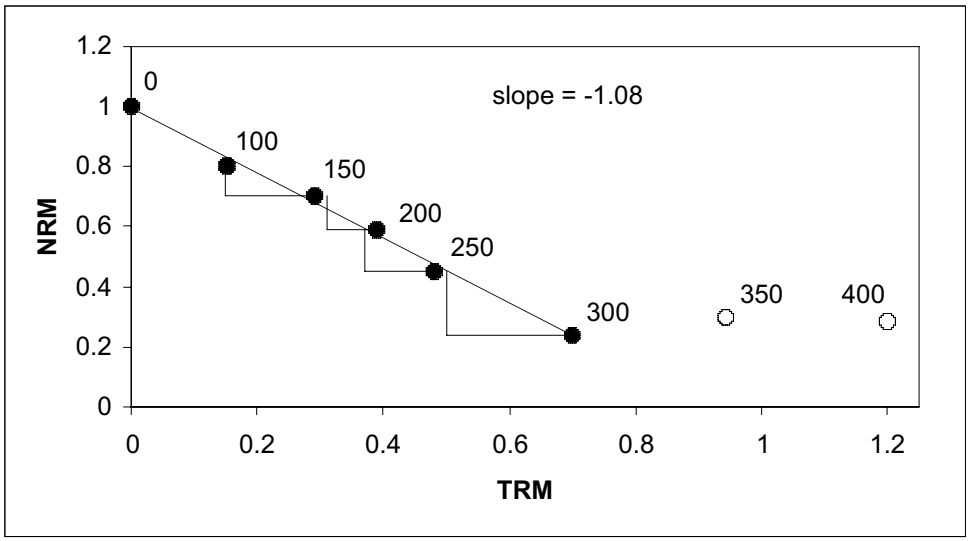

Figure 2.5: Synthetic example of a NRM-TRM plot, filled circles represent points used to calculate the best-fit line whereas hollow circles are those rejected.

Figure 2.5 shows an example of a NRM-TRM plot, with pTRM checks after every heating step, which loses linearity above 300°C. The pTRM 'triangles' indicate the results of the pTRM checks and clearly pass, i.e. their free end is close to the proceeding point. The palaeointensity estimate from this sample would thus be equal to 1.08 (the slope of the best-fit straight line) multiplied by the laboratory field. As observed in figure 2.5, it is usual for values of TRM and NRM to be normalised to the 0 (NRM) measurement.

2.4.2.1 Acceptance criteria

Coe *et al*. (1978) derived several statistical parameters used in this and many other studies. The calculations for the f, g, q, and β values are given in appendix 3. They also suggested that the following minimum criteria be applied to palaeointensity estimates before they are accepted and included in a site average (SA).

- The best-fit line must be defined by at least 4 points. This ensures that 4 separate estimates comprise the determined palaeointensity.
- The f-value must be greater than 0.15.
- The points defining the line must display no systematic curvature such that any segment spanning at least half the line has a slope different from the entire line by greater than 20%.
- Anomalous points in amongst those used to calculate the best-fit line must not be omitted unless experimental error is proven.
- Segments contaminated by secondary components of magnetisation must be avoided.

Selkin and Tauxe (2000) also developed the following criteria to be used in conjunction with that of Coe *et al*. (1978).

- The ratio (β) of the standard error of the slope of the best-fit straight line to the slope itself must be less than 0.1.
- The discrepancy between each pTRM check and the original value must be less than 10% of the length of the best-fit line through the data.
- The quality factor, q must be greater than unity.
- The standard deviation of the SA must be less than 25% of the value of the SA itself.

Both sets of criteria will be discussed in the context of the results presented in chapters 4 and 5. Generally, neither were used to dismiss data outright so as to allow some discussion of poor data to occur. Subsequent to the palaeointensity analyses being performed, a reliability (R) factor was developed empirically to allow comparison between palaeointensity estimates. This is calculated from the number of the properties shown in table 2.3 that the portion of the estimate possesses.

Reliability Factor
• A component believed to be a TRM is definitely isolated
• No pTRM impedance or initial steep slope (§ 4.3.3) is observed prior to or during the segment of the NRM-TRM plot used to calculate the estimate
• pTRM check discrepancies are less than 20%
• pTRM check discrepancies are less than 10%
• NRM check discrepancies are less than 10%
• All criteria proposed by Coe *et al*. (1978) are satisfied
• The β value is less that 0.10
• Measurements of χ_{RT} exhibit no significant (> 10%) changes below the maximum temperature measurement used to calculate the estimate.

Table 2.3: Properties comprising the R (reliability) factor.

The R factor will be quoted alongside all estimates together with its maximum possible value (to take account of experiments that did not measure NRM checks etc.). It will generally not be discussed with the results as their individual properties

are more important; it is stressed that the R factor is not intended as the 'last word' on the reliability of estimates but as a means of comparison between them. The R factors associated with most recently published palaeointensity estimates are usually 5 or above. Arguably, the R factor associated with an estimate should equal its maximum value before being pronounced reliable. In this study, those estimates with $R < 5$ are treated with healthy scepticism and those with $R < 3$ are generally not considered.

Coe *et al*. (1978) also proposed a system of weighting the contribution of each palaeointensity estimate to the mean estimate using its q factor. This system was not used in this study because of the strong, and in some cases unjustifiable, bias it can place on certain estimates. Each mean palaeointensity estimate will be displayed with its standard deviation as uncertainty bounds.

The average palaeointensity for a sampling site is converted into a virtual dipole moment (VDM; intensity equivalent of VGP) to allow it to be compared with results from different palaeolatitudes. These site average (SA) VDMs are the primary data used in tha analyses described chapters 7 and 8.

2.4.3 Problems associated with the Thellier method

The difficulties associated with absolute palaeointensity analysis are manifold. Although Thellier's method is the most successful in minimising failure-rate and drawing attention to unreliable recorders, it is nevertheless fraught with problems. Despite the support of intensive preliminary analyses (§ 2.2 and § 2.3) and rigorous sample selection, non-ideal behaviour is commonplace.

There are four main causes of samples behaving non-ideally during the Thellier experiment although they are often intrinsically combined. These are alteration in the laboratory, alteration over geological time, lack of SD material, and the primary magnetisation not being a TRM.

Much (well-deserved) attention has already been placed on laboratory-induced magnetic alteration (§ 2.1.6). In this study, some preliminary rock magnetic experiments were aimed at assessing the temperature at which such alteration is triggered so that the Thellier experiments could focus below it.

Natural alteration is usually expressed as a secondary magnetisation and therefore identifiable from the palaeodirectional analysis as well as rock magnetic experiments.

A Thellier experiment giving ideal results requires, amongst other things, all the remanence carriers to be single domain (SD). To illustrate the problems encountered when this condition is not met, it is easiest to first discuss TRM theory for MD grains and its implications for Thellier analysis and then introduce the hybrid conditions encountered in PSD grains. This shall be done in § 2.4.4.

The primary magnetisation of an igneous rock is usually assumed to be a TRM although this is not always the case. Studies indicate that deuteric oxidation is generally completed above the Curie temperature (§ 2.1.5) but there is very little, short of a detailed petrographic study of each sample, that can be done to confirm this.

Of even greater concern than samples failing to give results from the Thellier experiment and the associated time wasted, are those samples yielding inaccurate or even spurious estimates despite displaying almost ideal behaviour.

This can occur in numerous ways. An example of how alteration in the laboratory can hypothetically not affect NRM-TRM plot linearity or pTRM checks is given § 5.3.4. Additionally, McClelland (1996) showed theoretically that a CRM overprint in SD grains can have to same (non-) effect up to temperatures of 400°C. Such an overprint should be identifiable from the rock magnetic analyses but the addition of

a thermal component making it a TCRM could produce the same effect and may not be so noticeable.

The final problem associated with the Thellier method of palaeointensity estimation is that of differences in cooling rate between when the TRM was acquired naturally and that when it was acquired in the laboratory. The intensity of TRM in SD grains increases with cooling time by about 7% per order of magnitude (Dodson and McClelland Brown, 1980; Halgedahl *et al*., 1980; Fox and Aitkin, 1980). In slow-cooled plutonic rocks, the difference due to this effect could be as much as 40% although it is very difficult to estimate (Dodson *et al*., 1978). The implication of this for palaeointensity estimation is that the NRM-TRM plot tends to become steeper and the ancient field strength is overestimated. TRM intensity in MD grains displays the opposite response to SD grains although the effects are less (McClelland Brown, 1984). The effect of cooling rate differences for TRM held in PSD grains has not been tested.

2.4.4 TRM theory in MD grains: implications for the Thellier method

A unified theory explaining all aspects of TRM behaviour in MD grains has not yet been presented. Such a model should explain all of the following observed features (Shcherbakova *et al*., 2000):

1. The linear dependency of pTRM intensity on the imposed field.
2. The failure of pTRMs to obey the law of additivity and independence.
3. The existence of a 'pTRM tail.'
4. The dependency of pTRM intensity and other features on thermal prehistory.

From a practical perspective, point 1 means that it is hypothetically possible to recover an accurate palaeointensity from samples containing only MD grains. Effectively, points 2, 3, and 4 make this process more complex and difficult than in samples containing only SD grains.

There are three likely sources of TRM in MD grains (Dunlop and Özdemir, 1997), wall-pinning is regarded as the most important of these in general circumstances. The effectiveness of this mechanism in retaining remanence depends on the state of the MD grain. Large homogenous grains owe their hysteresis properties to pure *magnetocrystalline anisotropy* and have correspondingly low microcoercivities. Equally large but inhomogeneous or highly stressed grains can have deep potential wells allowing *magnetostrictive anisotropy* to dominate. Samples with a predominance of such grains can have coercivities comparable to those with SD grains (Shcherbakova *et al*., 2000).

MD grains do not obey Thellier's law of independence (§ 2.4.1). This is hardly surprising given that the same domain walls are responsible for recording different pTRMs and that the many walls present in a single grain are expected to interact with one another. A further complication arises from the fact that a demagnetising field due to surface poles acts on any grain with non-zero magnetisation. The effect of this field is not important for SD grains, which are usually magnetised along their easy axis, but causes (assemblages of) MD grains to be demagnetised of a portion of the total TRM more readily than to acquire a new pTRM beneath the same temperature. This means that the intensity of the pTRM lost is greater than that of a new pTRM imparted over the same temperature interval. The implications of this for the Thellier analysis are crucial, each point measured during the experiment between room temperature and T_C falls below the 'true' straight line leading to a convex-down pattern on the NRM-TRM plot (Levi, 1977). The end points (NRM = 1, TRM = 0; NRM = 0, TRM = 1) of the analysis will be correct, but as laboratory-induced alteration is usually effective before T_C of the sample has been reached, the second of these is usually unobtainable and consequently the palaeointensity cannot be calculated.

The impression given by the phenomena described above may be that the pTRM acquired between two temperatures ($T_1 > T_2$) is entirely removed by thermal

demagnetisation to the higher of these together with an extra portion of the total TRM. This is not the case however: a pTRM imparted between T_1 and T_2 is not removed by thermal demagnetisation to T_1 but retains a tail which can only be removed by demagnetisation to T_C in true MD grains.

Dunlop and Özdemir (2000) gave a more succinct definition of the behaviour of MD grains to thermal demagnetisation. They describe each pTRM as having a high and low tail defined by the spectrum of blocking temperatures, $f(T_B)$. The width of $f(T_B)$ increases with mean grain size but is still significant in PSD grains of 20 μm. The high and low tails are symmetric about T_B and are both removed by modest *AF demagnetisation* suggesting that they have a common cause. Unfortunately, this cause is presently unknown but may be associated with nucleation of new domains during pTRM acquisition and their denucleation during thermal demagnetisation (Dunlop and Özdemir, 2000).

Shcherbakova *et al*. (2000) showed that the thermal history of PSD and MD grains affects the properties of the pTRMs they subsequently acquired. Those acquired when a field is applied at some point during cooling from T_C ($pTRM_A$), obey the law of additivity but have larger pTRM tails than those acquired by heating from room temperature to the upper T_B and cooling back to room temperature ($pTRM_B$). The difference in intensity between the two total pTRMs was shown to be equal to the intensity of the tail of $pTRM_A$. Based on this observation, Shcherbakova *et al*. (2000) argued that it is the process of heating from room temperature to the upper blocking temperature that increases the (un)blocking temperature of the pTRM carriers above the original upper T_B. Thus, thermal demagnetisation itself causes the tail to be present in samples containing $pTRM_A$ by increasing the unblocking temperature. The same process increases the blocking temperature during the $pTRM_B$ heating cycle before the magnetisation can be acquired thus precluding this portion retaining it.

PSD grains occupy the size range between true SD (0.1 μm) and MD (> 10 – 20 μm) grains and display hysteresis parameters intermediate between the two. However, this intermediate behaviour is probably best regarded as a combination of MD characteristics (i.e. remanence derived from domain wall pinning) and a hard SD-like component (Xu and Dunlop, 1994). The source of this hard component is far from certain although the moments of the domain walls themselves may be partly responsible. Another possible explanation is that some of the grains in a PSD assemblage are metastable SD well above the SD size threshold. See Dunlop and Özdemir (1997) for a detailed discussion. The important aspect of PSD behaviour to this study is that samples displaying intermediate PSD hysteresis properties (§ 2.2.2.1) can produce linear NRM-TRM plots in a Thellier experiment (Perrin, 1998).

3. Geological Background

3.1. Introduction

This chapter intends to provide a background setting for the rock units studied in this project in addition to a brief discussion on their petrology and geological history.

All the rock units sampled for the purpose of this study were intrusive bodies cropping out in Eastern Australia. This area was chosen because of its widespread, well-dated igneous activity throughout the late Palaeozoic and Mesozoic, its well-constrained *APWP* through this time, and its position in the southern hemisphere from which palaeointensity data remain scarce.

Basaltic lavas are the most common igneous source of palaeomagnetic data. This is because their high iron content and fine grain size makes them stable and strong recorders of the palaeofield. However, palaeointensity estimation requires the magnetic minerals in the rock units to exhibit at least a partial resistance to chemical alteration upon heating in the laboratory. This attribute is maximised in rocks that are *deuterically oxidised*. Cooling at depth, normally over longer periods of time, intrusive rock units are more prone to this beneficial process and thus are preferred targets for this study. Intrusives also have a number of further advantages over lavas. The longer cooling time means that an intrusive unit averages out the *secular variation* (SV) of the magnetic field to a greater extent than a lava flow, which provides only a high resolution spot-reading of the field. In certain cases it has been shown that SV has been completely averaged out by a slow-cooled intrusion so that only the GAD field was recorded (McClelland and Briden, 1996). An intrusion is also less likely to be chemically altered subsequent to formation than a lava flow.

Maghaematisation is a low temperature oxidation process caused by weathering, it overprints the primary TRM with a CRM and renders the palaeointensity

unobtainable. Lavas flow directly onto the surface of the Earth and are therefore prone to this adverse process for longer than an intrusion formed at the same time.

Permian and Mesozoic intrusions in eastern Australia were preferentially selected for sampling on the basis of the following criteria:

- Their age was well-constrained.
- They crystallised during a time period of sparse VDM data coverage.
- They exhibited palaeomagnetic stability in previous studies.

§ 3.2 provides a brief introduction to pertinent aspects of eastern Australia's geological history, § 3.3 and § 3.4 then deal with the two primary field localities before describing the sampled units themselves.

3.2 The geological history of Eastern Australia

The single piece of continental lithosphere upon which the Australian nation stands also comprises the islands of New Guinea to the north separated from Australia by the Sahul Shelf. However, only the "Island continent" itself will be considered here.

Australia has a surface area of 8×10^6 km^2 and is characterised by its global isolation, generally low relief (a product of long term exposure above sea level) and widespread aridity.

Together with Antarctica, India, Africa, and South America, Australia was part of the supercontinent Gondwanaland from at least the early Ordovician (Van der Voo, 1993). Plate tectonics allowed the brief coalescence of all continental lithosphere to form Pangea in the mid-late Triassic (Veevers, 1989). Widespread dispersion of the continents was initiated in the mid-Jurassic when the large terrane of India split from the north coast of Australia. Following separation from Antarctica 45 Myr ago,

Australia finally emerged as a single continent and has subsequently moved towards the equator (Windley, 1996).

For the purpose of geological description, it is useful to divide the country into two geographically distinct zones separated by the Tasman line (see figure 3.1). The Western Shield and its associated basins cover approximately two-thirds of Australia's surface area. However, this area is not relevant to this study and consequently will not be described.

The majority of continental material east of the Western Shield was accreted to the craton during the Phanerozoic. Prior to this, the thick, shallow water Adeladian succession was formed in the eastern part of the South Australian (SA) state during the late Proterozoic. This was deformed in the Cambrian into the Delamarian orogeny as a consequence of generation and subsequent subduction of a palaeo-Pacific Ocean. The cycle of ocean generation followed by ocean-ocean collision and subduction was repeated in the Ordovician forming the Tasman geosyncline along the entire east margin of the craton and triggering extensive deposition and widespread acid magmatism. Following a prevalent interval of block-faulting spanning the Silurian and most of the Devonian, Chilean-type subduction was initiated at the eastern margin in the late Devonian resulting in the formation of a magmatic orogenic arc.

Terrestrial deposition in parts of the Tasman geosyncline continued into the Carboniferous, while more eastern areas were subject to marine deposition. The Carboniferous was also a period of extensive acid and basic pluton emplacement and volcanism in New South Wales (NSW) and Queensland (QLD). Widespread deposition continued into the Permian when much of the coal of the region was generated. The Hunter-Bowen Orogeny, a major but localised tectonic event uplifted the QLD basins and allowed granitoid intrusion in the late Permian.

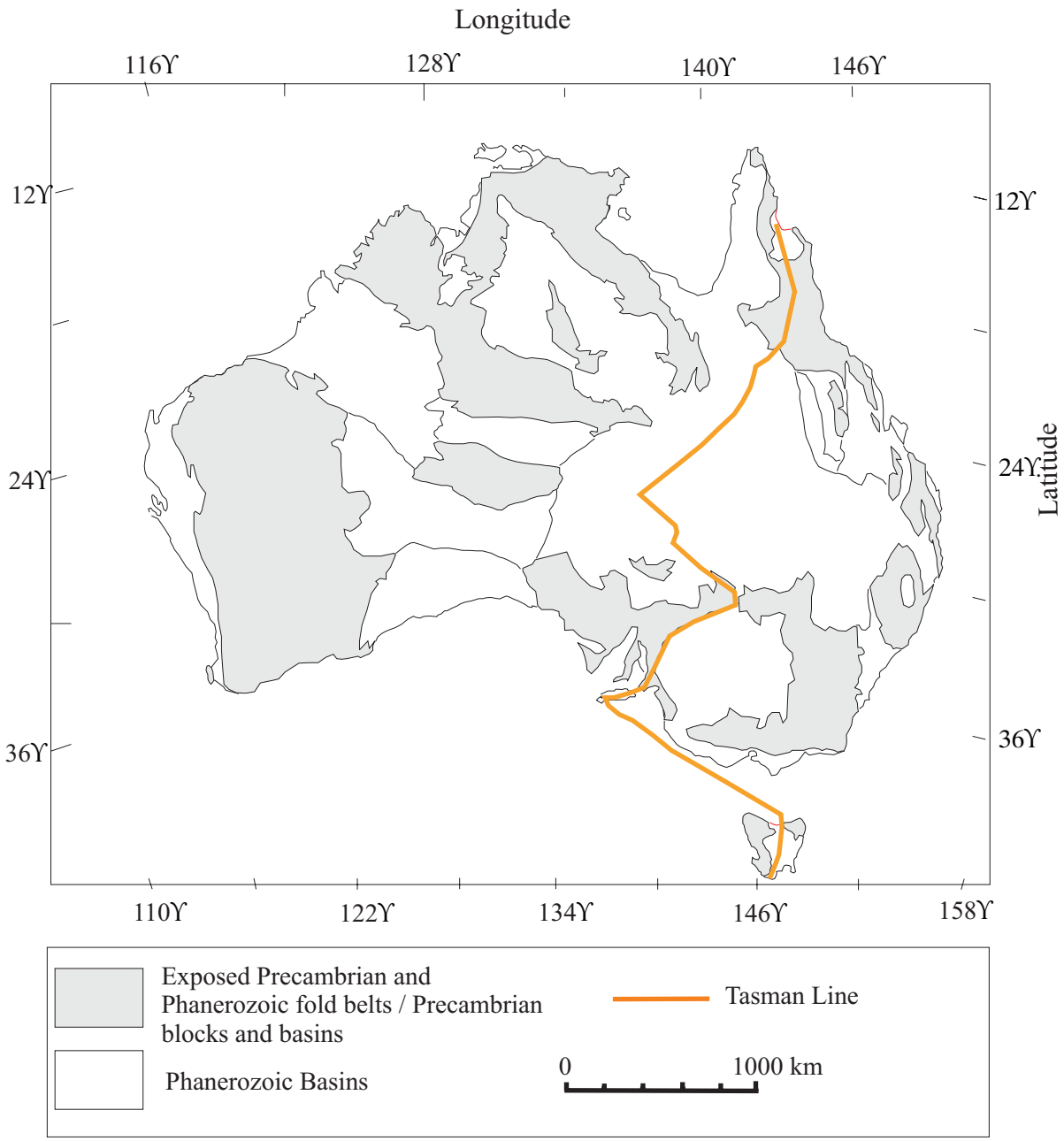

Figure 3.1 Australia's major geological units. Redrawn from Veevers (1984).

Basins formed during the Palaeozoic, particularly the Great Artesian Basin, were developed further in the Mesozoic. Terrestrial deposition was dominant until epeiric seas inundated the continent during the Cretaceous. Seafloor spreading and a Mariana-type subduction replaced the long established ocean-continent collisional boundary along the eastern margin. This rifted New Zealand and the Lord Howe Rise away from the continent creating the Tasman Sea (§ 3.2.2) in the late Cretaceous.

Eastern Australia experienced widespread, mafic volcanism in the Cenozoic. The locus of the central volcanic province migrated south, 16 degrees of latitude, between 33 Ma and 6 Ma resulting from the Australian plate moving over stationary hotspots in the underlying mantle (Wellman and McDougall, 1974b). Abundant and widespread lava fields may also be related to hotspot activity. The tectonic regime throughout the Cenozoic was epeirogenic however, and this igneous province displays better correlation with the areas most affected by uplift (Veevers, 1984).

3.2.1 The Tasman Sea rifting event

The most recent, major tectonic event to affect Eastern Australia has had significant consequences for palaeomagnetic studies in the area, and is therefore worthy of attention.

The Tasman Sea separates New Zealand and Lord Howe's Rise from southeastern Australia. Rifting occurred between 73.6 Ma and 52 Ma (Gaina *et al.,*1998) However, prior to this, the region was subject to a prolonged history of development as is the case with most continental margins (Moore *et al.*, 1986). This may have taken the form of igneous activity and continental lineament initiation as far back as the late Permian / Triassic (Ringis, 1975, Scheibner, 1975).

Raam (1968) was first to point out that regional metamorphism had affected marginal areas with temperatures exceeding 70°C. This was later supported by

studies of vitrinite reflectance of Sydney Basin coal measures (Middleton and Schmidt, 1982) which estimated that present-day surface coal had experienced palaeotemperatures in the range of 60°C to 249°C since it formed in the Permian.

Moore *et al.* (1986) showed that basement apatites up to 130km from the margin were subject to fission track resetting due to thermal activity in the period 80 – 100 Ma. This supported the 90 Ma estimate of Schmidt and Embleton (1981) inferred from the palaeomagnetic direction of overprinting in many southeastern Australian rocks. From the time-temperature relationship for thermoviscous remanent magnetisation (*TVRM*) in SD grains (Pulliah *et al.* 1975), a maximum temperature of 200°C for 3 Myr was inferred. In some rocks however, the temperature of overprinting appeared too high to be explained by the Pulliah *et al.* model. This discrepancy was later demonstrated to be due to either partial chemical overprinting or the physical effects of MD grains (Dunlop *et al.*, 1997b). Further palaeomagnetic studies showed that the overprint is also evident in igneous rocks and coals from the south of the Bowen Basin, although not as pervasive as in those closer to the margin (Lackie and Schmidt, 1996). In the north of the basin, the direction of overprinting was found to be shallower suggesting a younger age. These directions were all normal polarity, however, and this is consistent with acquisition during the CNS (83 – 118Ma). This may suggest that, in the absence of any known Tertiary reheating event affecting the area, the NRM of these samples may have been affected by the 90 Ma event.

Moore *et al.* (1986) concluded that the evolution of the continental margin was governed by thermal rather than mechanical processes and that doming uplift accompanied by elevated temperatures in the region was responsible for magnetic and fission track resetting during the period 80-100 Ma. Following this uplift, erosion rapidly removed all Jurassic and possibly some Triassic sediments from the Sydney Basin, cooling the area and leaving an exposure pattern similar to that witnessed today (Middleton and Schmidt, 1982).

The rifting that followed this event 10-20 Myr later was initially interpreted as a simple two-plate spreading system (Weissel and Hayes, 1977, Mutter and Jongsma, 1978, Shaw, 1978). However, Gaina *et al.* (1998) showed that several strike-slip faults and failed rifts in the basin illustrated that rifting propagated from south to north and could not be reconciled with such a simple model. Their study was based on gravity, magnetic, bathymetry and seismic investigations, in addition to age and affinity characterisation of dredged rocks. This comprehensive treatment of the basin led to the conclusion that 13 blocks of continental margin were separated from eastern Australia by both extensional and strike-slip movement in the late Cretaceous / early Tertiary. It was this complex process which generated the Tasman Sea, the Lord Howe and Middleton basins, and several failed rift systems.

3.3.The Sydney Basin

3.3.1 Background

The Permo-Triassic Sydney Basin, on the eastern coast of central NSW, is located between the Lachlan and New England fold belts (figure 3.2). It developed in the earliest Permian as part of a linear foredeep system incorporating the Bowen Basin (Herbert, 1976, 1980a), between the western craton and an eastern Pacific-rim orogen. The complete Sydney Basin succession is estimated to comprise approximately 4800m of sediment (Mayne *et al.*, 1974). It thickens to the north-east in the Hunter Valley region adjacent to the New England basement and thins to the east of here where it is overlain by the Jurassic and Cretaceous sediments of the Gunnedah Basin, which is itself a component of the Great Artesian Basin.

The basement consists of sequences continuous into the New England and Lachlan fold belts to the north/north-east and south/west respectively. The New England sequence, referred to as the 'Kuttong' Group, spans the Carboniferous and is expected to underlie the north-east of the Sydney Basin. It comprises lava flows, tuffs and meta-sediments derived from this material.

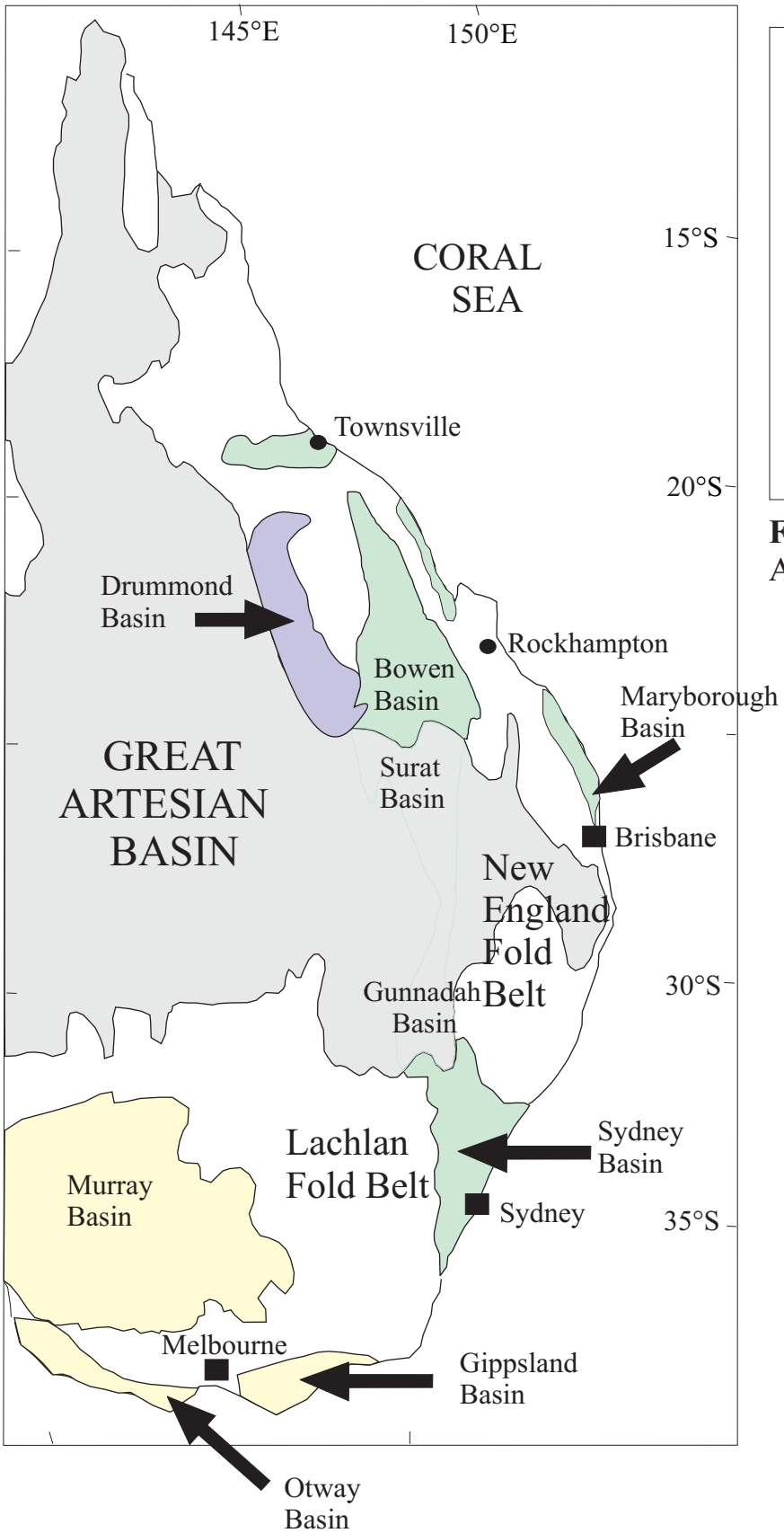

Figure 3.2 Overview of Eastern Australian geology.

Cat.	Formations	Lithology	Known extent
TRIASSIC: Sythian to Ladinian (245-225 Ma)			
14	Wianamatta	Sandstone and shales	Central-eastern portion of basin
13	Hawksbury	Sandstone	Central-eastern portion of basin
12	Narrobeen	Medium-coarse sands and shales	Thick across entire basin except southern tip
Upper Kazanian to Tatanian (265-245 Ma)			
11	Newcastle	Coal measures and medium-coarse sandstone	Entire basin except southern tip
10	Warratah and Dempsey	Coal and fine-medium sandstone	Entire basin except southern tip
9	Four Mile Creek	Coal and fine-medium sandstone	Entire basin except southern tip
8	Upper Wallis Creek	Coal and fine-medium sandstone	Entire basin except southern tip
7	Lower Wallis Creek	Coal and fine-medium sandstone	Entire basin except southern tip and far north-west
Samakian to Kazanian (285-265 Ma)			
6	Mulbring and Berry	Siltstone and fine sands	Prominent in all eastern areas
5	Muree and Nowra	Sandstones and conglomerates	Coastal, prominent in south and north-east
4	Branxton and Wandrawandrian	Sand and siltstone	Entire basin except north-west, deep in north-east
3	Greta and Snapper Point	Coal and fine-medium sandstone	Entire basin except north-west
2	Rutherford and Farley	Silts, fine sands and conglomerates	Entire basin except west
PERMIAN: Early Samakian (285-290 Ma)			
1	Lochinvar and Allandale	Sands, shales and volcanics	Coastal, prominent in south

Table 3.1: Stratigraphic units of the Sydney basin (from Mayne *et al.* , 1974)

The Lachlan fold belt sequence is Ordovician to Carboniferous in age and consists of sediments interspersed with felsic lavas and widely intruded by granites. In addition to forming the basement of the western part of the Sydney basin, this sequence also supplied much of the material comprising the basinal sediments. The Lachlan basement series is gently folded and forms an unconformity with the virtually flat-lying Permo-Triassic sequence above.

3.3.1.1. Stratigraphic History

The Sydney Basin sequence spans the Permian and early mid-Triassic and can be divided into 14 units or 'categories' which are temporally similar but pervade large areas of the basin. The categories as defined by Mayne *et al.* (1974) are given in table 3.1.

The environment throughout the depositional history of the basin can be loosely described as a fluctuating marine transgression followed by a fluctuating regression. A shallow sea forming in the basinal area was responsible for creating the oldest rocks before a major advance produced the formations in categories 2, 4 and 6 (see table 3.1). Minor regressions during this time were responsible for the deposition of category 3 and 5 formations before the advance halted in the Kazanian, (260-265 Ma) and a major regression ensued. The retreating sea left behind a complex, marginal system which allowed the extensive Illawarra, Tomago and Singleton (categories 7-10 collectively) and Newcastle coal measures to develop, while minor transgressions allowed deposition of the Dempsey formation and a marine tongue. The Hunter-Bowen orogeny at the end of the Permian initiated a process of delta progradation that terminated coal formation and allowed production of the final three formations which dominate the surface geology of the Sydney Basin. Although originally regarded as fluvial and lacustrine sediments (Mayne *et al.*, 1974), these were recently shown by Herbert (1997) to be sensitive to low order variations in sea-level changes. He concluded that the Narrobeen and Wianamatta formations were deposited in transitional estuarine conditions on a coastal plain, and that the

Hawkesbury sandstone was deposited in an extensive alluvial plain during a marine lowstand.

The north-western margin of the Sydney Basin is host to a small succession of Jurassic sediments (the Coliana and Piliga formations). Several lines of evidence suggest that basin-wide deposition continued through the late Triassic and into the Jurassic. These are derived from studies of coal rank (Middleton and Schmidt, 1982), source detritus in the Great Artesian Basin and comparison with the Clarence Basin to the north (Mayne *et al.*, 1974). Present-day surface rocks were buried under between 1 and 3 km of cover (Middleton and Schmidt, 1982) prior to an episode of rapid erosion in the late Cretaceous (see §3.2.2).

Three major source areas for the detritus making up the sediments in the Sydney Basin have been identified (Ward, 1972). These were: the New England fold-belt to the north-east, the Lachlan fold-belt to the west, and the offshore uplift to the east.

3.3.1.2 Igneous activity

Geochronological investigations compiled by Carr and Facer (1980) and added to by Embleton *et al.* (1985) identified three main pulses of activity responsible for the widespread igneous rocks in the Sydney Basin. Although magmatism was unlikely to have halted for longer than 10Ma, distinct intervals are observed with maxima at 50Ma, 190Ma and 250Ma (figure 3.3).

The earliest of these pulses comprised submarine latite eruptions and the emplacement of intermediate and basic plutonic intrusions. The potassium-rich nature of these rocks is believed to be representative of the culmination of a period of subduction (Emblton *et al.,* 1985) in the late Permian / early Triassic.

Figure 3.3: Histogram of published K-Ar ages for igneous rocks in the Sydney basin (redrawn from Embleton *et al*., 1985)

The late Triassic / Jurassic pulse of intrusive activity was synchronous with the final stages of stabilisation of the Tasman orogenic zone when a tensional regime existed across the whole of the supercontinent (McDougall and Wellman, 1976). The activity itself was mafic (alkaline and tholeiitic) and intermediate in character, and confined mainly to high-level intrusions (dykes, sills and plugs).

The Tertiary pulse of activity was the most extensive and formed many basaltic high level intrusions and lava flows. It was synchronous with the separation of Australia and Antarctica in the early Tertiary (Cande and Mutter, 1982) and plume activity was also contributory (Wellman and McDougall, 1974b).

3.3.2 Sampled Intrusions

3.3.2.1 Moss Vale Intrusions

During the June 1997 field season, two alkali-intrusions were sampled from the Moss Vale region in the Southern Highlands, 45km west of Woolongong in the Sydney Basin (see figure 3.4).

The tholeiitic Gingenbullen dolerite (GB) intrudes the flat-lying Wianamatta formation (category 14, table 3.1) and so is stratigraphically constrained to post-Triassic. This was confirmed by McDougall and Wellman (1976) who reported K-Ar ages for the GB averaging 172 ± 5 Ma from pyroxene and plagioclase samples. The Gibraltar microsyenite (GS) intrudes the older Hawkesbury sandstone and was K-Ar dated at 178 Ma by Evernden & Richards (1962).

The Gingenbullen dolerite (lat. 34.5°S, long. 150.3°E) is a 80m thick sill with horizontal dimensions of approximately 2km by 1km and is composed of crudely columnar quartz-dolerite (Thomas *et al.,* 2000). Seven sites comprising 43 oriented cores were extracted from the Gingenbullen Mountain quarry through its entire thickness.

The GS intrusion (lat. 34.5°S, long. 150.4°E) between Mittagong and Bowral is a 200m thick asymmetric laccolith composed of aegerine-augite microsyenite, deuterically oxidised in places, with thin pegmatite veins (Boesen *et al.* 1961). Although a reasonable spatial coverage of the intrusion was achieved, owing to suitable outcrop being restricted by housing development and intense weathering in parts, sampling was limited to four sites (24 oriented cores).

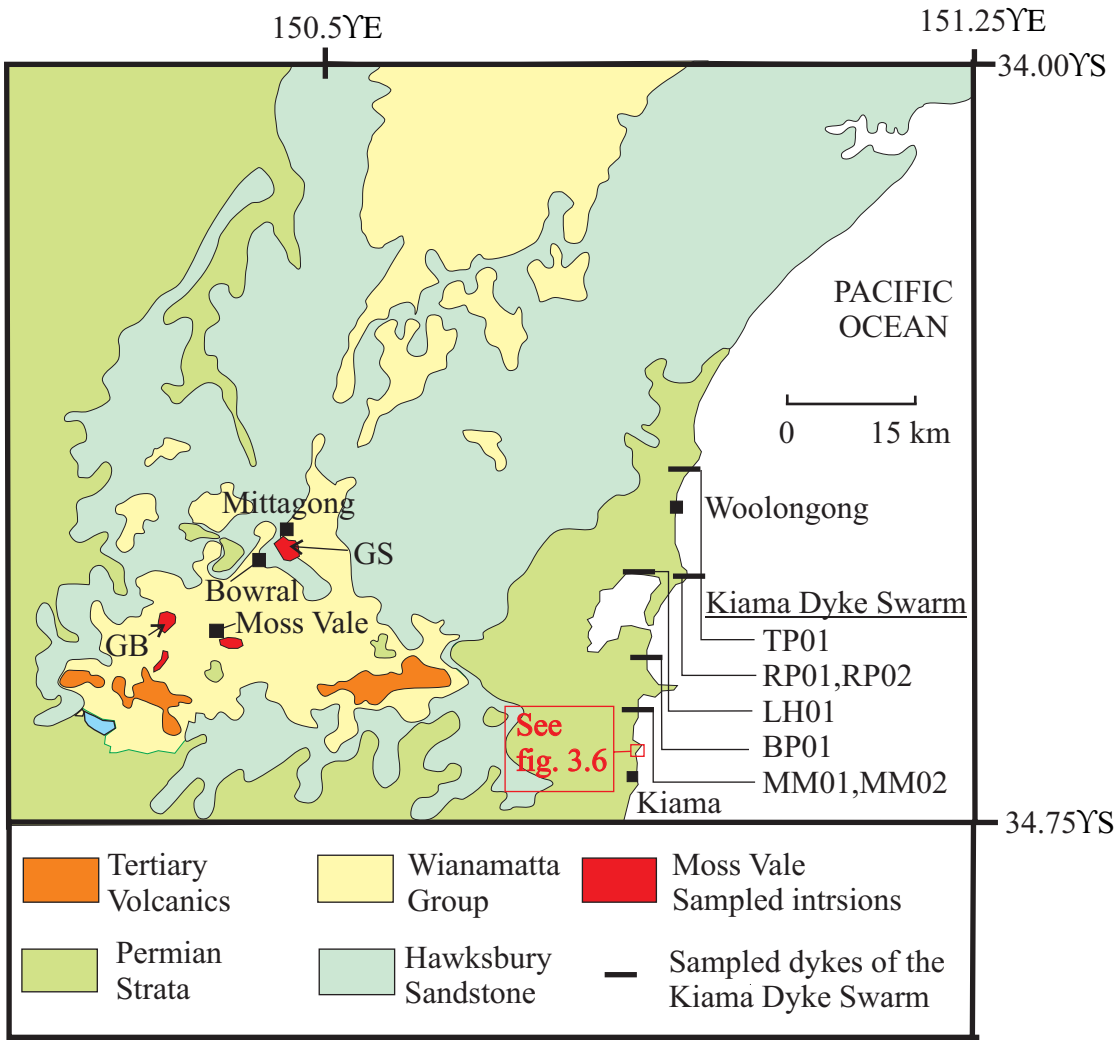

Figure 3.4: Simplified geological map of the southern Sydney Basin showing location of the Kiama Dykes and Moss Vale Intrusions

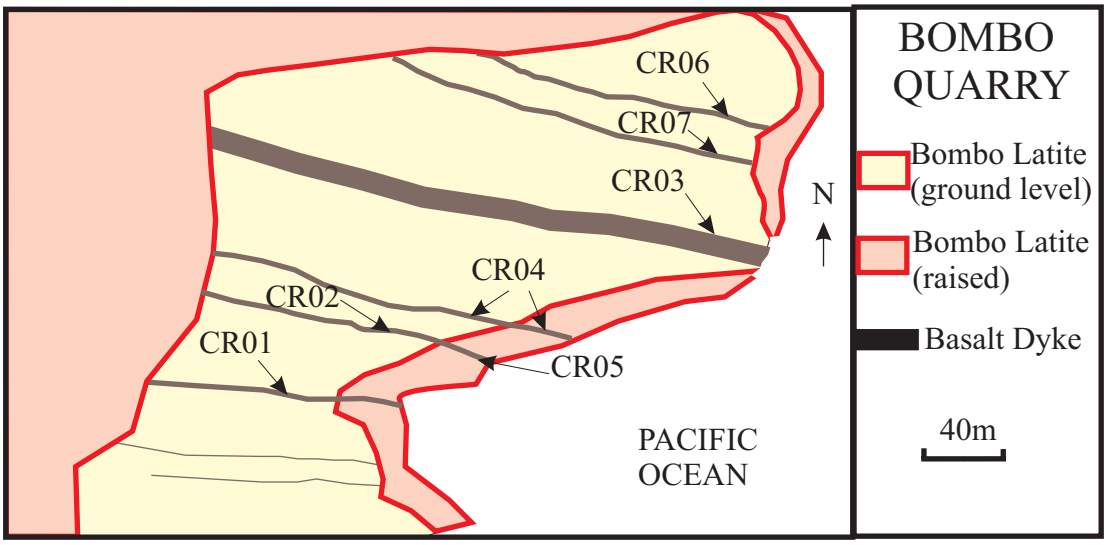

Figure 3.6: Schematic diagram of northern part of Bombo Quarry showing positions of Cathedral Rocks sampling sites

Site	Locality	No. of cores	Lat°S/ Long°E	Wall rock	Description of basaltic dyke rock	Strike	Width (m)
BP01	Barrack Point	8	34.56 / 150.87	Budong Sandstone	Very coarse-grained, green-grey, surface weathered.	095°	2.0
CR01	Cathedral Rocks	8	34.65 / 150.87	Bombo Latite	Very coarse-grained in central 80cm, finer-grained edges, grey-green with captured xenoliths (CR08), strong flow structures.	075°	0.7
CR02	Cathedral Rocks	5	34.65 / 150.87	Bombo Latite	Medium-grained, dark grey, fractured.	095°	2.5
CR03	Cathedral Rocks	8	34.65 / 150.88	Bombo Latite	Medium-grained, blue-grey with feldspar phenocrysts, severely fractured.	105°	10.0
CR04	Cathedral Rocks	8	34.65 / 150.88	Bombo Latite	Medium-grained, blue-grey with feldspar phenocrysts and vesicles, flow patterns.	100°	0.9
CR05	Cathedral Rocks	3	34.65 / 150.89	Bombo Latite	Same dyke as CR02, strong flow structures.	075°	2.5
CR06	Cathedral Rocks	7	34.65 /150.89	Bombo Latite	Medium-grained, dark grey, fractured, mild surface weathering.	100°	0.6
CR07	Cathedral Rocks	8	34.65 / 150.90	Bombo Latite	Medium-grained with vesicles, grey, fractured, relatively fresh.	100°	0.4
CR08	Cathedral Rocks	3	34.65 / 150.90	Bombo Latite	Coarse-grained xenoliths (~5-10cm) in western part of CR01 dyke	-	-
LH01	Lake Hights	0	34.49 / 150.86	Dapto Latite	Fine grained, very weathered.	-	1.3
MM01	Minnemurra	4	34.63 / 150.86	Bombo Latite	Medium-grained, severely fractured and weathered with iron-stained phenocrsts	100°	0.5
MM02	Minnemurra	4	34.63 / 150.86	Bombo Latite	Medium-grained, dark grey, severely fractured	115°	0.6
RP01	Red Point	5	34.50 / 150.92	Budong Sandstone	Light grey, coarse grained	100°	1.2
RP02	Red Point	3	34.50 / 150.92	Budong Sandstone	Coarse grained, light grey-green, weathered	102°	1.0
TW01	Towradgi Point	0	34.39 / 150.92	Pheasant's Nest	Coarse grained, blue-grey.	095°	-

Table 3.2: Summary of sites sampled from Kiama dyke swarm. N.B.No. of cores refers to oriented cores extracted in situ.

3.3.2.2 Kiama and Newcastle dyke swarms

During the March, 1999 field season, basalt dykes were sampled in two distinct regions along the coast of the Sydney Basin, the principal localities of which are shown in figure 3.5. The Cathedral Rocks (CR) locality comprised 8 sites in 6 dykes, and the relationship between these is illustrated in figure 3.6. Tables 3.2 and 3.3 give details of the dykes sampled at each site.

The sampled Kiama dykes (KD) comprised 15 approximately east-west trending, varyingly weathered, basalt dykes intruded into the flat-lying Shoalhaven group (incorporating category 6, table 3.1) of sandstones and latite flows. It was not possible to drill oriented cores at sites LH01 and TP01 but unoriented hand samples were collected from these for the purpose of palaeointensity recovery. To avoid the hazard of magnetic anisotropy, sampling was avoided in areas of a dyke where significant flow banding was observed.

Embleton *et al.* (1985) produced an age of 199 ± 3 Ma from K-Ar dating on biotite and kaersutite samples from the xenoliths which formed our CR08 site. Given the similar orientations of the sampled dykes and their close proximity, it is likely that they were all intruded close to this time.

The sampled Newcastle dykes comprised 5 basalt units intruding late Permian / Triassic sediments in the coastal region south, and within 50km of, Newcastle (figure 3.5). They form part of a predominantly NW-SE trending dyke system, extending south to Broken Bay, with fewer interspersed NE-SW dykes. Maxwell (1990) geochemically analysed samples from 8 of these dykes reporting that all the primary (NW-SE) oriented units gave signatures indicative of continental alkali basalts, but two of the three dykes displaying secondary orientations were tholeiitic in composition. From field evidence, he conjectured that those dykes with secondary orientations were younger than the rest and were likely formed during the Tasman rifting event between 82Ma and 60 Ma. He postulated that the primary dyke set was formed during a period of crustal stretching along a NE-SW axis, 10-30 Myr prior to

rifting. This concurs with Embleton *et al.*'s (1985) K-Ar ages for three of these primary units which included a 90.1 ± 1.5 Ma age estimate for the Little Red Head dyke sampled for this study.

Recently, a K-Ar age of 91 Ma was recovered from the NE-SW trending dyke at Norah Head (NH01; Sutherland pers. Comm.) which does not support the conclusions of Maxwell (1990). Palaeomagnetism provides an excellent opportunity to independently investigate the emplacement history of this suite of dykes.

Site	Locality	No. of cores	Lat°S/ Long°E	Wall rock	Description of basaltic dyke rock	Strike	Width (m)
NE01	Newcastle	9	32.93 / 151.79	Tomago sandstone	Coarse-grained, grey with feldspar phenochysts, fresh.	168°	1.0
NH01	Norah Head	10	33.28 / 151.62	Narrabeen sandstone	Medium-grained, grey with significant alteration in parts, heavily jointed	030°	1.8
LR01	Little Red Head	10	32.97 / 151.74	Newcastle conglomerate	Coarse-grained, grey, relatively fresh.	150°	1.2
CH01	Catherine Hill Bay	10	33.17 / 151.67	Newcastle conglomerate	Medium-grained, grey-green, significant alteration, high degree of surface weathering and fracturing.	035°	1.0
CH02	Catherine Hill Bay	5	33.17 / 151.67	Newcastle conglomerate	Medium-grained, dark grey-blue, some alteration, high degree of fracturing.	035°	0.7

Table 3.3: Summary of sites sampled from Newcastle dyke swarm.

3.3.2.3 Bawley Point Gabbro

The Bawley Point Gabbro (BPG) intrudes the early Permian Conjola formation (category 4, table 3.1) along 7 km of coastline approximately 25 km south of Ulladulla (fig. 3.5 and 3.7). The east-west extent of the intrusion is at least 6 km incorporating Brush Island, 3 km's from the coast.

Vallance (1969) first reported it to be a coarse-grained essexite remarking that it was petrographically similar to the Milton Monzonite, near Ulladulla. Evernden and Richards (1962) had reported K-Ar dates for the latter of 93Ma and BPG was

presumed to be contemporaneous. These were superseded by Facer and Carr (1979) who reported Permo/Triassic ages for both intrusions, dating the BPG at 241 ± 4 Ma. Although accessible outcrop was limited to coastal parts of the intrusion, it was possible to sample its entire north-south extent. Forty-one oriented cores, primarily from wave-cut platforms, were extracted at six sites, the names and locations of which are displayed in figure 3.7.

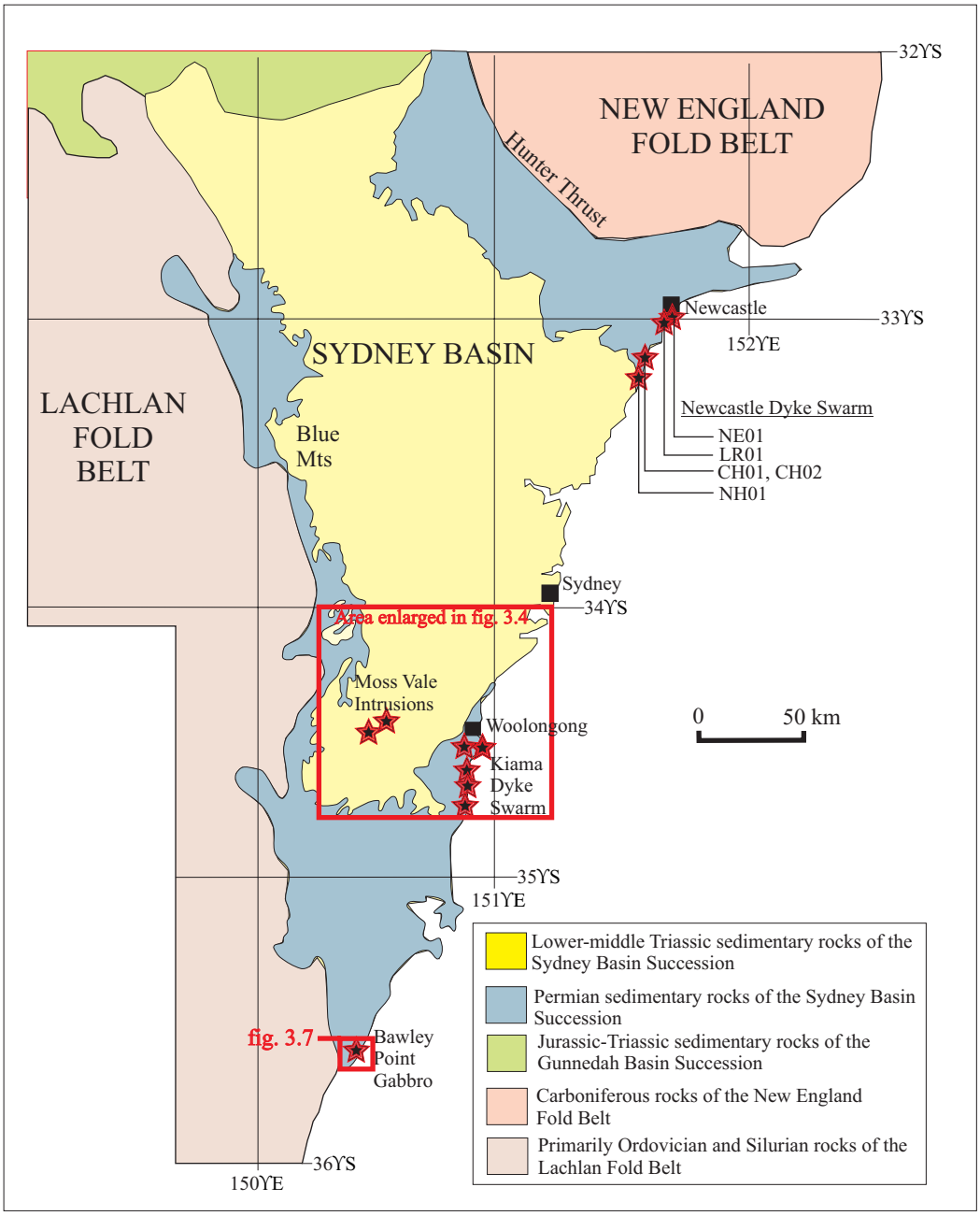

Figure 3.5: Simplified Geological map of Sydney Basin and surrounding area showing location of sampled intrusions (stars).

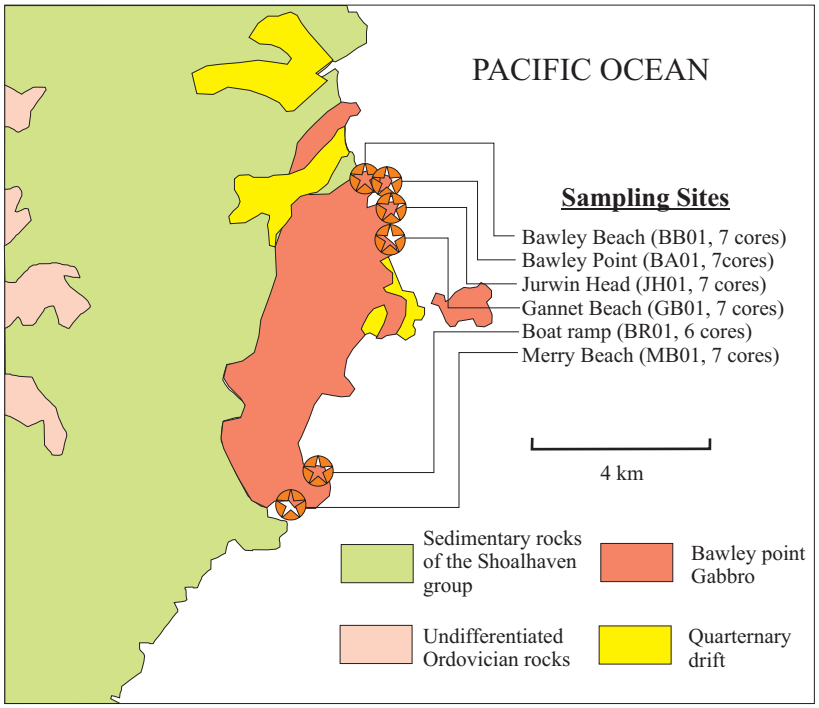

Figure 3.7: Map showing sampling sites within the Bawley point gabbro and surrounding geology.

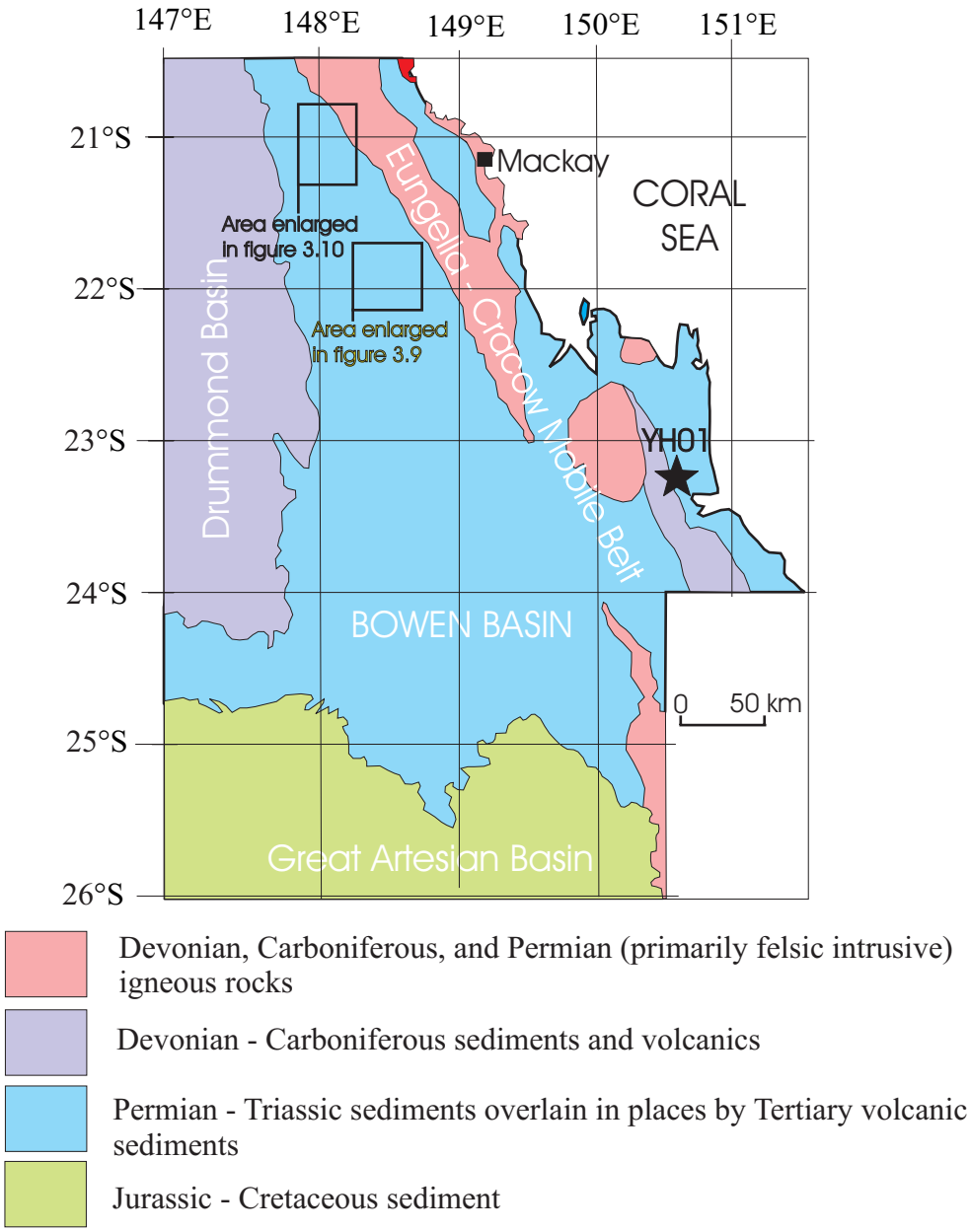

Figure 3.8: Simplified geological map of the Bowen basin region showing the location of the Yeppoon Highway (YH) gabbro and areas enlarged in other geological maps.

3.4. The Bowen Basin

3.4.1 Background

The Permo-Triassic Bowen Basin is a narrow, elongate basin extending north-south between latitudes 20° and 25°S in eastern central Queensland (See figure 3.8). It is bounded on all sides by basement highs although the Cretaceous-Jurassic Surat Basin conceals its southern extent (figure 3.2).

3.4.1.1 Tectonic and depositional history

In the past, numerous models have been presented to account for the formation of the Bowen Basin (e.g. Hammond, 1987, Mallet *et al.*, 1988). However, it is now widely accepted that it is a retro-arc foreland basin (Baker *et al*, 1993).

The New England orogen to the east of the Bowen Basin originated from collision of the palaeo-Pacific plate with the Gondwana craton in late Devonian-Carboniferous times (Murray, 1987). When subduction was reinitiated in the late Carboniferous-early Permian, the composite Bowen-Gunnadah-Sydney Basin formed.

Fielding *et al.* (1990b) document three periods of tectonic development. Firstly, back-arc extension through the early Permian created north-south trending graben and half-graben depocentres down the length of the present basin. Following a brief hiatus, there was a period of passive thermal subsidence until the early late Permian when the volcanic arc was reactivated allowing compression to dominate. During this stage, some of the existing normal faults were reversed and volcanolithic-rich sediments from the eastern margin spread over the entire basin (Baker *et al.*, 1993). This final protracted event, termed the Hunter-Bowen Orogeny, shortened, uplifted and eroded the basin, finally closing it in the mid-Triassic.

During the Permian, the depositional environment within the basin was controlled by a marine transgression followed by regression. The early Permian environment was primarily alluvial and lacustrine before marine inundation generated deltaic conditions. This transgression continued into the late Permian flooding virtually the entire basin and allowing marine and coastal sediments, notably the Back Creek Group, to be deposited. A transition from passive to flexural subsidence in the late Permian, traced using submarine mass-wasting deposits by Fielding *et al.* (1997), was responsible for the basin-wide regression. The extensive Blackwater Group was deposited in the deltas, coastal areas and alluvial plains left behind. These marginal conditions persisted until the Mid-Triassic and were responsible for deposition of the Rewan, Clematis and Moolayember Groups. The uplift associated with the Hunter-Bowen Event allowed up to 3km of sediments to be eroded (Fielding *et al.,* 1990b).

3.4.1.2 Igneous Activity

Central and southern eastern Queensland has been affected by phases of granite emplacement during the Devonian, Carboniferous, Permian, Triassic and Cretaceous periods (Webb & McDougall, 1968).

Permo-Carboniferous plutonism was confined to the eastern margin of the Bowen Basin and formed the Connors Arch complex in the north and the Auburn Complex in the south. These complexes are considered remnants of the northern-most part of the New England Orogen (Pattison, 1990).

Widespread plutonic activity from late Permian to mid-Triassic times was a product of the Hunter-Bowen Orogeny. Emplacement occurred over the western portion of the Auburn complex and in a north-south linear belt extending from Marlborough to northern New South Wales.

Igneous activity within the Bowen Basin itself was confined to the Cretaceous and Tertiary with magmatism in the Cretaceous comprising three primary phases of

exclusively intrusive activity (Webb & McDougall, 1968). The first of these (142 Ma-120 Ma) emplaced gabbroic to granodioritic plutons, dykes, and sills into every rock unit in the basin up to and including the Rewan Group (Pattison, 1990). This period of intrusion was likely contemporaneous with uplift of the Connors Arch (Dickens and Malone, 1973). The two later phases of activity (118 Ma- 112 Ma and ~70 Ma) emplaced granitic and trachytic plutonic and hypabyssal intrusions at isolated but widepsread locations (Pattison, 1990).

Magmatism in the Tertiary was predominantly extrusive and associated with the Central Volcano province (see §3.2.1). The major phase of this volcanic episode was between 31 and 27 Ma.

3.4.2 Sampled Intrusions

This section documents the suite of intrusive rocks sampled in the north-east portion of the Bowen Basin during the June 1998 field season.

3.4.2.1 The Bundarra and Eungella granodiorites

Numerous petrologically related units are observed to intrude the Nebo Syncline approximately 100km west to south-west of Mackay. They range in composition from granite to gabbro and may form part of a differentiated series (Malone *et al.*, 1964).

Age estimates, using a variety of techniques on samples from a spectrum of the intrusives, concur at early Cretaceous times (Pattison, 1990) strongly suggesting that the entire suite was roughly synchronous.

The Bundarra Granodiorite (BD) is a stock, ~30km^2 in area, which intrudes undifferentiated sandstone and siltstone of the Blackwater group. Its composition ranges from leuco- granite to alkali granite and approaches syenite in places.

Pattison (1990) reported fission track age estimates varying from 98Ma to 130Ma from samples of apatites, sphenes, and zircons. Estimates derived from the latter mineral were regarded as the most reliable and produced an average estimate of 127Ma, consistent with K-Ar estimates obtained by nearby units (Webb & McDougall, 1968).

The locations of the four sampling sites (from which 19 oriented cores were extracted) are illustrated in figure 3.9. Sampling was restricted by severe weathering, therefore fresh unoriented hand samples were also taken where possible. Reasonable lateral sampling coverage was attained; samples obtained at site BD01 were observed to be considerably more felsic than those collected at the other sites.

Figure 3.10 shows the locations and names of six more sampled intrusions collectively referred to as the Eungella Granodiorites. The largest and most easterly of these was Mount Barker (MB), a biotite-hornblende granodiorite which intrudes the Permian, Lower Bowen Volcanics group. Lack of exposure and access difficulties limited sampling to just one severely weathered site (7 oriented cores) from the 10km^2 stock. Potassium-Argon dating conducted on biotite and hornblende samples by Webb & McDougall (1968) gave consistent results averaging 123Ma for the intrusion.

The five smaller intrusions, sampled to the west of MB, are presumed to be contemporaneous. They consist of granodioritic bodies, 0.25 km^2 to 4 km^2 in area. Thirty-four oriented cores were taken from seven sites, which were generally less weathered than that at Mt. Barker (MB01).

Finally, during the June 1998 field season, the Yeppoon Highway (YH) gabbro, situated between Rockhampton and Yeppoon (figure 3.8) was also sampled. This intrusion is stratigraphically constrained to late Permian. Unfortunately, limited access to outcrop restricted sampling to just one site of seven cores.

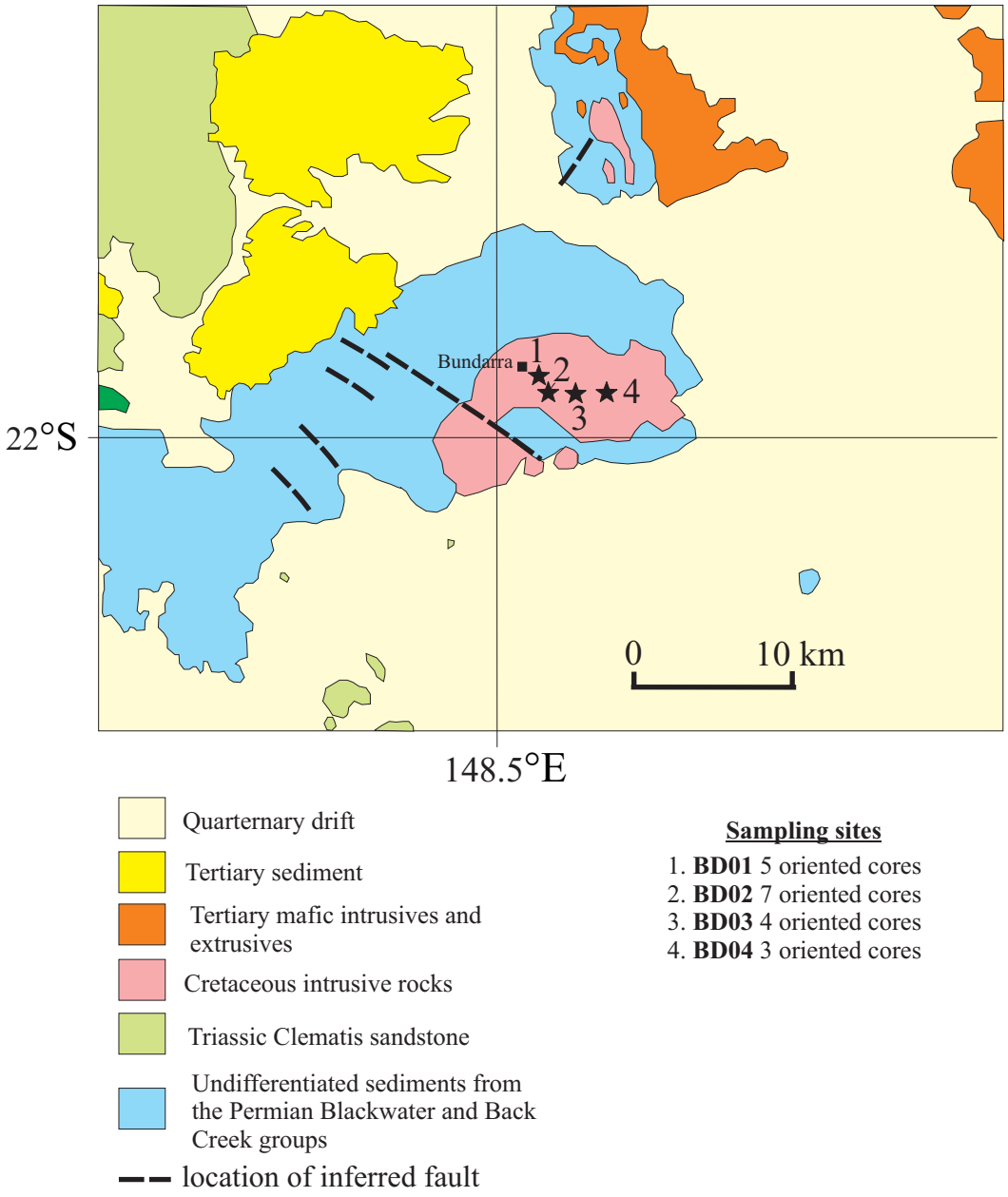

Figure 3.9: Map of sampling sites in the Bundarra granodiorite, and surrounding geology.

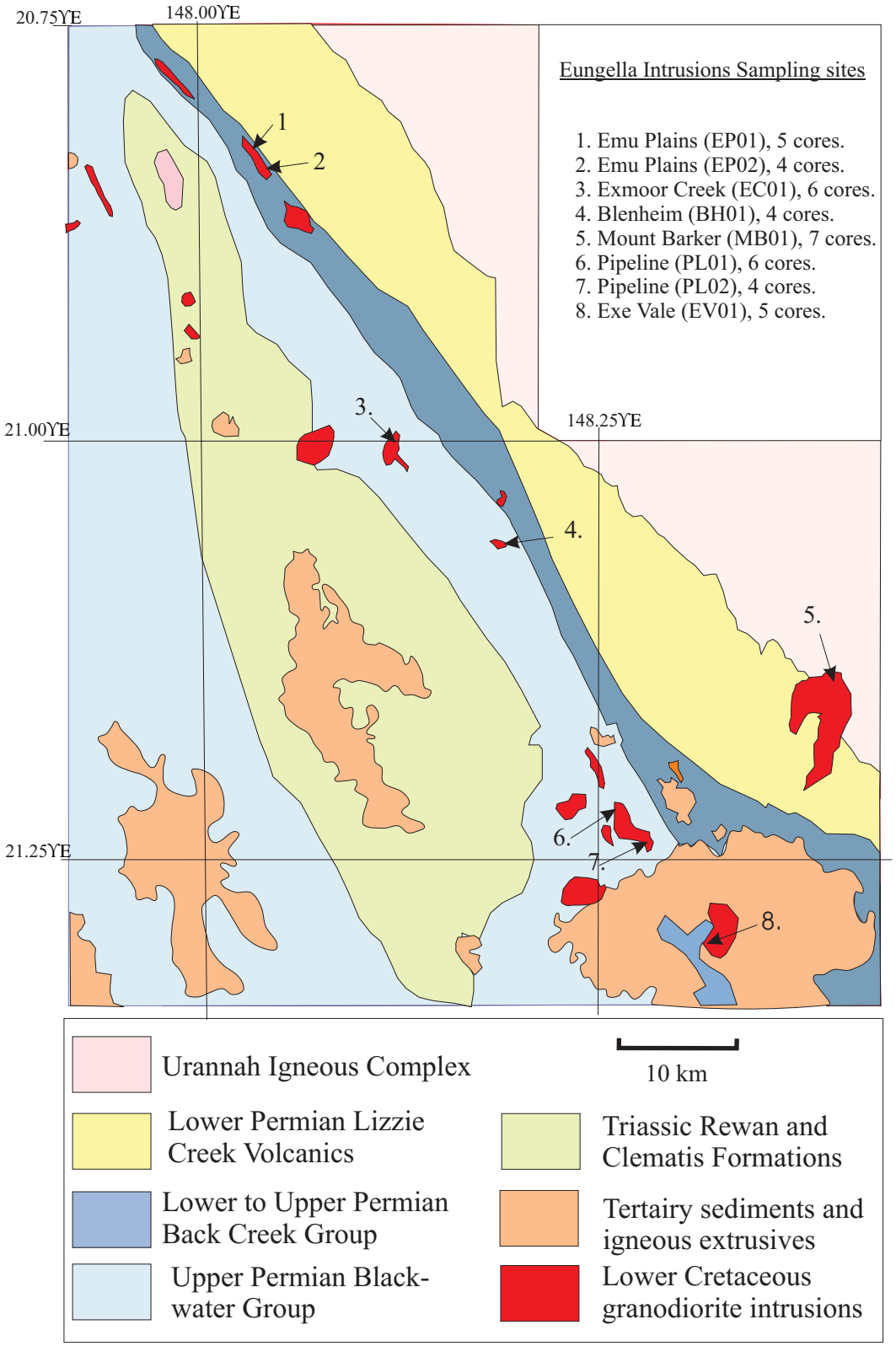

Figure 3.10: Simplified geological map of part of the Nebo Syncline showing locations of sampled Eungella Intrusions

4. Results of the experimental study on Australian igneous rocks

4.1 Previous Australian palaeomagnetic studies

As was discussed in § 2.3, the conversion of mean remanence direction into VGPs allows magnetisations acquired at different locations to be compared. Palaeomagnetic poles of the same age should coincide providing that there has been no relative motion between the two formation localities. All the intrusions sampled for this study are from Eastern Australia, and since the island continent has remained intact since these intrusions formed in the Permian (§ 3.2), VGPs recovered from them can be compared directly with palaeomagnetic poles derived from other rocks magnetised anywhere in Australia.

Van der Voo (1993) grouped Australian palaeopoles with Q ≥ 3 together into those displayed in table 4.1.

Age group	λ_{pole}	ϕ_{pole}	N	K	A_{95}
37-66	-61	121	7	38	10
67-97	-56	138	1		
98-144	-41	158	6	17	17
145-176	-48	169	6	29	13
177-195	-48	177	3	562	5
216-232	-32	170	1		
233-245	-31	158	2		
246-266	-36	141	3	37	21
267-281	-46	122	1		
282-308	-62	142	2		
309-365	-84	321	1		

Table 4.1: Palaeopole groups from Australia since the Devonian as defined by Van der Voo (1993).

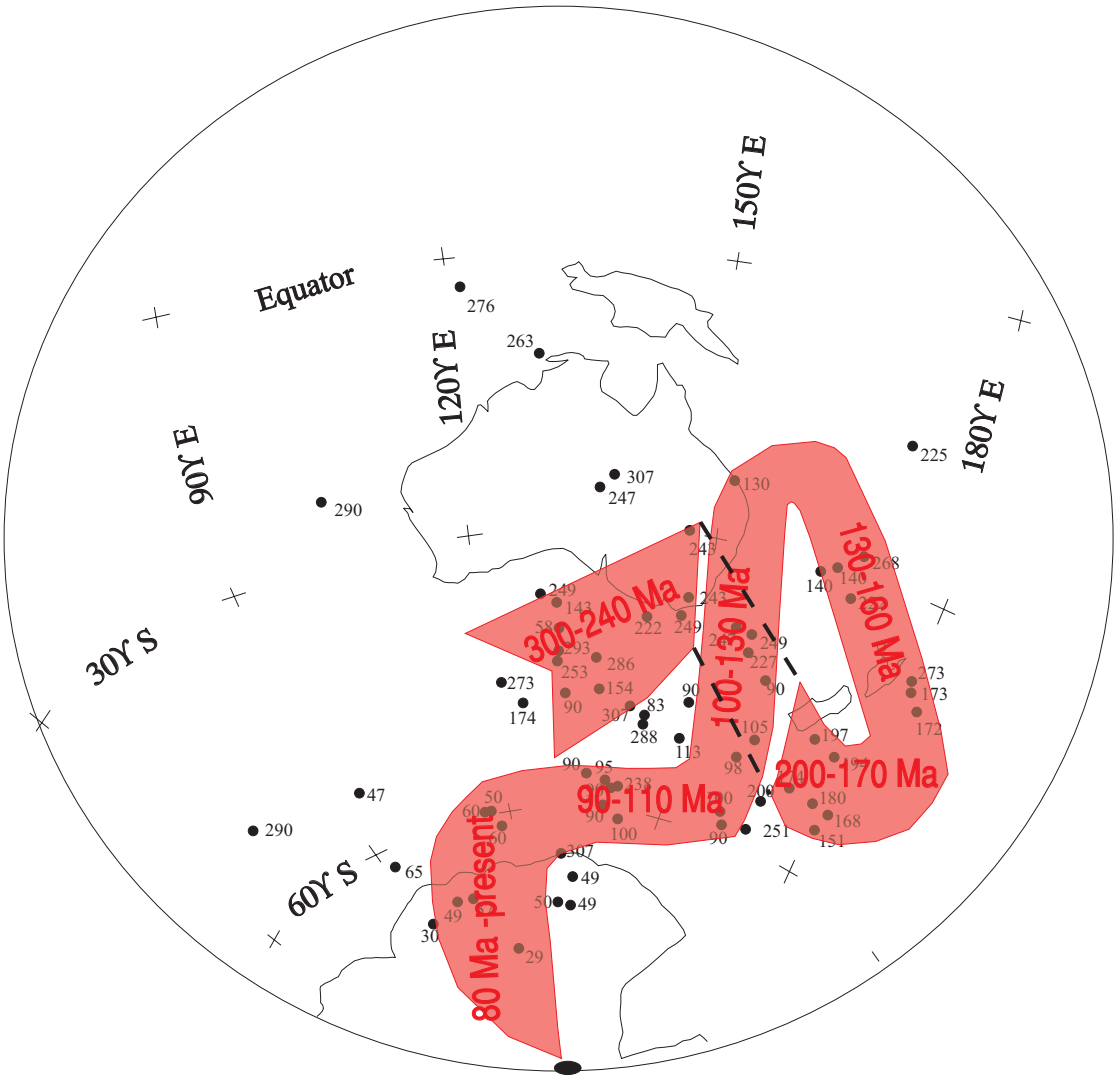

Figure 4.1: Australian APWP (0 - 300 Ma) with poles normalised to reverse polarity. Poles are listed in appendix 4.

Appendix 4 gives the position and dispersion of all published palaeopoles ranging in age from the Permian to the mid-Tertiary produced from studies of Australian rocks. The APWP used to constrain the ages of components of remanence isolated in this study is derived directly from these data (figure 4.1) rather than the grouped poles adopted by Van der Voo (1993) whose grouping may be too severe in swamping out the important fine-scale features of Australia's APWP such as the 'Corel Sea Loop' linking Permian and Cretaceous palaeopoles.

Attempts to extract palaeomagnetic information from some of the intrusions analysed in this study have been made previously. In most cases, however, these involved the AF as opposed to thermal demagnetisation technique used here together with more limited rock magnetic analyses or none at all. The only exception to this is the study conducted by Schmidt (1990) on the Kiama dyke swarm, which employed thermal demagnetisation together with high and low temperature measurements of susceptibility. However, the sampling and measuring carried out on this suite of intrusions for the purpose of the present study were far more extensive.

No palaeointensity experiments have been attempted on any of the intrusions described in this chapter prior to this study. Published palaeointensity studies performed on Mesozoic Australian rocks are somewhat rare. The primary attraction of Eastern Australia as the source of samples for this study was, together with the abundance of Mesozoic intrusions, the potential to recover palaeointensity data from the Earth's southern hemisphere where estimates remain somewhat sparse.

4.2 The Moss Vale Intrusions

Two intrusions were sampled from the Moss Vale-Mittagong region of the southern Sydney basin (see § 3.3.2.1 for details). The results from the Gingenbullen dolerite

(GB; 7 sites) and the Gibraltar microsyenite (GS; 4 sites) were also presented in Thomas *et al*. (2000).

4.2.1 Rock magnetic analysis

Several GB and GS samples were subject to thermomagnetic, hysteresis, χ_{LT}, and IRM acquisition and demagnetisation analyses. The hysteresis and thermomagnetic parameters observed for the site samples are shown in table 4.2.

Figure 4.2 shows representative thermomagnetic curves for GB and GS samples. GB site samples showed relatively consistent behaviour, there was a single Curie temperature between 490°C and 565°C indicating that low titanium titanomagnetite was the dominant phase. The cooling curve was generally a different shape than the heating curve (convex-down rather than convex-up) and crossed over the heating curve at low temperatures resulting in a higher js at low temperatures (figure 4.2a). Thermomagnetic curves from the four GS site samples were more varied in shape although all displayed a similar high T_C between that of magnetite and haematite but with M_S too high to be titanohaematite. One explanation is that the dominant magnetic mineral is maghaemite; this explanation is particularly appealing for sample GS03 which exhibits an inflexion in its heating curve at ~380°C often characteristic of maghaemite (Readman and O'Reilly, 1970). Nevertheless, maghaemite is usually observed to break down to haematite at ~ 500°C and there is little evidence of a much less magnetic phase forming at this temperature. Another plausible explanation is then that the assemblage contains a mixture of magnetite and haematite, the latter of which is largely destroyed upon heating to 700°C (figure 4.2c and d).

Sampling site	M_{RS}/M_S	Hc (mT)	H_{CR}/H_C	RS	ΔM_s	T_C (°C)
GB01				2.0	0.23	550
GB02	0.11	11	2.52	0.9		
GB03				1.2		565
GB04				0.7	0.04	510
GB05	0.10	6	2.17		0.01	495
GB06	0.10	6	2.23	0.6	-0.02	490
GB07				0.7	-0.1	505
GS01	0.22	13	3.12	0.8	-0.31	640
GS02	0.27	26	2.45	0.7	0.04	640
GS03	0.16	13	2.98	0.9	0.47	640
GS04				0.7	4.09	625

Table 4.2: Hysteresis and thermomagnetic parameters for site samples from the four Moss Vale intrusions. M_{RS} is saturation remanence, M_S is saturation magnetisation, RS is the ratio of susceptibility at liquid nitrogen temperature to that at room temperature, ΔM_s is the difference between saturation magnetisation at 100°C after heating to above TC expressed as a fraction of the initial M_s.

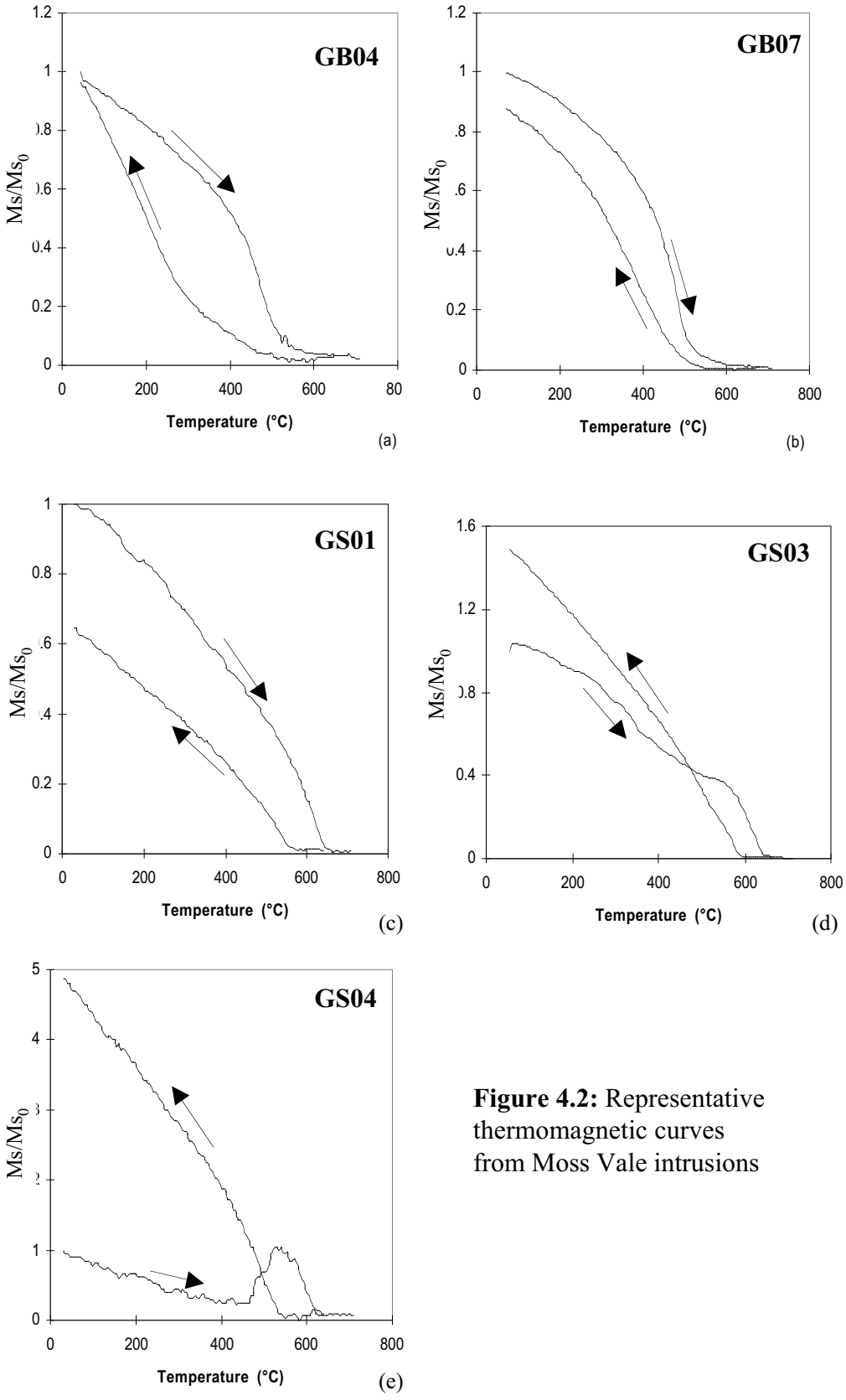

Figure 4.2: Representative thermomagnetic curves from Moss Vale intrusions

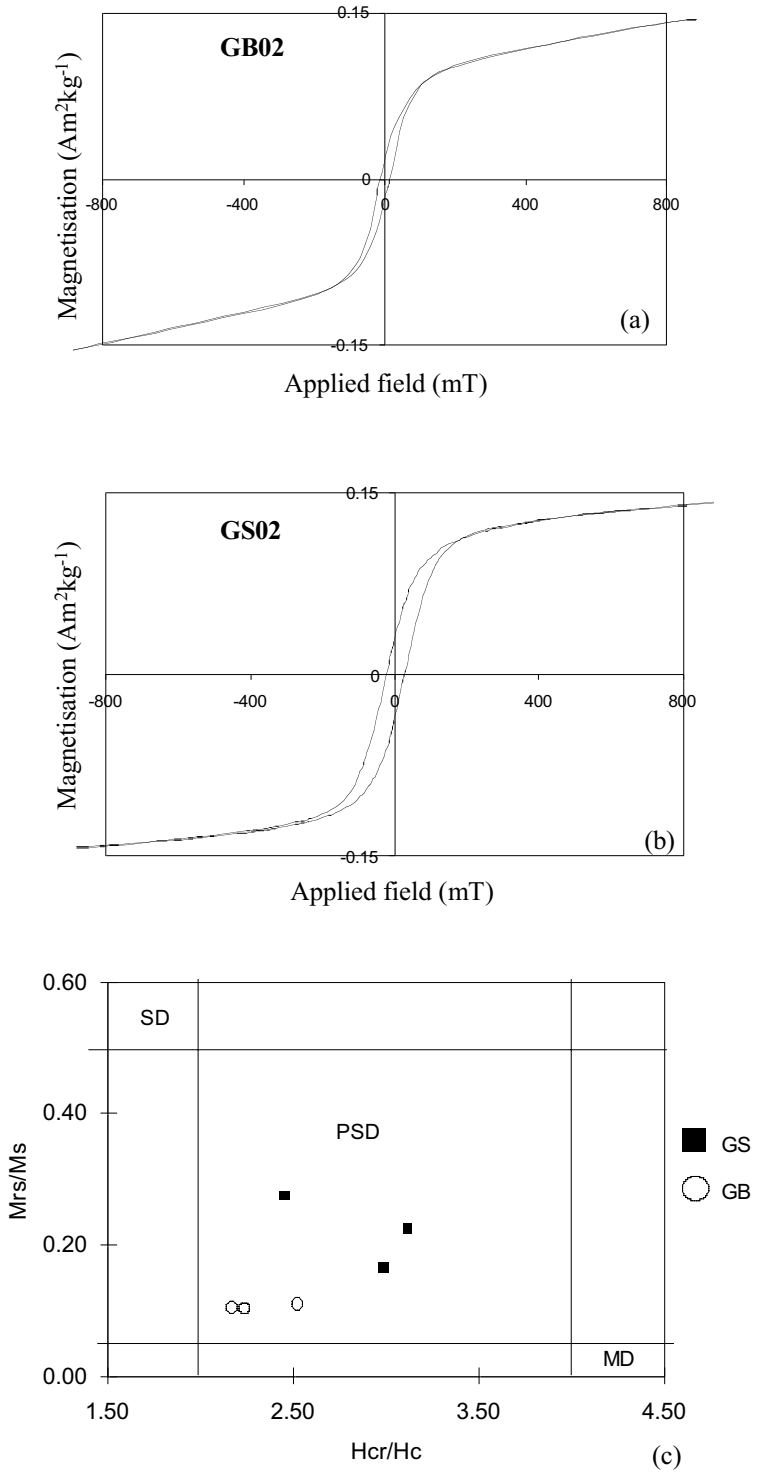

Figure 4.3: (a)-(b) representative hysteresis loops for the two Moss Vale intrusions. (c) Positions of all samples measured on a Day plot.

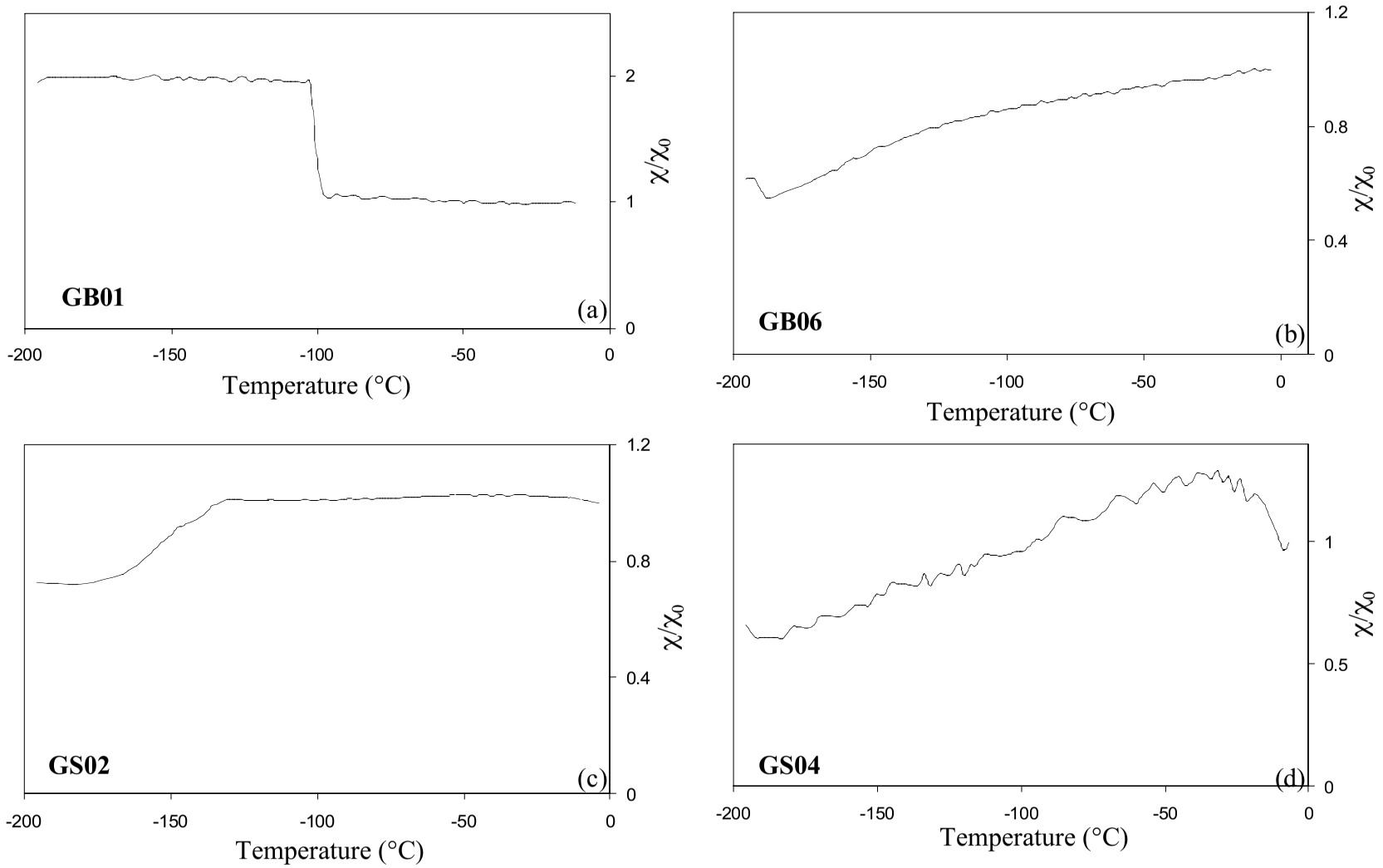

Figure 4.4: Representative χ_{LT} curves for GB and GS samples

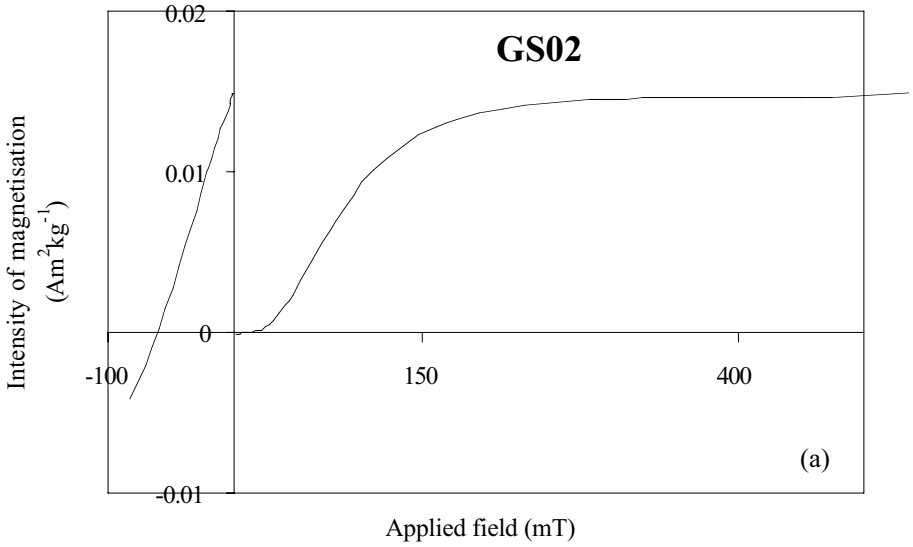

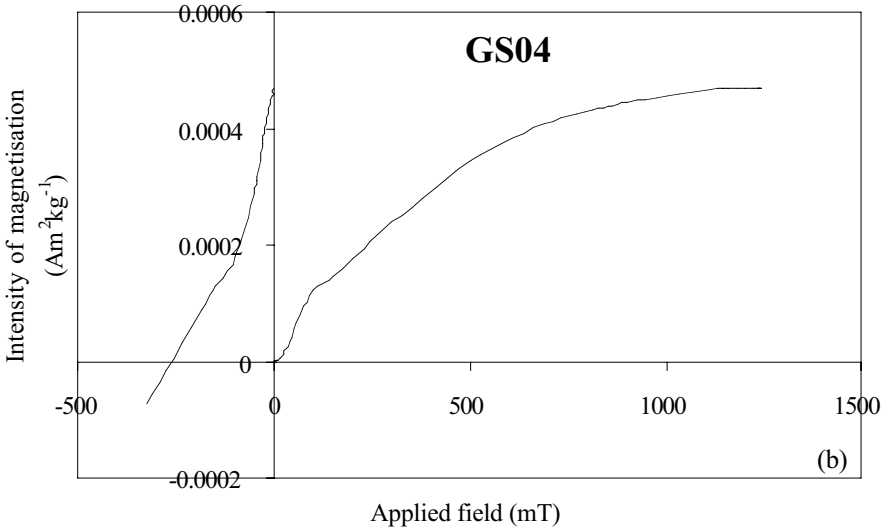

Figure 4.5: Representative partial remanent hysteresis curves for GS site samples

The thermomagnetic curve of GS04 (figure 4.2e) suggests that pyrrhotite and haematite are present during the heating curve. The former mineral alters to magnetite above 450°C and once again, the haematite component is largely removed prior to the sample cooling from 700°C.

Representative hysteresis loops from both intrusions are shown in figure 4.3. All samples measured plotted in the PSD region of the Day plot (figure 4.3e; Day *et al*., 1977) which is the usual case for igneous rock samples. The ratio M_{RS}/M_S is a much more reliable indicator of mean grain size than H_{CR}/H_C (Dunlop and Özdemir, 1997) and there was considerable variation between the samples within the PSD region. The GB samples comprised of generally lower coercivity material (MD or SP grains) than GS samples. Hysteresis loops tend to be dominated by the magnetically softest material in a sample and this can often drown out the signal from a harder phase. Therefore, the GB samples could not be ruled-out as stable palaeomagnetic recorders on this evidence alone.

Low temperature susceptibility (χ_{LT}) analysis revealed a wide range of behaviour between and within the GB and GS intrusions. Samples from sites GB01 and GB03 exhibited a sharp fall in χ at -100°C and 135°C respectively, about which the profile was relatively flat (figure 4.4a). This suggested that both samples contained a mineral with its Curie temperature at this point. This mineral is most likely a high Ti ($x > 0.8$) titanomagnetite or titanohaematite.

The other measured GB samples all displayed a gradual increase in χ over the temperature range (figure 4.4 (b)). This behaviour can be interpreted as indicating either a dominance of mid-range PSD grains, or a combination of SP and PSD grains. The lack of a peak in the profile and the moderate RS value does seem to preclude a significant MD contribution however. The cause of the slight rise below

180°C is not clear but may be the product of the superposition of more than one type of behaviour.

Samples from sites 1, 2, and 3 of the GS exhibited behaviour between that typical of SD and MD grains, which suggests a PSD dominated assemblage (figure 4,4 (c)). The unusual χ_{LT} profile displayed by the sample from site GS04 (figure 4.4 (d)) is presumably a product of the dominant pyrrhotite phase.

Several samples from each site of the GS intrusion were subjected to the IRM acquisition and demagnetisation analysis to ascertain the dominant remanence carriers. All samples from sites 1 to 3 displayed a single, strong ferromagnetic phase saturating at relatively low fields (< 400 mT; figure 4.5 (a)). The field at which half the saturation IRM was acquired ranged from ~ 50 mT to 80 mT suggesting that fine PSD and SD grains were the dominant remanence carriers.

The partial remanence hysteresis curve produced by samples from site GS04 gave values of saturation IRM more than an order of magnitude lower than those of the rest. They also saturated at much higher fields (> 1000 mT) and displayed inflexions on both the acquisition and demagnetisation curves (figure 4.5 (b)). The last of these behavioural aspects indicates that the remanence is carried by two phases of roughly equal importance. The softer of these components is likely to be provided by the pyrrhotite observed earlier while haematite probably provides the harder component. It is plausible that both haematite and pyrrhotite are present in the samples from sites GS01-03 and that their signal is swamped by the much stronger magnetite phase.

In summary, the samples from the GB are dominated by low Ti titanomagnetite PSD grains that are prone to moderate alteration on heating above their Curie temperature. The average grain size of the remanence carriers was not known precisely because of the apparent disagreement between the hysteresis and the χ_{LT} analyses.

The thermomagnetic criterion (Shcherbakova *et al*., 2000; § 2.2.4) was conducted on five GB samples in an attempt to further constrain it. For a pTRM between 300°C and T_R, the tail was an average of 11% of the total pTRM. Indicating that the dominant remanence carriers with $T_B < 300°C$ were large PSD grains. The tail check was repeated on a pTRM imparted between 500°C and T_R, and although empirically-based guidelines were not available, the average tail value of 2% is very low suggesting finer remanence carriers at higher temperatures. It should be pointed out however, that before both of these experiments were performed, the samples were demagnetised by heating to above T_C. This may have served to reduce the effective grain-size through thermal alteration. The presence of SP grains in GB samples could explain the low ratios of both M_{RS}/M_S and H_{CR}/H_C and the rising χ_{LT} profiles but is not certain.

The presence of Ti-poor titanomagnetite in all samples, coexisting with Ti-rich phases in some, strongly suggests that (oxy)exsolution was an important process during the initial cooling of the GB intrusion.

The likely presence of haematite in samples from the GS suggests that *deuteric oxidation* was intense in this felsic intrusion. The pTRM tail check gave an average value of just 3%, further supporting the notion that fine PSD to SD grains dominate the assemblage. Thermal alteration was evident in the thermomagnetic curves although the temperature at which it occurred was not ascertained. Pyrrhotite is a common accessory mineral in igneous rocks although it does not usually dominate the remanence (Dunlop and Özdemir, 1997). The reason for a lack of magnetite in site GS04 alone is not clear but it shows that initial composition and / or cooling processes differed through the intrusive body.

4.2.2 Palaeodirectional analysis

One sample from almost every core from each site of the GB and GS intrusions was subject to step-wise thermal demagnetisation to above T_C of the dominant magnetic

mineral. This was undertaken in 50°C steps up to 500°C, followed by smaller interval temperature steps to above 600°C.

Figure 4.6 shows two OVPs from the analysis of the Gingenbullen dolerite. The two almost anti-parallel components clear in these plots were evident in every sample analysed. The component of magnetisation occupying the lower blocking temperature (LBT) portion of the samples was directed up and generally to the north, indicating a normal polarity field was responsible for imparting it. The component occupying the higher blocking temperature (HBT) portion was a reverse polarity magnetisation that displayed greater inter-site dispersion. Additionally, most GB samples held a small viscous overprint that was usually removed by 150°C.

Appendix 5 gives the directions of magnetisation in each sample from the Moss Vale intrusions; table 4.3 summarises this information, giving the site means together with the overall means and VGPs for the four intrusions. Site 1 was omitted from the GB mean direction calculations because $k < 10$ for both components, indicating poor precision and questionable reliability.

The southern hemisphere VGP produced by the mean direction of the LBT component (53°S, 143°E) plots on the Australian APWP close to poles caused by the thermal event affecting south-eastern Australia from 80 – 100 Ma (figure 4.7; § 3.2.2). It therefore seems likely that the LBT component is another example of the ~ 90 Ma magnetic overprint observed in many rocks in the Sydney Basin (Lackie and Schmidt, 1996). Middleton and Schmidt (1982) inferred that the maximum temperature reached in the basin was 250°C and yet the LBT component looks to occupy the blocking temperature spectra up to at least 450°C in many samples. This discrepancy requires that the LBT component cannot be a true TRM but must either be a TVRM or a TCRM.

Site	$\overline{\Delta T\,(^{\circ}C)}$	N	Dec (°)	Inc (°)	k	α_{95}
	LBT Component					
GB01*	150 - 450	6	45	-68	5.7	28
GB02	150 - 400	6	26	-74	53.9	9
GB03	150 - 450	4	344	-74	31.6	17
GB04	100 - 300	5	257	-87	11.1	24
GB05	150 - 300	6	349	-87	21.9	15
GB06	100 - 350	7	25	-69	26.9	12
GB07	100 - 350	5	41	-82	18.4	18
Mean		6	13	-80	71.3	8
VGP	53°N, 323°E (dp=15, dm=15)					
	HBT Component					
GB01*	500 - 560	7	107	74	9.9	20
GB02	450 - 560	6	128	78	86.6	7
GB03	500 - 580	3	102	85	53.7	17
GB04	400 - 560	5	279	83	21.6	17
GB05	400 - 560	6	192	81	16.9	17
GB06	450 - 560	7	209	58	18	15
GB07	450 - 580	4	183	75	31.8	17
Mean		6	190	80	35.1	12
VGP	54°S, 145°E (dp=22, dm=23)					
GS01*						
GS02	150 - 350	4	196	75	80.1	10
GS03	150 - 350	7	191	70	756.6	2
GS04*	200 - 530	2	76	75	5.4	-
Mean		2	193	72	387.9	13
VGP	66°S, 133°E (dp=20°, dm=23°)					
MV01	0 - 300	9	4	-71	17.1	13
VGP	69°N, 325°E (dp=13°, dm=15°)					
SF01	0-250	6	178	-68	30.7	11
VGP	5°S, 329°E (dp=15, dm=18)					

Table4.3: Summary of results from palaeodirectional analyses of Moss Vale intrusions. An asterix denotes a result omitted from the mean calculation. $\overline{\Delta T}$ is the average temperature range from which the directions were taken

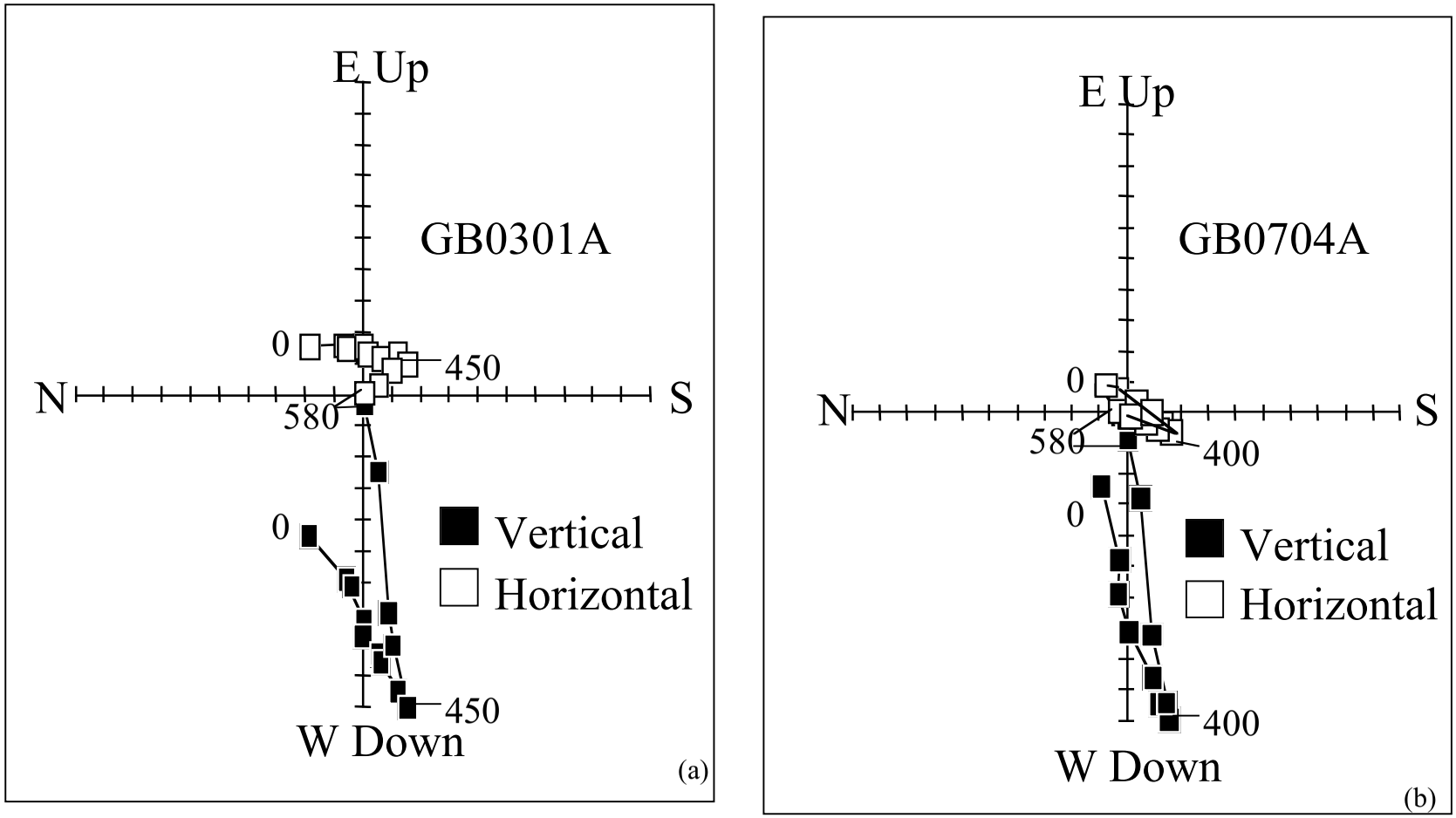

Figure 4.6: Representative OVPs from GB samples

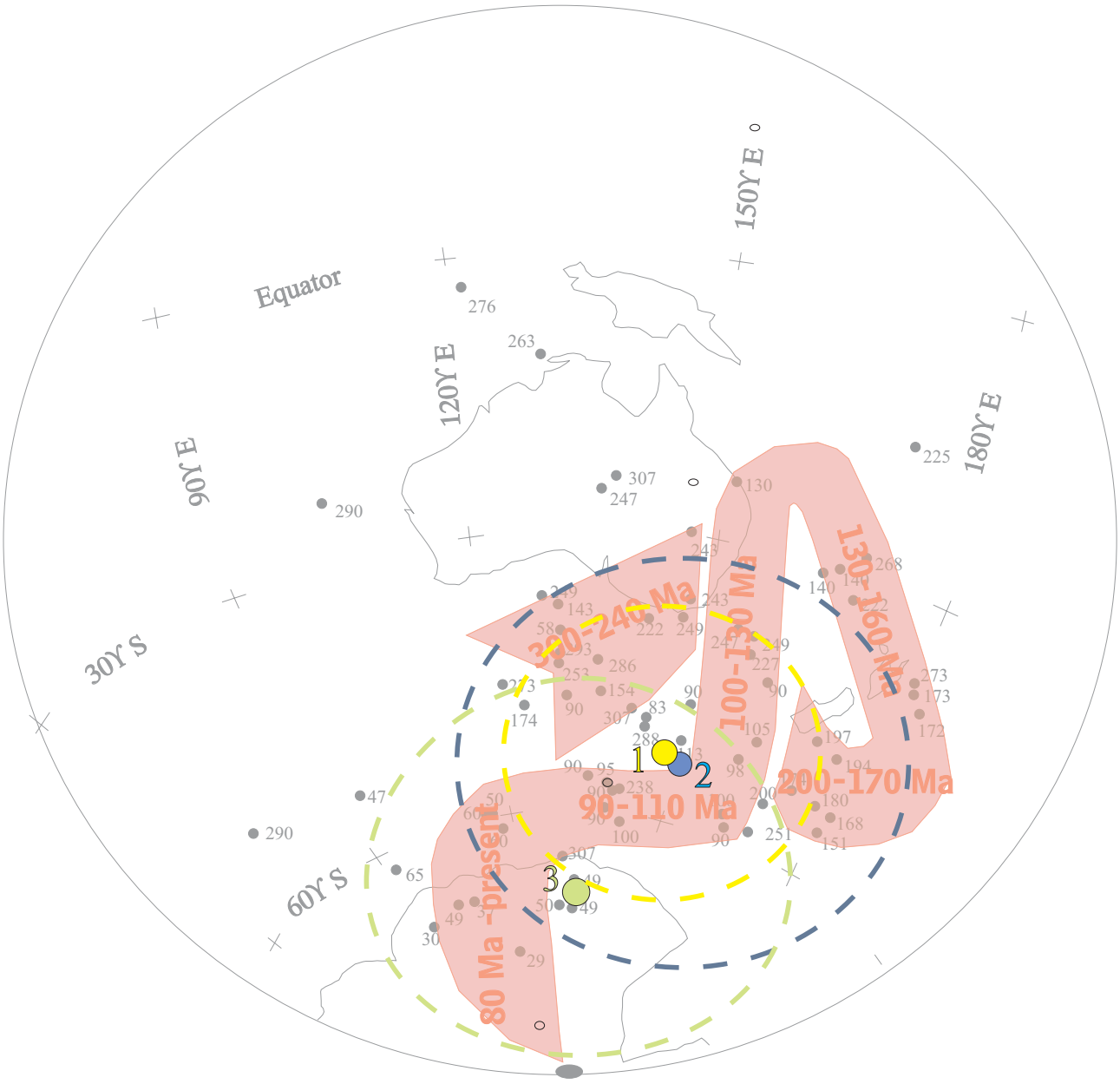

Figure 4.7: Australian APWP showing VGPs (normalised to reverse polarity) measured from Moss Vale intrusions. 1. GB LBT, 2. GB HBT, 3. GS.. Dashed ellipses showing 95% confidence limits.

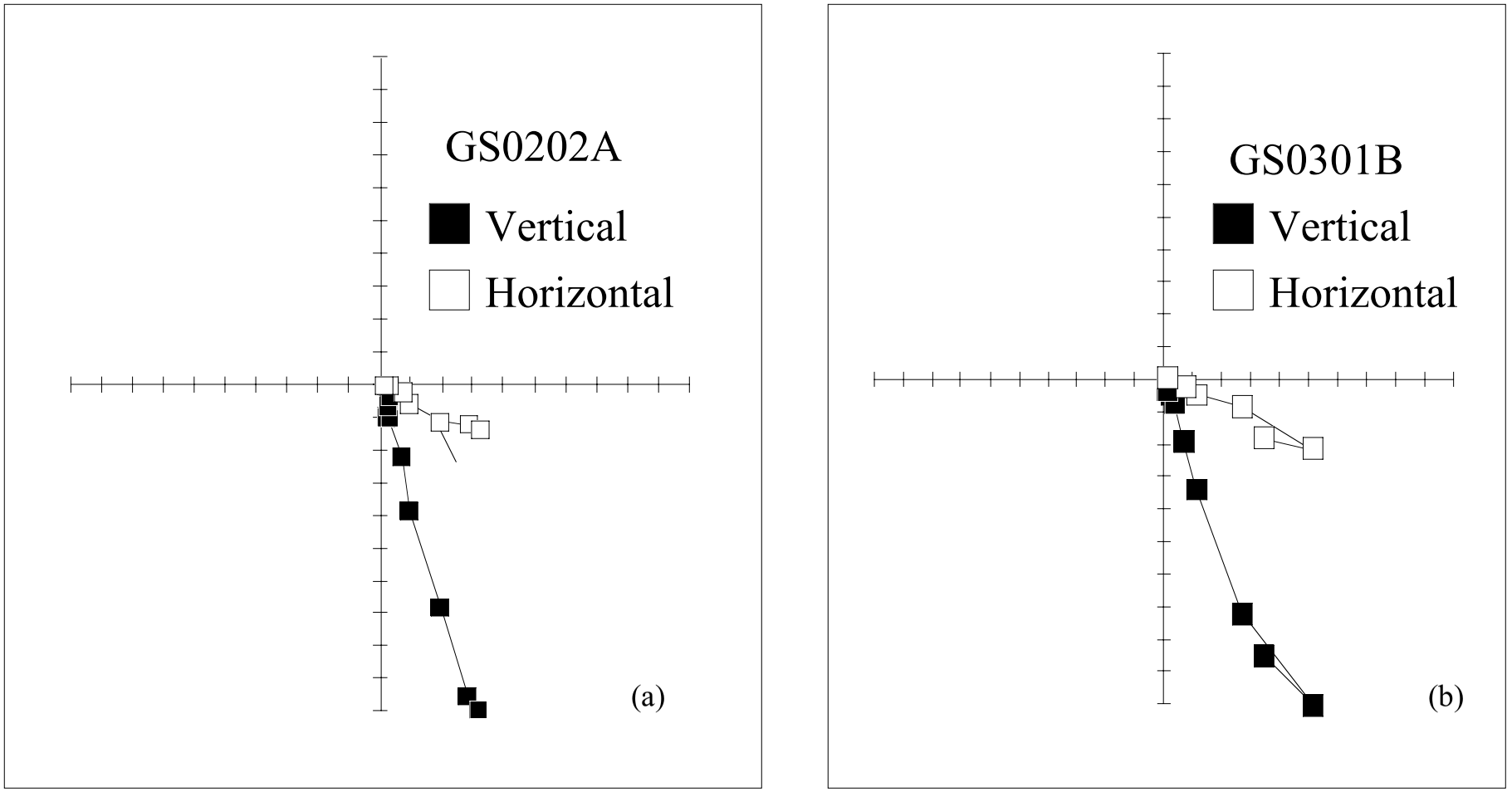

Figure 4.8: Representative OVPs from GS samples

Pullaiah *et al*. (1975) generated time-temperature curves for TVRM based on the theory of relaxation time in SD grains by Néel (1949). These however, predict an unrealistically high palaeotemperature for the GB. The temperature range of the LBT component found in this study was similar to that found in many samples extracted from the Milton Monzonite (Dunlop *et al*., 1997a). These samples had similar hysteresis parameters (M_{RS}/M_S, H_C) to GB samples inferring moderate to large PSD grains were predominant. Dunlop *et al*. (1997b) explained the anomalously high unblocking temperatures as an aspect of non-SD behaviour and this serves as an adequate explanation for the GB as well. In the case of the Milton Monzonite however, there was good reason to suspect that the overprint did not have chemical origin. In the absence of this for the GB, it was not possible to favour either the TVRM or TCRM explanation for the high maximum unblocking temperatures over the other.

Boesen *et al*. (1961) calculated a mean direction of remanence for the GB of (191 / +80) while Schmidt (1976) carried out further AF demagnetisation and isolated a hard component with mean direction (156 / +79) from samples taken from the central part of the intrusion. This is the first study of the GB using thermal demagnetisation and yields a HBT component very similar to that observed by Boesen *et al*. (1961).

The mean direction provided by the HBT component of sites GB02 to GB07 was almost exactly anti-parallel to that of the LBT component, but the timing of the overprint event during the CNS precludes the higher temperature component forming at this time. It is unfortunate that, because of the Coral Sea loop in the APWP, the poles for 90 Ma are close to those for the mid-Jurassic. Nevertheless, the VGP produced from the HBT mean direction may be too far west to represent an uncorrupted primary magnetisation. If site GB01 is included in the mean calculation, then the VGP moves to 52°S, 153°E which is closer to that produced by Schmidt's (1976) study (52°S, 164°E) but not nearly so well constrained. The exaggerated scatter of the results produced by this study compared to that by Schmidt (1976)

could be interpreted as a product of the different type of demagnetisation technique used. Components of pTRM held in large PSD grains exhibit pTRM tails above their blocking temperature (§ 2.4.4), which makes their removal by thermal demagnetisation difficult. This problem is not encountered by AF demagnetisation which can remove softer components and leave harder ones intact. It is therefore possible that the HBT component measured in this study is the primary TRM (as measured by Schmidt (1976)) with a slight bias resulting from the tail of the overprint.

Figure 5.8 shows OVPs from two GS samples: a small VRM was usually removed by demagnetisation to 150°C after which a convergent reversed component resided above this to ~500°C. Any remanence in the GS samples with $T_{UB} > 500°C$ was generally too weak to give a coherent signal. Samples from GS01 differed from the others in that they had very strong remanence magnetisations in apparently random directions. This type of behaviour strongly suggested that lightening bolts had imparted IRMs to all the samples from this site and that their results were meaningless. Samples from GS04 appeared to be unstable palaeomagnetic recorders: only two samples held a recoverable remanence and these differed significantly from one another.

The mean direction for the GS intrusion given in table 5.2 corresponds to a VGP of Tertiary age (figure 4.7) and is somewhat removed from the VGP (59°S, 210°E) found by the study of the GS by Schmidt (1976). Unfortunately this average is derived from only two sites and a total of just 11 samples and therefore cannot be relied upon to have averaged out palaeosecular variation (PSV) sufficiently to allow a meaningful comparison with other Australian poles.

The results, described so far, of the experiments performed on the samples from the four Moss Vale intrusions gave mixed indications of each sample sets potential for successful Thellier analysis. In the GB samples, it may be somewhat difficult to isolate a pure TRM whereas in the GS samples it is difficult to ascertain whether the

ChRM is even primary, let alone a TRM. Both sets of samples displayed a significant contingent yielding consistently directed components, this is the absolute minimum requirement for a palaeointensity analysis to be conducted.

4.2.3 Palaeointensity analysis

Samples from both intrusions were subjected to the Thellier method of palaeointensity analysis with pTRM checks after every alternate double heating step but no NRM checks.

The Thellier method, in 50°C steps from 100°C to 600°C, was applied to twenty GB samples selected from all sites. All GB samples generated NRM-TRM plots with steep *positive* slopes for the portion of the blocking temperature spectrum occupied by the overprint and shallower negative slopes for that in which the ChRM resided (figure 4.10).

It was decided that the first part of the NRM-TRM plot should be analysed as usual because the remanence residing here was largely thermal in origin and the results were of interest. Samples were adjudged to give a reasonable estimate if they fulfilled the criteria given by Coe *et al*. (1978; § 2.4.2), with the exception of that excluding portions affected by secondary magnetisations. Examples of NRM-TRM plots of LBT components giving acceptable palaeointensity estimates are shown in figure 4.11.

As can be seen in table 4.4, if the criteria requiring $\beta < 0.1$, $q > 1$, as suggested by Selkin and Tauxe (2000) are used, all of the palaeointensity estimates from the GB overprint would be discarded. As it stands, the individual uncertainties tend to be very high, the estimate of GB0605B is discarded simply because it is incomparably high. pTRM checks were limited to one per estimate and three of these have discrepancies (both low and high) greater than 10%.

The LBT component was not expected to behave well in a Thellier experiment: it cannot be a pure TRM and it is most likely carried by large PSD grains. Both of these factors are expected to cause a palaeointensity estimate to be erroneously high: part of the NRM is of non-thermal origin and the portion of the NRM-TRM plot may be the initial section of a convex-down curve. Therefore, the estimates presented above are tentatively proposed as a maximum limit on the strength of the palaeofield at 90 Ma.

For the purpose of investigation, pTRM checks were largely ignored in the analysis of the GB HBT component NRM-TRM plots, examples are given in figure 4.12. The details of the nine samples that passed the criteria of Coe *et al.* (1978) are given in table 4.5. Although q values were moderate, the pTRM check values were mostly observed to be extremely high relative to the original measured pTRM. It therefore seems likely that thermal alteration increased their capacity to acquire TRM at high temperatures causing the resulting estimates to be low. Only two samples have values of β sufficiently low to be accepted by the criterion of Selkin and Tauxe (2000) and only one site-average VDM (that from GB02) has a standard deviation of $< 25\%$ which is another of their minimum requirements. These are then, rather low quality results, which have reasonable q factors largely as a consequence of their high f factors. The likelihood of these palaeointensity estimates, and others presented in this chapter, being reliable is investigated in chapter 5 and discussed in chapter 9.

Thirteen samples from sites GS02, 03 and 04 were chosen because they appeared to be relatively unaffected by weathering and subjected to the Thellier method in 40°C heating steps from 100°C to 460°C. Several samples from site GS03 behaved reasonably well in the analysis (figure 4.13). Once the small VRM had been removed by ~140°C, there was often a linear portion on the NRM-TRM plot comprising at least four points. Above 300°C, the OVPs clearly indicate the acquisition of a CRM with T_{UB} greater than the current heating temperature.

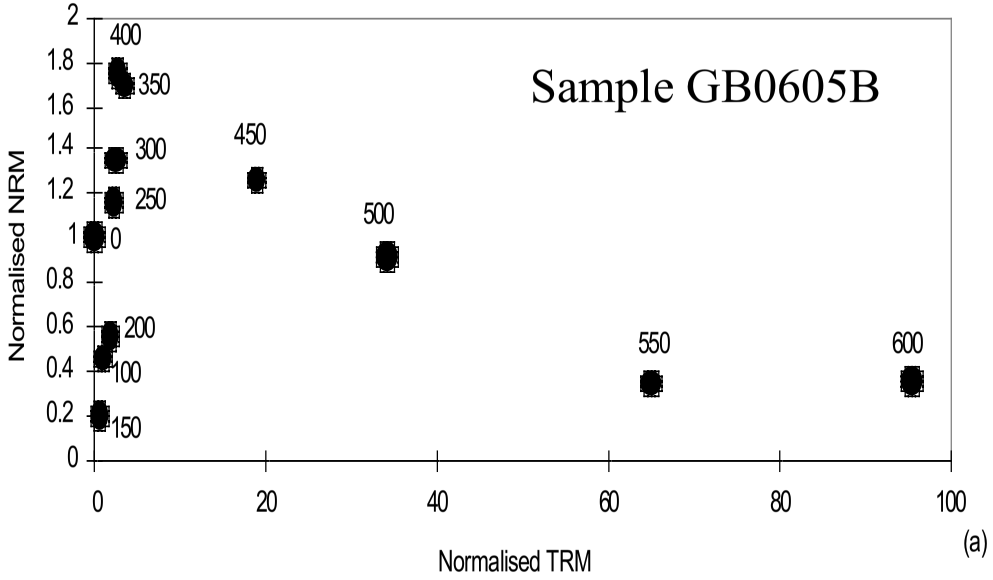

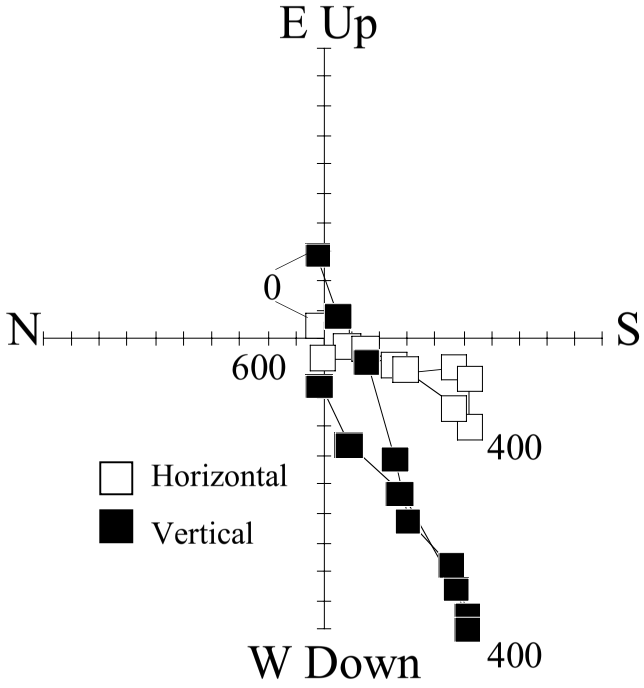

Figure 4.10: NRM-TRM plot and accompanying OVP for GB sample, numbers represent temperatures.

Sample	ΔT	N	f	g	β	q	pTRM check discepancy	R(6)	H_{PALAEO} (μT)	Site mean VDM (10^{22} Am^2)
GB102B	250-450	5	0.52	0.48	0.16	1.6	0.04	3	28 ± 18	4.9 ±0.9
GB105B	250-400	4	0.27	0.62	0.17	1.0	-0.16	2	36 ± 38	
GB404B	200-350	4	0.21	0.52	0.16	0.7	0.04	4	27 ± 40	3.5
GB501B	200-350	4	0.25	0.95	0.22	1.1	0.15	2	46 ± 44	6.2 ± 0.4
GB504B	200-350	4	0.40	0.65	0.13	2.1	-0.06	3	50 ± 24	
GB605B*	200-350	4	0.65	0.89	0.25	2.3	-0.06	3	98 ± 42	14.9
GB704B	200-350	4	0.19	0.67	0.38	0.3	0.14	2	25 ± 78	4 ± 0.9
GB707B	200-350	4	0.25	0.58	0.16	0.9	0.09	3	35 ± 38	
Mean									35 ± 10	4.7 ±1.2

Table 4.4: Accepted results (except for that marked with asterisk) from the LBT component of GB samples. The R factor has a maximum value of 6.

Sample	Δ T	N	f	g	β	q	Mean pTRM check discepancy	Max pTRM check discepancy	R(6)	H_{PALAEO} (μT)	Site mean VDM (10^{22} Am^2)
GB201B	400-600	5	0.94	0.61	0.13	4.3	25%	36%	2	13.0 ± 2.9	1.7 ± 0.1
GB202B	400-600	5	0.94	0.54	0.11	4.7	23%	42%	2	11.5 ± 2.5	
GB203B	400-600	5	0.98	0.55	0.16	3.5	26%	45%	2	12.0 ± 3.3	
GB402B	350-550	5	0.84	0.72	0.08	7.4	37%	37%	4	5.8 ± 0.8	0.8
GB501B	400-600	5	0.98	0.71	0.11	6.1	14%	23%	2	8.7 ± 1.4	1.2
GB602B	400-600	5	0.88	0.61	0.19	2.8	30%	44%	2	7.0 ± 2.5	1.2 ± 0.4
GB603B	400-600	5	0.88	0.65	0.14	4.1	31%	46%	2	7.6 ± 1.8	
GB604B	400-550	4	0.84	0.58	0.11	4.4	64%	64%	2	9.2 ± 2.1	
GB605B	400-550	4	0.68	0.49	0.08	4.2	20%	20%	3	3.3 ± 0.8	
Arithmetic mean										8.7 ± 3.1	1.2 ± 0.4

Table 4.5: Accepted results from the HBT component of the GB samples. The R factor has a maximum value of 6

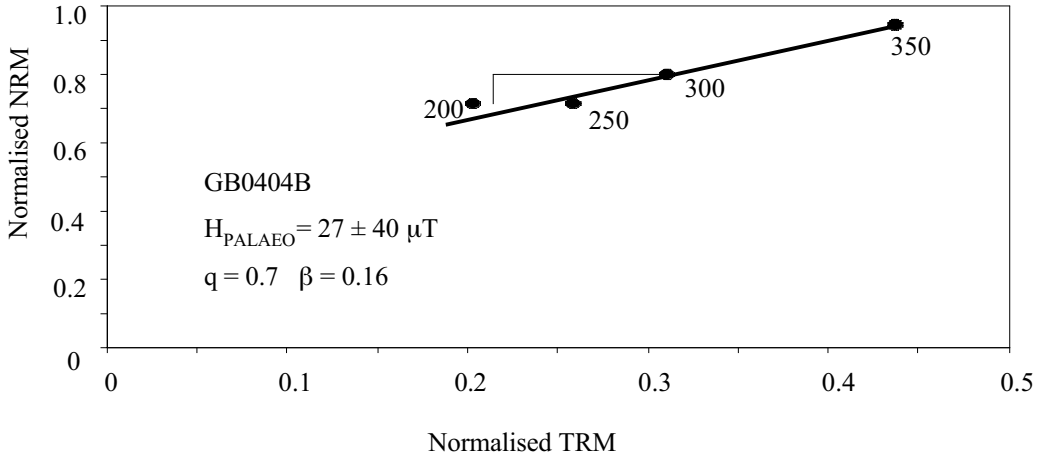

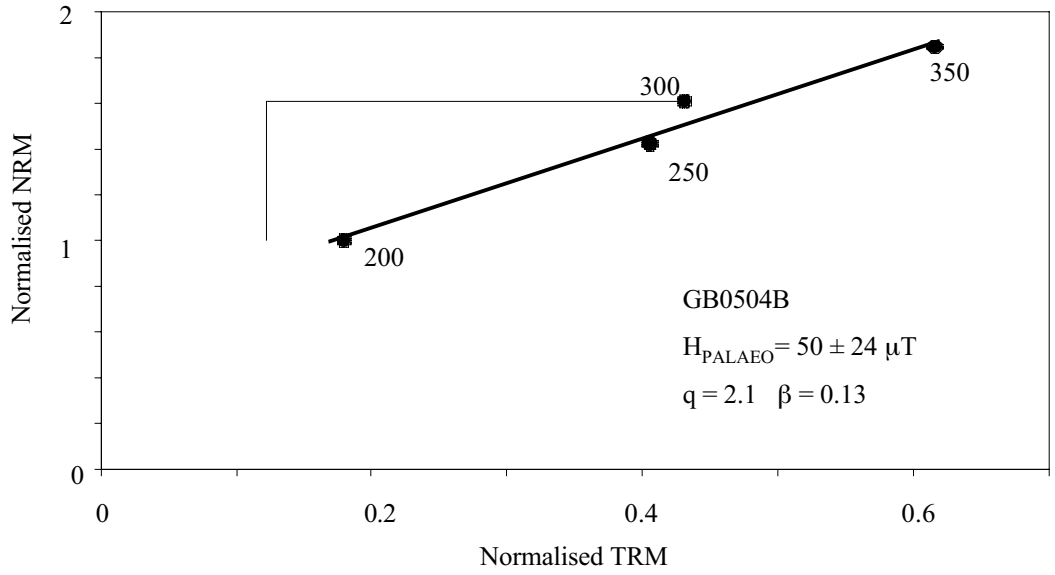

Figure 4.11: Low temperature portion of NRM-TRM plots for two samples yielding estimates for LBT component

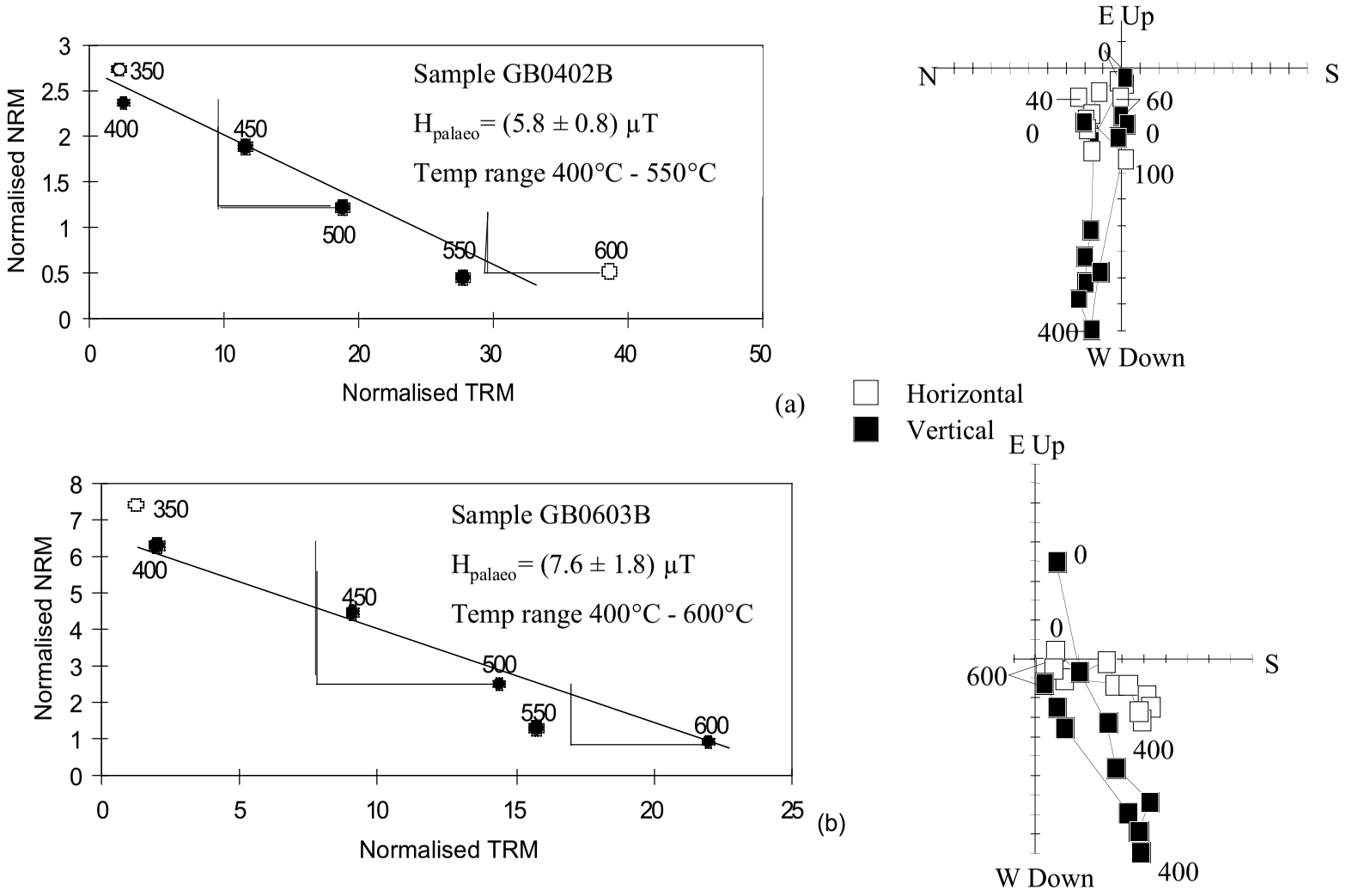

Figure 4.12: NRM-TRM plots produced by HBT component in two samples from the GB intrusion shown with accompanying OVPs. Hollow circles on the NRM-TRM plots represent points not used to calculate the best-fit straight line.

Sample	ΔT	N	f	g	β	q	Mean |pTRM check discepancy|	Max pTRM check discepancy	R(6)	H_{PALAEO} (μT)	Site mean VDM (10^{22} Am^2)
GS21D	180-300	4	0.44	0.64	0.08	3.8	21%	-21%	4	35.5 ± 9.5	5.0
GS32C	100-300	6	0.85	0.76	0.04	16.9	6%	-11%	5	28.8 ± 1.7	
GS34D	140-300	5	0.66	0.70	0.07	6.8	17%	-17%	5	26.7 ± 3.9	
GS35C	180-300	4	0.34	0.63	0.03	8.4	26%	-26%	4	24.3 ± 2.9	3.9 ± 0.5
GS36C	140-300	5	0.63	0.67	0.10	4.1	9%	-9%	6	28.1 ± 6.8	
GS37D	140-300	5	0.64	0.73	0.08	5.1	8%	-8%	6	21.2 ± 4.2	

Table 4.6: Details of palaeointensity estimates from the GS intrusion that passed the criteria of Coe (1976). The R factor has a maximum value of 6

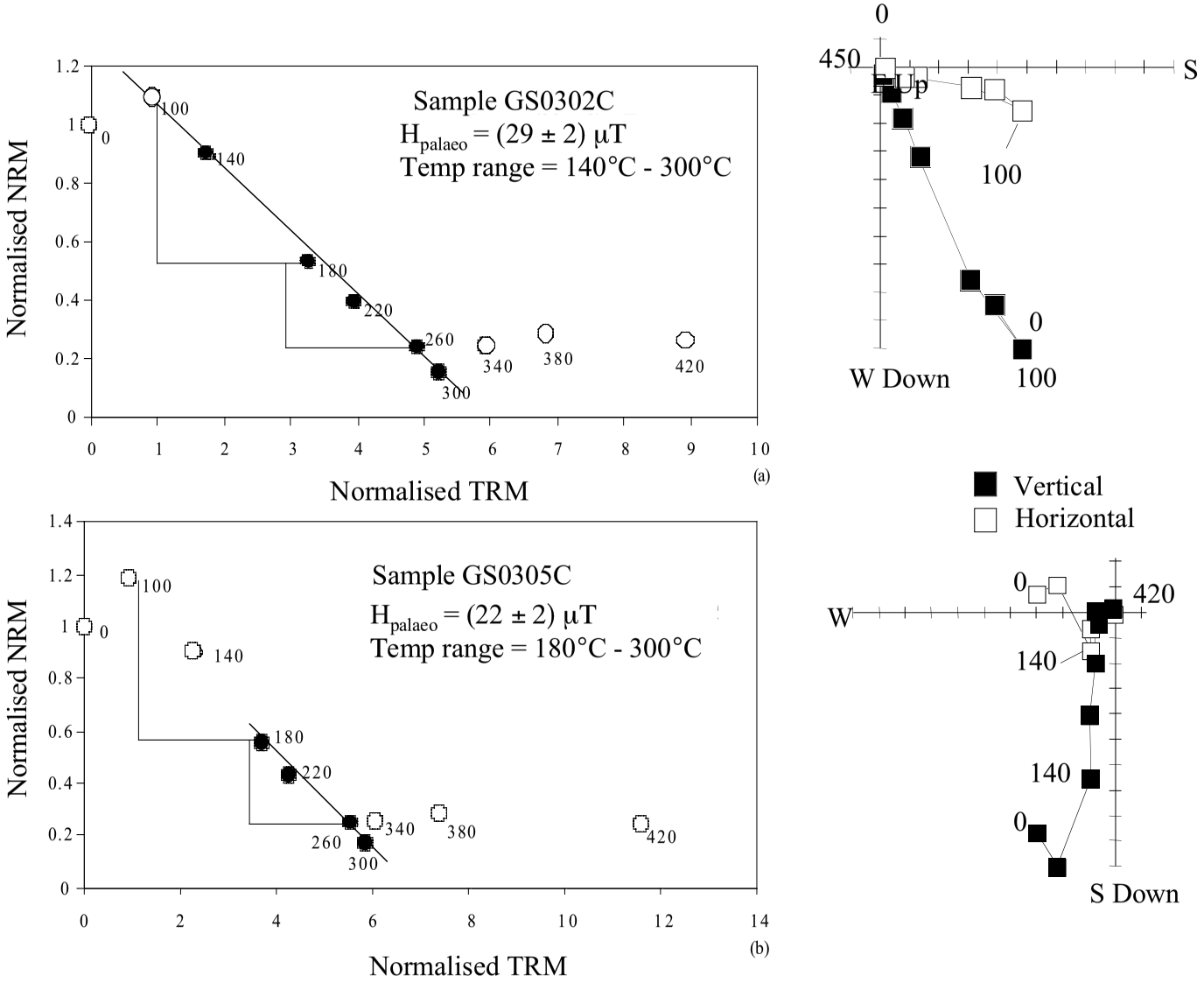

Figure 4.13: NRM-TRM plots produced by two samples from the GS intrusion shown with accompanying OVPs. Hollow circles on the NRM-TRM plots represent points not used to calculate the best-fit straight line.

The six samples that passed Coe's criteria are listed in table 4.6. The criteria suggested by Selkin and Tauxe (2000) are largely satisfied with the exception of that regarding pTRM checks. It is worth noting that, although the pTRM checks do tend to be rather low, the two samples that do pass this criterion (GS0306C and GS0307D) are not discernible from the others in the estimates they produce.

The mean direction of magnetisation of the actual components used in the GS03 mean VDM calculation translate to a VGP at 27°S, 190°E (dp=20°, dm=23°). This is a very long way away from the Tertiary portion of the Australian APWP but within errors of mid-Jurassic poles. Hence it seems that samples taken away from the surface of site GS03 may record a primary remanence.

4.3 The Kiama and Newcastle Dyke Swarms

These two suites of intrusions were introduced in § 3.3.2.2 and the details of the individual sites were given in tables 3.2 and 3.3 and figures 3.5 and 3.6.

4.3.1 Rock magnetic analysis

The following rock magnetic methods were applied to at least one sample from sites in the KD swarm: hysteresis, thermomagnetic and low temperature susceptibility (χ_{LT}). χ_{LT} analysis was not necessary for the ND sites because the results from the hysteresis and thermomagnetic analyses were conclusive. Additionally, some samples from both suites were subjected to repeated hysteresis measurements after cyclic heating to progressively higher temperatures. This was performed to assess the likelihood of thermal alteration occurring during the Thellier analysis. Finally all samples were subjected to χ_{RT} measurements after every heating stage of the palaeodirectional and palaeointensity analyses.

Sampling site	χ_{RT} $10^{-6}m^3/kg$	M_{RS}/M_S	Hc (mT)	H_{CR}/H_C	ΔM_s	T_C (°C)	RS
BP01	6881	0.02	1	1.68	-0.16	550	
CR01	5925	0.17	13	1.92	0.05	580	0.48
CR02	6557	0.12	8	0.92	-0.39	530	0.54
CR03	5967	0.05	5	0.99			
CR04	3753	0.16	12	1.97			
CR05	7131	0.12	8	2	-0.58	535	0.5
CR07	6781	0.11	7	2.01	-0.16	520	0.55
CR08	721	0.08	7	2.1	-0.16	550	0.46
MM01	4454	0.14	7	1.95	-0.74	610	0.76
MM02	1704	0.1	5	1.82			
RP02	3986	0.06	4	1.89	-0.095	550	
TP01	1911	0.06	5	1.99			

Table 4.7: Measured rock magnetic properties of KD samples

Sampling site	χ_{RT} $10^{-6}m^3/kg$	M_{RS}/M_S	Hc (mT)	H_{CR}/H_C	ΔM_s	T_C (°C)
CH01	1742	0.09	5	2.48	23.59	565
CH02	1862	0.13	5	2.08	1.87	270
LR01	4032	0.08	5	2.06	0.11	380
NE01	4287	0.05	3	2.05	0.24	465
NH01	2923	0.13	8	2.02	0.88	175

Table 4.8: Measured rock magnetic properties of ND samples

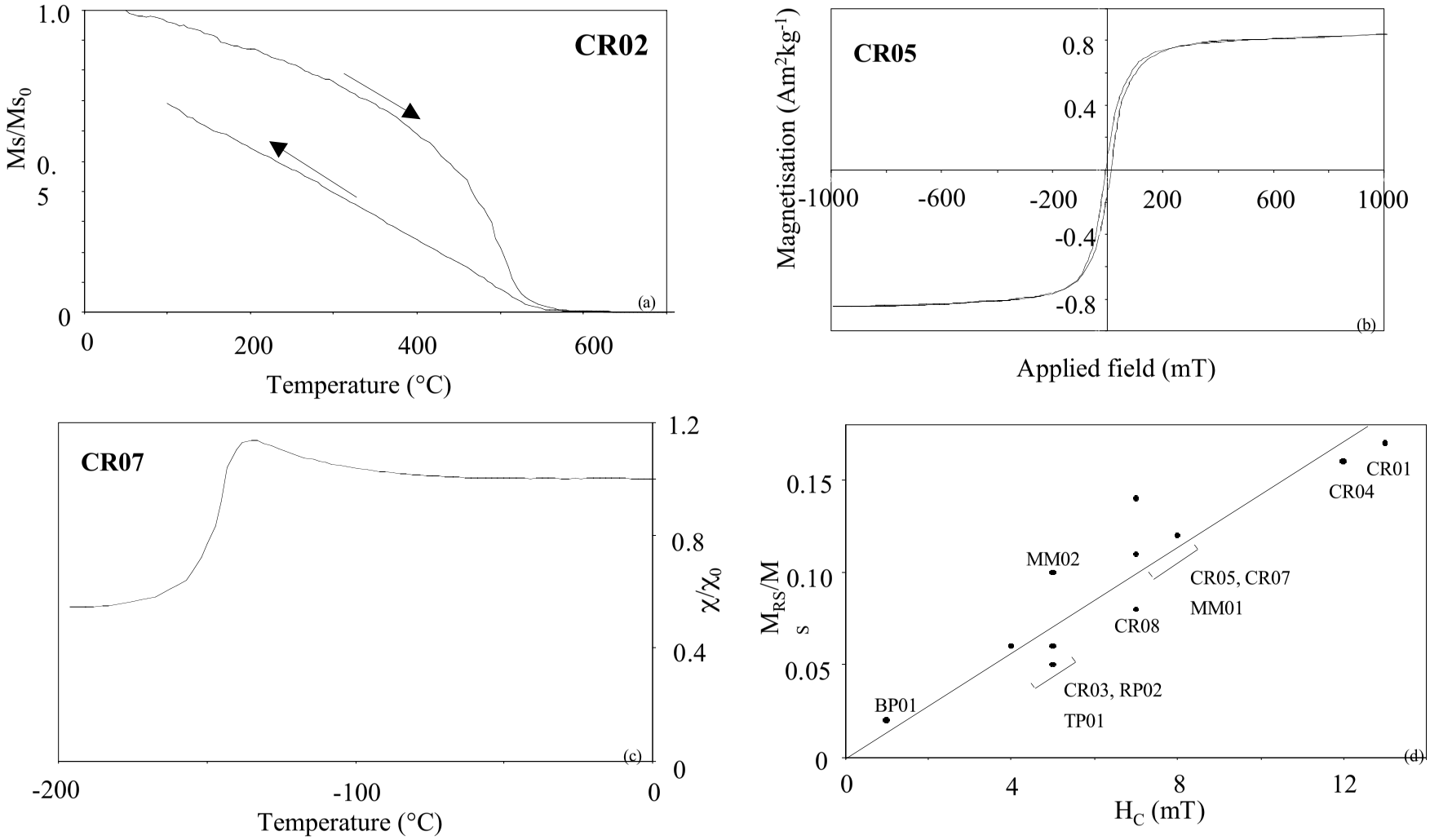

Figure 4.14: Representative plots from rock magnetic analyses of CR (a) thermomagnetic profile. (b) Hysteresis plot. (c) χ_{LT} profile (d) Hysteresis parameters from all KD sampling sites.

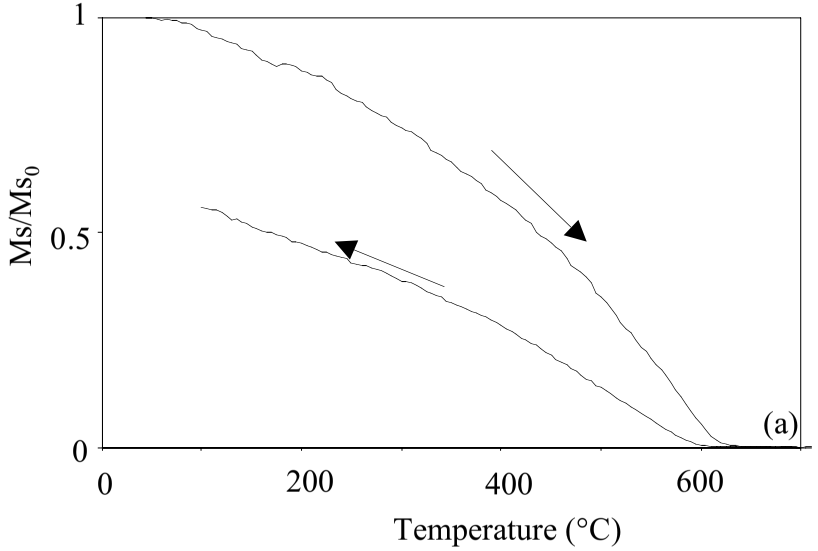

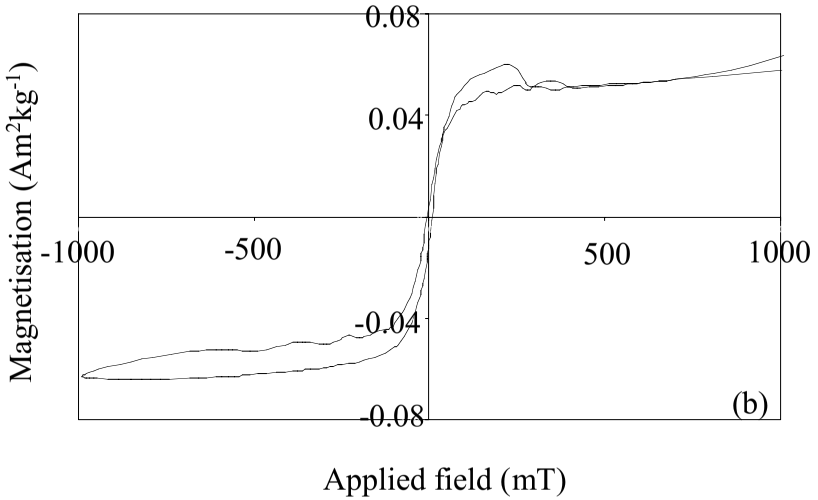

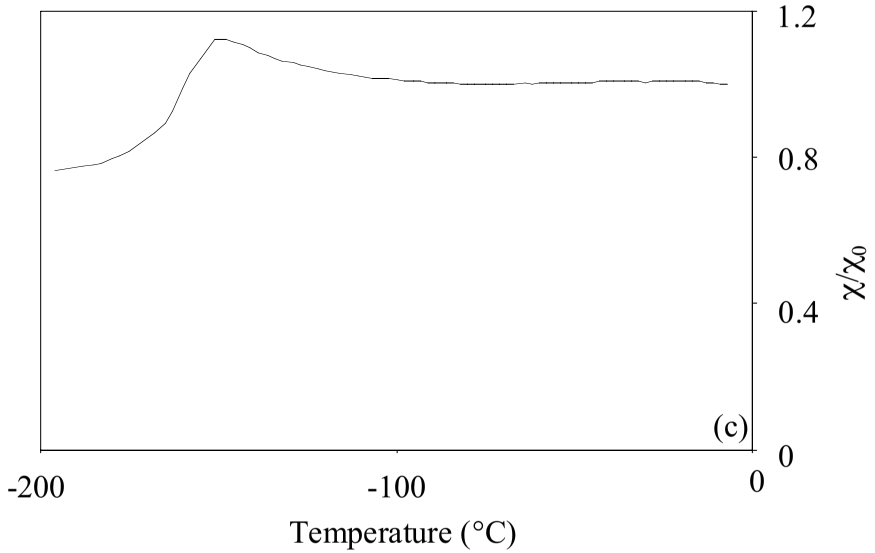

Figure 4.15: plots from rock magnetic analyses of a sample from site MM01. (a) thermomagnetic curve. (b) hysteresis plot. (c) χ_{LT} profile.

The magnetomineralogy of the KD samples was relatively consistent (table 4.7). Samples from all Cathedral Rock (CR) sites as well as those from Barrack Point (BP) and Red Point (RP02) produced similar thermomagnetic, hysteresis and χ_{LT} plots (figure 4.14(a)-(c)). These suggested that Ti-poor titanomagnetite grains ranging in size from PSD to true MD dominated the ferromagnetism of the samples. Significant alteration, resulting in a loss of magnetisation intensity and a change in its temperature dependence, was generally observed to have occurred during heating to 700°C in the thermomagnetic analyses.

The hysteresis properties of all KD samples were found to follow a more linear pattern when H_C rather than H_{CR}/H_C (as in a standard Day *et al.* (1977) plot) was plotted against M_{RS}/M_S (figure 5.14(d)). The sample from site BP01 was the only one observed to fall into the 'true MD' size range (Dunlop *et al.*, 1997b). A high presence of SP grains is an alternative explanation for some of the very thin hysteresis loops observed. To discover if SP grains were present in significant proportions in the KD samples, an analysis of frequency dependent susceptibility (§ 2.2.2.3) was performed. The measured susceptibilities at low and high frequencies differed by less than 2% in all samples suggesting that SP grains were not significant.

The sample taken from site MM01 displayed considerably different behaviour to the others during thermomagnetic and hysteresis analysis (figure 4.15 (a) and (b)). Although the measured hysteresis loop was rather noisy, it was clearly discernible as 'wasp-waisted' (Tauxe, 1998). This implies that the sample has either two comparable magnetic phases or two distinct grain size distributions (Roberts *et al.*, 1995). The thermomagnetic curve displayed no evidence of two Curie temperatures; similarly SP grains cannot comprise a component of the ferromagnetism. The χ_{LT} profile (figure 4.15(c)), together with the slight peak in the thermomagnetic heating curve at ~ 200°C, are suggestive of a mixture of MD and SD grains and therefore this seems a probable explanation for the wasp-waisted hysteresis loop. The ferromagnetic mineral itself is likely to be maghaemite as it has a Curie temperature

greater than that of magnetite and altered to a less magnetic derivative (haematite) upon cooling. It should be noted that the MM01 sample was taken from the bottom of a core and therefore the presence of maghaemite at this site may not be confined to the surface.

ND samples displayed hysteresis properties ranging from true MD to large PSD grain size (table 4.8 and figure 4.16(b) and (d)). Samples from the two Catherine Hill Bay (CH) sites displayed humps in their heating curves (figure 4.16(a)) although that from site CH02 also displayed a phase with T_C = 270°C on the heating curve. Both samples (and especially that from CH01) showed an increase in M_S on the cooling curve and the ferromagnetic content in the CH01 sample was sufficiently low to allow the paramagnetic minerals to significantly affect the hysteresis loop. Thermomagnetic analysis of the other samples displayed a single T_C phase altering to a more magnetic, higher T_C phase upon cooling (figure 5.16(c)). This behaviour is indicative of titanomagnetite with a moderate Ti content suggesting that these dykes cooled too quickly to allow (oxy) exsolution to occur. Oxidation did occur during the thermomagnetic analysis however, and would be very likely to occur during thermal demagnetisation in a palaeomagnetic study. The CH01 sample may contain a significant proportion of pyrrhotite while that of CH02 may contain a mixture of titanomagnetite and pyrrhotite.

Figure 4.17 (a) and (b) show the effects on hysteresis properties of cycling certain samples to progressively higher temperatures. Unsurprisingly, most of the samples appear to show progressive shifts to a lower effective grain size (higher values of M_{RS}/M_S and H_C). Although it is difficult to know exactly what constitutes a 'significant change' in the properties, it was apparent that, excepting the CR01 and perhaps the LR01 samples, all had shifted noticeably in their properties after heating to 400°C and above. Excepting samples from CH01 and NE01 (the latter of which there is insufficient information for), it appears that the samples survived heating to 300°C without experiencing severe modification in their abilities to retain a remanence.

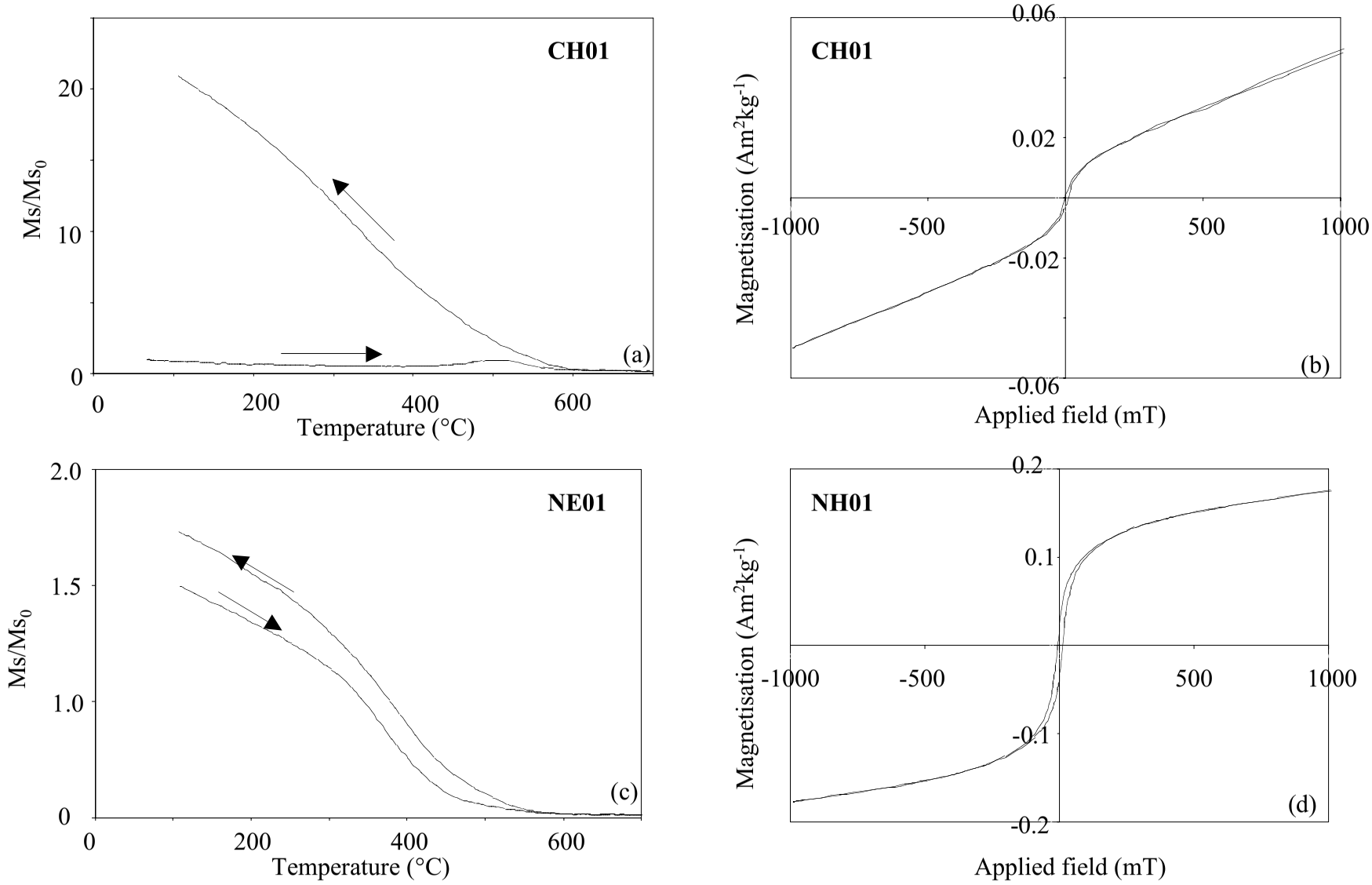

Figure 4.16: Representative plots from thermomagnetic ((a) and (c)) and hysteresis ((b) and (d)) curves.

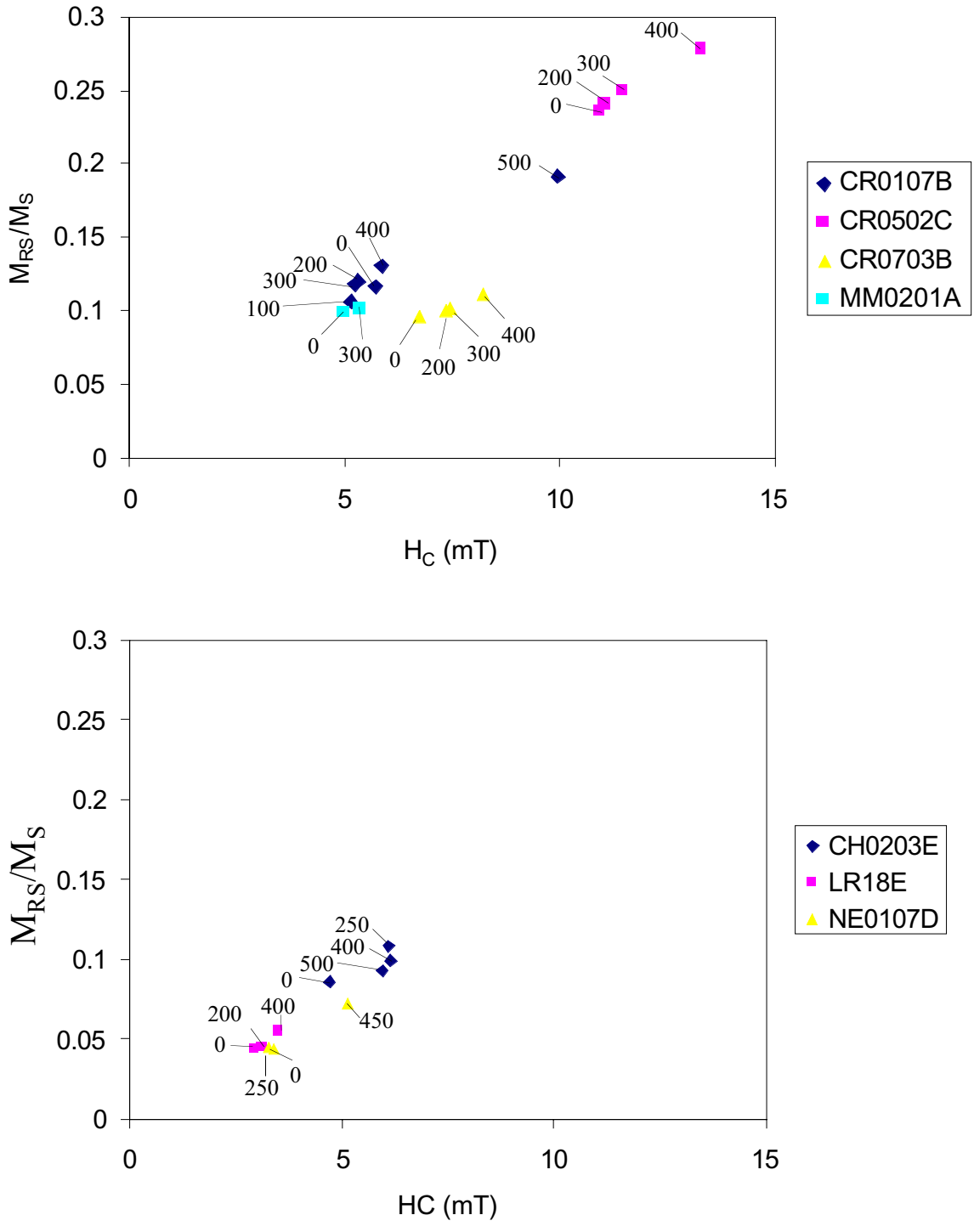

Figure 4.17: Plots of hysteresis properties after heating to the temperatures indicated for (a) Kiama dyke samples, (b) Newcastle dyke samples.

The rock magnetic analyses described in this section did not in general purport to samples from either the KD or ND swarms being suitably stable palaeomagnetic recorders for Thellier analysis. The large effective grain-size of most of the samples could require the Thellier method to be applied across entire blocking temperature spectra in order to be certain of a reliable estimate. This itself would require that the samples be free from magnetic overprints and entirely resistant to laboratory induced alteration during the Thellier analysis. The results of the rock magnetic analyses presented here suggested that the second of these criteria at least, may not be fulfilled.

4.3.2 Palaeodirectional analysis

One 'A' (top of core) sample from virtually every site of both the KD and ND swarms were subject to palaeodirectional analysis in the form of thermal demagnetisation and principle component analysis. The demagnetisation steps were at 50°C intervals from 100°C to 500°C followed by 30°C to 580°C or 640°C in some cases.

Most KD samples gave OVPs which, after removal of a spurious component at relatively low temperatures (~ 150ºC), appeared to contain a single, normal polarity, convergent component (figure 4.18 (a) and (b)). However, some samples from sites BP01, CR01, CR08 and RP01 also displayed a reversed polarity high blocking temperature (HBT) component residing above 400 - 500ºC (figure 4.18 (c)). Additionally, figure 4.18 (d) shows a clear example of a sample displaying at least two separate components with the same polarity. This feature was suspected in many more samples (especially those from site CR04) but was very difficult to identify with certainty.

Schmidt (1990) performed thermal demagnetisation on seven of the Kiama dykes and reported that five of them gave stable consistent ChRMs with a steep normal polarity to the NNW (average direction: 332/-77 (k=102, α95=8)). This direction yields a VGP consistent with other early Jurassic palaeopoles (figure 4.19). Two other dykes however, were reported to give mean directions shifted towards the Cretaceous direction of magnetisation (i.e. further east) and with increased scatter. Schmidt (1990) therefore drew attention to the likelihood of overprinting by the 90 Ma thermal event affecting the Sydney basin.

Appendix 5 lists the directions of magnetisation in the KD samples measured here and table 4.9 shows the site and overall mean directions. The mean direction of all the sites is relatively precise but corresponds to a VGP closer to previously calculated Cretaceous rather than Jurassic palaeopoles (figure 4.19). Applying a criterion to the site mean directions requiring k > 30 leaves 5 sites (marked with *) which combine to give a VGP closer to that reported by Schmidt (1990) but still within errors of Cretaceous palaeopoles as is that of Schmidt (1990) (figure 4.19). From the OVPs of three samples from CR04, it was possible to isolate the normal polarity HBT component; these gave a mean VGP position at 67ºN, 318ºE (dp = 12º, dm = 14º) which suggests that a CRM was imparted at either Cretaceous or early Tertiary times. This high temperature CRM is evident, as a shearing to the east of the ChRM component, in many samples but is extremely difficult to remove because it usually overlaps with the (assumedly) primary TRM. With regard to the palaeointensity analysis described in the next section, samples had to be inspected for overprinting of the TRM individually. Nevertheless, from this study it is apparent that those samples from sites CR02, CR04, CR05, CR07, and RP02 have the greatest probability of retaining an uncorrupted primary TRM in at least part of their blocking temperature spectra.

The reversely magnetised HBT component displays very poor inter-site consistency (table 4.9), therefore it is difficult to ascertain the time at which it was acquired. The fact that it occupies a similar part of the blocking temperature spectra as the normal

polarity HBT means that it could have been acquired through the same mechanism (low temperature oxidation), and therefore at the same time. The implication of this presumption is that the CRM overprint could not have formed during the CNS (83 –118 Ma).

Samples from different sites (dykes) of the ND swarm behaved quite differently from one another. OVPs generated by CH01 and NH01 samples were generally noisy: overprints with apparently random directions were present up to ~ 400ºC after which a reverse polarity ChRM remained until above 500ºC (figure 4.20 (a)). The ChRM directions from each site were somewhat inconsistent leading to large uncertainties in their mean directions (table 4.10). Samples from CH02 were more stable palaeomagnetic recorders and, although they still displayed a random overprint, it was removed by demagnetisation to ~150ºC leaving steep reversed polarity ChRMs discernible up to 560ºC (figure 4.20 (b)).

Samples from site LR01 also yielded noisy OVPs although two distinct components were isolated in several cases. The first of these was normal polarity and occupied the blocking temperature spectrum up to ~ 450°C, the second, reversed, component was observed, in four of the seven samples analysed, only after demagnetisation to at least 530°C (figure 4.20(c)). The mean direction of this ChRM is very poorly constrained because of its variation between samples, nevertheless it was similar to those from CH and NH samples and was included in the first of the reversed polarity mean calculations (table 4.10).

OVPs produced by thermal demagnetisation of the NE01 samples were simpler to interpret as only one normal polarity component was discernible. Unfortunately, it was not possible to state with any certainty whether this component was the ChRM because the plots became noisy as the remanence of the samples grew weaker. Figure 4.20(d) is an example of a clear OVP from this site. The mean direction of magnetisation from this site has only a moderate uncertainty attached to it because of the reasonable number of estimates it comprises of.

Site	$\overline{\Delta T}$ (°C)	N	Dec (°)	Inc (°)	k	α_{95}
BP01	100-450	6	6	-73	22	10
CR01	100-500	6	24	-62	12	31.6
CR02*	200-580	3	327	-77	1411	3
CR03	150-500	5	359	-68	28	15
CR04	150-450	8	315	-82	22	11
CR05*	100-530	3	319	-81	787	4
CR06	350-530	4	13	-71	18	15.1
CR07*	100-450	7	347	-85	51	9
CR08*	100-400	3	354	-68	153	10
MM01*	150-560	4	356	-79	114	9
MM02*	200-530	4	4	-77	271	6
RP01	300-560	4	18	-73	18	16
RP02*	250-500	2	326	-61	265	15
Mean		13	355	-75	70	5
VGP		63ºN 336ºE (dp = 8, dm = 9)				
Mean (*)		7	341	-76	77	6
VGP (*)		59ºN 347ºE (dp = 10, dm = 11)				
	HBT Component					
BP01	500-580	4	324	71	10	22
CR01	400-500	1	204	66		
CR08	400-500	3	168	69	1425	2
RP01	500-580	1	12	86		
Mean		4	214	83	17	17
VGP		46ºS 140ºE (dp = 33, dm = 33)				

Table 4.9: Site mean directions for Kiama dykes. Only those marked with asterisk are used in the calculation of the second mean

Site	$\overline{\Delta T}$ (°C)	N	Dec (°)	Inc (°)	k	α_{95}
CH01*	350-530	4	299	84	29	17
CH02*	150-560	5	229	86	97	8
LR01	530-600	4	261	81	6	29
NH01*	450-580	7	270	79	10	20
Mean		4	268	83	356	5
VGP		33ºS, 135ºE (dp =10 , dm =10)				
Mean (*)		3	271	84	267	8
VGP		32ºS, 138ºE (dp =15 , dm =16)				
CH Mean		2	272	86	370	
VGP		33ºS, 142ºE				
LR01	150-450	7	359	-73	63	8
NE01	150-450	7	7	-78	16	13
Mean		2	2	-76	455	
VGP		60ºN, 330ºE				

Table 4.10: Newcastle dyke (ND) site and overall mean directions

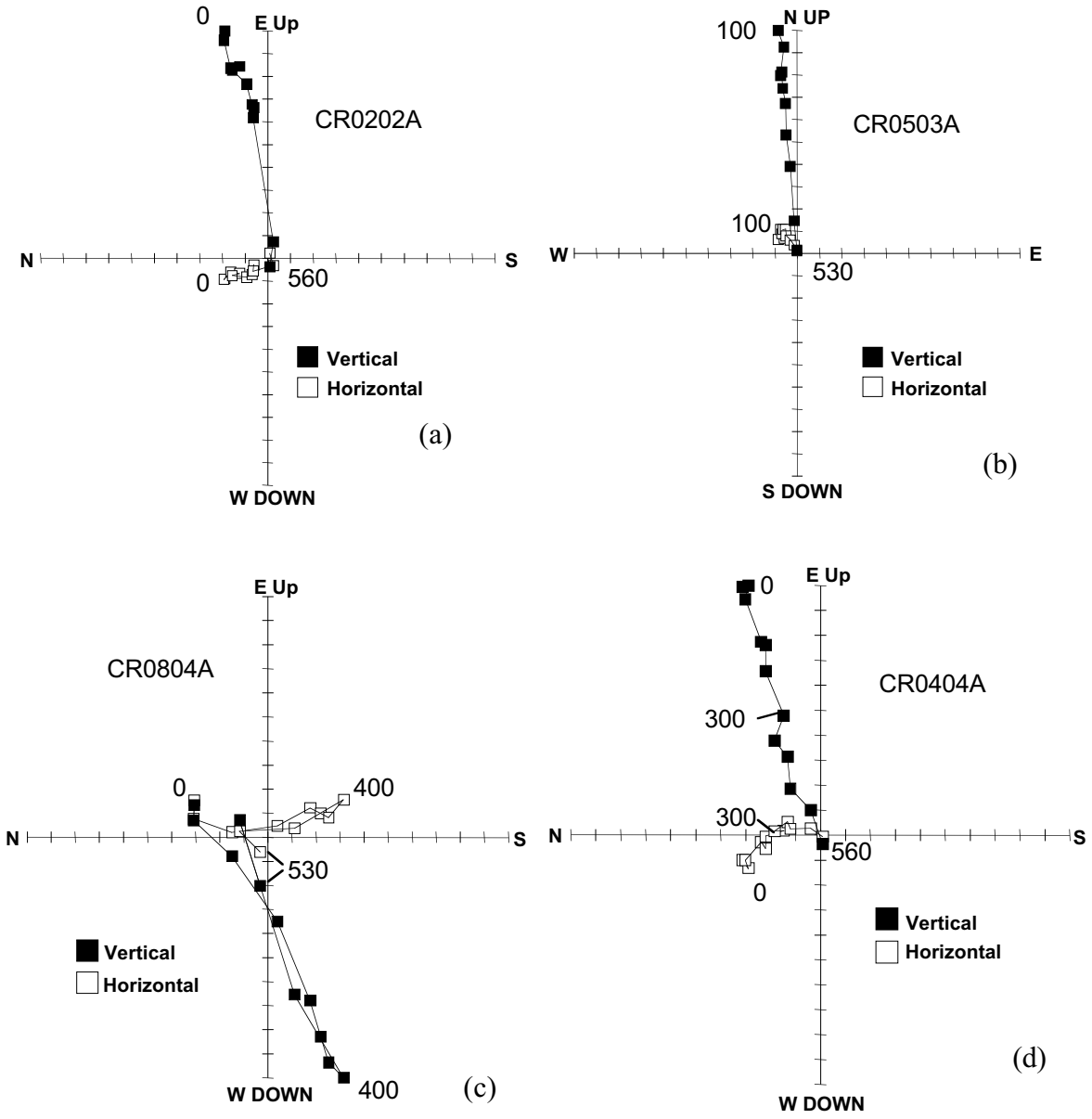

Figure 4.18: Representative OVPs from the palaeodirectional study of KD samples

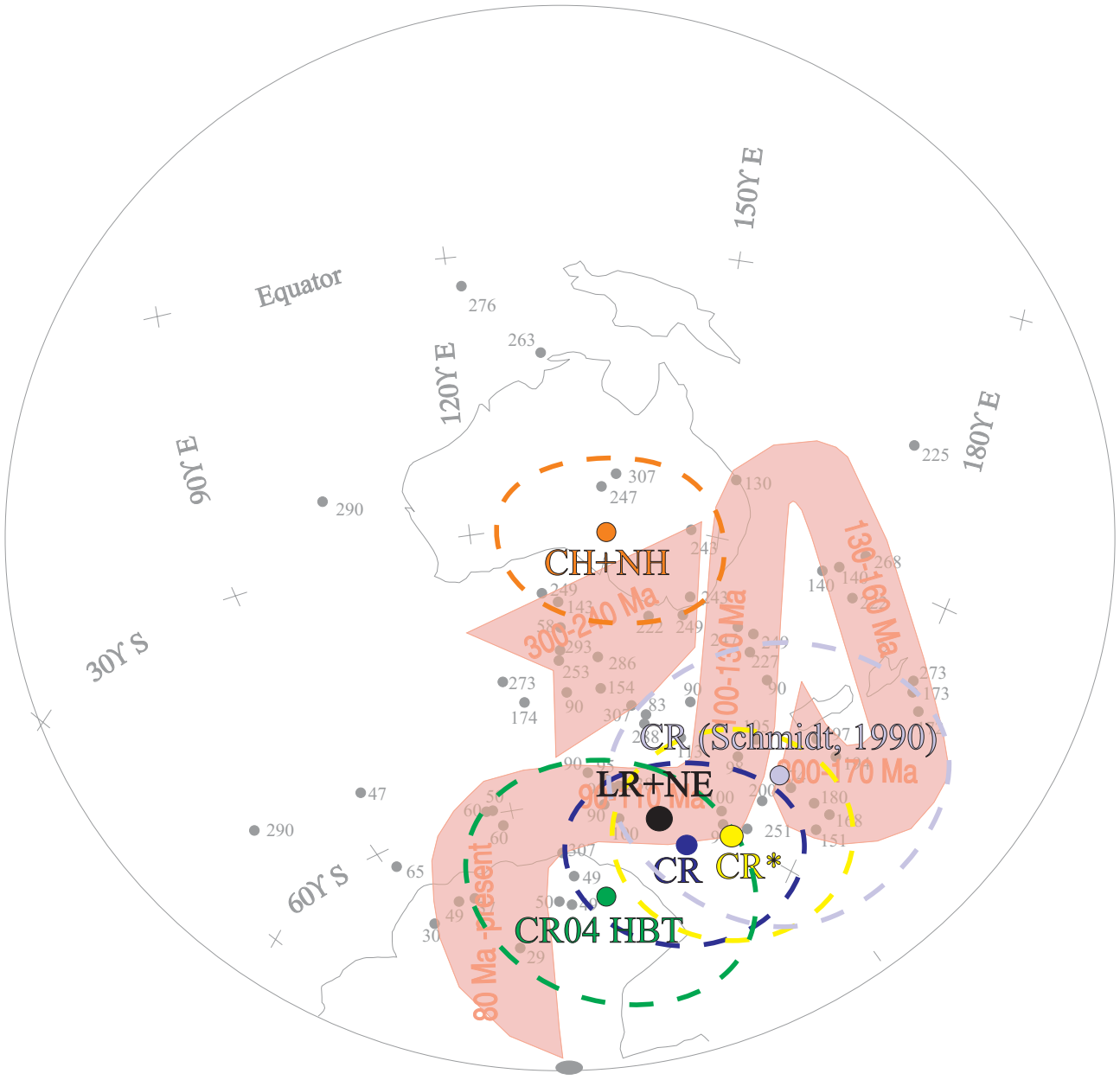

Figure 4.19: Australian APWP showing VGPs (normalised to reverse polarity) measured from Kiama and Newcastle dykes. Dashed ellipses show 95% confidence limits.

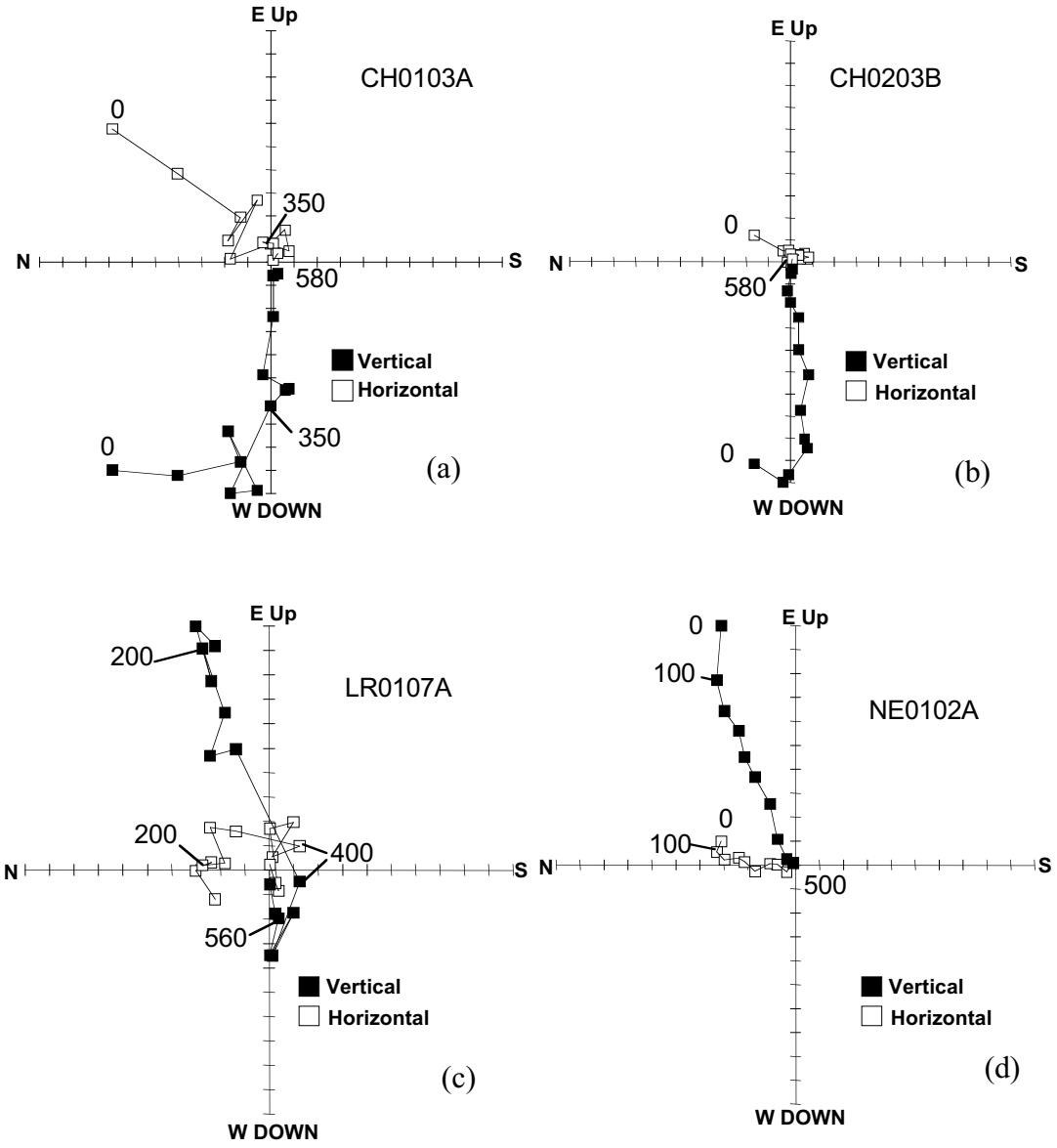

Figure 4.20: Representative OVPs from the palaeodirectional study of ND samples

A surprising result emerging from samples of all ND sites except NE01 was the presence of measurable components of remanence after demagnetisation above T_C of the site samples as measured by thermomagnetic analysis (table 4.8). One explanation that accounts for this is that the M_S signal from the harder remanence carriers was entirely drowned out of the thermomagnetic curves by the necessarily more voluminous higher Ti phase. Another explanation is that the ChRM magnetisation was a CRM or VRM acquired during or after demagnetisation in the laboratory. This second explanation is the most appealing to account for the scattered ChRMs of LR01 and NH01. Using Watson's test for randomness (Watson, 1956) both of these clusters of directions reject the null hypothesis of complete randomness at 95%, however this test is somewhat biased for small N and stray fields in the laboratory may not be expected to impart randomly directed magnetisations to orderly aligned samples. The ChRMs of the CH samples are directed too consistently to have been acquired in the laboratory. It is difficult however to explain the observed ChRMs of the NH01 and LR01 samples and therefore these directions must be treated with some caution.

From field observations and geochemical analysis, Maxwell (1990) concluded of the ND swarm that those dykes with NW-SE trends (LR and NE in this study) were plume originated and formed between 90 Ma and 110 Ma, whereas those with NE-SW trends (CH and NH in this study) post-dated these and were continental tholeiites. The conclusion of the relative ages of the two sets of dykes was based on a field observation: a dyke of the latter trend intruded an undated dyke with the former trend at Norah Head. However, this is not supported by a recent radiometric study of the NH dyke which produced a K-Ar age of 91 Ma (Sutherland, pers. comm.) suggesting that the two suites of dykes were emplaced simultaneously.

The reversed polarity of the ChRM component in NH01 samples is not consistent with the notion of the dyke forming at 91 Ma as radiometric dating suggests. Consequently, if this age is correct, this component must be an overprint acquired in the late Cretaceous or Tertiary. However, although it is not precise, the VGP

associated with this component (31°S, 127°E) is far-removed from other palaeopoles from these times but close to those from the Permian and Triassic. One explanation for this contradiction is that argon was allowed to escape from minerals in the NH samples during the 90 Ma thermal event causing the K-Ar age to be reset at this time.

The two mean directions that can be treated as the most reliable are those produced by the CH site means and NE and LR (LBT) site means. The VGPs associated with these directions plot at Permo-Triassic and mid-Cretaceous portions of the Australian APWP respectively (figure 4.19). Allowing for both insufficient sampling of PSV and uncertainties in the pole positions, it is still not possible for palaeomagnetism to support the notion of the CH dykes forming after the NE dyke at least. It is possible that the minor NW-SE trending dyke at Norah Head was not part of the same suite as the others sharing this trend.

The dyke sampled as LR01 in this study was K-Ar dated at 90.1 ± 1.1 Ma by Embleton *et al*. (1985). Although the reversed ChRM mean direction corresponds to a VGP (34°S, 131°E, dp = 54°, dm = 56°) close to palaeopoles measured previously at the Permo-Triassic boundary, the huge uncertainty associated with it would enable it to be placed almost anywhere on the APWP. Therefore although it is plausible that the K-Ar date, as well as most of the blocking temperature spectra in the LR01 samples, was reset by the 90 Ma thermal event, a more likely explanation at this stage is that the ChRM was acquired as either a secondary CRM in the Tertiary or a VRM/CRM in the laboratory.

The simplest explanation which is consistent with the results produced by the palaeodirectional study of the Newcastle dykes is as follows. The NE-SW trending dykes formed during the first pulse of igneous activity in the Sydney basin, between 230 Ma and 260 Ma (§ 3.3.1.2) as reported by Embleton *et al*. (1985). The dykes with the NW-SE trends analysed here however, formed as part of the large-scale thermal event that affected much of Eastern Australia prior to the rifting of the

Tasman Sea (§ 3.2.2). Samples from each of the dykes retain (albeit poorly in the case of the Norah Head dyke) a primary magnetisation (most likely a TRM) across a significant portion of their blocking temperature spectra. However, the next section will produce a small but significant piece of evidence that casts some doubt on this interpretation.

4.3.3 Palaeointensity Analysis

The Kiama dykes Thellier analysis was the largest single experiment performed in this study; sixty-one KD samples were subjected to nine double heating steps from 100°C and 410°C with pTRM and NRM checks after each. Some samples from each site were measured with the exception of those from sites CR06, RP01, and RP02, which were excluded because of the lack of samples available after the two previous analyses and the palaeomagnetic instability indicated by these.

Unfortunately, thermal alteration of the samples during the analysis was prevalent at relatively low temperatures. This did not appear to take the form of laboratory CRM acquisition but rather expressed itself in dramatic changes (frequently reductions) in the capacity of samples to acquire pTRM in portions of their blocking temperature spectrum. This frequently occurred before the ChRM of the sample could be isolated and was easily recognisable by a loss of linearity in the NRM-TRM plots (figure 4.21).

The NRM-TRM plots featured in figure 4.21 both display evidence of a phenomenon commonly observed in KD samples: the presence of ultra-high (UH) pTRM checks. These are defined as pTRM check values (indicated by the unattached end-point of the right-angles) that are not only higher than the pTRM value that they should be similar to, but also the pTRM gained by the preceding remagnetisation step (i.e. the pTRM check right-angle appears to the right of the point to which it is fixed; figure 4.21). This is clearly an unusual result and signifies that, for the example of a UH 100°C pTRM check:

$$|151\text{-}102| > |151\text{-}150|$$

using the convention described in § 2.4.2. This implies that the pTRM check demagnetisation stage (102) to 100°C removes more remanence than was imparted during the remagnetisation stage (151) to 150°C and shows unambiguously that alteration occurred during one of these stages.

Thermal alteration of the magnetic properties of KD samples, such that the pTRM acquired during a certain remagnetisation stage was less than that acquired during the previous remagnetisation stage to a lower temperature, was very common and is evident in figure 4.21 (a) and (b). This signified a dramatic loss in pTRM acquisition and could be caused by either the destruction of magnetic material or, more probably, by the shifting of the T_B spectrum toward a magnetically 'harder' configuration. Every analysed sample from sites BP01, CR01, CR02, CR04, and MM02 (18 samples) were discounted because this type of alteration (termed pTRM impedance from hereon) was affective prior to isolation of a sufficient part of the ChRM.

All eleven samples from sites TP01 and LH01 were not considered as palaeointensity recorders because of difficulties in removing IRM overprints and isolating a stable ChRM, the CR03 sample was also discounted because there was a large increase in pTRM capacity prior to ChRM isolation. Some samples from sites CR05, CR07, CR08 and MM01 did produce results worthy of some discussion however.

Two samples from CR05 provided estimates that satisfied the criteria of Coe *et al*. (1978) and did not exhibit pTRM impedance (table 4.11 and figure 4.22(a)). Five other samples experienced pTRM impedance at 280°C. Although it could not be justified by observed experimental error, this point was ignored on the NRM-TRM plots (figure 4.22(b)) and the resulting estimates provided by these five are shown

for completeness in table 4.11. The results are generally of low quality and none satisfy all of the criteria required by Selkin and Tauxe (2000); the relatively high consistency of their estimates is interesting to note however.

All nine CR07 samples exhibited pTRM impedance to some extent during the Thellier experiment. This was sufficient to make the possibility of reliable palaeointensity estimation altogether untenable for seven of these, NRM-TRM plots from the remaining two are given in figure 4.23. The 100, 150 and 190 pTRM checks were missing because of experimental error and some of the pTRM checks from the selected portion of the CR0708B plot were ultra-high. Furthermore, it was not clear if, in the case of this latter sample, the ChRM was isolated over the portion of NRM that was used for the estimate. Nevertheless, the results from both samples and their associated statistical values are given in table 4.12. It is apparent from the large degree of scatter (high β value) that even if misgivings arising from the discussion given above were to be ignored, these results should still be treated with the utmost caution.

The results from three of the four CR08 (xenolith) samples were discarded because of problems isolating the ChRM and pTRM impedance, the details of the remaining sample can be seen in table 4.12 and figure 5.24 (a). The result would be rejected using the criteria of Selkin and Tauxe (2000) because one of the pTRM checks is 12% deviant from the original value; however, the Coe statistics are quite acceptable.

Finally, three low quality estimates were provided by samples from the MM01 site (table 5.12 and figure 5.24 (b)). These should be treated with especial caution because of the suspicion that maghaemite is the primary ferromagnetic mineral (§ 5.3.1) and therefore that the remanence is a CRM. The direction of remanence in the three samples was steep upwards and to the south-west and this corresponds to pole positions somewhat later in the Jurassic than 200 Ma. This does not in itself mean

that the magnetisation is secondary however, as the dykes at Minnemurra could have formed somewhat later than those at Cathedral rocks.

A further test of the dominant domain state of grains within each sample is the Koenigsberger ratio (Q) defined as:

$$Q = \frac{M_{NRM}}{\chi H}$$

where: M_{NRM} is the intensity of the NRM acquired in field H, and χ is room temperature susceptibility. Obviously this cannot be calculated in this case, however it may be estimated by substituting M_{TRM} (calculated from the x-intercept of the best-fit line) and H_{LAB} into the equation for the natural terms. The laboratory Koenigsberger ratio (Q_L) is shown with the estimates. It is expected to range from < 1 in MD dominated assemblages to > 10 for SD grains (Dunlop and Özdemir, 1997).

The values of the Q_L observed in KD samples were rather low (tables 4.11 and 4.12), furthering suspicions regarding their validity as palaeointensity recorders. However, no evidence of convex-down slopes, except in sample CR0801B (figure 4.21(b)), was observed in their NRM-TRM plots.

The Newcastle dyke Thellier analysis was confined entirely to samples from sites LR01 and NE01. These samples appeared much fresher than the rest and both retained an apparently primary remanence over a significant, relatively low temperature portion of their blocking temperature spectra. A total of 42 samples were subjected to nine doubling heating steps between 100°C and 420°C, several more were demagnetised further to 450°C and 480°C, NRM and pTRM checks were performed after every measurement.

The results from 15 of the 24 LR01 and 9 of the 18 NE01 samples were discarded all together because of difficulties isolating the TRM component before major alteration

was observed to have occurred. In particular, several samples displayed behaviour similar to that observed in Jurassic basalts by Kosterov and Prévot (1997), whereby NRM was removed very easily at low temperatures without concomitant TRM acquisition. This resulted in a ridiculously high estimate for the low temperature portion and rendered the higher temperature portion invalid because of the prior alteration of magnetic properties. The behaviour termed earlier as pTRM impedance was also observed to be a facet of these steep slopes (e.g. figure 4.25(a)).

The results of samples that displayed this initial steep slope as clearly as the example given in figure 4.25(a), together with those that exhibited very noisy NRM-TRM and orthogonal vector plots (e.g. figure 4.25(b)), were rejected outright. However the results of many more samples, particularly those from site LR01, were somewhat more ambiguous. The definition of pTRM impedance, i.e. the loss of NRM between two demagnetisation stages whilst the higher temperature remagnetisation imparts less pTRM than that previously, was met frequently at low to moderate temperatures. This produced NRM-TRM plots that were somewhat noisy for the initial part of the estimate but with the steep slope far less prominent than in those that were rejected outright (e.g. figure 4.26(a)).

In those samples that did not appear to contain a significant overprint, estimates were extracted from the portion of their blocking temperature spectra prior to pTRM impedance affecting the NRM-TRM plot (e.g. figure 4.26(b)). Estimates comprising less than four points were not accepted in this analysis.

Table 4.13 shows all the recovered palaeointensity estimates and their associated statistical parameters. While only those estimates that satisfied the criteria stipulated by Coe *et al*. (1978) are presented, only three estimates also fully satisfied the criteria proposed by Selkin and Tauxe (2000), the NRM-TRM plots of two of these are shown in figure 4.27. Once again, low values of Q_L were recorded but little evidence of convex-down NRM-TRM plots were observed.

The results from sample LR0105D (figure 5.27(a)) were especially interesting for a number of reasons. The first was that the 450°C point could be incorporated into the current estimate, providing more certainty, without altering its value. The reason for its omission was purely its associated pTRM check discrepancy (-15%), which would make it unacceptable by the criteria of Selkin and Tauxe (2000). This could be considered as preliminary, empirical justification for easing the pTRM check requirement slightly.

The second interesting observation is that the isolated, low to moderate T_B component is clearly of reversed polarity. This is in contrast to every other sample from the LR01 site measured in this and the palaeodirectional analysis. Stages of sample and data preparation that might have resulted in the direction of this component of remanence being misrepresented were re-checked for mistakes, none were found. The experimental stage could not have been the cause because the measurements were systematically anomalous for this sample only.

There are several other reasons to suspect that this direction is genuine. The first is that the component structure within sample LR0105D is distinctly different to that within the other samples from the same core, and indeed those within most other LR01 samples. As was discussed in § 4.3.2, many LR01 samples retained a reversed polarity ChRM which was isolated by 500°C. After demagnetisation to just 420°C (the minimum limit in this analysis) however, the OVPs of most samples showed a very weak magnetisation and the commencement from a normal to reversed polarity component. The OVP of the LR0105D sample was, although somewhat noisy, distinctly different to this: the origin was not approached by the vertical component despite demagnetisation to 480°C. Alternatively stated, there was no sign of another component of magnetisation in this anomalous sample.

The second reason to expect that the reversed polarity component in sample LR0105D is genuine is that its direction is not antipodal to the normal polarity component in other samples but is instead entirely consistent with the reverse

polarity site mean directions given in table 4.10. As figure 4.28 illustrates, this direction is more westerly and steeper than the LR01 LBT mean. Its exact coincidence with the LR01 HBT mean direction must be regarded as somewhat coincidental given the large uncertainty in the position of the latter, however its proximity to the well-defined CH direction can be taken a little more seriously.

It is interesting to note that the LR0105D sample, of all the samples from site LR01, exhibits the best behaviour during the Thellier experiment as this suggests that the reversed component is more likely to be a pure TRM. If this were true, the conclusions founded at the end of the previous section would be refuted as the Little Red Head dyke could not have formed during the CNS. The revised history of the dyke would then be that it formed at a similar time to the Catherine Hill Bay, and probably Norah Head, dykes but was magnetically overprinted (most likely by a TVRM) at 90 Ma. This sample may be anomalous only in the sense that it does not possess the magnetically soft, easily overprinted, component of grain sizes ubiquitous in this basalt dyke.

No matter how convincing it is however, the evidence from a single sample is insufficient to draw conclusions upon. Instead it should be regarded as sufficient to cast some doubt on the conclusions made from the palaeodirectional and geochronological analyses. The error in the latter of these could itself be explained by the escape of argon from the rock system during the re-heating event (Fowler, 1990). A further palaeomagnetic study, utilising a more sensitive magnetometer to reduce noise, on the HBT component of the LR dyke is required before firm conclusions can be made. If the HBT component in the LR01 samples was proved to be primary then it would be reasonable to assume that the NE01 samples, having more MD-like properties (table 4.8) and being derived from a dyke of a similar trend, were contemporary but completely overprinted by the event at 90 Ma.

Because of the component's reversed polarity, the palaeointensity estimate from sample LR0105D was treated separately to the rest of those from site LR01.

Sample NE0107B is also worthy of special mention as it provides the only estimate with a maximum possible R factor (table 4.13 and figure 4.27(b)). Several other NE01 samples also behaved better in the Thellier experiment than sample LR0105D. Using the same argument as that given for the reversely magnetised LR01 sample, this would suggest that the NE01 samples were more likely to be carrying a primary TRM. However, this argument is not without flaws: McClelland (1996) showed theoretically that a sample containing only a CRM component could behave perfectly in a Thellier experiment up to 400°C.

Because only three samples fulfilled the criteria stipulated by Selkin and Tauxe (2000), these criteria were relaxed a little for the purpose of investigation. Four further samples were identified which had values of $\beta \leq 0.15$ and whose maximum pTRM discrepancy was less than or equal to 15%. The mean values comprising these estimates were found to be largely unchanged from those comprising all the estimates however.

Unfortunately, the VDM estimates presented in table 4.13 must be treated a little cautiously because of doubts over the primary nature of the components. Providing than the experiment is confined to temperatures below the maximum absolute temperature a rock reached during the acquisition of a TVRM, the Thellier method should give an accurate estimate when performed on an assemblage of SD grains. The primary remanence carriers with low blocking temperatures in these samples are very unlikely to be SD grains however and the re-heating event was expected to cause temperatures to be elevated by a maximum of 250°C (Middleton and Schmidt, 1982). Therefore, if the normal component is secondary, these estimates cannot be accurate.

Sample	ΔT	N	f	g	β	q	Mean |pTRM check discepancy|	Mean |NRM check discrepancy|	Max pTRM check discepancy	Max NRM check discrepancy	Q_L	Temp (χ_{RT} alteration)°C	R (8)	H_{PALAEO} (μT)	Site mean VDM (10^{22} Am^2)
CR0501B	320-410	4	0.20	0.64	0.24	0.54	7%	4%	-13%	-5%	0.5	None	5	64 ± 117	7.4±1.7
CR05H1A	100-415	9	0.30	0.84	0.08	3	14%	-	27%	-	0.2	None	5	46 ± 15	
CR0501C*	190-410	7	0.26	0.79	0.17	1.2	14%	4%	54%	-6%	0.5	None	3	66 ± 55	8.2 ± 1.2†
CR0502B*	320-410	4	0.16	0.63	0.08	1.2	11%	3%	-14%	-4%	0.7	None	5	59 ±49	
CR0503B*	190-410	6	0.31	0.76	0.07	3.3	11%	3%	18%	-5%	0.5	None	5	74 ± 22	
CR05H1B*	240-410	5	0.25	0.74	0.14	1.4	9%	4%	18%	-5%	0.5	410	3	59 ± 42	
CR05H1C*	240-410	5	0.24	0.73	0.15	1.2	14%	5%	23%	-7%	0.5	None	2	59 ± 50	

Table 4.11: Palaeointensity estimates from KD site CR05. * denotes samples that experienced pTRM impedance at 280°C. † This mean is comprises all 7 estimates. The R (reliability) factor has a maximum value of 8.

Sample	ΔT	N	f	g	β	q	Mean |pTRM check discepancy|	Mean |NRM check discrepancy|	Max pTRM check discepancy	Max NRM check discrepancy	Q_L	Temp (χ_{RT} alteration)°C	R (8)	H_{PALAEO} (μT)	Site mean VDM (10^{22} Am^2)
CR0703B	100-280	5	0.16	0.79	0.27	0.47	8%	3%	27%	7%	0.7	410	3	47 ±100	7.1 ±1.3
CR0708B	280-380	4	0.17	0.44	0.13	0.56	12%	5%	28%	8%	0.4	None	3	61 ± 108	
CR0801B	240-380	5	0.41	0.34	0.07	2	5%	-	12%	-	1.2	None	5	36 ± 18	5.6
MM0103B	0-190	4	0.25	0.59	0.38	0.39	14%	7%	21%	7%	1.1	150	4	72 ± 185	8.2 ±1.4
MM0104B	0-240	5	0.18	0.69	0.28	0.44	6%	9%	16%	-13%	1.9	150	3	53 ± 119	
MM0104C	0-240	5	0.19	0.66	0.25	0.51	8%	9%	16%	-13%	1.8	150	3	56 ± 111	

Table 4.12: Palaeointensity estimates from KD sites CR07, CR08 and MM01

Sample	ΔT	N	f	g	β	q	Mean |pTRM check discepancy|	Mean |NRM check discrepancy|	Max pTRM check discepancy	Max NRM check discrepancy	Q_L	Temp (χ_{RT} alteration)°C	R(8)	H_{PALAEO} (μT)	Site mean VDM (10^{22} Am^2)
LR0105D†	100-420	9	0.5	0.78	0.05	7.5	3%	12%	7%	-20%	2.4	None	5	9 ± 1	1.2
LR0103C	150-350	6	0.53	0.76	0.14	2.9	15%	4%	30%	9%	0.7	310	3	28 ± 10	2.3 ± 1
LR0106C*	100-380	8	0.57	0.8	0.14	3.3	5%	8%	-8%	17%	1.1	None	5	14 ± 4	
LR0106D*	150-380	7	0.4	0.75	0.13	2.3	7%	2%	14%	4%	0.8	350	4	22 ± 10	
LR0107B	150-350	6	0.33	0.64	0.14	1.5	8%	5%	16%	8%	0.8	None	5	20 ± 14	*2.3 ± 0.8
LR0107D*	270-420	5	0.48	0.61	0.09	3.2	10%	5%	12%	9%	1.2	None	6	12 ± 4	
LR0108B	270-450	6	0.21	0.8	0.17	1	15%	13%	-52%	-30%	0.9	420	2	14 ± 14	
LR0108C	270-420	5	0.25	0.49	0.16	0.79	11%	90%	-15%	23%	1.3	None	4	8 ± 10	
NE0104C	100-350	7	0.71	0.55	0.12	3.4	16%	12%	38%	-30%	0.6	None	4	27 ± 8	5.3 ± 1.4
NE0104D	270-380	4	0.65	0.55	0.12	3.2	8%	12%	20%	-33%	0.6	350	3	27 ± 9	
NE0106B	190-380	6	0.71	0.62	0.09	4.7	9%	1%	22%	-2%	0.4	None	5	50 ± 11	
NE0106C*	100-380	7	0.8	0.75	0.1	6.1	5%	8%	9%	-21%	0.4	None	6	43 ± 7	
NE0107B*	100-310	5	0.44	0.67	0.07	4.1	2%	4%	4%	-9%	0.3	None	8	37 ± 9	*5.4 ± 1.4
NE0107C*	100-350	6	0.59	0.69	0.09	4.7	6%	4%	-11%	14%	0.4	None	6	27 ± 6	
NE0108B	0-190	4	0.42	0.67	0.17	1.6	17%	2%	20%	3%	0.5	None	6	47 ± 28	
NE0108C	0-350	8	0.72	0.79	0.15	3.7	10%	6%	18%	-14%	0.4	None	4	50 ± 14	

Table 4.13: Palaeointensity estimates from ND samples. R factors were calculated assuming that the TRM component was normal polarity * denotes estimate with β and maximum pTRM check discrepancy < 15% and mean VDM calculated from these estimates, †estimate singled out for reasons given in the text.

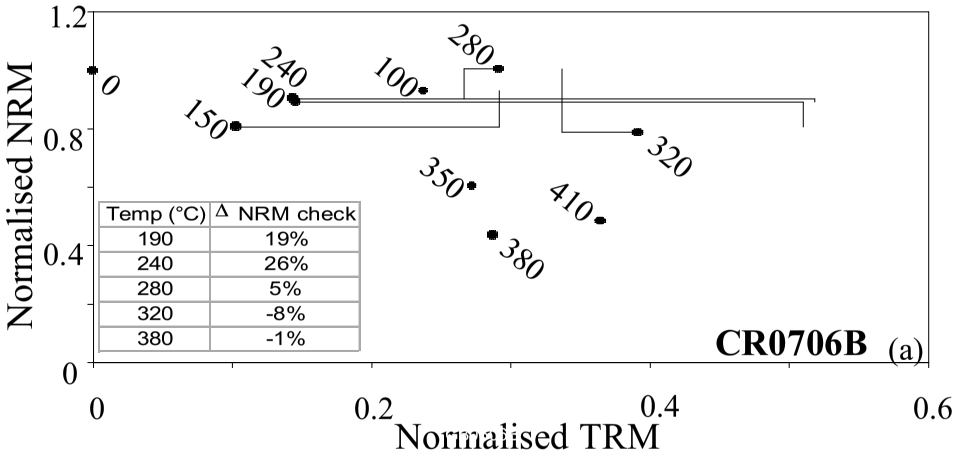

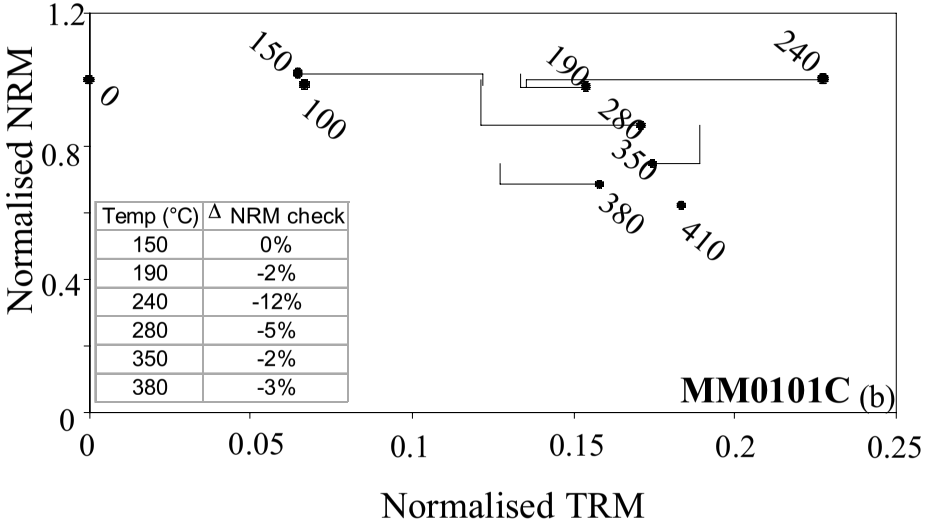

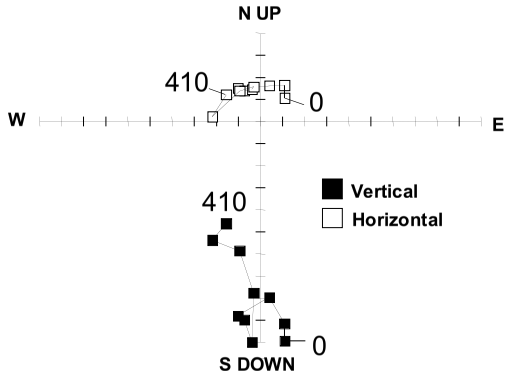

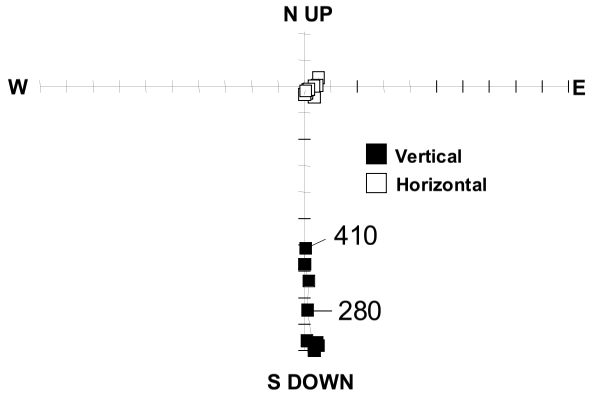

Figure 4.21: NRM-TRM plots and accompanying OVPs for representative KD samples exhibiting repeated alteration of pTRM capacity during a Thellier experiment

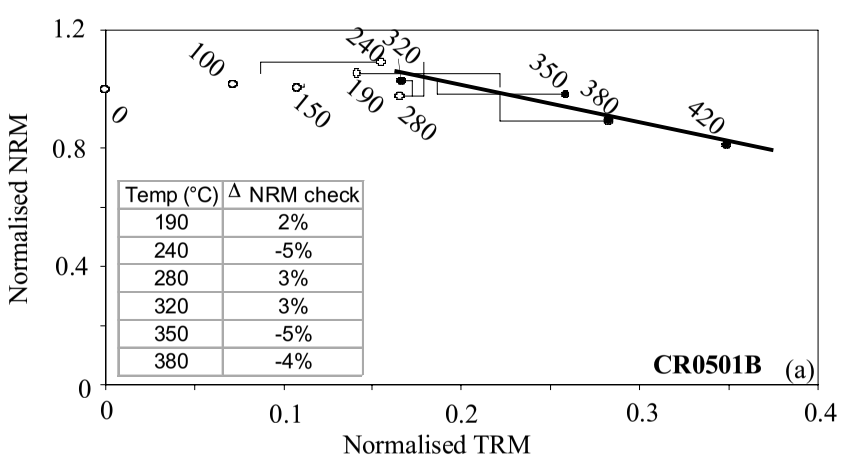

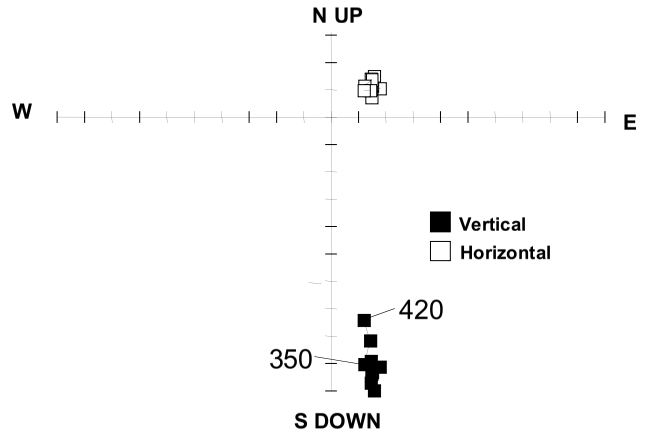

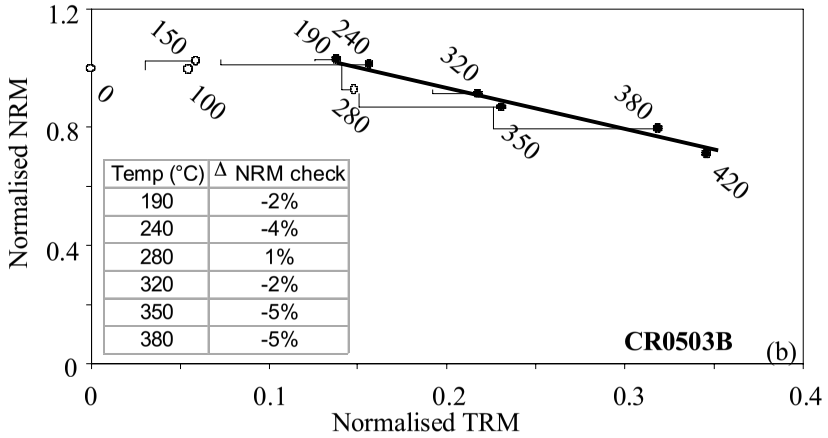

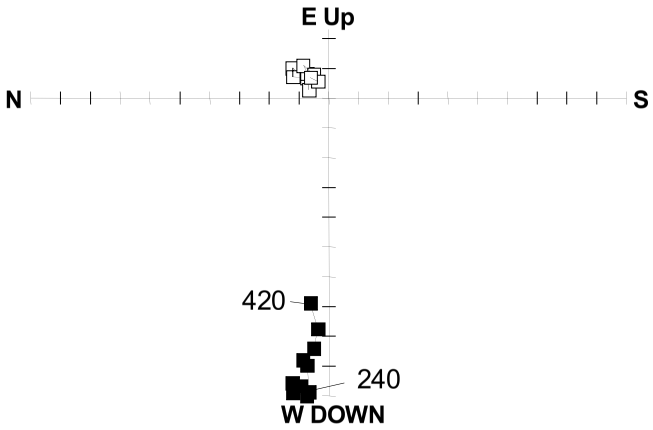

Figure 4.22: NRM-TRM plots and accompanying OVPs for representative CR05 samples. In (b) the 280 point is excluded from the estimate because it falls off the line comprising the estimate. Filled (unfilled) points are those used (not used) to calculate the line.

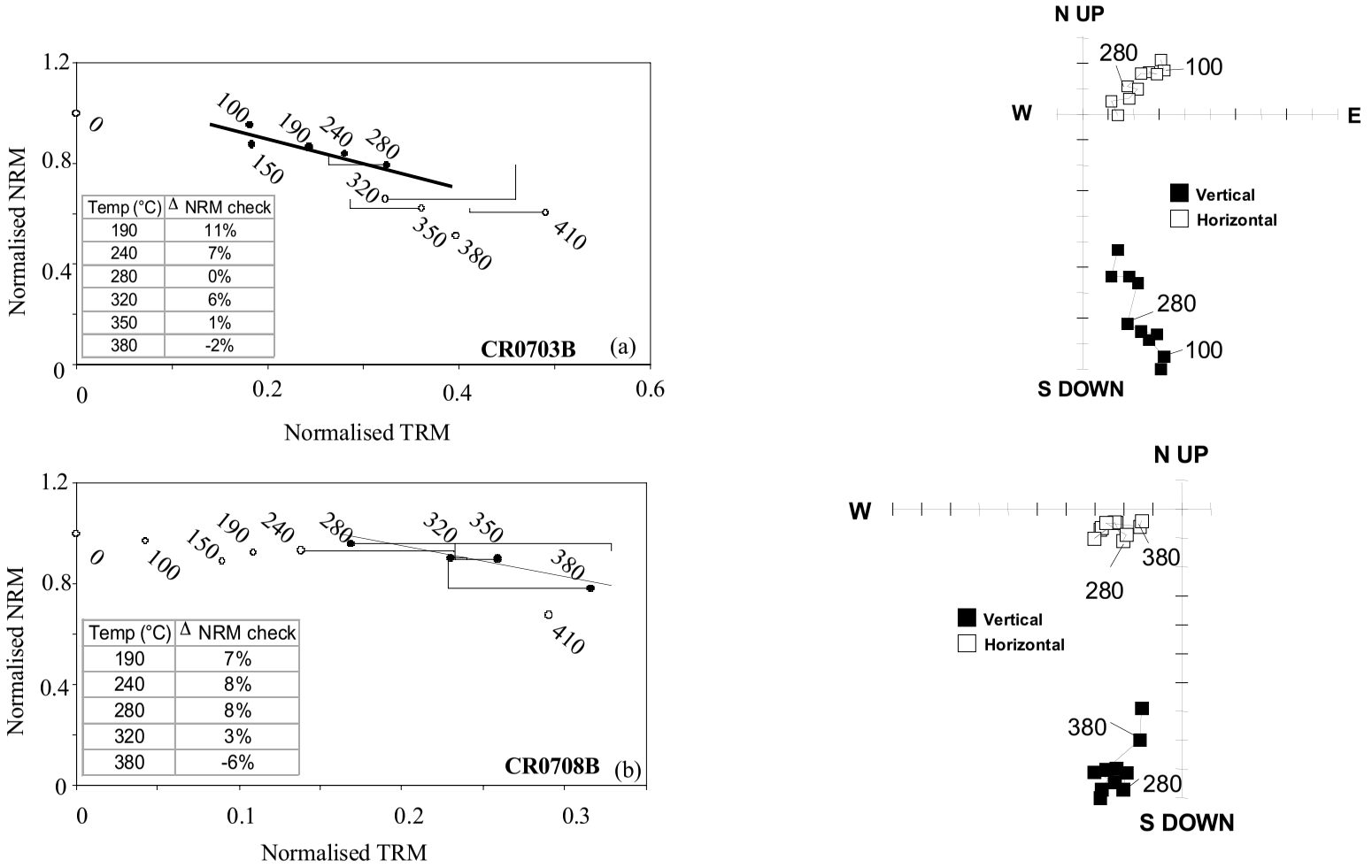

Figure 4.23: NRM-TRM plots and accompanying OVPs for best CR07 samples. Filled (unfilled) points are those used (not used) to calculate the line.

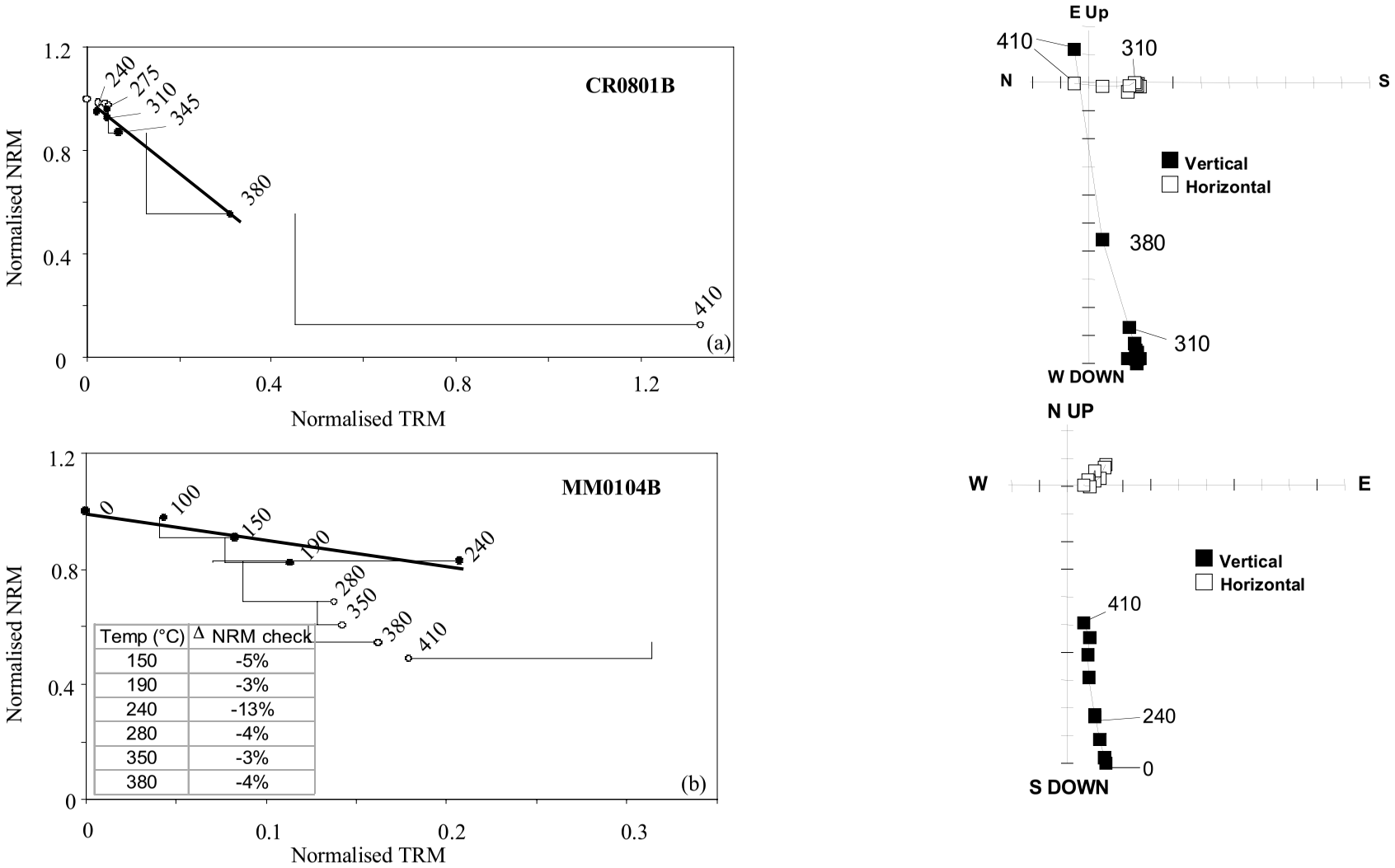

Figure 4.24: NRM-TRM plots and accompanying OVPs for representative CR08 and MM01 samples. Filled (unfilled) points are those used (not used) to calculate the line.

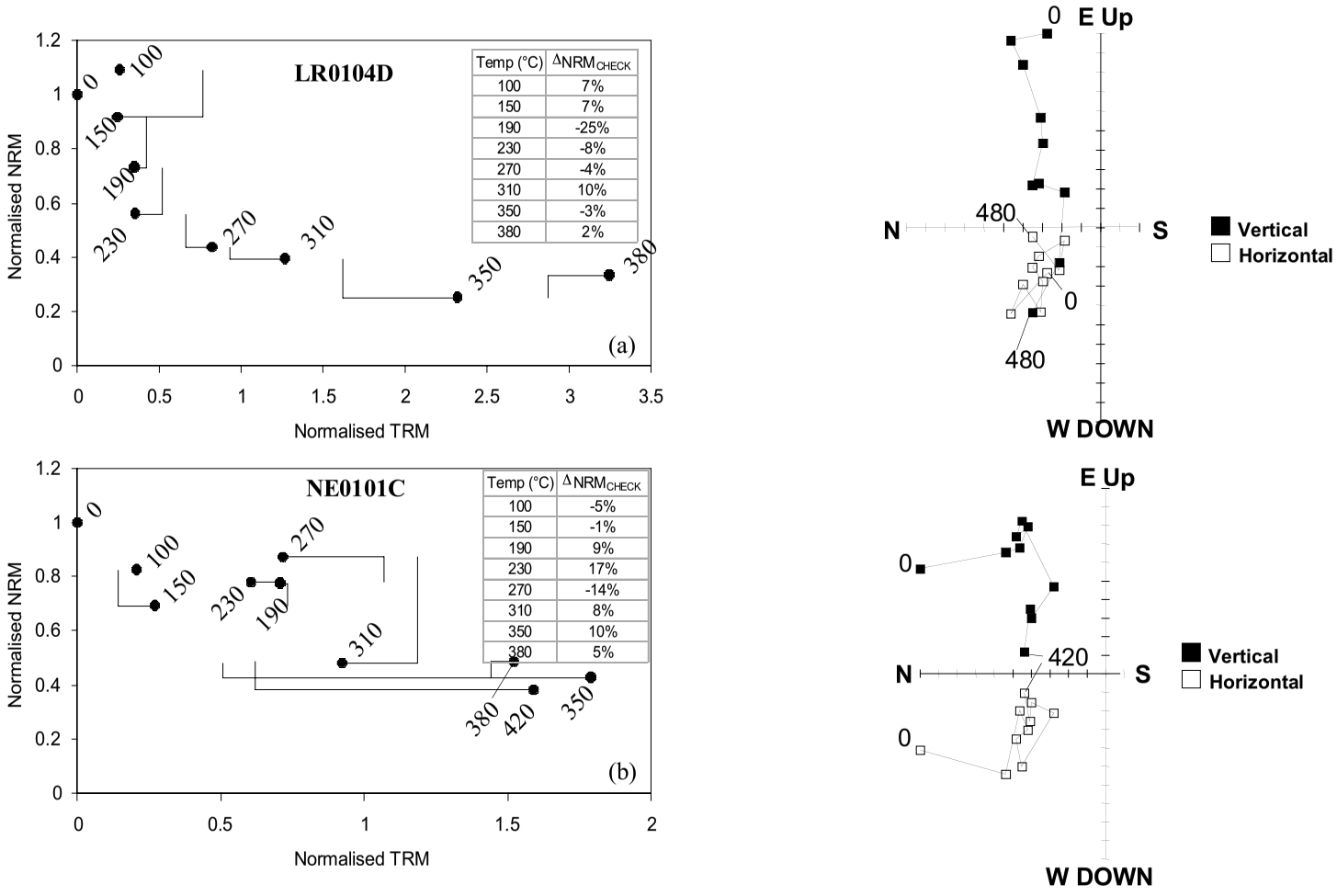

Figure 4.25: Examples of NRM-TRM plots and OVPsfor ND samples that were rejected outright.

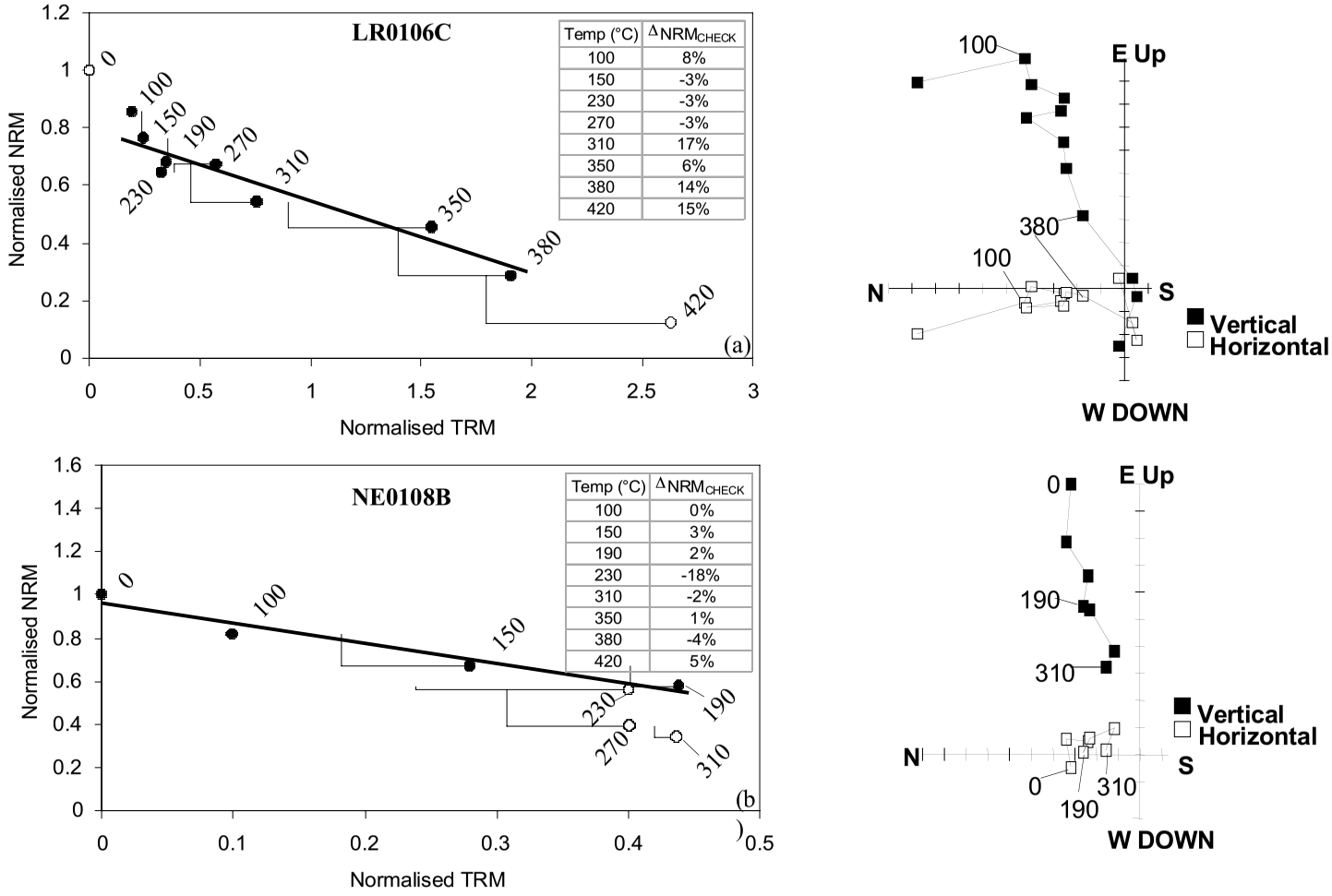

Figure 4.26: Examples of NRM-TRM plots and OVPs for ND samples from which palaeointensity estimates were extracted despite them demonstrating non-ideal behaviour. Filled (hollow) circles represent used (discarded) points.

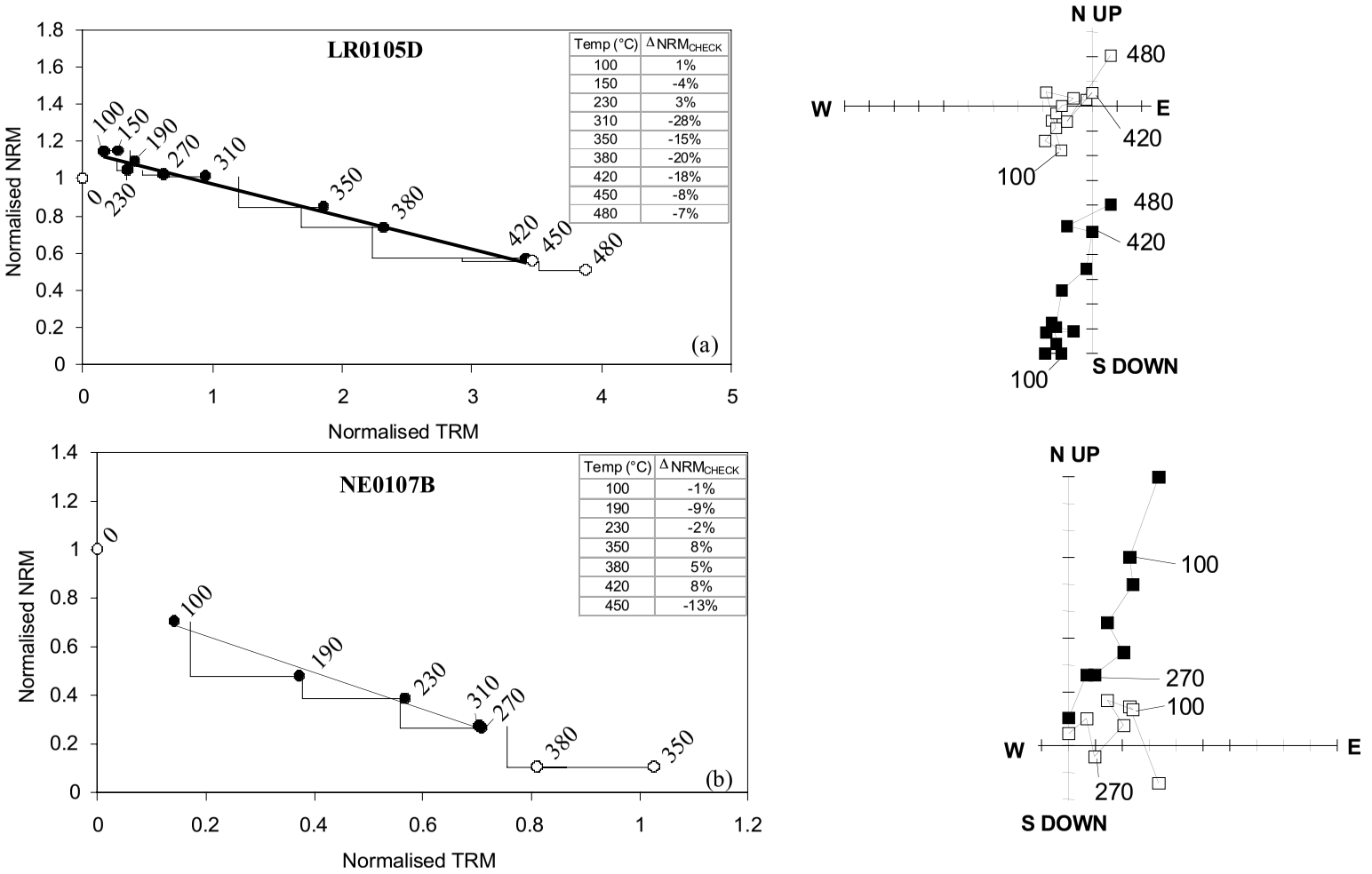

Figure 4.27: Examples of NRM-TRM plots and OVPs for 2 of the 3 ND samples which fulfilled the criteria required by Selkin and Tauxe (2000). Filled (hollow) circles represent used (discarded) points.

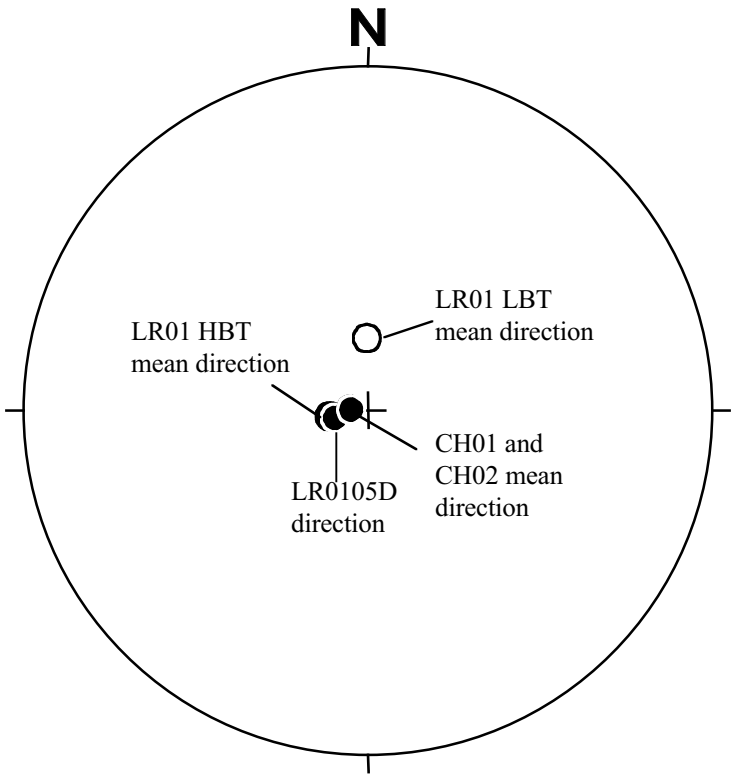

Figure 4.28: Circular plot showing the normal (hollow circles) and reversed (filled circles) ChRM directions from various ND samples used in the Thellier analysis.

4.4 The Bawley Point Gabbro

The early-Triassic BPG was described in § 3.3.2.3; figure 3.7 shows the locations of the six sampling sites adopted by this study. There were no previously published rock magnetic or palaeomagnetic analyses of the body.

In this study, the rock magnetic analysis was conducted after the palaeodirectional analysis. It is for this reason that the rock magnetic experiments were focussed on samples from certain sites (those with the greatest palaeomagnetic stability) while those from others were ignored. However, for consistency, the analyses will be reported in the usual order.

4.4.1 Rock magnetic analysis

Thermomagnetic, hysteresis and χ_{LT} analysis was performed on samples from BPG sites. The GB01 site was excluded from this because of the general failure of its samples to retain a meaningful remanence (§ 4.4.2). The thermomagnetic criterion was applied to samples from all sites however. The results from these analyses are summarised in table 4.14.

All samples behaved similarly in the different rock magnetic analyses. Curves produced by thermomagnetic analysis, although somewhat noisy, strongly suggested that Ti-poor titanomagnetite was the dominant ferromagnetic mineral in the BPG samples. Upon cooling from 700°C, a small change of shape was evident in the curve indicating that some alteration had taken place (figure 4.29(a)). The relatively high Curie temperatures indicated that, as expected, the intrusion cooled slowly enough for the original titanomagnetite to exsolve to its end-members.

Sampling site	χ_{RT} $10^{-6}m^3/kg$	M_{RS}/M_S	Hc (mT)	H_{CR}/H_C	RS	Δj_s	T_C (°C)	pTRM $tail_{300}$ (%)
BA01	9482				0.91	-0.13	535	21
BB01	9469	0.00	0.4	1.19	1.03			23
BR01	6216	0.04	4.5	1.98		-0.19	530	14
GB01	7824							14
JH01	4838	0.03	3.2	2.06		0.24	535	16
MB01	2810	0.05	6.1	2.00	1.13			16

Table 4.14: Results of rock magnetic analysis on BPG samples

Site	$\overline{\Delta T\ (^\circ C)}$	N	Dec (°)	Inc (°)	k	α_{95}
	LBT Component					
BA01	100-300	5	005	-71	66	10
BB01*	0-150	3	106	-75	5	67
BR01	100-300	4	314	-78	31	17
GB01	0-200	2	223	-67	112	24
JH01*	100-350	3	259	-60	21	27
MB01	100-350	5	355	-68	158	6
Mean		4	323	-80	18	22
VGP		50°N, 348°E (dp=15, dp=15)				
	HBT Component					
BA01	530-610	4	211	69	159	7
BB01*	250-530	3	112	57	22	27
BR01	350-580	3	218	58	74	14
GB01	500-580	4	337	56	54	13
JH01	450-530	3	064	84	607	5
MB01	450-560	4	302	83	115	9
Mean		5	262	81	12	23
VGP		20°S, 152°E (dp=44, dm=45)				

Table 4.15: Site and overall mean directions from components of remanence recorded in BPG samples. * denotes site mean not used in overall calculation.

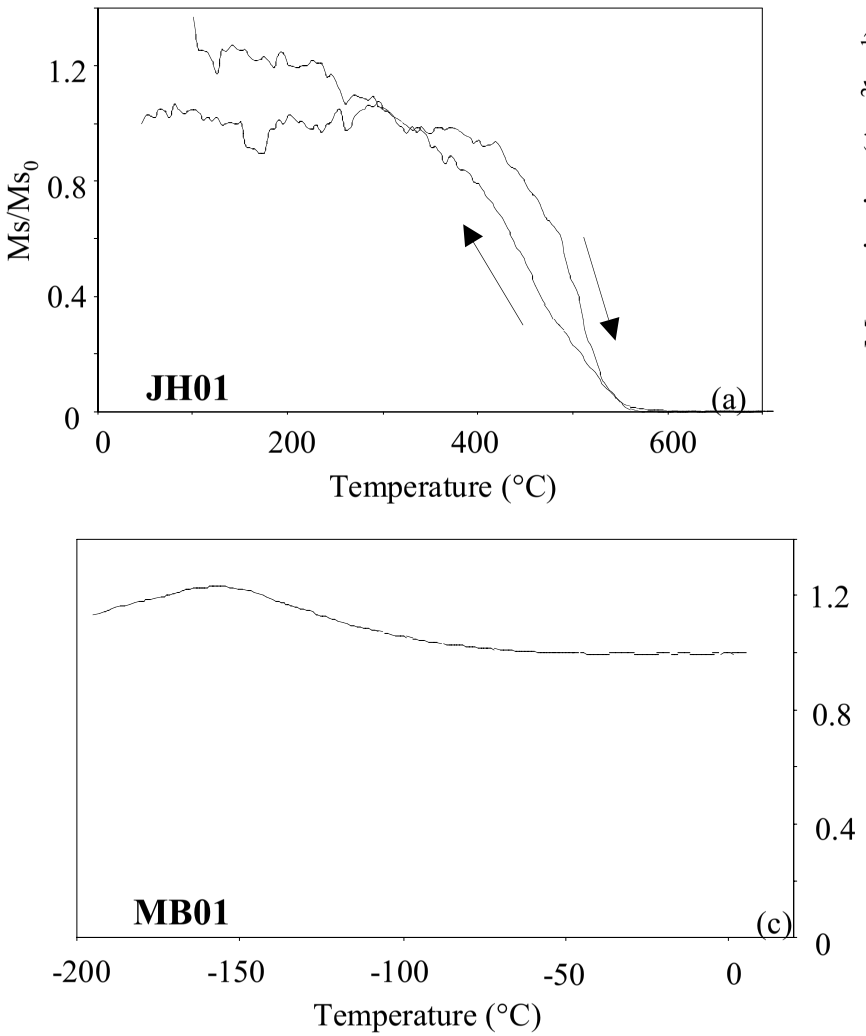

Figure 4.29: Representative plots of results from (a) thermomagnetic (b) hysteresis (c) χ_{LT} analyses of BPG samples.

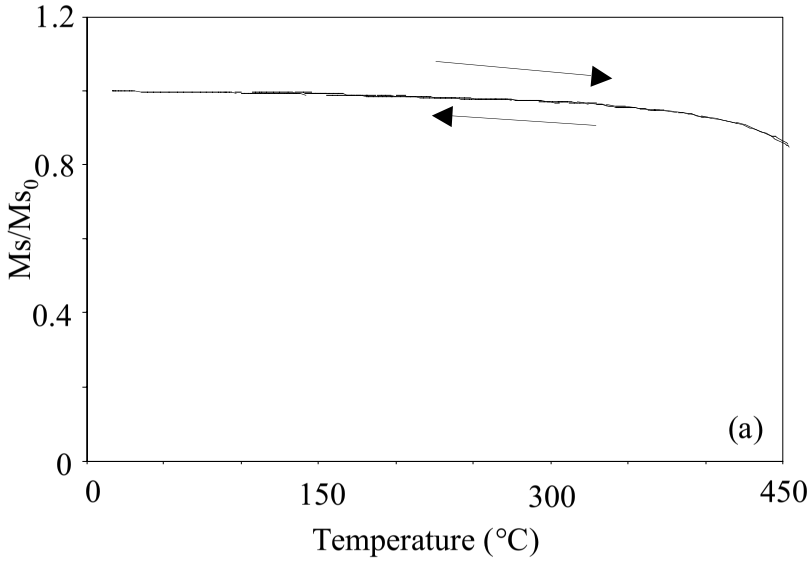

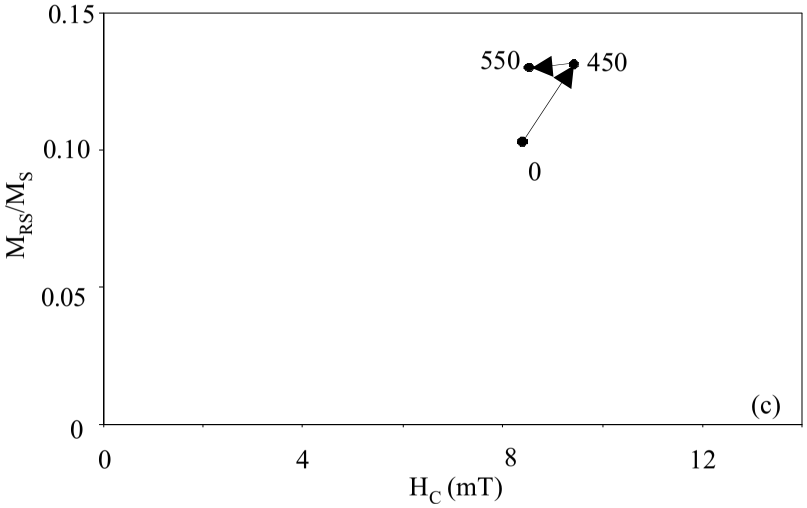

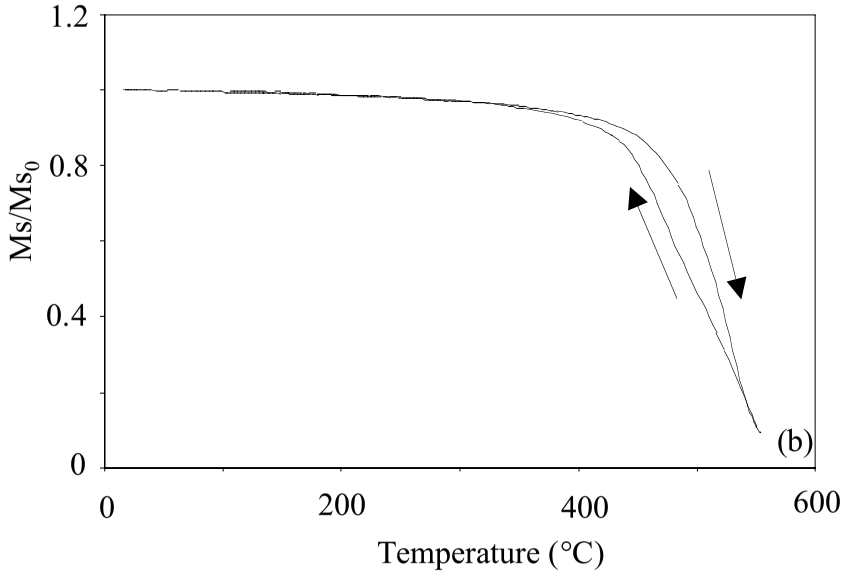

Figure 4.30: plots of (a) thermomagnetic analysis to 450°C, (b) thermomagnetic analysis to 550°C, (c) hysteresis parameters measured at room temperature prior to and after each heating cycle (to temperature shown) for sample **MB0105B**.

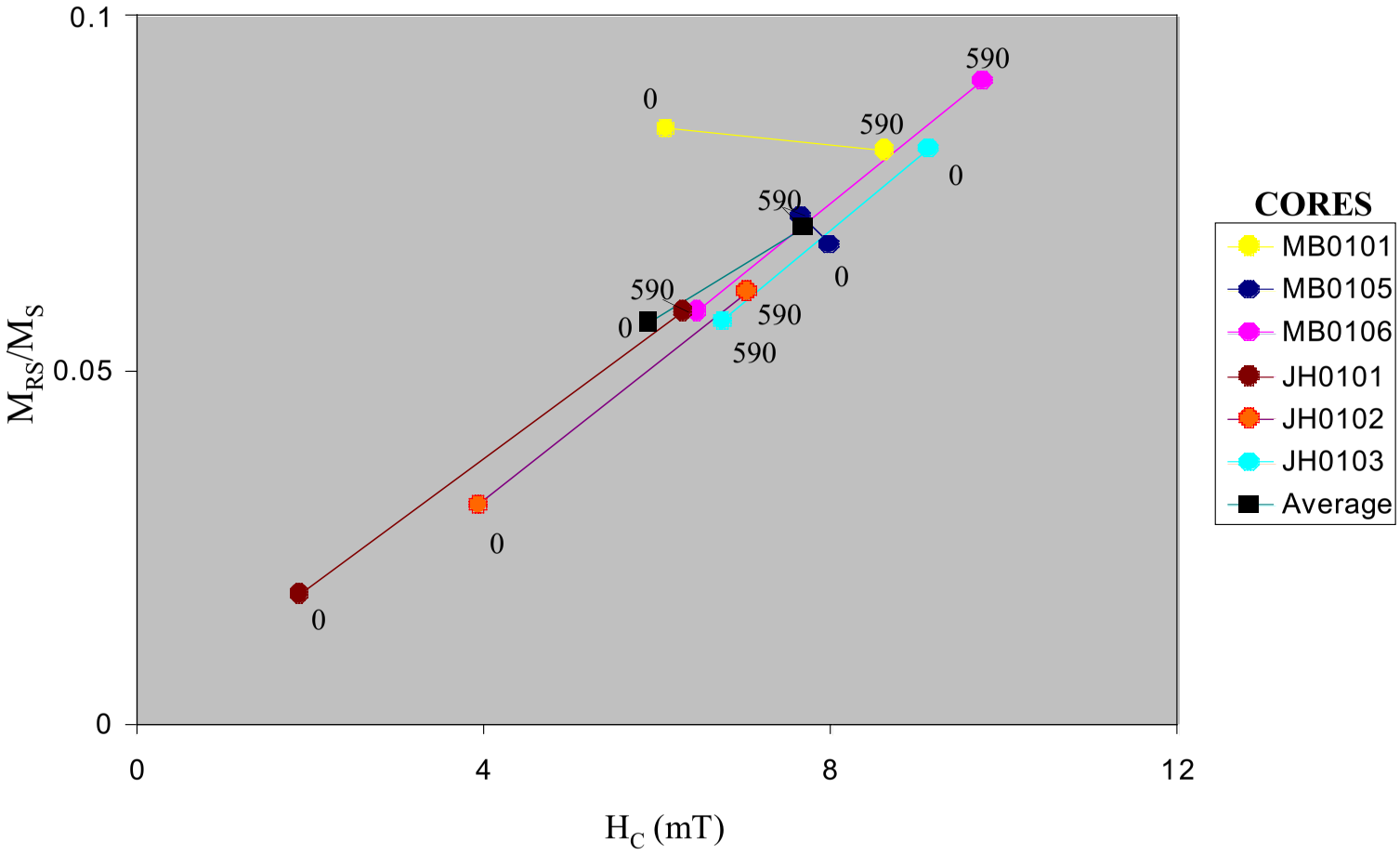

Figure 4.31: Plot showing variation of hysteresis parameters between pairs of samples from the same core one of which has been heated to 590°C previously (denoted by 590) and one of which has no received no pre-treatment (denoted by 0).

The hysteresis loops produced by some of the BPG samples were exceptionally thin (figure 4.29(b)) indicating that either MD or SP was the dominant grain size. However, the measured susceptibilities of all samples at high and low frequencies were less than 10% different to one another suggesting that the latter of these was not significant. The thermomagnetic criterion supported this interpretation, the tail due to a pTRM between 300°C and T_R was large enough to signify that MD (tail > 15%) and large PSD grains resided in this portion of the blocking temperature spectrum (table 4.14). The χ_{LT} curves produced by the BPG samples (figure 4.29(c)) were of the type termed group 3 by Senanayake and McElhinny (1981) who claimed that these were produced by MD Ti-poor titanomagnetite. It is not clear however, if it is these types of curves, or those with a much lower RS value (e.g. figure 4.14(c); Radhakrishnamurty, 1977) that indicate MD in a mixed domain state (Thomas, 1992).

A further MB sample was subjected to hysteresis measurements at room temperature and after thermomagnetic cycling to 450°C and 550°C. Figure 4.30 shows that, although the thermomagnetic cooling curves retained a similar shape as the heating curves during both heating cycles, the hysteresis parameters were altered significantly once the sample was heated to 450°C.

Finally, two samples from each of three cores from sites MB01 and JH01 were selected for room temperature hysteresis analysis. One of each core had previously been heated to above T_C while the other had received no pre-treatment. Figure 4.31 shows the variation in hysteresis parameters between the pairs of samples. One would expect to find that the treated samples plot further to the top right of the chart if thermal alteration is significant because this process generally reduces effective grain size. Although this is true of three of the core samples, the measurements from the remaining samples combine to make the result of this experiment inconclusive. This ambiguity is probably a product of intrinsic small-scale variations in hysteresis properties between untreated samples from the same cores. Samples from the MB0105 core were used in both this analysis and that discussed in the previous

paragraph. Comparing the properties of the untreated samples in both figure 30(c) and figure 31 shows that significant variation in the ratio of M_{RS}/M_S existed. This ambiguity aside, the average variation of properties shown in figure 5.31 together with the results of the previous experiment do suggest that some alteration of hysteresis properties is expected in MB and JH samples after they are heated to high temperature.

4.4.2 Palaeodirectional analysis

Approximately six samples from each sampling site of the BPG were subject to thermal demagnetisation in 50°C intervals from 100°C to 500°C and then in 30°C intervals to 610°C.

The OVPs generated by the measurements made after each demagnetisation step were generally noisy making it difficult to perform principle component analysis. Nevertheless, the blocking temperature spectra of many samples were observed to contain two components of remanence. The component that resided in the lower temperature region (LBT component; ~ 0-350°C) always displayed a normal polarity whilst that in the higher temperature region (the HBT component; ~ 450-560°C) was reversed. Figure 4.32 gives two examples of OVPs which clearly display the two components.

Appendix 5 lists the recovered components of remanence for each sample and table 4.14 displays the calculated mean directions. In many samples it was not possible to isolate a reliable component of remanence: IRM overprints were common and M.A.D values were often very high. This sometimes necessitated the use of a circular rather than orthogonal vector plot to determine the ChRM direction.

Site mean directions for both components are quite widely scattered (figure 4.33) and although the directions themselves have reasonable precision parameters, they have moderate to large uncertainties because of the small number of estimates that

comprise them (table 4.14). The sites marked with asterisks were not used to calculate the overall means because of their unacceptably poor precision. Despite this, the overall means are still poorly constrained. The VGP resulting from the LBT mean is close to palaeopoles calculated from magnetisations acquired in the mid-Cretaceous (figure 4.34) suggesting that it may be have been caused by the 90 Ma thermal event affecting the Sydney Basin. Unfortunately, the large uncertainties associated with this VGP preclude a detailed discussion as to its origin.

On the basis of the very poorly constrained mean HBT direction, it was decided to analyse the site mean directions in discrete groups. The BA01 / BR01 and JH01 / MB01 site mean directions are close to one another. The VGP generated by the first of these clusters was 62°S, 91°E: close to the Tertiary portion of the Australian APWP (figure 4.34). This suggests that the HBT component in these samples may be a CRM formed by weathering in this period. The VGP corresponding to the JH01 and MB01 site means was 29°S, 149°E. This is located close to Australian palaeopoles of late Permian / early Triassic age which suggests that this component in these samples may be of primary origin.

The VGPs associated with the outlier site mean directions (BB01 and GB01) were far removed from the Australian APWP signifying that these directions are probably composites of more than one component.

The large effective grain size of remanence carriers in the BPG samples, as identified by the rock magnetic analysis, causes them to be poor palaeomagnetic recorders. While the samples from sites JH01 and MB01 are candidates for retaining a primary TRM in a small high temperature portion of their blocking temperature spectra, it was decided that the predominance of MD-like grains and the susceptibility of the samples to thermal alteration in the laboratory made them entirely unsuitable for palaeointensity analysis.

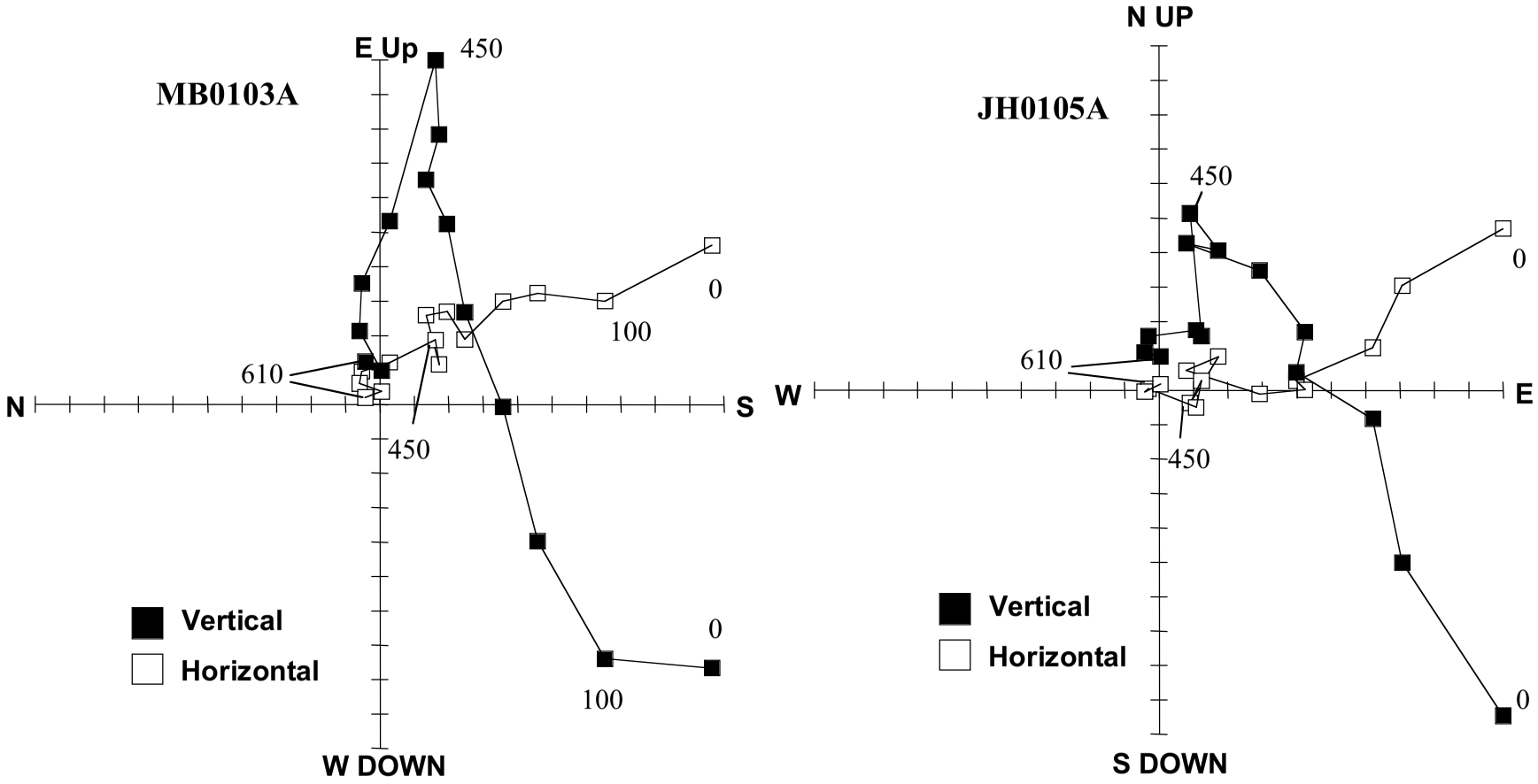

Figure 4.32: OVPs derived from palaeodirectional analysis of BPG samples which clearly display the two components.

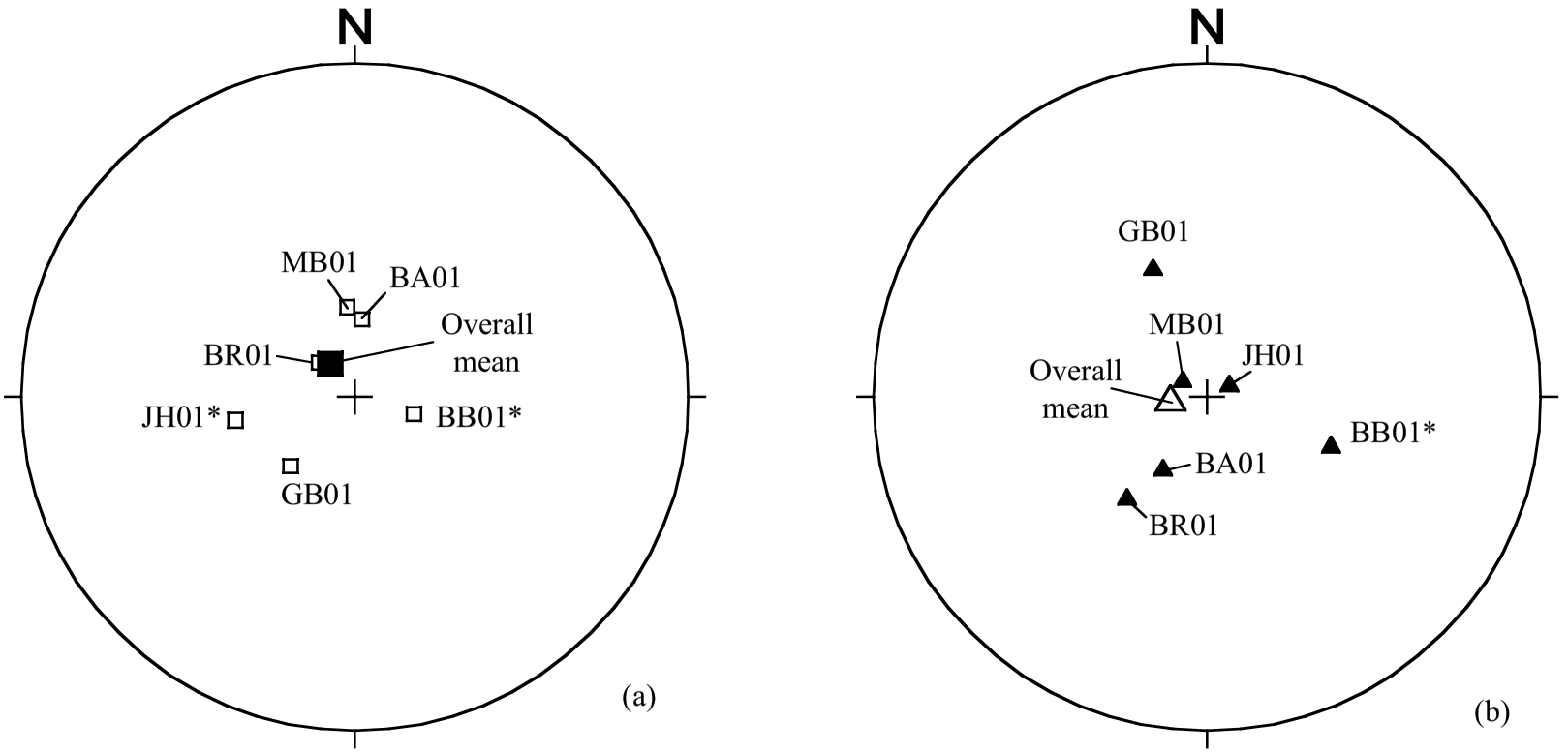

Figure 4.33: (a) LBT site mean directions in upper hemisphere and (b) HBT site mean directions in lower hemisphere for the Bawley Point gabbro. Points are annotated with their site name, * denotes a direction not used to calculate the overall mean

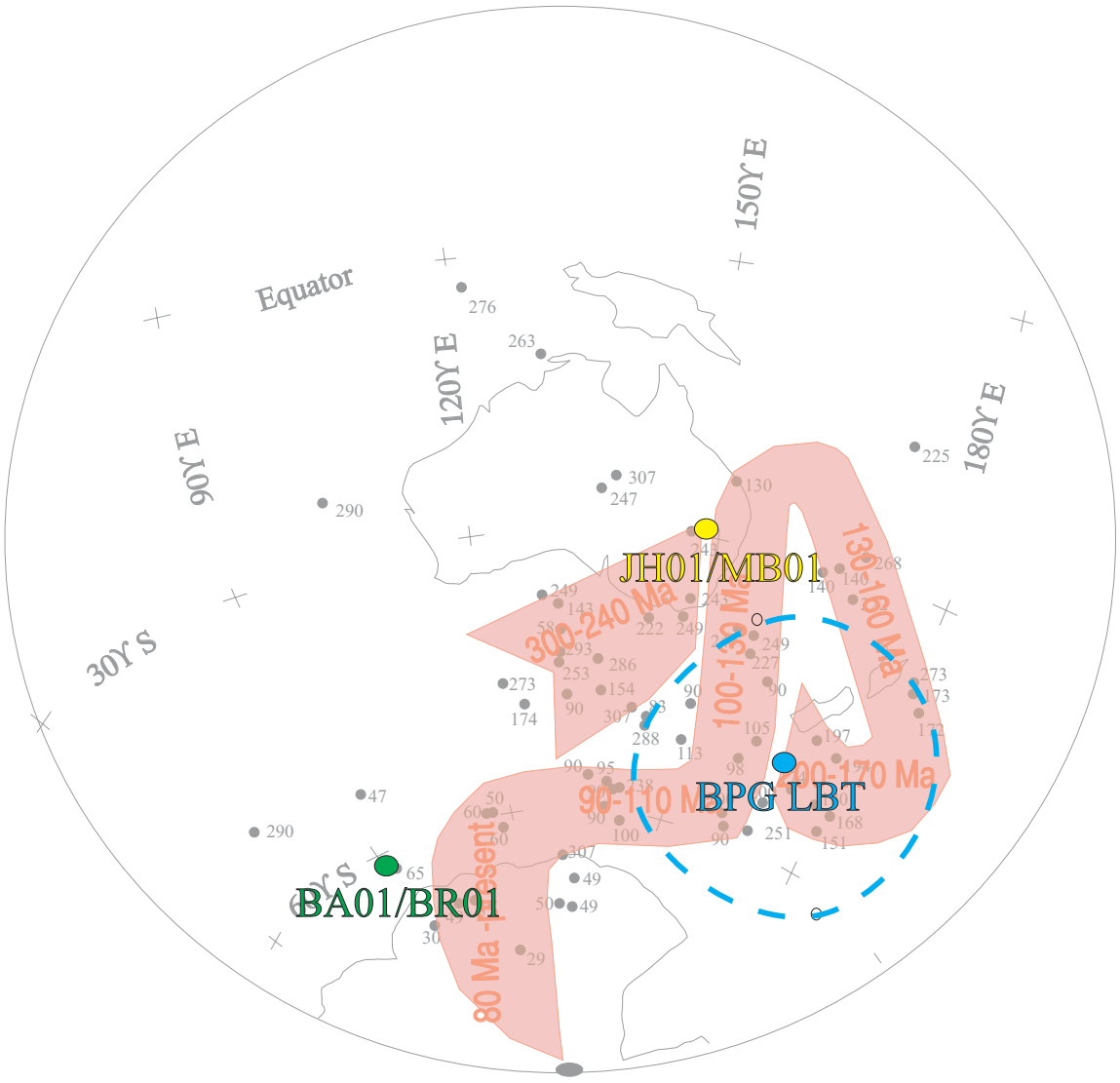

Figure 4.34: Australian APWP showing VGPs (normalised to reverse polarity) measured from Bawley point gabbro samples. Dashed ellipse show 95% confidence limit for estimate

4.5 The Bundarra and Eungella granodiorites

These two suites of Bowen Basin intrusions were discussed in § 3.4.2.1. Sampling of the Bundarra (BD) granodiorite was restricted to four sites consisting of 22 oriented cores and a number of unoriented hand samples. Samples from site BD01 appeared considerably more felsic than the others. Six of the Eungella granodiorite (EG) intrusions were sampled at eight sites, the details of which are given in figure 3.9 and 3.10.

4.5.1 Rock magnetic analysis

Thermomagnetic, hysteresis, and χ_{LT} analyses were conducted on at least one sample from most sampling sites of the BD and EG intrusions. A problem encountered while analysing the granodiorite samples was that, not entirely unexpectedly, some of them were too weak to allow certain analyses to be effective.

It was observed that samples from site BD01 had M_S and χ_{RT} values approximately two orders of magnitude less than samples from the other sites of this intrusion (table 4.16). Unfortunately, this precluded effective analysis using either the thermomagnetic or χ_T techniques as the equipment used was insufficiently sensitive. However, hysteresis loops produced by the samples exhibited parameters clearly within the PSD range of the Day *et al*. (1977) plot in addition to a considerable paramagnetic component (figure 4.35(a)). These were observed to be in stark contrast to those produced by the samples from sites BD02, 03 and 04, which were very thin (figure 4.35(b)). Once again, a test of the frequency dependence of susceptibility was performed on samples from these last three sites, proving decidedly negative. Therefore, it appears that MD grains dominated entirely the hysteresis properties of these samples (table 4.16).

Thermomagnetic analysis of samples from sites BD02 and BD03 produced strong evidence that pure magnetite was their dominant ferromagnetic mineral and that this altered little upon heating to 700°C (figure 4.36(a)). This suggests that the original

cooling rate of the intrusion was low enough to allow the primary titanomagnetite to fully exsolve to its end members.

The χ_{LT} curves produced by samples from sites BD03 and BD04 were of the classic MD- type as described by Radhakrishnamurty *et al*. (1977) with very low RS values (figure 5.36(b) and table 4.16). The BD02 site sample however, produced a much flatter profile with the peak at –150°C just evident, the reason for this inconsistency was not clear.

Table 4.17 summarises the rock magnetic properties of the EG site samples, once again, several samples were too weak to provide meaningful results from either the thermomagnetic or χ_{LT} experiments. Samples from sites EC01 and MB01 both have Curie temperatures above that of magnetite but displayed no inflections on the heating curve. Both exhibit significant alteration on their cooling curves, the MB01 sample alters to a marginally higher Curie temperature phase upon cooling (figure 4.37(a)). The sample from site EP01 did display an inflection on the heating curve and this, coupled with the less magnetic phase observed on the cooling curve, strongly suggests that maghaemite (altering to haematite at ~ 400°C) is the dominant ferromagnetic phase (figure 4.37(b)).

The hysteresis loops produced by the samples varied between being distinctly characteristic of PSD (figure 4.38(a)) to characteristic of MD, those produced by samples from sites PL01 and EV01 especially (figure 4.38(b)) displayed significant paramagnetic components.

Sampling site	χ_{RT} (m^3kg^{-1})	M_S (Am^2kg^{-1})	M_{RS}/M_S	Hc (mT)	H_{CR}/H_C	ΔM_s	T_C (°C)	RS
BD01	16	0.004	0.14	16.3	1.95			
BD02	2109	0.283	0.02	3.5	2.15	-0.08	580	0.96
BD03	2530	0.179	0.01	1.5	1.48	-0.08	580	0.35
BD04	2427	0.262	0.02	1.5	1.78			0.35

Table 4.16: Thermomagnetic and hysteresis properties of BD site samples

Sampling site	M_S (Am^2kg^{-1})	M_{RS}/M_S	Hc (mT)	H_{CR}/H_C	ΔM_S	T_C (°C)	RS
EC01	0.240	0.11	6	1.89	-0.31	615	0.91
EP01	0.280	0.15	17	2.00	-0.51	575	1.09
EV01	0.003	0.11	5	2.17			
MB01	0.307	0.04	8	1.89	-0.15	595	0.7
PL01	0.012	0.11	8	1.73			

Table 4.17: Thermomagnetic and hysteresis properties of EG site samples

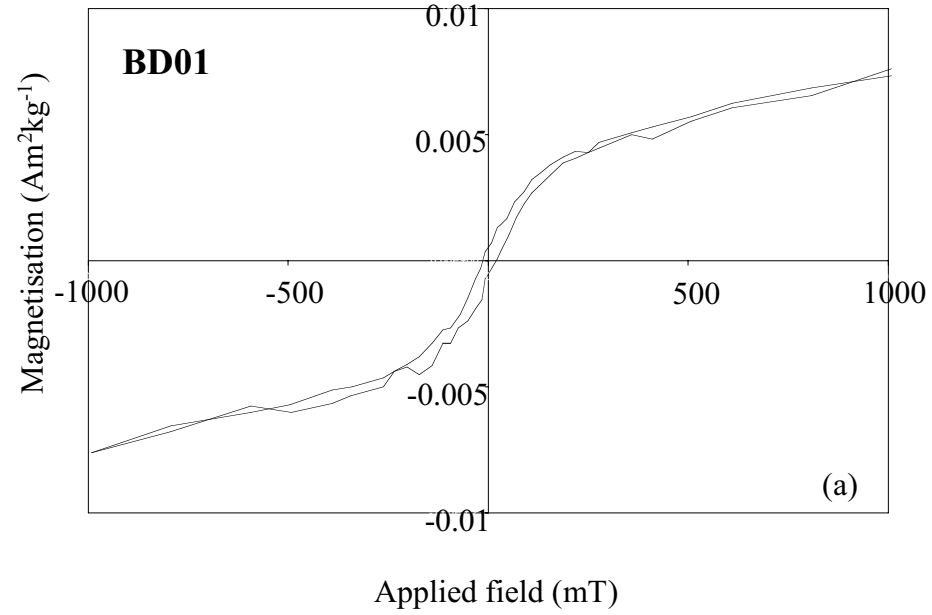

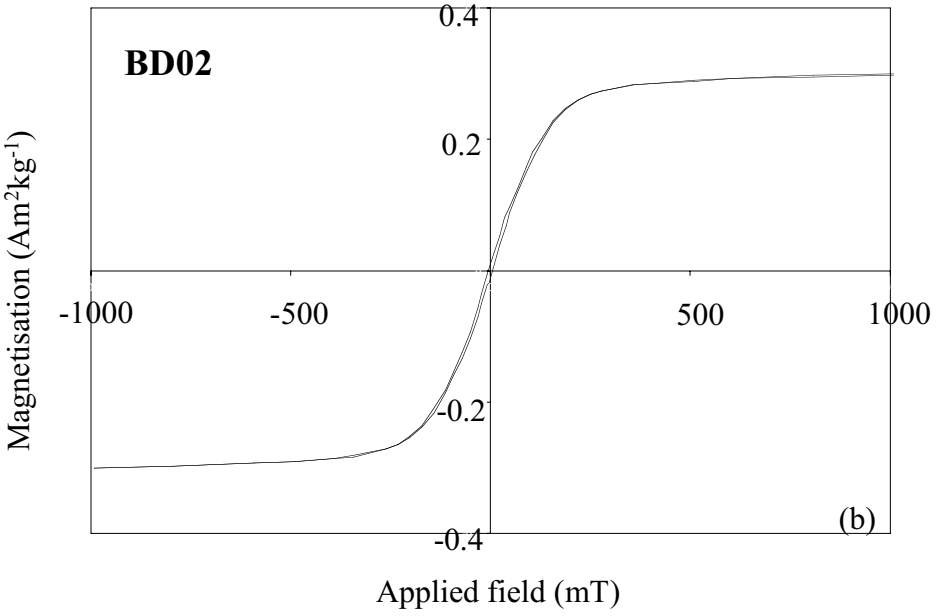

Figure 4.35: Representative hystersis loops produced by samples from the BD granodiorite

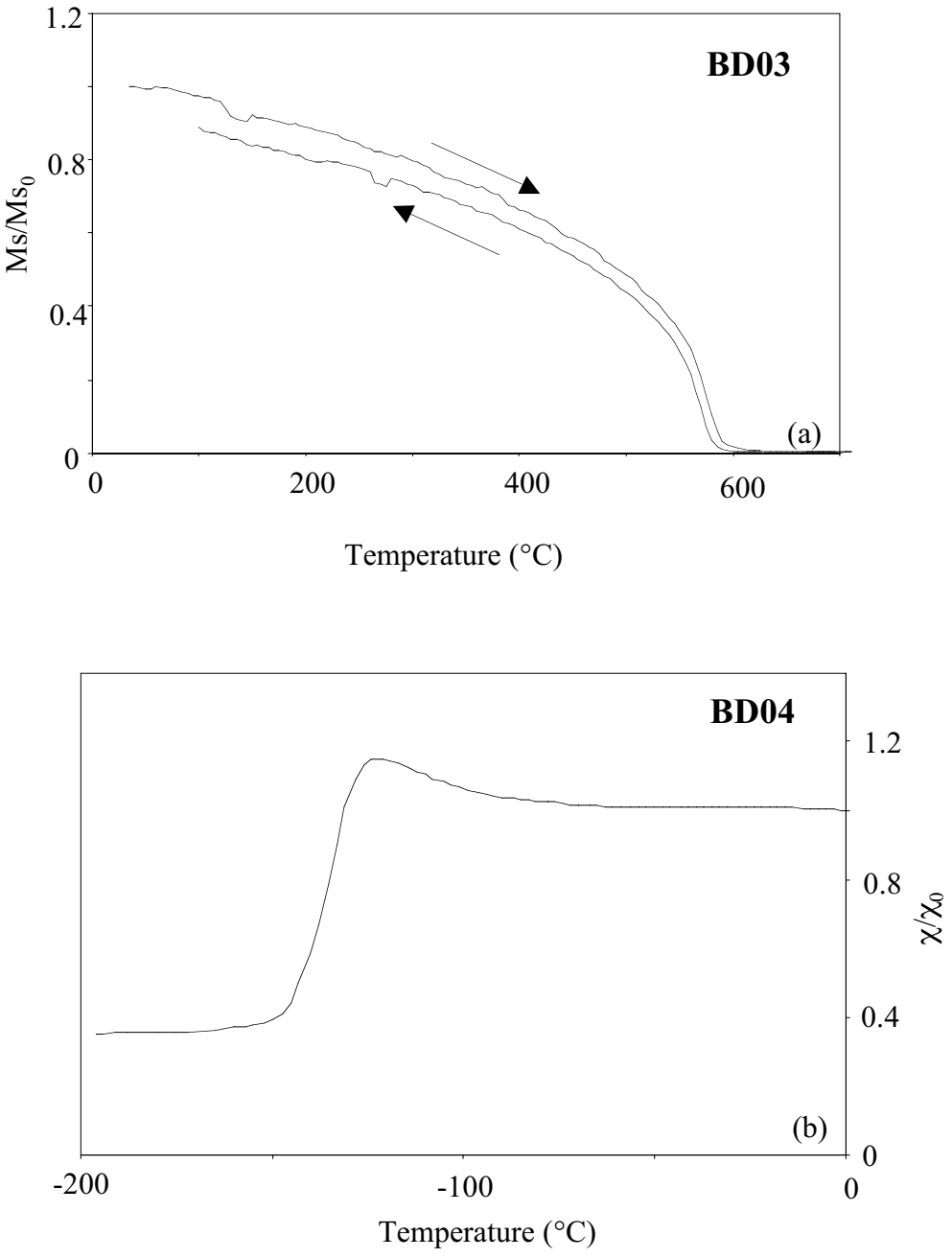

Figure 4.36: Representative (a) thermomagnetic and (b) curve produced by samples from the BD granodiorite. N.B. the distortions observed in the thermomagnetic curves are expected to be a result of the measuring apparatus itself.

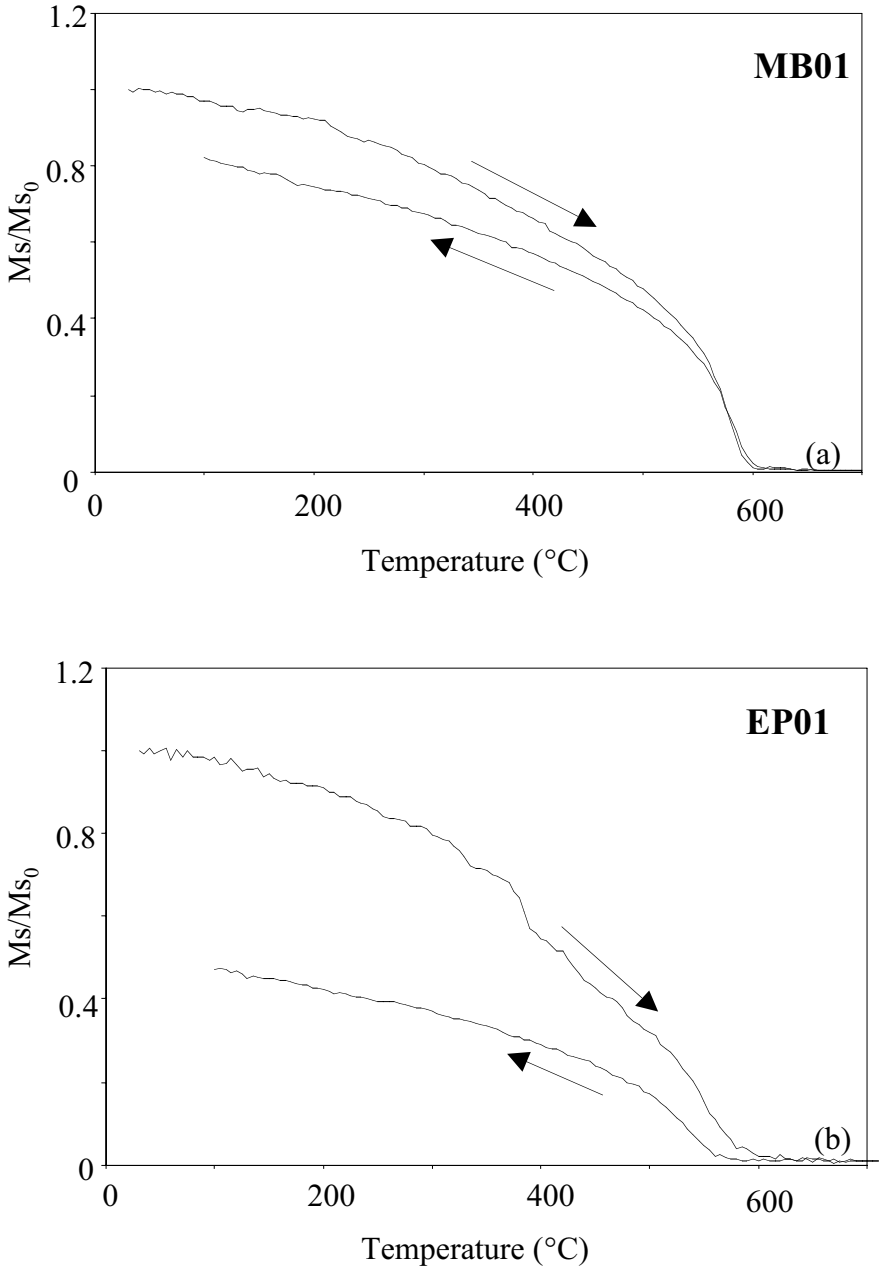

Figure 4.37: Thermomagnetic cyrves produced by samples from EG granodiorite.

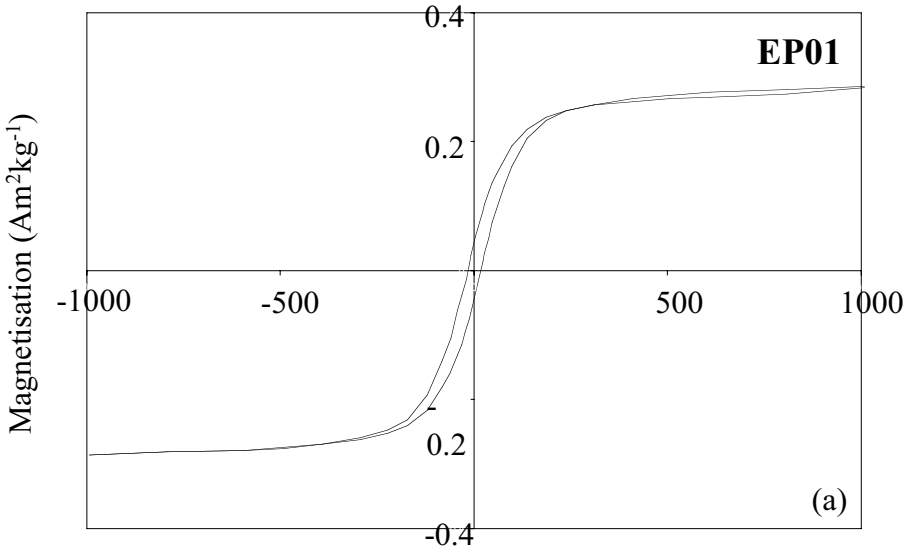

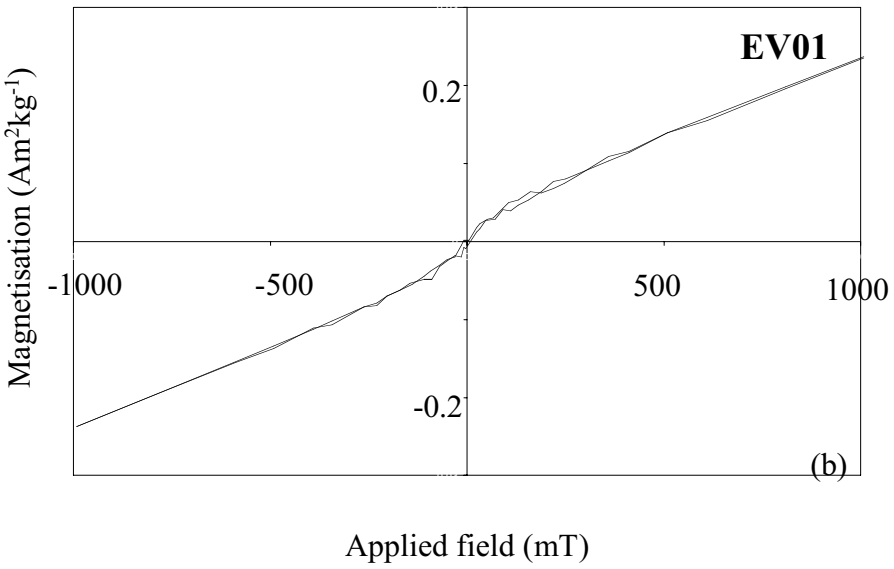

Figure 4.38: Hysteresis loops representing extremes of EG sample behaviour

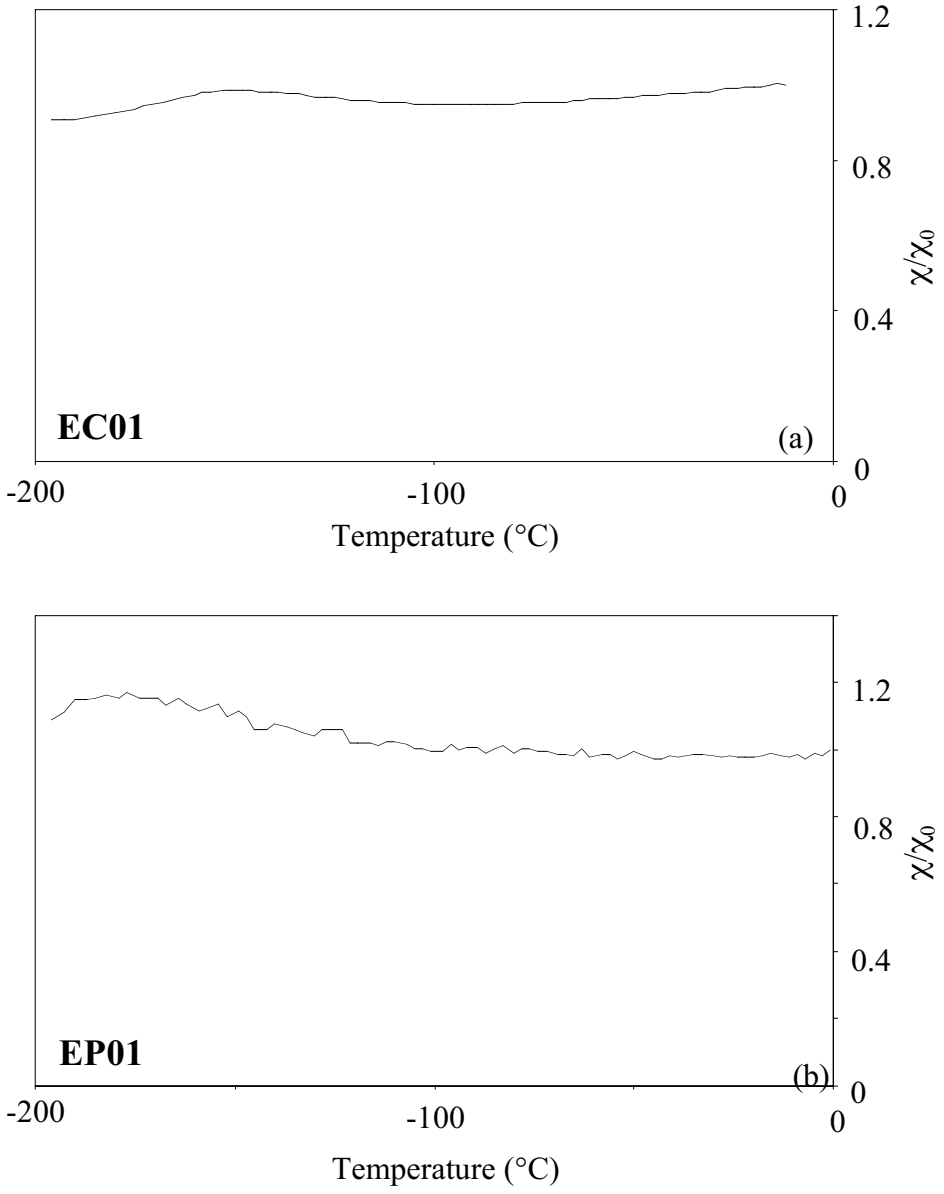

Figure 4.39: χ_{LT} cyrves produced by samples from EG granodiorite.

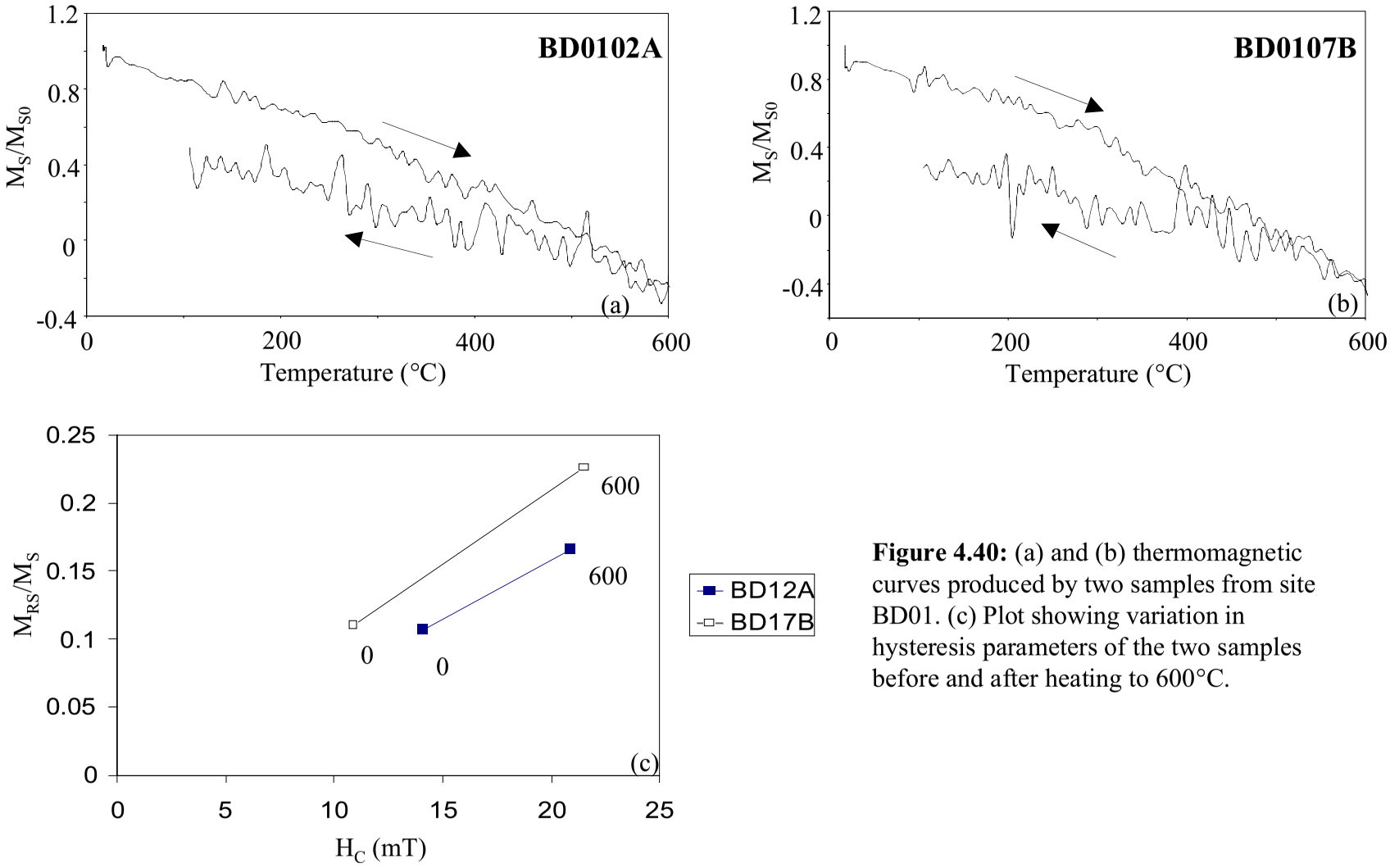

Figure 4.40: (a) and (b) thermomagnetic curves produced by two samples from site BD01. (c) Plot showing variation in hysteresis parameters of the two samples before and after heating to 600°C.

The results of the χ_{LT} experiments were varied, the sample from MB01 displayed a MD profile similar to those exhibited by BD03 and BD04 samples. The samples from sites EC01 and EP01 displayed much less variation however, and the profile of the latter sample exhibited the peak in χ at a lower temperature than is usually observed (figures 4.39(a) and (b)). This may be caused by the presence of some titanium in the lattice of the maghaemite crystals (Radhakrishnamurty, 1985).

The final rock magnetic study performed aimed to discover if samples from site BD01 suffered alteration upon heating to 600°C. Thermomagnetic analysis was conducted on two BD01 samples using a variable field translation balance (VFTB). Although the resulting curves were still rather noisy (figures 4.40(a) and (b)), it was possible to discern that the saturation magnetisation was reduced for both samples upon cooling (the reason for the negative values of M_S recorded by the instrument was not known). Furthermore, the variation in the hysteresis properties of the samples prior to and after the heating cycle showed unambiguously that significant alteration had taken place (figure 4.40(c)).

4.5.2 Palaeodirectional analysis

Stepwise thermal demagnetisation, in intervals of 50°C from 100°C to 500°C and then of 30°C to 590°C, was applied to sixteen BD samples derived from all four sites. Considering the predominance of MD grains in the samples inferred from the rock magnetic analysis and the weak remanence encountered, the OVP's produced by the measurements of remanence were remarkably clear. However, IRM overprinting was frequently observed.

All samples exhibited a normal polarity low blocking temperature component (LBT) that required demagnetisation up to 500°C to remove it in many cases. However, in samples from site BD01, a reverse polarity ChRM was also present above this (figure 4.41(a)). Figure 4.41(b) shows the OVP of a sample displaying parallel normal polarity components at both high and low temperature portions of its

blocking temperature spectrum. This behaviour suggests that these components are chemical and thermal (pTRM or TVRM) respectively in origin, but were acquired at the same time.

Normal polarity components of magnetisation were observed in four BD samples measured by Lackie and Schmidt (1996) who reported a VGP at 11°N, 345°E (dp=15, dm=16). This is somewhat removed from the mean VGP found from this study (table 4.18) which plots to the east of the early Jurassic portion of the Australian APWP (figure 4.42). Nevertheless the large uncertainty associated with the mean LBT direction precludes a meaningful comparison with other palaeopoles. It is quite possible that this normal component is a product of the 90 Ma thermal event. If so, its non-Cretaceous direction can be accounted for by the insufficient number of samples of questionable palaeomagnetic stability recording it. Certainly, Lackie and Schmidt (1996) found normal polarity overprints in most igneous rocks of the Bowen Basin although many of these did not have mid-Cretaceous directions (§ 3.2.2).

The reversed HBT component observed in samples from sites BD01 and BD02 was somewhat better constrained and produced a VGP within errors of the mid/late-Jurassic portion of the APWP (figure 4.42). This may be the primary remanence suggesting that the intrusion was emplaced slightly before the early-Cretaceous time that the fission track estimates of Pattison (1990) inferred. It would be necessary to measure more samples with the reliability of those from site BD01 to confirm this however.

Samples from site BD01, despite their very low intensities of magnetisation, produced the clearest OVPs. This is obviously a result of the smaller effective grain size that they exhibited in the hysteresis analyses. The essentially MD nature of the samples from other sites allowed them to be easily overprinted. Consequently, the observed scatter of directions between these samples is probably due to each recorded ‘component’ actually being a composite of a number of overlapping

components. By this logic, the mean direction of the normal components from site BD01 is likely to be the most reliable. Unfortunately, this is comprised of only two estimates because of IRM overprinting from lightening strikes in the other samples. The VGP it produces is located at 30°N, 3°E, which is close to the being antipodal to the VGP produced by the ChRM. This may suggest that the sample cooled over a sufficient time for a geomagnetic reversal to occur and that the LBT component in BD01 samples is also primary.

Thermal demagnetisation of the EG samples was continued up to 680°C because of the surviving remanence present above T_C of magnetite. Samples taken from sites BH01 and EP02 were excluded from the palaeodirectional analysis because of the extremely low intensities (< 5 _ 10^{-8} Am^2kg^{-1}) of their NRMs. For those samples analysed, recoverable components of magnetisation were usually limited to high temperature (> 550°C) portions of the blocking temperature spectra. At lower temperatures, the OVP usually displayed either randomly directed IRM overprints or significantly curved plots indicating overlapping components. The results from some samples of most sites had to be discarded because of total IRM overprinting (see appendix 5), additionally, samples from EC01 had a tendency to develop strong CRM components once they were demagnetised beyond 560°C.

Meaningful isolated components were difficult to recognise in many EG samples because they were confined to high T_B's and tended to be very weak, therefore circular rather than orthogonal vector plots were employed in recovering the ChRM of samples from all sites except EV01 and MB01. Samples from the latter of these sites behaved distinctly differently to the rest, carrying almost the entire remanence in a very narrow range of blocking temperatures above 560°C (figure 4.43). Haematite was the likely stable remanence carrier in these samples and was probably also present in samples from most of the other intrusions. It appears, however, that a small amount of coexisting magnetite was sufficient to effectively mask the dominance of this mineral in the results of the hysteresis and thermomagnetic analyses.

Site	$\overline{\Delta T}$ (°C)	N	Dec (°)	Inc (°)	k	α_{95}
	LBT component					
BD01	0-500	2	271	-76	455	
BD02	0-300	3	321	-51	7	52
BD03	0-590	1	252	-76		
BD04	0-250	3	284	-67	8	47
Mean		4	293	-70	25	19
VGP	31ºN, 18ºE (dp =28 , dm =33)					
	HBT component					
BD01*	530-590	4	120	73	81	10
BD02*	200-530	1	74	78		
BD04	250-590	2	117	-25	5	
Mean*		2	101	76	88	
VGP	25ºS, 177ºE					

Table 4.18: Site and overall mean directions from components of remanence observed in samples from the BD granodiorite

Site	$\overline{\Delta T}$ (°C)	N	Dec (°)	Inc (°)	k	α_{95}
EC01	590-650	2	009	76	8	
EP01	0-560	1	000	-44		
EV01*	300-500	2	010	-80	267	
MB01*	560-680	6	354	-80	759	2
PL01	620-680	6	170	69	12	20
PL02	590-650	3	122	64	8	48
Mean(*)		2	002	-80	1447	
VGP	41ºN, 327ºE					

Table4.19: Site and overall mean diresctions from sites of the EG intrusions

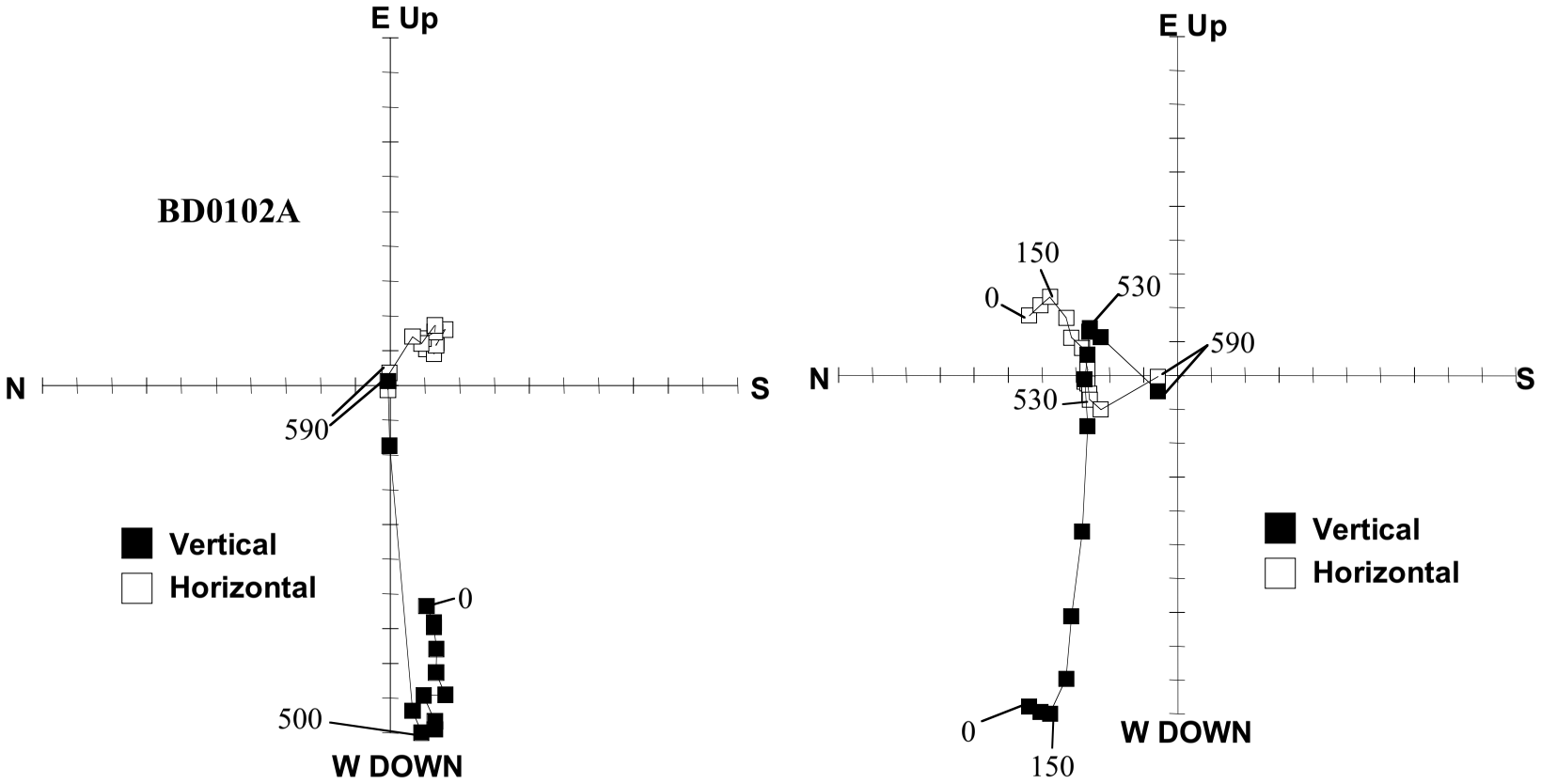

Figure 4.41: Clear examples of OVPs produced by BD samples described in text.

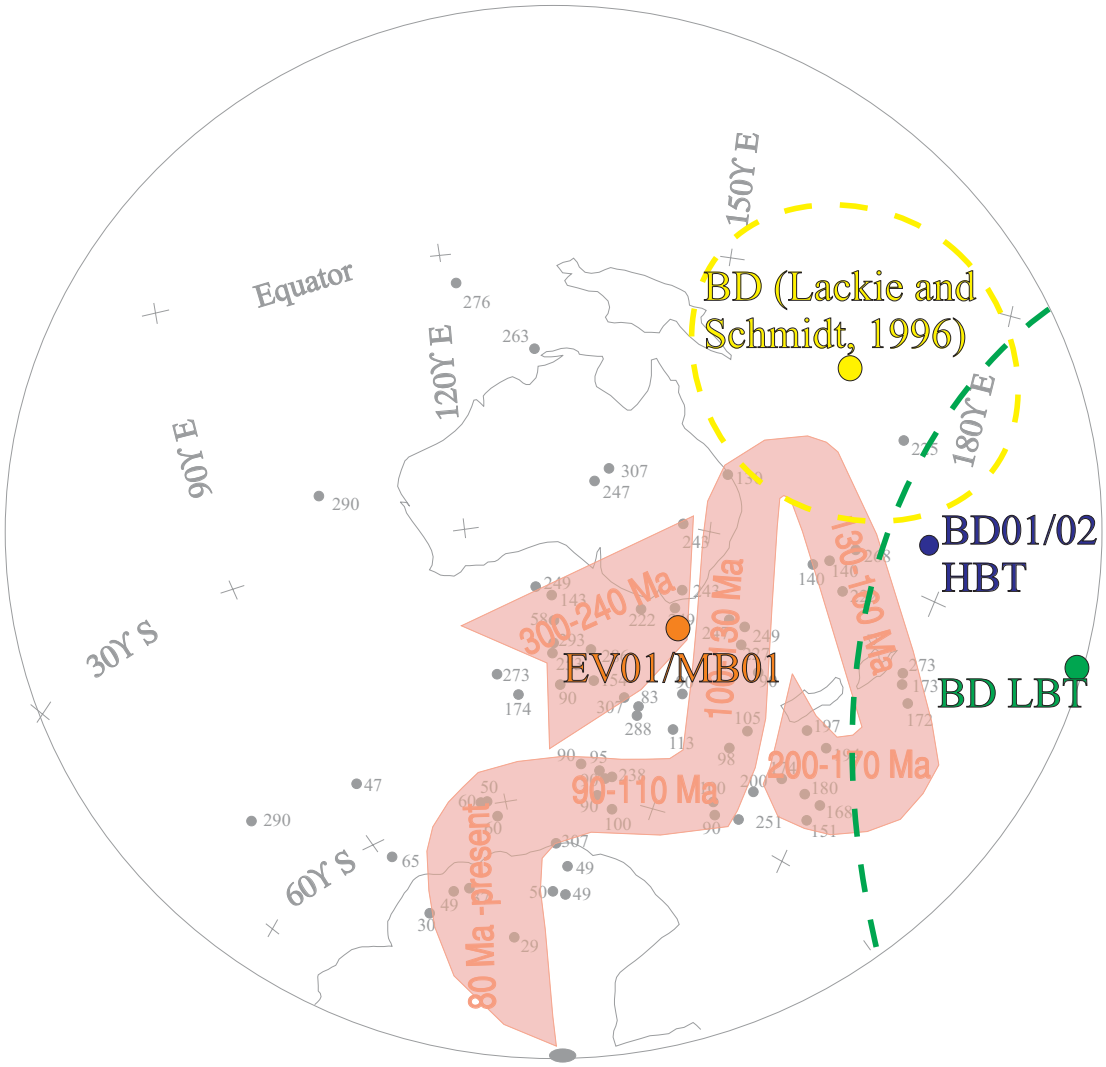

Figure 4.42: Australian APWP showing VGPs (normalised to reverse polarity) measured from Bundarra and Eungella granodiorites. Dashed ellipses are 95% confidence limits.

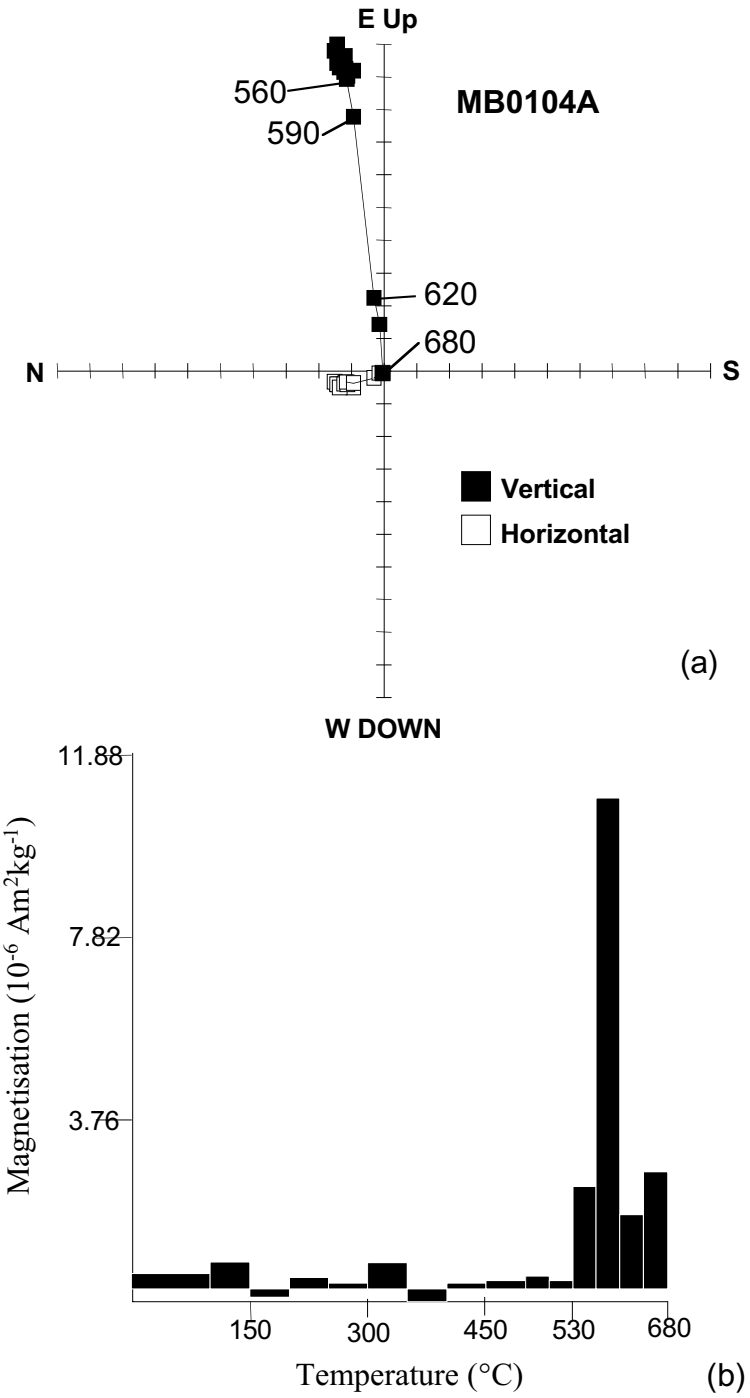

Figure 4.43: (a) OVP produced by thermal demagnetisation of the Mount Barker granodiorite sample MB0104A. (b) Plot of blocking temperature spectrum of sample MB0104A.

Because of the noise inherent in the measurements of remanence of many samples and the widespread IRM overprinting, site mean directions tended to be very poorly constrained (table 4.19). ChRM components of both normal and reverse polarity were observed, although the site means of the latter were insufficiently precise to warrant discussion. The single recoverable component from EP01 had the same direction as the present field suggesting that a VRM may have overprinted the entire blocking temperature spectrum.

The normal polarity ChRM directions from EV01 and MB01 samples combined to give well-constrained site mean directions and a pole close to the lower Cretaceous portion of the Australian APWP (figure 4.42). This in itself suggested that this remanence may have been primary. However, the samples from site MB01 appeared very weathered and, although haematite was inferred from the palaeodirectional study, it was not certain that maghaemite could not also be a contributor. Therefore polished thin sections were prepared from three of the Mt Barker (MB01) samples to allow alternative analyses. Raman microspectroscopy directed at the opaque crystals in the sections failed to show any evidence of maghaemite but repeatedly produced spectra indicative of haematite and, to a lesser extent, magnetite (de Faria *et al*., 1997). AF demagnetisation was also performed on one MB01 sample and it was found that less than 10% of the remanence was removed by demagnetisation to 150 mT, which strongly suggested that haematite was the dominant remanence carrier.

Observation of the thin sections using transmitted light microscopy showed that most of the opaque crystals had formed in fractures and were secondary. These had not formed as a result of weathering but of whole-rock recrystallisation by a hydrothermal event involving temperatures in excess of 300°C, which was likely to have occurred shortly after the intrusion had been emplaced. The combined evidence strongly suggests that the ChRM of the MB samples is a CRM contained in authigenic haematite formed shortly after emplacement. The surviving large grains of magnetite in the samples define the hysteresis loops and dominate the

thermomagnetic curves due to their much higher capacity to acquire induced magnetisation however.

Due to the paucity of EG samples carrying a reliable primary remanence, no palaeointensity work was performed on this suite of rocks.

4.5.3 Palaeointensity analysis

A Thellier analysis was performed on 16 samples from all four sites of the Bundarra granodiorite. Unfortunately sampling at site BD01 was restricted because of the seemingly inappropriate composition of the rock, consequently only two samples from this site remained to perform this analysis on. In addition to these, a number of core samples from site BD02 were also included together with five unoriented hand samples collected from sites BD03 and BD04.

It was decided to employ double heating steps at intervals of 50°C throughout the entire blocking temperature spectrum with pTRM checks after every other double step. Unfortunately, the analysis failed absolutely for all but one sample. The cause of the failure was widespread reduction in the capacity of the samples to acquire pTRM beginning at low (<200°C) temperatures. This was the same as the 'pTRM impedance' observed in many KD samples (§ 4.3.3) and although it did not always cause the pTRM gained at a higher temperature to actually be less than the previous measurement, it frequently caused the initial portion of the NRM-TRM plot to be ridiculously steep (figure 4.44).

A large and sudden increase in pTRM was often observed after the 580°C remagnetisation step (figure 4.44(b)), which gave the overall impression of an extreme convex-down NRM-TRM plot. A convex-down plot is expected to result from a Thellier analysis of a sample containing only MD grains (§ 2.4.4). However, the ratio of the initial to the final slope in this analysis often reached several tens: far greater than that observed by experiments on crushed magnetite known to be MD

(Levi, 1977; Shcherbakova *et al*., 2000). Therefore, although the large average grain-size of the BD samples probably plays a role in producing a steep initial slope, the dominant process is thought to be laboratory-induced magnetic alteration.

Pure magnetite is unlikely to oxidise at such low temperatures and consequently this alteration is unlikely to involve changes in the chemical composition of the grains. Instead, physical alteration, possibly through irreversible changes of microstress within the grains, appears more likely. This type of alteration may induce not only the pTRM impedance effect but could also cause large portions of NRM to be lost as domain rearrangement occurs (Kosterov and Prévot, 1997). This concurs with the results found here where, frequently, over half of the NRM is lost by demagnetisation up to only 350°C.

Only one sample did not suffer from pTRM impedance prior to the isolation of the samples ChRM, its NRM-TRM plot and OVP are shown in figure 4.45. Unfortunately the sample was not oriented in situ and therefore, one has no way of knowing if the convergent component had a direction that indicated that it was primary. It was observed that a loss of NRM without accompanying pTRM gain occurred during the 350°C step. The statistics accompanying the full 0-500 estimate are favourable to those accompanying the 0-300 estimate (table 4.20) although both pass the criteria of Coe *et al*. (1978) and Selkin and Tauxe (2000), including that regarding pTRM checks. However, the estimates do differ significantly and as this behaviour (albeit more extreme) has caused so many samples from the same suite to fail, it would be safer to truncate the line above 300°C and take the latter estimate.

Sample	ΔT	N	f	g	β	q	Max pTRM check discepancy	Mean |pTRM check discepancy|	Temp (χ_{RT} alteration)° C	R(7)	H_{PALAEO} (μT)	VDM (10^{22} Am^2)
BD04H2A	0-500	9	0.82	0.86	0.09	8.1	-7%	3%	580	5	74 ± 9	10.4
	0-300	5	0.39	0.73	0.10	2.9	2%	1%		5	56 ± 20	7.9

Table 4.20: Two possible palaeointensity estimates and accompanying statistics for only non-failing BD sample

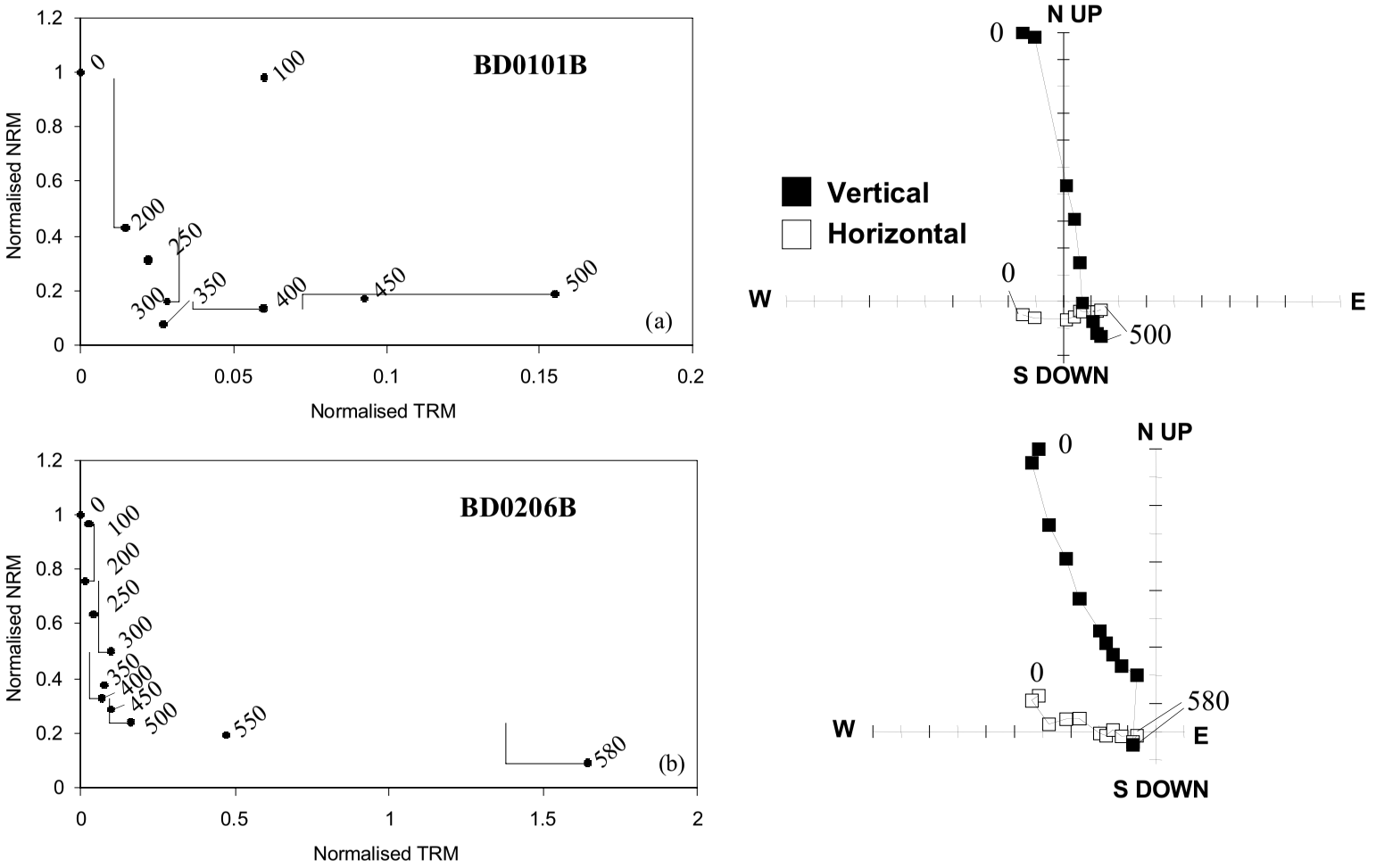

Figure 4.44: NRM-TRM plots and accompanying OVPs for BD samples failing to give reliable palaeointensities because they exhibit pTRM impedance.

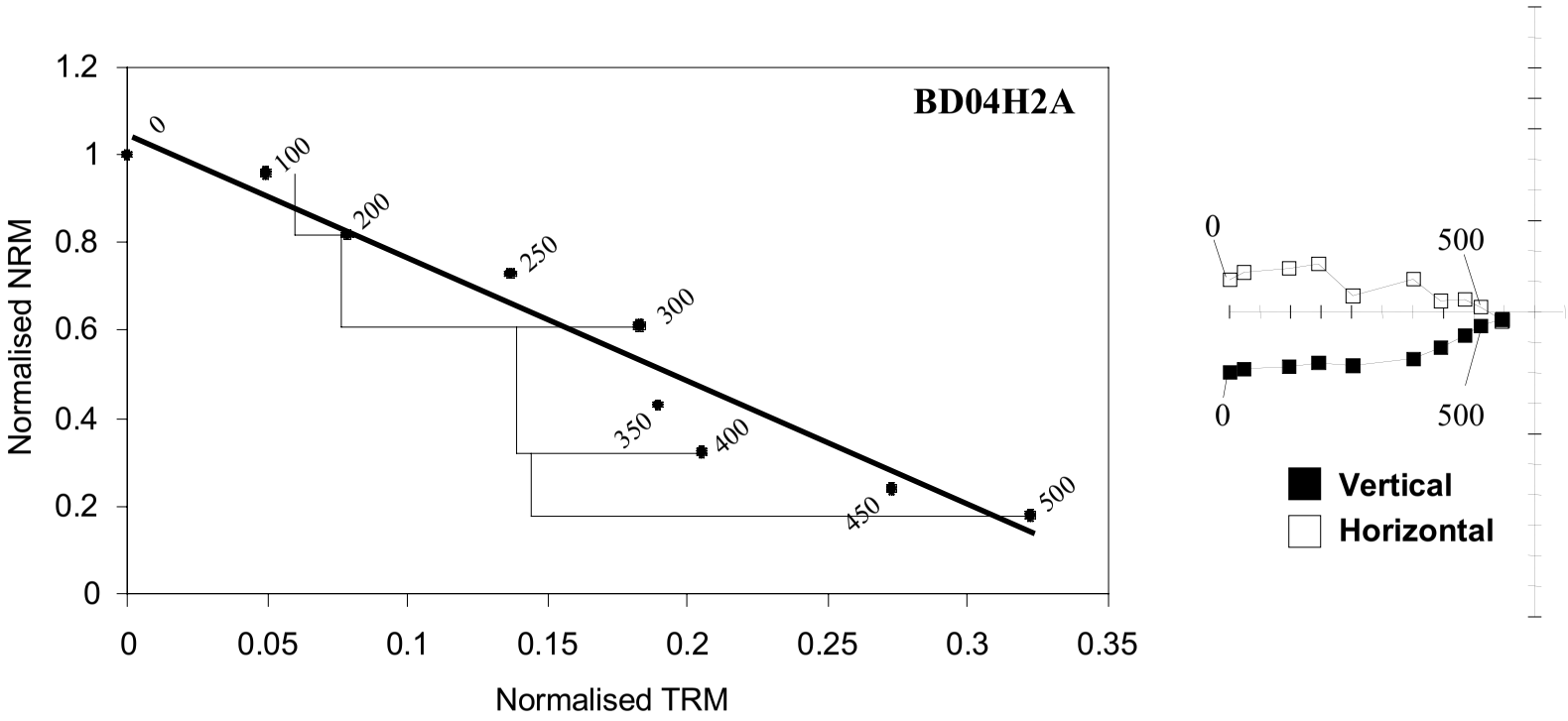

Figure 4.45: NRM-TRM and orthogonal vector plots for the single BD sample that did not suffer from pTRM impedance prior to the isolation of the ChRM

4.6 The Yeppoon highway gabbro

Seven cores were extracted from a single site in the late Permian gabbro on the Yeppoon Highway (YH) (§ 3.4.2.1). As only fourteen samples were recovered, a Thellier experiment was performed immediately on all of these with the intention of recovering palaeodirectional information from the results of this analysis. Unfortunately, there was no opportunity to perform any preliminary rock magnetic experiments.

The YH samples were subjected to double heating step at the following temperatures: 100°C, 200°C, 270°C, and 320°C followed by 40°C intervals up to 480°C or 510°C after which demagnetisation was observed to be complete. Most remagnetisation steps were followed by a pTRM and NRM check. In contrast to what one would expect to encounter in a mafic intrusion, the remanent magnetisation of the samples was observed to be weak (between 1 and 5 _ 10^{-6} Am^2kg^{-1}). The resulting OVPs of the NRM were somewhat noisy, although at least two normal polarity components were evident in most samples (figure 4.46). However, the noise became enhanced as the samples were demagnetised and consequently, a reliable direction for the ChRM was not recoverable in many. Similarly, the low blocking temperature portion of the OVP often exhibited curvature, indicating that more than one component were residing in it.

Appendix 5 lists the directions of the recognised in components in all samples and table 4.21 gives the mean directions. The LBT component is relatively well defined but produces a VGP that is well removed from established Australian palaeopoles since the Permian. This suggests either that the overprint was imparted at a time of extreme SV or, more likely, that the measured directions are actually a composite of multiple normal components of magnetisation.

Two samples displayed shallow westward ChRM directions, these did not correspond to a meaningful VGP position and therefore are absent from table 4.21.

The other ChRM directions were very steep and relatively well grouped. This VGP is positioned on the APWP at a point that could correspond with either a late Permian or early Cretaceous time of magnetisation. As there is no reason to suspect that the YH gabbro was overprinted in the early Cretaceous, it is reasonable to assume that this direction component is the primary remanence.

The type of alteration termed pTRM impedance here was fortunately not prevalent in the results of this Thellier analysis. The largest single problem faced was that there were insufficient measurements in the parts of the blocking temperature spectra in which the distinguishable components resided. Estimates that comprised three or more points on the NRM-TRM plot were recorded despite the criterion of Coe *et al*. (1978) requiring that $N \geq 4$ (figure 4.47).

Two samples definitely did exhibit pTRM impedance prior to the isolation of the ChRM, another (sample YH0104A) may have also although the shallow direction of the ChRM in this sample means that its results should be treated with suspicion regardless. The estimates associated with the LBT component are of little practical use because its mean direction does not conform to any post-Permian direction measured before in Australia. However, these are displayed in table 4.22 for completeness although none of them fulfil the combined criteria of Coe *et al*. (1978) and Selkin and Tauxe (2000). The four estimates recovered from the HBT component are displayed in table 4.23. The values of β were generally better than those observed in the LBT estimates, however low f and g values ensured that the q values were, with one exception, not wholly preferable.

Even after excluding sample YH0104A from the mean calculation, for the reasons given above, the mean VDM for the late Permian is relatively high, approaching the present-day value ($7.9 \_ 10^{22}$ Am^2; Merrill *et al*., 1996).

Site	$\overline{\Delta T}$ (°C)	N	Dec (°)	Inc (°)	k	α_{95}
	LBT component					
YH01	100-320	9	256	-56	23	11
VGP	3ºN, 22ºE (dp =11 , dm =16)					
	HBT component					
YH01	400-480	6	350	-85	36	11
VGP	34ºN, 333ºE (dp =22 , dm =22)					

Table 4.21: Mean directions of remanence components in YH samples

Sample	ΔT	N	f	g	β	q	Mean |pTRM check discepancy|	Max pTRM check discrepancy	Mean |NRM check discrepancy|	Max NRM check discrepancy	R(7)	H_{PALAEO} (μT)	Site mean VDM (10^{22} Am^2)
YH0101A	100-320	4	0.30	0.63	0.27	0.7	6%	13%	9%	-14%	3	24 ± 34	4.5 ± 2.1
YH0102A	100-270	3	0.48	0.37	0.10	1.8	30%	-37%	3%	4%	3	36 ± 20	
YH0102B	100-270	3	0.33	0.47	0.13	1.2	5%	7%	11%	-14%	3	30 ± 24	
YH0104B	100-270	3	0.74	0.40	0.16	1.8	23%	30%	6%	-6%	2	38 ± 22	
YH0105A	100-320	4	0.59	0.61	0.25	1.5	21%	-40%	6%	-22%	2	26 ± 18	
YH0105B	100-360	5	0.38	0.69	0.29	0.9	8%	26%	5%	-9%	3	12 ± 14	
YH0106A	0-200	3	0.40	0.48	0.19	1.0	9%	-9%	7%	9%	4	22 ± 22	
YH0106B	200-320	3	0.18	0.48	0.17	0.5	13%	-26%	9%	-12%	1	8 ± 14	

Table4.22: Palaeointensity estimates and associated statistics for LBT component in YH samples

Sample	ΔT	N	f	g	β	q	Mean |pTRM check discepancy|	Max pTRM check discrepancy	Mean |NRM check discrepancy|	Max NRM check discrepancy	R(7)	H_{PALAEO} (μT)	Site mean VDM (10^{22} Am^2)
YH0101A	400-480	3	0.47	0.22	0.10	1.0	24%	37%	5%	-6%	4	76 ± 76	7.5 ± 2.6
YH0102A	400-480	3	0.65	0.45	0.00	680.9	24%	25%	7%	-17%	3	57.3 ± 0.1	
YH0102B	400-480	3	0.4	0.29	0.15	0.3	40%	63%	12%	-21%	2	30 ±100	7.1 ± 3.0†
YH0104A*	360-440	3	0.41	0.26	0.13	0.8	25%	-32%	6%	-11%	1	66 ± 82	

Table 4.23: Palaeointensity estimates and associated statistics for HBT component in YH samples. * denotes sample in which low level pTRM impedance was observed at 360°C. † mean excluded sample marked with *.

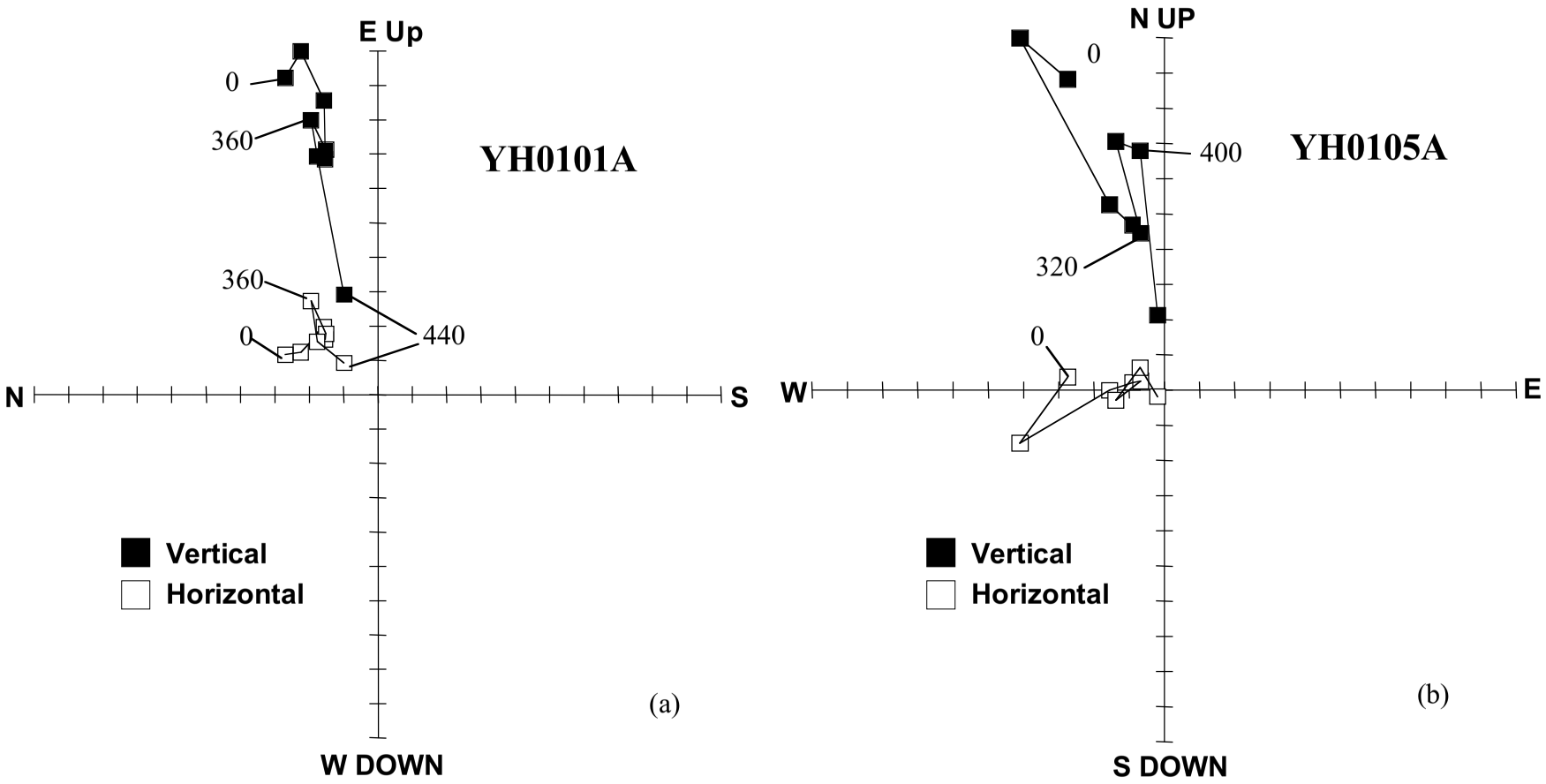

Figure 4.46: Representative OVPs produced by palaeodirectional analysis of YH samples.

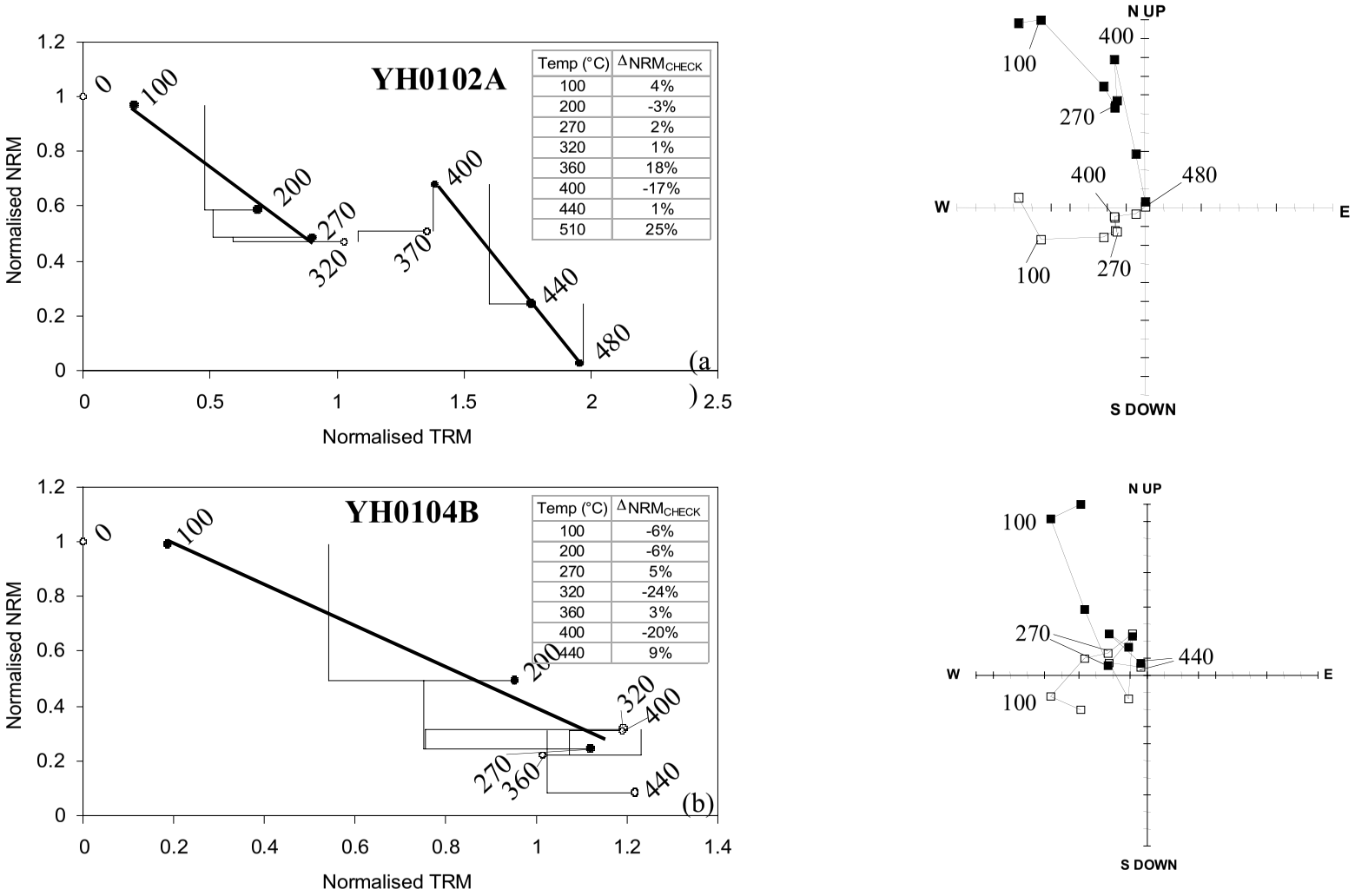

Figure 4.47: NRM-TRM plots and accompanying OVPs for two representative YH samples. Filled (hollow) circles represent used (discarded) points.

4.7 Discussion

During this study, a total of ten suites of intrusive rocks, varying considerably in mineralogy and grain size, were subjected to some palaeomagnetic and / or rock magnetic analysis. Consequently, the results presented in this chapter offer a good opportunity to discuss both the suitability of different igneous rocks for palaeomagnetic analysis, and the usefulness of different experimental techniques in assessing this potential and acquiring the information itself. This discussion section will be segmented into aspects concerning the three primary categories of analysis, as was done for the individual rock suites themselves. A discussion of the potential significance of the palaeointensity results themselves for the global dipole moment record will be reserved until chapter 9.

The techniques employed during the rock magnetic analyses involved, almost exclusively, monitoring the variation of the properties associated with total (i.e. induced plus remanence) rather than just remanent magnetisation. This is expected to create problems in the analysis of samples in which the primary remanence carriers coexist with a magnetically soft component that plays little part in carrying the remanence but, because of its higher susceptibility and saturation magnetisation, dominates the response of the sample to imposed fields. In such instances, thermomagnetic, hysteresis and all susceptibility analyses can be expected to provide the information (Curie temperature, domain state and susceptibility to alteration) primarily or even solely about the palaeomagnetically less important, softer phase.

This problem of misinformation was encountered frequently in this study but its most striking incidence was regarding the samples from the Mt Barker (MB) granodiorite. These contained virtually all their remanence in haematite, with a narrow unblocking temperature range between 560°C and 680°C (figure 4.43). The only hints from the rock magnetic tests that haematite existed in the measured samples were that the indicated Curie temperature (595°C) was slightly above that of

pure magnetite (this could have been construed as evidence for maghaemite however), and that the coercivity (8 mT) was slightly higher than that normally associated with such a low ratio (0.04) of remanent to saturation magnetisation. The picture supplied by the rock magnetic analysis (strengthened by the χ_{LT} profile) was that of an assemblage of either MD maghaemite or MD magnetite together with a possible haematite component, apparently of little significance. It was only realised during the palaeodirectional analysis that it was the MD magnetite that was largely insignificant.

Another noteworthy case of under-representation of the principal remanence carriers in the rock magnetic analysis was that of the Newcastle dykes. Thermomagnetic analysis of three of the site samples (that of CH02, LR01, and NH01) produced Curie temperatures between 175°C and 380°C indicative of titanomagnetite with a moderate to high titanium content, this was itself an unusual result that will be discussed later. However, the palaeodirectional study isolated, albeit somewhat noisily, components of remanence extending to above 550°C. Clearly, the ferromagnetic phase that retained the high temperature portions of these components had a much lower contribution to the observed saturation induced magnetisation than the titanomagnetite.

The simple solution to the problem discussed above is to use rock magnetic techniques that solely measure the remanence properties of a sample. These include AF demagnetisation, IRM acquisition, temperature dependent remanence measurement and the thermomagnetic criterion. The problem with the last of these is that the samples may alter dramatically during the course of the experiment rendering the results invalid.

Rock magnetic techniques based on the properties relating to the induced magnetisation of samples have been used to great effect in this and many other studies. However, it is necessary to bear in mind that they may not always provide the complete picture.

Intrusives, as opposed to extrusives, were targeted by this study for a number of reasons (§ 3.1). One of these was that deuteric oxidation was expected to occur frequently causing samples to contain pure magnetite and / or haematite which are more resistant to chemical alteration in the laboratory than their titanium enriched equivalents. This was the case for BD and GS samples; most other samples exhibited Ti-poor titanomagnetite as the primary phase, indicating that some oxyexsolution at least had occurred. The exceptions to this were the ND samples, which contained titanomagnetite with significant titanium content. This was very likely a primary phase in the rocks and indicates that the dykes must have been intruded at a very high level in order that cooling was fast enough not to allow exsolution to be completed.

Intrusions were also sampled in preference to lavas because of the greater probability of them not containing maghaemite and a CRM overprint as a consequence. This reasoning appears to have been justified as only 3 sites from the 44 analysed are suspected of suffering from the effects of low temperature oxidation.

The effects of the thermal event proceeding the rifting of the Tasman Sea were called upon repeatedly to explain normal polarity components of magnetisation that overprinted the ChRM in many samples. This was especially prevalent in many of the samples studied here because of the large PSD / MD component of grain-sizes encountered in them. Consequently, thermal demagnetisation in excess of 400°C was sometimes required before the TVRM (or TCRM) was removed. This study has served to establish even further, the effectiveness of this event in recording itself, to some extent, in the palaeomagnetic signatures of eastern, and not just south-eastern, Australia. It may also be construed that it has produced evidence against the suitability of intrusive rock (due to their high average grain size) from this region, and formed prior to 90 Ma, for palaeointensity analysis.

As a consequence of the Cretaceous thermal event, the VGP position for Australia at this time, as with most others since the Triassic at least, is relatively well constrained. This alone however, did not allow the age of isolated components of remanence to be ascertained easily however. This is because the APWP for Australia through the Mesozoic era, by virtue of the Corel Sea loop, is somewhat limited in spatial extent. This has the potential of being especially problematic for magnetisations acquired in the Triassic and Cretaceous when the APWP crosses (figure 4.1) and non-unique age estimates are possible. This did not cause any particular problems in this study however. Instead problems regarding the cramped nature of the Australian APWP were encountered when VGPs were derived from mean directions of remanence with moderate to large associated uncertainties, and could be placed with equal (95%) confidence on portions of the APWP representing variations in time exceeding 100 Myr.

The results of many samples were discarded from the palaeodirectional analysis because their NRM was completely overprinted by IRM due to lightening strikes. Unfortunately this is a largely inescapable annoyance encountered in many palaeomagnetic studies. The two suites of intrusions that were most hampered by this phenomenon were the EG granodiorites and the BPG. The former of these was located within tropical latitudes, where lightening storms are more frequent, and both were very exposed. IRM acquisition probably presented more of a problem in this study than in many because of the high contents of MD / large PSD grains encountered in the samples, which are overprinted easier and can corrupt the entire blocking temperature spectrum.

With the exception of the relatively well-behaved Gibraltar microsyenite, the results of this study largely reinforce the preconception that felsic intrusions are poor palaeomagnetic recorders (Butler, 1992). While many of the more mafic samples also exhibited noisy component structures during demagnetisation, the low intensity of magnetisation encountered in many of the EG and BD samples served to accentuate this and caused the recovery of directions to be made very difficult.

Surprisingly, BD01, the site containing possibly the weakest samples studied in the palaeodirectional analysis, provided, where IRM overprinting was not evident, good directional information. This suggests that not all felsic intrusions should be avoided for palaeomagnetic studies. Unfortunately, no straightforward criteria for sample selection, prior to rock magnetic analysis, can be identified from this study.

The results from the palaeointensity analyses were somewhat discouraging considering the large amounts of laboratory time required to acquire them. Ultimately, there was no single set of estimates that could be presented as wholly reliable by virtue of them possessing every attribute required by contemporary acceptance criteria (i.e. a maximum R factor). The certainty that a TRM is completely isolated is an unavoidable requirement of successful Thellier analysis and therefore closed to argument and improvisation. Other criteria, especially those proposed by Selkin and Tauxe (2000), are much less well founded however. Given that so startlingly few of the estimates presented in this chapter met with these strict criteria, some investigation into their applicability to these samples and their measurement was warranted. This investigation was the primary aim of the analysis described in chapter 5 and the issue receives further attention in chapter 9.

Sixty-five percent of Thellier results obtained during this study were rejected outright. Notwithstanding the uncertainty in the acceptance criteria discussed above, this quantity of measured samples failing to give palaeointensity estimates that would meet with any sensible criteria (e.g. those advocated by Coe *et al*. (1978)) may still seem excessively high. This was not in fact the case, a high (> 50%) failure rate for studies employing the Thellier method is a generally expected result and one that must be offset against the importance of gaining reliable estimates.

.

The relatively high content of large ferromagnetic grains present in the assemblages of many of the samples measured during this study did add to the problems associated with palaeointensity estimation somewhat. Frequently, it was not possible to remove extensive overprints and isolate the supposed primary component before

the NRM-TRM plot produced by the sample indicated that significant alteration had occurred.

The type of alteration encountered in this study was so frequently pTRM impedance (as it was named in this chapter), that it is worth examining this form of non-ideal behaviour a little more closely. Firstly, it must be stated that, although pTRM impedance is an intuitive name for a form of alteration whereby NRM demagnetisation so outstrips pTRM remagnetisation, a more accurate term may in fact be NRM annihilation. The point being that the pTRM acquisition capacity of a sample may be relatively unaffected while NRM is lost at a catastrophically high rate as a result of the alteration.

Unless such pTRM as is acquired is confined entirely to the part of the blocking temperature spectrum above the temperature reached by the subsequent pTRM check stage, the affect of pTRM impedance (*sensu stricto*) would be to cause the result of the pTRM check to be low relative to the original value. However, if NRM annihilation occurred during only the demagnetisation stage, the pTRM check value should be unaffected.

The values of the pTRM checks performed after pTRM impedance (*sensu lato*) was observed to occur in this study were usually (but not always) low relative to their expected values suggesting that the original interpretation of their cause is the correct one. With respect to both pTRM and NRM checks, the terms low, acceptable and high are somewhat subjective. The 10% level of acceptance advocated by Selkin and Tauxe (2000) was used as a yardstick in discussing the results produced by this study although its appropriateness was unclear. The extent to which these errors could be attributed purely to experimental uncertainties and consequently overlooked was another reason for performing the analysis described in the next chapter.

It was stressed earlier that the R factor (§ 2.4.2) was not intended as a quantitative measure of the reliability of an estimate. Some of the properties that count towards its value are unquestionably more important than others, and only estimates with maximum R factors would conventionally be regarded as wholly reliable. However, it was because so few of the estimates produced from this study satisfied this criterion that an objective means of comparing estimates, in the context of their apparent reliability, was developed. To facilitate the use of the R factor as a guide, the site average (SA) VDM estimates in table 4.24 are presented in order of decreasing mean R factor.

It will be shown in chapter 5 that the question of reliability is a complex one. The R factor is an indicator of the reliability of an estimate *as assessed by conventional criteria*. However, work presented in chapter 5 raises concern over the appropriateness of applying rigid criteria, in their current form, to the results of all palaeointensity analyses. The significance of this for the results presented in this chapter will be discussed in chapter 9.

Site	Component	Age (Ma)	VDM (10^{22} Am^2)	$\overline{R}$	$\sigma(H_{EST})/H_{EST}$	N
NE01*		90	5.4 ± 1.4	6.6 (8)	26%	3
NE01		90	5.3 ±1.3	5.25 (8)	26%	8
GS03		178	3.9 ± 0.5	5.2 (6)	13%	5
BD04	0-300	~127	7.9	5(7)		1
CR05*		200	7.4 ± 1.7	5 (8)	23%	2
CR08		200	5.6	5 (8)		1
LR01*	Normal	90	2.3 ± 0.8	5 (8)	35%	2
LR01	Reversed	~245	1.2	5 (8)		1
CR07		200	7.1 ± 1.3	4.5 (8)	18%	2
LR01	Normal	90	2.3 ± 1	4.1 (8)	43%	7
GB04	HBT	172	0.8	4 (6)		1
GB04	LBT	90	< 3.5	4 (6)		1
GS02		178	5.0	4 (6)		1
CR05		200	8.2 ± 1.2	4 (8)	15%	7
MM01		~200	8.2 ± 1.4	3.3 (8)	17%	3
GB06	LBT	90	< 14.9	3 (6)		1
YH01*	HBT	~250	7.1 ± 0.3	3 (7)	42%	3
YH01	LBT	post-250	< 4.5 ± 2.1	2.6 (7)	47%	8
GB01	LBT	90	< 4.9 ± 0.9	2.5 (6)	18%	2
GB05	LBT	90	< 6.2 ± 0.4	2.5 (6)	6%	2
GB07	LBT	90	< 4 ± 0.9	2.5 (6)	23%	2
YH01	HBT	~255	7.5 ± 2.6	2.5 (7)	35%	4
GB06	HBT	172	1.2 ± 0.4	2.25 (6)	33%	4
GB02	HBT	172	1.7 ± 0.1	2 (6)	6%	3
GB05	HBT	172	1.2	2 (6)		1

Table 4.24: All site average (SA) estimates produced by this study in descending order according to their R factor. Maximum possible R factor is shown in parentheses.
* denotes the mean of a preferentially selected subset of estimates

5. An Experimental Evaluation of the Thellier Method

5.1 Introduction

Despite the efforts of Coe *et al*. (1978) and Selkin and Tauxe (2000) to develop acceptance criteria, there is still some confusion surrounding the issue of what constitutes a reliable palaeointensity result.

The reliability of an estimate is generally judged by the statistical parameters associated with it (e.g. q, β, etc.) as well as the level of repeatability in the pTRM and NRM checks. Coe *et al*. (1978) developed these parameters but proposed no acceptance criteria based upon them specifically. The criteria of Selkin and Tauxe (2000), regarding them and the maximum allowable pTRM check discrepancies, were described in § 2.6.2 and referred to numerous times in chapter 4.

These were developed from Thellier analyses of submarine basalt glass (SBG) samples. The ferromagnetic content of these rocks was shown to usually consist of entirely SD Ti-poor titanomagnetite (Pick and Tauxe, 1994). It is therefore, not entirely unexpected that the criteria would appear somewhat strict when applied to the samples used in this study, which have a much larger average grain size and are therefore much more prone to non-ideal behaviour. However, these facts alone do not justify the adoption of more relaxed criteria. If the samples used here are, in actuality, almost wholly unreliable as palaeointensity recorders, then the criteria of Selkin and Tauxe (2000) are appropriate. The experiment described in this chapter was performed with the aim of contributing further to the argument over acceptance criteria.

This chapter presents the results of a simulated Thellier experiment conducted on a variety of samples that had previously been given a complete laboratory TRM. The aim of this analysis was to investigate the behaviour of the samples and the accuracy

of their results, in an experiment where the ideal result was known. The primary objective was to provide new acceptance criteria, regarding values of statistical parameters and maximum allowable pTRM and NRM check discrepancies, based upon *empirical* evidence of what constitutes sufficient reliability.

5.2 Experimental analysis

5.2.1 Procedure and initial results

A total of 14 samples, from 4 suites of intrusions described in chapter 3 and already analysed using the Thellier method on their NRM (chapter 4), were selected for use in a second, simulated Thellier analysis. Beforehand each was fully demagnetised by heating to 700°C and cooling in a zero field.

The remanence measured after this process was used to ascertain a minimum limit on the random errors produced by measuring. This limit was found to be ~ 1% of the TRM generated by cooling the sample from above T_C in a field of 50 μT. To allow for summation of errors in the analysis to come, differences between measured values and their checks greater than 4% of the total TRM were initially regarded as significant.

Before the full TRM was imparted, the samples were first subjected to the pTRM tail check described by Shcherbakova *et al* (2000) to help ascertain their domain state. Each was given a pTRM between 300°C and room temperature (T_R) and then demagnetised to the same temperature. The measured remanence after demagnetisation (the tail of the pTRM) was determined as a percentage of the remanence prior to demagnetisation. The results of the test are indicated in table 5.1, only two samples were found to have a significant tail (> 4%; Shcherbakova *et al*., 2000) indicating that PSD rather than SD grains (as in the rest) were the dominant remanence carriers below 300°C.

Sample	pTRM tail	Q	χ alteration	final TRM
CR0107A	1.1%	12.8	> 400°C	1.17
CR0502A	1.6%	18.8	> 400°C	1.52
CR0503A	1.4%	15.6	> 400°C	1.06
CR0703A	12.3%	19.1	N/A	0.93
GB0107C	-1.0%	5.9	N/A	1.02
GB0606B	-1.1%	7.7	N/A	1.01
GB0703B	-1.6%	13.5	N/A	0.88
GS0205B	8.6%	7.6	N/A	0.89
GS0206B	-0.1%	7.6	N/A	0.91
GS0301C	1.5%	7.6	N/A	0.90
GS0302A	-2.0%	8.1	N/A	0.91
LR0109B	-1.1%	10.2	> 400°C	1.15
NE0101C	-0.9%	11.4	> 400°C	1.02
NE0105B	-0.2%	13.2	> 400°C	1.10

Table 5.1: Initial results for all samples investigated. Q is the Koenigsberger ratio, final TRM refers to measured TRM, normalised to initial NRM, after the 600°C remagnetisation stage and should equal 1.

It is usually necessary to estimate the Koenigsberger ratio (Q) value from experimental results because H is not known (§ 4.3.3), however in this case the 'NRM' is actually a laboratory TRM. Values of Q for the samples used in this analysis are given in table 5.1, it is expected to range from < 1 in MD dominated assemblages to > 10 for SD grains (Dunlop and Özdemir, 1997).

Once the samples had been given an 'NRM' they were subject to a Thellier experiment, with 100°C steps and pTRM and NRM checks at every stage. The laboratory field applied to the samples during remagnetisation stages had the same strength and direction as that used to impart the 'NRM.' The experiment was continued up to 600°C at which temperature the NRM was completely removed. After every heating step and subsequent measurement, the room temperature susceptibility (§ 2.4.2.3) was measured allowing a continuous check for alteration of bulk magnetic properties. The temperature at which significant (> 10%) changes in this parameter were observed are indicated in table 5.1 and appendix 6.

Sample CR0703A has a relatively large pTRM tail suggesting that PSD grains are the remanence carriers between 300°C and room temperature (T_R) but has a very high Q ratio. This could be because both PSD and SD grains are present in the assemblage. Most other samples seem to be dominated by SD and small PSD grains and therefore should display linear NRM-TRM plots.

Significant alteration of magnetic properties as denoted by changes in χ of > 10% is confined to temperatures > 400°C in less than half of the samples. Interestingly, these changes, which are all increases, are evident in those samples that also display an increase in TRM capacity (final TRM > 1) by 600°C suggesting that the same grains are responsible. Those samples which display a decrease in TRM capacity (final TRM < 1) are not accompanied by a significant change in susceptibility. Magnetic susceptibility is inversely proportional to coercivity and so is dominated by the softer remanence carriers in an assemblage. It is possible therefore that changes in bulk susceptibility of a sample can occur independently of changes in its capacity to acquire a TRM. A plausible explanation for the observation made here is that significant increases in χ reflect alteration affecting the entire magnetic assemblage (possibly oxidation), while significant decreases in TRM capacity are due to alteration of the high coercivity grains alone. This highlights the need to employ caution when using susceptibility measurements alone as a check on alteration during a real Thellier experiment.

5.2.2 Results of the Thellier analysis

Table 5.2 gives the estimates and their associated statistical parameters when no criteria are applied and all the points were used. Most of the samples gave estimates within 10% of the actual value and the application of a simple criterion requiring the maximum curvature to be less than 30% removes three of the worst estimates (along with a reasonably accurate estimate). However, the estimate produced by sample GB0703B, despite being somewhat inaccurate, was accompanied by good all-round statistics and could not be filtered out by any reasonable criteria.

Sample	H_{EST} (μT)	ΔH_{EST}	g	q	β	Max pTRM check	Max NRM check	Mean pTRM check	Mean NRM check	Max curvature	R(8)
CR0107A	43.9	-12%	0.78	7.2	0.11	-7%	5%	-1.7%	0.3%	52%	5
CR0502A	34.8	-30%	0.81	6.6	0.12	-6%	5%	-2.3%	0.6%	51%	5
CR0503A	52.7	5%	0.84	5.6	0.15	13%	-2%	2.8%	-0.9%	47%	4
CR0703A	54.6	9%	0.47	14.1	0.03	5%	-4%	1.9%	-1.2%	4%	8
GB0107C	48.9	-2%	0.81	14.1	0.06	5%	-3%	1.9%	-0.6%	21%	7
GB0606B	48.2	-4%	0.81	14.8	0.05	10%	-4%	3.9%	-1.3%	21%	7
GB0703B	58	16%	0.69	18.7	0.04	4%	-2%	3.5%	-1.3%	4%	8
GS0205B	56	12%	0.47	15.3	0.03	8%	-4%	4.2%	-1.4%	5%	8
GS0206B	54.5	9%	0.42	20.6	0.02	8%	-2%	4.2%	-0.8%	4%	8
GS0301C	55.2	10%	0.52	8.6	0.06	12%	-5%	4.8%	-1.4%	17%	7
GS0302A	54.9	10%	0.51	12.3	0.04	12%	-2%	5.5%	-0.6%	12%	7
LR0109B	44	-12%	0.81	8.6	0.09	7%	-5%	4.0%	-1.4%	32%	6
NE0101C	50.5	1%	0.7	6	0.11	7%	-3%	3.9%	-1.1%	21%	5
NE0105B	49.2	-2%	0.69	4.8	0.14	19%	-3%	6.5%	-1.4%	22%	5

Table 5.2: Estimates and their associated statistical parameters when all points are used. ΔH_{EST} refers to the inaccuracy of the estimate relative to the known 'palaeointensity'. pTRM and NRM check figures refer to the discrepancies between the check and the original value. The maximum curvature value refers to the criterion introduced by Coe et al. (1978) and should be less than 20%.

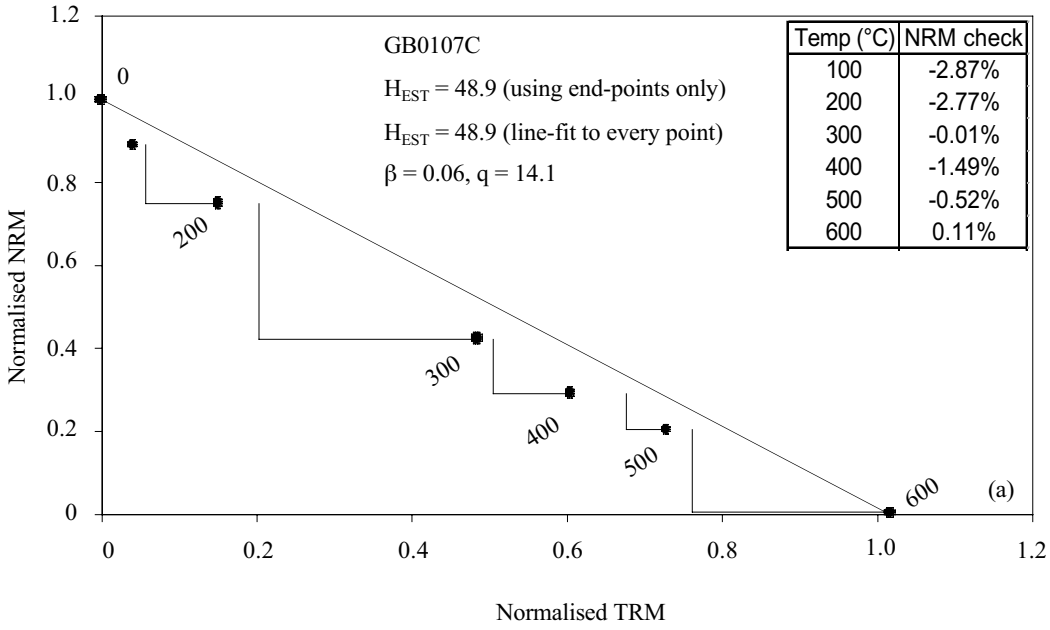

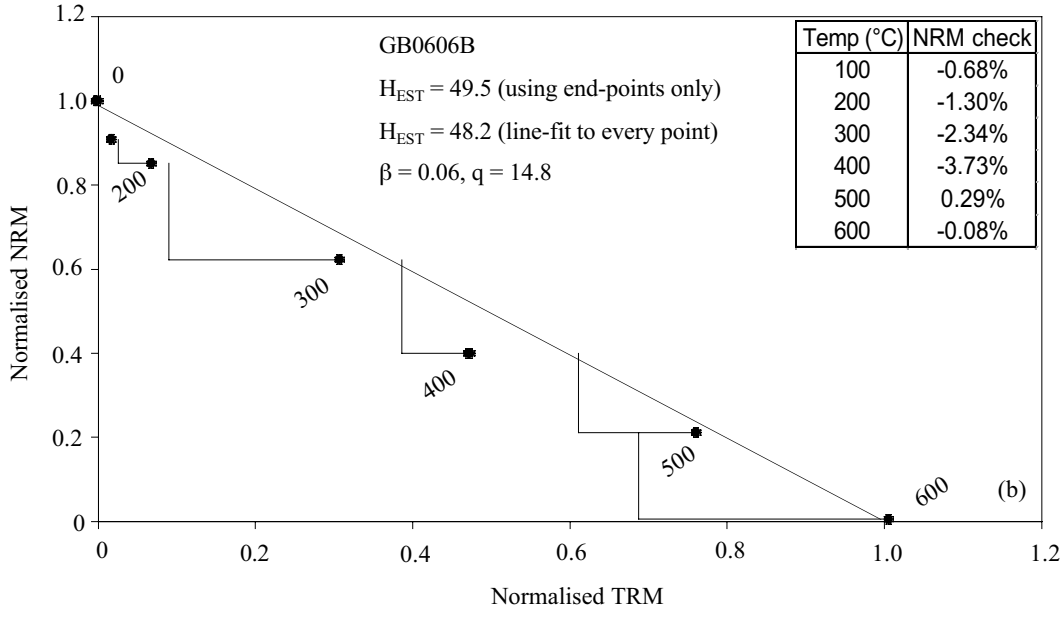

Figure 5.1: NRM-TRM plots for two samples giving accurate overall estimate.

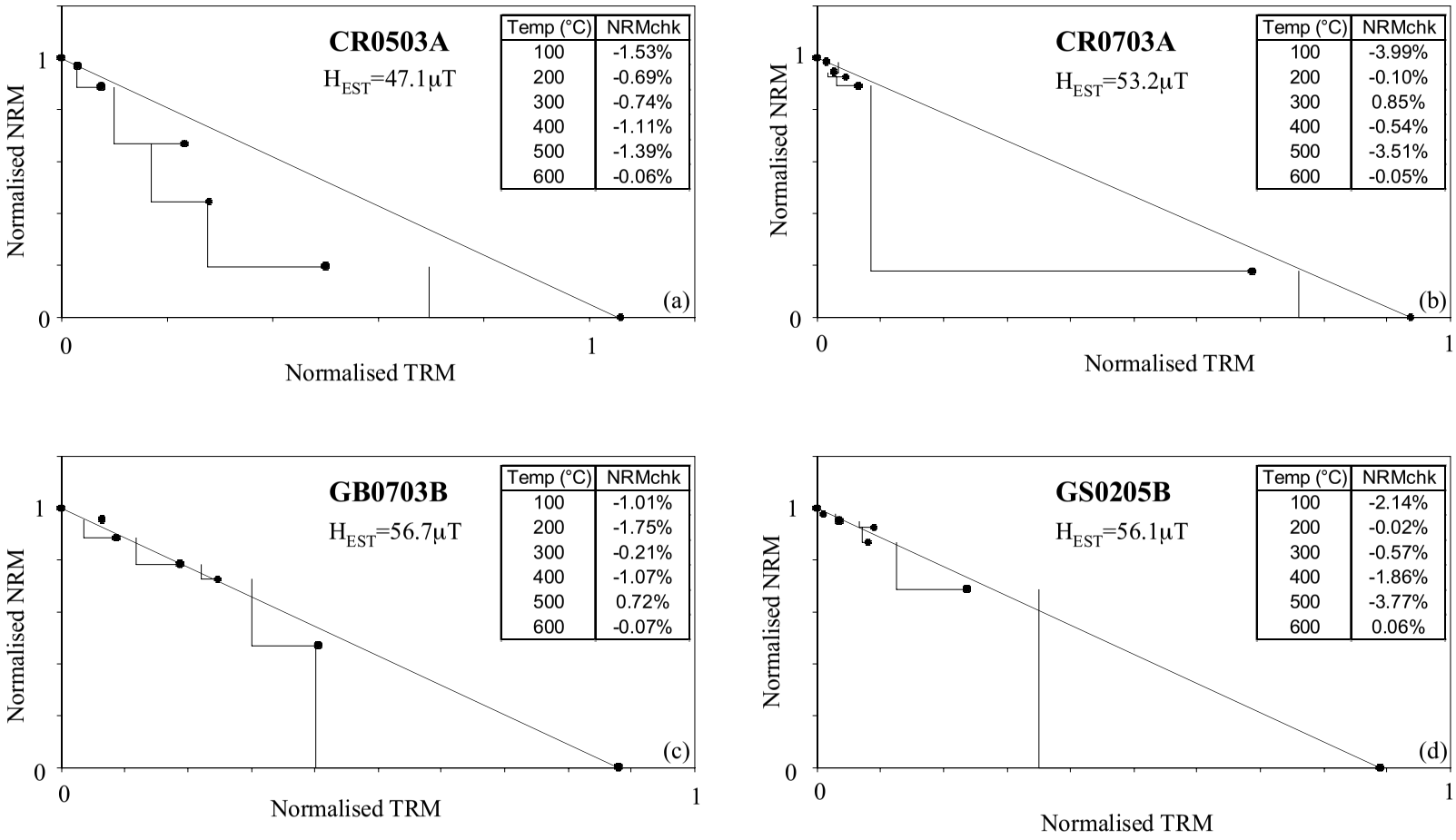

Figure 5.2 (a) - (j): Full NRM-TRM plots of ten samples included in the Thellier analysis (see figures 5.1 and 5.3 for rest). H_{EST} refers to the estimate of field strength that results if just the two end points are used. Heatings were done in 100°C steps.

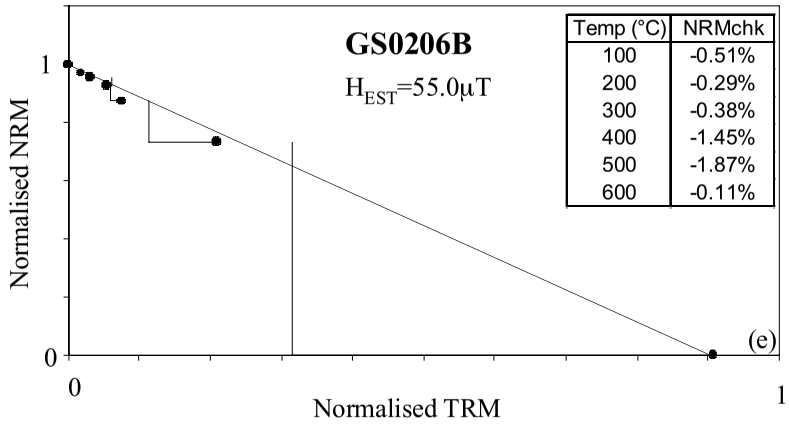

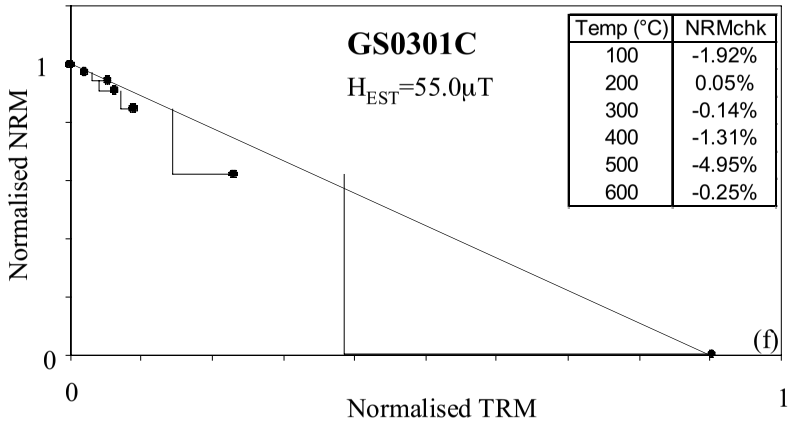

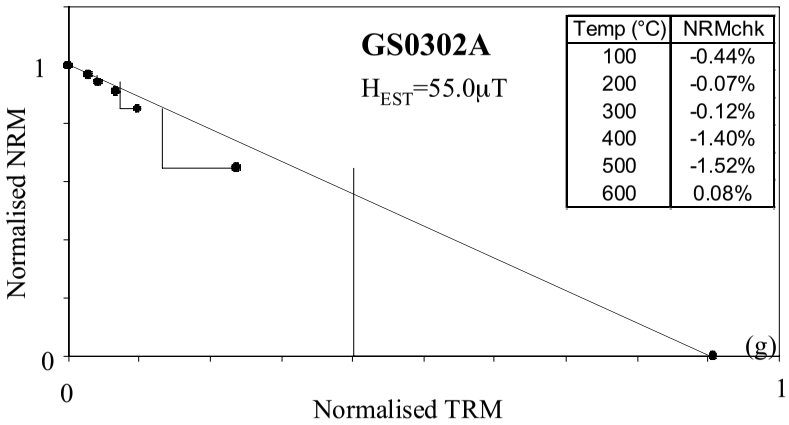

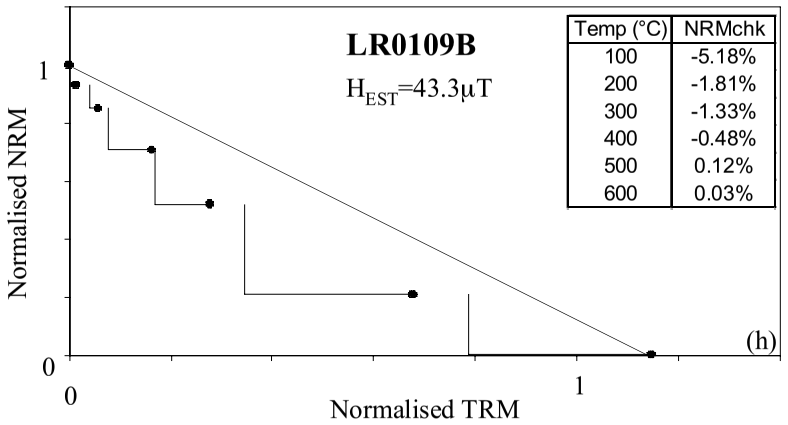

Figure 5.2 (cont'd).

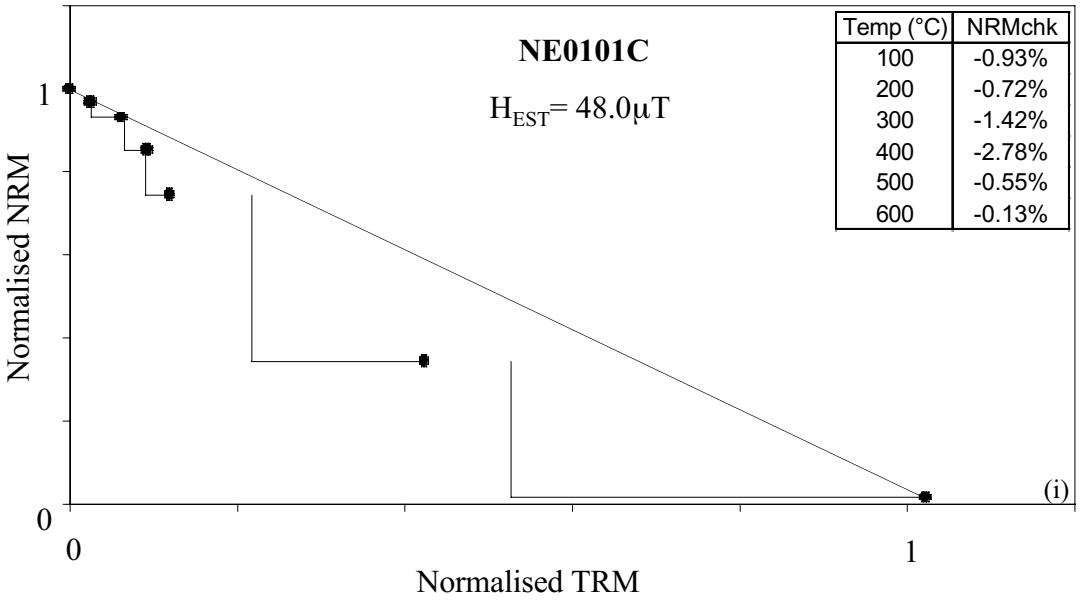

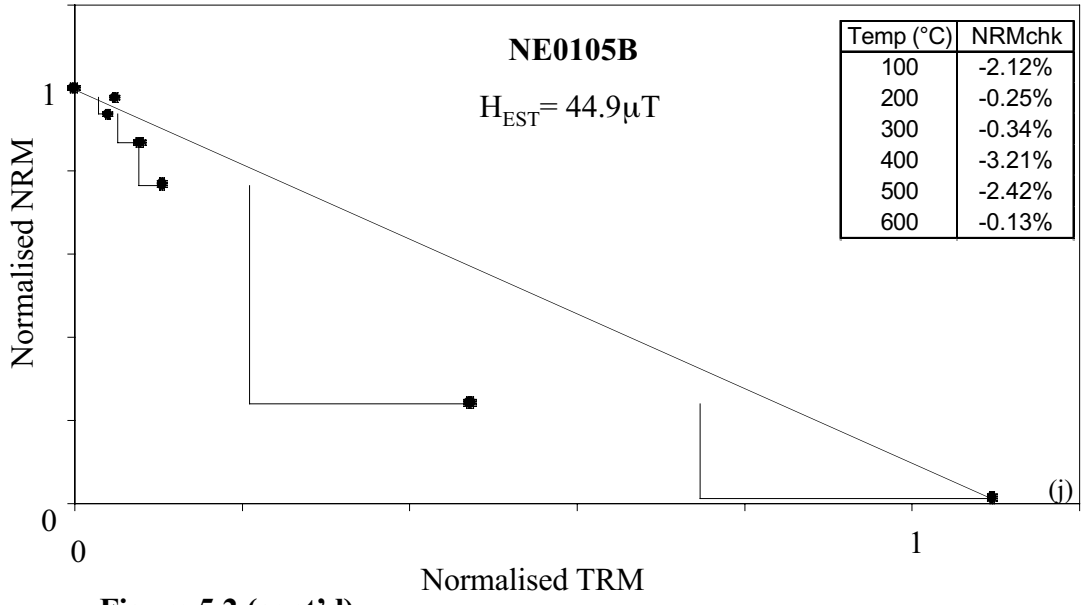

Figure 5.2 (cont'd).

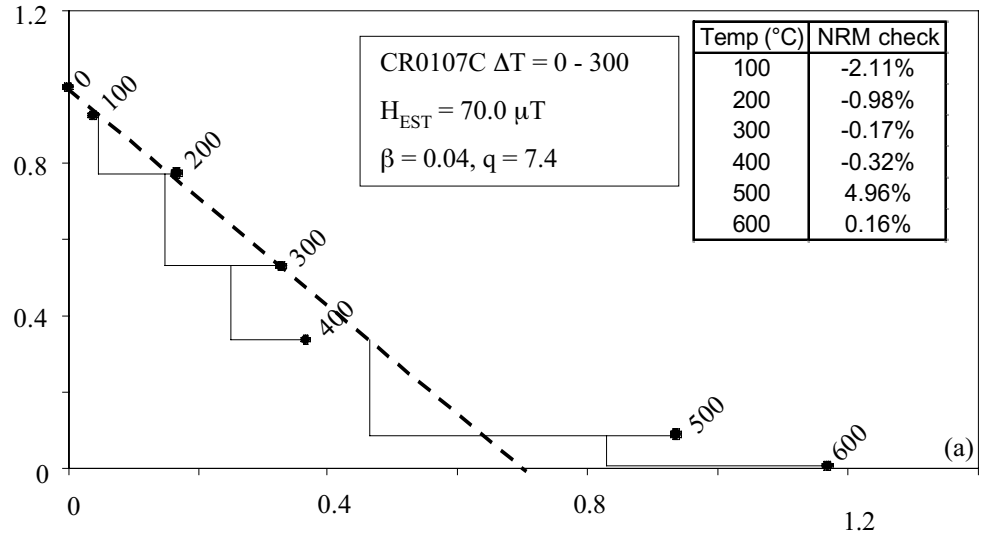

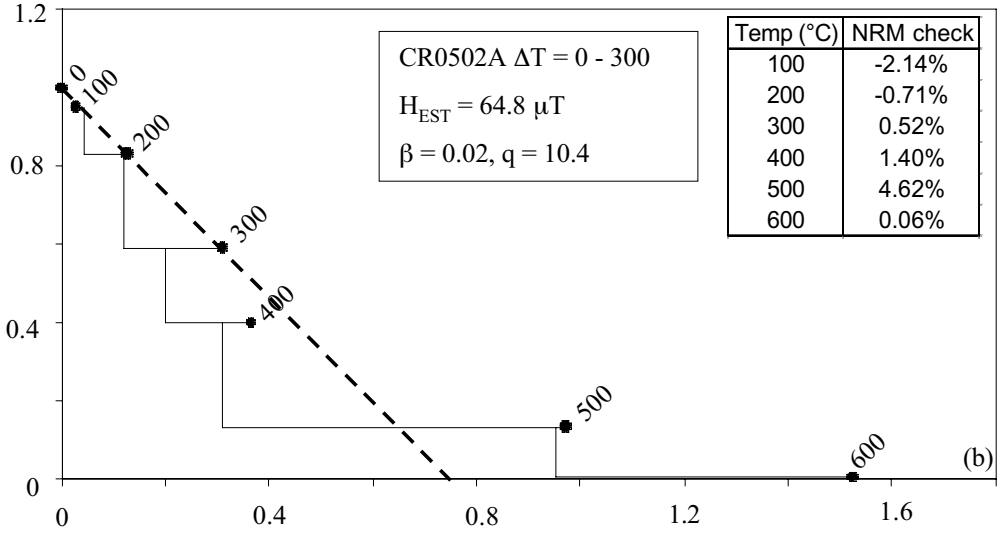

Figure 5.3: Examples of NRM-TRM plots for two samples that display linear low temperature portions with an artificially high slope.

It is interesting to note that the four estimates achieving a maximum R factor are offset from the true value by ~ 10% while others with lower R factors are more accurate. This suggests that, in this instance, the application of rigid acceptance criteria should be questioned. Further support for this notion is provided later in this section although a full discussion is not given until chapter 9.

Allowing for an error of 4% in the final TRM, only three samples give totally reliable estimates through the entire temperature range of the experiment (table 5.1). One of these (NE0101C) also displays a significant increase in its susceptibility and would normally be discarded from an analysis on this basis. NRM-TRM plots of the two samples that give unquestionably reliable estimates are shown in figure 5.1. In both of these, all the points between 0 and 600 fall below the (true) line joining the two end-points. Additionally most of the pTRM checks are higher than the initial pTRM values and the NRM checks are lower. These general characteristics were also observed in the NRM-TRM plots of every other sample except two (figure 5.2). Changing conditions that could produce these results will be discussed in § 5.3.

Despite also displaying convex-down plots, samples CR0107A and CR0502A differed from the rest in exhibiting significant low and high pTRM check and NRM check discrepancies respectively. Given that the field used during the experiment was parallel to that used in imparting the original TRM, high NRM checks could be diagnostic of CRM formation in the laboratory and would explain the very large observed pTRM acquisition at high temperature. Nevertheless, if the plots are truncated before they lose linearity and the portion 0°C to 300°C is retained, estimates can be recovered that, on the basis of q and β values and the minimal pTRM and NRM check discrepancies, appear reliable (figure 5.3). These estimates are however, 30 – 40% higher than the real value. It is a concerning observation that in a real Thellier analysis both of these samples would be assumed to be recording reliable estimates.

Figure 5.2 suggests that this surprising observation may be repeated in the results of other samples. To test this, a set of criteria were applied to the results requiring the NRM-TRM plot to be truncated at 300°C or above ($N \geq 4$) so that $\beta < 0.10$ and the maximum pTRM check discrepancy was less than 10%. Those passing are given in table 5.3 and necessarily have a maximum associated R factor of 8.

Sample	H_{EST} (μT)	q	β	ΔT	Max pTRM check	Max NRM check	Mean pTRM check	Mean NRM check
CR0107A	70.0	7.4	0.04	0-300	1.6%	-2.1%	1.5%	1.6%
CR0502A	64.8	10.4	0.02	0-300	0.7%	-2.1%	0.6%	1.4%
CR0503A	71.8	4.4	0.04	0-300	1.6%	-1.5%	1.2%	1.1%
CR0703A	59.2	8.8	0.02	0-500	1.8%	-4.0%	0.9%	1.8%
GB0703B	57.9	2.5	0.08	0-400	2.2%	-1.7%	2.2%	1.0%
GS0205B	65.5	3.2	0.06	0-500	3.3%	-3.8%	1.3%	1.7%
GS0301C	84.7	1.2	0.09	0-400	0.5%	-1.9%	0.3%	0.9%
GS0302A	75.0	9.8	0.02	0-500	2.5%	-1.5%	1.3%	0.5%
LR0109B	81.6	5.3	0.06	0-400	2.1%	-5.2%	1.3%	2.2%

Table 5.3: The results of those portions of NRM-TRM plots that pass the criteria described in text.

The result of unquestionably accepting those estimates fulfilling these criteria is obviously disastrous yielding a mean value some 40% higher than reality and outside of error bounds.

After excluding the two samples that may have acquired a CRM during the experiment, the remaining samples were generally observed to give their most accurate estimate if every point between 0°C and 600°C was used to obtain it. The criterion requiring that the maximum curvature in the slope be less than 30% is by far the most effective at removing the inaccurate estimates (table 5.2). The mean estimate is then 52 ± 4 μT, which is quite acceptable. There is very little difference between the estimates derived from best-fit lines through all the points and those just connecting the end points (table 5.1). The mean of the (filtered) estimates taken from this latter group is 53 ± 4 μT.

5.2.3 Discussion

The results from the simulated Thellier analysis were somewhat surprising. It was expected that thermally stabilised SD remanence carriers would exhibit linear NRM-TRM plots through most of their blocking temperature spectra and that pTRM and NRM check discrepancies would take the form of random errors around the zero value. Instead, convex down NRM-TRM plots were generally produced with a tendency for high and low pTRM and NRM checks respectively.

Before it is possible to conceive any criteria that would be applicable to the results of a Thellier experiment on samples carrying a true NRM, it is necessary to investigate the cause of the non-ideal behaviour in these samples. In particular, the likelihood of encountering the convex-down plots, which cause the estimates to be high when the plot is truncated below T_C, in untreated samples needs to be ascertained.

The next section is concerned with explaining the occurrence of the non-ideal behaviour observed in the results of this experiment. The implications of these results to studies of samples in which the field intensity is unknown is addressed in § 5.4.

5.3 Discussion of non-ideal behaviour

5.3.1 Possible causes of non-ideal behaviour

All but three (CR0107A, CR0502A, and CR0503A) of the samples primarily displayed pTRM checks higher and NRM checks lower than the original values (appendix 6). A further sample (GB0606B) also displayed a single, significantly low pTRM check at 500°C. Additionally, the sample LR0109B may also be considered separately from the others: the exaggerated curvature it exhibits and the low estimate

it provides suggests that significant irreversible alteration affected it during the experiment.

Each of the remaining 9 samples give reasonably accurate estimates (within 12%; table 5.2) and exhibit similar behaviour, which will be referred to from here on as quasi-multi-domain (QMD) behaviour, on account of its similarity with that observed in MD grains (§ 2.4.4).

While the rock magnetic methods used in this analysis were limited in number, they both targeted the remanence carriers directly and gave no indication of a significant MD fraction. However, because of their origin as alteration products rather than as primary crystals, it is possible that the remanence carriers observed in these samples are not non-interacting SD grains dominated by shape anisotropy, but MD grains governed by magnetostrictive anisotropy with correspondingly high coercivities (§ 2.6.4). If this were true, it is not clear if it could be responsible for generating this non-ideal behaviour (§ 5.4).

Hill and Shaw (2000) observed behaviour very similar to that found here in recent Hawaiian lava samples recording the known geomagnetic field. They tentatively proposed the cause as a high temperature CRM formed during initial cooling of the lava. This is unlikely to be the cause in this instance. It is difficult to imagine chemical changes occurring in so many annealed samples during the cooling phase of laboratory treatment. The remanence is very likely a pure TRM.

Irreversible chemical and/or physical alteration induced in the laboratory seems an unlikely culprit for producing QMD behaviour. The alteration would have to act in two opposite senses during the experiment with fortunate coincidence providing the mechanism for them approximately cancelling one another out. Irreversible alteration is dominant at high temperatures for samples CR0107A and CR0502A and may play a secondary role in other samples but cannot be the primary cause of the behaviour that is being investigated.

Hypothetically, reversible alteration could explain the behaviour although a physical mechanism to account for it is somewhat elusive. The capacity of most of the samples to acquire TRM between T_C and T_R after the Thellier experiment is similar to that prior to it. It is only the capacity of the samples to retain TRM at temperatures below T_C that has changed significantly through the experiment. Reversible alteration could cause the total remanent magnetisation of the sample to remain essentially constant while its blocking and unblocking temperature spectrum alters progressively through the experiment.

5.3.2 An examination of models to explain the behaviour

An explanatory model for QMD behaviour must include: the high pTRM check/low NRM checks, the abrupt loss of NRM without concomitant acquisition of pTRM at low temperature, the reverse at high temperatures, and the non-modification of total TRM acquisition capacity. A series of models with the potential for explaining QMD behaviour will be examined here.

5.3.2.1 Absolute changes in pTRM capacity

Two similar techniques for correcting NRM-TRM plots for irreversible alteration were advocated by Valet *et al*. (1996) and McClelland and Briden (1996). These assume that the anomalous position of a point is a function of the cumulative anomalies of each pTRM check calculated prior to that point and use NRM checks to show that alteration is restricted to grains with T_{UB} below the current temperature of demagnetisation. There are two major problems with such techniques. The first is that there is no check for the type of alteration that occurred in this analysis. Marginally low NRM checks would be taken as meaning that the NRM had undergone no alteration, and the high pTRM checks would be inferred to mean that pTRM capacity had increased relative to the NRM through the experiment. The

opposite is true for QMD samples at low temperatures, and therefore the correction would tend to push the points away from their true value.

The second problem with this type of correction technique is that a point is only corrected for alteration that occurred between T_R and the temperature that the subsequent pTRM check heating stage reached. For example, a 300°C point defined by 300 and 301 measurements and followed by a 202 pTRM check stage would only be corrected by the alteration observed to occur between T_R and 200°C. If there had been any change in pTRM capacity between 200°C and 300°C, this could not be accounted for.

Table 5.4 shows the effect of applying the correction on the intensity estimates and β values of all the samples. In most cases, it is observed to lower the β value, and consequently make the estimate appear most reliable, while making the estimate itself more inaccurate. This would obviously be a disastrous result for a normal Thellier analysis attempting to obtain reliable estimates.

The major exceptions to this observation are the results from sample LR0109B which are both improved markedly. Although the correction does not generate a perfectly linear plot (figure 5.4), it does suggest that the exaggerated curvature evident in the NRM-TRM plot of this sample is primarily a product of irreversible alteration in its capacity to acquire pTRM, rather than the QMD effect.

Sample	H_{EST} (μT)	Δ H_{EST} (μT)	β	Δ β
CR0107A*	44.8	1.1	0.11	0.01
CR0502A*	33.2	-1.5	0.13	0.00
CR0503A*	53.7	1.4	0.09	-0.06
CR0703A	53.1	-1.2	0.01	-0.02
GB0107C	53.3	4.8	0.03	-0.03
GB0606B*	51.7	3.7	0.05	0.00
GB0703B	63.1	6.1	0.07	0.03
GS0205B	58.6	3.2	0.02	0.00
GS0206B	60.3	6.3	0.02	0.00
GS0301C	60.2	5.4	0.01	-0.05
GS0302A	66.6	11.9	0.01	-0.03
LR0109B*	50.4	6.6	0.07	-0.02
NE0101C	57.1	7.0	0.09	-0.02
NE0105B	60.7	12.0	0.07	-0.07

Table 5.4: Revised estimates using the correction for absolute alteration proposed by Valet *et al*. (1996) and McClelland and Briden (1996). The differences in results between those using the uncorrected data for all temperature steps are also shown. Asterisk denotes sample not displaying pure QMD behaviour

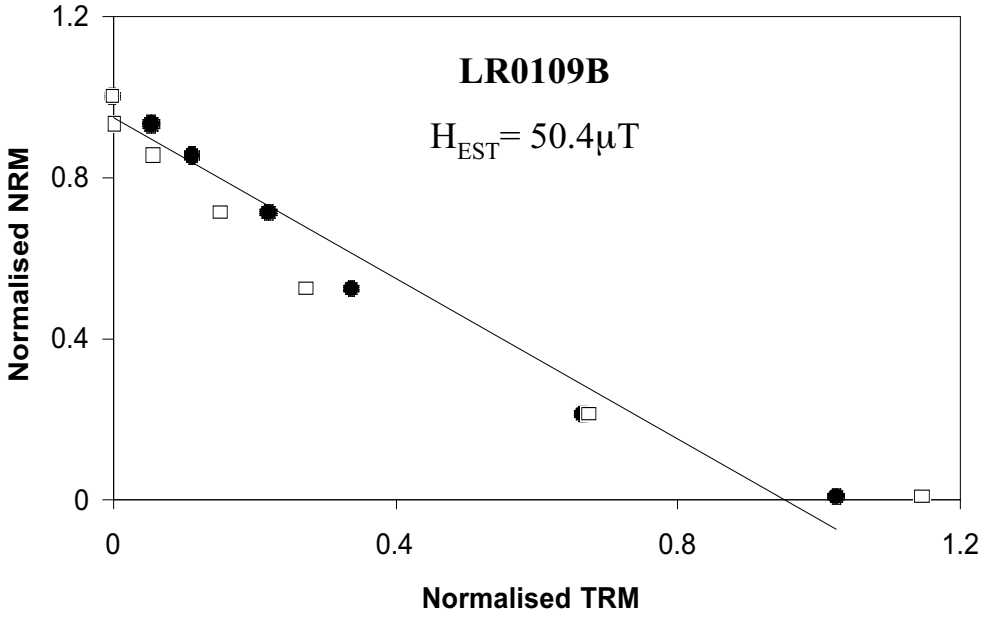

Figure 5.4: NRM-TRM plots for samples before (squares) and after (circles) correction for absolute changes in pTRM capacity was applied to sample LR0109B. Quoted palaeointensity is that from best fit line (shown) through all the corrected points.

5.3.2.2 Progressive NRM removal

An artificially steep slope together with high pTRM checks and low NRM checks can be explained by alteration in which every second heating step to the same temperature (i.e. the remagnetisation step) further demagnetises some remanence but does not replace it sufficiently with pTRM during cooling.

The sequence of events would then be:

- 100 demagnetisation – NRM lost
- 101 remagnetisation – more NRM lost, pTRM acquired
- pTRM gained at 100°C is determined by 101 – 100 and is low
- 103 NRM check – pTRM (and possibly some more NRM) lost, 103 < 100
- 200 demagnetisation – NRM lost
- 201 remagnetisation – more NRM lost, pTRM acquired
- 102 demagnetisation – pTRM acquired below 100°C during 201 (and perhaps more) is removed
- pTRM check is calculated from 201-102, providing that 102 removed at least what is should (i.e. 102 measurement is less than or equal to its unaltered value) then the pTRM check will appear high relative to the value of 101-100 to which it is compared.

If, as this model assumes, the capacity of each sample to acquire pTRM is unimpeded by the alteration, then the only cause of the steep slope is the loss of NRM during the remagnetisation step. It then follows that if each pTRM point is calculated by subtracting the NRM check, rather than the original NRM, from the remagnetisation measurement (e.g. 101 – 103 rather than 101 – 100), then the slope should be corrected or, if excess NRM loss also occurred during the NRM check as well, actually be made shallow.

This correction was attempted for all samples and it was found that, although the slope was brought marginally closer to unity, the correction was grossly insufficient except for the 100°C point of a few samples. This implies that although progressive NRM removal may be a factor in some aspects of this behaviour, the dominant process responsible for generating the initial steep portions is the loss of pTRM acquisition capacity below the heating temperature. Simply, pTRM acquisition during the remagnetisation stage is inhibited.

The only explanation for the low NRM checks is that NRM is being progressively removed subsequent to the original demagnetisation step. Although this process is not the dominant cause of the initial steep slope observed in QMD samples, it may be causing the pTRM checks to appear higher than the original pTRM imparted.

If this is the case, then the anomaly between a pTRM check and the original should be *at least* corrected by making allowances for the NRM reported missing by the NRM checks. For example, at 100°C: (101-100) + (100-103) should be greater than or equal to (201-102). If all the excess NRM loss occurred during the remagnetisation heating stage (101 and 201 in this example), the two should be equal. If some further NRM loss occurred between the first remagnetisation stage (101) and the NRM check measurements (103), then the correction would overcompensate and the new pTRM check would be less than the revised pTRM. Table 5.5 shows the results for all the samples.

Temp (°C)	CR0107A*	CR0502A*	CR0503A*	CR0703A	GB0107C	GB0606B*	GB0703B
100	-1.7%	-0.8%	-2.4%	-4.0%	-1.0%	-1.4%	0.1%
200	-2.8%	-1.5%	1.9%	-2.4%	2.6%	0.4%	0.8%
300	-7.8%	-10.7%	-7.0%	-0.6%	2.1%	5.5%	3.7%
400	9.3%	-4.1%	-1.6%	1.7%	5.6%	10.3%	4.2%
500	-5.8%	2.6%	17.9%	3.9%	2.8%	-7.0%	0.3%
Temp (°C)	GS0205B	GS0206B	GS0301C	GS0302A	LR0109B*	NE0101C	NE0105B
100	-1.1%	1.7%	0.0%	2.0%	-3.2%	-1.7%	-2.8%
200	3.6%	1.9%	-1.9%	2.7%	0.2%	0.9%	-1.6%
300	1.0%	1.5%	-0.3%	0.7%	-0.2%	-1.2%	-0.7%
400	2.6%	2.6%	4.1%	1.9%	6.0%	7.0%	7.0%
500	8.0%	8.7%	10.8%	14.9%	11.2%	9.8%	24.9%

Table 5.5: pTRM minus pTRM checks when former is corrected for excess NRM loss by alteration during the remagnetisation stage. Asterisk denotes sample not exhibiting pure QMD behaviour.

This technique appears partially effective at low temperatures but is certainly not at higher ones; large positive anomalies remain for many samples especially at 400°C and 500°C showing that pTRM checks are still high after this correction. Consequently, progressive NRM removal during the remagnetisation may play a minor role in causing all features of QMD behaviour but is definitely not the primary cause of either the convex-down plots or the high pTRM checks.

5.3.2.3 Demagnetisation bias

Throughout this study, pTRM checks are calculated by subtracting the pTRM check demagnetisation stage measurement from the higher temperature remagnetisation stage, e.g. 201 – 102 for the 100°C pTRM check. Therefore, a high pTRM check value could result from stage 102 removing more pTRM than was acquired during 101. This is consistent with the tendency, evident in the steep initial slopes of QMD NRM-TRM plots, of TRM to be removed easier than it is acquired during this experiment.

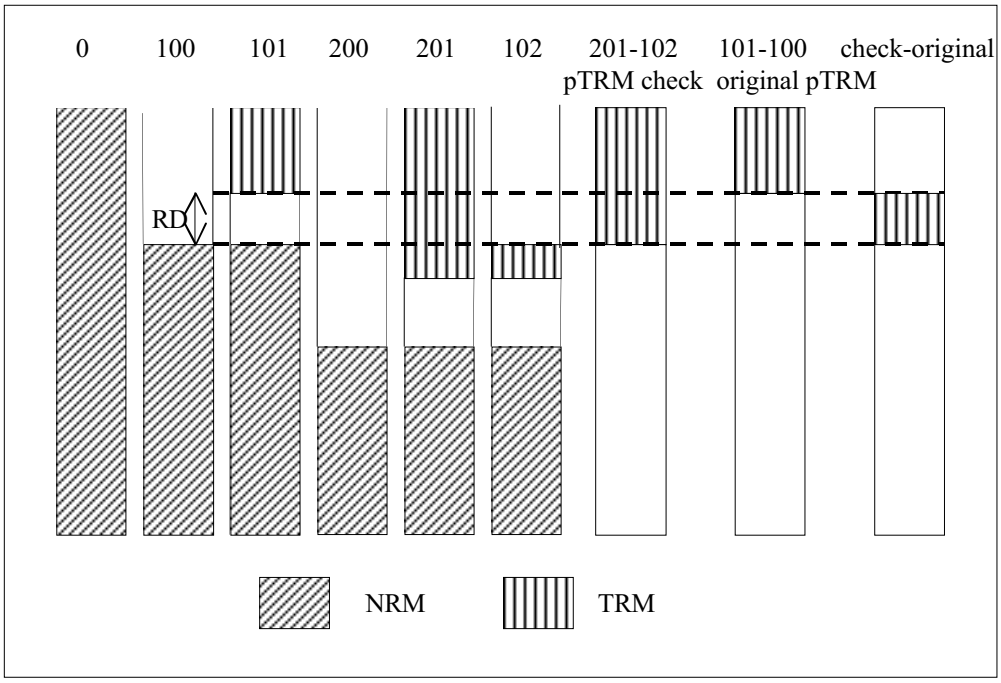

Figure 5.5: Schematic diagram showing that the pTRM check anomaly is the same as the RD experienced by the initial demagnetisation stage if demagnetisation bias is present.

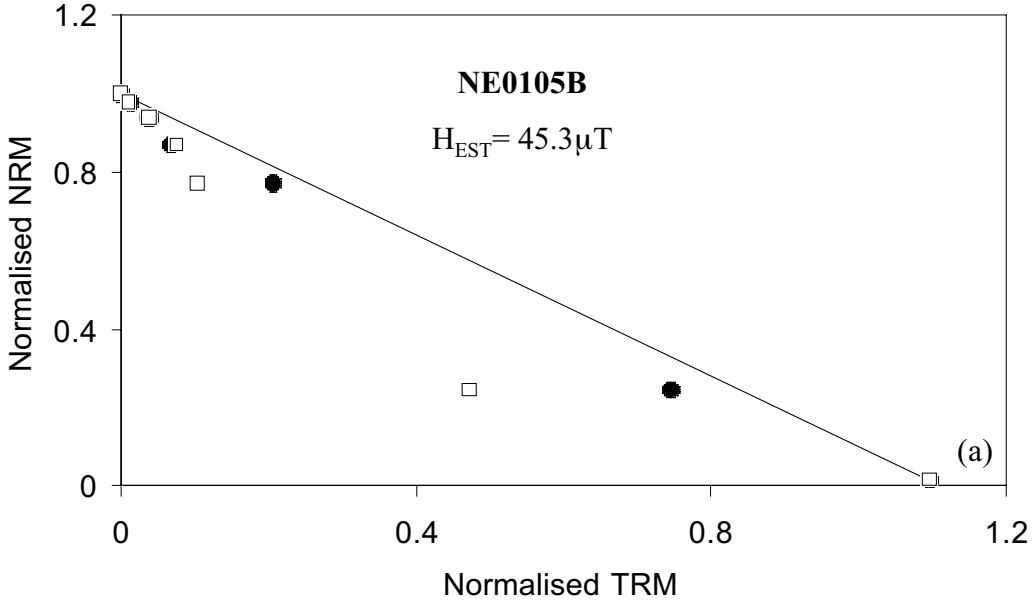

Figure 5.6 (a) - (i): NRM-TRM plots for QMD samples before (squares) and after (circles) the demagnetisation bias correction. Lines are joining the end points of the plot, quoted palaeointensities are those from best fit line through all the corrected points.

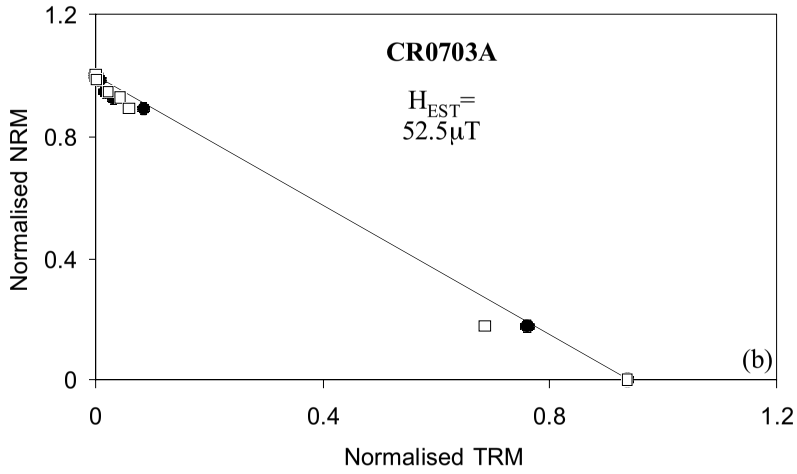

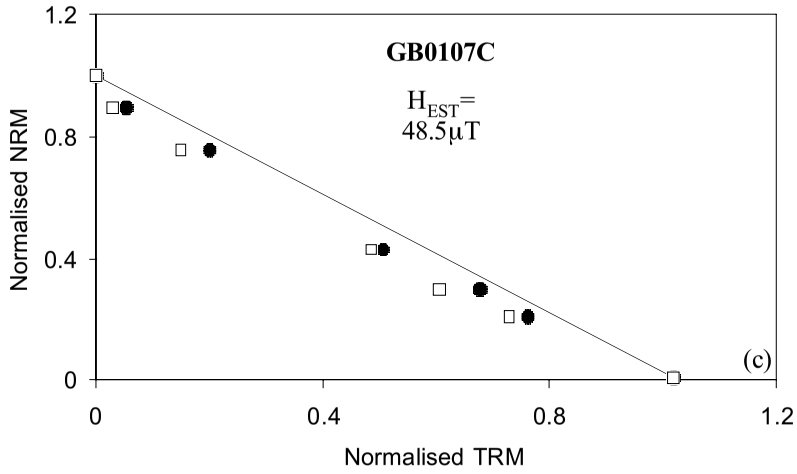

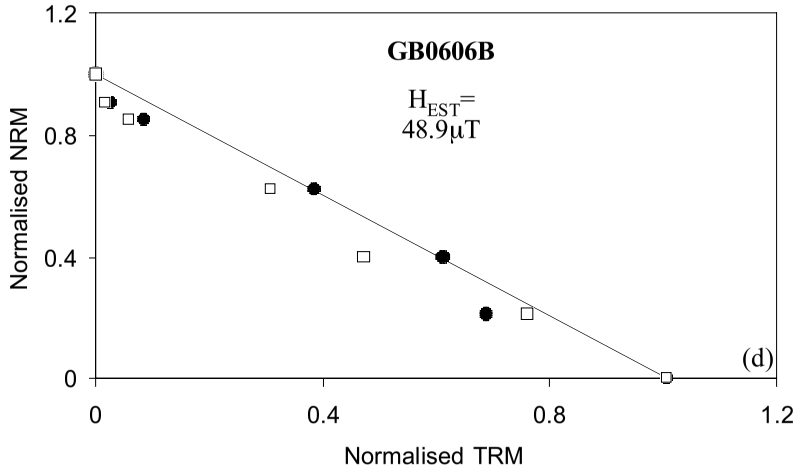

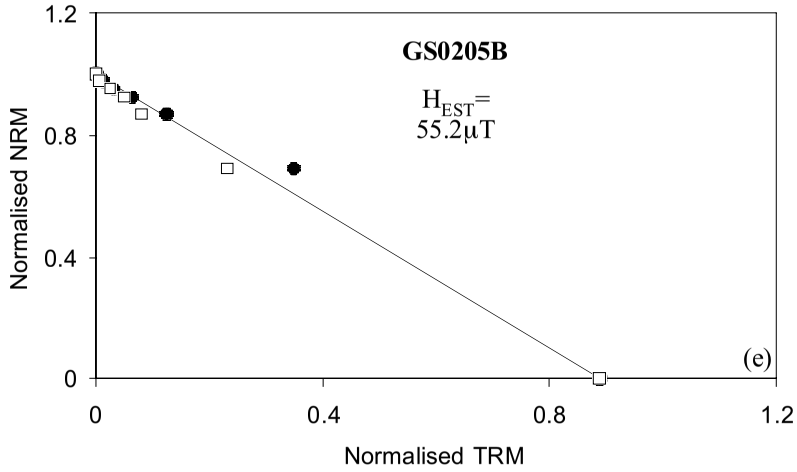

Figure 5.6 cont'd

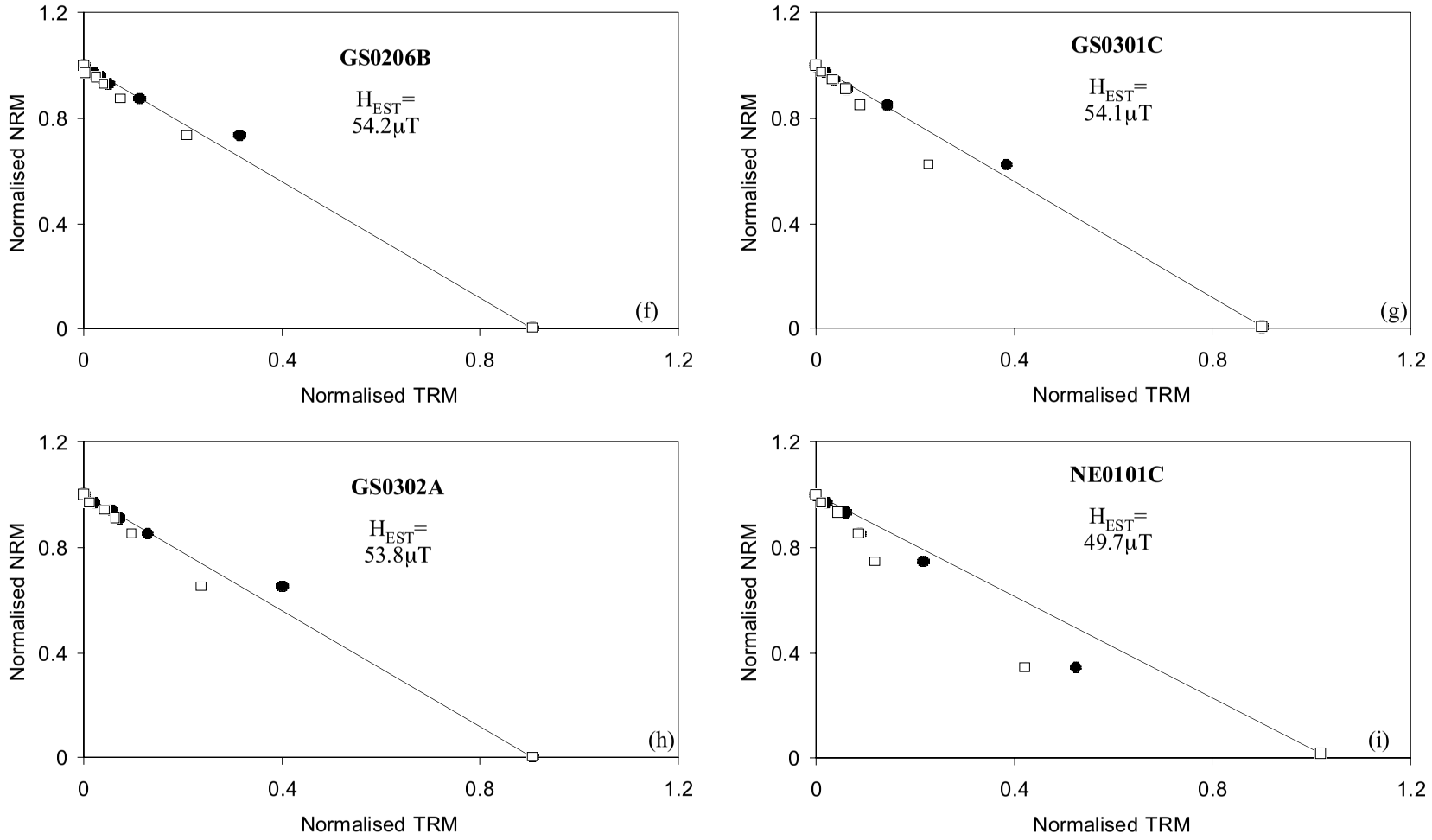

Figure 5.6 cont'd

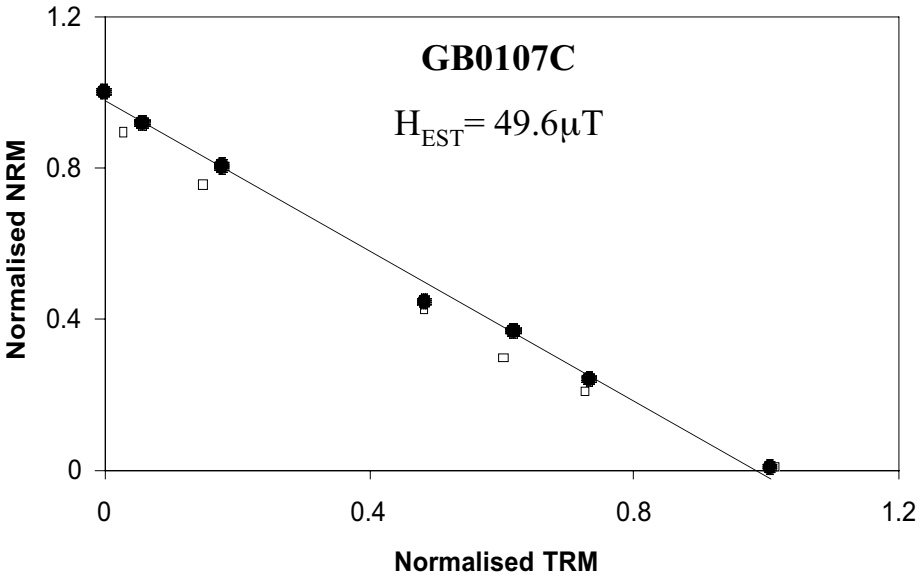

Figure 5.7: NRM-TRM plots for samples before (squares) and after (circles) corrections for demagnetisation bias and progressive NRM removal were applied to sample GB0107C Quoted palaeointensity is that from best fit line (shown) through all the corrected points.

	Before correction				After correction			
Sample	H_{EST} (μT)	β	Max $\|d_{TRM}\|$	Mean d_{TRM}	H_{EST} (μT)	β	Max $\|d_{TRM}\|$	Mean d_{TRM}
CR0107A*	43.7	0.11	0.41	-0.19	45.4	0.13	0.31	-0.20
CR0502A*	34.7	0.12	0.55	-0.28	34.4	0.14	0.61	-0.32
CR0503A*	52.3	0.15	0.35	-0.17	49.3	0.10	0.35	-0.17
CR0703A	54.3	0.03	0.09	-0.04	52.5	0.02	0.04	-0.02
GB0107C	48.6	0.06	0.12	-0.10	48.5	0.04	0.08	-0.06
GB0606B*	48.0	0.06	0.13	-0.08	48.9	0.05	0.11	-0.05
GB0703B	57.0	0.03	0.06	-0.02	58.0	0.04	0.07	0.00
GS0205B	55.5	0.02	0.04	-0.03	55.2	0.04	0.07	0.01
GS0206B	54.0	0.02	0.04	-0.03	54.2	0.04	0.07	0.01
GS0301C	54.8	0.06	0.12	-0.04	54.1	0.03	0.04	0.00
GS0302A	54.6	0.04	0.08	-0.03	53.8	0.04	0.08	0.01
LR0109B*	43.9	0.09	0.28	-0.18	43.0	0.07	0.21	-0.13
NE0101C	50.1	0.11	0.26	-0.10	49.7	0.06	0.16	-0.06
NE0105B	48.7	0.14	0.37	-0.13	45.3	0.04	0.10	-0.05

Table 5.6: Estimates and parameters for each sample prior to and after demagnetisation biasing correction. Asterisk denotes sample not displaying definite QMD behaviour

If this were the case, the discrepancy between the pTRM check and the original pTRM would be a measure of the extent to which demagnetisation was favoured over remagnetisation at the temperature of the check, a value called the remanence deficit (RD) here. Assuming that the same value of RD is retained during the pTRM check stage (102 in this example) as that during the initial demagnetisation stage (100 in this example), it could be used to correct the NRM measurement and generate an accurately sloping NRM-TRM plot. There is therefore a diagnostic test to show whether 'demagnetisation bias' is the dominant source of QMD. This correction obviously relies upon each sample reaching the same temperature during numerous heating phases. This was ensured by holding the oven at the maximum temperature for a sufficient time (> 30 minutes) to allow the entire sample to warm, and always placing the sample in the same position within the oven.

Figure 5.5 shows that adding the pTRM check discrepancy to the 101 measurement will yield the correct slope. This process, termed the demagnetisation bias correction here, was performed at every temperature step for all the samples. Figure 5.6 gives examples of corrected NRM-TRM plots. Although in certain cases the correction appeared insufficient (e.g. for samples NE0101C and NE0105B), and in others to over-correct (especially the 500 point for the GS samples), generally it appeared to be very effective in moving the points towards the line connecting the end-points of the plots. Figure 5.7 shows the effect of applying both the progressive NRM removal and demagnetisation bias corrections simultaneously to sample GB0107C, it is only this sample that can be argued to be fully corrected by these.

The deviation (d_{TRM}) of the each point from the end-point line along the TRM axis was measured before and after the correction was applied. The mean and maximum values of this are given for each sample together with the β parameter, before and after the correction was applied in table 5.6. The mean value of d_{TRM} was observed to drop in almost every instance as the points moved closer to, and to either side of, the end-point line. This was not always the case for the maximum value of d_{TRM} however, which was increased where over-correction occurred. The value of β can

also be seen to be lower for most samples as a result of the correction. The palaeointensity estimate itself tended not to be altered significantly however, this was expected because the slopes of the original best-fit and end-point lines were also similar to one another (tables 5.1 and 5.2).

Consequently, the demagnetisation biasing process is a candidate for being the dominant cause of QMD behaviour. If the progressive NRM removal (§ 5.3.2.2) process is also contributory, its correction would act to bring the points of those currently under-corrected samples, further towards the line connecting the end-points. This is not, however, the case for the GS samples, which were overcorrected to varying extents by the demagnetisation biasing correction. An investigation of these samples, in particular, forms the basis of the next section.

5.3.2.4 Cumulative progressive NRM removal

GS samples consistently produced over-estimates of the field, despite displaying some of the lowest values of β prior to any correction. It is likely therefore, that some limited process of irreversible alteration affected the samples during the experiment. It was observed that the final TRM measurement of these samples was low by an amount similar to their total NRM check anomalies. A process of alteration called cumulative progressive NRM removal (CPNR) may be responsible for this behaviour.

CPNR is very different to progressive NRM removal: the latter entailed an erroneously low measured pTRM because of NRM removal that occurred solely during that remagnetisation stage. Cumulative progressive NRM removal infers that the remanence carriers that retained this removed NRM are entirely destroyed and consequently that there is a progressive reduction in the capacity of the sample to acquire and retain remanence.

A correction, whereby the NRM value of every point was increased by the cumulative (negative) discrepancies in the NRM checks recorded so far was attempted. The results for all the samples are given in table 5.7.

	Before correction				After correction			
Sample	H_{EST} (μT)	β	Max $\|d_{NRM}\|$	Mean d_{NRM}	H_{EST} (μT)	β	Max $\|d_{NRM}\|$	Mean d_{NRM}
CR0107A*	43.7	0.11	0.35	-0.13	44.8	0.09	0.31	-0.13
CR0502A*	34.7	0.12	0.36	-0.15	36.6	0.11	0.34	-0.17
CR0503A*	52.3	0.15	0.33	-0.13	49.7	0.14	0.30	-0.14
CR0703A	54.3	0.03	0.09	-0.03	51.6	0.03	0.07	-0.01
GB0107C	48.6	0.06	0.11	-0.08	45.2	0.04	0.09	-0.07
GB0606B*	48.0	0.06	0.13	-0.07	43.8	0.04	0.09	-0.06
GB0703B	57.0	0.03	0.07	-0.02	55.6	0.03	0.05	0.00
GS0205B	55.5	0.02	0.05	-0.02	51.4	0.01	0.01	0.00
GS0206B	54.0	0.02	0.04	-0.03	51.7	0.01	0.02	-0.02
GS0301C	54.8	0.06	0.13	-0.04	50.4	0.03	0.07	-0.02
GS0302A	54.6	0.04	0.09	-0.03	52.7	0.03	0.06	-0.02
LR0109B*	43.9	0.09	0.24	-0.13	41.3	0.08	0.17	-0.09
NE0101C	50.1	0.11	0.25	-0.08	47.0	0.10	0.21	-0.07
NE0105B	48.7	0.14	0.33	-0.10	44.9	0.13	0.28	-0.08

Table 5.7: Estimates and parameters for each sample prior to and after cumulative progressive NRM removal correction. Asterisk denotes sample not displaying definite QMD behaviour

The deviation (d_{NRM}) of each point, along the NRM axis, from the corrected end-point line was calculated after the correction was applied and this was compared with the same parameter for the uncorrected points about their uncorrected end-points line. All of the QMD samples exhibited smaller mean values of d_{NRM} following the correction, and most also had smaller maximum d_{NRM} and β values. However, it was only the 4 GS samples and CR0703A that exhibited an improved estimate (figure 5.8). Therefore it would be a dangerous correction to apply when one is not certain that CPNR is the cause of the low NRM checks and it is currently not clear how such certainty could be acquired

CPNR appears to explain most of the irreversible alteration that causes five of the QMD samples to record a high intensity estimate. However, its correction does not entirely eliminate the convex-down shape of the plot in all those samples for which it improves the estimate (figure 5.8), suggesting that demagnetisation bias may also have a role in causing these samples to be non-ideal.

In examining the results given in table 5.7, the five samples that benefited from the application of this correction were identified only on the basis of them previously over-estimating the field and subsequently providing a more accurate estimate. This would obviously not be a usable criterion in a standard palaeointensity experiment and therefore it is worth examining the samples to discover if there are any other diagnostic features of CPNR.

All five of these samples displayed unblocking temperature spectra distinctly skewed towards high temperatures but there is no obvious reason why this should indicate that they are prone to this type of alteration. Another striking feature is that they all possess reduced convex-down shape in their NRM-TRM plots and, as a consequence, lower values of d_{TRM} and d_{NRM} prior to any correction (tables 5.4 and 5.5). This may seem counter-intuitive given that both CPNR and demagnetisation biasing act to displace the points in the same sense, and that these five samples may be prone to both of these processes. However, its explanation lies in the fact that only the former of these processes causes the final, high temperature point to be offset and that this has the effect of straightening the plot. In the context of standard Thellier analyses, it is very instructive to realise that, in certain cases, it is the most linear plots that should be suspected of exhibiting irreversible alteration!

CPNR may be expected to hamper pTRM checks in the exactly the same way as progressive NRM removal did (§ 5.3.2.2) rather than having a cumulative effect. However, table 5.5 showed that individual NRM check discrepancies were insufficient to account for their pTRM counterparts in all the samples. This constitutes further evidence that some other process, most likely demagnetisation bias, was also contributory in causing the non-ideal behaviour.

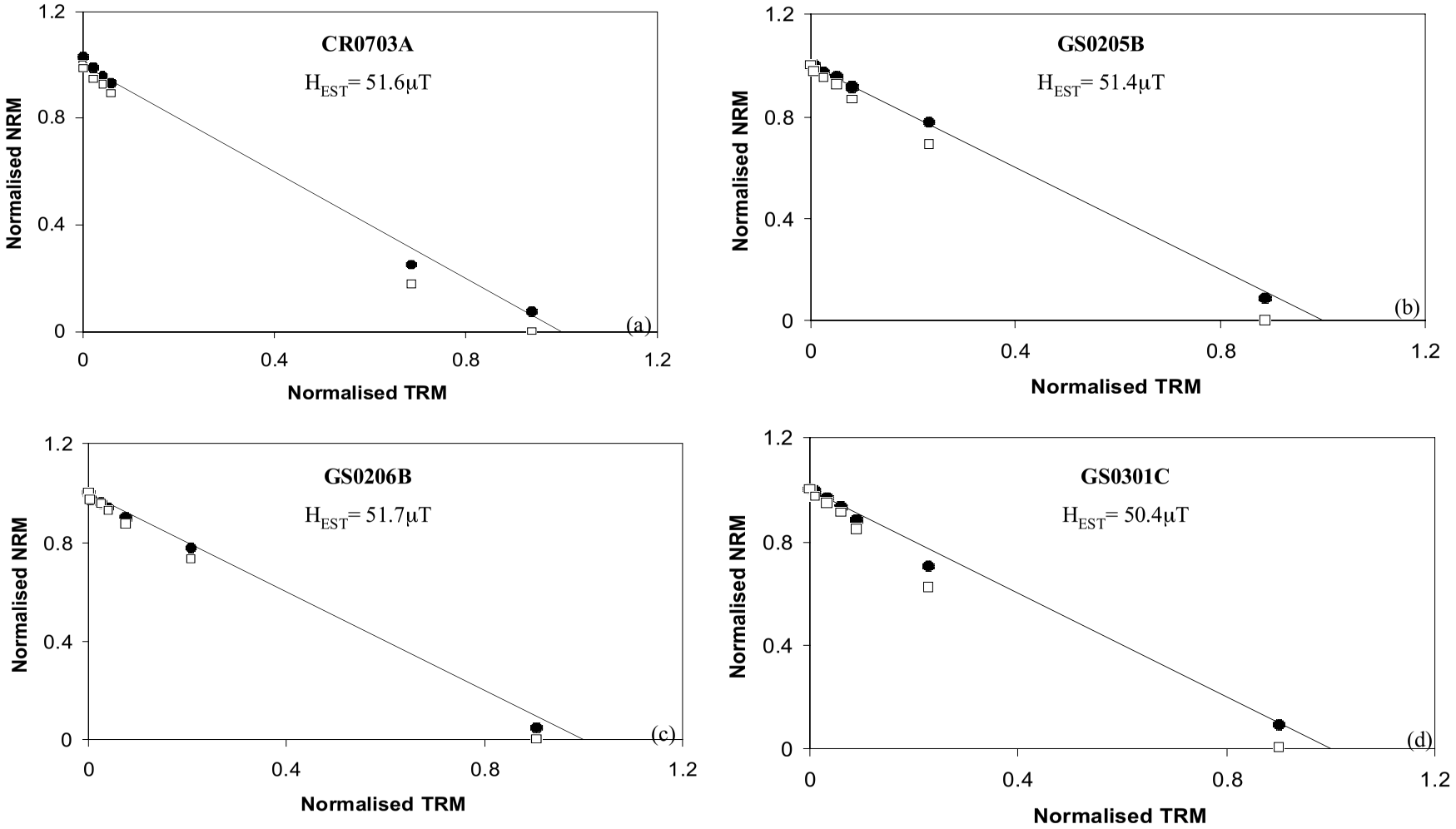

Figure 5.8 (a) - (d): NRM-TRM plots for certain QMD samples before (squares) and after (circles) the cumulative progressive NRM removal correction. Lines shown are those which would give a perfect estimate, quoted palaeointensities are those from best fit line through all the corrected points.

5.3.4 Discussion

Four models of non-ideal behaviour were advocated and tested in the previous section with varying degrees of applicability to the samples. The results suggested that demagnetisation bias was the dominant cause of QMD behaviour. They also showed that no single process was sufficient to account for the non-ideal behaviour of any sample in its entirety.

The four tested models constitute every mode of non-ideal behaviour generation, which are both feasible and correctable. However, it is also plausible that further types of alteration could have occurred that did not announce themselves in non-ideal behaviour, except in the sense of an inaccurate estimate. A hypothetical example of such a process is given in table 5.8. If this behaviour continued in the same manner to the Curie temperature, the plot would be 'ideal' (linear, passing pTRM and NRM checks) but the slope of the line would give an estimate that was high by an unquantifiable amount. While it can only be hoped that such a situation is extremely rare in reality, it constitutes an alternative explanation, albeit an unlikely one, for the behaviour of sample GB0703B and others. Its mentioning here also serves to highlight the fact that this analysis has not, and could not have, taken every feasible process of non-ideal behaviour generation into account.

Portion of BTS	Stage of experiment								
	0	100	101	200	201	102	300	301	202
0-100	N		T-A		T-A			T-A	
100-200	N	N	N		T-A	T-A		T-A	
200-300	N	N	N	N	N	N		T-A	T-A
300-400	N	N	N	N	N	N	N	N	N

Table 5.8: Blocking temperature spectrum (BTS) of sample during a hypothetical Thellier experiment in which progressive alteration only occurs at temperatures: $Temp_{pTRM\ check} < Temp_A < Temp_{remag}$. N = NRM, T = TRM, A = alteration to TRM.

Despite this, the analysis appears to have been successful in accounting for the single dominant process causing non-ideal behaviour in ten of the fourteen measured samples. With retrospect, it is now possible to identify features in the NRM-TRM plots of these that are likely to be diagnostic of the process affecting them. Table 5.9 summarises these; it was decided that quantitative measures (e.g. values of β and $|d_{NRM}|$) would be largely overlooked as diagnostic features because of the potential for other incidences of the same processes observed here to vary considerably in their severity.

Dominant process	Samples	Diagnostic features
CRM formation	CR0107A, CR0502A	High NRM checks coupled with extreme increases in measured pTRM and exaggerated curvature
Absolute changes in pTRM capacity	LR0109B	Changes in shape of plot are equal in direction and magnitude to pTRM check discrepancies.
Progressive NRM removal	None	Low NRM checks, pTRM checks are high and point is offset by equal amount to that at same temp
Demagnetisation bias	GB0107C,GB0606B,	Convex-down plot with moderate (~20%) curvature, high pTRM checks
Cumulative NRM removal	CR0703A, GS0205B, GS0206B, GS0301C, GS0302A	Low NRM checks, pTRM checks are high by equal amount to that at same temp, point is offset by cumulative total

Table 5.9: Diagnostic features evident in NRM-TRM plots of samples which exhibit non-ideal behaviour as a result of one dominant process

Table 5.10 summarises the positive consequences of applying the appropriate correction to those samples, whose behaviour is dominated by one process. The mean field estimate is corrected to within 2% of the true value and its standard deviation is reduced by a factor of three to within 3% of the mean value.

	Pre-correction		Corrected	
Sample	H_{EST} (μT)	Mean $d_{N/TRM}$	H_{EST} (μT)	Mean $d_{N/TRM}$
CR0703A	54.6	-0.03	51.6	-0.01
GB0107C	48.6	-0.10	48.5	-0.06
GS0205B	55.5	-0.02	51.4	0.00
GS0206B	54.0	-0.03	51.7	-0.02
GS0301C	54.8	-0.04	50.4	-0.02
GS0302A	54.6	-0.03	52.7	-0.02
LR0109B	43.9	-0.13	50.4	-0.09
Mean	52.3 ± 4.4	-0.05	51.0 ± 1.3	-0.03

Table 5.10: Intensity estimates and deviations from end-point line for each sample before and after the appropriate correction had been applied.

5.4 Implications for Thellier studies of untreated samples

The analysis described in this chapter constitutes a preliminary investigation into the causes of certain aspects of non-ideal behaviour during a Thellier experiment. Perhaps the single most surprising result was that despite the extensive pre-treatment they had received, every measured sample exhibited noticeable, and often systematic, non-ideal behaviour to a certain degree.

Most other studies employing the Thellier analysis to estimate the intensity of a known laboratory field have been performed on artificially prepared samples of constant grain size (e.g. Levi, 1977; Xu and Dunlop, 1995a). None have reported non-ideal behaviour as complex and intricate as that that was observed here. It may be that such complex behaviour only occurs in real igneous rocks, which have much more complicated grain-size distributions, mineralogy, and grain/domain interactions than size-filtered assemblages.

It is necessary for this section to discuss these findings in the context of Thellier analyses performed on untreated samples in which the ancient field strength is sought.

Unfortunately, this analysis did not shed any light on the effects of the process referred to as pTRM impedance (chapter 4) on palaeointensity determination. This alteration process may only be evident in meta-stable grains, which are prone to changes in their stress regime at low temperatures. Consequently, it would not be expected to be evident in thermally treated samples.

The most concerning outcome of this analysis is the set of results presented in table 5.3 which, under normal circumstances, would be assumed to be accurate because of their moderate to high q values and low pTRM and NRM check discrepancies. It is important to note that this behaviour, namely over-steep linear low temperature portions with passing pTRM checks, is not exhibited by just one particular rock type. At least one sample from each rock suite fulfils the conventional criteria and gives a high estimate. The peculiar pre-treatment of these samples, relative to those in nature, is expected to make the magnetic grains more resistant to laboratory alteration and to decrease their average domain state. Therefore the presence of this phenomenon in the results of a simulated experiment suggests that it may also occur in some conventional experiments as well. This notion is further supported by Hill and Shaw's (2000) observations of similar behaviour exhibited in recent Hawaiian lavas.

Table 5.2 provides the estimates and associated parameters derived from the whole NRM-TRM plot of every sample analysed. Thirteen of the fourteen samples provide estimates within 16% of the true value, which will be regarded here as an acceptable margin in the case of a standard Thellier analysis. However, the three modes of irreversible alteration discussed in the last section are likely to have been far less potent in these than they would be in samples that had received no pre-treatment. Therefore, it is possible to gain some insight into values of parameters that indicate that, although some irreversible alteration did occur, it was not sufficient to force the total estimate to be inaccurate by a significant amount (in this case 16%).

Samples CR0503A and NE0105B produced some of the worse parameters observed and yet both provided estimates within 6% of the true value. Accepting this at face

value, a reasonable set of acceptance criteria would be: (1) All points from NRM-TRM plot are used, (2) $q > 4$, (3) $\beta < 0.15$, (4) Maximum pTRM check discrepancy < 20%, (5) No NRM checks are high by greater than (say) 3%, (6) maximum NRM check discrepancy > -6%, (7) maximum curvature < 50%.

Criterion (1) would require that most natural samples be treated by low-temperature or AF demagnetisation prior to the experiment and after every subsequent remagnetisation stage. This requirement makes the results of this analysis somewhat inapplicable to the palaeointensity results presented in chapter 4, which all displayed secondary magnetisations, often to a high degree.

The other criteria are rather relaxed compared to those proposed by Selkin and Tauxe (2000) or even Coe *et al*. (1976). However, the two samples upon which they are based may have been affected by numerous processes of irreversible alteration and therefore it could be argued that the correct estimate was a product of them effectively cancelling one another out. The implication of this would be that, in another instance of irreversible alteration, the estimate could be made much less accurate while its associated parameters satisfied these criteria.

Unfortunately, the results of this analysis alone can not define any whole-scale criteria more effective or convincing than these because five of the samples associated with the best parameters (GB0703B and the GS samples) produce some of the most inaccurate estimates. The most reliable criteria that can be presented from this analysis are (5) and (7), which relate to laboratory CRM formation.

Acceptance criteria for results have previously been proposed on the premise that some non-ideal behaviour is inevitable in a Thellier experiment, and that a limit must be set on the level this can reach before the estimate is rendered unusable. This non-ideal behaviour is usually assumed to be in the form of 'noise' superimposed onto perfect SD behaviour, i.e. linear plot with passing pTRM and NRM checks. However, this approach had to be modified to understand the behaviour of the

samples analysed here: pTRM and NRM check discrepancies were regarded, not as random noise, but as quantitative functions of the magnitude and style of the non-linearity in the TRM-NRM plots. The checks themselves often only constituted a few percent of the length of the plot, and would have been dismissed as random noise using the criteria of Selkin and Tauxe (2000) when, actually, they were critical to correcting the plot itself.

Obviously, if this approach were to be adopted in the analysis of natural samples, much more experimental work and theoretical consideration than this chapter provides is required. The remainder of this section is concerned with preliminary discussion regarding the relevance of the observations made here, and the possible application of corrections to results produced by untreated samples in general. Limited discussion regarding the implications of this study for the results specifically presented in chapter 4, is reserved for chapter 9.

Because of how the latter is calculated, one would expect NRM check discrepancies to cause pTRM check discrepancies but not necessarily vice versa. If the two were observed to be equal in magnitude, then one could be reasonably certain that one of the two processes termed progressive and cumulative progressive NRM removal were solely responsible for the non-ideal behaviour of a sample.

As table 5.11 attests, if CPNR is the dominant process acting upon a sample, it is usually clear that it, rather than progressive NRM removal, is responsible for the low NRM checks. Because of its generally weak effects, progressive NRM removal is not

	Progressive NRM removal			Cumulative NRM removal		
Sample	Max $\lvert d_{NRM} \rvert$	Mean d_{NRM}	H_{EST} (μT)	Max $\lvert d_{NRM} \rvert$	Mean d_{NRM}	H_{EST} (μT)
CR0703A	0.05	-0.03	53.3	0.07	-0.01	51.6
GS0205A	0.02	-0.01	56.2	0.01	0.00	51.4
GS0206A	0.03	-0.02	55	0.02	-0.02	51.7
GS0301C	0.07	-0.03	55	0.07	-0.02	50.4
GS0302A	0.07	-0.03	55	0.06	-0.02	52.7

Table 5.11: Estimates and deviations of four samples suffering from cumulati
progressive NRM removal after the two NRM removal corrections

the dominant alteration process in any of the samples observed here. However, it must be a secondary process in every sample (except those in table 5.11) displaying low NRM checks.

Only one sample (GB0107C) was shown to exhibit non-ideal behaviour primarily because of demagnetisation bias. However, the corrected NRM-TRM plots of most of the other samples suggested, through convex-down plots and high pTRM checks, that this phenomenon also contributed to their behaviour. The linearity of the NRM-TRM plots of all of the QMD samples benefited from the application of the correction despite their estimates being relatively unchanged.

This type of behaviour is typical of that expected from samples dominated by MD grains (§ 2.6.4). Xu and Dunlop (1995a) performed Thellier experiments on 135 μm grains of MD magnetite and observed, somewhat surprisingly, that the pTRM checks passed despite the convex-down plot generated. However, it is the manner in which pTRM checks are calculated throughout this study, i.e. by demagnetisation and vector subtraction rather than the imparting of a fresh pTRM, that allows demagnetisation bias to be evident in the pTRM checks as well as the shape of the NRM-TRM plot.

Demagnetisation bias requires that T_B is higher than T_{UB} for each grain in an assemblage. This contradicts both theory and experiment for an assemblage of non-interacting SD grains but is a recognised aspect of MD behaviour during a Thellier experiment. However, the two rock magnetic experiments performed on the samples used in this study generated no evidence of MD grains.

There is then a confusing contradiction, one explanation mentioned earlier could be that the dominant remanence carriers are large grains that are strongly heterogeneous because of the repeated alteration they have been subject to. It is not known if grains whose coercivity were entirely dominated by stress could possess the demagnetisation bias of magnetocrystalline anisotropic MD grains without also

sharing the tendency to possess pTRM tails and exhibit high induced magnetisation. Further experimental work in the form of detailed rock magnetic and microscopic analyses is required to investigate this matter further.

If this was the cause of demagnetisation bias in these samples, how likely is it to occur in natural samples that exhibit SD like behaviour to rock magnetic analyses targeted at their remanence carriers? The subdivision of titanomagnetite, by ilmenite lamellae, into distinct regions that behave like elongate SD grains is believed to be common in basalt lavas (Senanayake and McElhinny, 1981). Magnetostrictive anisotropy may well be a factor in controlling the remanence of these grains (Thomas, 1992) and therefore demagnetisation bias could be expected to occur frequently in nature. The results from this analysis are far too limited to form any conclusions on this issue. It is worth bearing in mind however, that both Tanaka and Kono (1991) and Hill and Shaw (2000) observed similar behaviour in untreated samples from basalt lava flows.

The demagnetisation bias correction has enormous potential for application to results from standard Thellier experiments. In particular, the inferred relationship between pTRM check discrepancies and convex-down plots represents a possible mechanism of recognising and correcting for MD behaviour in samples. At present there is no direct means of showing that a convex-down plot is a product of MD grains and not due to irreversible alteration. Furthermore, if MD grains are known to dominate the assemblage, in order that an accurate palaeointensity estimate can be recovered, the sample must be free from secondary overprints and no alteration must occur upon heating to T_C so that the end-points of the plot can be used. If the demagnetisation biasing correction is proved correct, these exacting requirements will be negated. Each point can be moved to its correct position through addition of its pTRM check discrepancy providing no alteration has occurred prior to the pTRM check measurement. Obviously, the demagnetisation bias theory and correction require more research before they can become accepted.

It is evident from the results of this analysis that GS and Newcastle (NE and LR) samples produced consistently high and low overall estimates respectively. These traits may well be a product of the magnetomineralogical characteristics of these particular rock suites. Palaeointensity studies are frequently concerned with only a single rock suite and therefore, although the correction may suggest that demagnetisation biasing is the dominant cause of the observed non-ideal behaviour, the mean estimate will be offset from the true value.

In this analysis, samples exhibiting QMD behaviour and passing the criteria defined above are inaccurate by a maximum of only ~ 10%, which is an acceptable even for the mean estimate. Much more empirical evidence is required to show if this would be the case in all instances however.

5.5 Conclusions

1. Non-ideal behaviour in Thellier experiments is exhibited by samples appearing to comprise dominantly SD grains that are thermally annealed to some extent.

2. Using every point on the plot, or using only the full NRM and TRM points to produce an estimate yielded a far more accurate mean than applying any criteria (including those based on pTRM and NRM checks) that truncated certain plots at a temperature below T_C.

3. In many samples, non-ideal behaviour (specifically convex-down plots and high pTRM checks) may not be primarily a result of irreversible alteration of the ferromagnetic grains within them.

4. Samples in this experiment in which the non-ideal behaviour is partially or principally a component of ‘demagnetisation bias’ are recognisable by their QMD behaviour. The fundamental features of this behaviour are: (1) points between the full NRM and TRM points fall exclusively below the line connecting

these two points on the NRM-TRM plot; (2) no pTRM check is low by > 3% and the average pTRM check is high; (3) no NRM check is high by > 3%. Additionally, the application of the demagnetisation bias correction reduces the mean and maximum deviation of the points about the line connecting the end-points on the NRM-TRM plots.

5. The demagnetisation bias correction may allow correction of convex-down plots produced by samples containing predominantly MD grains although further work is necessary to verify this (§ 10.2)

6. Small amounts of NRM may be progressively removed each time a sample is reheated to the same temperature. Correction using NRM check measurements is at least partially effective although a method of discriminating between progressive NRM removal and CPNR has not been developed.

7. The monitoring of room temperature susceptibility (χ_{RT}) for significant changes after each heating step was effective at highlighting those samples that undergo the most dramatic increases in TRM capacity. However, it must not be used as a sole indicator for significant alteration occurring during a Thellier experiment.

8. The method of correcting NRM-TRM plots through use of the anomalies between pTRM checks and the original values as suggested by Valet *et al*. (1996) and McClelland and Briden (1996) was, for the most part, counter-effective in this analysis. The plots appeared less scattered, but shifted the slope away from that that would give the correct estimate.

It would be unjustifiable to presume that the conclusions reached from this one analysis are applicable to all or most analyses of natural samples. Nevertheless, a number of observations are important to note in the context of all Thellier analyses. The most important is that illustrated in table 5.3. Further studies are urgently required to ascertain how commonplace the disastrous conditions met in the 9 of

these 14 samples that display steep initial plots are in nature. As stated earlier, behaviour similar to that observed here was noted by Hill and Shaw (2000) when they used the microwave palaeointensity technique on samples from a recent Hawaiian lava flow to estimate the known field intensity. They suggested the presence of a high temperature CRM as a plausible explanation for two-slope NRM-TRM plots. This serves as a likely explanation when the NRM is primary but is not credible for the samples analysed here in which the grains had already been stabilised by heating to above T_C several times in the laboratory.

In order that future Thellier palaeointensity analyses (of natural and pre-treated samples) can contribute to the debate presented in this section, the experimental procedure needs to be carefully prescribed. The double-heating steps should each be followed by a pTRM and NRM check, and must continue to above T_C. Additionally, the laboratory field must have a component in the same direction as the 'natural' field in order that low NRM checks can be unambiguously associated with NRM destruction and not CRM formation.

A brief discussion of its implications of this analysis for the results presented in chapter 4 will be given in the overall discussion section (chapter 9).

6. Background to the global geodynamic system

6.1 The Geomagnetic field

As its navigational usage throughout human history attests, the geomagnetic field is predominantly dipolar in nature and close to alignment with the Earth's rotation axis. Approximately 90% of the present field (fig. 6.1(a)) can be accounted for by placing a single dipole source at the centre of the Earth and inclining it 11.5° with respect to the rotation axis. The rest of the field must be accounted for by non-dipole sources, which produce the additional non-dipole field (NDF, fig. 6.1(b)) surplus to the dipole field. A power spectrum of the spherical harmonic description of the present field shows that terms with degree $l < 14$ (where $l=1$ is a dipole, $l=2$ is a quadrupole etc.) originate in the core, while those of higher frequency are manifestations of permanently magnetised crustal bodies (figure 6.1(c)). Terms with $l > 14$, which do originate in the core, do not penetrate the mantle.

Implicit to palaeomagnetism is the fact that the time-averaged field is that produced by a *geocentric axial dipole* (GAD). This implies that there is a direct relationship between latitudinal position on the Earth and the inclination of the field at any one site averaged over sufficient time, an assumption that is critical in tectonic reconstruction.

A recent study of the entire palaeomagnetic database by Kent and Smethurst (1998) presented evidence that while the GAD hypothesis was valid during the Cenozoic and Mesozoic, prior to 250 Ma directions are skewed towards shallow inclinations. This would be the case if the source of time-averaged field included quadrupole and octupole ($l = 2$ and $l = 3$) components.

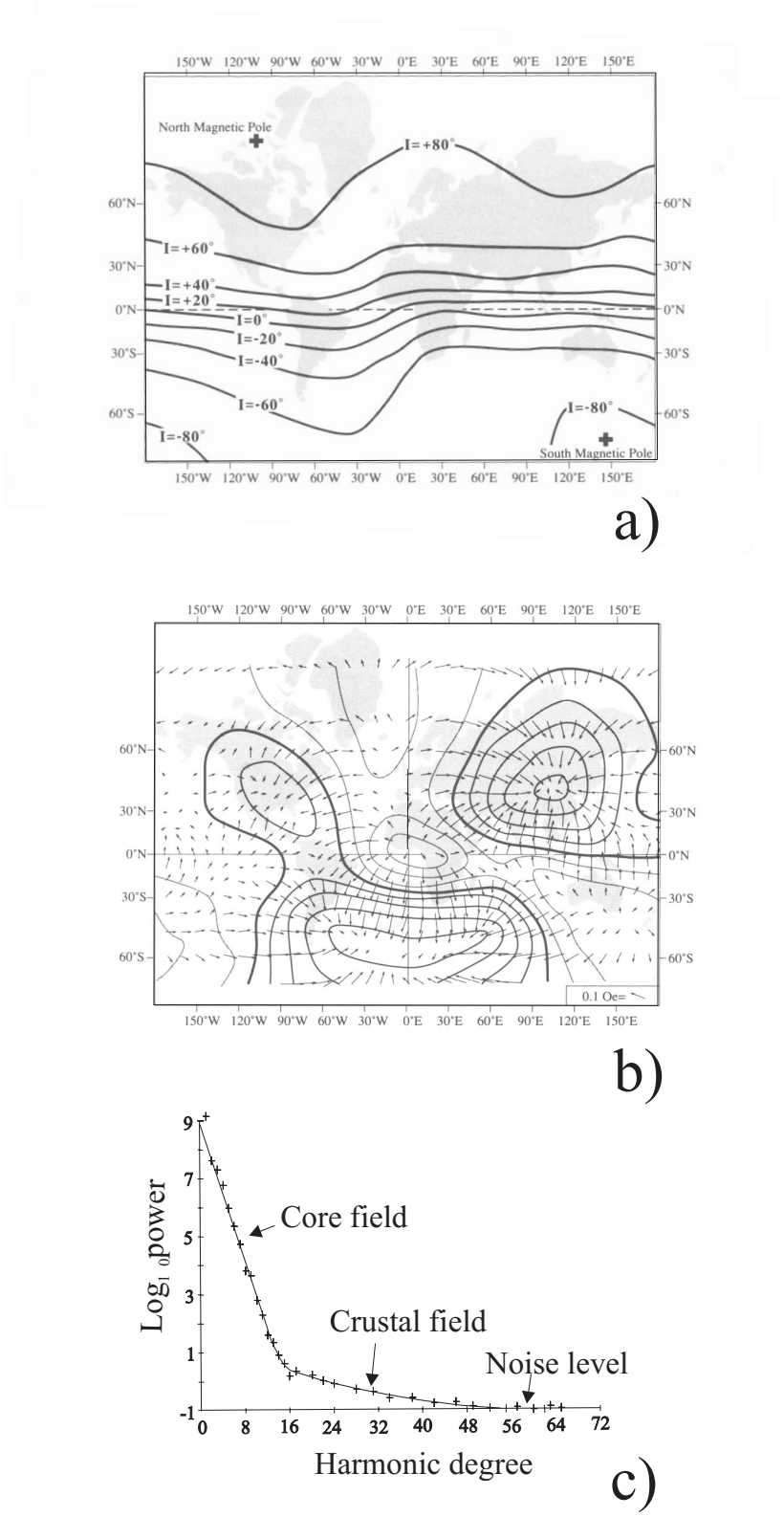

Figure 6.1: (a) Isoclinic chart showing variation of magnetic inclination over the surface of the Earth (Butler, 1992). (b) Isodynamic chart showing intensity (horizontal and vertical components) of the present non-dipole field (NDF) (Butler, 1992). (C) Power spectrum of present geomagnetic field (redrawn from

6.1.1 Secular variation

In addition to being spatially complex, the geomagnetic field is also temporally variant over a huge range of time-scales. Variations with periods greater than ~ 1 year are termed collectively as *secular variation* (SV) and are primarily a facet of core processes. More rapid variations are normally associated with external influences from the solar wind and its interaction with the magnetosphere. SV is usually considered to vary on time-scales up to 10^5 years (Dormy *et al*., 2000) ; time-scales of up to 10^9 years have been observed in the palaeomagnetic record but are assumed to be associated with the influence of lower mantle convection and inner core growth (see § 6.4) rather than an intrinsic feature of the geodynamo.

Global compilations of secular variation have been made from observatory, historical, archaeomagnetic, lake and ocean sediment and lava palaeomagnetic data. Despite the wealth of data extending over several timescales, SV remains too complex to be described in a single model (e.g. Bullard *et al*., 1950; Creer, 1977).

Fisk (1931) observed that NDF intensity and NDF SV was anomalously low in the region of the Pacific Ocean; this feature has since been termed the Pacific non-dipole low or Pacific Dipole Window. This and other persistent features in the NDF were reported by Bloxham and Gubbins (1985, 1986) and Jackson *et al*. (2000) from downward continuation of a record of secular variation from 1590 to present, produced using mariners' navigational documents.

Runcorn (1992) proposed increased electrical conductivity in the lower-most mantle beneath the Pacific to explain the non-dipole low as well as preferred transition paths (§ 6.4). This is broadly supported by seismic shear wave data (Lay *et al.*, 1998, Lay, 1995) which displays a distinctly different signature beneath the central Pacific than beneath the Pacific rim and other areas. If heterogeneity in the D'' layer (§ 6.3.1) is influencing the geodynamo, it must have been occurring over a period of at least a few million years and hence should be supported by palaeomagnetism.

However, despite several such studies in the area (Doell and Cox, 1972; Coe *et al*., 1978; McElhinney *et al*., 1996b; Tanaka, 1999), the question of its presence over the last 5 Myr has not been resolved.

6.1.2 Reversals and excursions

The realisation that the geomagnetic field had reversed polarity many times in the past was key to the plate tectonic revolution in Earth sciences. This phenomena is illustrated best in marine magnetic anomalies (MMA's) where through the process of constant renewal, oceanic crust acts as a 'tape recorder' of the geomagnetic polarity. Elsewhere, sedimentary and lava sequences can be correlated with one another and used to extend the geomagnetic polarity time scale beyond the oldest surviving oceanic crust (~160 Ma), albeit with increasing uncertainty.

At present, the field is in a 'normal' polarity state with the north pole axial dipole near the south geographic pole, hence the north pole of a magnet is attracted towards the north geographic pole. In a 'reversed' state, the axial dipole (and possibly nondipole components as well) is in the opposite sense, the method of transition between these two states is not fully understood at present.

Palaeomagnetic records of transitions (lasting ~ 4–5kyr) are preserved in rapidly deposited sedimentary and volcanic successions. Studies by Hillhouse and Cox (1976), Mankinen *et al*. (1985), and Prévot *et al.* (1985), indicate that low palaeointensities (approximately one-third of pre-transitional values), dominance of non-dipole components, and extremely rapid SV may all be features of polarity transitions.

Between reversals, the intensity of the field has been argued to vary systemically by Valet and Meynadier (1993) who presented relative palaeointensity variation from sediments formed over the past 4 Myr.

In any palaeomagnetic record, if there is deviation of the VGP greater than 45° from the time averaged mean without a consequent polarity shift, an *excursion* is said to have occurred (Verosub, 1977). Similar to reversals, these are often observed to coincide with a drop in intensity (e.g. Tauxe and Hartl, 1997) which is consistent with the notion of them being aborted reversals. It is not clear if reversals are mere extremes of SV or a result of entirely separate processes in the core. It appears that excursions bridge this gap as they are not distinct from SV beyond the arbitrary 45° VGP deviation cut-off.

Recent analyses of palaeomagnetic records from the Bruhnes and upper Matuyama chrons (Langereis *et al*., 1997, Lund *et al*., 1998) suggest that excursions and reversal excursions occurred more frequently than previously thought (~30-100 kyr). Gubbins (1999) argued that the geomagnetic field in the outer core undergoes full reversal during a reversal excursion. However, it is only if these new conditions are sustained for long enough (3 kyr) for the field within the inner core to change polarity by diffusion, that the geomagnetic field becomes stable in the new polarity.

6.1.3 Reversal frequency since the Carboniferous

Phillips and Cox (1976) used spectral analysis to show that there was no dominant periodicity in the magnetic reversal record. This means that to a first approximation the reversal process is random on short time scales. The record can then be described as a Poisson distribution (McFadden, 1984a) in which the timing of each event (reversal) has no relationship with the time since the last event. This cannot be entirely true, since the reversal event itself can take 5000 years to be completed the instantaneous reoccurrence of the event is therefore not possible. However, McFadden and Merrill (1993) have shown that with a slight modification to account for this, the Poisson process appears to provide an adequate description of the reversal record over short time intervals.

Over longer time intervals, reversal frequency is clearly non-stationary. Figure 6.2(a) shows that there were two distinct intervals in the last 400 Ma when the reversal process effectively ceased. These are called the Cretaceous Normal Superchron (CNS; 83.0 – 121 Ma) and the Permo-Carboniferous Reversed Superchron (PCRS; 262 – 320 Ma; see later).

Figure 6.2(b) shows the smoothed reversal frequency since the mid-Jurassic from the compiled time scales of Cande and Kent (1995) and Channell *et al*. (1995). From this it is clear that reversals occur more frequently at times long before and after the CNS than at times close to it. This variation has been interpreted in two different ways. McFadden (1984a) estimated the varying mean reversal frequency and incorporated it into a gamma process describing the distribution of reversals. When this reversal frequency estimate is plotted against time, its variation appears to be quite smooth coming into and going out of the CNS. The variation is also asymmetric about the CNS (McFadden and Merrill, 1997) with the fall in reversal frequency prior to the CNS being steeper than the recovery afterwards.

Gallet and Hulot (1997) plotted the duration of each polarity interval against the order of its occurrence and found strong evidence for three discrete periods of reversal frequency behaviour. Interval length did not vary greatly and there was no overall trend from the start of the record (158 Ma) to 130 Ma (Period **A**). Period **B** (130 – 25 Ma) represents a time of significant variation in the interval length. It rose quickly to a maximum (the CNS) and appears to have fallen steadily since this time. During period **C**, the polarity duration record is once again in a stationary regime although the mean duration of intervals is slightly shorter than that in period A (0.23 Myr compared to 0.29 Myr). The boundaries of the three periods are marked on figure 6.2 (b).

Gallet and Hulot (1997) proved that the means of representing reversal frequency used by McFadden (1984a) generated plots that appeared to show continuous

variation by producing a similar plot from synthetic data incorporating a non-stationary period surrounded by two stationary periods.

Constable (2000) presented a new analysis of reversal frequency based on the non-parametric adaptive kernel density estimate. 95% confidence limits, placed on the temporal locations of modes and antimodes in the record, could not reject the hypotheses of either McFadden and Merrill (1997) or Gallet and Hulot (1997).

Earlier than 158 Ma, the reversal chronology is much more poorly known because of the absence of marine magnetic anomalies. However, a quasi-continuous record can be inferred back to 330 Ma from compilation of sedimentary records (Opdyke and Channell, 1996). The Permo-Carboniferous reversed superchron (PCRS) is a reoccurring feature in magnetostratigraphic studies although its boundaries, especially its base, are not fully resolved. One of the most reliable studies were made from successions in the Canadian Maritime Provinces (Divenere and Opdyke, 1990, 1991a), they indicate that the boundaries of the PCRS are at 262 Ma and 320 Ma, these shall be used in this study. A more recent study using the SHRIMP technique on zircons (Roberts *et al*., 1996) supported this, placing the top of the PCRS at 263 Ma. After the superchron, the data suggests that reversal frequency increased rapidly in the late Permian and perhaps continued increasing very gradually through the Triassic.

The overturn time of the geodynamo is 500 years and the longest time-scale it operates on is ~5 kyr (Gubbins, 1999), therefore it is unlikely that any inherent process within the core could be responsible for such long period oscillations. These variations are therefore assumed to be due to the mantle's influence in dictating boundary conditions for the geodynamo (see § 6.3).

6.2 Mantle and lithosphere dynamics

6.2.1 Introduction

Thermal convection drives mantle motion with an overturn time of approximately 10^8 years. The heat flux from the core is thought to contribute only 10% of the Earth's heat budget (Davies, 1998) with the rest coming from radioactive sources within the mantle itself. The main driving force of mantle convection is the density excess at the surface caused by conductive cooling of the lithosphere.

The mantle is traditionally divided into an upper and lower region by prominent seismic reflectors at 440 and 660 km. These are thought to indicate the boundaries of a transition zone with olivine and garnet undergoing solid-state phase change at 440 km and a change in structure of perovskite at 660 km. No agreement has yet been reached on the dynamic role of this zone (see §6.2.4).

The other seismically distinct zone within the mantle is the approximately 200km thick, D'' layer just above the core-mantle boundary (CMB). This layer is noticeably slower than the mantle above it and appears to have severe topography (> 50 km) in places (Earle and Shearer, 1997). Additionally, it appears to display lateral heterogeneity as indicated by travel-time differences in P and S waves travelling through the layer. The significance of these and other features of D'' are discussed in § 6.3.1.

6.2.2 Plate-scale convection

The outer solid Earth is split into numerous lithospheric plates incorporating the crust and underlying viscous upper mantle. These plates represent a cool thermal boundary layer, the motion of which forms the dominant component in mantle convection.

Subduction occurs at destructive plate boundaries where two plates collide and a trench forms. Mid-oceanic ridges (MORs) form at constructive boundaries where plates are moving away from one another and new crust is formed. The topography of MORs and the variation in lithospheric thickness either side of them is consistent with a passive upwelling along these boundaries rather than any buoyancy driven separation (Sclater and Francheteau, 1970). This implies that the main driving force in plate tectonics is the pull of the negatively buoyant lithospheric plate (slab) as it falls through the mantle.

The low density of continental lithosphere precludes it following the oceanic lithosphere it is attached to into the mantle, consequently when one continent collides with another subduction halts (Eide and Torsvik, 1996). The changing position of continents with respect to one another is therefore a primary feedback process affecting convection in the entire mantle.

What follows is a brief summary of plate tectonic evolution during the period in which dipole moment variation will be analysed (Devonian to present). A protracted period of subduction dominated the Palaeozoic allowing numerous continental collisions to occur. By the early Devonian (400 Ma), Baltica and Laurentia had already collided with one another forming Laurussia, and Gondwana and Asia were moving towards this. The formation of the supercontinent Pangaea was completed by the late Carboniferous (~ 320 Ma; Yale and Carpenter, 1998) as Gondwana collided with the recently formed Laurasia.

Pangaea remained intact until the mid-Jurassic, during which time it had rotated slowly and steadily and the continents gradually adjusted their configuration (Muttoni *et al*., 1996). Separation between North America and Europe began at ~180 Ma (Klitgord and Schouten, 1986), most of the other continents followed suit in the Cretaceous. By the end of the Cretaceous, of all the separate continents observed today, only Antarctica and Australia remained attached. In addition to the separation of these two landmasses, India also made its journey to the base of Asia in the

Tertiary (70 – 45 Ma; Lee and Lawver, 1995). On the present globe, the Atlantic and Indian Oceans are expanding at the expense of the Pacific, Africa is rifting away from the Middle East and Australia is moving northwards.

6.2.3 Mantle plumes and large igneous provinces

Large igneous province (LIP) is an umbrella term encompassing all igneous activity that is not directly attributable to plate tectonics. Together they are responsible for between 5 and 10% of the current surface heat and magma flux (Davies, 1988; Sleep, 1990). However, transient LIPs in the past may have contributed a great deal more over a relatively short time (e.g. Tarduno *et al*., 1991).

The entire Earth is cooling, the mantle can transfer heat from its interior to the atmosphere by convection involving the lithosphere, whereas the core can only conduct heat away from its upper surface. The corollary of this is that a hot thermal boundary layer is likely to form at the base of the mantle. Both theory and experimentation shows that a thermal boundary layer at the base of the mantle would eject material episodically in the form of plumes (Griffiths and Turner, 1998). The boundary layer would swell in an area to some critical volume before generating sufficient buoyancy to overcome the higher viscosity of the overlying material. A spherical plume 'head' would then break away from the layer and begin rising through the mantle followed by a narrow conduit or 'tail' linking the head to the boundary layer. The plume head would grow as it progressed up through the mantle both from a supply of material from its feeder tail and from incorporation of surrounding material.

This 'head and tail' morphology of plumes has been advocated to explain commonly observed spatial and temporal links between two types of LIPs: flood basalts and hot-spot island chains (Richards *et al*., 1989). In this simple model the mantle head produces the flood basalt where the plume first reaches the base of the lithosphere, subsequently the laterally near-stationary plume tail is responsible for creating an

intermittent trail of hot-spot islands as the plate moves over it. This explanation has received much criticism (see below) and given that some hot-spot chains (notably Hawaii) have no associated flood basalt and vice-versa, it is unlikely to provide a complete model of plume behaviour.

In addition to providing an explanation for intra-plate magmatism, plumes have also been advocated as a cause of continental rifting (White and McKenzie, 1989; Hill, 1991; Courtillot *et al*., 1997). Anderson (1994) has pointed out however, that most spreading ridges are located at pre-existing lithospheric sutures and not randomly located as would be expected from a pure plume model. Courtillot *et al*. (1999) accounted for the coincidence of rift events with flood basalts and areas of weak lithosphere by proposing a 'mixed scenario of active/passive rifting.' They state that a plume must be present and plate forces must be favourable in order for the rift to occur, its precise location and that of its accompanying flood basalt is influenced by local lithospheric heterogeneity.

The necessity of mantle plumes to explain any lithospheric phenomena has repeatedly been called into question. The notion of hot spots as a source of non-tectonic volcanism can be replaced by that of 'wet spots' in which a part of the mantle is enriched with volatiles (H_2O, CO_2) (Green and Falloon, 1998).

Anderson (1992a,b), Heller *et al*. (1996) and Smith and Lewis (1999) have attacked plume theory over the extent to which it impinges on the dominant plate tectonic processes. They put far more emphasis on heterogeneity within the lithosphere as the causal factor behind mantle upwelling and continental rifting, claiming that insulation of the upper mantle by supercontinents is responsible for generating hot regions which later penetrate the lithosphere at points of weakness.

In an excellent review paper on the topic of large igneous provinces, Coffin and Eldholm (1994) concluded that no single model may exclusively explain the generation of the whole range of LIPs. Rather it is perhaps better to examine the

specifics of each LIP and find a model that fits all the observed data rather than trying to fit a generic model of LIP emplacement to all of them.

Using a simple melt estimate model, they showed that continental flood basalts and oceanic plateaus are likely to have at least part of their origin in the lower mantle, the sources of most of the smaller LIPs however can be accommodated in the upper mantle. They particularly favoured upper mantle sources for persistent LIPs as they found it unlikely that a plume tail from the deep mantle could persist for 100 Myr. However, this may not be consistent with geochemical arguments (§ 6.2.5)

6.2.4 The role of the 660 km transition

The extent to which the transition zone affects the mode of convection within the mantle is not agreed upon although a gradual convergence of theories is currently emerging. Originally the layer was considered as a boundary to mantle convection stopping interaction between the upper and lower mantle and this theory persists for some (e.g. Wen and Anderson, 1997). At the other extreme, some believe that the layer has little effect on convection and the two parts of the mantle mix freely. Both theories have some strong observational evidence which suggests that the truth lies somewhere between these extremes.

The chemical transformation believed to characterise moving down through the 660 km boundary is:

$$Mg_2SiO_4 \text{ (spinel)} \longrightarrow MgSiO_3 \text{ (perovskite)} + MgO$$

This is an endothermic reaction with a negative Clapeyron slope of the phase equilibrium curve. This means that the pressure at which the transformation occurs is inversely proportional to the temperature of the material, the significance being that any down-welling cold lithosphere will have to be deeper in the mantle than the surrounding material before it adopts the same denser structure. This implies a

buoyancy force will oppose the sinking motion of subducted slabs once they reach the boundary, and this may be sufficient to halt the downward progress altogether.

Upwelling hot material, presumably in the form of mantle plumes will face the same problem in the opposite sense. Subducting slabs and to a lesser extent plumes, are the most dynamic form of heat transfer in the mantle. If the 660 km boundary is sufficient to halt their progress, then weaker, passive circulation cells will certainly be kept apart. Consequently, there is a theoretical basis for entirely segregated mantle convection.

Numerical studies have attempted to investigate the effectiveness of the boundary in halting both cold sinking anomalies and their hot rising counterparts although their accuracy is hampered by uncertainty in the precise value of the Clapeyron slope. In the most realistic case of a three-dimensional model with variable viscosity, the 'slab' clearly does penetrate the boundary although it is delayed for a time there (Davies, 1998). This picture is generally supported by seismic evidence (Creager and Jordon, 1988; Vidale and Garcia-Gonzalez, 1988; Zhou *et al*., 1990; Zhou and Clayton, 1990) which indicate the presence of cold, dense slab material below 660 km. In some cases they also claim to have observed a deflection along the boundary (Zhou and Anderson, 1989). Additionally, Steinberger (2000a) predicted the present locations of slabs at depths of greater than 1700 km and found the predictions in reasonable agreement with the geoid and regions of fast seismic velocities.

The emerging picture is then one of the 660 km boundary being 'leaky' and allowing slabs to penetrate once enough pressure has accumulated.

A recent study by Cizkova *et al*. (1999) showed that the observed seismic signal in the lower mantle could be explained without the need for slab penetration if there exists a thin low viscosity layer just below the 660 km boundary. In such a case,

downwellings in the upper mantle would thermally interact with the lower mantle to trigger downwellings below the boundary but no mass would be transferred.

The most recent numerical study of the capability of upwellings to penetrate the 660 km boundary was conducted by Marquart *et al*. (2000). They found that if the plume head was not large enough (radius > 100 km) to penetrate immediately, heat diffused from it and allowed secondary penetration some time later. They concluded that the spinel – perovskite boundary was unlikely to constitute a barrier to plumes of the size thought to generate many LIPs.

A recent high-resolution tomographic study of the plume beneath Iceland was conducted by Foulger *et al*. (2000). They observed that the high velocity cylinder beneath the hotspot broadened out below 250 km depth inferring that the base (and source) of the plume was the transition zone.

Even if the mantle is currently undergoing whole-scale convection, this does not imply that this was always the case. In the early portion of the Earth's history when the upper mantle was a lot hotter than present, it would have had a much lower viscosity and therefore would have convected faster than at present (Griffiths and Turner, 1998). Consequently, plates would have been younger (warmer), thinner and more ductile when they were subducted and lack the momentum to penetrate the transition zone.

Davies (1995b) produced a numerical model to show that up to 1 billion years ago, slabs would have been incapable of penetrating the spinel - perovskite boundary. Because heat could only be transferred across the boundary by conduction, the upper mantle would have cooled a lot quicker than the lower mantle. A large temperature difference would have developed which would be removed episodically by a catastrophic exchange of upper and lower mantle material, similar to that observed in non-penetrative numerical models (Davies, 1998). It should also be stated that there are some numerical models of the present mantle (e.g. Tackley *et al*., 1993)

that also exhibit accumulation of slabs at 660 km followed by avalanching but on a more frequent basis.

6.2.5 Compositional heterogeneity in the mantle

Seismic observations and heat flow arguments provide the argument for whole-mantle convection whereas geochemical observations tend to favour the layered model. If the entire mantle were convecting as a single entity, one would expect to find homogeneous geochemical signatures from igneous rocks derived solely from the mantle, this is not the case. Mid-oceanic ridge basalts (MORB) tend to be depleted in incompatible elements and are similar to one another while mafic rocks associated with plumes tend to contain enriched material and are heterogeneous.

Davies (1998) draws attention to the distinction between stirring and mixing and claims that the mantle has not transferred mass in its present form for long enough to achieve homogeneity. He claims that geochemical signatures for MORB and hot spot island basalts are consistent with the plausible notion that the upper mantle comprises well mixed and therefore homogenous material, whereas the lower mantle is less depleted and has not been as well mixed.

Both Campbell (1998) and Kogiso *et al*. (1997) claim that hotspot material is derived from the D'' region (§ 6.3) and that this material is enriched from subducted slabs that have sunk to the base of the mantle. Campbell (1998) also claimed that the lower mantle away from D'' was slightly depleted because of entrainment into rising plume heads.

Kellogg *et al*. (1999) produced an alternative theory of compositional stratification, which they argued accounted for several pieces of evidence not supported by other models. They reasoned that the amount of heat generation within D'' would have to be unrealistically high to account for the heat flux observed at the surface. They also

pointed to the seismic and geochemical argument that there is no reason for a compositional boundary at 660 km (Jackson, 1998; Jackson and Rigden, 1998).

They overcame these problems by proposing a model in which the mantle is still divided into three compositionally distinct regions with D" intact, but rather than the division between upper and lower mantle occurring at 660 km, it occurs deep (~1600 km) in the lower mantle. The layer, which accounts for 20 to 30% of the total volume of the mantle, is enriched in radiogenic sources and is modelled as just 4% less dense than the material of the upper mantle. It is proposed that just above this layer lies a transition zone which consists of depleted mantle and enriched relic slabs, the nature of which accounts for the complex and varying compositions of the hot-spot islands it sources.

Some evidence for this layer exists in the form of seismic tomography profiles (van der Hilst *et al*., 1997; van der Hilst and Kárason, 1999), and numerical modelling proves that such a layer would have remained chemically distinct from the rest of the mantle for the duration of Earth's history. The model also indicates that the introduction of a slab from above would generate large topography in the layer either side as it penetrates down to the CMB.

It must be stressed that the Kellogg *et al*. model is far from acceptance in the mantle-studying community although it is arguably the most consistent with observation.

6.2.6 Discussion

Beyond the fact that the motion of lithospheric slabs is the dominant component of (at least upper) mantle convection, there exists little general consensus on the form that processes throughout the mantle take and how they are represented at the surface. Plate-scale convection represents ~ 90% of the heat transfer at the from the Earth's interior to the surface, Anderson (1994) claims that plumes cannot simply be superposed onto this system and remain unaffected. He argues that feedback

processes inherent in a top-cooled system like the mantle precludes a secondary feature of convection such as plumes independently affecting the governing processes (e.g. causing rifting).

The debate over whole and / or layered mantle convection could continue for some time although, as stated earlier, strong evidence on both sides favours the development of some hybrid model.

How important are these unresolved issues with respect to the present study? The two extreme modes of mantle convection are outlined below alongside their impacts for crustal-core interaction:

1. **Whole mantle convection, plumes are critical:** Some residue of all subducted plates settles on the CMB; all intra-plate igneous activity is a direct result of plumes rising from the just above the CMB. Every element of crust / uppermost mantle interaction also bears some relation to a preceding or subsequent event in the lower-most mantle which is likely to affect the core. It should therefore be possible to draw a correlation between every plate tectonic / LIP event with changes in the geomagnetic field record.

2. **Layered mantle convection, plumes are negligible:** All subducted slabs are retained in the upper mantle; all LIP activity is due to anomalous pre-existing lithospheric and asthenospheric conditions. Presumably hot upwellings and especially cold slabs at 670 km would have some interaction with the flow below the transition zone which may in turn affect the flow at the base of the mantle. Therefore it is possible that correlation could exist between some events in the geological record and those in the palaeomagnetic record.

Therefore even case 2 above does not preclude events in the lithosphere having some relationship with the palaeomagnetic record. The majority of evidence concurs with the notion of upper / lower mantle interaction. Even if slabs and plumes do not

penetrate, it has been demonstrated by numerical models that they initiate significant flows at the other side which will likely impede to some extent on the corresponding boundary of the mantle (Cizkova *et al*., 1999; Marquart *et al*., 2000).

The apparent lack of firm knowledge of mantle processes should not be regarded as a barrier to deducing the level of coupling between crustal processes and the geomagnetic field. On the contrary, there is an opportunity to discriminate between mantle models by discovering the relationship between the two surrounding layers and using this information to provide constraints.

6.3 The Global geodynamic system

6.3.1 The core-mantle boundary region

The core and mantle meet at an interface with the largest density contrast in the planet. Despite intensive multi-disciplined research into the region of mantle just above this boundary, its precise nature remains enigmatic. This section aims to provide a brief overview of currently popular theories regarding the lowermost mantle (LMM), for a detailed review see Gurnis *et al*. (1998).

The D'' layer corresponds to a flattening of the seismic velocity distribution in the lowest 200 – 300 km of the lower mantle. A temperature contrast of approximately 1000-2000 K exists between the core and lower mantle (Williams, 1998), therefore the D'' layer must be, at least in part, a thermal boundary layer. However, seismic studies of the layer also display significant lateral heterogeneity and anisotropy requiring a more complex explanation.

There are three plausible explanations for its origin. The first is that it is a 'graveyard' for relict slabs, the second that it contains primordial material, and the third that it is a product of core-mantle interactions. At present, experimental and theoretical research is not well-placed to discriminate against any of these

possibilities, rather it points to a very complex system which could be influenced by all three (Tackley, 1998). If, as discussed in § 6.2, D'' material is entrained into upwellings then the layer obviously needs replenishing by some process and cannot be purely primordial.

Seismic tomographic studies support the notion of some slabs reaching the CMB and spreading along it (van der Hilst *et al*., 1998) and this model is also compatible with the observed seismic heterogeneity and horizontal anisotropy in D'' (Kendall and Silver, 1998). However, it need not be the only explanation.

The LMM also contains an ultra-low velocity zone (ULVZ), 5-40 km thick at the base of D'' (Garnero and Helmberger, 1995; Mori and Helmberger, 1995). This seismological feature (10% reduction in P and S wave velocities) is noticeably absent from some areas, suggesting that it is either not present or thinner than the resolution of the studies allow (a few km). It was originally attributed to the presence of partial melt (Williams and Garnero, 1996; Revenaugh and Meyer, 1997), however another possibility is that it is a transition zone, between the core and mantle (Garnero and Jeanloz, 2000). The large uncertainties associated with the studies of diffracted waves used in this region means that either of these explanations or a combination of them both are plausible at present. However, geochemical arguments tend to favour the presence of partial melt to account for the signature.

The correlation between locations of hot-spots at the surface of the Earth and the distribution of the ULVZ at the base of the mantle is significant at the 99% confidence level (Williams *et al*., 1998). Additionally, there may be an anti-correlation with areas shown by tomography to contain fast (cold) anomalies in the lower mantle (Lay *et al*.,1998; figure 6.3). Therefore it is possible that the ULVZ is a feeder zone for hotspots.

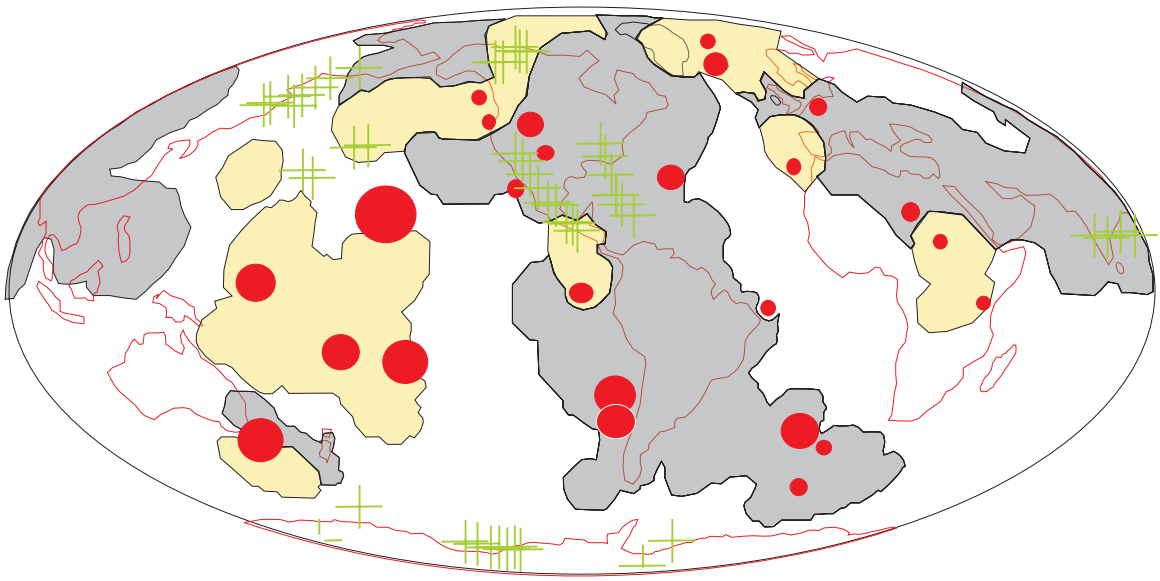

Figure 6.3: Mollweide projection of globe showing where ULVZ has been detected (yellow shading), whe it is absent (grey shading), hotspots at surface (red circles) and lower mantle density anomalies (crosses) corresponding to subducted material (redrawn from Lay *et al*. (1998)).

This was supported by the study of Russell *et al*. (1998) who intensively mapped D" anisotropy at the location where the Hawaiian plume is thought to originate. They found large changes in shear-wave velocity and anisotropic polarisation over short distances and interpreted them as indications of small-scale dynamics corresponding to a lateral flow of material in D" towards the plume base and then up into the plume column itself.

Most of the inferences made about the LMM are far from certain because of the many and complex factors involved. Importantly though, much of the current thinking seems to favour the concept of a relationship between lithospheric processes (subduction and LIP emplacement) and conditions at the very base of the mantle.

6.3.2 Convection in the outer core

Before discussing the mechanisms through which the mantle may affect the geomagnetic field, it is necessary to briefly describe the energy sources for the geodynamo itself. The geodynamo is powered by convection of liquid iron within the outer core. The question remaining is therefore: what provides the energy for this convection?

The liquid in the outer core is an iron-rich alloy, the other constituent element(s) is (are) poorly constrained but must be lighter than iron to fit seismic density estimates (Poirier, 1994). Theoretical studies on the thermal evolution of the core estimate that the inner core has grown from nothing in the last 2 Gyr (Buffet *et al*., 1996; Labrosse *et al*., 1997; Lister and Buffet, 1998). This has occurred because the core has been continuously losing primordial heat, allowing iron to separate from the lighter element(s) and freeze at the inner core boundary (ICB). The residual iron-deficient alloy is then a buoyant entity at the base of the outer core and rises to the surface. It is this release of gravitational energy which causes the 'compositional

convection' believed to be the primary source of energy for the present geodynamo (Loper, 1978a).

Thermal convection is the other candidate for powering the geodynamo. Energy for this process is derived from primordial heat, latent heat release and possibly radiogenic heat produced by a yet unknown quantity of potassium in the outer core (Parker *et al*., 1996). Estimates of Carnot efficiencies are subject to large uncertainties but indicate that thermal convection probably accounts for approximately 20% of the power to the geodynamo with the rest coming from compositional convection (Lister and Buffet, 1995).

Palaeomagnetic evidence suggests that the geodynamo was operative up to 1.5 Gyr before the inner core had begun forming (Hale and Dunlop, 1984). The strength of compositional convection is proportional to the surface area of the inner core, hence thermal convection must have been dominant in the past. This is plausible since the core will have been much hotter in the past and hence the heat flow across the CMB will have been higher. This last point is particularly significant: the vigour of thermal convection is entirely dependent on the heat flux out of the core. This is controlled not only by the amount of heat released into the core but also by lower mantle temperature and thermal conductivity.

Given the high conductivity of liquid iron, it is feasible that at times the heat flux at the CMB could be less than that conducted up the core's adiabat. Such conditions would not only halt thermal convection, but would result in the circulation of warm material back down into the core through compositional convection expending energy otherwise used to power the geodynamo (Loper, 1978b).

Buffett *et al*. (1996) showed analytically and numerically that inner core growth was proportional to the heat flow through the CMB. For all inner core radii, the total (i.e. thermal and compositional) efficiency of convection is proportional to the heat flux across the CMB. Therefore, homogenous changes in CMB heat flux dictated by the lowermost mantle will directly affect the vigour of core convection and thus the

strength of the geodynamo. Cooler (or higher conductivity) lowermost mantle conditions will strengthen the geodynamo (and probably the observed magnetic field), hotter conditions will weaken it. The possible implications of lowermost mantle heterogeneity (static and dynamic) for the geodynamo are poorly recognised but will be discussed in the next section.

6.3.3 Plausible mechanisms of core-mantle interaction

In attempting to recognise how the geomagnetic field reacts to mantle influence, it is first necessary to identify all the possible ways D'' can affect the geodynamo. In addition to thermal (temperature and heat conductivity) effects, the mantle may also influence flow within the core through heterogeneity in electrical conductivity, gravitational force and topography. The extent to which these factors influence the geodynamo is, at present very uncertain. However, although secular variation may be strongly influenced by them all, it seems likely that only thermal core-mantle interaction will cause the major shifts in geodynamo regime that the present study aims to identify. Hence, only thermal interactions will be discussed from this point on.

As discussed above, the temperature and thermal conductivity of the lowermost mantle control the heat flux out from the core and are therefore of critical importance. Homogenous changes in heat flux across the CMB directly affect the vigour of convection within the core (§ 6.3.2), this is likely to have direct consequences for geomagnetic field strength and possibly for reversal rate (Glatzmaier and Roberts, 1997). Such boundary-wide shifts in lower mantle conditions have been invoked in a number of hypotheses linking crustal and geomagnetic events (e.g. Loper and McCartney, 1986; Larson and Olson, 1991; Eide and Torsvik, 1996). These hypotheses will be discussed further in § 6.3.4.

Another scenario is that core convection is controlled through dynamic thermal heterogeneity at the CMB. This is supported by palaeomagnetic evidence of non-

dipole features persisting for millions of year (Gubbins and Kelly, 1993; Johnson and Constable, 1995, 1997, 1998; Kelly and Gubbins, 1997), and from the positional correlation of seismic heterogeneity in the lowermost mantle with flux lobes at the CMB (Giardini *et al*., 1987).

Su *et al*. (1994) interpreted seismic heterogeneities inferred from tomography in the lowermost mantle, as evidence for temperature anomalies there. If these anomalies are due purely to thermal heterogeneity, they suggest temperature variations of hundreds of Kelvin over distances of approximately 1000 km. Given that Bloxham and Gubbins (1987) have shown that temperature anomalies above 1 K at the CMB would drive thermal winds in the outer core, it is not difficult to imagine the extent to which the geodynamo would be affected if this were the case.

The patterns of core–flow induced and the manner in which geomagnetic field generation would be affected by different heterogeneous boundary conditions are difficult to investigate. Nevertheless a number of numerical studies have recently approached the problem; the results of the most complete study performed by Glatzmaier *et al*. (1999) will be discussed here.

This used a sophisticated, self-consistent numerical model, incorporating both compositional and thermal convection, and was run 8 times for at least 100,000 years of simulation time with different heat flux patterns maintained on the outer boundary in each case. Of the many observations made from this study, the following are worthy of note:

1) Dynamos subject to significant equatorial asymmetry were generally less stable in terms of dipole latitude and moment.
2) High polar heat flux resulted in generation of the most stable and efficient fields. For inverse heat-flow patterns (low polar heat flux), the field fluctuated much more rapidly and in one case died away all together.
3) Dynamos subject to both homogeneous and seismically inferred boundary conditions had a qualitatively similar reversal frequency to that of the

geodynamo. However, the dispersion of calculated VGP's and duration of transition in the former case was more 'Earth-like' than that in the latter.

4) Significant changes in heat-flux were necessary to obtain noticeable changes in reversal frequency.

The first two points are intuitively appealing: in the first case the dynamo prefers equatorially symmetric heat flow patterns, as this is how the flow within the core is naturally, consequently asymmetry upsets the equilibrium. Furthermore, as a result of the rapid rotation of the core, simulations suggest that convection tends to favour columnar axial flow (Glatzmaier and Roberts, 1995a; Sarson *et al*., 1998), this is especially the case for the Glatzmaier-Roberts (G-R) dynamo model. As demonstrated in this study, one suspects that high polar heat flux would favour this mode and stabilise the dynamo and conversely, that heat flux concentrated at the equator / mid-latitudes would do quite the opposite.

Glatzmaier *et al*. (1999) used point 3 here to argue that the seismic heterogeneity observed at the base of the mantle might not be representative of heat-flux at the CMB. Instead the heterogeneities may be due more to compositional rather than thermal anomalies or alternatively, that the warmer regions of D'' may have higher thermal conductivity (possibly as a result of partial melting) which would tend to equilibrate heat-flux over the entire CMB.

However, it must be remembered that the G-R model, despite being self-consistent, could be in an entirely different regime to the geodynamo (Zhang and Gubbins, 2000b). All current numerical models need the retarding action of viscosity to stabilise the solutions they produce. However, in the real geodynamo the effects of viscosity are thought to be negligible (Dormy *et al*., 2000). Consequently, although the G-R model generates a magnetic field dominated by an axial dipole, and is capable of spontaneous polarity reversal, it should not be assumed to accurately represent the geodynamo.

The uncertainty surrounding the reliability of numerical models of the geodynamo is highlighted in their inconsistencies with one another. Several self-consistent, three-dimensional models of the geodynamo, producing 'Earth-like' fields, have been developed separately (e.g. Glatzmaier and Roberts, 1995a; Kuang and Bloxham, 1997; Christensen *et al*., 1998). However, Dormy *et al.* (2000) observed that they did this via significantly different mechanisms (i.e. styles of fluid flow). Given that fluid velocity fields capable of generating a magnetic field similar to the geomagnetic field may be highly non-unique, it is not reasonable to assume that the geodynamo would react identically (or even similarly) to the G-R model when subject to certain patterns of heat flux heterogeneity.

The same caution that should be applied to point 3 is also applicable to point 4. Consequently, while present uncertainties remain, self-consistent numerical models are of limited use in predicting the response of the geodynamo to dynamic boundary conditions. A greater insight may instead be achieved by asymptotic studies (§ 8.2.4) in the correct parameter regime.

6.3.4 Previously proposed global geodynamic models

The plausibility of causal links between lithospheric and geomagnetic events has been established in § 6.2 and § 6.3, prior to this sub-section. The remainder of this chapter is a discussion of previous interpretations of relationships between the geological and palaeomagnetic records. Several of these models will also be discussed, where relevant to the global dipole moment record, in chapter 9.

The first hypotheses to link geomagnetic field behaviour with events observed at the Earth's surface were based on correlations of intra-plate volcanic and / or tectonic events with cycles in reversal frequency (Vogt, 1972; Jones, 1977; Sheriden, 1983, 1986; Loper and McCartney, 1986). Although most of these correlations have since been shown to be based on spurious data (Merrill *et al*., 1996), they formed the basis

for the popular belief that changes in the thickness of D'' (through the release of plumes), trigger shifts in geomagnetic reversal rate.

Larson (1991) reported a 50% to 75% increase in ocean-crust formation between 120 Ma and 80 Ma and advocated a series of major CMB-derived plumes reaching the surface as the cause. These plumes were responsible for generating up to 8 oceanic plateaux and constituted what Larson (1991) termed a 'superplume episode'. Anderson (1994) rebuked this however, claiming that lithospheric conditions triggering shallow upwellings was a more likely explanation (see § 6.2). Larson (1991) also claimed that the initial pulse of material (120 Ma – 125 Ma) was responsible for a global increase in plate motion. This was achieved either by dynamic separation of the plates by the plumes, or a lowered asthenospheric viscosity caused by plume heating. This itself was dismissed by Heller *et al.* (1996) who claimed crustal production increased only in the Pacific while the motion of other oceanic plates actually slowed during this time.

This supposed superplume coincided with the onset of the CNS, a fact that Larson and Olson (1991) attributed some significance to. They also showed that LIP production had fallen since the peak at 120 Ma to a low at 20 Ma and has risen since and suggested an inverse correlation with reversal frequency for the last 120 Myr. They proposed that the sudden thinning of D'' and consequent increased heat – flux across the CMB triggered a transition in the geodynamo from a weaker oscillatory state into a strong stable state (the CNS). This assumption was based on numerical studies of the variation of reversal rate with *magnetic Reynolds number* (R_m) for two numerical models of the dynamo (Braginskii and Roberts, 1987; Olson and Hagee, 1990). These showed that an increased R_m, the result of the higher convection velocities associated with enhanced CMB heat-flux, impeded the reversal process. This is supported by the more sophisticated G-R dynamo which tends to exhibit more unstable behaviour when its efficiency is reduced (Glatzmaier and Roberts, 1997). However, this is not the case for all numerical dynamos, the model of Sarson

and Jones (1999), which is constructed in a lower *Rayleigh number* regime, displays a positive correlation between Ra and reversal frequency (Sarson, 2000).

Plumes are expected to take 20 – 30 Myr to rise from the base of the mantle to the lithosphere (Loper, 1992). Larson and Olson (1991) explained the synchronicity of extensive volcanism with the onset of the CNS by stating that the thinning of D'' triggered a decrease of reversal frequency cumulating in the CNS just as the plume reached the surface.

Larson and Kincaid (1996) later adjusted the model by supposing the following course of events: Gondwanaland broke up at approximately 130 Ma, this lead to massive subduction and slab penetration at the 660 km discontinuity. They used a simple 2-dimensional fluid dynamical model to show that the discontinuity is advected surfacewards by hot counter-flow resulting from the introduction of cold material into the lower mantle. The resulting volcanism was shown to be quasi-synchronous with the arrival of the slab material at the CMB, resulting in increased heat-flux across out of the core and hence the onset of the CNS.

However, Loper (1992) claimed that the lower mantle has a very long (10^9) natural time-scale and that D'' has considerable thermal inertia. This implies that following an episode of plume flux from D'', the heat flux from the core changes only very slowly and therefore so would the geomagnetic response.

Eide and Torsvik (1996) also invoked changes in total heat flux across the CMB as the trigger for a superchron. They point out that the onset of the PCRS was coincident with the final amalgamation of Pangaea and that approximately 200 Myr of subduction preceded this. Three dimensional studies of mantle convection (Tackley *et al*., 1993; Honda *et al*., 1993) suggest that ponding of subducted material occurs at the 660 km discontinuity, a prolonged episode of which can result in catastrophic 'mantle flushing' after which the slabs descend to the CMB. Eide and Torsvik (1996) proposed that this had occurred several times prior to the late

Carboniferous which, through the lateral spreading of slab material at the CMB, developed a cold blanket there. The final flushing episode occurred as the continents coalesced and the pieces of subducted oceanic crust detached themselves. Assumedly, the increased heat flux at the CMB triggered the PCRS in the same way that the thinned D'' triggered the CNS in the model of Larson and Olson (1991).

Eide and Torsvik (1996) also make brief references to the relationship of *true polar wander* (TPW) to their model. A study by Van der Voo (1994) indicated that there was likely a period of rapid TPW from late Ordovician to late Devonian times. Eide and Torsvik (1996) claim that the large-scale subduction, continental assembly at the equator, and catastrophic flushing events at this time, and consistent with their model, could induce such an interval. Courtillot and Besse (1987) compared geomagnetic reversal rate with TPW since 200 Ma and found that a period of low TPW coincided with the major interval of decreasing reversal frequency (110-170 Ma) and that due to continental insulation, lithospheric velocities were also low at this time. Conversely during periods of high TPW, the mantle was in a more active state as the continents were moving towards one another and reversal rate was increasing. They proposed the causative link between core and mantle to be, once again, the emitting of plumes from a thick D'' layer. The layer is either inactive, thin and getting thicker or thick and thinning itself by releasing instabilities. In this instance they used the 'cold blob' instability mechanism of McFadden and Merrill (1986) to trigger reversals and stated that these would be more frequent when D'' was thicker and therefore more unstable.

This model is different to those of Loper and McCartney (1986) and Larson and Olson (1991) in that they disregard heat-flux across the CMB and instead look to the simultaneous generation of instabilities at either side of it. They point to the release of a particularly large instability at the end the CNS which manifested itself on the surface as the Deccan traps at the Cretaceous – Tertiary boundary. In light of research conducted since Courtillot and Besse (1987), this simple model appears to be refutable. Larson (1991) has shown that greater LIPs (presumably derived from

larger D'' instabilities) were emplaced on ocean floors in the 40 Myr preceding this event. This time should be quiescent in order that no instabilities were released into the core and a superchron could be maintained.

Prévot *et al*. (2000) recently compiled an updated record of TPW using only data from igneous recorders. They found a somewhat different variation of TPW over the last 200 Myr with standstills from 0 – 80 Ma and 150 - 200Ma and a dramatic peak at 110 Ma.

They interpreted the coincidence of rapid TPW with excessive volcanism and an inhibition of the reversal mechanism as a signal of a major mantle reorganisation event in the early Cretaceous. TPW is believed to be caused by mass reorganisation within the planet, they argue therefore that the remarkable stasis in this phenomena before and after the event suggests stable, layered convection in the mantle occurred at these times. This was punctuated by a dramatic mixing of the two layers caused by catastrophic avalanching of cold dense material through the 660 km 'boundary' as reported in the numerical models of Tackley *et al*. (1993), Honda *et al*. (1993) and Davies (1995b).

This is consistent with the claim by Gallet and Hulot (1997) that the rapid shift in the reversal record from stationary to non-stationary behaviour they observed at 130 Ma (§ 6.1.3) was likely to have been caused by the arrival of a slab (or series of slabs) in the LMM.

Perhaps one of the most convincing pieces of evidence of correlation between tectonic processes and the palaeomagnetic record comes from wavelet analysis of the reversal record (Ricou and Gibert, 1997). This indicated ten discrete discontinuities in reversal frequency since 158 Ma superposed onto the 10^8 year variation. Each one of these corresponds to the formation or abandonment of a MOR greater than 2000 km in length, the magnetic events being delayed by only 3.1 ± 1.7 Ma.

Previously, Ricou (1995) had noted distinctive plate tectonics patterns responsible for Tethys Ocean generation and termination, and observed that switches between the two were quasi-synchronous with the two most recent superchrons. To explain both the long and short-term coincidences of crustal and geomagnetic events, a system of load-distribution equilibration at the CMB was proposed. Hence, as the lateral distribution of mass in the crust / upper mantle undergoes change, the topography at the CMB adjusts itself to counteract it. This mechanism has not yet been proved viable but remains one of the few possible ways in which the crust and core could interact without whole-mantle transfer of heat and / or mass which would necessitate a greater time difference between events.

7. An objective statistical analysis of the global dipole moment record

7.1 Introduction and previous analyses

The present study aimed to assess the relationship between long-term (10^7 -10^8 year) variation in geomagnetic poloidal field strength and other global processes involving the core and the mantle. A prerequisite for this was obviously a sound awareness of the extent and type of geomagnetic intensity variation over a time greater then 100 million years. The statistical analysis described here was performed with the objective of answering the following basic questions with respect to trends in field strength: 'What has definitely occurred?' and 'what is likely to have occurred?' Care was taken to approach the analyses objectively, using only information provided by the data themselves.

An answer to a third important question, 'What has definitely not occurred?' required the data to be analysed in the context of information about (and particularly timings of) processes not self-evident in the VDM record itself. As such analyses are implicit to the interpretation of the data, they are reserved for chapter 8.

Absolute palaeointensity estimates are derived from the primary TRM of rocks with ages spanning the last 3.5 Gyr. These are usually combined with the inclination of the palaeofield to calculate the VDM (§ 2.4.2) and allow direct comparison of estimates from different locations. If palaeodirectional information is not available, as with samples from ocean cores etc., then palaeofield inclination must be calculated from the palaeolatitude of the rock unit (estimated from plate reconstructions), assuming an axial dipole. Dipole moments generated using this technique are referred to as virtual axial dipole moments (VADM's) and are subject to greater imprecision than VDM's because they do not allow for dipole wobble. Both VDMs and VADMs are used, without

discrimination, in the study described in this chapter in preference to field intensity due to their interchangeable nature.

Some statistical analysis of the whole or large parts of the VDM record has been performed previously (e.g. Kono and Tanaka, 1995b; Perrin and Scherbakov, 1997) allowing the following major observations to be made:

- At present, the limited VDM data set does not clearly display any overall trend with time since 3.5 Ga (Kono and Tanaka, 1995b).
- Much of the Mesozoic is characterised by persistent low dipole moment values (approximately one-third of the present-day value). This Mesozoic dipole low (MDL) was first reported by Prévot et al. (1990) and has since been supported by numerous studies. Its boundaries and the method of transition from this period to the present state remain unconstrained however. Perrin and Shcherbakov (1997) used latitudinal dependency of field strength to show that the dipole structure of the field was maintained through this period. They also showed that the MDL was highly unlikely to be a product of insufficient sampling of a field similar to that that has prevailed for the last 23 Ma.
- Secular variation (SV) of the field, as denoted by the standard deviation as a percentage of the mean VDM, is much greater for the period 10-0 Ma than for 10-0 Kyr (Kono and Tanaka, 1995b). This suggests that most fluctuations in the dipole field occur on a period of 10^6 years or more. Perrin and Shcherbakov (1997) showed that 100 Myr averages of the VDM record up to 300 Ma suggested a direct relationship between standard deviation and VDM mean. However, they acknowledged that this result was compromised by a similar relationship exhibited between standard deviation and the number of points comprising the mean.

Selkin and Tauxe (2000) performed the most recent analysis of the VDM record using only data that were acquired by the Thellier method employing pTRM checks and passing the criteria given in § 2.4.2. They concluded that there was no long-term variation of dipole moment between 0.3 and 300 Myr and that a mean value of $\sim 5 \times 10^{22}$ Am^2 was maintained.

The present study used two databases as its source of data. The first of these was compiled by Tanaka *et al*. (1995) and later updated by Perrin and Shcherbakov (1997) and Perrin *et al*. (1998). It contains all published palaeointensity site averages (referred to as SA data from here on), applying no selection criteria. The record was made more comprehensive by the addition of missing submarine basalt glass (SBG) SA data published in Selkin and Tauxe (2000).

It was decided that this analysis would not include any of the SA estimates presented in chapter 4. This was done primarily in the spirit of fairness, none of these results were published at the time this analysis was begun and many had not yet been determined. Nevertheless, the experimental part of this study was primarily concerned with adding to our knowledge of dipole moment variation during the Mesozoic. Therefore some discussion of the data it produced in the context of this study is necessary. This will be given in § 9.3.

The pooled set, used in this analysis, contained over 1700 data but some filtering was required in order to allow the study to focus on analysing trends of $10^7 – 10^8$ years and to remove unreliable and unusable data. The data used satisfied the criteria listed below which are justified in the subsequent paragraphs:

1. An age between 10 and 400 Ma, either of radiometric or stratigraphic origin must be specified.
2. A VDM or VADM must be calculated from either the inclination of the magnetisation or inferred from palaeolatitude.
3. The polarity of magnetisation must not be specified as transitional.
4. The method of palaeointensity acquisition must be either Thellier or Shaw or a combination using one or both of these methods.

The period 10 – 0 Ma contains 29% of the data, is heavily skewed towards younger ages, and has been rigorously studied previously by Kono and Tanaka (1995b). It was decided therefore, that these data would be omitted. Conversely, data aged older than 400 Ma are very scarce and sufficiently widely distributed to render an analysis, even of 10^8 year trends, untenable. Therefore, only the period 400 – 10 Ma, with an average data frequency of 1.6 points / Myr, was

assessed in the present study. As discussed earlier field strengths are dependent on latitude at the time of magnetic acquisition, therefore VDM and VADM values are required to allow comparison of palaeointensity results from different locations on the globe.

The strength of the poloidal field is believed to fall substantially for several thousand years during a geomagnetic polarity transition (e.g. Prévot *et al*., 1985). As this is not a facet of the long-term variation we are seeking, but rather a short-live phenomena associated with the reversal process itself, data known to be derived from these periods were omitted from this study. This does not guarantee that the surviving record is free from transitional intensity estimates because it can be difficult to assess the polarity of magnetisation in samples that are older than several million years old. For the purpose of this study it is assumed that, given that the geomagnetic field occupies a transitional state for less than 5% of its time (Tauxe and Hartl, 1997) and the estimates are randomly spaced in time, the effects of rogue transitional data are slight.

Finally, the Thellier method is widely regarded as the most reliable method of estimating palaeointensity (Prévot *et al*., 1990; Prévot and Perrin, 1992). The modified Shaw (1974) method (Rolph and Shaw, 1985), although lacking theoretical support and prone to producing SA data with large scatter, has been shown in practice to give similar results to the Thellier method (Thomas, 1992). Data acquired using this method were considered acceptable in the analysis of Kono and Tanaka (1995b) and were not removed before the present analysis. Other methods of palaeointensity acquisition (e.g. Wilson, 1961; Van Zijl *et al*., 1962) are considerably less reliable than Shaw's, consequently estimates recovered using these methods were not used in this analysis except where they were used in conjunction with either the Thellier or Shaw method.

Following the application of the four-stage filter outlined above, 713 SA data remained with which to perform the analysis. This set contained no data known to be unreliable or inappropriate. However, it was decided that a sub-set of data passing a fifth criterion – namely that the SA must be derived from two or more

estimates resulting in a standard deviation less than 10% of the mean – would be given elite status. Self-consistency is an important quality for sight averages to display, an SA is generally produced from sample estimates close to one another in a rock unit and therefore should not be subject to variation of geomagnetic origin. 420 data (58.9% of the total) were judged to be more reliable than the rest by virtue of their low standard deviations, the uses for this selected site average (SSA) subset are described in the following sections.

7.2 Overview of data

Figures 7.1 and 7.2 adequately represent the first-order features of the ASA (all site average) and SSA data respectively. The considerable scatter of VDM data observed between estimates of similar ages (figs 7.1(a) and 7.2(a)) is unlikely to be due entirely, or even primarily, to the imprecision of estimates in the records. Rather, it is largely caused by "rapid" variation of the dipole moment, which occur on too short a time-scale ($< 10^6$ year) to be caused by the major mantle processes of interest to this study. The variations in the magnitude of this scatter over longer periods however, could provide important information concerning the evolution of the geodynamo and are discussed later.

The effect of applying the self-consistency criteria to the data is to lower the standard deviation not least by removing all the outlier estimates in the early and late Tertiary. These estimates may well be erroneous and their absence in the SSA data instils some confidence in this discriminative process.

Figures 7.1(b) and 7.2(b) highlight two of the major problems faced when attempting to interpret the current VDM record: scarcity and uneven distribution of the data. The inequality in data representation is such that variation in the dipole moment with periods greater than 10 Myr could cause a significant bias in any analysis of the total data set. This is best illustrated by examining the distributions of the SSA data by VDM and age (figs. 7.2(c) and 7.2(b) respectively). The former histogram suggests a bi-modal distribution of estimates, this feature was observed by Perrin and Shcherbakov (1997) in their

selected data and described by them as being typical of a chaotic system governed by highly non-linear equations. In reality, the second peak in the distribution ($9 – 14 \_ 10^{22}$ Am^2) is caused by the large number (42% of the total) of internally consistent values from the period 340 – 260 Ma. Consequently, a distinction needs to be drawn between the distribution of internally consistent VDM estimates with ages 400 – 10 Ma, shown in figure 7.2(c), and the actual distribution of dipole moments during this period.

Figure 7.3(a) displays the quantity of data omitted from the SSA record in each 20 Myr age bin. The large number of omissions in the periods 20-0 Ma and 60 – 80 Ma is shown to be largely proportional to the amount of ASA data (figure 7.3(b)). Nevertheless, ignoring the period 240 – 200 Ma (where there are no SSA data), data from the period 120 – 10 Ma appear to be more prone to failing the internal consistency test than those from the rest of the record. This is largely due to the many single sample estimates within this period which were automatically rejected from the SSA record. Later it will be shown that, with the exception of certain periods, SSA data is sufficiently abundant to test inferences made using the ASA record.

The large scatter evident in the VDM record and other direct observational studies (e.g. Constable *et al*, 1998) indicates that the dipole moment varies substantially on time-scales shorter than those we are aiming to identify, and has done this to some extent, for the entire period of this study. Additionally, non-dipole features of the field can remain approximately static for at least 400 years (Jackson *et al*, 2000) and possibly much longer (§ 6.1.2) causing VDM estimates to deviate from the real dipole moment. While most palaeointensity studies provide estimates from more than one site, very few are able to average SV sufficiently to produce a *palaeomagnetic dipole moment* (McFadden and McElhinny, 1982). Therefore, the VDM record is clearly prone to being biased towards those studies which published the most SA data when, in terms of representation of the long-term trends of the field, such biasing may not be justified.

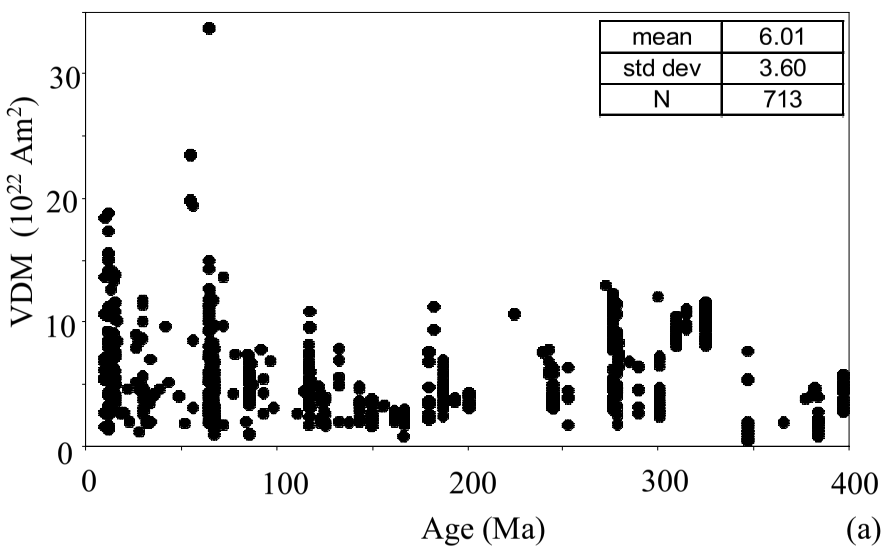

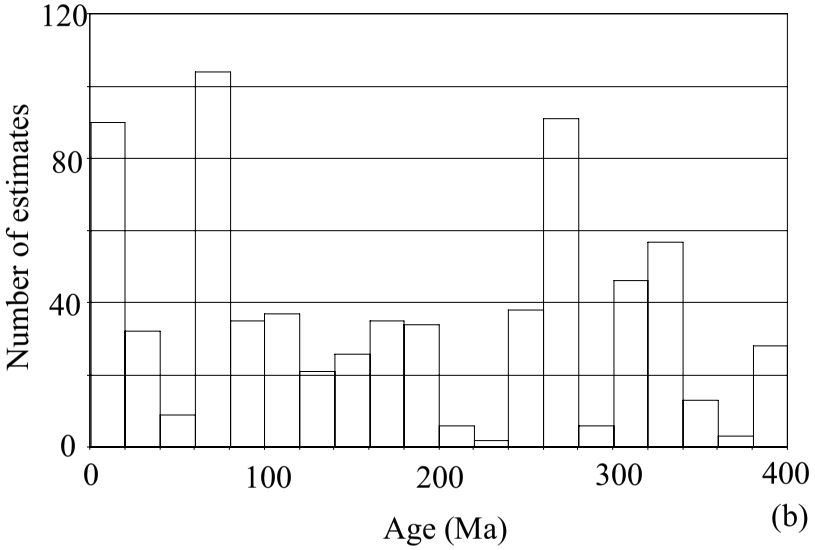

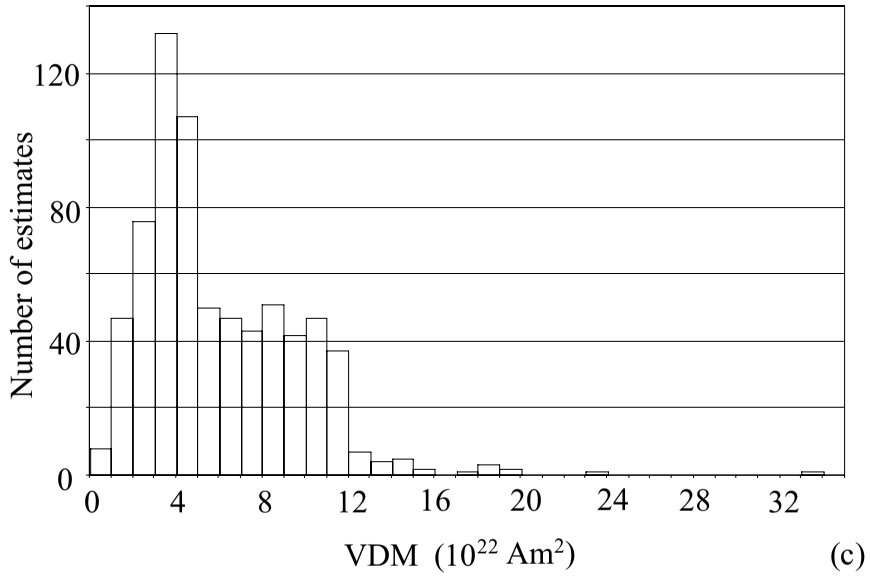

Figure 7.1: All site average (ASA) data plotted to show (a) VDM versus age, (b) age distribution in 20 Myr bins, (c) VDM distribution in 1 _ 10^{22} Am^2 bins.

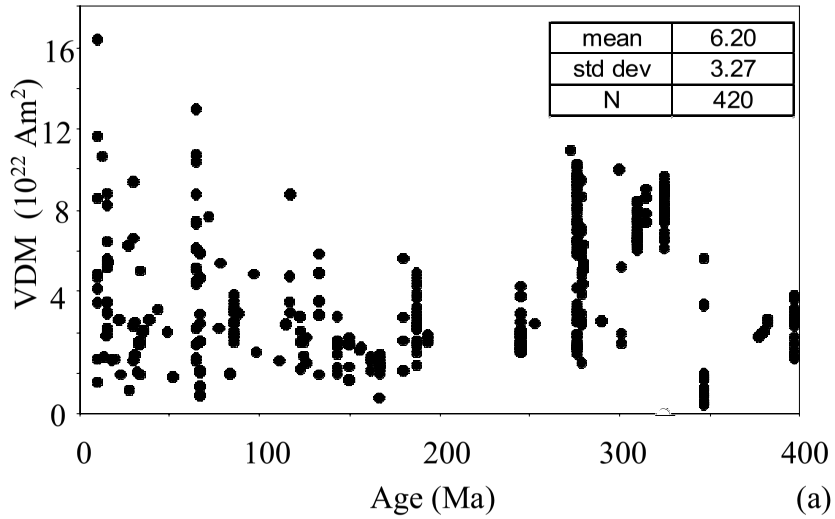

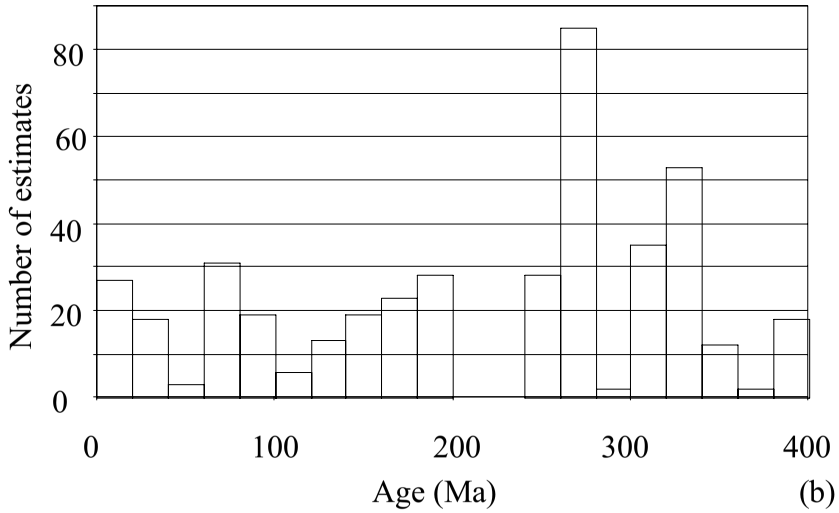

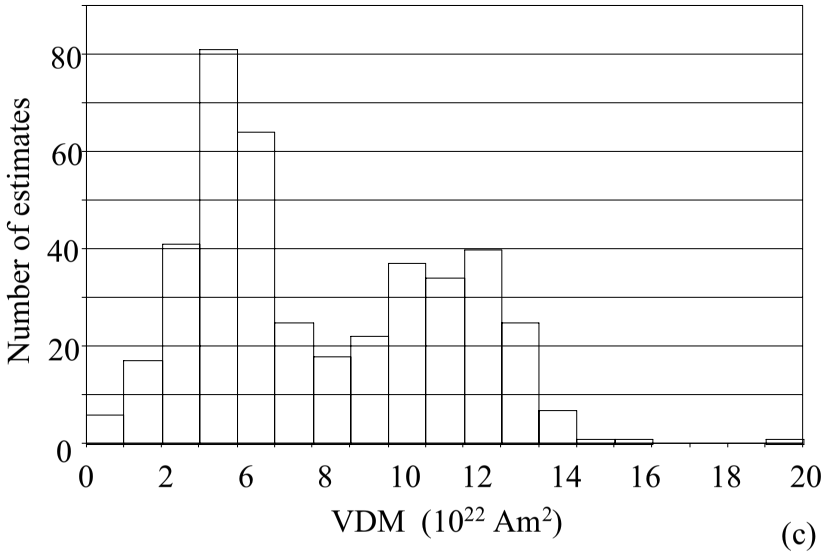

Figure 7.2: Selected site average (SSA) data plotted to show (a) VDM versus age, (b) age distribution in 20 Myr bins, (c) VDM distribution in 1 _ 10^{22} Am^2 bins.

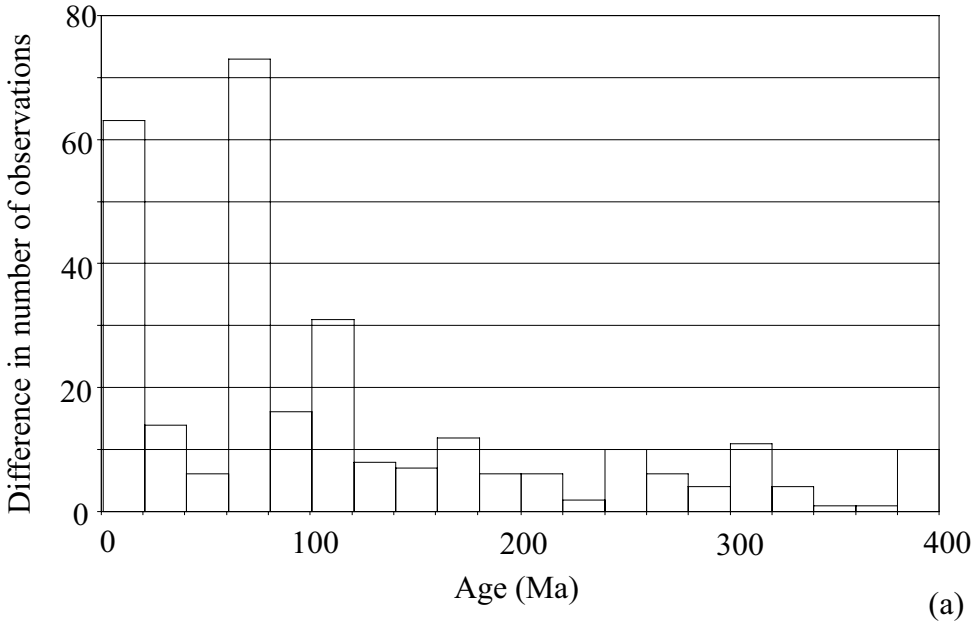

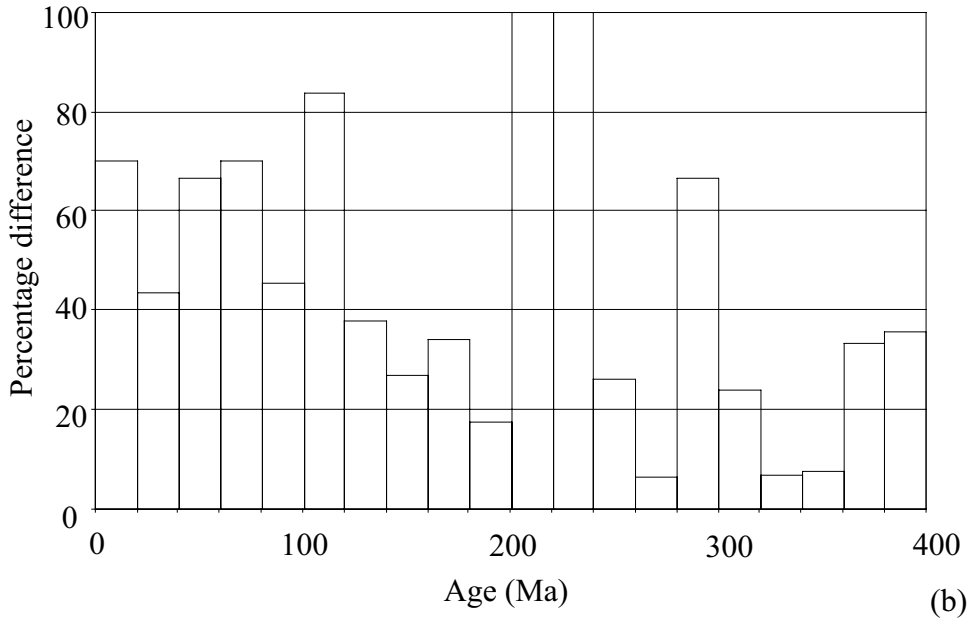

Figure 7.3(a): differences between ASA and SSA expressed as number of observation and (b) percentage of ASA data not present in SSA data.

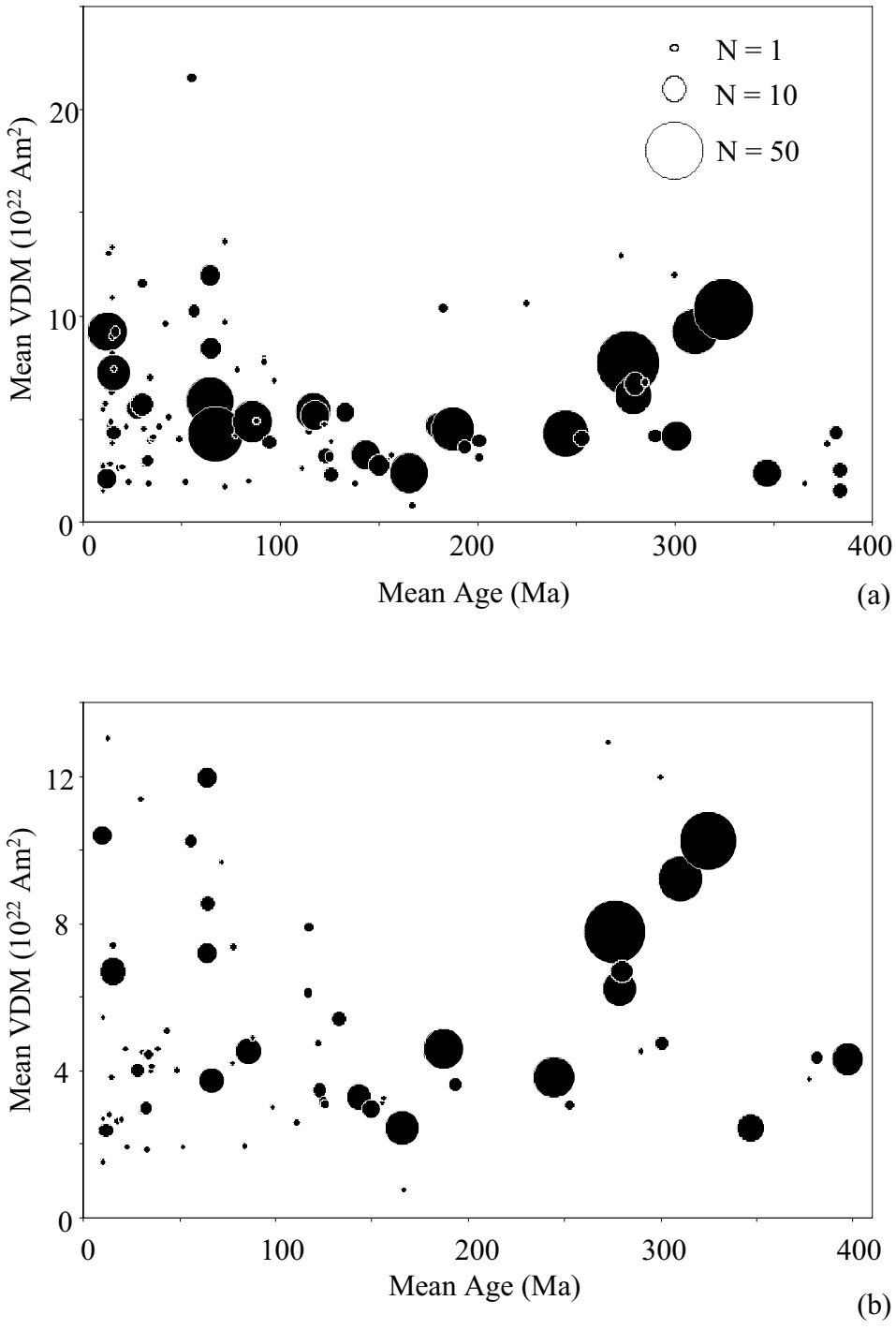

Figure 7.4: Mean VDM versus mean age for (a) all RS data, (b) selected RS data.

Although greater numbers of SA data produced from a single study increases the probability that short-term dipole variation has been averaged out, problems may occur when SA data from more than one study are averaged. Consider the following scenario involving two lava successions formed at roughly the same time.

The first succession contained individual flows formed every fifty years for 1kyr, during which time a flux lobe of low geomagnetic intensity was centred upon the region. However, the second succession consists of flows produced every ten thousand years for 50 kyr. Assuming that every flow produces a good quality SA estimate, it is clear to see that a simple average of these estimates will be heavily biased towards the much more restricted study. This problem cannot be easily overcome, the amount of dipole moment variation in (say) 1 Myr is unknown for poorly sampled time periods, therefore a reliable assessment of the extent to which a study has averaged out short-term fluctuations cannot be made.

An alternative approach was used here. Estimates passing both of the following criteria were grouped into 'Rock Suites' (RS) and are listed in appendix 7:

1. The age estimates must place the SA data within 5 Myr of each other and the uncertainty in this estimate must be sufficient to allow the estimates to be contemporary.
2. The location of the sampling sites must be within 5º latitude and 5º longitude of one another.

These criteria are admittedly somewhat arbitrary; they are likely to be over–strict but were applied in order to make certain that secular variation of the dipole moment is no-longer a biasing factor.

Obviously it would be neither fair nor sound practice to over-apply statistical analysis to data arranged in this way: a RS datum acquired from just one SA estimate would carry the same weight as one which averaged many data. However, it is worth noting that *every RS average is a spatially and / or*

temporally distinct representation of the dipole moment. The usefulness of the RS grouping system is therefore in allowing the data to be presented in a more interpretable way, helping to illustrate where SA biasing may be a problem, and in providing some verification of results obtained from the record of SA estimates.

For completeness, the primary statistical parameters of the RS data are given in table 7.1.

	μ_{VDM}	σ_{VDM}	N
All SA	6.00	3.60	711
Selected SA	6.20	3.27	420
All RS	5.61	3.46	109
Selected RS	5.01	2.88	73

Table 7.1: mean, standard deviation and number of estimates for representations of VDM data in the period 400 – 10 Ma.

7.3 Evolution of the dipole moment

The plots of mean VDM against mean age for all and selected RS estimates (figures 7.4 (a) and (b)) confirm the basic pattern observed in the equivalent SA plots. That is:

- The inferred mean value (largely controlled by the highest individual values) rises quasi-continuously from a minimum between 167 and 180 Ma to a maximum between 10 and 67 Ma.
- There is a suggestion of a gradual decrease in mean value from a maximum between 325 and 347 Ma to the minimum mentioned above. This appears to have been initiated by a rapid transition from persistently low values of VDM from 400 Ma to at least 347 Ma.
- The variation of the lowest values of VDM with time is clearly much less than that of the highest values. An obvious corollary of this is that the short-term variation in dipole moment is proportional to the mean.

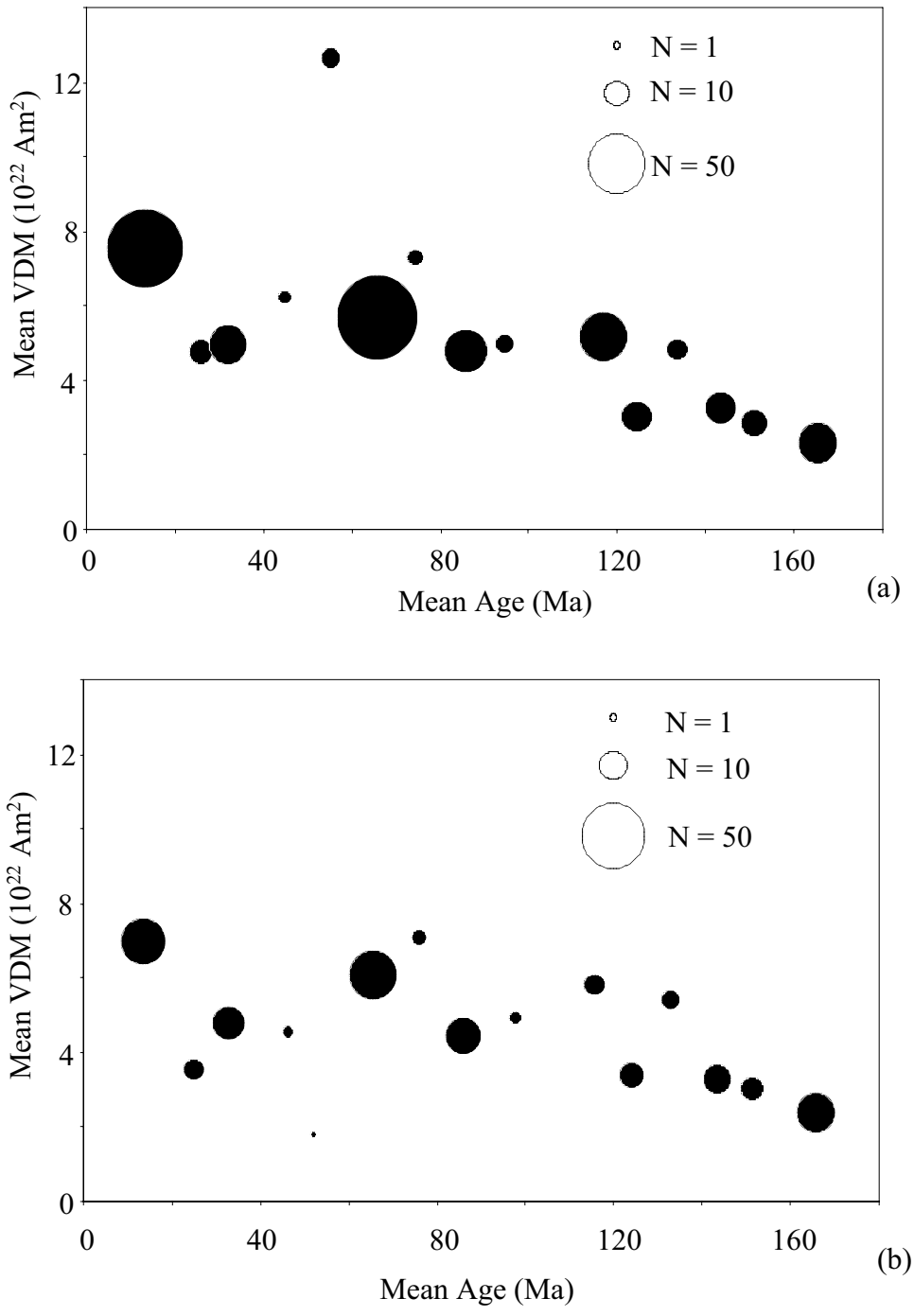

Figure 7.5: Mean VDM estimates in 10 Ma age bins since 167 Ma for (a) ASA data and (b) SSA data.

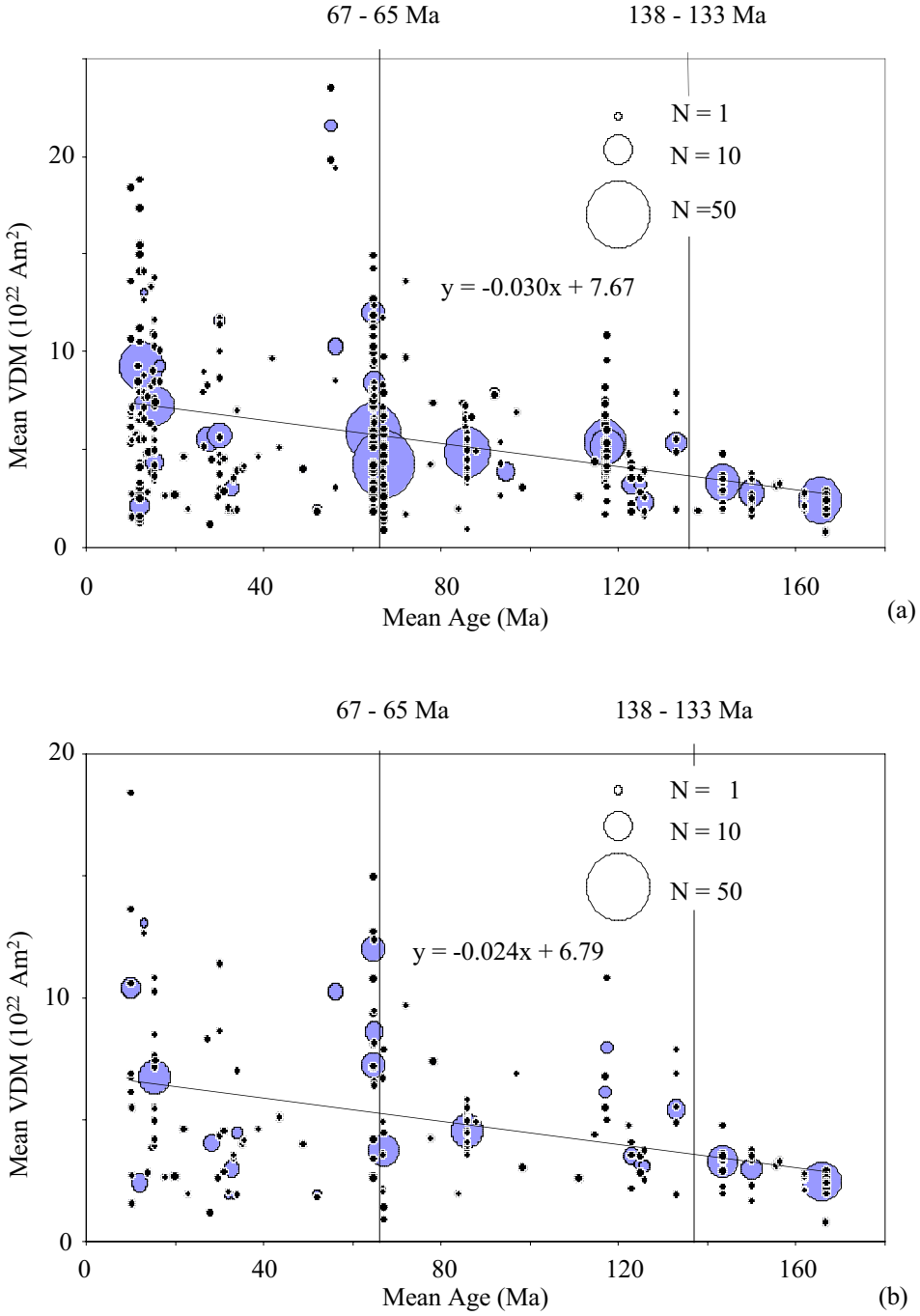

Figure 7.6: Plots of SA (black) and RS (blue) data with ages 167 - 10 Ma for (a) all data, (b) selected data. The equation is that of the regression line (through the SA data) shown, the vertical lines signify the partitions suggested by ANOVA.

7.3.1 The period 167 – 10 Ma

The estimates in this period were grouped into 10 Ma bins, the variation in the mean VDMs through time (figure 7.5) affords us the clearest picture of the estimated dipole moment behaviour during this period. It is still difficult to ascertain from these plots whether there was a continuous or punctuated evolution throughout the period, certainly there appears to be a reduction in the rate of increase from 119 – 10 Ma, relative to 167 – 120 Ma. This is supported by the RS data (figure 7.4) which exhibit a much larger scatter in low values during this period. Figure 7.4 (a) especially shows little change in the slope of its highest values but a great reduction in the slope of the lowest VDM data. However, this could easily be an artefact due to the large number of RS data with low N in the later period.

The manner of transition from low to high VDM was investigated using a simple but effective method to reveal whether a continuous or punctuated variation was preferred. Firstly, a linear regression was applied to all the SA data in this period (figure 7.6(a)). The mean squares of the regression (MS_R) is equal to the sum of the squares of the regression line (SS_R) due to there being only 1 degree of freedom (see Davies, 1973 for more details). The mean squares of the deviation of the data around the regression (MS_D) is calculated by:

$$MS_D = \frac{SS_D}{N-2}$$

Where SS_D is the sum of the squares of the deviation about the regression and N is the total number of data. The F value is the ratio of the variance of two groups of data and in this case is a measure of the likelihood that the slope of a linear regression is not zero (i.e. that the data follow a trend and are not random). It is calculated from:

$$F_{regress} = \frac{MS_R}{MS_D}$$

and obviously becomes higher as the fit of the data to the regression line is improved. The F value from linear regression in the period 10 – 167 Ma is 60.2 for the ASA data, and 32.2 for the SSA data. As expected, this is sufficient to rule out the null hypothesis that the slope is zero with greater than 99% confidence.

Single-step analysis of variance (ANOVA) is a means of assessing the difference between two random samples drawn from normal populations. In the case of SA VDM estimates, samples often appear closer to being drawn from log-normal populations, however there are a sufficient number of data in each sample used in this study for ANOVA to be effective. The necessary equations are listed below:

$$MS_A = \frac{SS_A}{m-1}$$

$$MS_W = \frac{SS_W}{N-m}$$

$$F_{ANOVA} = \frac{MS_A}{MS_W}$$

where, MS_A and SS_A are the mean squares and sum of squares respectively between the samples, MS_W and SS_W are the mean squares and sum of squares respectively within the samples, m is the number of samples, and N is the total number of data in all samples. In this case F is proportional to the likelihood that the samples are drawn from different populations. When the data are split into two samples (m = 2), the number of degrees of freedom used to calculate the significance of the F value is the same for both the ANOVA and regression analyses. This allows a direct comparison of F values to indicate which of the methods of variation, i.e. continuous linear change or a single punctuation, more accurately describe the evolution of the dipole moment.

Crucial to this comparison is the position of the partition of the data into the two samples used by the ANOVA analysis. The optimum position of this partition

was found by progressively moving it along the age axis and observing where the maximum F_{ANOVA} value was reached. The results for the ASA data set and their meanings are given below:

- From ANOVA of data between 10 Ma and 167 Ma, a maximum F value (64.2) was attained when the partition was between 65 and 67 Ma. This is not significantly greater than that calculated from the regression analysis but does indicate that there is a large difference between data either side of this partition.

- The data between 67 Ma and 167 Ma were then analysed with the results: $F_{regress} = 24.0$ and $F_{ANOVA} = 43.0$ when the partition was between 122.4 Ma and 133 Ma. Another peak in the value of F_{ANOVA} (40.2) occurred when the partition was moved to between 133 Ma and 138 Ma. Clearly, a jump between low and high values at either of these intervals is a significantly better way of explaining the evolution of VDM estimates through this period than a continuous transition.

- An analysis of the data between 10 Ma and 122.4 Ma gave $F_{regress} = 12.8$ compared to $F_{ANOVA} = 25.8$ when the partition was in the optimum position between 65 Ma and 67 Ma. Once again, a punctuated evolution was preferred.

The same progressive analysis on the SSA data set yielded qualitatively identical results with the following exceptions:

- In the 167 – 67 Ma period, ANOVA indicated that the partition should be between 133 Ma and 138 Ma.
- In the 133 – 10 Ma period, although ANOVA, with partitioning between 65 Ma and 67 Ma, gave a significantly higher F value than regression (7.9 compared to 4.1), both were much lower than those attained in all other analyses ($F_{regress}$ was only just significant at the 95% level). This indicates that SSA VDM evolution through this period is smaller and less direct than

the other periods analysed. The results are still significant however, and figure 7.4 (b) shows more clearly that an increase definitely took place.

Three major segments of data emerge from the ASA and SSA records as a consequence of these analyses. These are 65 – 10 Ma, 122.4 / 133 – 67 Ma, and 167 –123 / 138 Ma. It was decided that the segments would be kept consistent for both the ASA and SSA data sets and this was achieved by placing the partition between the second and third segments between 133 Ma and 138 Ma for both sets of data. This is easy to justify from both the small difference between F_{ANOVA} values with the partition at this position rather than the optimum in the ASA record, and qualitatively through observation of the data relative to this partition on figure 7.6.

With the dipole moment record in its current state, it can not be concluded that these three segments represent distinct periods of consistent dipole behaviour because the position of the inferred boundaries are particularly sensitive to the SA data close to them and there are large gaps within the segments. However, the data compartmentalising described here is a lot less arbitrary than introducing partitions every (say) 10 Ma as is usually done (e.g. Selkin and Tauxe, 2000). Some form of partitioning is necessary to allow the variation of the data through the record to be assessed (§ 7.3.3).

The ANOVA versus regression test was performed on the SSA data set applying partitions at the two boundaries specified above. The two analyses now possessed different degrees of freedom and consequently, the F values could not be directly compared. However, a comparison of the probabilities of each failing to reject the null hypothesis of random distribution ($1 \_ 10^8$ for ANOVA and $7 \_ 10^8$ for regression) shows that punctuated increase is favoured over linear increase at the 95% confidence limit. However, it is stressed that much more high quality data is needed before the punctuated increase model can be confirmed and the position of the partitions constrained.

It is clear to see that the behaviour of the mean dipole moment varies between the Tertiary and the Jurassic. Nevertheless it is useful to have quantitative support from statistical tests and the segmentation of the record allows this. The K-S test (see § 7.3.3 below) was used to compare ten random samples of VDM estimates from the 65 – 10 Ma segment with those from the 167 – 138 Ma segment. The greatest probability of the two being drawn from the same distribution was found to be $\sim 10^{-20}$ for all the data and $\sim 10^{-13}$ for the selected data set.

7.3.2 The period 400 – 180 Ma

Despite the fact that a single long-term trend is suggested through much of the data older than 180 Ma, it would not have been feasible to apply similar analyses to these estimates. The record suffers from large sections of poor or absent coverage and the limited number of RSs present, even in well-represented sections, means that the SA data tends to be confined to the narrow vertical strips noticeable on figures 7.1 (a) and 7.2 (a). Therefore it is extremely likely, that the sampling density distribution, rather than the data themselves, would generate the divisions.

It was a simple matter to divide the record into age-defined subsets by eye using the distributions of both SA and RS data. This process was done on the basis of grouping similar (in both VDM and age) data. This had the disadvantage of being somewhat arbitrarily controlled by age distribution and subjectivism. However, it allowed data analysis to handled easier than if they were all together. The segments chosen are indicated on figures 7.7 (a) and (b) and are discussed in the next section.

7.3.3 Analyses of individual segments

What follows is a discussion of each segment defined in the last two sections and illustrated in figures 7.6 and 7.7. Figures 7.8 – 7.16 enable a closer look at the features of the individual segments to be made.

The non-parametric Kolmogorov – Smirnov (KS) test (Davies, 1973) is a useful means of assessing the likelihood that two samples are drawn from the same distribution. The K-S statistic itself is simply the maximum deviation between 2 cumulative distribution functions (C_{N1} and C_{N2}):

$$dn = \max_{-\infty<x<\infty} \left| C_{N1} - C_{N2} \right|$$

The probability that two samples drawn from the same distribution will deviate by dn is given by:

$$P = 2\sum_{i=1}^{\infty}(-1)^{i-1} e^{-2i^2 N dn^2}$$

Where N is the number of observations. The K-S test will be used on data in every segment to compare the sample distribution with that expected by both Gaussian and log-normal distributions with the same mean and standard deviations.

<u>65 – 10 Ma</u>

65 - 10 Ma	μ_{AGE}	μ_{VDM}	σ_{VDM}	N_{SA}	N_{RS}	N_{RS} / N_{SA}	$P_{GAUSSIAN}$	$P_{LOG\text{-}NORMAL}$
All data	32.8	7.05	4.65	183	53	29%	0.02	0.90
Selected data	33.5	6.22	3.66	65	32	49%	0.39	0.83

Table 7.2: Summary of data from the segment 10 –65 Ma. $P_{GAUSSIAN}$ and $P_{LOG\text{-}NORMAL}$ are the probabilities, calculated using the K-S test, of the sample being derived from a Gaussian / Log-normal distribution with the same mean and standard deviation.

Data from this period are higher on average and more scattered than in most segments. This period is also anomalous in the sense of having a large number of RS data relative to SA data which suggests that extremes of SV are, for the most part, of less concern here than elsewhere. The mean VDM and its standard deviation alter significantly upon application of the self-consistency filter, the large reduction in N attests to the large quantity of lower quality data in this segment.

Figure 7.8 reveals large temporal breaks in the record, particularly the periods 26 – 16 Ma and 55 – 35 Ma. This complicates the interpretation of the most interesting feature to be drawn from these data: the very low gradient of the regression line. This line is clearly 'anchored' to the clusters of data at the temporal extremes of the segment, however both of these are produced from numerous RSs. Thus, there is a strong suggestion that, although the behaviour of the dipole moment in the interior of this segment is poorly constrained, there was very little trend through the segment. A simple method of further confirming or refuting this suggestion was employed. The data were split at 37.5 Ma and the distributions of all and selected data before and after this time were compared. It was found that the K-S test could not distinguish between them at the 95% confidence limit, reinforcing the premise outlined above.

The data in the 10-65 Ma segment are clearly drawn from a log-normal distribution which concurs with the results of McFadden and McElhinney (1982) for the period 5 – 0 Ma.

133 – 67 Ma

133 - 67 Ma	μ_{AGE}	μ_{VDM}	σ_{VDM}	N_{SA}	N_{RS}	N_{RS} / N_{SA}	$P_{GAUSSIAN}$	$P_{LOG\text{-}NORMAL}$
All data	93.4	4.63	2.17	144	23	16%	0.42	0.32
Selected data	95.7	4.54	1.97	52	18	35%	0.53	0.20

Table 7.3: Summary of data from the segment 133 – 67 Ma.

The average VDM in this segment is significantly lower than that in 65 – 10 Ma, displaying a concomitant reduction in the scatter of the estimates. This long period also displays pronounced periods of insufficient representation (figure 7.9,

noticeably during the Cretaceous normal superchron (CNS; 108 – 83 Ma), and the 10 Myr preceding it. Fortunately, there is still a relatively high percentage of RS data in the period as a whole.

Once again, the gradient of the regression line is not significantly different from zero and the K – S test cannot discriminate between the distributions of all and selected data from the first and second halves of the segment.
The distribution that the data in this segment are drawn from is not obvious. While the histograms (especially that for all the data) retain the long tail to the right, they do not peak as far to the left as those in the 65 – 10 Ma. The K-S test favours the Gaussian distribution in both cases but cannot rule out log-normal as a possibility.

<u>167 – 138 Ma</u>

167 - 138 Ma	μ_{AGE}	μ_{VDM}	σ_{VDM}	N_{SA}	N_{RS}	N_{RS} / N_{SA}	$P_{GAUSSIAN}$	$P_{LOG\text{-}NORMAL}$
All data	155.6	2.68	0.75	52	7	13%	0.93	0.88
Selected data	156.4	2.76	0.72	38	6	16%	0.90	0.46

Table 7.4: Summary of data from the segment 167 – 138 Ma.

This segment contains significantly less RS data than the two previously described, and consequently is intermittent in its coverage (figure 7.10). The mean VDM and its standard deviation are much lower than average although a significant (~ 0.4 / 10 Myr) trending increase in VDM is inferred. This is verified by a K-S comparison of the two halves of the segment which rules out a common distribution with greater than 99% confidence.

The K-S test prefers the Gaussian as a distribution for the data in this segment, owing to the lack of a high-value tail. However, this and the log-normal distribution become more similar as the standard deviation becomes smaller.

201 – 180 Ma

201 - 180 Ma	μ_{AGE}	μ_{VDM}	σ_{VDM}	N_{SA}	N_{RS}	N_{RS} / N_{SA}	$P_{GAUSSIAN}$	$P_{LOG\text{-}NORMAL}$
All data	187.9	4.60	1.72	50	6	12%	0.16	0.82
Selected data	187.3	4.48	1.24	32	3	9%	0.97	0.90

Table 7.5: Summary of data from the segment 201-180 Ma.

The mean VDM and standard deviation in this segment are similar to those in the 133 – 67 Ma, indeed the K – S method cannot discriminate between them. Nevertheless, the increasing trend of the VDM through this period seems to preclude any symmetry about a minimum at ~ 170 Ma. This inferred trend, especially that in the selected set, must be treated with caution however. The age interval is not large and the bulk of the data are concentrated towards the centre of the period. Much more data from this segment, and for the preceding 40 Myr, are necessary before anything more than very long-term variation in the dipole moment can be supposed.

Regarding the frequency distribution of VDM data, the high-value tail of the unselected histogram is eliminated by the internal consistency criterion. In this case therefore, it appears that inaccurate measurement is responsible for the log – normal distribution.

253 – 240 Ma

253 - 240 Ma	μ_{AGE}	μ_{VDM}	σ_{VDM}	N_{SA}	N_{RS}	N_{RS} / N_{SA}	$P_{GAUSSIAN}$	$P_{LOG\text{-}NORMAL}$
All data	245.7	4.24	1.34	39	3	8%	0.05	0.27
Selected data	245.3	3.83	0.78	28	2	7%	0.47	0.77

Table 7.5: Summary of data from the segment 253 – 240 Ma.

This segment is particularly lacking in RS data, the selected set being dominated by just one. The mean VDM is slightly lower than that of 201 – 180 Ma but the distribution is noticeably more log-normal. The evolution of the dipole moment from the period 253 – 180 Ma (with a necessary total disregard of the period between 201 and 240) was explored in the same manner as the three earlier

segments. The regression line displayed only a very slight negative slope (0.09 / 10 Myr) but the K – S method distinguished the two segments with 99% confidence due to their difference in shape.

285 – 273 Ma

285 - 273 Ma	μ_{AGE}	μ_{VDM}	σ_{VDM}	N_{SA}	N_{RS}	N_{RS} / N_{SA}	$P_{GAUSSIAN}$	$P_{LOG\text{-}NORMAL}$
All data	277.4	7.35	3.08	92	5	5%	0.22	0.10
Selected data	277.3	7.58	3.03	85	4	5%	0.29	0.11

Table 7.6: Summary of data from the segment 285 – 273 Ma.

This segment contains a relatively large number of data concentrated into a short age span. Despite the relatively low proportion of RS data, enough are present to represent this central portion of the period well. The histograms produced by the data are very dispersed although the mean values of the three primary RSs are relatively constant.

301 – 290 Ma

301 - 290 Ma	μ_{AGE}	μ_{VDM}	σ_{VDM}	N_{SA}	N_{RS}	N_{RS} / N_{SA}	$P_{GAUSSIAN}$	$P_{LOG\text{-}NORMAL}$
All data	298.6	4.54	2.38	19	3	16%	0.42	0.98
Selected data	298.6	6.20	3.54	5	3	60%	0.86	0.95

Table 7.7: Summary of data from the segment 301 – 290 Ma.

Although this segment contains an adequate 3 RS data, the number of SA data retained in the selected record is very small. The mean VDM is also shown to change significantly in the selected set, as the one point with high VDM exerts more influence.

325 – 310 Ma

325 - 310 Ma	μ_{AGE}	μ_{VDM}	σ_{VDM}	N_{SA}	N_{RS}	N_{RS} / N_{SA}	$P_{GAUSSIAN}$	$P_{LOG\text{-}NORMAL}$
All data	319.8	9.90	0.98	89	2	2%	0.23	0.23
Selected data	319.5	9.85	0.96	83	2	2%	0.32	0.34

Table 7.8: Summary of data from the segment 325 – 310 Ma.

This segment is particularly striking for a number of features. Firstly, the mean VDM is higher than any other segment and this is coupled to a standard deviation that is very low. Hence it obviously does not conform to the general feature exhibited by most segments where the two are proportional (see § 7.3.4). Additionally, the large number of data are derived from just 2 RSs, although one would expect that such a large number of SA data would preclude insufficient representation of SV. Finally only a very small fraction of the data are not regarded as internally consistent at the 10% level.

397 – 347 Ma

397 - 347 Ma	μ_{AGE}	μ_{VDM}	σ_{VDM}	N_{SA}	N_{RS}	N_{RS} / N_{SA}	$P_{GAUSSIAN}$	$P_{LOG\text{-}NORMAL}$
All data	377.2	3.15	1.78	44	7	16%	0.57	0.12
Selected data	376.5	3.56	1.83	32	4	13%	0.49	0.07

Table 7.9: Summary of data from the segment 397 – 347 Ma.

The period 375 – 350 within this segment is severely lacking data and could have justified the splitting of the segment presented here in two. This aside, the data represents a phase of general low dipole moment prior to a rapid increase between 347 Ma and 325 Ma. There is a reasonable presence of high quality data and the proportion of RSs is adequate in the earliest part at least. There is a suggestion of a decreasing trend in dipole moment through the segment (gradient of regression = 0.4 / 10 Myr). This is surprising in the context of the sudden increase that occurred after the end of the period, however the trend is somewhat tenuous at present given the lack of data in the bulk of the segment.

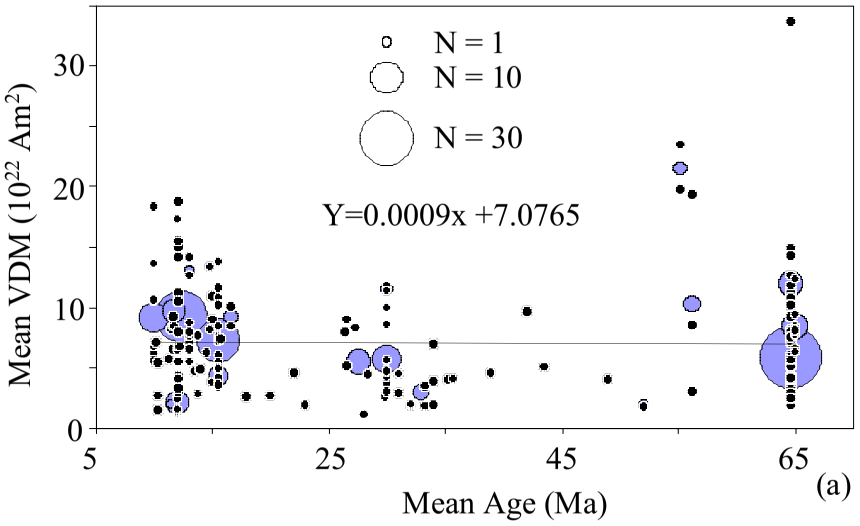

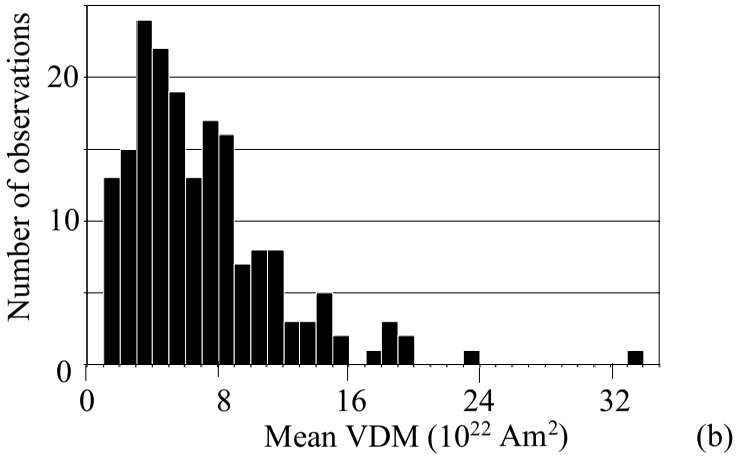

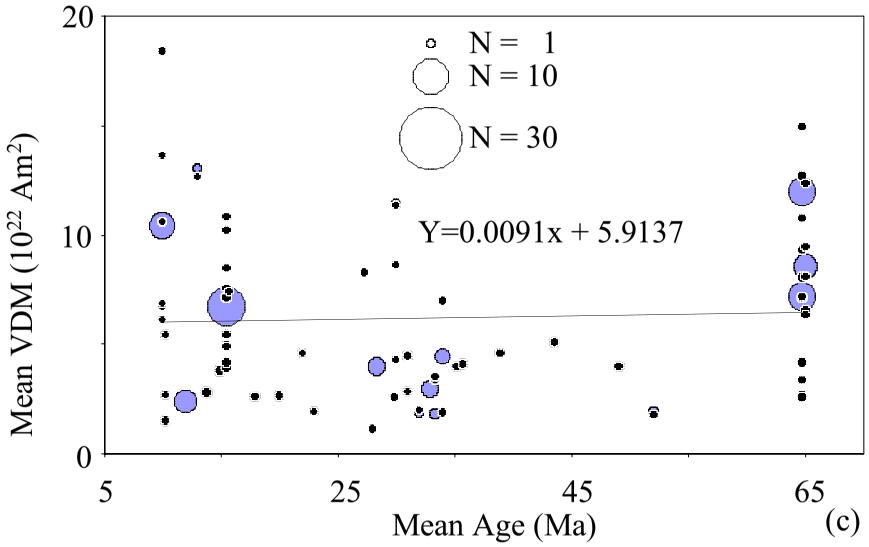

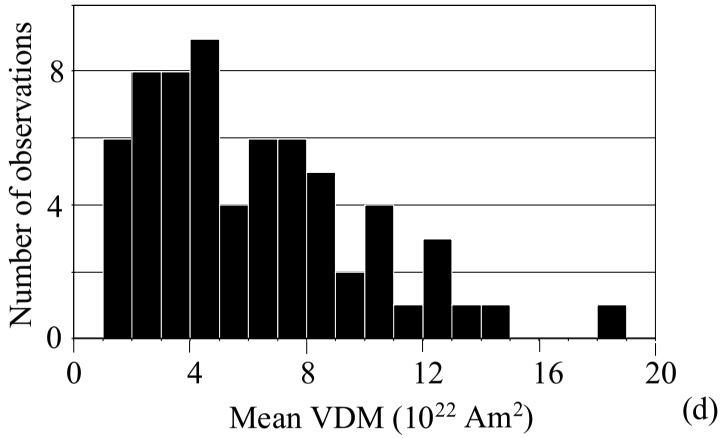

Figure 7.8: Plots of SA (black) and RS (blue) data with ages 65 - 10 Ma for (a) all data and (c) selected data. Regression line is given with equation. The distribution of SA data is shown in (b) for all SA data and (d) for selected SA data.

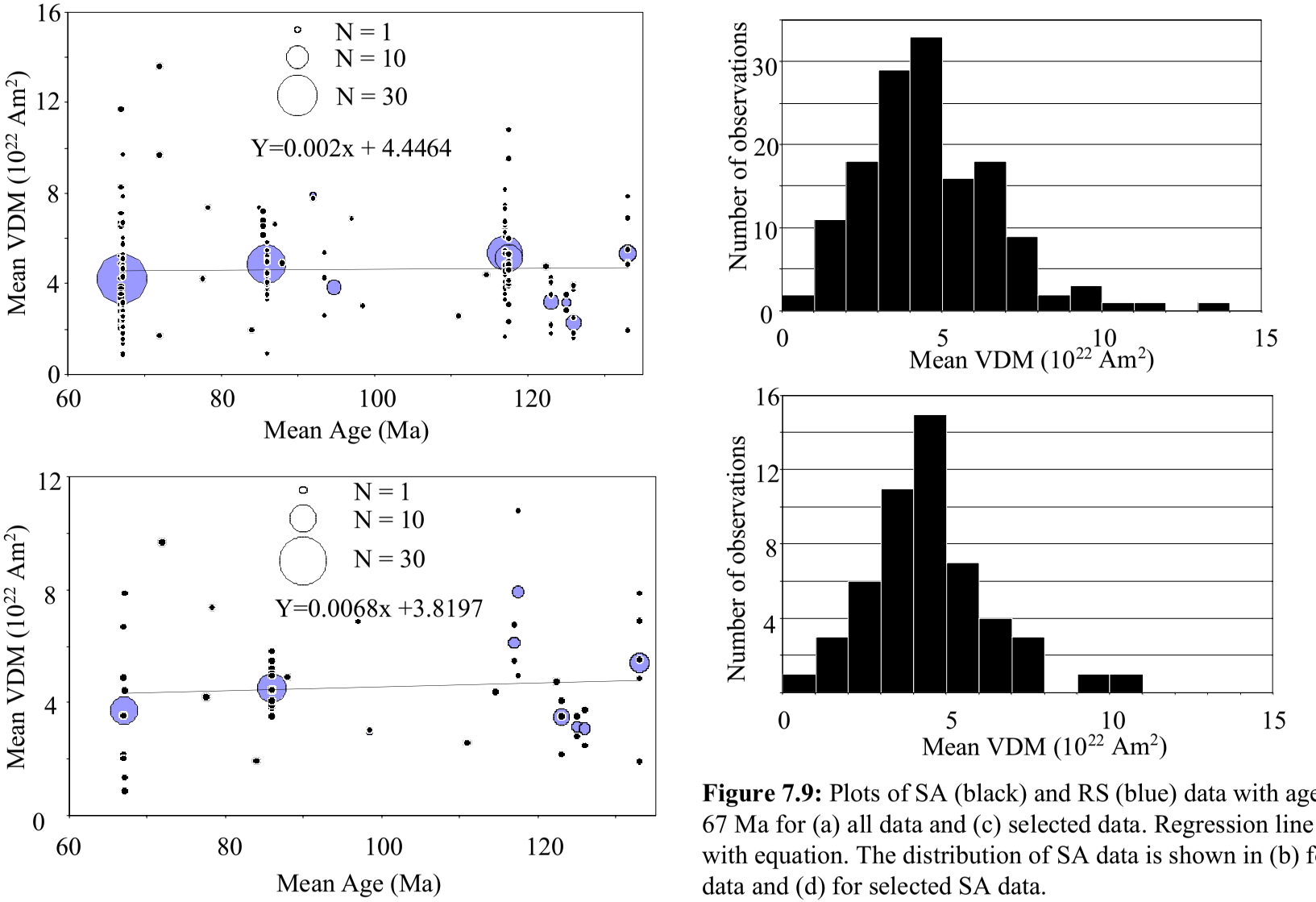

Figure 7.9: Plots of SA (black) and RS (blue) data with ages 133 - 67 Ma for (a) all data and (c) selected data. Regression line is given with equation. The distribution of SA data is shown in (b) for all SA data and (d) for selected SA data.

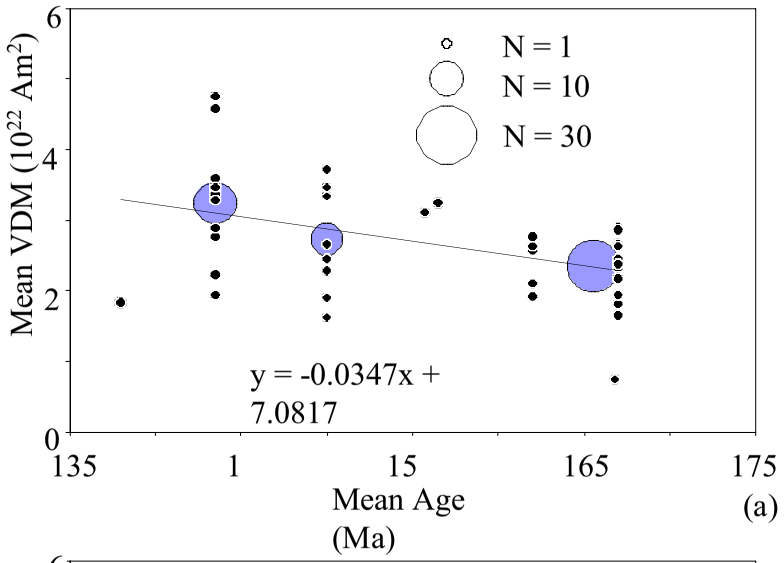

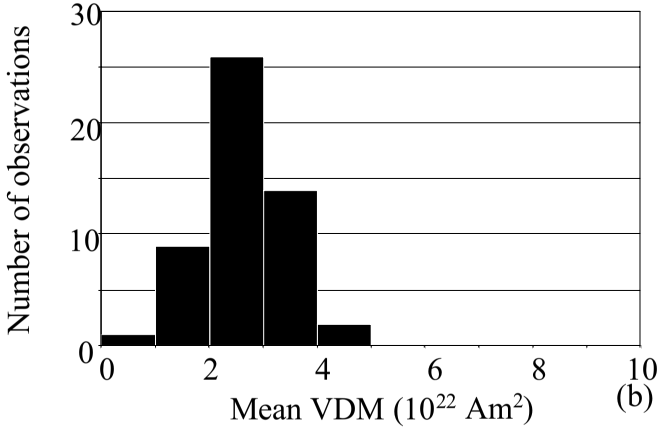

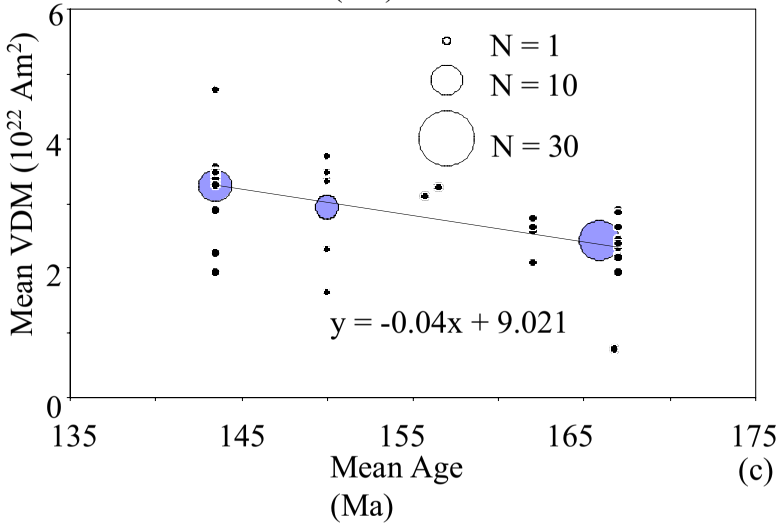

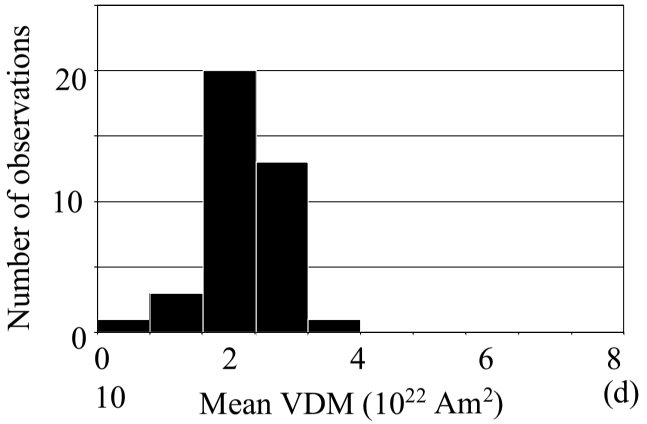

Figure 7.10: Plots of SA (black) and RS (blue) data with ages 167 - 138 Ma for (a) all data and (c) selected data. Regression line is given with equation. The distribution of SA data is shown in (b) for all SA data and (d) for selected SA data.

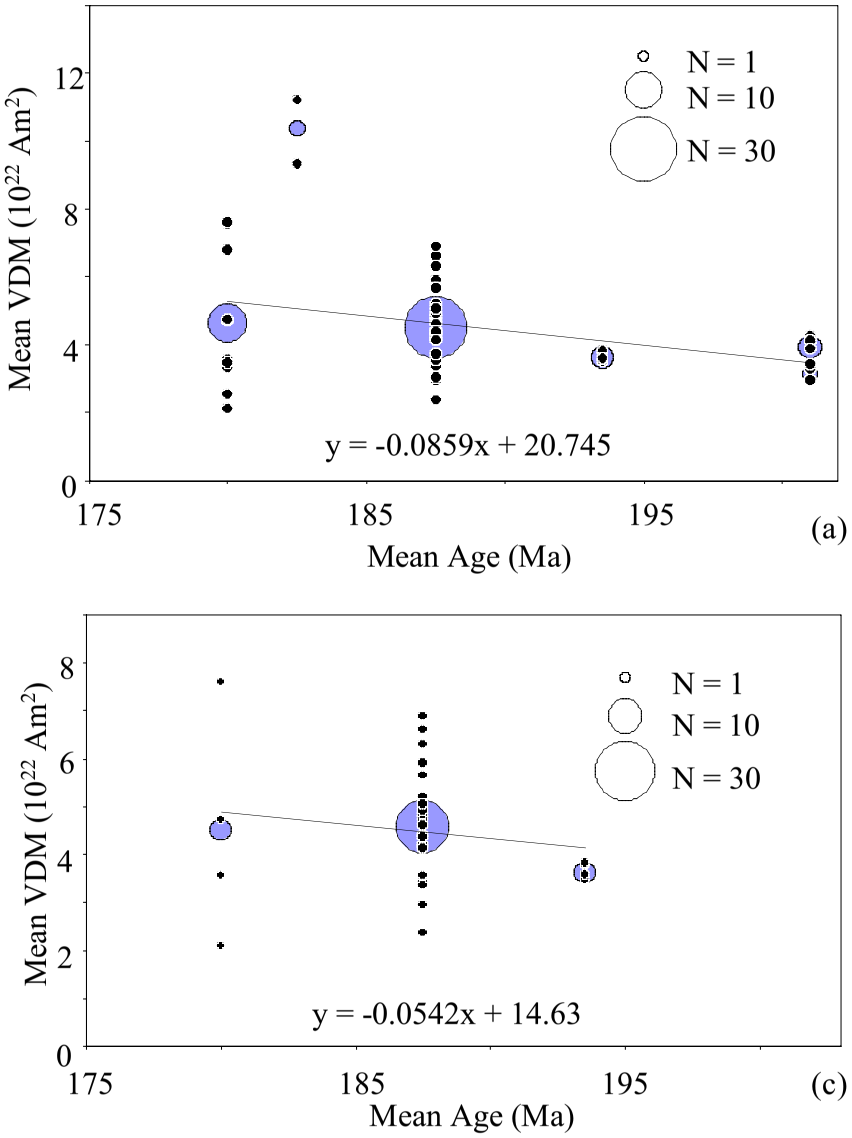

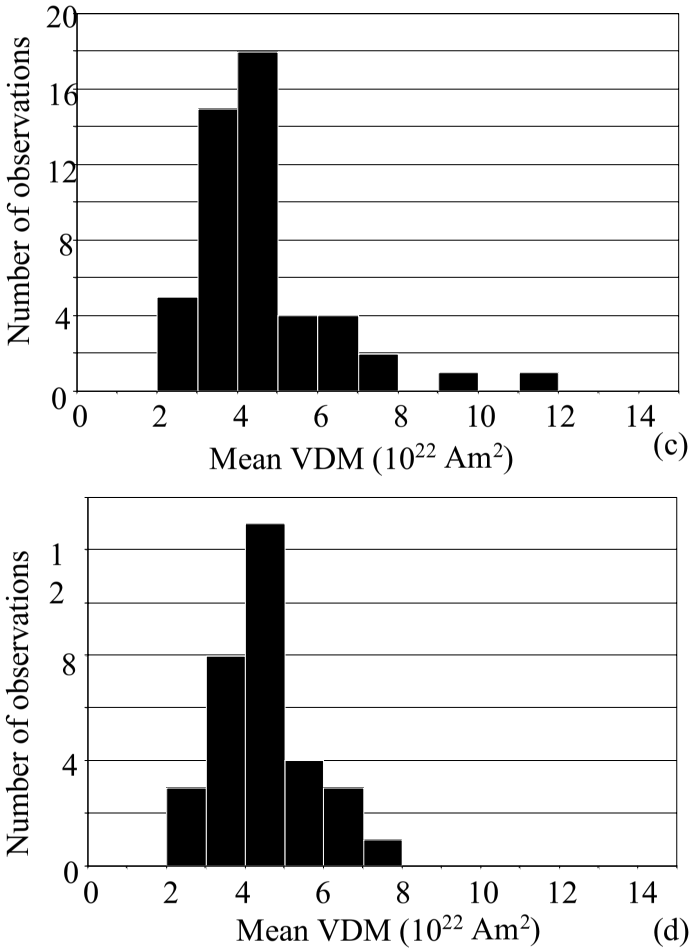

Figure 7.11: Plots of SA (black) and RS (blue) data with ages 201-180 Ma for (a) all data and (c) selected data. Regression line is given with equation. The distribution of SA data is shown in (b) for all SA data and (d) for selected SA data.

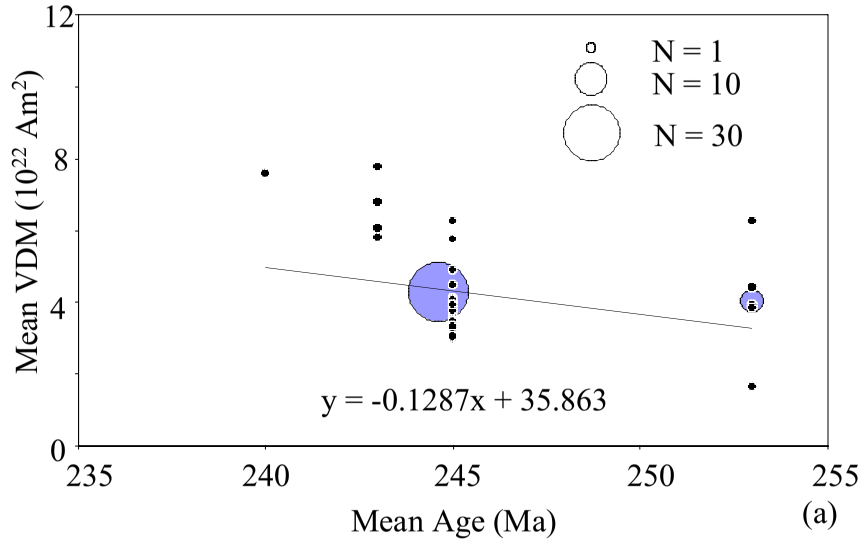

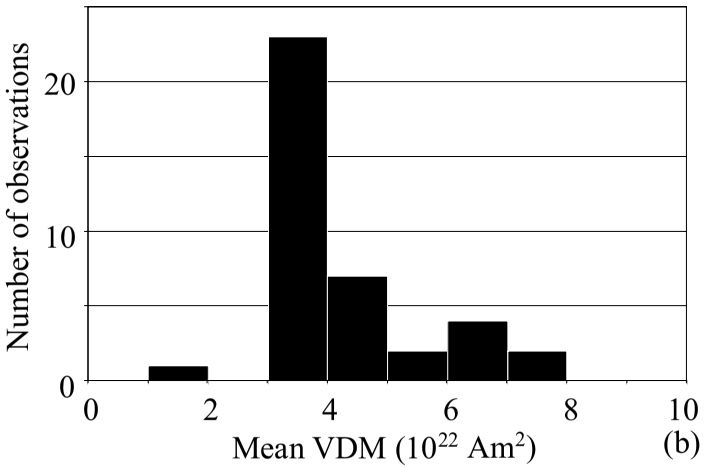

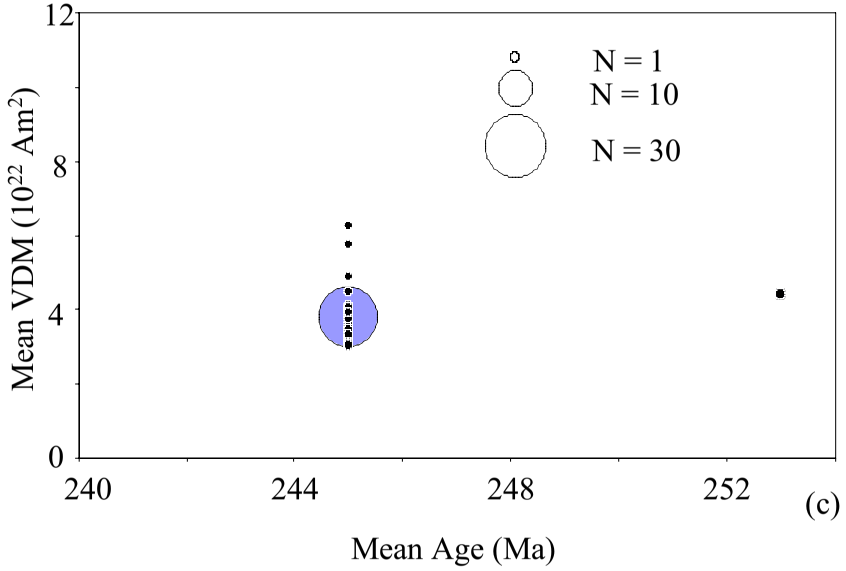

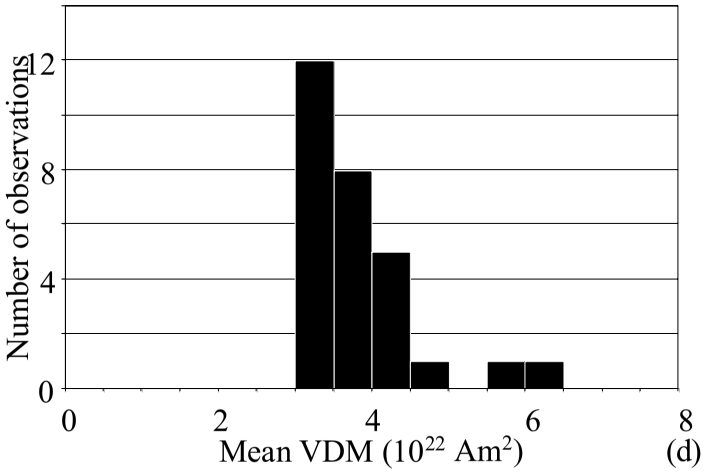

Figure 7.12: Plots of SA (black) and RS (blue) data with ages 253 - 240 Ma for (a) all data and (c) selected data. Regression line is given with equation. The distribution of SA data is shown in (b) for all SA data and (d) for selected SA data.

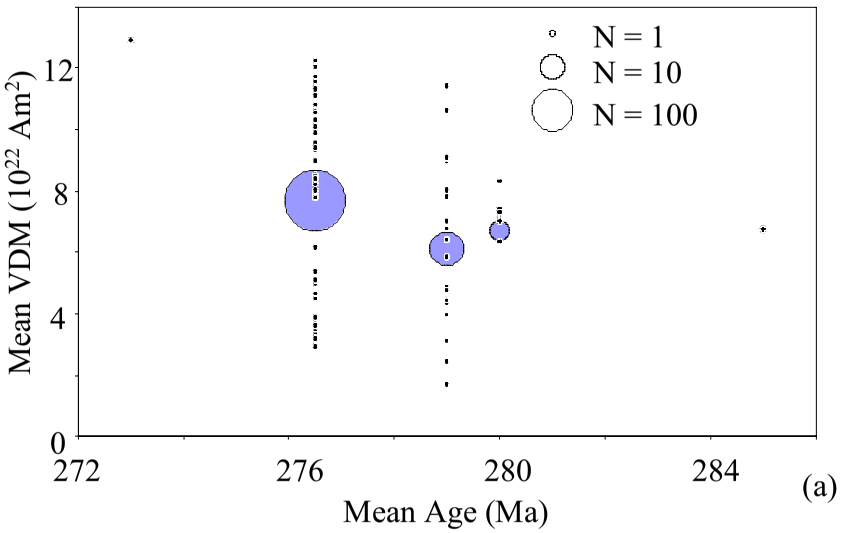

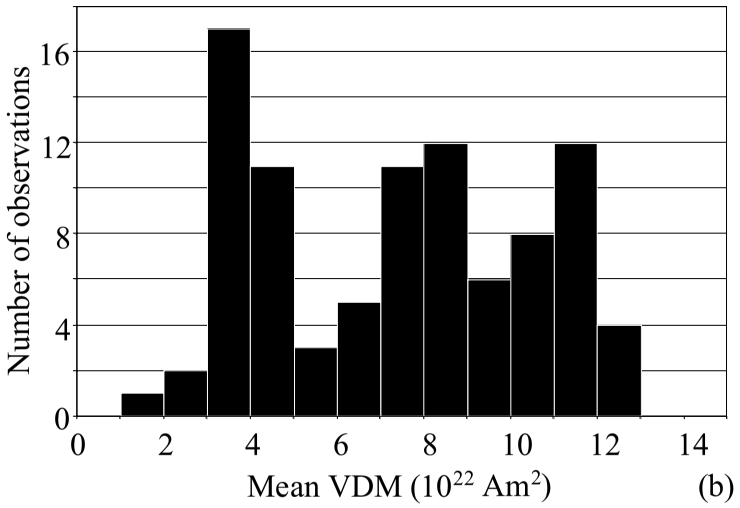

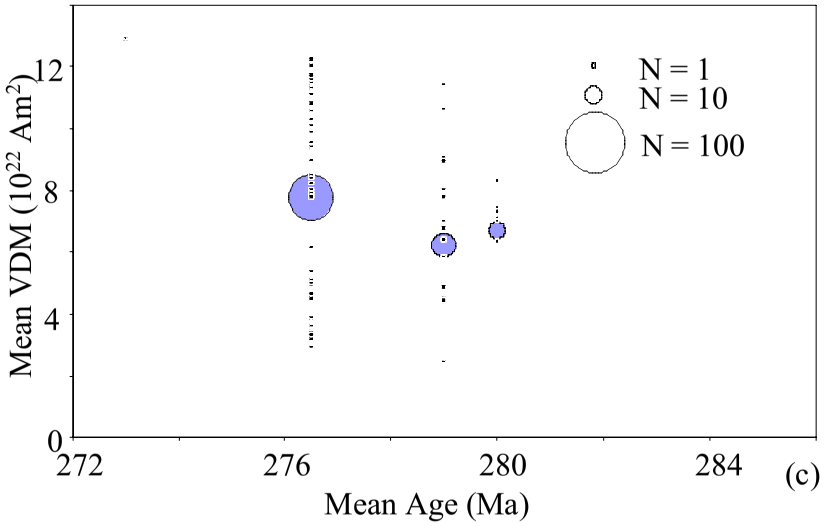

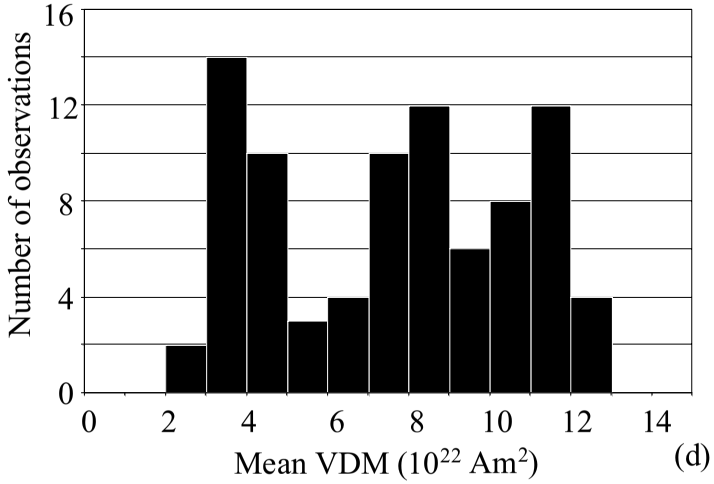

Figure 7.13: Plots of SA (black) and RS (blue) data with ages 285 - 273 Ma for (a) all data and (c) selected data. The distribution of SA data is shown in (b) for all SA data and (d) for selected SA data.

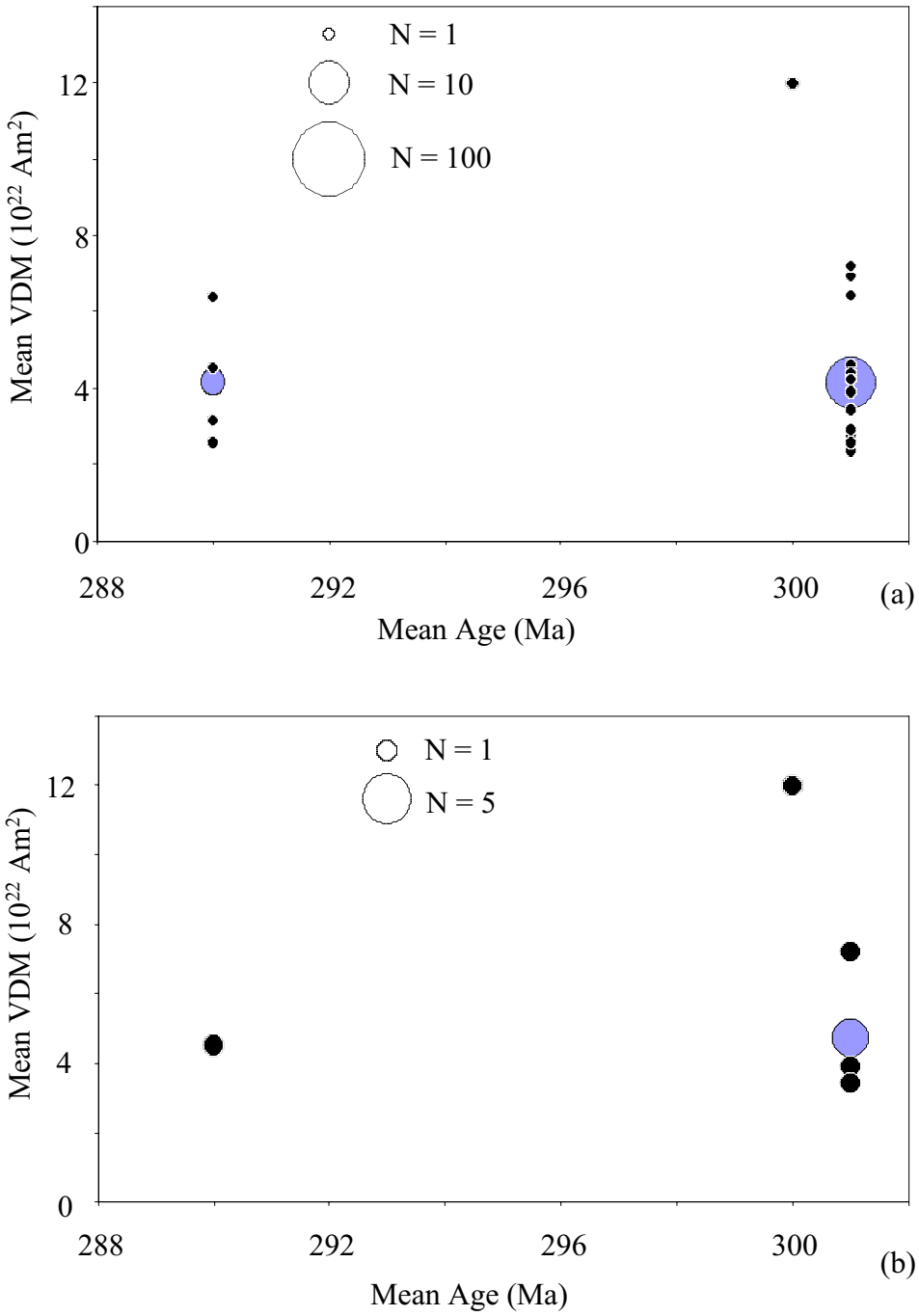

Figure 7.14: SA (black) and RS (blue) estimates in the period 301 - 290 Ma for (a) all data, (b) selected only data.

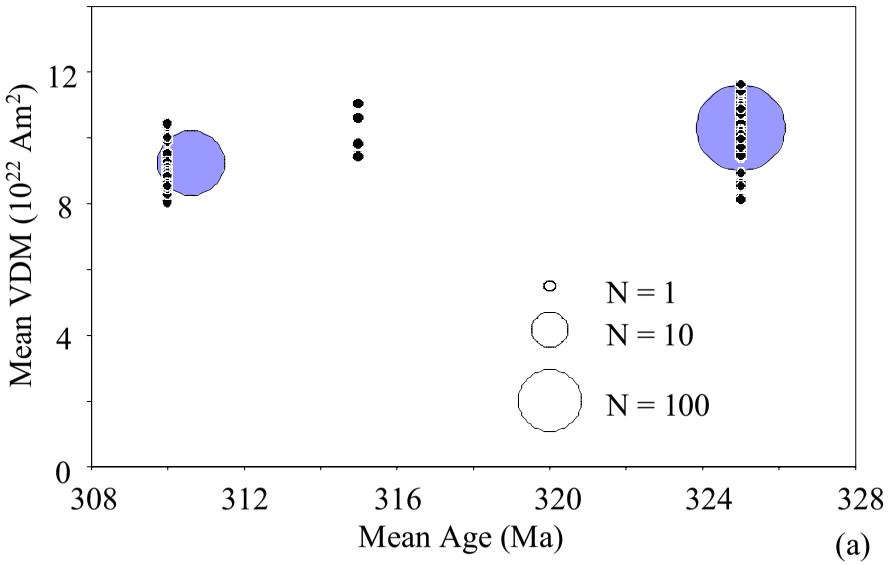

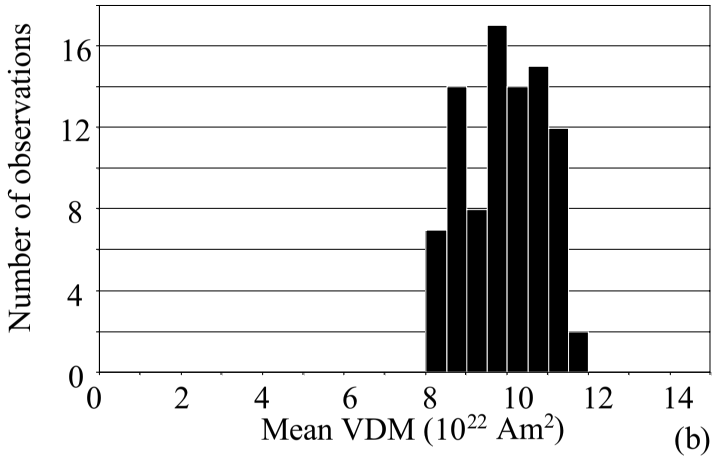

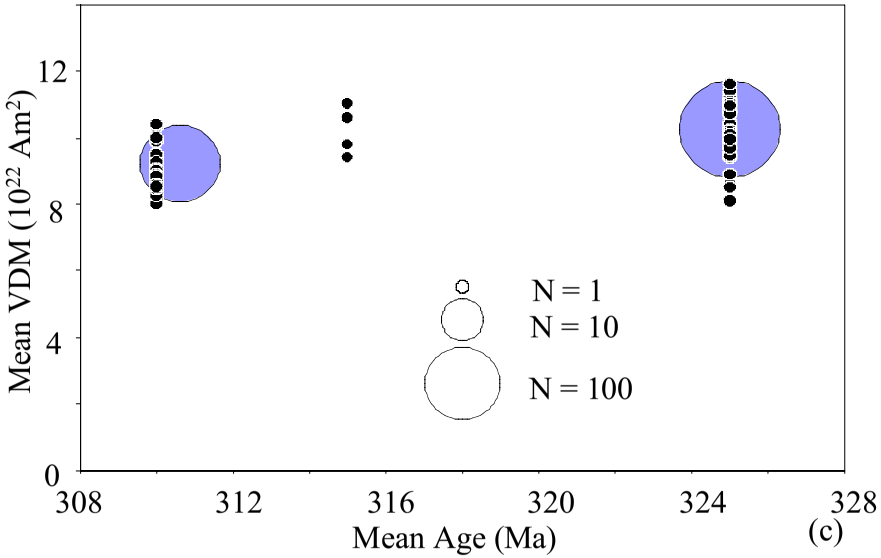

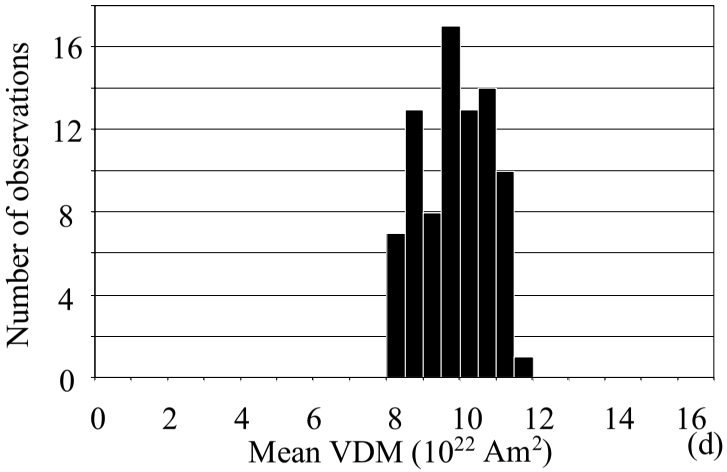

Figure 7.15: Plots of SA (black) and RS (blue) data with ages 325 - 310 Ma for (a) all data and (c) selected data. The distribution of SA data is shown in (b) for all SA data and (d) for selected SA data.

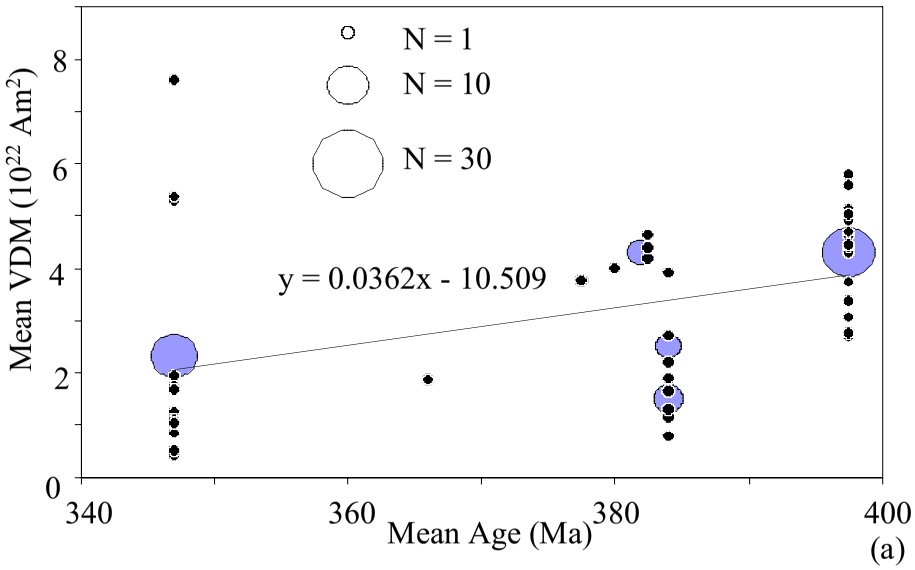

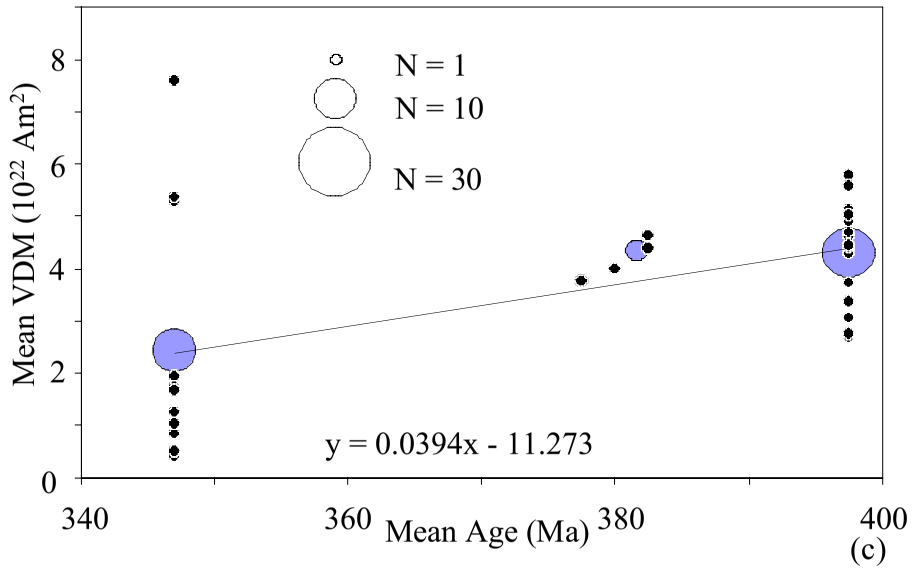

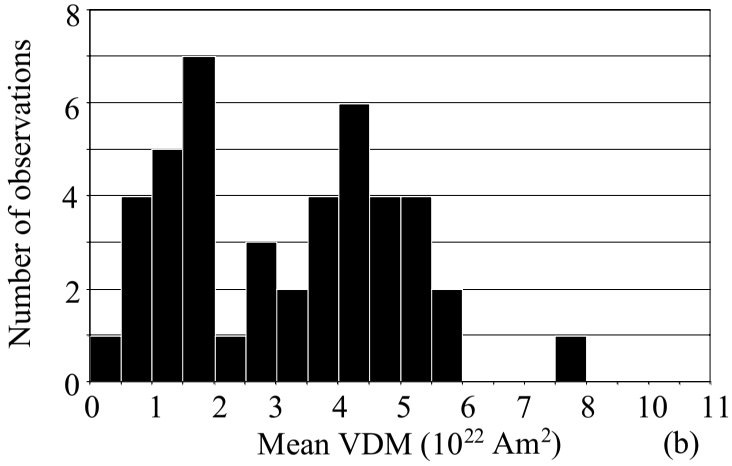

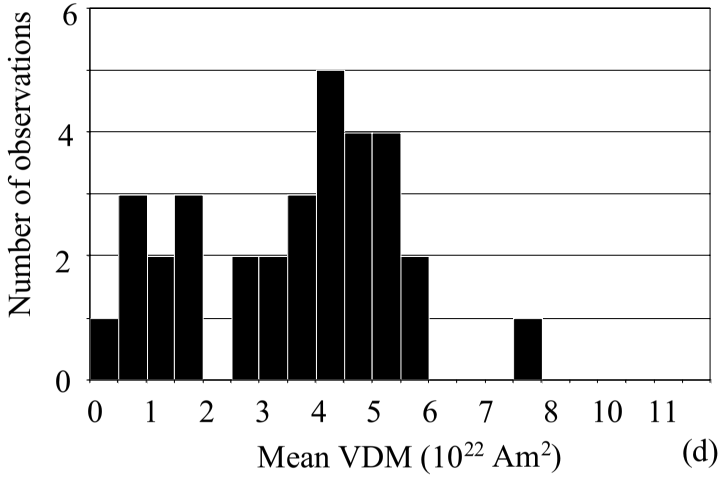

Figure 7.16: Plots of SA (black) and RS (blue) data with ages 397 - 347 Ma for (a) all data and (c) selected data. Regression line is given with equation. The distribution of SA data is shown in (b) for all SA data and (d) for selected SA data.

7.3.4 Variation of standard deviation

The relationship between mean VDM and its standard deviation, as investigated by Perrin and Shcherbakov (1997; §7.1) for arbitrary 100 Ma intervals, was assessed again using the categories defined in this study. The segment 325 – 310 Ma was excluded from this analysis as it is an obvious outlier; possible reasons for this are discussed later. Figure 7.17(a) and (c) testify that a positive correlation exists between mean VDM and standard deviation, however once again this was jeopardised by some correlation existing between standard deviation and the number of estimates in the segment. This was most significant for the complete data set and implied that it was possible that low standard deviation was caused by insufficient representation of the variation.

To allow this uncertainty to be overcome, another analysis was performed. The selected data set was used because the scatter of data within segments was less likely to be caused by imprecise estimates. In addition to the segment 325 – 310 Ma, 301 – 290 Ma was also excluded due to the severe paucity of data within it. From the remainder, the period 253 – 240 was that comprising the smallest number of data (N = 28). To allow an unprejudiced comparison, a random selection of 28 SA data was extracted from each of the other segments and a mean and standard deviation calculated from each. This was repeated five times to ensure consistency; the results are plotted on figure 7.18 and show unambiguously that a positive correlation between mean VDM and standard deviation exists.

This is an important result in itself but the plot also provides a few more points of interest. Firstly, those periods falling above the regression line tend to have a greater percentage of RS to SA data than those that fall below. This is entirely consistent with the notion of inter-RS variation being greater than intra-RS variation and highlights the usefulness of grouping data into rock suites to help in assessing likely SV averaging. Secondly, the linear relationship, approximated here by a regression line, clearly intercepts the x-axis above zero. This implies that theoretically, if the mean VDM falls below a certain level, fluctuation

ceases. Additionally, it indicates that it is not valid to compare VDM distributions by expressing the standard deviations as a percentage of the mean because this figure would rise with mean VDM although a linear relationship between the two was followed.

Finally it is worth noting that, although the scatter of the points on figure 7.18 is observed to be greater for high values of mean and standard deviation, this is unlikely to reflect an inherent aspect of dipole moment behaviour. Rather, it is likely that it arises by coincidence from inconsistent sampling density. The two segments that reside in the top right-hand corner of figure 7.18 both have large numbers of SA data from which random selections were made, therefore their statistical parameters are liable to vary more between samples than the other segments with less data.

The relationship between mean dipole moment and its standard deviation can be understood qualitatively by examining the ASA or SSA plots of VDM versus age (figures 7.1(a) and 7.2(a)). For most of the record, the lowest values of SA data are relatively constant; it is the variation in the maximum limit that causes the mean to change. Such a situation implies that any temporal mean will contain a greater range of values (and consequently higher standard deviation) when its value is increased.

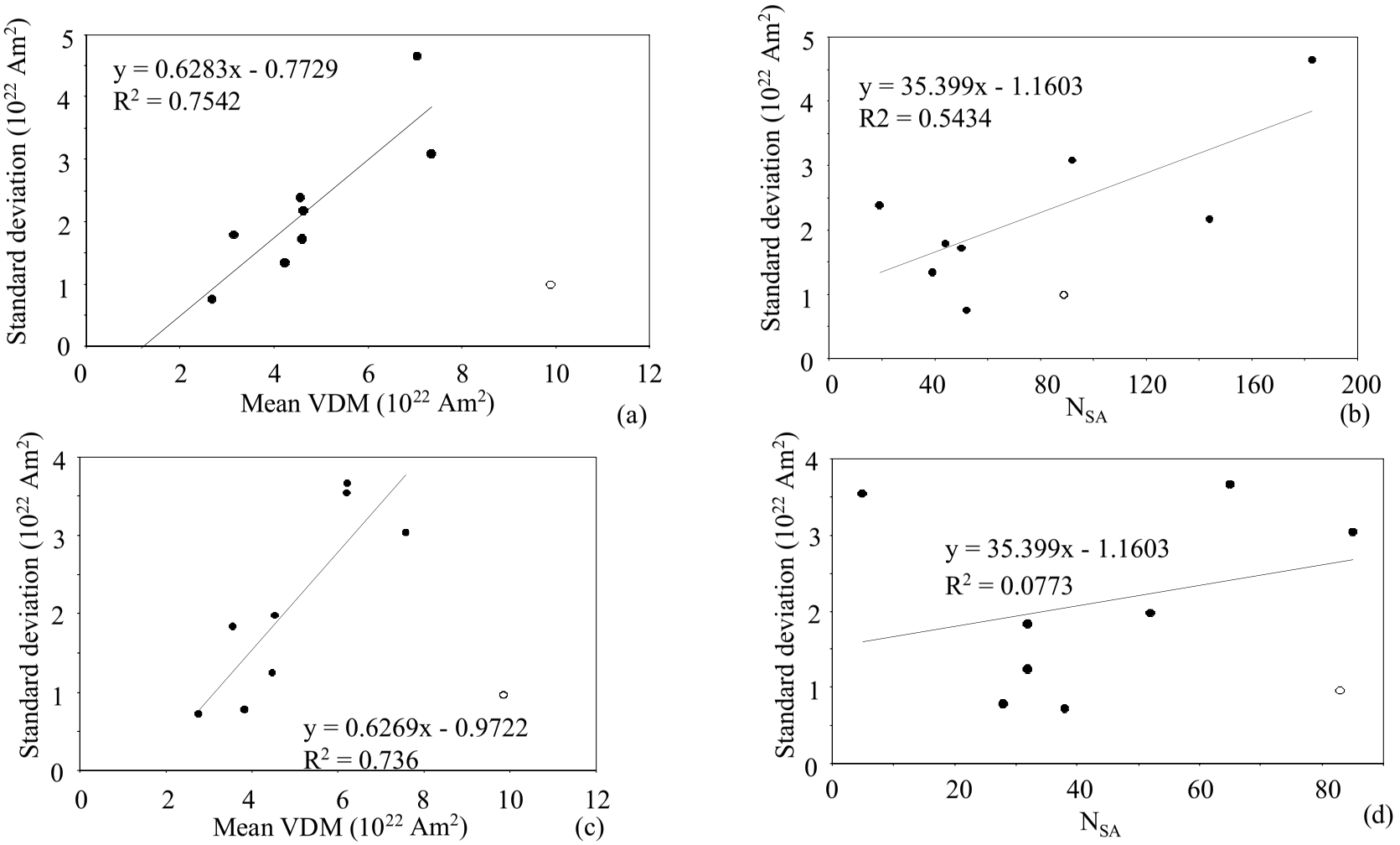

Figure 7.17: Standard deviation of mean SA VDM data in each segment plotted against (a and c) the mean VDM and (b and d) number of SA data. Hollow points represent the period 325 - 310 Ma which was excluded from this study.

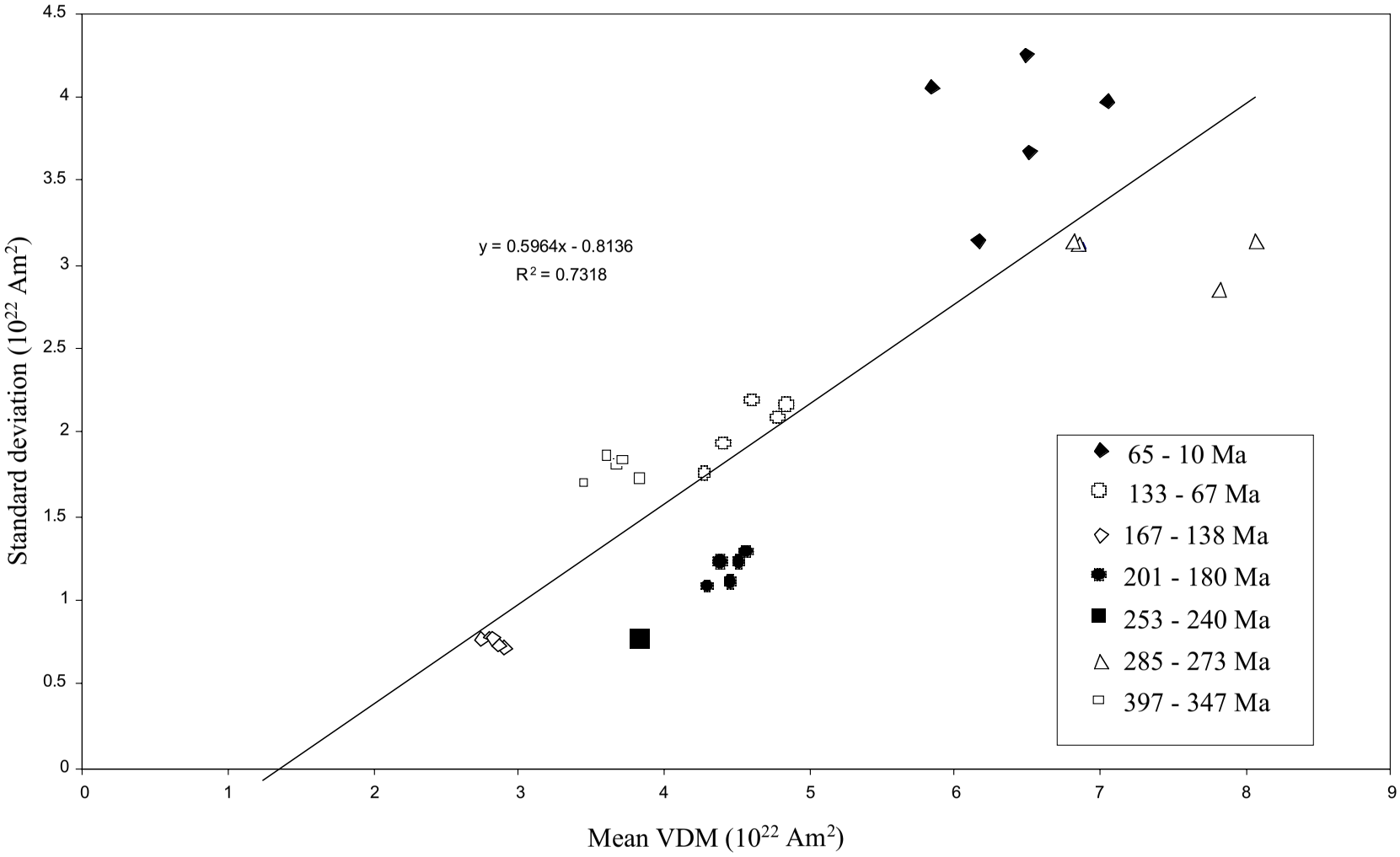

Figure 7.18: Mean VDM plotted against standard deviation for five random selections of 28 SSA data from each segment indicated on the diagram.

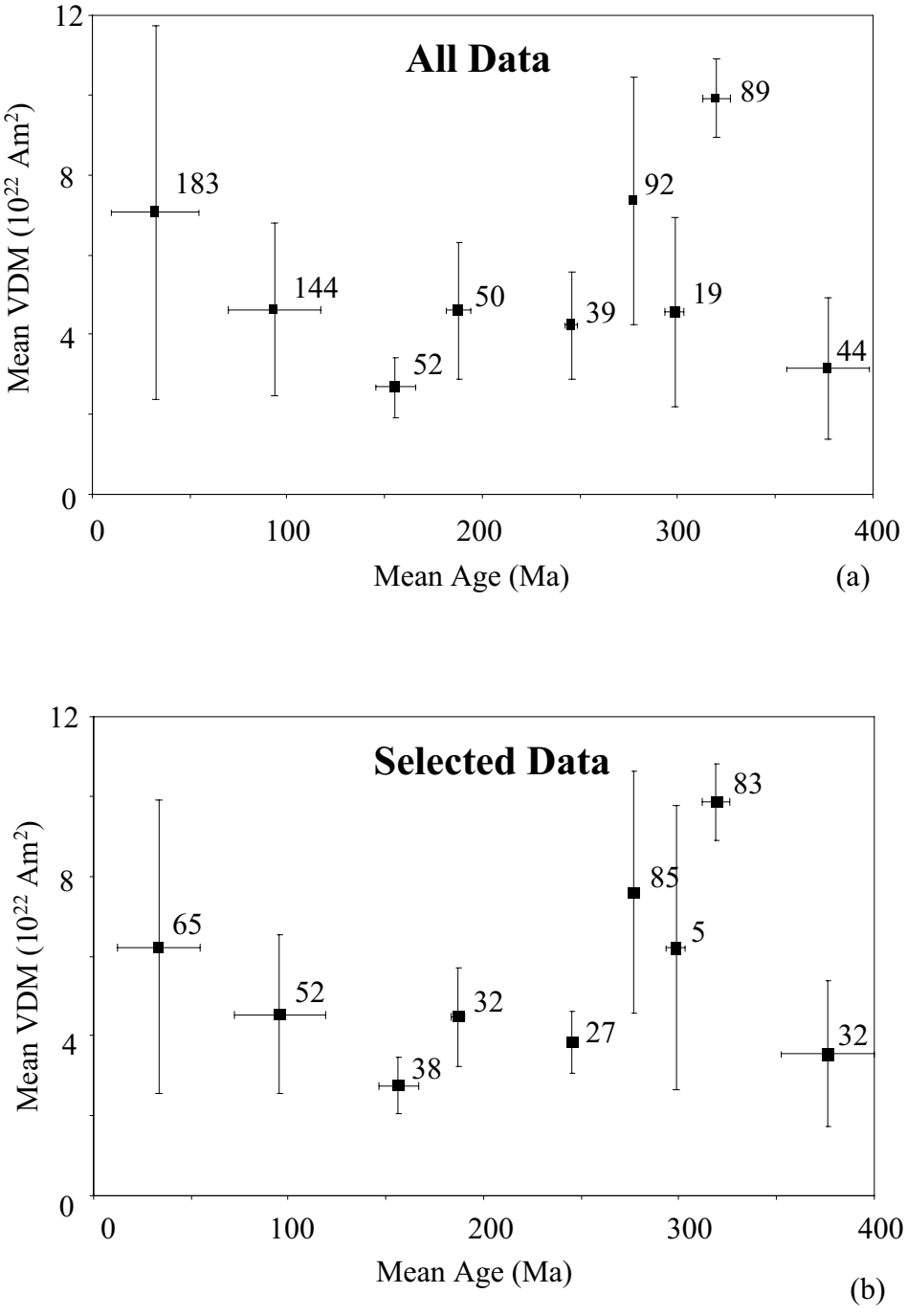

Figure 7.20: Segment mean VDM results versus mean age. Error bars indicate one standard deviation, the number of SA data each mean is derived from is indicated.

7.4 Discussion and conclusions

Figure 7.20 shows the evolution of the dipole moment through the period 400 – 10 Ma as defined by segment means. Quite surprising is the closeness with which the means defined by the selected data follows those defined by the complete data set. The only exception to this rule is the segment 301 – 290 which was discussed in the last section.

These plots show, beyond doubt, that there has been variation of the average dipole moment over periods of hundreds of millions of years since the Devonian. The clearest first-order features are the increase in dipole moment since the mid-Jurassic and the decrease beginning in the Carboniferous. It is not presently possible to identify the time of culmination of this second trend but it is likely to be between 170 Ma and 245 Ma. From this, it can be inferred, from both the ASA and SSA data, that the gradient of a linear decrease from the Carboniferous would be between approximately 0.5 and 0.8 _ 10^{22} Am^2 / 10 Myr. This is high compared to the measured gradient of the regression line through the period of increasing dipole moment 167 – 10 Ma (0.3 _ 10^{22} Am^2 / 10 Myr). These crude calculations suggest asymmetry around the minimum value of dipole moment. The period of time in which the field was in its weaker state prior to the Carboniferous is very poorly constrained. It was almost certainly low between 380 and 400 Ma (see figure 7.16) but may have continued to be so until 345 Ma. This places the gradient of increase following it between 1.2 and 3.0 _ 10^{22} Am^2 / 10 Myr, considerably higher than the other trends. It must be stressed that although these variations are referred to as 'trends,' they are presumed to be neither linear nor continuous. Unfortunately due to the intermittent nature of the coverage, it was not possible to investigate the style of progression through the Palaeozoic as was done in the 167 – 10 Ma period.

Much of this analysis is plagued by insufficient and heterogeneous representation of the data. This is problematic on two levels represented by the number of SA data and number of RS data. Those associated with the first of these are obvious: temporal gaps in the record and insufficient averaging of short-term variation.

Those directly related to paucity of RS data are somewhat subtler but potentially more damaging. In the period 167 – 10 Ma, SA data are shown to cover a wide range of values – very low values are present even when the mean value is high. This is much less the case in the period 325 – 180 Ma, causing a reduction in the standard deviation of segments from this period (§ 7.3.4). Without acknowledging the low proportion of RS to SA data in these segments, it would be easy to assume, on the grounds of comparable numbers of SA data, that the dipole (moment) was exhibiting different behaviour. Of course that is not to say that the behaviour of the dipole *is* the same in these two periods, merely that our current knowledge of RS distribution offers an alternative explanation.

It is not clear if the obvious statistical anomaly evident in segment 325 – 310 Ma can be explained as a result of insufficient RS representation. Certainly, the proportion of RS to SA data is exceptionally small (table 7.8) but it is the lack of variation between the large number of SA data within the 2 RSs which is more surprising. The very high proportion of internally self-consistent estimates strongly suggests that the field was accurately recorded.

A closer examination of the data in this period reveals that spatial representation is limited: both rock suites comprised SA data from lava flows and baked contacts in Uzbekistan (Solodovnikov, 1992a, 1992b, 1992c). Consequently there are two plausible explanations for these results; the first is that they represent, without bias, a global regime of dipole moment behaviour not observed elsewhere in the record. This is not altogether unlikely given that they herald the onset of the longest period of constant polarity in the last 400 Myr. The second possibility is that a window of low SV persisted in this region for at least 15 Myr. This feature would be the Carboniferous equivalent of the disputed Pacific dipole window (§ 6.1.2) and would most likely reflect D'' heterogeneity. Clearly data of similar age but from outside of Asia are urgently required to address this problem.

Below is a summary in point form of the primary observations arising from this analysis. Observations expressed as points 1 to 5 are presented with greater confidence than in points 6 to 10.

1. The mean dipole moment has varied significantly on a maximum time-scale in excess of 10^8 years during the period 400 – 10 Ma.
2. The mean dipole moment when averaged from a significant (28) number of estimates forms a positive linear relationship with the standard deviation of those estimates. This is because the maximum limit of the SA value controls the mean while the minimum remains relatively constant.
3. The mean dipole moment rose from a minimum of between 2 and 3 _ 10^{22} Am^2 in the period 180 – 167 Ma, to between 6 and 7 _ 10^{22} Am^2 at approximately 65 Ma.
4. The mean dipole moment fell from a maximum value probably in excess of 8 _ 10^{22} Am^2 in the period 325 – 310 Ma to the low value given above in the mid – Jurassic.
5. The mean dipole moment was less than 5 _ 10^{22} Am^2 in the early Devonian, this situation may have persisted into the early Carboniferous.
6. The data suggest that there was little overall evolution in the dipole moment through the period 65 – 10 Ma.
7. The data suggest that there was little overall evolution in the dipole moment through the period 133 – 67 Ma.
8. The data suggest that there was a gradual increase (0.4 _ 10^{22} Am^2/ 10 Myr) in mean dipole moment through the period 167 – 130 Ma.
9. Observations 6, 7, and 8 combine to give the impression of an initially gradual increase followed by two sudden increases in dipole moment (at 138-133 Ma and 67 – 65 Ma) separated by a long period of stasis.
10. The data suggest that the transition mentioned in observation 4 occurred mainly between 325 Ma and approximately 240 Ma.

7.4.1 Future work

The problems associated with inadequate data representation have been emphasised throughout this chapter. Table 7.11 lists the periods in which the acquisition of more data would most benefit the analysis of the VDM data set studied here. Needless to say, the addition of reliable data to any part of the

record is of inestimable use in further constraining the observations reported above.

Period (Ma)	Importance
55 – 16	Confirming or refuting the non-evolution of the dipole moment in the period 65 – 10 Ma
120 – 80*	Confirming or refuting the non-evolution of the dipole moment in the period 67 - 133 Ma and in constraining dipole moment behaviour in the CNS
180 – 167*	Locating the Jurassic minimum dipole moment more precisely
240 – 200	Establishing the behaviour of the field between two inferred periods of relatively low dipole moment
310 – 285	Confirming or refuting a reinstated low field regime during this period of the PCRS
325 – 310	Further investigation of the anomalously small variation reported in this period
375 – 350	Constraining the gradient of the pre-PCRS rise in dipole moment

Table 7.11: The benefits gained by the acquisition of data in specific temporal periods of the 400 – 10 Ma VDM record. Asterisk denotes a period supplemented by results presented in chapter 4 and discussed in § 9.3.

8.0 Interpretation of the global dipole moment record

8.1 Introduction

It will be apparent from chapter 6 that any model that hopes to satisfy all the observational and theoretical evidence relevant to the global dynamic system in its entirety will be immensely complex. It is well beyond the scope of this study to proffer such a model. Indeed, it is unforeseeable any model claiming to be encompassing will be accepted while fundamental uncertainties about mantle convection and geomagnetic field generation remain.

Instead, this chapter aims to bring the concept of an acceptable model closer to reality by introducing a further constraint that it must consider. The dipole moment record has rarely been used to constrain global dynamic processes primarily because of its sparseness. However, Perrin and Shcherbakov (1997) and chapter 7 illustrated that there are some long-term features in the record that can be presented with a degree of certainty. In this chapter these features will be discussed in the context of other indicators of global processes.

An accurate VDM estimate is a measurement of the average geomagnetic poloidal field strength (hereon referred to as PFS) truncated above harmonic degree 14 (Cain *et al*., 1974). Reliable information regarding its variation through the past is of great importance in constraining the global processes described in chapter 6. However, care must be taken not to use PFS as a proxy for other variables without good reason. The PFS does not necessarily reflect the efficiency of the geodynamo in generating a magnetic field because the ratio of poloidal to toroidal field may have altered or there may have been shift in the distribution of the Gauss coefficients. Similarly, PFS may not be directly proportional to the vigour of convection in the core because the style (and hence efficiency) of magnetic field generation in the geodynamo may be dependent on the Rayleigh number.

Shifts in the power spectrum of the poloidal field are unlikely to be significant away from reversals and excursions. These would be expected to influence observable non-dipole components as well as those that aren't evident at the surface, but the axial dipole has been shown to dominate for at least the last 250 Ma (Kent and Smethurst, 1998). Therefore in this chapter dipole moment is assumed to reflect PFS, but not necessarily total magnetic energy, *per se*.

Although a testable hypothesis explaining the long-term variation of mean PFS is proposed in § 8.5, firm conclusions regarding the internal and external processes affecting the geodynamo were not attainable because of the imperfect dipole moment record and theoretical uncertainties.

8.2 The relationship between dipole moment and reversal frequency

The non-stationarity in the reversal record is the most obvious indication of geomagnetic response to external influence. Because the variation occurs on a timescale of 10^8 years, it is usually assumed that it is regulated by changing conditions at the CMB. Although there have been numerous models, described in § 6.3, correlating changes in reversal rate with global geological phenomena, very few referred to the dipole moment record. However both must be present in an encompassing model. With this objective in mind, and from the perspective of studying geodynamo processes alone, a comparison of dipole moment and reversal frequency variation is necessary.

There is a huge disparity between superchrons, which last for tens of millions of years, and the longest chrons, lasting for ~ 3 Myr (Opdyke and Channell, 1996). This suggests that the geodynamo has two different regimes, one in which it reverses (every 500 kyr on average) and one in which it does not. Therefore, in the following comparison of reversal frequency and dipole moment variation, superchrons will be regarded separately (in § 8.2.2) from the rest of the record.

8.2.1 Reversal frequency and dipole moment variation outside of superchrons

The mid-Jurassic to present time interval in which the reversal record is relatively well constrained coincides with the 167 – 10 Ma interval of the dipole moment record discussed in some detail in the last chapter. Therefore a reasonable qualitative comparison can be made (figure 8.1). The dashed lines representing dipole moment trends must of course be treated with some caution because of the large gaps present. For example, it would obviously not be valid to assume that the mean dipole moment did not vary within the 133 – 167 Ma segment as, in particular, the middle of the CNS is poorly represented. However, it can be claimed with some confidence that the dipole moment did not evolve consistently between the start and end of this segment. At any rate, the CNS itself is not included in this first discussion (but see § 8.2.2).

A clear insight can be derived from examining the beginning and end of the entire (160 – 10 Ma) period. Reversal frequency is similar but mean dipole moment is higher, by greater than 50%, towards the end of the period. Moreover, reversal frequency appears to have completed a half-period of oscillation whereas the mean dipole moment has retained a single trend. Qualitatively, it is highly unlikely that these observations are influenced by poor data representation (figure 7.6), therefore they strongly suggest that the mean dipole moment does not follow a simple, direct relationship with reversal frequency.

The relevance of this observation to the earlier parts of both records is difficult to ascertain because most of the dipole moment measurements fall into either the PCRS or the period 400 – 330 Ma in which the reversal frequency is poorly constrained. One comparison that may be valid is that of the variation between the late Permian / early Triassic (253 – 240 Ma) and the early Jurassic (201 – 180 Ma). The reversal rate is expected to range from near minimum to near maximum between these segments, but the mean dipole moments differ by less that 20%. This observation is

not as well founded as that described above because of the lack of VDM data (particularly those exhibiting internal consistency) in the 253 – 240 Ma segment (figure 7.12).

A comparison of the transitions between segments of consistent behaviour for the two parameters is difficult even for post-Jurassic time because of the large gaps in the dipole moment record. It is feasible that a local transition in dipole moment exists between 15 Ma and 27 Ma (see figure 7.8), coincident with the 25 Ma transition in reversal frequency, but considerably more data from this interval are required before this is known. In the reversal record however, this boundary is more the termination of a gradual process of renewal than a dramatic shift in regime and so a sharp boundary may not be expected.

Of greater importance is the rapid shift of reversal frequency behaviour from stationary to non-stationary at 130 Ma. This is within the errors of the 138 – 133 Ma boundary when it is suggested that the mean dipole moment experiences a shift in behaviour from low and trending upwards to higher and stationary. It is interesting to note that the stationary and non-stationary phases of the two parameters appear to occur in the opposite order about their respective boundaries. More VDM estimates are required from the period 145 – 125 Ma to establish the timing and significance of any boundary between these segments.

A greater transition in dipole moment behaviour appears to occur at the Cretaceous-Tertiary boundary and this does not have its equivalent in the reversal frequency record. However, this 'boundary' may itself only be a consequence of the temporal distribution of VDM estimates around it (see chapter 7).

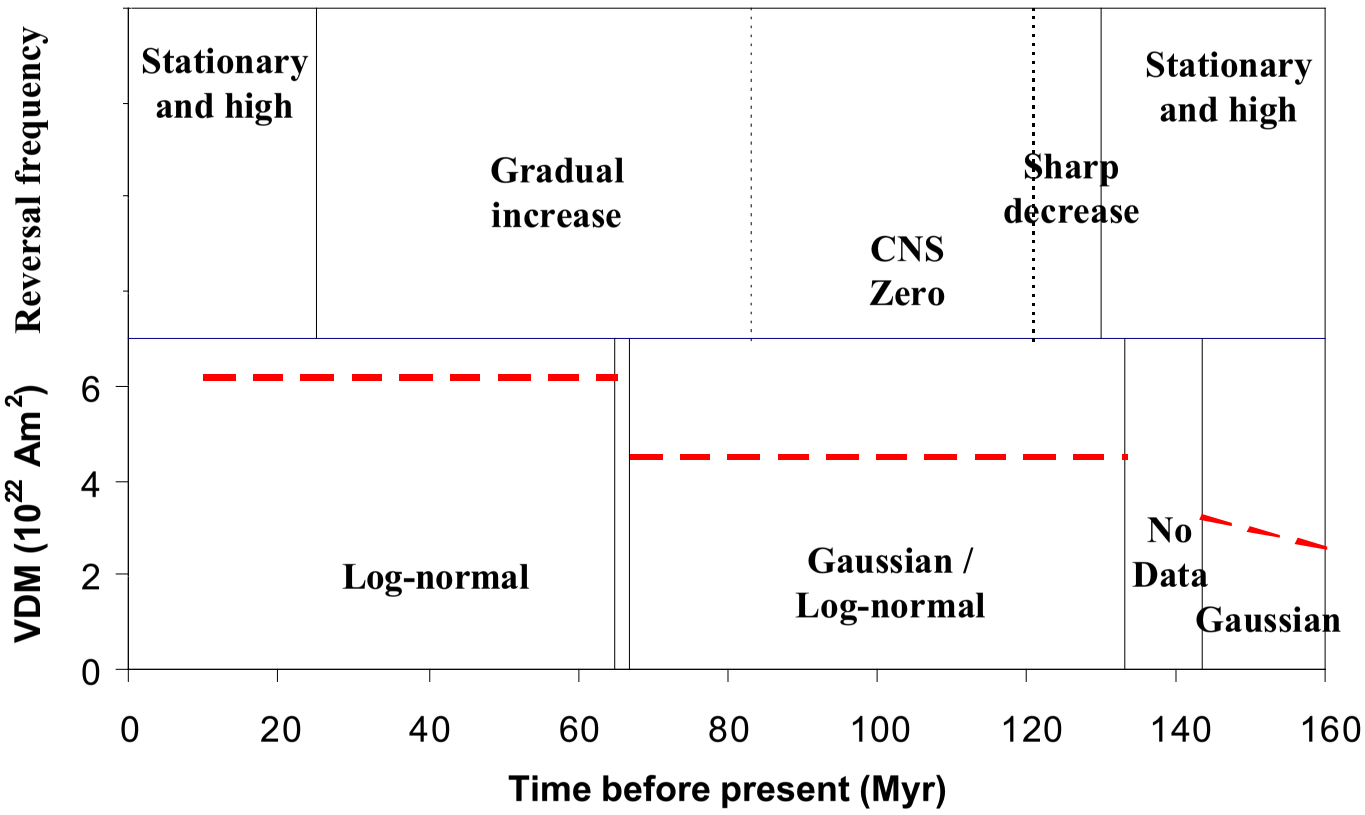

Figure 8.1: Schematic diagram displaying primary features of the dipole moment and reversal frequency variation since the mid-Jurassic.

8.2.2 The mean dipole moment during the superchrons

As stated earlier, the superchrons appear to represent periods of time when the geodynamo was in a distinctly different regime. The strength of the dipole moment has generally been expected to reflect this. Loper and McCartney (1986) and Courtillot and Besse (1987) assumed that reversals were caused by instabilities forming in the core and that their generation rate is proportional to the vigour of convection in the core. A superchron therefore, was necessarily a low energy state with attendant low poloidal field strength.

Larson and Olson (1991) argued that in the kinematic dynamo models of Olson and Hagee (1990) and Braginsky (1976), increased Rm suppressed the reversal process. Consequently, they expected the cessation of the reversal process to be accompanied by anomalously high poloidal field strength. The numerous models of Glatzmaier *et al*. (1999) also appear to support this notion.

The parameters of the data from within the CNS are given in table 8.1 and plots of the data are shown on figure 8.2.

121-83 Ma	μ_{AGE}	μ_{VDM}	σ_{VDM}	N_{SA}	N_{RS}	N_{RS} / N_{SA}	$P_{GAUSSIAN}$	$P_{LOG\text{-}NORMAL}$
All data	102.6	4.993	1.75	72	11	15%	0.88	0.38
Selected data	94.1	4.804	1.68	25	9	36%	0.48	0.66

Table 8.1: Summary of data from the CNS. $P_{GAUSSIAN}$ and $P_{LOG\text{-}NORMAL}$ are the probabilities, calculated using the K-S test, of the sample being derived from a Gaussian / Log-normal distribution with the same mean and standard deviation.

It is clear from figure 8.2 that the bulk of the period has particularly poor data coverage, nevertheless there are enough RS data to allow some analysis of the whole CNS. In particular, it is important to identify any differences in the distribution of data within the CNS with that around it. With this objective in mind, comparisons of

these data and those from the same segment (133 – 67 Ma) excluding the CNS were performed. The K-S test relies on an equal number of data in both distributions therefore it was necessary to make numerous random selections from the remaining data in this segment.

Figure 8.3 shows the cumulative distribution functions of the two sets of data. The K-S test for the ASA gave probabilities ranging from 0.004 to 0.12 with the average somewhat beneath 0.05. Therefore, although it is not possible to unequivocally rule out the null hypothesis that the samples are from the same distribution, there is a reasonably strong suggestion that they are. Figure 8.3(a) gives some insight into possible differences between the two, notably the CNS data is lacking in low VDM estimates relative to the samples taken from outside. This is responsible for increasing the mean VDM of the CNS data to slightly above that of the rest of the segment.

A comparison of the SSA data is more informative (figure 8.3(b)). The K-S test generally gives probabilities of less than 0.01 due to the significantly higher standard deviation of the data outside the CNS. Although the difference in spread of the two samples is skewed towards the lower values, there are significant differences at higher values as well. The distribution of SSA data for the CNS is influenced heavily by one rock suite, which comprises 44% of the data clustered tightly around a mean value. This coupled with the chasm in the record between 88 Ma and 115 Ma means that the observations made from the selected data set must be treated with some caution.

Table 8.2 and figure 8.4 display the primary features of the dipole moment data from the PCRS. The large number of high quality SA data for this period is encouraging, unfortunately the low number of rock suites compromises this to some extent.

320-262 Ma	μ_{AGE}	μ_{VDM}	σ_{VDM}	N_{SA}	N_{RS}	N_{RS} / N_{SA}	$P_{GAUSSIAN}$	$P_{LOG\text{-}NORMAL}$
All data	287.7	7.39	2.96	143	9	6%	0.05	0.0003
Selected data	286.9	7.95	2.76	122	8	7%	0.04	0.0001

Table 8.2: Summary of data from the PCRS.

The bi-modal distribution of the data is interesting because it is not primarily a product of separate low and high rock suites but rather is evident within the distributions of several of the rock suites.

The special case of the data in 315 – 310 Ma was discussed in the last chapter, the removal of this single rock suite increases the standard deviation but does not significantly affect the shape of the distribution.

The variation of ASA data (figure 8.4(a)) with age suggests a dip in dipole moment in the bulk of the PCRS superposed onto a general decreasing trend. The data responsible for this dip all but disappear when the selection criterion is applied but the overall trend is exaggerated. However this trend is anchored to just one rock suite at the early end of the superchron.

A quantitative comparison of the PCRS data with any other period of the dipole moment record would be somewhat pointless, as the mean VDM is so high. That of the segment, 65 – 10 Ma approaches it but the very large difference in N_{RS} / N_{SA} for the two groups may be significant in causing the shapes of their distributions to be so obviously different. Nevertheless, it is worth noting that PCRS is similar to the CNS in the sense that its standard deviation is relatively low and there is a virtual absence of very low (< 2 _ $10^{22}Am^2$) VDM estimates.

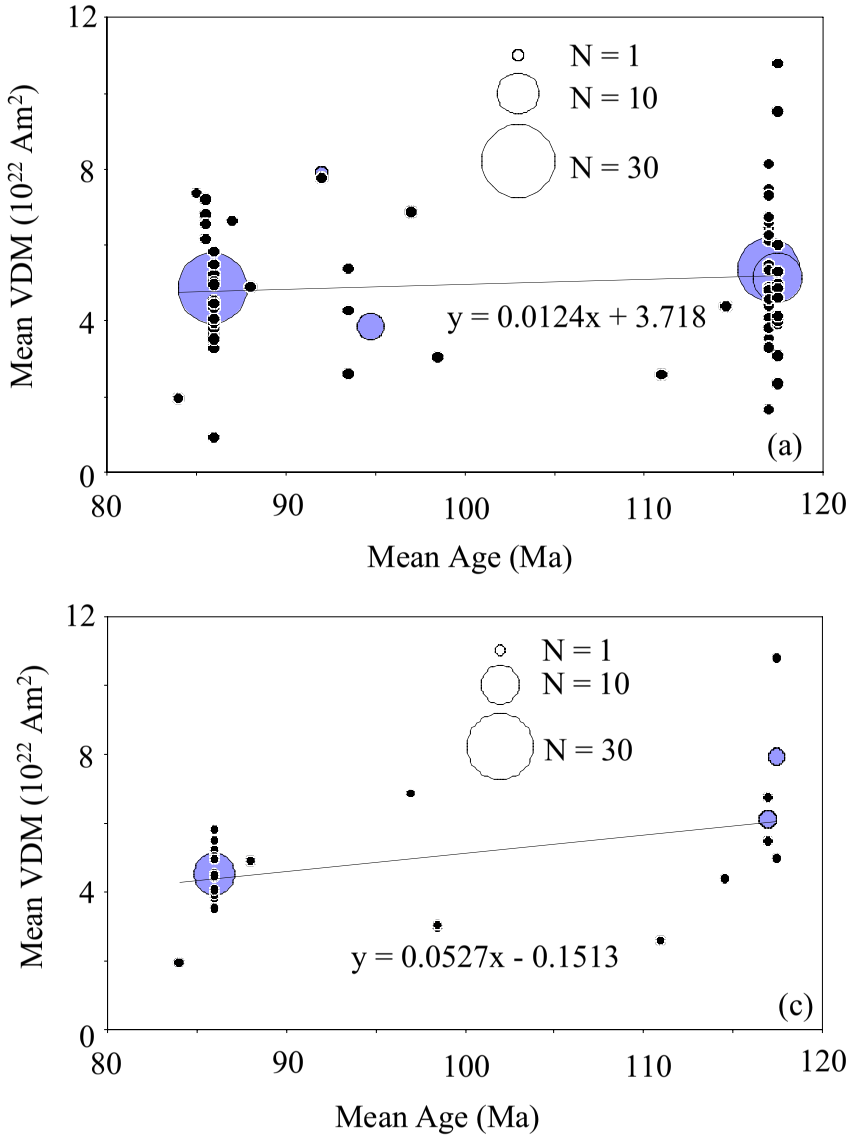

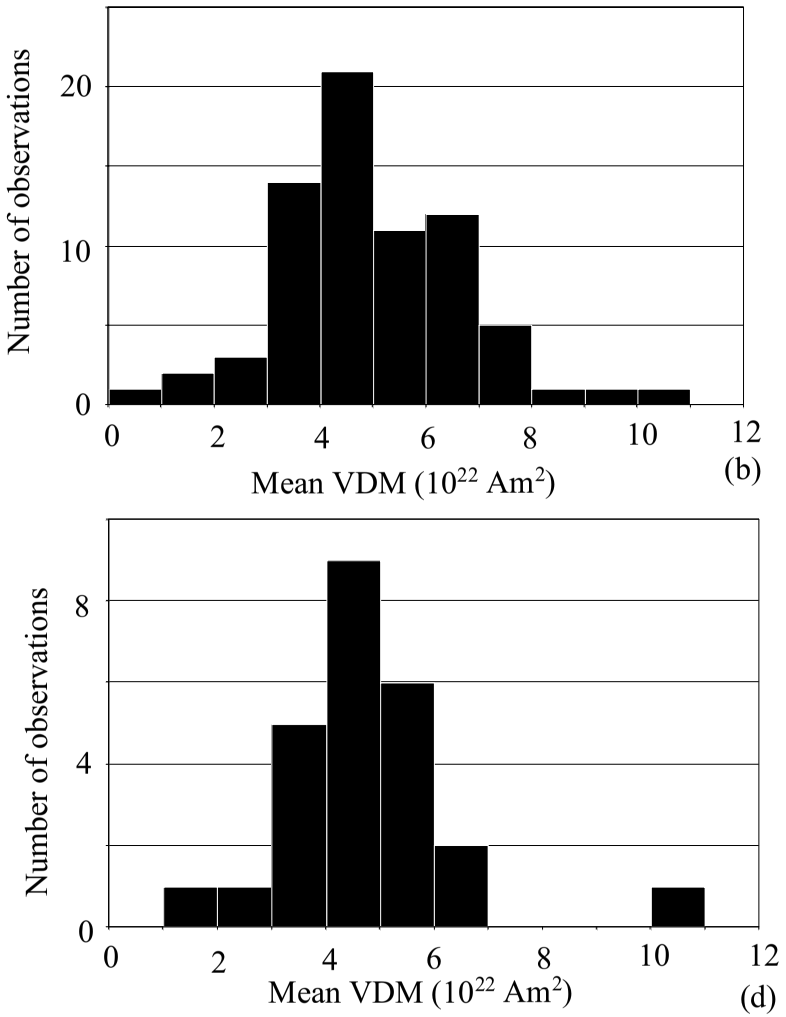

Figure 8.2: Plots of SA (black) and RS (blue) data from the CNS for (a) all data and (c) selected data. Regression line is given with equation. The distribution of SA data is shown in (b) for all SA data and (d) for selected SA data.

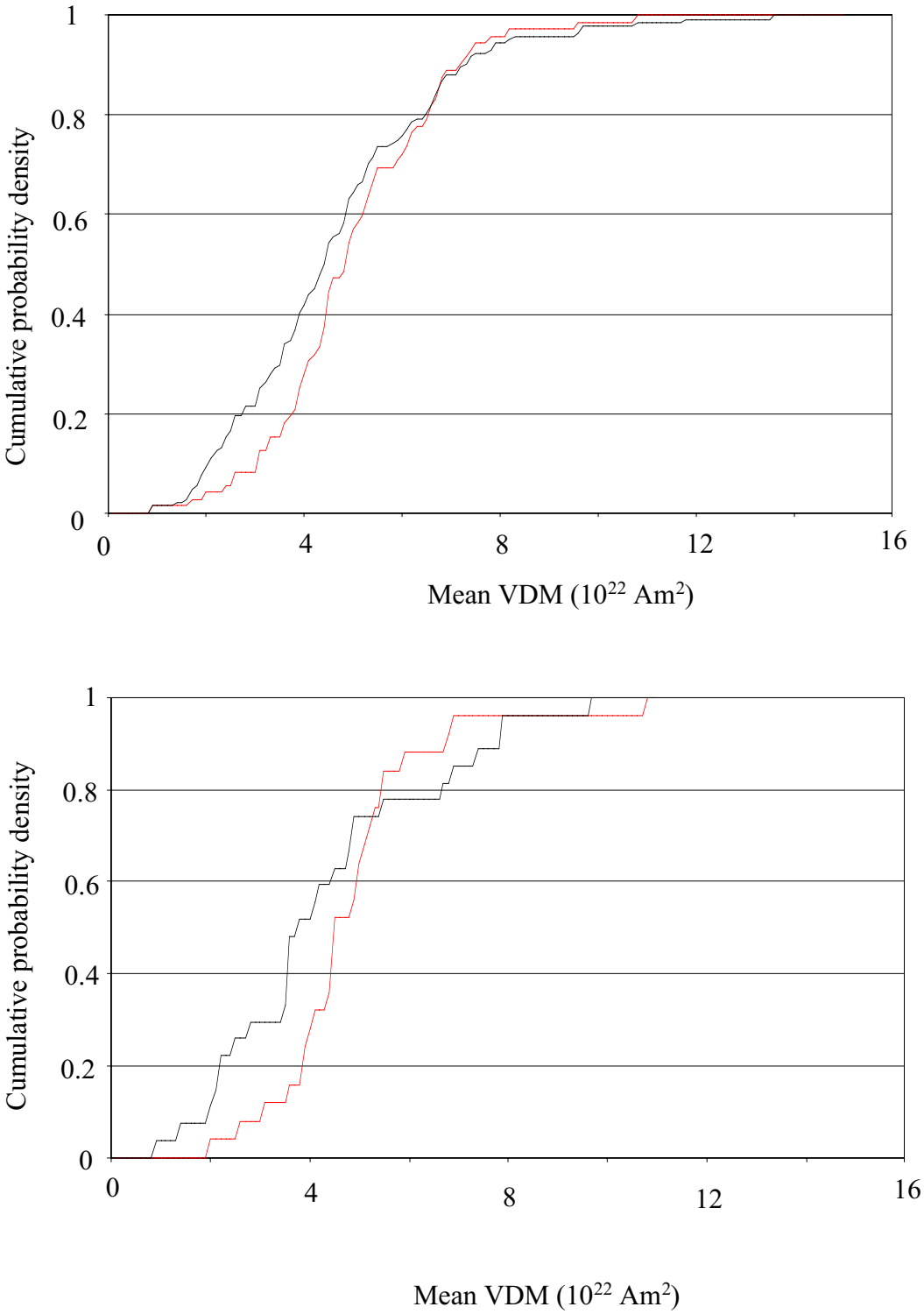

Figure 8.3: Cumulative distribution function of SA data in the CNS (red line) and functions of data from 133 - 67 Ma segment, excluding CNS data (black lines). (a) all data, (b) selected data only.

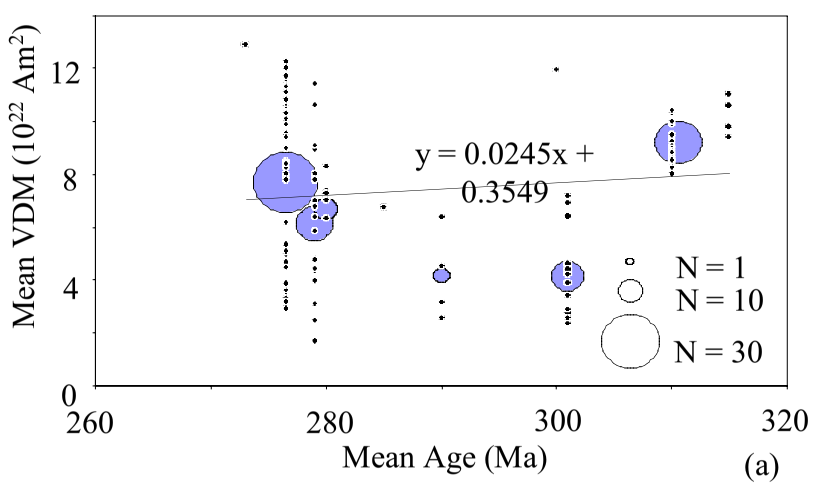

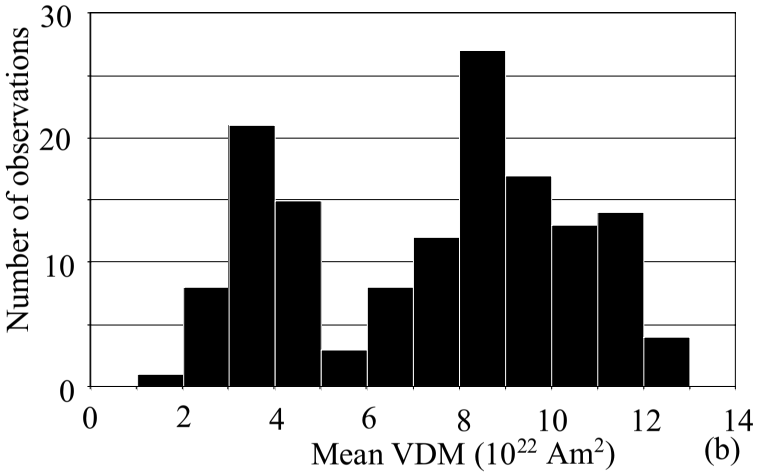

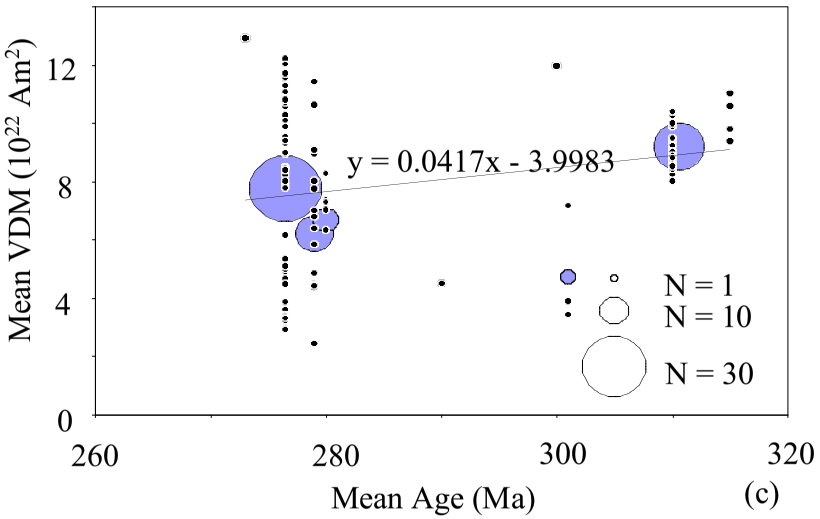

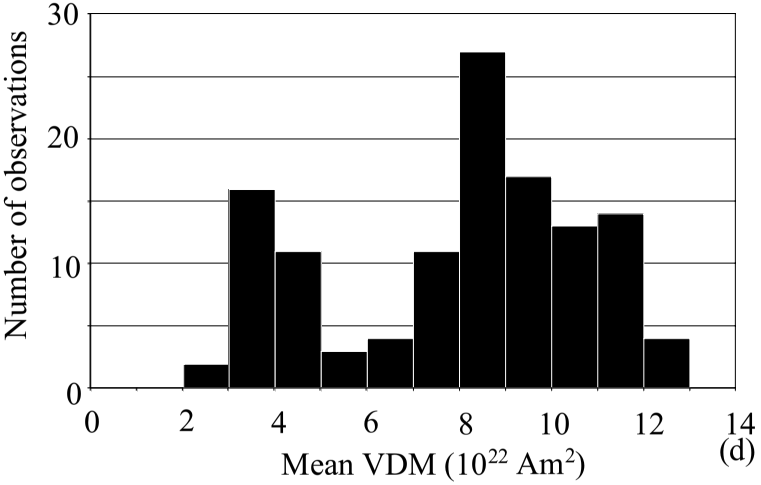

Figure 8.4: Plots of SA (black) and RS (blue) data from the PCRS for (a) all data and (c) selected data. Regression line is given with equation. The distribution of SA data is shown in (b) for all SA data and (d) for selected SA data.

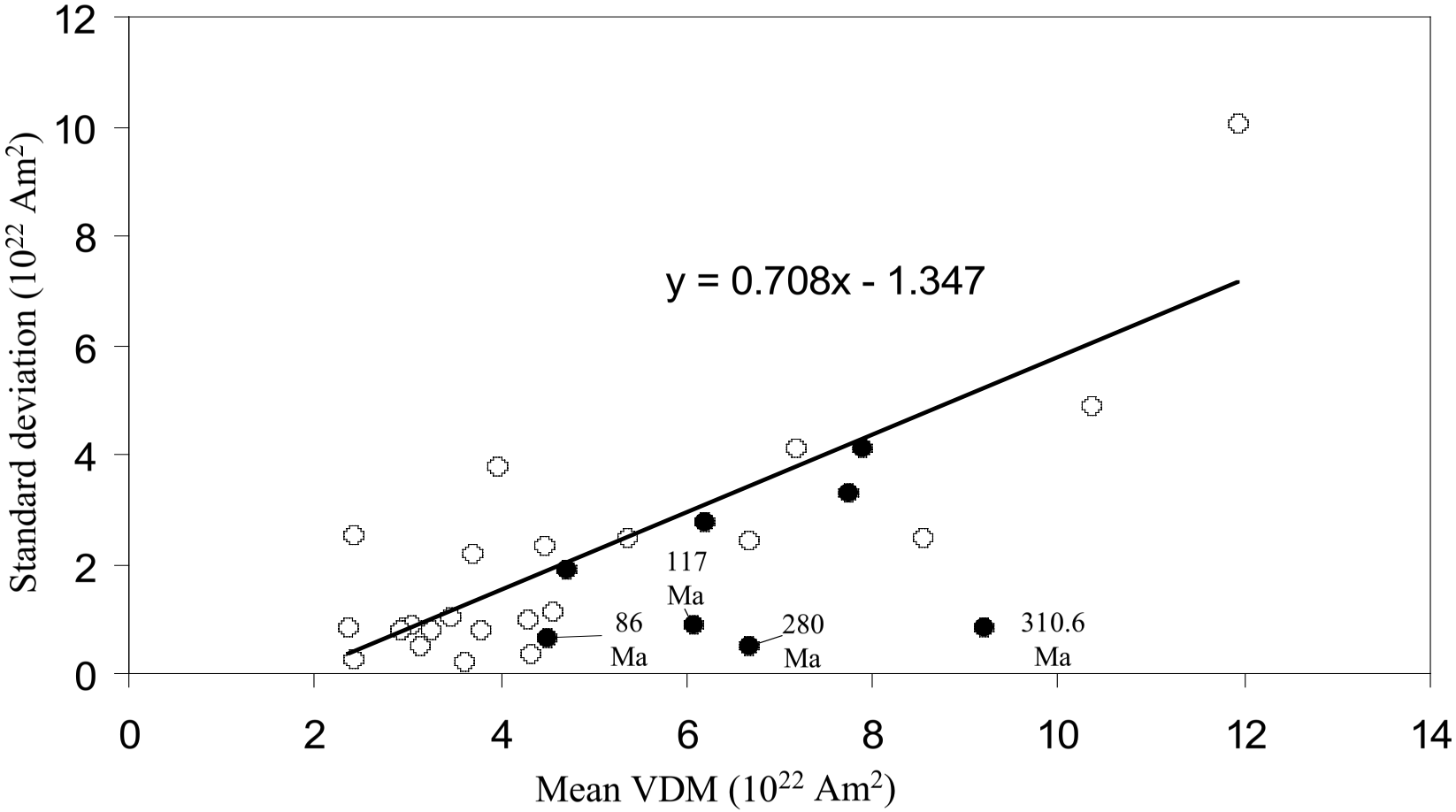

Figure 8.5: Selected data rock suite parameters from during (black) and outside(white) superchrons. The regression line was calculated using the white points only. The 325 rock suite was excluded from this plot because of the uncertainty in its age.

The rock suite dated at 325 Ma was not included in this analysis of the PCRS as it is dated before the onset of the superchron. Its 20 Ma uncertainty in age however, places it well within errors of the superchron, additionally all 57 SA data points that comprise it record a single (most likely reversed) polarity. The effect of incorporating this RS into the PCRS group is to hugely increase the higher of the two peaks in the distribution, increasing the mean and lowering the standard deviation.

Both the CNS and PCRS data sets contained rock suites comprised of tightly clustered SA data. To investigate the significance of this, the mean and standard deviation of the selected RSs were plotted against one another (figure 8.5). Clearly, several superchron RSs have anomalously low standard deviations. However there are no obvious differences (e.g. N, age, etc.) between those and the RSs closer to the non-superchron regression line.

8.2.3 Discussion

The first question that should be addressed in this section is that of whether there is any correlation of PFS and reversal frequency. The vicinity of the transitions in behaviour of the two parameters in the late Jurassic suggests that both were perturbed at this time. It is quite possible that, as both records improve, more synchronous transitions will emerge. Nevertheless, beyond this tenuous link the dipole moment record clearly does not display any first-order correlation with reversal frequency but appears to vary on a time-scale of roughly twice as long.

It seems intuitive that the dipole moment should obey a simple, possibly linear, relationship with reversal frequency and some numerical simulations appear to support this (e.g. Glatzmaier *et al*., 1999). A discussion of the possible causes of change to the two parameters is necessary to illustrate how this could not be the case.

Poloidal field is generated by helicity in the outer core, which in turn is a result of the meridional (as opposed to zonal) flow due to convection. Therefore it follows logically that changes in the PFS represent changes in the vigour and style of meridional flow in the core.

Our knowledge of the cause or causes of geomagnetic field reversals is far from certain. McFadden and Merrill (1986) concluded from statistical analysis of polarity intervals that the process responsible for generating reversals was independent from that responsible for 'normal' geodynamo action. However, no evidence for their proposed 'cold blob' instabilities (§ 6.3) has been reported for reversing dynamo models. Rather, geodynamo simulations suggest that reversals are a natural consequence of fluctuations inherent to the non-linear interaction of processes operating within the system.

Even within the simulations themselves, it is difficult to diagnose the cause of a single polarity reversal because of the immensely complex behaviour they exhibit at all times. Sarson (2000) postulated a simple kinematic mechanism, frequently observed in simulations, to account for reversals. The meridional flow in dynamo models tends to support stable modes in $\alpha\omega$ *dynamos* that would otherwise oscillate (Roberts, 1972). Fluctuations in this flow, caused by variation in thermal and magnetic forces, allows this oscillatory behaviour to occasionally dominate and could therefore be responsible for reversals (Sarson, 2000). He noted that Glatzmaier *et al*. (1999; see § 7.4) found that dynamos subject to high polar heat flux, favouring meridional circulation, exhibited less time dependency.

However, this mechanism appears to favour correlation between PFS and reversal frequency. If the meridional circulation is strong, not only are oscillatory conditions inhibited, but the poloidal field is stronger too.

Another theory that may explain geomagnetic reversals and excursions is that the geodynamo is intrinsically unstable causing the magnetic field to collapse frequently

and allowing it to reverse and undergo excursions. Zhang and Gubbins (2000a,b) showed that the critical Rayleigh number (R_C) is hugely sensitive to small fluctuations in the poloidal field strength in a strong-field Taylor-state (zero viscosity) dynamo making it very unstable. This state is then replaced by a weak field state in which there is a geostrophic rather than magnetogeostrophic balance. The viscosity, despite being very small, then plays a necessary role in balancing the Coriolis force allowing the convection to occur on a time and length scale several orders of magnitude less than in the strong-field regime. This type of convection would also be unstable because it would not transport heat sufficiently and thus there could exist a vacillation of the geodynamo between strong and weak field states consistent with the palaeomagnetic record of reversals and excursions.

Gubbins and Zhang (in prep.) later proposed that when the geodynamo entered the weak field state, convection would be controlled by lateral variation at the CMB and would therefore remain large-scale. During these times, when reversals and excursions were allowed to take place, the heterogeneity imposed by the lowermost mantle would heavily influence the core-flow and hence the likelihood of a reversal.

If the data studied here are at all valid, the process responsible for controlling the mean PFS must act independently of the process responsible for changing the susceptibility of the poloidal field to polarity reversals. The model of Gubbins and Zhang essentially allows these processes to be operative at different times. Assuming this model to be true, two fundamental questions remain:

- What process is responsible for controlling PFS when the geodynamo is in the strong field state?
- How could this process act independently of the lateral thermal heterogeneities at the CMB responsible allowing both the geodynamo to enter the weak field weak state and the subsequent reversal of the field?

Plausible answers to these questions will be discussed later in the context of further evidence described in subsequent sections.

Whatever process allows geomagnetic reversals to occur does not appear to operate during superchrons (Opdyke and Channell, 1996). These periods are not highly distinctive in the dipole moment record however. Contrary to previous propositions (Larson and Olson, 1991; Loper and McCartney, 1986), the superchrons do not appear to exhibit a uniquely different mean poloidal field strength from that of 'normal' times. Excepting the absence of low results, the VDM measurements through the CNS are relatively similar to those before and after the period. Similarly, the means of the VDM measurements from the two superchrons are very different. Furthermore, long term variation of the PFS appears to operate within the PCRS and remain unperturbed during the CNS. These observations constitute further evidence that the process responsible for allowing reversals is largely decoupled from that generating the poloidal field.

The scarcity of very low VDM estimates in both superchrons may be significant, however as it suggests that these values may be associated with reversals. It is difficult to provide a minimum threshold below which the dipole moment indicates that the field is prone to reversal. An ASA of less than 1 _ 10^{22} Am^2 is present in the CNS period although this may be inaccurate.

The entire record is purged of SA data known to be from transitional periods when the dipole moment drops by as much as an order of magnitude (Gubbins, 1994). Although there are probably unreported transitional estimates in the record, this is unlikely to explain the disparity between the relative amounts of CNS and non-CNS estimates in the region of 0 – 4 _ 10^{22} Am^2.

Collapses of the dipole field into the weak field state are expected to occur as often as every thousand years (Gubbins, pers. Comm.). However, they are unlikely to be well-represented in the dipole moment record presented here because the

accompanying direction of the poloidal field is likely to have been anomalous (relative to the rest of the rock suite) and consequently the estimates would be reported as transitional or unreliable. Upon inspection, most low VDM estimates have similar directions to those comprising the rest of the rock suite.

The poor representation of these low values in the superchrons does suggest that these low values are associated with reversals; a plausible explanation is that they were recorded at times when the poloidal field retained its dipole direction but was descending into, or recovering from, a collapse. Logically, this implies that the geodynamo entered the weak field state far less often (possibly not at all) during superchrons. However, this is difficult to reconcile with the concept of an intrinsically unstable dynamo promoted by Zhang and Gubbins (2000a). Is it feasible that the CMB conditions are such during superchrons that the geodynamo loses its inherent instability? There are no obvious alternative explanations for why there should be such a disparity in low VDM estimates between the reversing and non-reversing periods.

It would be useful to discover whether there is any correlation between low values of dipole moment and reversal frequency outside of superchrons. This would help discriminate between two processes that possibly control reversal frequency. The first is that high reversal frequency is simply a consequence of the geodynamo collapsing more frequently and having more opportunities to reverse. The alternative is that imposed CMB conditions dictate how likely the field is to reverse once it is in the weak field state, and that the frequency of dynamo collapse is as high at all times outside superchrons. Neither of these processes are pertinent to superchron periods assuming that dynamo collapse is far less commonplace.

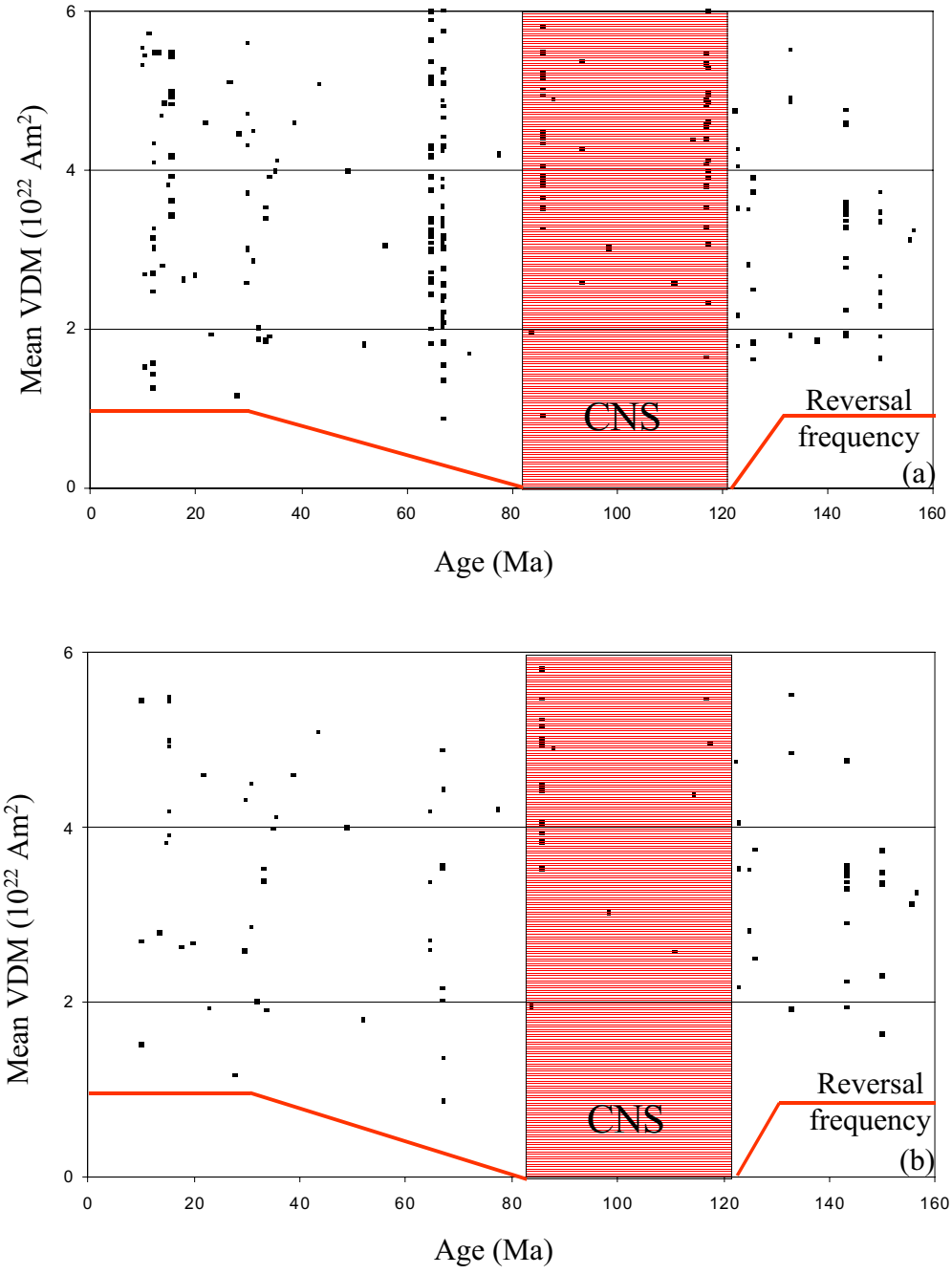

Figure 8.6: (a) Low ASA VDM estimates between 10 Ma and 158 Ma, red line shows variation in reversal frequency schematically. (b) same for selected data only.

Figure 8.6 allows a detailed qualitative comparison of low VDM estimates and reversal frequency. Taking any arbitrary upper limit between 2 and 4 _ 10^{22} Am^2, there is no obvious difference between estimates from close to the superchron on both sides, and those further away. Clearly more data are needed to verify this but, presently, the record tentatively suggests that the poloidal field may not be weak any more frequently at times of high reversal frequency than at other times. If the assumption of low estimates being related to collapses is true, it implies that the geodynamo is equally prone to collapse at all times outside of superchrons.

Another interesting observation made from figure 8.6 is that, prior to the CNS (160 – 122 Ma), the PFS does not reach as low values (< 1.5 _ 10^{22} Am^2) as those after the CNS. This is a product of the very low standard deviation of the segment 167 – 133 Ma but its significance is unclear given that reversal frequency is approximately the same as in the segment 65 – 10 Ma.

8.3 The relationship between dipole moment and true polar wander (TPW)

TPW is the movement of the entire mantle relative to the rotation axis and is calculated by combining the APWP of lithospheric plates with the APWP for hotspots. This method relies implicitly on the assumption that hotspots are stationary within the mantle and offer a reference frame for this shell. Non-zero TPW is thought to represent mass redistribution within the mantle forcing variation in the Earth's moment of inertia.

The most recent study of TPW for the last 200 Myr was conducted by Prévot *et al*. (2000) using only high quality palaeomagnetic poles from igneous rocks. They reported results very different from those of Courtillot and Besse (1987; § 6.3.4) who studied the same interval. Periods of standstill were reported between the present and 80 Ma and 200 – 150 Ma. Between these intervals there was motion of the rotation axis reaching a dramatic peak (5° / Myr) at approximately 110 Ma.

Using palaeomagnetic data from just Pacific seamounts, Sager and Koppers (2000) also found evidence for a short-lived, extremely rapid episode of TPW in the late Cretaceous (~ 84 Ma) without requiring that the 'static hotspot' assumption be made.

Prévot *et al* (2000) noted the quasi-correlation between this observed variation of TPW, geomagnetic reversal frequency and mid-Cretaceous plume activity (see below). They attributed this major reorganisation of material in the mantle in the Cretaceous to a period of catastrophic avalanching of accumulated slab material through the 660 km transition zone (§ 6.2.4). Prior and subsequent to this period, they postulated that the absence of TPW reflected episodes of stable layered convection.

Clearly, as with reversal frequency, the timescale of reported variation in TPW is approximately half that of PFS. The two intervals during which there is no TPW are coincident with parts of the dipole moment record that exhibit quite different behaviour. There is no suggestion that the important transitions in TPW behaviour are synchronous with possible transitions in PFS behaviour and therefore no direct coupling in between the processes responsible for generating them is implied.

This is somewhat surprising as one would imagine that such major events in the mantle impinging on the CMB and causing a decrease in reversal rate would affect the poloidal field generated by the geodynamo. However it is worth remembering that both reversal frequency and dipole moment records exhibit transitions in behaviour between ~140 Ma and 130 Ma. This suggests that both may have experienced delayed responses to the sudden increase in TPW at 150 Ma, although in the case of the dipole moment record the response was a single, relatively slight shift in behaviour. Similarly, there may have been a small transition in mean PFS ~15 Myr after the TPW event ended at 80 Ma. However, it is not clear whether 10 Myr is sufficient time for the effects of descending slabs to be felt at the CMB.

These arguments aside, the whole concept of measured global TPW must be treated with some caution. The premise that hotspots are stationary markers in the mantle is based on the assumption that they are all plume-derived. While this is accepted by many, there still remains a contingent of Earth scientists who use several different aspects of observational evidence to argue that most or all LIPs are spatially controlled by lithospheric conditions and have upper-most mantle origins (Anderson, 1998a,b; Sheth, 1999; Smith and Lewis, 1999). If, as some of these claim, hotspot trails are a product of progressive lithospheric fissuring, then the mode of TPW calculation used by Prévot *et al* (2000) is invalid.

8.4 The relationship between dipole moment and Large Igneous Province (LIP) emplacement

Large igneous provinces are believed by some to be manifestations of plumes derived from the lower-most mantle (Richards *et al*., 1991), others argue that their position and extent is controlled entirely by lithospheric processes and that they originate in the upper mantle (e.g. Anderson, 1998a,b). Coffin and Eldholm (1994) take the conservative view that each LIP much be viewed separately and that there may be a variety of causes, see § 6.2.3 for further discussion.

Larson (1991) analysed oceanic crustal production versus time since 150 Ma and found that both oceanic plateaux emplacement and Pacific Ocean ridge spreading was markedly increased during the period 120 – 80 Ma. He attributed this to the crustal impingement of one or more 'superplumes' from the CMB and noted the synchronicity of the CNS. Larson and Olson (1991) found a very similar temporal pattern of crustal production resulted when all LIPs were analysed and concluded that mantle plumes controlled reversal frequency. Figure 8.7 shows the three records together with the geomagnetic reversal frequency, a qualitative correlation is hard to dismiss.

Prior to 125 Ma, crustal production in the form of LIPs was relatively minor but consistent. There are no existing LIPs reported before 250 Ma in the period of our study (Yale and Carpenter, 1998).

Clearly, the correlation of LIP emplacement with reversal frequency precludes a simple relationship with PFS. However, the onset of the 'superplume' is close to the 138 – 133 Ma transition in the dipole moment record and the noticeable peak in crustal production at 65 Ma is coincident with a further transition. This suggests that factors which may control the geomagnetic reversal frequency may also perturb the ability of the geodynamo to generate poloidal field.

Yale and Carpenter (1998) also regarded giant dyke swarms (GDS) as mantle plume signatures, these are evident throughout the geological record since 350 Ma, prior to this there was an absence of GDS and LIPs since 500 Ma. Tatsumi *et al*. (2000) claimed that belts of metamorphosed basalts (greenstone) in Japan suggested a giant plume erupted in the Pacific between 300 and 350 Ma. This would coincide with the rapid increase in PFS observed in the dipole moment record between these times.

Yale and Carpenter (1998) observed an ~500 Myr cyclicity in the occurrence of GDS and LIPs since 3 Ga. They proposed therefore that these are proxies for supercontinent aggregation, the potential effect of this phenomenon on PFS is discussed in the next section.

If, as Tatsumi *et al* (2000) claim, there was a Pacific superplume in the Carboniferous then there is a good case for these large scale upwellings causing the reversal process to halt. Using simple thermal arguments, Loper (1992) claimed that CMB temperature would change very slowly in response to a significant thermal upwelling and therefore plume initiation would not cause sudden changes in the geomagnetic reversal frequency. Consequently, both Larson and Kincaid (1996) and Gallet and Hulot (1997) preferred the arrival of slab material at the CMB as a mechanism for rapidly reducing the tendency of the geodynamo to reverse. Gallet

and Hulot (1997) also claimed that this mechanism was consistent with the much more gradual restoration of reversal frequency as the cold slab material at the CMB was slowly reincorporated into mantle convection.

Large-scale subduction and superplumes are not mutually exclusive indicators or causes of changes in geomagnetic reversal frequency. Larson and Kincaid (1996) presented a two-dimensional model of the mantle in which the 660 km thermal boundary layer was advected upwards causing widespread volcanism as slab penetration occurred. Three dimensional models of a partially layered mantle have also shown that penetration of slabs into the lower mantle (which may be catastrophic) is expected to result in some form of counter-flow which could manifest itself at the surface as extensive volcanism (Tackley, 2000).

There is some evidence suggesting that periods of increased LIP emplacement are coincident with some of the instances when the behaviour of the mean PFS shifted from one domain to another. This implies that the process responsible for producing LIPs may also be capable of perturbing the geodynamo in such a way as to effect the generation of the poloidal field. The absence of first order correlation between these two parameters however, suggests that there is not a single mantle process controlling them both.

8.5 The relationship between dipole moment and supercontinent formation

The dominant process in mantle convection is plate tectonics. This itself is largely controlled by subduction of oceanic lithosphere into the upper mantle and probably through the 660 km transition zone (see § 6.2.4 for further discussion).

The discussion of mantle dynamics given in § 6.2.6 concluded that it was probable that features of mantle convection which caused major crustal events would also

effect the lowermost mantle (LMM). Significant changes in LMM conditions are themselves likely to cause variations in the observed geomagnetic field (McFadden and Merrill, 1995). Logically linking these factors, one would expect to find a signature of the major plate tectonic events evident in the dipole moment record.

There are three obvious periods broadly describing different stages of tectonic activity in the last 400 Myr (§ 6.2.2).

- **320 Ma + :** Period of coalescence, high and variable plate speeds.
- **320 Ma – 180 Ma:** Period of supercontinent maintenance, low and steady plate speeds.
- **180 – Present Ma:** Period of separation and independent motion, high and variable plate speeds.

The boundaries of these periods have a very strong time correlation with the two major transitions of behaviour recorded in the dipole moment record (chapter 7). The final assembly of Pangaea was well within errors of the onset of high PFS evident in the dipole moment record as the large RS at 325 Ma. The 167 – 138 Ma segment has the lowest mean dipole moment and displays a continuous increasing trend. Consequently, the lowest mean field strength, signifying the transition of mean PFS from a decreasing trend or stable state to one of gradual increase was at or just before the beginning of this segment. This is coincident with the initial reinstatement of widespread subduction of the Pacific as Pangaea began to separate.

The anomalous nature of the 325 – 310 Ma segment was discussed in § 8.5, the two rock suites that comprise this may record a stationary spatial anomaly in the geomagnetic field. It is worth restating the point first made in chapter 8 that further data of this age from outside of Asia are urgently required to confirm that the dipole moment high at this time was a global feature, and that a sharp increase in PFS did take place in the early Carboniferous. For the purpose of this study however, it is assumed that the measured high mean VDM, if not the standard deviation, was

representative of global PFS at this time. Even if, these two rock suites were shown to be unrepresentative, the basic pattern of PFS variation, upon which most of the conclusions of this chapter are based, would remain intact although the model presented in § 8.5.1 would require some modification.

Assuming the action of accreting material onto continents to be negligible, average plate velocity, subduction and ridge production are equivalent parameters for the Earth. Therefore, subduction was far less prevalent once Pangaea was established than before and after. The primary role that subduction plays in the wholesale transfer of heat through the mantle was discussed in § 6.3, a consequence of this is that the average mantle-wide temperature is expected to be strongly reliant on the global prevalence of subduction.

8.5.1 A simple model of core-mantle-crust interaction

The model described in this section is consistent with the main features of PFS variation since the Devonian as identified in chapter 7. It relies on the following implicit assumptions.

- Mean PFS (and hence measured dipole moment) is inversely proportional to the temperature of the lowermost mantle (LMM). This is easy to imagine if one assumes that core convection (especially meridional flow) is proportional to the temperature difference between the upper and lower boundaries of the outer core.
- The temperature of the lowermost mantle is inversely proportional to the quantity of subducted material penetrating the 660 km transition.
- For reasons given below, layered mantle convection operated prior to the formation of Pangaea and whole mantle convection operated once the continents dispersed.

A cartoon showing the basic evolution of the mantle implied by the model is given in figure 8.8. The stages of the model are:

- **Devonian to earliest Carboniferous.** The continents are drawing together. The upper mantle is cool and becoming more so as rapid subduction takes place. The lower mantle is convecting separately, heat may only be transferred upwards by conduction through the transition zone. The lower mantle average temperature is relatively high and hence the heat flux out of the core is low. PFS was low (figure 8.8(a)).
- **Mid- to late Early Carboniferous.** Final assembly of the continents takes place. Ongoing subduction further cools the upper mantle and this together with slab delamination after continent-continent collision (Eide and Torsvik, 1996) causes a series of avalanches of cold material through the transition zone into the warm lower mantle. This decreases the temperature throughout the lower mantle dramatically and results in CMB heat-flux and hence geomagnetic PFS increasing markedly (figure 8.8(b)).
- **Late Carboniferous to Early Jurassic.** Pangaea remained intact, subduction was limited to that due to supercontinent rotation and readjustments of the configuration of the continents (Muttoni *et al.*, 1996). The upper mantle became progressively warmer because of the scarcity of slab material to allow heat generated by radioactivity and the cooling of the core to be removed, and the insulation effect of the supercontinent. Consequently the transfer of heat across the transition zone by conduction was weak and the lower mantle grew warmer. Heat flux from the core diminished, as did PFS (figure 8.8(c)).
- **Mid-Jurassic to present.** Pangaea began to break-up, the cold subducted slabs fell straight through the warm upper mantle and had more momentum upon reaching the transition zone than in the Devonian. This coupled with the even higher temperatures in the lower mantle allowed the slabs to pass through the transition zone relatively freely. The upper and lower mantle became gradually cooler as subduction continued and new zones formed. The heat flux from the core gradually increased and with it so did mean PFS (figure 8.8(d)).

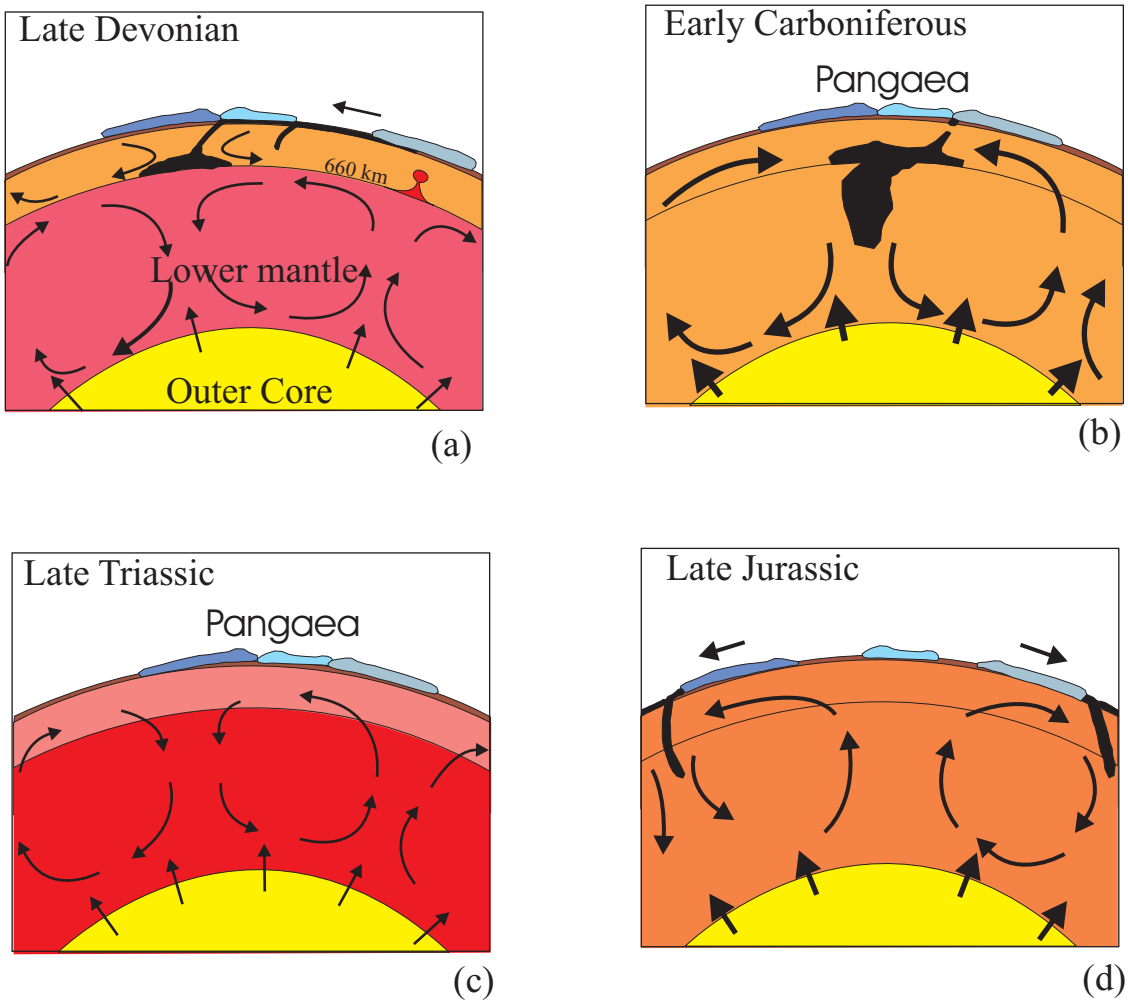

Figure 8.8: Cartoon of Earth cross-section showing qualitative stages of the model presented in § 8.5. (a) Coalescence of continents, cool upper mantle, slabs do not have sufficient momentum to penetrate the 660 km transition, the lower mantle is warm and therefore CMB heat-flux is low. (b) Final assembly of Pangaea, temperature difference between upper and lower mantle becomes large enough to cause catastrophic flushing of cool upper mantle material through the 660 km transition. Subsequently, the lower mantle cools quickly and CMB heat flux increases markedly. (c) Pangaea is maintained, the whole mantle becomes warmer, and CMB heat flux diminishes. (d) Pangaea separates, falling slabs have sufficient momentum to penetrate the 660 km transition and begin cooling the lower mantle. CMB heat-flux gradually increases.

8.6 Discussion

Long term variation in PFS as recorded in the global dipole moment record has a longer timescale of variation than geomagnetic reversal frequency, LIP emplacement, and TPW for at least the last 150 Myr. The specific mantle processes controlling these observed features may perturb the capability of the geodynamo to generate poloidal field strength but certainly do not control it. However, mean PFS has varied on a timescale indicative of hundreds of millions of years and therefore is likely to be controlled by changes in the lowermost mantle.

The variation of mean PFS exhibits a strong time correlation with supercontinent formation and dispersal. This is best explained by invoking subduction and counter-flows as mechanisms linking major crustal and geomagnetic phenomena. The model described in the last section is consistent with the entire dipole moment record and is based upon plausible mantle mechanisms. However, it does not attempt to take all observed and implied global phenomena into account.

Superchrons are initiated at some time after both increases in PFS are observed to begin. The onset of the PCRS is synchronous with the amalgamation of Pangaea at 320 Ma, Eide and Torsvik (1996) attributed it to a blanket of cold material flushed through the transition zone and coating the CMB, this interpretation is not in disagreement with the model presented here. Larson and Kincaid (1996) argued that the CNS too was triggered by the arrival of slab material at the CMB. In their model, the break-up of Gondwanaland at ~130 Ma causes part of the Pacific plate to cascade into the lower mantle. A large plume forms as counter-flow causing the extensive Pacific volcanism observed for the mid-Cretaceous. Gallet and Hulot (1997) also argued that the arrival of slab material at the CMB was the most plausible mechanism for generating the observed pattern of reversal frequency since 158 Ma. Hotspot activity is suspected to have been widespread in the mid-Carboniferous (Tatsumi *et al.*, 2000), suggesting that one or more large plumes may

have formed as counter-flows to the lithospheric avalanching proposed to have occurred at this time as well.

To first order then, the model presented here is not in qualitative disagreement with those previously proposed to account for superchrons and superplumes. It is however, necessary to examine the timings of the processes advocated to explain the variation in PFS observed. Implicit to the model is the notion that there was just one relatively short-lived episode of mantle flushing between 300 and 400 Ma. It is not possible to well-constrain the date and duration of this event because of the small number of rock suites dated between 320 and 375 Ma and the large uncertainties in their age. All that the model implies for certain is that between 375 and 400 Ma, the lower and upper mantle convected separately, but between then and 305 Ma (minimum uncertainty bound for age of 325 Ma RS), cold material had reached the CMB. This is quite consistent with the timings of 'mantle-flushing' advocated by Eide and Torsvik (1996).

The gradual increase in PFS following the break-up of Pangaea is constrained to have begun between 180 and 146 Ma (from the 4 Ma age uncertainty of the 150 Ma RS). This allows ample time for the effects of increased subduction commencing with the initial rifting of the Atlantic at 180 Ma to begin affecting the lowermost mantle.

Davies (1995b) presented a numerical model showing that layered mantle convection followed by catastrophic avalanching of material may have been active 1 Gyr ago when the Earth was warmer. Based upon indirect evidence of PFS variation, it is proposed here that a similar situation existed in the 80 Myr leading up to the final amalgamation of Pangaea. Qualitatively, the inferred low temperature of the upper mantle at this time justifies this. A critical test will be ascertaining, through numerical models of the mantle, whether conditions can be such that layered mantle convection can exist prior to supercontinent formation, catastrophic avalanching can

occur near the point of final coalescence, and whole mantle convection can resume upon break-up.

The need to employ caution in using dipole moment as a proxy for core and LMM conditions was highlighted § 8.1. However, in the model presented in § 8.5, PFS is assumed to be directly proportional to the vigour of core convection, which is itself assumed to be inversely proportional to the average temperature of the LMM. This is justified in this case by the principle of Ockham's razor (that the simplest explanation is usually correct) and by the VDM data itself. The timescale of mean PFS variation is sufficiently long since the Permian at least, that total CMB heat flux variation, itself controlled by average lower mantle temperature, is the simplest and most plausible mechanism for controlling it.

Imposed upon the long-timescale variation of PFS are the shorter timescale variations in reversal frequency. It was not an aim of this study to delineate the cause(s) of long term variation in geomagnetic reversals, however some discussion of how this parameter can vary separately from PFS is warranted.

An active mechanism of polarity reversal, derived from a part of the dynamo action responsible for generating the magnetic field, is not favoured by the results of this study because it is difficult to de-couple reversal frequency from PFS (Sarson, 2000; Glatzmaier *et al*., 1999). The recent hypothesis of Zhang and Gubbins (2000a,b) that the geodynamo is intrinsically unstable may be more compatible with this notion (§ 8.2.4).

If reversals do occur when the geodynamo is in a weak field state, either the susceptibility of the geodynamo to such collapses, the likelihood of reversals occurring once this state has been achieved, or a combination of them both must control reversal frequency. These factors are likely to be a function of lateral variations in thermal conditions at the CMB (Gubbins, pers. Comm.). Consequently, it may be that the frequency of reversals is controlled only by *relative* differences in

heat flux across the CMB whereas mean PFS responds only to variations in the *total* heat flux. It is beyond the scope of this study to provide theoretical backing for this hypothesis.

For most of this chapter, it is the time-averaged (> 10 Myr) PFS that has been discussed. It is worth noting however, that minimum values of VDM remain largely consistent through sufficiently sampled periods, and therefore that it is more appropriate to refer to changes in the range of PFS rather than its mean value. This notion is supported by the observed correlation of mean and standard deviation discussed in § 7.3.4.

PFS varies on several different time-scales superposed onto one another in the VDM record. It is confined to a maximum value that is defined by the temperature of the LMM in the model presented here, and a minimum value somewhere above zero. Most of the short-term variation (of geomagnetic origin) observed in the record is likely to be due to fluctuations associated with the process of dynamo action. An exception to this is when the VDM is less than $4 \_ 10^{22}$ Am^2 and the field may be in the temporal vicinity of a polarity reversal. The relationship between mean VDM and its standard deviation appears to be linear (figure 7.18). This implies that the field does not display any obvious tendency to vary its stability relative to its mean value; i.e. when the maximum allowable value of PFS is altered, the field does not become more or less focussed about its mean value. This may not be the case in superchrons when the tendency of the field to fluctuate may be reduced (§ 8.2.3). The addition of further data from within and around superchrons is required to verify this before any interpretation can be made.

In order that the model presented in § 8.5.1 can be introduced as a potentially viable explanation for crustal-core interaction, it is necessary that it can be tested. The most obvious test that must be conducted is on the dipole moment record itself, upon which the model is based. It is critically important that reliable new palaeointensity

data continues to be produced so that the simple pattern of variation implied by the present record can be substantiated.

9. Discussion

9.1 Part 1 Discussion

Chapter 4 concerned the generation and interpretation of results produced using the techniques outlined in chapter 2 on the samples described in chapter 3. A primary finding of chapter 4 was that the combination of techniques and samples utilised in this study almost unerringly failed to produce palaeointensity estimates that justified unequivocal acceptance by *conventional* criteria.

It may be argued that the samples and the use of only thermal demagnetisation in this study contributed to the paucity of unambiguously reliable estimates, through the medium of the large average magnetic grain size of the samples. However, the same medium can also be used to argue for a relaxation in the criteria conventionally used to assess reliability. Samples with large effective grain sizes are likely to produce noisier NRM-TRM plots, just as they do OVPs. This could explain high degrees of scatter and large pTRM and NRM check discrepancies without having to infer that the samples were altogether incapable of providing an accurate (if somewhat imprecise) palaeointensity estimate. Therefore, it is argued that none of the estimates presented in table 4.25 deserve outright dismissal and that all of them are worthy of the consideration that will be given in § 9.3.

Obviously, the reliability of the estimates must govern the seriousness of the consideration given and the R factor is a useful guide for this purpose. However, it is not an absolute measure. For example, the estimates produced by the NE01 samples have some of the highest R factors observed in this study. Nevertheless, until the targeted component is proved to be a TRM, they must be regarded with more suspicion than those estimates that undoubtedly satisfy this criterion but have a lower associated R factor.

Because of the extremely interesting results described in chapter 5, the discussion regarding the estimates presented in table 4.24 cannot end here. The potential significance of the results of the simulated Thellier experiment for the results presented in chapter 4 and Thellier studies, generally, is best illustrated in table 5.3. Simply, any Thellier palaeointensity study using the conventional analytical approach, and in possession of the information recovered from the rock magnetic analyses, would present these significant overestimates as accurate and precise. Although many samples displayed systematically high pTRM checks, this was not always the case at low temperatures (figure 5.3) and therefore there exists no simple criteria for discriminating against these results in real Thellier experiments.

As stated in chapter 5, conventional analyses of Thellier data assume ideal behaviour and apply criteria to allow for a certain level of non-systematic deviation from this. However, this approach simply does not work for the results presented in chapter 5. This raises two questions that require addressing urgently:-

How common is this behaviour in samples that have received no thermal pre-treatment?

How can it be identified and corrected for?

Unfortunately this study can answer neither fully. The low temperature portion can be made over-steep by a host of processes including demagnetisation biasing, (cumulative) progressive NRM removal, absolute changes in pTRM capacity and the hypothetical 'invisible' type of alteration illustrated in figure 5.8. It is likely that at least some of these processes operate in normal Thellier analyses. Although most of these are theoretically identifiable from concomitant check discrepancies, the combination of two or more processes together with the extra noise generated by untreated samples would make their recognition (and correction) an extremely difficult exercise.

The obvious guard against subtle non-ideal behaviour is to apply stricter acceptance criteria. This would not work for these samples because the check discrepancies and degrees of scatter are so close to zero. The only largely effective criterion that was to require the entire blocking temperature to be used to find the estimate. The problems that would arise from indiscriminately applying this criterion to the results of real analyses were discussed in § 5.5; one would first need to show that irreversible alteration was not highly significant. While this itself may be feasible, the likelihood of encountering untreated samples that do not exhibit irreversible alteration upon heating to T_C is rather low.

Clearly, much more research, based upon the guidelines given in § 5.5, is required into non-ideal behaviour produced during Thellier experiments. This will allow the likelihood of over-estimates occurring in untreated samples, together with methods of recognition and correction, to be ascertained.

The results presented in chapter 5 are highly significant because they show that rigid acceptance criteria are not always appropriate or useful in highlighting the most accurate estimates. The subsequent analysis was also successful in providing explanations for some aspects of the non-ideal behaviour observed. In particular, the development of the demagnetisation biasing model and correction may ultimately provide a means of extracting palaeointensity estimates from samples containing only MD grains, which also exhibit alteration at some stage during heating in the laboratory.

Similarly, the significance and possible uses of NRM checks were assessed. The analysis indicated that discrepancies of just a few percent were sufficient to explain notable inaccuracies in the recovered estimate. However, it was not possible to develop a means of discriminating between the processes referred to as progressive NRM removal and CPNR operating on a sample.

The reliability of the estimates presented in chapter 4, in the context of conventional acceptance criteria, has already been discussed. How do the results of the simulated Thellier experiment and subsequent analysis effect the conclusions formed from this discussion?

Obviously, the full answer to this question can not be provided until further research is performed. The observations and inferences made from the evaluation of the Thellier analysis tended to deal with pTRM and NRM check discrepancies an order of magnitude smaller than those observed in the results presented in chapter 4. Large random errors, the occurrence of catastrophic alteration (e.g. pTRM impedance), and secondary overprints associated with the 'natural' results effectively serve to preclude the meaningful application of the Thellier evaluation results to most of these.

The best example of consistency between the two studies is the NRM-TRM plot produced by sample CR0801B (figure 4.24(a)), which could conceivably indicate QMD behaviour. It may be significant that this sample, derived from a xenolith in a dyke, experienced a thermal history similar to the pre-treatment received by the samples used in the simulated Thellier experiment (i.e. reheating to above T_C).

Unfortunately, no NRM checks were performed on this sample, and it was not completely demagnetised; its laboratory Koenigsberger ratio indicated that large PSD grains dominate its assemblage. The correction when applied across the maximum possible extent of the blocking temperature spectrum caused the estimate to alter by over 30% (table 9.1 and figure 9.1). All the associated parameters were observed to improve and therefore the correction could be said to have worked. However, a greater density of points across the samples blocking temperature spectrum and NRM checks would be required to verify its success.

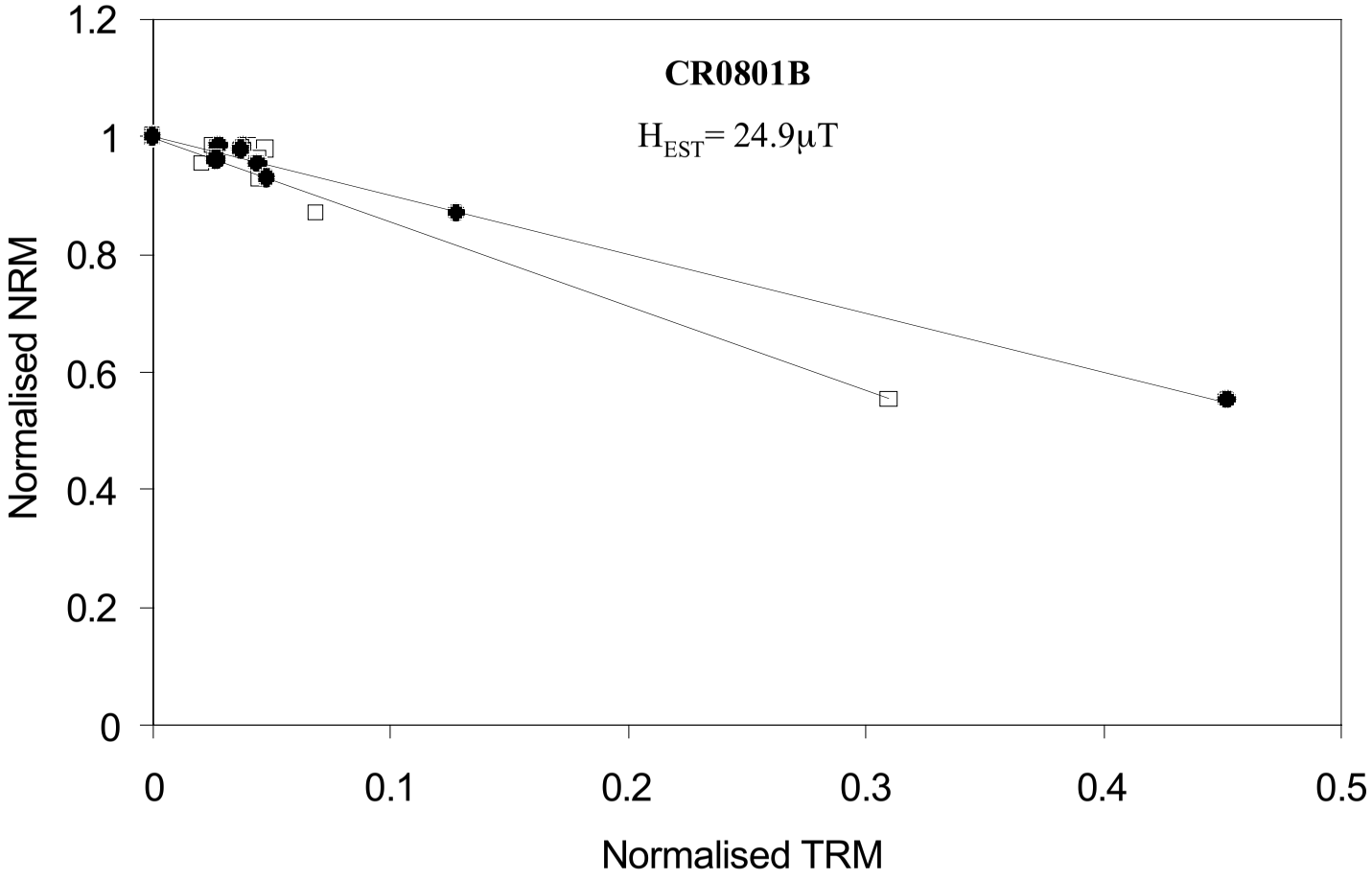

Figure 9.1: NRM-TRM plot for sample CR0801B before (squares) and after (circles) demagnetisation bias correction is applied. Quoted palaeointensity is that from best fit line (shown) through all the corrected points. Best-fit line through uncorrected points is also shown for comparison.

	Before correction					After correction			
Sample	H_{EST} (μT)	β	Max $\lvert d_{TRM}\rvert$	Mean d_{TRM}	ΔT	H_{EST} (μT)	β	Max $\lvert d_{TRM}\rvert$	Mean d_{TRM}
CR0801B	37.7	0.06	0.033	-0.006	0-380	24.9	0.04	0.023	-0.001

Table 9.1: Estimate and parameters for sample CR0801B prior to and after demagnetisation bias correction.

QMD behaviour was generally not observed in the NRM-TRM plots of the samples analysed in chapter 4. Nevertheless, it may have been exhibited less obviously by samples other than CR0801B and escaped notice. However, even if this were the case, one could argue that the inaccuracies produced by the use of a limited portion of the NRM-TRM plot may not have been quite as severe as those observed in chapter 5 (table 5.3). This is because the retained portions of NRM-TRM plots were generally towards the centre of the blocking temperature spectrum of untreated samples so as to avoid secondary magnetisations at low temperature, and catastrophic alteration at high temperature. Due to the shape of a convex-down plot, the slope used would therefore be intermediate in value of those at higher and lower temperatures. Because this central portion represents a transition in slopes, an exaggerated scatter of points about the line may also be expected.

9.2 Part 2 Discussion

The aspect of this study represented in part 2 of this thesis aimed to assess the dipole moment record in the context of certain geodynamic systems and their hypothesised interaction.

While this study does not represent the first attempt to analyse the variation of dipole moment over hundreds of millions of years, it is probably the most detailed and far-reaching. It was stated in § 7.1 that Selkin and Tauxe (2000) performed some statistical analysis on the record of estimates produced with passing pTRM checks with ages between 250 Ma and the present. Their primary conclusion of interest to this study, was that no long-term evolution of the dipole moment had occurred over this period.

However, by requiring that pTRM checks were employed in acquiring the measurements, they excluded 1324 estimates from the updated database of Perrin *et al*. (1998) and 443 from the ASA data-set used in this study. They justified this rather extreme filtering exercise by showing that the distribution of their selected data-set differed from that of the *entirely unfiltered* palaeointensity database at the 95% confidence level. However, the K-S test employed here (figure 9.2) showed that the SBG RS data-set was not distinguishable from the SRS data-set used in this study at the 95% confidence level. This suggests that the wholesale exclusion of estimates that were produced before the usage of pTRM checks became common practise may not be justified.

Consequently, it is argued here that the conclusions of this study are more valid than those produced by the Selkin and Tauxe (2000) because they have grounding in approximately twice as many estimates.

The variation of the ASA and SSA dipole moment records over long timescales was shown to be highly significant (§ 7.3.1). This itself is a supporting argument for the reliability of the data-set. There are no obvious reasons, except geomagnetic intensity variation, for the dipole moment record to display trends in time. Given the large amount of data present in the ASA data-set (711 estimates split in 109 rock suites), a significant proportion of wholly unreliable estimates would result in a random distribution through time and this is clearly not the case.

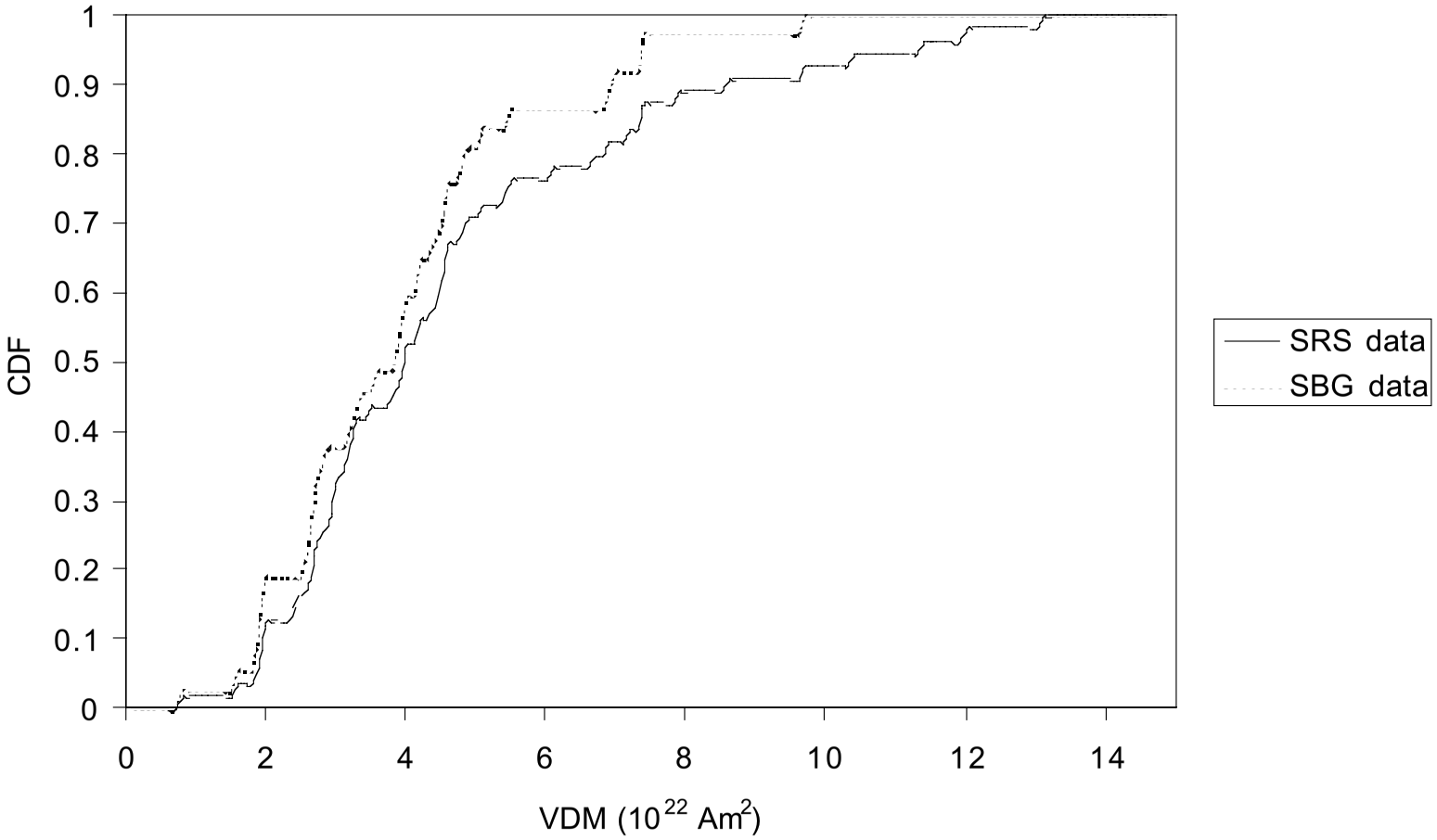

Figure 9.2: CDF functions for selected RS and SBG RS data

The long timescale variation evident in the dipole moment record strongly suggests that conditions at the CMB may influence the generation of PFS in the outer core. Our knowledge of *magnetohydrodynamics* and the LMM is currently not sufficient to directly explain the mechanism for this. Therefore it is necessary to search for possible relationships between geomagnetic behaviour and observed or inferred mantle processes and extrapolate these to likely causal factors.

The results of applying this process to the dipole moment record were presented in chapter 8. The supercontinent amalgamation-dispersal cycle was the only mantle process, evident at the lithosphere, that operated on a timescale as long as that exhibited by the dipole moment record. A model of core-mantle interaction was developed and the causal factors inferred were that subduction (when the slab penetrated the 660 km transition) acted to lower the temperature of the entire mantle, and that the capacity of the geodynamo to generate poloidal field was directly proportional to the total heat-flux through the CMB.

This model also has significant implications for our understanding of mantle processes and these must be proved viable (§ 10.1) before the proposed system can be confirmed.

It is now beyond question that long-period change in reversal frequency and PFS are decoupled at first order. The former appears to vary on a shorter timescale which it may share with the other primary mantle processes, namely LIP emplacement and TPW. In previously proposed models of core-mantle-lithosphere interaction, there has been a tendency for processes such as plume eruption (Larson and Olson, 1991) and the arrival of a slab at the CMB (Gallet and Hulot, 1997) to be regarded in isolation as causal processes for geomagnetic variation. However, the mantle itself is likely to operate using a host of feedback systems (Anderson, 1998a) and therefore the actual global geodynamic system will most likely require explaining in the context of all major geological phenomena.

This approach may appear to preclude the observation of largely uncorrelated reversal frequency and dipole moment records. However, this is not necessarily the case. Significant LIP emplacement and TPW events may be synchronous with transitions in PFS behaviour (§ 8.3 and § 8.4) although more reliable information regarding both of these mantle processes and the dipole moment record are required to verify this. Regardless of the eventual findings, an explanation of how different processes, acting simultaneously at the top of the CMB, can dominantly affect different aspects of geodynamo behaviour is required.

This problem was partly discussed in chapter 8 where it was proposed that heterogeneity in heat flux across the CMB may control reversal frequency while total heat flux controls PFS. This explanation may well prove to be a gross oversimplification but is sufficient at present.

The lack of first-order correlation between reversal frequency and PFS is also interesting in the context of the geodynamo process itself. Most numerical models of the geodynamo that exhibit polarity reversals do so dynamically suggesting that these and excursions are simply a product of the highly time-dependant (chaotic) nature of the field generation process. However, this seems to imply that PFS and reversal frequency should bear some relation to one another (Glatzmaier and Roberts, 1997; Sarson, 2000). Consequently, the notion that reversals only occur when the field collapses into a weak-field state (Zhang and Gubbins, 2000a,b) was considered as an alternative explanation. The compatibility of this theory with the observations remains to be seen. Suffice to say that, at present, they are not incompatible.

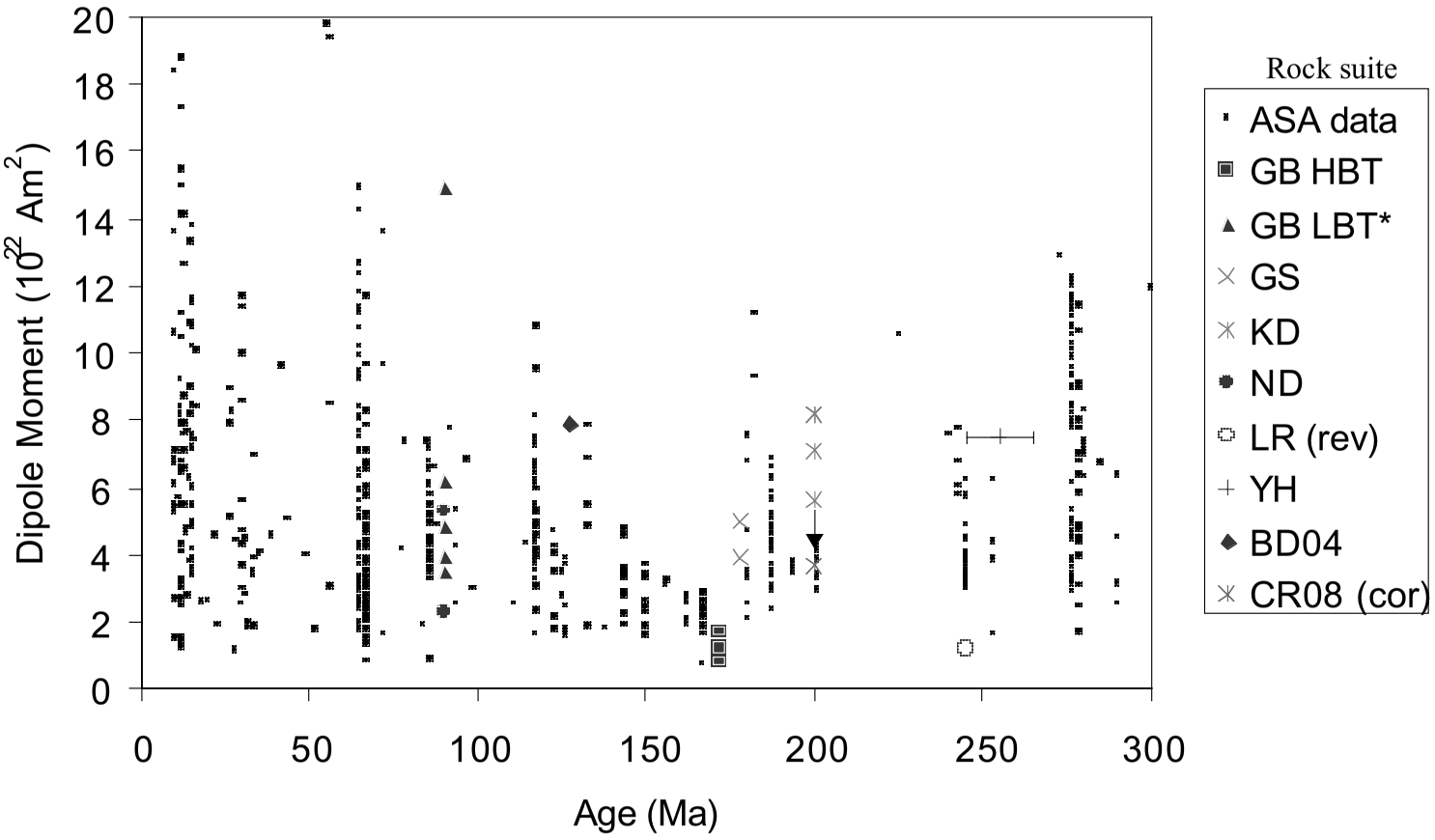

Figure 9.3: VDM (truncated above 20 _ 10^{22} Am^2) versus age plot for ASA data and VDM estimates presented in chapter 4 (table 4.24) *GB LBT estimates represent maximum limits of dipole moment.

9.3 Overall discussion

It is necessary to engage in some discussion of how the results presented in part 1 relate to the analysis and interpretation presented in part 2.

The first and most important requirement is to judge the consistency of the palaeointensity estimates produced by this study (chapter 4) with the conclusions based on the analyses of the secondary dipole moment record (chapters 7 and 8).

All the SA VDM estimates produced by this study (table 4.25), with the exception of that produced by YH LBT, which had very limited age constraint, are plotted in figure 9.3. When more than one estimate was produced from a site (e.g. CR05, NE01), only that with the higher N was plotted although there was generally little difference.

At first glance, the estimates produced by this study appear to fit in well with the general pattern of the ASA data. However, some discussion of each of the rock suite estimates is warranted.

The estimates produced by the HBT component of the GB intrusion had low associated R factors and were presented somewhat cautiously because of the high degree of failure exhibited by the pTRM checks. The alteration that possibly occurs at high temperature would be likely to cause GB samples to underestimate the palaeointensity; the same effect would also be achieved if demagnetisation bias were a contributor to the non-ideal behaviour.

Although the GB HBT estimates themselves are extremely low, they are certainly not inconsistent with the current dipole moment record. They are observed to extend the trend of the 133 – 167 Ma segment of the record back to 172 Ma almost linearly.

The VDMs produced from the GB LBT estimates are expected to be higher than the actual dipole moment because time as well as temperature was responsible for imparting the remanence. Consequently they are presented as maximum limits of the dipole moment at the time they were acquired. Although one of the GB LBT SA estimates does appear to be anomalously high, the other four are comparable to most others acquired at this time. They combine to suggest that PFS was less than two-thirds of its present value through most of the CNS.

The GS samples were presented as reasonably reliable palaeointensity recorders in chapter 4. The VDMs they produced were significantly higher than those of the quasi-contemporaneous GB HBT estimates, however this does not necessarily imply alteration affecting either set of samples. The GS estimates fit in well with the RS at 180 Ma and if one accepts the results of this and the GB HBT study, then the punctuated increase in dipole moment since the Jurassic is constrained to have been initiated between 178 Ma and 172 Ma.

The reliability of the estimates produced by the KD samples are open to question because of the pTRM impedance frequently observed. While they are generally higher than contemporary estimates, they fit in well with the notion of a gradual decrease in mean dipole moment through the early Jurassic. The effect of the demagnetisation bias correction on the single CR08 estimate is to place it within the range of the two RSs at 201 Ma. However, this may well be coincidence.

The SA estimates derived from the ND sites would be regarded as some of the most reliable if it were not for the slight doubt over them possessing a primary TRM (§ 4.3.3). Disregarding this for the present, the two estimates are well within the range of others from the 67 – 133 Ma segment. Although the LR01 estimate is rather low, it is not sufficient to be highly conspicuous in a period lacking polarity reversals (§ 8.2.2).

The VDM provided by the single reversely magnetised sample from the ND sites is sufficiently low to be associated with the reversal process however. A possible implication of this is that its remanence was acquired in a time of extreme SV and that therefore, its direction (and consequently its inferred age) is not meaningful. The ND samples urgently require further study to address uncertainties associated with them. For the present, it should be borne in mind that the estimates from either the normal or reversed, and not both, are likely to be correct.

The single YH (HBT) estimate is shown with x-axis error bars on figure 9.3 indicating that its age is constrained by stratigraphy only to the late Permian. The value of the VDM is intermediate of the mean values of ASA data either side and therefore it is conformable with the notion of progressive decrease through the Permo-Triassic.

The BD04 (0-300) SA comprises of only one estimate with no supporting directional information and therefore must be treated cautiously. Although it is one of the higher estimates within its segment (167 – 138 Ma), it is not particularly conspicuous.

Consequently, the dipole moment estimates produced by this study do not challenge any of the conclusions formed in chapters 7 and 8 and support them in several instances. This, in turn, suggests that many of the estimates presented in table 4.24 are *approximately* correct.

It must be remembered that the differences in cooling rate the samples experienced in nature and the laboratory serves to offset the estimated field strength from reality (§ 2.4.3). Although attempts to correct for this in the GB and GS samples were made (Thomas *et al*., 2000), they were not mentioned in this thesis because of the very large uncertainties in natural cooling time. Another problem is that it was seldom clear whether the PSD grains encountered in the samples studied here behaved more like SD or MD grains in acquiring remanence and consequently, the appropriate correction to apply was not known. The effect will be largest in the slower cooled

rocks (GB, GS, YH, BD) and could oppose the offset caused by alteration in the experiment. The offset in the estimates provided by the very high level intrusions (i.e. the Newcastle and Kiama dykes) would probably be less than 20%.

For the most part, features observed in the dipole moment record were qualitatively consistent in both the ASA and SSA data-sets. It is worth investigating the effectiveness of the criterion used to discriminate between these in filtering the SA estimates produced by this study.

Only two of the estimates presented in table 4.24 have standard deviations of less than 10% of their value. Surprisingly, both of these also have very low Reliability factors ($R < 3$) so the self-consistency criterion would fail to select those estimates conventionally regarded as most reliable. The criterion itself is based upon the sound assumption that a set of reliable estimates from the same site will be similar in value because random error is the sole cause of any observed scatter. However, the absence of a criterion requiring a minimum number of estimates (above two) to comprise the SA may allow apparent self-consistency to be achieved by coincidence; the two 'selected' SA data in table 4.24 are comprised of only two and three estimates respectively.

An improved SSA criterion, based solely upon the estimates displayed in table 4.24, and assuming the R factor to be effective, would be to require that the SA is comprised of at least four estimates and that the associated standard deviation was less than 35% of its value. This would reject all SAs except those with R greater than 5.

This criterion obviously needs to be tested and refined using other data-sets before it is used in an analysis of the dipole moment record. In particular, the 35% maximum limit on standard deviation does appear rather generous and may be indicative of the fact that none of the SA estimates used to derive it can be accepted unequivocally, even by conventional criteria. The important observation to stress here is that the

current criterion used for defining the SSA data-set may allow some estimates of dubious reliability to be regarded with inappropriate confidence.

Before a synthesis can be reached, both a thesis (sensu stricto) and an antithesis must be proposed. The results of this study could be regarded as representing aspects of both of these.

The uncertainties, highlighted by part 1 of this study, that relate to the reliability of palaeointensity estimates and the problems that were encountered in avoiding these act to reduce, to some extent, the confidence that can be placed on the analysis and subsequent interpretation of the global dipole moment record. This does not imply that the study is lacking in completeness: all non-theoretical studies are inherently incomplete, rather that it offers a balanced argument.

In particular, the results presented in table 5.3 pose questions concerning the reliability of many estimates, even those that would conventionally be accepted unequivocally. To illustrate this, it is worth highlighting sample NE0107B and stressing that its high quality palaeointensity estimate is derived from an NRM-TRM plot (figure 4.27(b)) not dissimilar to those of CR0107C and CR0502A in the simulated Thellier experiment (figure 5.3). This could be used as an argument against the conclusions formed from part 2 of this study. However, the same counter that was against the strict filter employed by Selkin and Tauxe (2000; § 9.2) can be used again here. A data-set dominated by *wholly unreliable* estimates would produce a record randomly distributed through time. This is clearly not the case. Additionally, it must be stressed that the extent to which the non-ideal behaviour exhibited by the samples studied using the simulated Thellier experiment is shared by samples containing a TRM acquired in nature, cannot be ascertained from the results of this study. The fact that the xenolith sample analysed in § 5.3 and § 9.1 was one of the few that appeared to produce a QMD plot suggests that it may only be a characteristic of rocks that have been extensively reheated.

Finally, despite the quantitative nature of the investigation, most of the conclusions formed from the statistical analyses of the dipole moment record were based upon the qualitative features that it displayed. There is no reason to suspect that types and extent of non-reliability are biased to any particular time periods of the record, and the rock suite method was used effectively to ascertain the significance of features identified. Therefore, it is argued that most of the conclusions are valid regardless of the number of offset estimates in the record because the quantity of independent data is, in most cases, sufficient to preserve *relative* variation accurately. The conclusions that must be treated with the most caution are those, already highlighted, which are based upon time periods represented by a limited number of rock suites.

10. Conclusions and future work

This study has been as successful in clearly pointing the way for further research as it has in providing answers to definitive questions, which is unsurprising considering the breadth of subject area undertaken by it. What follows is a list of the primary conclusions reached by this study in the order in which they were presented in the text, § 10.2 identifies the areas requiring future work and presents them in the same format.

10.1 Conclusions

1. Rock magnetic techniques that measure the total (remanent and induced) magnetisation of samples may completely overlook the dominant remanence-carrying component of a sample if there is a coexisting magnetically soft phase. Therefore, techniques that measure properties of remanent magnetisation only should be used whenever possible as a support for palaeointensity studies (§ 4.7).

2. Palaeointensity analysis of Mesozoic/Permian intrusive igneous rocks from eastern Australia produced estimates of field strength that, although not unequivocally acceptable by conventional criteria, were compatible with the global dipole moment record. Problems regarding many of the samples were centred on their large average grain size, which caused the NRM-TRM plots to be noisy and the primary component to be largely overprinted by the reheating event preceding the rifting of the Tasman Sea. Non-thermal methods of demagnetisation to remove this 90 Ma overprint would be useful in future studies of these types of rocks.

3. A type of alteration termed pTRM impedance in this study (§ 4.7) frequently occurred at relatively low temperatures in palaeointensity experiments and precluded samples from producing reliable estimates. The cause of this was

changes in the physical properties of the remanence carriers (likely to be adjustments in the stress regime of PSD grains). It could perhaps be predicted in future studies by room temperature hysteresis measurement after cyclic heating (Kosterov and Prévot, 1997) although this would need to be performed on a sample-by-sample basis.

4. Samples that have remanence properties within the SD range and produce NRM-TRM plots that satisfy all conventional criteria can significantly overestimate the intensity of a laboratory field used to impart a TRM. Conversely, samples producing NRM-TRM plots that do not satisfy all the criteria (they exhibit significant curvature and high pTRM checks) can give estimates accurate within 5%.

5. Causes of non-ideal behaviour evident in discrepancies between pTRM and NRM checks and their original values of less than 10% can be responsible for generating significant curvature of the NRM-TRM plot and overestimating the field intensity by 5 – 15%. However, both of these features were largely corrected in the analysis described in chapter 5.

6. A method was developed that may make it possible to use pTRM check discrepancies to correct for convex-down NRM-TRM plots produced by MD grains during a Thellier experiment. This 'demagnetisation bias' correction could be developed into an extremely useful tool for producing reliable palaeointensities from samples that would otherwise be discarded.

7. Poloidal field strength (PFS) recorded at the surface of the Earth has varied over tens and hundreds of millions of years, strongly suggesting that processes in the lowermost mantle (LMM) affect the capacity of the geodynamo to generate poloidal field. This variation expresses itself in the maximum limit of dipole moment measured at any one time while the minimum value remains relatively

constant. A consequence of this is that the mean dipole moment for a period of time is quasi-linearly proportional to its associated standard deviation.

8. Applying a criterion requiring that SA data have associated uncertainties of less than 10% of their mean value did not significantly alter the general pattern of the 400 – 10 Ma dipole moment record and therefore was largely unnecessary. However, in a future study it may be useful to include a criterion requiring that a minimum number of estimates comprise the SA (§ 9.3).

9. Relative to times before and after, there is presently a paucity of low (0 – 4 _ 10^{22} Am^2) VDM estimates and a virtual absence of very low (0 – 2 _ 10^{22} Am^2) estimates during the CNS period (121 – 83 Ma). This suggests that such values may be associated with the reversal process although they are unlikely to represent polarity transitions themselves.

10. The variation in the measured dipole moment may be punctuated rather than continuous since the late Jurassic with two transitions observed at 65 Ma and 133 Ma. These transitions may have been synchronous with much more dramatic changes in geomagnetic reversal frequency and corresponding proposed intervals of true polar wander (TPW) and large igneous province (LIP) emplacement. Beyond this unconfirmed correlation, these inferred mantle and geomagnetic signals appear entirely decoupled from the dipole moment record.

11. The primary features of the dipole moment record display a good temporal correlation with the formation of Pangaea and its subsequent break-up. A simple model that explains the current PFS observations was proposed. The primary assumptions were: PFS is proportional to total heat-flux from the core; the 660 km transition was a much more effective boundary to subducting slabs prior to Pangaea forming than afterwards; slabs entering the lower mantle act to increase heat flux through the CMB. For more details see § 8.5 and § 8.6.

10.2 Future work

1. A palaeodirectional analysis on samples from the Newcastle (NE01) and Little Red Head (LR01) dykes using non-thermal demagnetisation techniques and a cryogenic magnetometer should be undertaken. This should focus examining the HBT component so that the significance of sample LR0105D can be verified and the age of formation of this suite of dykes confirmed.

2. Simulated Thellier experiments should be performed on rock samples with extensive supporting rock magnetic experiments (all techniques used by this study) before and after palaeointensity analysis. Ideally, sub-samples taken from the cores should be subject to hysteresis and IRM acquisition / demagnetisation experiments, using a variable field translation balance (VFTB) after each heating step to a new temperature. The results of these should be assimilated and interpreted in the manner of chapter 5. The benefits of this series of investigation could be enormous, allowing a clearer insight into the causes of non-ideal behaviour during Thellier analysis and their prediction and correction. These investigations have the advantage of using any previously measured samples. The same series of experiments should also be performed on untreated samples from lava flows formed in a measured (geomagnetic) field to check that observed phenomena were not the sole result of the pre-treatment the samples had received.

3. Simulated Thellier experiments should be performed on size-filtered (synthetic or crushed) PSD and MD grains of annealed magnetite. This would allow the demagnetisation bias correction to be evaluated as a means of recovering a reliable palaeointensity estimate from a sample containing only MD grains which alter upon heating to their Curie temperature.

4. The addition of more reliable SA data to the dipole moment record for period 400 – 10 Ma is required. For a break-down of periods particularly requiring

more estimates, see table 7.11. The addition of extra data to this record is vital in confirming and constraining the features identified in chapter 7 and interpreted in chapter 8. However, there also appears to be a need to gain a clearer insight into what actually constitutes reliable estimates (see point 3 of this section) before the behaviour of PFS since the Devonian can be fully recognised. Assistance in this respect is also expected in the form of improved methods for acquiring palaeointensity estimates. Recent developments in this field include the microwave palaeointensity method (Hill and Shaw, 1999, 2000) and the application of the Thellier method to individual plagioclase crystals containing magnetic inclusions (Cottrell and Tarduno, 1999, 2000).

5. Further theoretical studies of the geodynamo should be undertaken to facilitate an understanding of how reversal frequency and mean poloidal field strength can be largely decoupled. The lack of correlation between these two variables is an important constraint for geodynamo theory that is not satisfied by the current generation of numerical models.

6. Numerical modelling of the mantle, incorporating continental crust, is required to investigate the effects of supercontinent formation on layered / whole mantle convection patterns. The plausibility of the hypothesis made in chapter 8 of the 660 km transition being far more effective as a barrier to subduction prior to supercontinent formation than after, needs to be evaluated.

Reference List

Anderson, D.L., 1994. Superplumes or supercontinents? Geology, 22, 39-42.

Anderson, D.L., 1998a. The EDGES of the mantle. From: Gurnis, M., Wysession, M., Knittle, E., Buffett, B., (eds.), The core-mantle boundary region, AGU, 255-272.

Anderson, D.L., 1998b. The scales of mantle convection. Tectonophysics, 284, 1-17

Baker, J.C., Fielding, C.R., de Caritat, P., Wilkinson, M.M., 1993. Permian evolution of sandstone composition in a complex back-arc extensional to foreland basin: the Bowen Basin, Eastern Australia. J. Sed. Petrol., 63, 5, 881-893.

Bailey, M.E., Dunlop, D.J., 1977. On the use of anhysteretic remanent magnetisation in paleointensity determination. Phys. Earth Planet. Int., 13, 360-362.

Bloxham, J., Gubbins, D., 1985. The Secular Variation of the Earth's Magnetic Field. Nature, 317, 777-781.

Bloxham, J., Gubbins, D., 1986. Geomagnetic field analysis. IV. Testing the frozen-flux hypothesis. Geophys. J. R. Atron. Soc., 84, 139-152.

Bloxham, J., Gubbins, D., 1987. Morphology of the geomagnetic field and implications for the geodynamo. Nature, 325, 509-511.

Boesen, R., Irving, E., Robertson, W.A., 1961. The Palaeomagnetism of some igneous rock bodies in New South Wales. J. Proc. Royal Soc. N.S.W., 94, 227-232.

Braginsky, S.I., 1976. On the neatly axially-symmetric model of the hydromagnetic dynamo. Phys. Earth Planet. Sci., 11, 191-199.

Braginskii, S.I., Roberts, P.H., 1987. A model-Z geodynamo. Geophys. Astrophys. Fluid Dyn., 38, 327-349.

Buffet, B.A., 2000. Earth's core and the geodynamo. Science, 288, 2007-2012.

Buffet, B.A., Huppert, H.E., Lister, J.R., Woods, A.W., 1996. On the thermal evolution of the Earth's core. J. Geophys. Res., 101, 7989-8006.

Bullard, E.C., Freedman, C., Gellman, H., Nixon, J., 1950. The westward drift of the Earth's magnetic field. Phil. Trans. R. Soc. London, A243, 67-92.

Butler, R.F., 1992. Paleomagnetism: magnetic domains to geological terranes. Blackwell Sci., pp 319.

Cain, J.C., Davis, W.M., Regan, R.D., 1974. An n = 22 model of the geomagnetic field. EOS, Trans. Am. Geophys. Union, 56, 1108.

Campbell, J.H., 1998. The mantle's chemical structure: insights from the melting products of mantle plumes. From: Jackson, I. (ed.), The Earth's Mantle: Composition, structure and evolution. Cambridge Univ. Press, 259-310.

Cande, S., Kent, D.V., 1995. Revised calibration of the geomagnetic polarity timescale for the late Cretaceous and Cenozoic. J. Geophys. Res., 100, 6093-6095.

Cande, S.C., Mutter, J.C., 1982. A revised identification of the oldest sea-floor spreading anomalies between Australia and Antarctica. Earth Planet. Sci. Lett., 58, 151-160.

Carr, P.F., & Facer, R.A., 1980. Radiometric ages of some igneous rocks from the Southern and southwestern Coalfield of New South Wales. Search, 11, 382-3.

Channell J.E.T., Cecca, F., Erba, E., 1995. Correlations of Hauterivian and Barremian (early Cretaceous) stage boundaries to polarity chrons. Earth Planet. Sci. Lett., 134, 125-140.

Christensen, U., Olson, P., Glatzmaier, G.A., 1998. A dynamo model interpretation of geomagnetic field structures. Geophys. Res. Lett., 25, 10.

Cizkova, H., Cadek, O., van den Berg, AP., Vlaar, NJ., 1999. Can lower mantle slab-like seismic anomalies be explained by thermal coupling between the upper and lower mantles? Geophys. Res. Lett., 26, 1501-1504.

Coe, R.S., 1967b. Palaeointensities of the Earth's magnetic field determined from Tertiary and Quaternary rocks. J. Geophys. Res., 72, 3247-3262.

Coe, R.S., Gromme, C.S., Mankinen, E.A., 1978. Geomagnetic paleointensities from radiocarbon dated lava flows on Hawaii and the question of the Pacific non-dipole low. J. Geophys. Res., 83, 1740-1756.

Coffin, M.F., Eldholm, O., 1994. Large Igneous Provinces: crustal structure, dimensions, and external consequences. Rev. Geophys., 32, 1-36.

Constable, C.G., 2000. On rates of occurrence of geomagnetic reversals. Phys. Earth. Planet. Int., 118, 181-193.

Constable, C.G., Parker, R.L., 1988. Statistics of the geomagnetic secular variation for the past 5 m.y. J. Geophys. Res., 93, 11569-11581.

Cottrell, R.D., Tarduno, J.A., 1999. Geomagnetic paleointensity derived from single plagioclase crystals. Earth Planet. Sci. Lett., 169, 1-5.

Cottrell, R.D., Tarduno, J.A., 2000. In search of high-fidelity geomagnetic paleointensities: A comparison of single plagioclase crystal and whole rock Thellier-Thellier analyses. J. Geophys. Res., 105, 23579-23594.

Courtillot, V., Besse, J., 1987. Magnetic field reversals, polar wander, and core-mantle coupling. Science, 237, 1140-1147.

Courtillot, V., Hofmann, C., Manighetti, I., Kidane, T., Tapponnier, P., 1997. Relations between plume birth and continental break-up: the case of the Ethiopian traps and the Afar depression. Terra Nova, 9, 522.

Courtillot V., Jaupart C., Manighetti I., Tapponnier P., Besse J., 1999. On causal links between flood basalts and continental breakup. Earth Planet. Sci. Lett., 166, 177-195.

Craeger, K.C., Jordon, T.H., 1988. Slab penetration into the lower mantle beneath the Mariana and other island arcs of the North-west Pacific. J. Geophys. Res., 91, 3573-3589.

Creer, K.M., 1977. Geomagnetic secular variation during the last 25000 years: An interpretation of the data obtained from rapidly deposited sediments. Geophys. J. R. Astron. Soc., 48, 91-109

Davies, G.F., 1995b. Penetration of plates and plumes through the mantle transition zone. Earth Planet. Sci. Lett., 133, 507-516.

Davies, G.F., 1998. Plates, plumes, mantle convection and mantle evolution. From: Jackson, I. (ed.), The Earth's Mantle: Composition, structure and evolution. Cambridge Univ. Press, 228-229.

Davies, J.C., 1973. Statistics and data analysis in geology. John Wiley and sons, pp646.

Day, R., Fuller, M., Schmidt, V.A., 1977. Hysteresis properties of titanomagnetites: grain-size and compositional dependence. Phys. Earth Planet. Int., 13, 260-267.

Dickens, J.M. & Malone, E.J. Geology of the Bowen Basin, Australia. Bureau of Mineral Resources, Geophysics and Geology, Bulletin, 130.

Divernere, V.J., and Opdyke, N.D., 1990. Paleomagnetism of the Maringouin and Shepody formations, New Brunswick – A Namurian magnetic stratigraphy. Can. J. Earth Sci., 27, 803-810.

Divernere, V.J., and Opdyke, N.D., 1991a. Magnetic polarity stratigraphy in the uppermost Mississippian Mauch Chunk formation, Pottsville, Pennsylvania. Geology, 19, 127-130.

Dodson, R.E., Dunn, J.R., Fuller, M., Williams, I., 1978. Palaeomagnetic record of a late Tertiary field reversal. Geophys. J. Roy. Astron. Soc., 53, 373-412.

Dodson, M.H., McClelland Brown, E., 1980. Magnetic blocking temperatures of single domain grains during slow cooling. J. Geophys. Res., 85, 2625-2637.

Doell, R.R., Cox, A.V., 1972. The Pacific geomagnetic secular variation anomaly and the question of lateral uniformity in the lower mantle. From: Robertson, E.C., (ed.), The Nature of the Solid Earth, McGraw-Hill, 245-284.

Dormy, E., Valet, J-P., Courtillot, V., 2000. Numerical models of the geodynamo and observational constraints. Geochem. Geophys. Geosyst., 1, paper no. 2000GC000062.

Dunlop, D. J., Özdemir, Ö., 1997. Rock magnetism: fundamentals and frontiers. Cambridge Univ., pp 573.

Dunlop, D. J., Özdemir, Ö., 2000. Effect of grain size and domain state on thermal demagnetization tails. Geophys. Res. Lett., 27, 1311-1314.

Dunlop, D.J., Özdemir, Ö., Schmidt, P.W., 1997a.
Dunlop, D.J., Özdemir, Ö., Schmidt, P.W., 1997b. Paleomagnetism and paleothermometry of the Sydney Basin 2. Origin of anomalously high unblocking temperatures. J. Geophys. Res. 102, B12, 27,285 – 27,295.

Earle PS, Shearer PM, 1997. Observations of PKKP precursors used to estimate small-scale topography on the core-mantle boundary. Science, 277, 667-670.

Eide, E.A., Torsvik, T.H., 1996. Palaeozoic supercontinental assembly, mantle flushing, and genesis of the Kiaman Superchron. Earth Planet. Sci. Lett., 144, 389-402.

Embleton, B.J.J., Schmidt, P.W., Hamilton, L.H., Riley, G.H., 1985. Dating volcanism in the Sydney Basin: Evidence form K-Ar ages and palaeomagnetism. From: Sutherland, F.L., Franklin, B.J., Waltho, A.E. (eds.). Volcanism in Eastern Australia. Geol. Soc. Aust. Publ. 1, 3-26.

Evans, M.E., McElhinny, M.W., 1969. An investigation of the origin of stable remanence in magnetite-bearing rocks. J. Geomag. Geoelec., 21, 757-773.

Evernden, J.F., & Richards, J.R., 1962. Potassium-argon ages in eastern Australia. J. Geol. Soc. Aust., 9 (1), 1-50.

Facer, R.A. &Carr, P.F., 1979. K-Ar dating of Permian and Tertiary igneous activity in the southeastern Sydney Basin, New South Wales. J. Geol. Soc. Aust., 26, 73-79.

De Faria, D.L.A., Venâncio Silva, S., de Oliveira, M.T., 1997. Raman microspectroscopy of some iron oxides and oxyhydroxides. J. Raman. Spectrosc., 28, 873-878.

Fielding, C.R., Gray, A.R.G., Harris, G.I., Salomon, J.A., 1990b. The Bowen Basin and overlying Surat Basin. Bureau of Mineral Resources, Geophysics and Geology Bulletin 232, 107-118.

Fielding, C.R., Stephens, C.J., Holcombe, R.J., 1997. Submarine mass-wasting deposits as an indicator of the onset of foreland thrust loading-Late Permian Bowen Basin, Queensland, Australia. Terra Nova, 9, 14-18.

Fisher, R.A., 1953. Dispersion on a sphere. Proc. Roy. Soc. Lond., A217, 295-305.

Fisk., H.W., 1931. Isopors and isoporic movement. Bull. Int. Geodet. Geophys. Union, No. 8, Stockholm Assembly 1930, 280-292.

Foulger, G.R., Pritchard, M.J., Julian, B.R., Evans, J.R., Allen, R.M., Nolet, G., Morgan, W.J., Bergsson, B.H., Erlendsson, P., Jakobsdottir, S., Ragnarsson, S., Stefansson, R., Vogfjord, K., 2000. The seismic anomaly beneath Iceland extends down to the mantle transition zone and no deeper. Geophys. J. Int., 142, F1-F5.

Fowler, C.M.R., 1990. The solid Earth: an introduction to global geophysics. Cambridge Univ. Press, pp 472.

Fox, J.M.W., Aitken, M.J., 1980. Cooling-rate dependence of thermoremanent magnetisation. Nature, 283, 462-463.

Gaina, C., Müller, D.R., Royer, J., Stock, J., Hardebéck, J., Symonds, P., 1998. The tectonic history of the Tasman Sea: A puzzle with 13 pieces. J. Geophys. Res. 103, B6, 12,413–12,433.

Gallet, Y., Hulot, G., 1997. Stationary and non-stationary behaviour within the geomagnetic polarity time scale. Geophys. Res. Lett., 24, 1875-1878.

Garnero, E.J., Helmberger, D.V., 1995. A very slow basal layer underlying large-scale low-velocity anomalies in the lower mantle beneath the Pacific: evidence from core phases. Phys. Earth Planet. Int., 91, 161-176.

Garnero, E.J., Jeanloz, R., 2000. Earth's enigmatic interface. Science, 289, 70-71.

Giardini, D., Li, X.-D., Woodhouse, J., 1987. Three-dimensional splitting of the Earth from splitting in free-oscillation spectra. Nature, 325, 405-411.

Glatzmaier, G.A., Coe, R., Hongre, L., Roberts, P.H., 1999. The role of the Earth's mantle in controlling the frequency of geomagnetic reversals. Nature, 401, 885-890.

Glatzmaier, G. A., Roberts, P.H., 1995a. A 3D convective dynamo solution with rotating and finitely conducting inner core and mantle. Phys. Earth Planet. Int., 91, 63-75.

Glatzmaier, G.A., Roberts, P.H., 1997. Simulating the geodynamo. Contemp. Phys., 38, 269-288.

Green, D.H., Falloon, T.J., 1998. Pyrolite: a Ringwood concept and its current expression. From: Jackson, I. (ed.), The Earth's mantle: composition, structure and evolution, Cambridge Univ. Press, 311-381.

Griffiths, R.W., Turner, J.S., 1998. Understanding mantle dynamics through mathematical models and laboratory experiments. From: Jackson, I. (ed.), The Earth's mantle: composition, structure and evolution, Cambridge Univ. Press, 191-227.

Grommé, C.S., Wright, T.L., Peck, D.L., 1969. Magnetic properties and oxidation of iron-titanium oxide minerals in Alae and Makaopuhi lava lakes, Hawaii. J. Geophys. Res., 74, 5277-5293.

Gubbins, D., 1994. Geomagnetic polarity reversals: a connection with secular variation and core-mantle interaction.

Gubbins, D., Kelly, P., 1993. Persistent patterns in the geomagnetic field over the past 2.5 Myr. Nature, 365, 829-832.

Gubbins, D., 1999. The distinction between geomagnetic excursions and reversals. Geophys. J. Int., 137, F1-F3.

Gurnis, M., Wysession, M.E., Knittle, E., Buffett, B.A., 1998. The core-mantle boundary region. Am. Geophys. Union, pp 334.

Hale, C.J., Dunlop, J., 1984. Evidence for an early Archaen geomagnetic field: a palaeomagnetic study of the Komati formation, Barberton greenstone belt, South Africa. Geophys. Res. Lett., 11, 97-100.

Halgedahl, S.L., Day, R., Fuller, M., 1980. The effect of cooling rate on the intensity of weak field TRM in a single domain magnetite. J. Geophys. Res., 85, 3690-3698.

Hammond, R., 1987. The Bowen Basin, Queensland, Australia: an upper crustal extension model for its early history. Bureau of Mineral Resources, Geophysics and Geology, Australia Record, 51, 131-139.

Heller P.L., Anderson, D.L., Angevine, C.L., 1996. Is the middle Cretaceous pulse of rapid sea-floor spreading real or necessary? Geology, 24, 491-494.

Herbert, C., 1976. The depositional development of the basin, from: An outline of the geology and Geomorphology of the Sydney Basin, Branagan, D.F. (ed.), 5-38. Science Press and University of Sydney department of geology and geophysics.

Herbert, C., 1997. Sequence stratigraphic analysis of Early and Middle Triassic alluvial and estuarine facies in the Sydney Basin, Australia. Aust. J. Earth, Sci., 44, 125-143.

Herbert, C., 1980a. Depositional development of the Sydney Basin, from: A guide to the Sydney Basin. New South Wales geological survey bulletin 26, 11-52.

Hill, M.J., Shaw, J., 1999. Palaeointensity results for historic lavas from Mt Etna using microwave demagnetization / remagnetization in a modified Thellier-type experiment. Geophys. J. Int., 139, 583-590.

Hill, M.J., Shaw, J., 2000. Magnetic field intensity study of the 1960 Kilauea lava flow, Hawaii, using the microwave palaeointensity technique. Geophys. J. Int., 142, 487-504.

Hill, R.I., 1991. Starting plumes and continental break-up. Earth. Planet. Sci. Lett., 104, 398-416.

Hillhouse, J., Cox, A., 1976. Bruhnes-Matuyama polarity transition. Earth Planet. Sci. Lett., 29, 51-64.

Honda, S., Balachandar, S., Yuen, D.A., Reuteler, D., 1993. 3-dimensional mantle dynamics with an endothermic phase-transition. Geophys. Res. Lett., 20, 221-224.

Hooper, P.R., 1990. The timing of crustal extension and the eruption of continental flood basalts. Nature, 345, 246-249.

Hunt, C.P., Moskowwitz, B.M., Banerjee, S.K., 1995. Magnetic properties of rocks and minerals. From: Ahrens, T.J. (ed.), Rock physics and phase relations: a handbook of physical constants, vol. 3. Am. Geophys. Un., 189-204.

Jackson, A., Bloxham, J., 1991. Mapping the fluid flow and shear near the core surface using the radial and horizontal components of the magnetic field. Geophys. J. Int., 105, 199-212.

Jackson, A., Jonkers, A.R.T., Walker, M.R, 2000. Four centuries of geomagnetic secular variation from historical records. Phil. Trans. R. Soc. London, A358, 957-990.

Jackson, I., 1998. Elasticity, composition and temperature of the Earth's lower mantle: a reappraisal. Geophys. J. Int., 134, 291-311.

Jackson, I., Rigden, S., 1998. Composition and temperature of the Earth’s mantle: seismological models interpreted through experimental studies of Earth materials. From: Jackson, I. (ed.), The Earth’s Mantle: Composition, structure and evolution. Cambridge Univ. Press, 405-460.

Johnson, C.L., Constable, C.G., 1995. The time-averaged geomagnetic field as recorded by lava flows over the past 5 million years. Geophys. J. Int., 122, 489-519.

Johnson, C.L., Constable, C.G., 1997. The time-averaged geomagnetic field: global and regional biases for 0-5 Ma. Geophys. J. Int., 131, 643-666.

Johnson, C.L., Constable, C.G., 1998. Persistently anomalous Pacific geomagnetic fields. Geophys. Res. Lett., 25, 1011-1014.

Jones, G.M., 1977. Thermal interaction of the core and mantle and long-term behaviour of the geomagnetic field. J. Geophys. Res., 82, 1703-1709.

Kellogg, L.H., Hager, B.H., van der Hilst, R.D., 1999. Compositional stratification in the deep mantle. Science, 283, 1881-1884.

Kelly, P., Gubbins, D., 1997. The geomagnetic field over the past 5 Myr. Geophys. J. Int., 128, 315-330.

Kendall, J.-M., Silver, P.G., 1998. Investigating causes of D'' anisotropy. From: Gurnis, M., Wysession, M.E., Knittle, E., Buffett, B.A., (eds.). The core-mantle boundary region. Am. Geophys. Union, 97-118.

Kent, D.V., Smethurst, M.A., 1998. Shallow bias of paleomagnetic inclinations in the paleozoic and Precambrian. Earth Planet. Sci. Lett., 160, 391-402.

Kirschvink, J.L., 1980. The least squares line and plane and the analysis of palaeomagnetic data. Geophys. J. Roy. Astron. Soc., 62, 699-718.

Klitgord, K.D., Schouten, H., 1986. Plate kinematics of the central Atlantic. From: Vogt, P.R., Tucholke, B.E. (eds.), The geology of North America, the western north Atlantic region. Geol. Soc. Am. Press, 351-378.

Knittle, E., 1998. The solid / liquid partitioning of major and radiogenic elements at lower mantle pressures: implications for the core-mantle boundary region. From: Gurnis, M., Wysession, M.E., Knittle, E., Buffett, B.A., (eds.). The core-mantle boundary region. Am. Geophys. Union, 119-130.

Kono, M., 1987. Changes in TRM and ARM in a basalt due to laboratory heating. Phys. Earth Planet. Int., 46, 1-8.

Kono, M., Tanaka, H., 1995b. Intensity of the geomagnetic field in geological time: a statistical study. From: Yukutake, T (ed.), The Earth's central part: it's structure and dynamics, Terrapub, 75-94.

Kogiso, T., Tatsumi, Y., Shimoda, G., Barsczus, H.G., 1997. High μ (HIMU) ocean island basalts in southern Polynesia: new evidence for whole mantle scale recycling of subducted oceanic crust. J. Geophys. Res., 102, 8085-8103.

Kosterov, A.A., Prévot, M., 1998. Possible mechanisms causing failure of Thellier palaeointensity experiments in some basalts. Geophys. J. Int., 134, 554-572.

Kuang, W., Bloxham, J., 1997. An Earth-like numerical dynamo model. Nature, 389, 371-374.

Labrosse S., Poirier J.P., LeMouel J.L., 1997. On cooling of the Earth's core. Phys. Earth Planet. Int., 99, 1-2.

Lackie, M.A., & Schmidt, P.W., 1996. Thermal events in the Sydney – Bowen Basin as defined by palaeomagnetism. Geol. Soc. Aust. Extended Abstracts 43, 319 – 328.

Laj, C. Mazaud, A., Weeks, R., Fuller, M., Herrero-Bervera, E., 1991. Geomagnetic reversal paths. Nature, 351, 447.

Langereis, C.G., Dekkers, M.J., de Lange, G.J., Paterne, M., van Santvoort, P.J.M., 1997. Magnetostratigraphy and astronomical calibration of the last 1.1 Myr from an eastern Mediterranean piston core and dating of short events in the Bruhnes. Geophys. J. Int., 129, 75-94.

Larson, R.L., 1991. Latest pulse of Earth: evidence for a mid-Cretaceous superplume. Geology, 19, 547-550.

Larson, R.L., Kincaid, C., 1996. Onset of mid-Cretaceous volcanism by elevation of the 670 km thermal boundary layer. Geol., 24, 551-554.

Larson, R.L., Olson, P., 1991. Mantle plumes control magnetic reversal frequency. Earth Planet. Sci. Lett., 107, 437-447.

Lay, T., 1995. Seismology of the lower mantle and core-mantle boundary. Rev. Geophys. Suppl., U.S. National Report to IUGG 1991-1994, 325-328.

Lay, T., Williams, Q., Garnero, E.J., 1998. The core-mantle boundary layer and deep Earth dynamics. Nature, 392, 461-468.

Lee, T, -Y, Lawver, L.A., 1995. Cenozoic plate reconstruction of Southeast Asia. Tectonophysics, 251, 85-138.

Levi, S., 1977. The effect of magnetite particle size on paleointensity determinations of the geomagnetic field. Phys. Earth Planet. Int., 13, 245-259.

Levi, S., Merrill, R.T., 1976. A comparison of ARM and TRM in magnetite. Earth Planet. Sci. Lett., 32, 171-184.

Levi, S., Merrill, R.T., 1978. Properties of single domain, pseudo single domain and multi domain magnetite. J. Geophys. Res., 83, 309-323.

Lie, X., Dziewonski, A. M., 1998. Global analysis of shear wave velocity anomalies in the lower-most mantle. From: Gurnis, M., Wysession, M.E., Knittle, E., Buffett, B.A., (eds.). The core-mantle boundary region. Am. Geophys. Union, 21-36.

Lister, J.R., Buffett, B.A., 1995. The strength and efficiency of thermal and compositional convection in the geodynamo. Phys. Earth Planet. Sci., 91, 17-30.

Lister, J.R., Buffett, B.A., 1998. Stratification of the outer core at the core-mantle boundary. Phys. Earth Planet. Int., 101, 1-2.

Loper, D.E., 1978a. The gravitationally powered dynamo. Geophys. J. Royal Astron. Soc., 54, 389-404.

Loper, D.E., 1978b. Some thermal consequences of a gravitationally powered dynamo. J. Geophys. Res., 83, 5961-5970.

Loper, D.E., 1992. On the correlation between mantle plume flux and the frequency of reversals of the geomagnetic field. Geophys. Res. Lett., 19, 25-28.

Loper, D.E., McCartney, K., 1986. Mantle plumes and the periodicity of magnetic field reversals. Geophys. Res. Lett., 13, 1525-1528.

Love, J.J., 1999. A critique of frozen-flux inverse modelling of a nearly steady geodynamo. Geophys. J. Int., 138, 353-365.

Lund, S.P. Acton, G., Clement, B., Hastedt, M., Okada, M., Williams, R., 1998. Geomagnetic field excursions occurred often during the last million years. EOS, Trans. Am. Geophys. Un., 79, 178-179.

Mallett, C.W., Hammond, R.L., Leach, J.H.J., Enever, J.R., Mengel, C., 1988. Bowen Basin – Stress, structure and mining conditions; assessment for mine planning. NERDDC Project 901, Final Report.

Malone, E.J., Oligers, F., Kirkegaard, A.G., 1964. Geology of the Mount Coolon 1:250000 Sheet , Queensland,. Ibid., 121.

Mankinen, E.A., Prévot, M., Grommé, C.S., Coe, R.S., 1985. The Steens Mountain (Oregon) geomagnetic polarity transition 1: directional history, duration of episodes, and rock magnetism. J. Geophys. Res., 90, 10393-10416.

Marquart, G., Schmeling, H., Ito, G., Schott, B., 2000. Conditions for plumes to penetrate the mantle phase boundaries. J. Geophys. Res., 105, 5679-5693.

Maxwell, S., 1990. Geochemical characterisation of dykes intruding the north-east Sydney Basin, Australia. From: Parker, A.J., Rickwood, P.C., Tucker, D.H., (eds.) Mafic dykes and emplacement mechanisms. A.A. Balkema, publ. no. 23, 415-419.

Mayne, S.J., Nicholas, E., Bigg-Wither, A.L, Rasidi, J.S., Raine, M.J., 1974. The geology of the Sydney Basin – a review. Bur. Min. Resour. geol. geophys. bull., 149, pp 136.

McClelland Brown, E., 1984. Experiments on TRM intensity dependence on cooling rate. Geophys. Res. Lett., 11, 205-208.

McClelland, E., 1996. Theory of CRM acquired by grain growth, and its implications for TRM discrimination and palaeointensity determination in igneous rocks. Geophys. J. Int., 126, 271-280.

McClelland, E., & Briden, J.C., 1996. An improved methodology for Thellier-type paleointensity determination in igneous rocks and its usefulness for verifying primary thermoremanence. J. Geophys. Res. 101, 21,995-22,013.

McDougall, I., Wellman, P., 1976. Potassium-Argon ages for some Australian Mesozoic igneous rocks. J. Geol. Soc. Aust., 23, 1-9.

McElhinny, M.W., McFadden, P.L., Merrill, R.T., 1996a. The time-averaged paleomagnetic field 0-5 Ma. J. Geophys. Res.,101, 25007-25027.

McElhinny, M.W., McFadden, P.L., Merril, R.T., 1996b. The myth of the Pacific dipole window. Earth Planet. Sci. Lett., 143, 13-22

McFadden P.L., 1984a. Statistical tools for the analysis of geomagnetic reversal sequences. J. Geophys. Res., 89, 3363-3372.

McFadden P.L., McElhinny, M.W., 1982. Variations in the geomagnetic dipole 2: statistical analysis of VDMs for the past 5 million years. J. Geomag. Geoelec., 34, 163-189.

McFadden, P.L., Merril, R.T., 1984. Lower mantle convection and geomagnetism. J. Geophys. Res., 89, 3354-3362.

McFadden, P.L., Merril, R.T., 1986. Geodynamo energy source constraints from paleomagnetic data. Phys. Earth Planet. Int., 43, 22-33.

McFadden, P.L., Merril, R.T., 1993. Inhibition and geomagnetic field reversals. J. Geophys. Res., 98, 6189-6199.

McFadden, P.L., Merril, R.T., 1995. History of Earth's magnetic field and possible connections to core-mantle boundary processes. J. Geophys. Res., 100, 307-316.

McFadden, P.L., Merril, R.T., 1997. Asymmetry in the reversal rate before and after the Cretaceous normal polarity superchron. Earth Planet. Sci. Lett., 149, 43-47.

McFadden, P.L., Merril, R.T., McElhinny, M.W., 1988. Dipole/Quadrupole family modelling of palaeosecular variation. J. Geophys. Res., 93, 11583-11588.

McFadden, P.L., Merril, R.T., McElhinny, M.W., Lee, S., 1991. Reversals of the Earth's magnetic field and temporal variations of the dynamo families. J. Geophys. Res., 96, 3923-3933.

McHone, J.G., 2000. Non-plume magmatism and rifting during the opening of the central Atlantic Ocean. Tectonophysics, 316, 287-296.

Merrill, R.T., McFadden, P.L., 1994. Geomagnetic field stability: Reversal events and excursions. Earth Planet. Sci. Lett., 121, 57-69.

Merrill, R.T., McElhinny, M.W., 1983. The Earth's Magnetic Field. Acad. Press, London, 401 pp.

Merrill, R.T., McElhinny, M.W., McFadden, P.L., 1996. The Magnetic Field of the Earth: Paleomagnetism, the Core, and the Deep Mantle. Acad. Press, London, 531 pp.

Michel, A. Chaudron, G., 1935. Etude du sesquioxide de fer cubique stabilisé. C. R. Acad. Sci. Paris, 201, 1191-1193.

Middleton, M.F., & Schmidt, P.W., 1982. Paleothermometry of the Sydney Basin. J. Geophys. Res., 87, B7, 5351 – 5359.

Moore, M. E., Gleadow, A. J.W., Lovering, J.F., 1986. Thermal evolution of rifted continental margins: new evidence from fission tracks in basement apatites from south-eastern Australia. Earth and Planet. Sci. Lett. 78, 255 – 270.

Mori, J., Helmberger, D.V., Localized boundary layer below the mid-Pacific velocity anomaly identified from a PcP precursor. J. Geophys. Res., 100, 20359-20365.

Murray, C.G., Fergusson, C.L., Flood, P.G., Whitaker, W.G., Korsch, R.J.,1987. Plate tectonic model for the Carboniferous evolution of the New England Fold Belt. Aust. J. Earth Sci., 34, 213-236.

Mutter, J.C.,& Jongsma, D., 1978. The pattern of the pre-Tasman sea rift system. Bull. Aust. Soc. Explor. Geophys. 9, 10-75.

Muttoni, G., Kent, D.V., Channell, J.E.T., Evolution of Pangaea: paleomagnetic constraints from the Southern Alps, Italy. Earth Planet. Sci. Lett., 140, 97-112.

Nagata, T., Arai, Y., Momose, K., 1963. Secular variation of the geomagnetic total force during the last 5000 years. J. Geophys. Res., 68, 5277-5282.

Néel, L., 1949. Théorie du traînage magnétique des ferromagnétiques en grain fins avec applications aux terres cuites. Ann. Géophys., 5, 99-136.

Néel, L., 1955. Some theoretical aspects of rock magnetism. Adv. Phys., 4, 191-242.

Olson, P.L., Hagee, V.L., 1990. Geomagnetic polarity reversals, transition field structure, and convection in the outer core. J. Geophys. Res.,95, 4609-4620.

Opdyke, N.D., 1962. Palaeoclimatology and continental drift. From: Runcorn, S.K., (ed.), Continental Drift. Acad. Press, London and New York, 41-65.

Opdyke, N.D., Channell, J.E.T., 1996. Magnetic stratigraphy. Acad. Press, pp346.

O'Reilly, 1984. Rock and mineral magnetism. Blackie, Chapman and Hall. 220pp

Özdemir, Ö., Banerjee, S.K., 1984. High temperature stability of maghaemite. Geophys. Res. Lett., 11, 161-164.

Parker, L.J., Atou, T., Badding, J.V., 1996. Transition element-like chemistry for potassium under pressure. Science, 273, 95-97.

Pattison, 1990. Igneous intrusions in the Bowen Basin. M.Sc. report for Queensland University of Technology.

Perrin, M., 1998. Paleointesity determination, domain structure, and selection criteria. J.Geophys. Res., 103, 30591-30600.

Perrin, M., Schnepp, E., Shcherbakov, V., 1998. Paleointensity database updated. Eos, 79, 198.

Perrin, M., Shcherbakov, V., 1997. Palaeointensity of the Earth's magnetic field for the past 400 Ma: evidence for a dipole structure during the Mesozoic low. J. Geomag. Geoelec., 49, 601-614.

Phillips, J.D., Cox, A., 1976. Spectral analysis of the geomagnetic reversal time scales. Geophys. J. R. Astron. Soc., 45, 19-33.

Pick, T., Tauxe, L., 1994. Characteristics of magnetite in submarine basaltic glass. Geophys. J. Int., 119, 116-118.

Poirier, J.P., 1994. Light elements in the Earth's outer core – a critical review. Phys. Earth Planet. Int., 85, 319-337.

Prévot, M., Derder, M.E., McWilliams, M.O., Thompson, J., 1990. Intensity of the Earth's magnetic field: evidence for a Mesozoic dipole low. Earth Planet. Sci. Lett., 97, 129-139.

Prévot, M., Mankinen, E., Grommé, C.S., Lecaille, A., 1983. High palaeointensities of the geomagnetic field from thermomagnetic studies on rift valley pillow basalts from the mid-Atlantic ridge. J. Geophys Res., 88, 2316-2326.

Prévot, M., Mankinen, E., Coe, R.S., Grommé, C.S., 1985. The Steens Mountain (Oregon) geomagnetic polarity transition 2. Field intensity variation and discussion of reversal models. J. Geophys. Res., 90, 10417-10448.

Prévot, M., Mattern, E., Camps, P., Daignieres, M., 2000. Evidence for 20° tilting of the Earth's rotation axis 110 million years ago. Eart Planet. Sci. Lett., 179, 517-528.

Prévot, M., Perrin, M., 1992. Intensity of the Earth's magnetic field since Precambrian time from Thellier-type intensity data and inferences on the thermal history of the core. Geophys. J. Int., 108, 613-620.

Pulliah, G., Irving, E., Buchan, K.L., Dunlop, D.J., 1975. Magnetization changes caused by burial and uplift. Earth Planet. Sci. Lett., 28, 133-143.

Raam, A., 1968. Petrology and diagenesis of Broughton Sandstone (Permian). Kiama District, New South Wales. J. Sediment. Petrol., 38, 319 – 331.

Radhakrishnamurty, C., Likhite, S.D., Sahasrabudhe, P.W.,1977. Nature of magnetic grains and their effects on the remanent magnetization of basalt. Phys. Earth. Planet. Int., 13, 289-300.

Radhakrishnamurty, C.,1985. Identification of titanomagnetites by simple magnetic techniques and application to basalt studies. J. Geol. Soc. India, 26, 640.

Readman, P.W., O'Reilly, W., 1970. The synthesis and inversion of non-stoichiometric titanomagnetites. Phys. Earth Planet. Int., 4, 121-128.

Revenaugh, J.S., Meyer, R., 1997. Seismic evidence of partial melt within a possibly ubiquitous low velocity layer at the base of the mantle. Science, 277, 670-673.

Richards, M.A., Duncan, R.A., Courtillot, V.E., 1989. Flood basalts and hot-spot tracks: plume heads and tails. Science, 246, 103-107.

Ricou, L.E., 1995. Tethys and Transit plate patterns viewed against long-term periodicity of magnetic field reversals. Phys. Earth Planet. Int., 87, 255-265.

Ricou, L.E., Gibert, D., The magnetic reversal sequence studied using wavelet analysis: a record of the Earth's tectonic history at the core-mantle boundary. Géophysique interne (Eng. Translation), 325, 753-759. Gibert, D., The magnetic reversal sequence studied using wavelet analysis: a record of the Earth's tectonic history at the core-mantle boundary. Géophysique interne (Eng. Translation), 325, 753-759.

Ringis, J., 1975. The relationship between structures on the south-east Australian margin and in the Tasman Sea, Bull. Aust. Soc. Explor. Geophys. 6, 39 – 41.

Roberts, A.P., Cui, Y., Verosub, K.L., 1995. Wasp-waisted hysteresis loops: mineral magnetic characteristics and discrimination of components in mixed magnetic systems. J. Geophys. Res., 100, 17909-17924.

Roberts J., ClaoueLong, J.C., Foster, C.B., 1996. SHRIMP zircon dating of the Permian System of eastern Australia. Aust. J. Earth Sci., 43, 401-421.

Roberts, P.H., 1972. Kinematic dynamo models. Phil. Trans. Royal. Soc. London, A271, 663-697.

Rolph, T.C., Shaw, J., 1985. A new method of palaeofield magnitude correction for thermally altered samples and its application to lower Carboniferous lavas. Geophys. J. Roy. Astron. Soc., 80, 773-781.

Runcorn, S.K., 1992. Polar path in geomagnetic reversals. Nature, 356, 654.

Sager, W.W., Koppers, A.A.P., 2000. Late Cretaceous polar wander of the Pacific plate: evidence of a rapid true polar wander event. Science, 287, 455-459.

Sarson, G.R., 2000. Reversal models from dynamo calculations. Phil. Trans. R. Soc. Lond. A, 358, 921-942.

Sarson, G.R., Jones, C.A., 1999. A convection driven geodynamo reversal model. Phys. Earth Planet. Int., 111, 3-20.

Sarson, G.R., Jones, C.A., Longbottom, A.W., 1998. Convection driven geodynamo models of varying Ekman number. Geophys. Astrophys. Fluid Dyn., 88, 225-259.

Scheibner, E. 1975. Relationship of transfer faults in the Tasman Sea to crustal fractures in New South Wales, from: Crust and Upper Mantle of south-east Australia Symposium Abstracts, Denham, D. (ed.). Bur. Miner. Resour., 81.

Sclater, J.G., Francheteau, J., 1970. The implications of terrestrial heat-flow observations on current tectonic and geochemical models of the crust and upper mantle of the Earth. Geophys. J. Roy. Astron. Soc., 20, 509-542.

Schmidt, P.W., 1976. The non-uniqueness of the Australian Mesozoic pole position. Geophys. J. R. astr. Soc. 47, 285 – 300.

Schmidt, P.W., 1990. An attempt to determine uplift of the Sydney basin, New South Wales, Australia, from the paleomagnetic signatures of dyke contacts from

Kiama. From: Parker, A.J., Rickwood, P.C., Tucker, D.H. (eds.), Mafic dykes and emplacement mechanisms. A.A. Balkema, publ. no. 23, 263-271.

Schmidt, P.W., Embleton, B.J.J., 1981. Magnetic overprinting in sotheastern Australia and the thermal history of its rifted margin. J. Geophys. Res., 86, 3998-4008.

Selkin, P.A., Tauxe, L., 2000. Long-term variations in palaeointensity. Phil. Trans. R. Soc. Lond. A, 358, 1065-1088.

Senanayake, W.E., McElhinny, M.W., 1981. Hysteresis and susceptibility characteristics of magnetite and titanomagnetite: interpretation of results from basaltic rocks. Phys. Earth Planet. Int., 26, 47-55.

Shaw, J., 1974. A new method of determining the magnitude of the palaeomagnetic field, application to five historic lavas and five archaeological samples. Geophys. J. Roy. Astron. Soc., 39, 133-141.

Shaw, R.D., 1978. Sea-floor spreading in the Tasman Sea: a Lord Howe Rise – eastern Australian reconstruction. Bull. Aust. Soc. Explor. Geophys. 9, 75-81.

Shcherbakova, V.V., Shcherbakov, V.P., Heider, F., 2000. Properties of partial thermoremanent magnetisation in PSD and MD magnetite grains. J. Geophys. Res., 104, 767-781.

Sheridan, R.E., 1983. Phenomena of pulsation tectonics related to the break-up of the eastern North American continental margin. Tectonophys., 94, 169-185.

Sheridan, R.E., 1986. Pulsation tectonics as the control of North American palaeooceanography. From: Summerhayes, C.P., Shackleton, N.J. (eds.), North American Palaeooceanography, Geol. Soc. Spec. Publ., 21, 255-275.

Sheth, H.C., 1999. Flood basalts and large igneous provinces from deep mantle plumes: fact, fiction, and fallacy. Tectonophysics, 311, 1-29.

Sleep, N.H., 1990. Hotspots and mantle plumes: some phenomenology. J. Geophys. Res., 95, 6715-6736.

Smith, A.D., Lewis, C., 1999. The planet beyond the plume hypotheseis. Earth Sci. Rev., 48, 135-182.

Solodovnikov, G.M., 1992a. Paleostrength of geomagnetic field in Middle-Late Carboniferous. Izv., Earth Phys. (Eng. Trans.),28, 327-331.

Solodovnikov, G.M., 1992b. Geomagnetic intensity in the middle Carboniferous of Uzbekistan. Izv., Earth Phys. (Eng. Trans.),28, 511-515

Solodovnikov, G.M., 1992c. Palaeointensity of the geomagnetic field in the lower Permian. Izv., Earth Phys. (Eng. Trans.), 28, 718-722.

Stacey, F.D., 1991. Effects on the core of structure within D''. Geophys. Astrophys. Fluid dyn., 66, 157-163.

Steinberger, B., 2000a. Slabs in the lower mantle: results of dynamic modelling compared with tomographic images and the geoid. Phys. Earth planet. Sci., 118, 241-257.

Su, W.-J., Woodward, R.L., Dziewonski, A.N., 1994. Degree 12 model of shear velocity heterogeneity in the mantle. J. Geophys. Res., 99, 6945-6980.

Tackley, P.J., Stevenson, D.J., Glatzmaier, G.A., Schubert, G., 1993. Effects of an endothermic phase transition at 670 km depth in a spherical model of convection in the Earth's mantle. Nature, 361, 699-704.

Tackley, P.J., 1998. Three-dimensional simulations of mantle convection with a thermo-chemical basal boundary layer: D"? From: Gurnis, M., Wysession, M.E., Knittle, E., Buffett, B.A., (eds.). The core-mantle boundary region. Am. Geophys. Union, 231-254.

Tackley, P.J., 2000. Mantle convection and plate tectonics: towards an integrated physical and chemical theory. Science, 288, 2002-2006.

Tanaka, H., 1999. Circular asymmetry of the paleomagnetic directions observed at low latitude volcanic sites. Earth Planets and space, 51, 1279-1286.

Tanaka, H., Kono, M., 1991. Preliminary results and reliability of palaeointensity studies on historical and ^{14}C dated Hawaiian lavas. J. Geomag. Geolec., 43, 375-388.

Tanaka, H., Kono, M., Uchimura, H., 1995. Some global features of palaeointensity in geological time. Geophys. J. Int., 120, 97-102.

Tarduno, J. A., Sliter, W.V., Kroenke, L., Leckie, M., Mayer, H., Mahoney, J.J., Musgrave, R., Storey, M., Winterer, E.L., 1991. Rapid formation of the Ontong-Java plateau by Aptian mantle plume volcanism. Science, 254, 399-403.

Tatsumi, Y., Tomomi, K., Ishizuka, H., Maruyama, S., Nishimura, Y., 2000. Activation of Pacific mantle plumes during the Carboniferous: evidence from accretionary complexes in southwest Japan. Geology, 28, 580-582.

Tauxe, L. 1998. Paleomagnetic principles and practice. Kluwer acad., pp 312.

Tauxe, L., Hartl, P., 1997. 11 million years of Oligocene geomagnetic field behaviour. Geophys. J. Int., 128, 217-229.

Thellier, E., Thellier, O., 1959. Sur l'intensité du champ magnétique terrestre dans la passé historique et géologique. Ann. Géophys., 15, 285-376.

Thomas, D.N., 1992. Rock magnetic and palaeomagnetic investigations of the Precambrian Gardar lava succession, South Greenland. Ph.D. Thesis, University of Liverpool, pp513.

Thomas, D.N., 1993. An integrated rock magnetic approach to the selection or rejection of ancient basalt samples for palaeointensity experiments. Phys. Earth Planet. Int., 75, 329-342.

Thomas, D.N., Biggin, A.J., Schmidt, P.W., 2000. A palaeomagnetic study of Jurassic intrusives from southern New South Wales: further evidence for a pre-Cenozoic dipole low. Geophys. J. Int., 140, 621-635.

Tucker, P., O'Reilly, W., 1980b. The laboratory simulation of deuteric oxidation of titanomagnetites: effects on magnetic properties and thermoremanence. Phys. Earth Planet. Int., 23, 112-133.

Valet, J.P., Meynadier, L., 1993. Geomagnetic field intensity and reversals during the past four million years. Nature, 366, 234-238.

Valet, J.P., Brassart, J., Le Meur, I., Soler, V., Quidelleur, X., Tric, E., Gillot, P.Y., 1996. Absolute paleointensity and magnetomineralogical changes. J. Geophys. Res., 101, 25029-25044.

Vallance, T.G., 1969. Mesozoic and Cenozoic igneous rocks. A: Central and southern New South Wales. From: Packham, G.H. (ed.) 513-529.

van der Hilst, R.D., Widiyantoro, S., Engdahl, E.R., 1997. Evidence for deep mantle circulation from global tomography. Nature, 386, 578-584.

van der Hilst, R.D., Widiyantoro, S., Creager, K.C., McSweeney, T.J., 1998. Deep subduction and aspherical variations in P-wavespeed at the base of Earth's mantle. From: Gurnis, M., Wysession, M.E., Knittle, E., Buffett, B.A., (eds.). The core-mantle boundary region. Am. Geophys. Union, 5-20.

van der Hilst, R.D., Kárason, H., 1999. Compositional heterogeneity in the bottom 1000 kilometers of the Earth's mantle: toward a hybrid convection model. Science, 283, 1885-1888.

Van der Voo, R., 1993. Paleomagnetism of the Atlantic, Tethys and Iapetus Oceans. Cambridge Univ. Press, pp 421.

Van der Voo, R., 1994. True polar wander during the middle Paleozoic. Earth Planet. Sci. Lett., 122, 239-243.

.

Van Zijl, J.S.V., Graham, K.W.T., Hales, A.L., 1962. The palaeomagnetism of the Stormberg lavas of South Africa, 1 and 2. Geophys. J. Royal Astron. Soc., 7, 23-39 and 169-182.

Veevers, J.J. (ed.), 1984. Phanerozoic Earth History of Australia. Oxford Sci. publ., pp 418.

Veevers, J.J., 1989. Middle-late Triassic singularity in the stratigraphic and magmatic history of the Pangean heat anomaly. Geology, 17, 784-787.

Verosub, K., 1977. Geomagnetic excursions and their paleomagnetic record. Rev. Geophys. Space Phys., 15, 145-155.

Vidale, J.E., Garcia-Gonzalez, D.E., 1988. Seismic observation of a deep slab. Geophys. Res. Lett., 15, 369-372.

Vogt, P.R., 1972. Evidence for global synchronism in mantle plume convection and possible significance for geology. Nature, 240, 338-342.

Ward, C.R., 1972. Sedimentation in the Narrabeen Group, southern Sydney Basin, New South Wales. J. Geol. Soc. Aust. 19, 393-409.

Watkins, N.D., Haggerty, S.E., 1967. Primary oxidation variation and peterogenesis in a single lava. Contrib. Min. Petrol., 15, 251-271.

Watson, G.S., 1956. A test for randomness of directions. Monthly Notices Geophys. J. Roy. Astron. Soc., 7, 160-161.

Webb, A.W., McDougall, I., 1968. The geochronology of the igneous rocks of eastern Queensland. J. Geol. Soc. Aust., 15(2), 313-346.

Weissel, J.K., Hayes, D.E., 1977. Evolution of the Tasman Sea reappraised. Earth Planet. Sci. Lett. 36, 77-84.

Wellman, P., & McDougall, I., 1974b. Cainozoic igneous activity in Eastern Australia. Tectonophysics 23, 49-65.

Wen, L.X., Anderson, D.L., 1997. Layered mantle convection: A model for geoid and topography. Earth Planet. Sci. Lett., 146, 367-377.

White, R.S., McKenzie, D.P., 1989. Magmatism at rift zones: the generation of volcanic continental margins and flood basalts. J. Geophys. Res., 94, 7685-7729.

Williams, Q., 1998. The temperature contrast across D''. From: Gurnis, M., Wysession, M.E., Knittle, E., Buffett, B.A., (eds.). The core-mantle boundary region. Am. Geophys. Union, 73-81.

Williams, Q., Garnero, E.J., 1996. Seismic evidence for partial melt at the base of the Earth's mantle. Science, 273, 1528-1530.

Williams, Q., Revenaugh, J., Garnero, E., 1998. A correlation between ultra-low basal velocities in the mantle and hot spots. Science, 281, 546-549.

Wilson, R.L., 1961. Palaeomagnetism in Northern Ireland, part 1: The thermal demagnetisation of natural magnetic moments in rocks. Geophys. J. Roy. Astron. Soc., 5, 45-58.

Wilson, R.L., Watkins, N.D., 1967. Correlation of petrology and natural magnetic polarity in Colombia Plateau basalts. Geophys. J. Roy. Astron. Soc., 12, 405-424.

Windley, B.F., 1996. The Evolving Continents (3rd edition). John Wiley & Sons, pp526.

Wu, Y.T., Fuller, M., Schmidt, V.A., 1974. Microanalysis of a N.R.M. in a granodiorite intrusion. Earth Planet. Sci. Lett., 23, 275-285.

Xu, S., Dunlop, D.J., 1994. The theory of partial thermoremanent magnetisation in multidomain grains. 2. Effect of microcoercivity distribution and comparison with experiment. J. Geophys. Res., 99, 9025-9033.

Xu, S., Dunlop, D.J., 1995a. Thellier paleointensity determination using MD and PSD grains (abstract). Eos (Trans. Am. Geophys. Un.), 76, F170.

Yale, L.B., Carpenter, S.J., 1998. Large igneous provinces and giant dyke swarms: proxies for supercontinent cyclicity and mantle convection. Earth Planet. Sci. Lett., 163, 109-122.

Zhang, K., Gubbins, D., 2000a. Is the geodynamo process intrinsically unstable? Geophys. J. Int. 140, F1-F4.

Zhang, K., Gubbins, D., 2000b. Scale disparities and magnetohydrodynamics in the Earth's core. Phil. Trans. R. Soc. Lond. A, 358, 899-920.

Zhou, H.W., Anderson, D.L., 1989. Search for deep slabs in the northwest Pacific mantle. Proc. Natl. Acad. Sci. USA, 86, 8602-8606.

Zhou, H.W., Anderson, D.L., Clayton, R.W., 1990. Modelling of residual spheres for subduction zone earthquakes 1. Apparent slab penetration signatures in the NW Pacific caused by deep, diffused mantle anomalies. J. Geophys. Res., 95, 6799-6827.

Zhou, H.W., Clayton, R.W., 1990. P and S wave travel time inversions for subducted slab under the island arcs of North-east Pacific. J. Geophys. Res., 95, 6829-6851.

Zijderveld, J.D.A., 1967. A.C. demagnetisation on rocks: analysis of results. From: Collinson, D.W., Creer, K.M., Runcorn, S.K. (eds.). Methods in palaeomagnetism. Elsevier, pp 254-286.

Appendix 1: Glossary of Terms

α^2 dynamo	Type of dynamo whereby both the *poloidal* and *toroidal* components of the magnetic field are generated by helical fluid flow
$\alpha\omega$ dynamo	Type of dynamo in which the poloidal magnetic field is generated by helical fluid flow and the toroidal field is generated by differential flow
AF demagnetisation	Technique of demagnetisation whereby samples are subject to an alternating magnetic field applied in random directions.
Anhysteretic Remanent Magnetisation (ARM)	Remanence acquired during *AF demagnetisation* when a small direct field imparts a bias to the alternating field.
Apparent Polar Wander Path (APWP)	A collection of temporally variant, spatially similar *palaeomagnetic poles*. These designate an imaginary path the time-averaged geomagnetic pole would have followed, over a time period, if the source area had remained stationary.
Blocking Temperature (T_B)	Temperature below which, the *relaxation time* of a *ferromagnetic* grain extends beyond laboratory time (~100s) and the grain acquires a *remanence.*
Blocking Temperature Spectrum	The range of *blocking temperatures* present in an assemblage due to the size/shape/*coercivity* range of the grains present there. Many samples have a T_B spectrum extending from T_R up to the *Curie temperature* of the constituent magnetic minerals.
Boussinesq approximation	Commonly used in fluid dynamics, this approximation demands that the fluid is incompressible and that temperature / composition anomalies alone cause changes in density.
Characteristic Remanent Magnetisation (ChRM)	The highest stability component of a material's *NRM.* I.E. the last component to be demagnetised. In igneous rocks, this is

	usually (though not always) the primary *TRM*.
Chemical Remanent Magnetisation (CRM)	Magnetisation acquired in grains as they grow from solution or are formed from alteration of pre-existing minerals, while subject to a field.
Chron	A period of time when the field is predominantly in a single polarity state. I.E. normal (N) or reversed (R).
Coercivity (H_C)	The field required to remove an anti-parallel *remanent magnetisation*.
Coercivity of remanence (H_{CR})	The back-field required to reorient the direction of magnetisation in sufficient remanence carriers so that once the field was removed, the net remanence of the sample was zero.
Critical single domain size	The maximum length of an SD grain, above which 2 or more *magnetic domains* are created. Between 0.05 and 0.08 μm for equidimensional magnetite but can be up to 1μm for highly elongate grains.
Critical superparamagnetic size	The minimum size of SD grains below which *superparamagnetism* is displayed. Between 0.025 and 0.03 μm for equidimensional magnetite at room temperature
Curie point (Tc)/ Curie temperature	The temperature above which a mineral ceases to be ferromagnetic. Can be indicative of mineral (e.g. magnetite, Tc=580°C, haematite, Tc=680°C).
Deuteric Oxidation	Oxidation occurring during the original cooling of an igneous rock.
Diamagnetism	Weak magnetism opposed to an inducing field, displayed by all materials, has its origin in orbit of electrons about the nucleus.
Dipole	The simplest source of a magnetic field consisting of a north and south pole separated by a distance d.
Dipole moment	See *magnetic moment.*

Domain	Volume of grain in which all atomic *dipole moments* are aligned.
Ekman Layer	A viscous layer adjacent to a no-slip ($\mathbf{v} = 0$) boundary. The fluid increases in speed away from the boundary and is twisted by the Coriolis force to produce an Ekman spiral. Ekman layers are the only part of the core in which viscosity is thought to play a part in core dynamics and they are expected to be less than 100m thick.
Ekman Number	The ratio of viscosity to coriolis force. The larger this number, the thicker the *Ekman* boundary *layers*.
Ferromagnetism	Strongest type of magnetisation, displays *hysteresis* properties.
Frozen flux assumption	Assumption made whereby magnetic flux only moves through advection by the infinitely conducting fluid in which it is present and does not diffuse. It is generally believed to be a good approximation in the time frame of SV, although it has recently being criticised (Love, 1999).
Geocentric axial dipole (GAD)	A dipole suspended at the centre of the Earth, parallel to the rotation axis.
Hysteresis	A feature of ferromagnetic materials whereby the material retains a *remanent magnetisation* in the absence of an applied field. This remanence can be removed by application of a back-field, equal to the *coercivity* of the material.
Induced magnetisation	The magnetisation of a substance due to a field acting upon it. Induced and remanent magnetisation combine to form the total magnetisation of a ferromagnetic material.
Isothermal Remanent Magnetisation (IRM)	Remanence acquired by material during short term application of a (strong) field at constant temperature. Lightning is a common natural source of IRM.

K value	Statistical measure of precision of a mean direction. Approaches infinity for the mean of tightly clustered directions.
Maghaemite/CD magnetite	(γFe_2O_3). Ferromagnetic mineral formed from low temperature oxidation of magnetite. Chemically identical to haematite but retains spinel atomic structure of magnetite. Usually metastable and breaks down to haematite (αFe_2O_3) on heating above 250°C.
Magnetic domain	A region of a ferromagnetic grain which has a single dipolar magnetisation.
Magnetic moment/ Dipole moment	The product of the magnetic charges in a *dipole* and the distance between them. Measured in A/m^2.
Magnetic Reynolds number (Rm)	Given by the equation vL / k_m where v is velocity, L is length scale and k_m is the magnetic diffusivity, it is a measure of both the effectiveness of the geodynamo and the appropriateness of the *frozen flux assumption.*
Magnetocrystalline anisotropy	Anisotropy dictated by the preference of ferromagnetic crystals to be magnetised along certain axes. Dominant source of *coercivity* in haematite and homogenous MD grains of magnetite.
Magnetohydrodynamics	A mathematical discipline involving the combination of fluid dynamics and electromagnetic theory. It is used to explain the processes operating within the geodynamo.
Magnetostatic energy (e_m)	The energy stored in a grain due to the effect of similar charges being adjacent to one another.
Magnetostrictive anisotropy	Magnetic anisotropy in a grain due to the spontaneous change in dimension of the crystal when it is magnetised. The strain dependence of magnetocrystalline anisotropy.
Mean angular deviation (MAD)	A statistic used in principle component analysis which defines the scatter of a set of points on an OVP around their best fit straight line.

Multidomain (MD)	The domain state of a large *ferromagnetic* grain which splits itself into several *domains* in order to reduce the overall *magnetostatic energy* of the grain. MD grains have a lower *coercivity* than SD grains.
Natural Remanent Magnetisation (NRM)	The total remanence of a material prior to laboratory demagnetisation. I.E. the vector sum of all components in a sample.
Orthogonal Vector Plot (OVP)	Chart designed for representation of components of magnetisation in a stepwise demagnetised sample (after Zijderveld, 1967). **(Appendix 1)**
Palaeomagnetic dipole moment	The average dipole moment for a period of several million years once the measuring imprecision has been removed and fluctuations within that period have been sufficiently averaged. Analogous to the *palaeomagnetic pole*.
Palaeomagnetic Pole	The mean position of a set of *VGP's* for a region covering a time span of 10^4 – 10^5 years, hence averaging out secular variation.
Palaeopole	Any *VGP* or *palaeomagnetic pole*.
Paramagnetism	*Induced magnetisation* in direction of applied field. Disappears once field is removed. Much weaker than *ferromagnetism*.
Partial Thermoremanent Magnetisation (pTRM)	A portion of a material's TRM held between two distinct *blocking temperatures*.
Poloidal Field	Part of magnetic field with a radial component. The only part of the geomagnetic field which can be observed.
Primary remanence	A remanence acquired at the time the rock formed.
Principle Component Analysis	Technique used to analyse components of magnetisation in a sample. The components reside in a discreet or overlapping *blocking temperature spectrum* which is isolated by stepwise demagnetisation and presented on an *OVP*.

Rayleigh number (Ra)	Dimensionless number used to quantify the vigour of convection. Must be above a critical value (Ra_c) for convection to occur.
Relaxation time (τ)	Time taken by any one grain to lose its direction of *remanent magnetisation* due to thermal agitation. Strongly temperature dependent.
Remanent Magnetisation / Remanence	Magnetisation which records the direction of a previous field acting on a material. Still present after original field is removed.
Rossby number	Ratio of inertial to Coriolis forces.
Saturation magnetisation (M_S)	The maximum magnetisation of a sample, acquired when all *magnetic moments* within an assemblage are oriented in the same direction. Measured in Amperes/metre.
Saturation remanence (M_{RS})	The maximum strength of a remanent magnetisation. Measured by first imparting a saturation magnetisation and subsequently removing the applied field.
Secondary magnetisation	Any *remanent magnetisation* in a sample that was acquired after the *primary remanence*.
Secular Variation (SV)	Temporal variation (T > 1 year) of the geomagnetic field (usually excluding reversals); assumed to have internal origin.
Shape anisotropy	Dominant source of coercivity in SD magnetite grains. Caused by an elongate grains preference for being magnetised along its long axis so that *magnetostatic energy* is minimised.
Single Domain (SD)	The domain state of a small grain in which the energy required to create separate domains is greater than the associated reduction in *magnetostatic energy.*
Superparamagnetism (SP)	Type of *ferromagnetism* in very small grains whereby the *relaxation time* is so short that the grain effectively behaves in a *paramagnetic* fashion but with attendant high strength.

Susceptibility (χ)	The relationship between *induced magnetisation* of a material and the applied field. Measured in m^3/kg.
Themoremanent magnetisation (TRM)	Magnetisation acquired by grains as they cool through their *blocking temperature* (T_B) while subject to a field.
Toroidal Field	Part of magnetic field with no radial component.
True Polar Wander (TPW)	The motion of the mantle with respect to the Earth's spin axis (or vice versa); calculated from the motion of the lithosphere's motion relative to spin axis (deduced from *APWP's*) together with the motion of the mantle relative to the lithosphere (assumed to be given by hot spot trails).
Unblocking temperature (T_{UB})	The temperature at which a group of *ferromagnetic* grains loses its remanence. $T_B=T_{UB}$ for *single-domain* grains.
Virtual Dipole Moment (VDM)	The geocentric d*ipole moment* that would give rise to the palaeofield strength measured at a point on the Earth's surface.
Virtual Geomagnetic Pole (VGP)	Position of geomagnetic S pole which would give rise to direction of *remanent magnetisation* of a sample in its current, in-situ location.
Westward Drift	Model of non-dipole field motion to account for *secular variation*

Appendix 2 – Interpretation of Orthogonal Vector Plots

Orthogonal vector plots (OVP's, figure A1.1) are the singular best method of graphically representing components of magnetisation. The remanence of a sample following each stage of thermal demagnetisation is plotted on two axes which allows the three dimensional vector to be represented on a two dimensional diagram. Principle component analysis can then be used to identify components of magnetisation (Kirschvink, 1980).

At first glance they are not simple to interpret. Important things to realise are:

-OVP's are comprised of two sets of axes, the horizontal set is represented by the cardinal compass points and the vertical set by the up and down axes and two compass points.

-Each horizontal (unfilled) point and vertical (filled) point represents the magnetisation of the sample after a demagnetisation step, the temperature of which is shown.

-The distance of a point from the origin is proportional to its relative intensity of magnetisation. Therefore a *ChRM* should always converge on the origin.

-Points forming straight lines indicate discrete components of magnetisation, whereas curves represent overlapping of multiple components in the *blocking temperature spectrum.*

-The direction of a component can be found by translating it so that the highest demagnetisation-field points are at the origin, then reading-off the direction of the line using the axes.

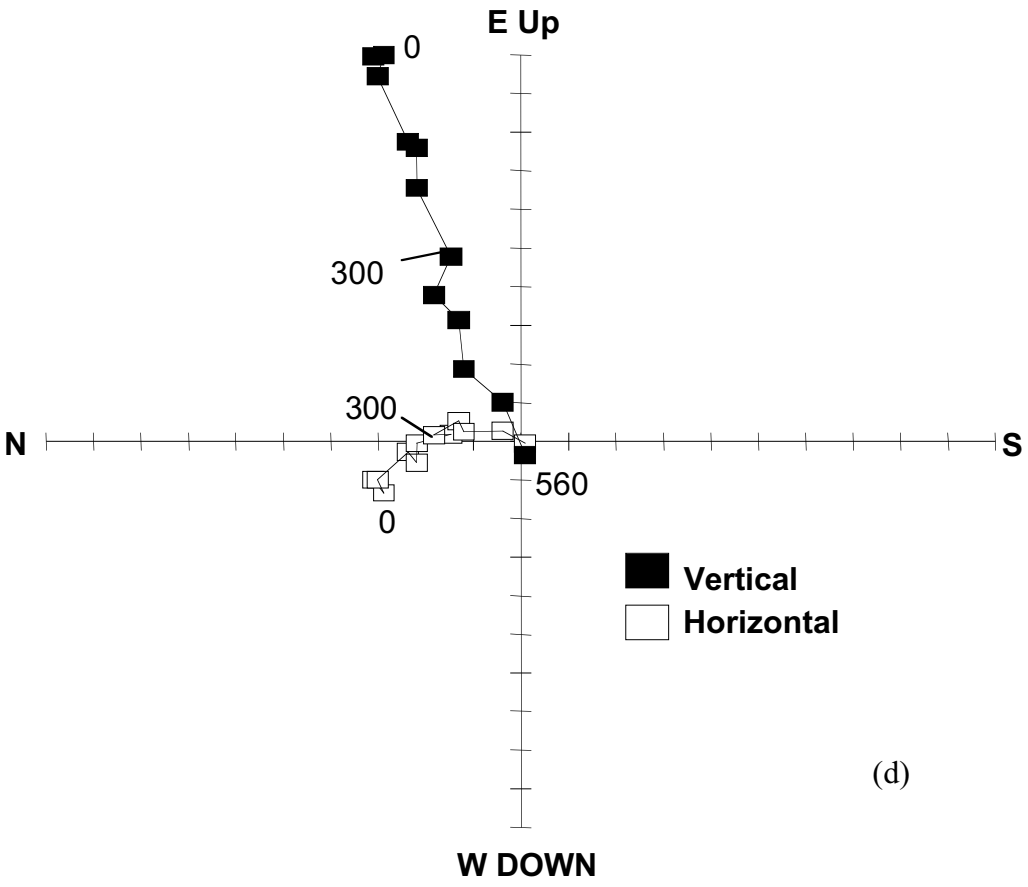

(d)

Figure A1.1: Example of a OVP. Numbers represent temperature of thermal demagnetisation.

Appendix 3: Coe's statistics

The statistics proposed by Coe *et al.* (1978) are widely quoted with palaeointensity results. The following section defines their calculation.

The **standard error of the slope** is calculated from:

$$\sigma_b = \left[\frac{2\sum_i (y_i - \bar{y})^2 - 2b\sum_i (x_i - \bar{x})(y_i - \bar{y})}{(N-2)\sum_i (x_i - \bar{x})^2} \right]^{1/2}$$

This standard error divided by the slope is a parameter called β and is useful measure of uncertainty.

The **f (fraction) value** is simply the fraction of total NRM used in calculating the palaeointensity.

$$f = \Delta y_T / NRM_{total}$$

where: $\Delta y_T = NRM_{max} - NRM_{min}$

NRM_{max} and NRM_{min} are the maximum and minimum NRM values used to calculate the palaeointensity and NRM_{total} is the maximum NRM of the sample (N.B. NRM_{total} may not be the 0 NRM measurement when secondary components are present).

The **g (gap) value** is a measure of the uniformity of the spacing (Δy) between each point's perpendicular projection onto the best fit straight line.

$$g = 1 - \overline{\Delta \bar{y}} / \Delta y_T$$

where: $\overline{\Delta \bar{y}} = (1 / \Delta y_T) \Sigma_{i=1}^{N-1} \Delta y_i^{\,2}$

Δy_T is the total length of the NRM segment used.

The value of g increases with uniformity of spacing; it is 1 for perfectly even spacing of points along the NRM axis.

The **q value** is an index of quality of a palaeointensity determination.

$$q = | b | f g / \sigma_b$$

where: b is the slope of the best-fit straight line and σ_b is its standard error.
It is usual for q values to be quoted alongside any palaeointensity determination. The reciprocal of q is a measure of the relative uncertainty of a palaeointensity measurement. This is multiplied by H_{pal} to determine an absolute uncertainty.

Appendix 4: Australian palaeopoles from Permian to mid-Tertiary times

Source: Palaeomagnetic database provided by the Norwegian Geological Survey at:
http://www.dragon.ngu.no/palmag/paleomag.htm

ROCKUNIT	MAG AGE RANGE		PLAT	PLONG	DP	DM	AUTHORS	YEAR
Lower Edie Porphyry	2	65	63	36	9,6	16,6	Manwaring,E.A.	1974
Kwikla Volcanics	2	65	34	55			Manwaring,E.A.	1974
Gabbro	2	65	42	220			Manwaring,E.A.	1974
Ferruginized sediments	5	35	78,2	349,5	6,1	7,6	Schmidt,P.W., Taylor,G., Walker,P.H.	1982
Perth Basin sediments	16	29	81,2	288,8	4,5	4,5	Schmidt,P.W., Embleton,B.J.J.	1976
Canaway Profile, Eromanga Basin	23	35	74,1	295,1	6,6	6,6	Idnurm,M., Senior,B.R.	1978
Liverpool, Springsure Volcanoes and Older Volcanics combined	25	35	68,9	272,4	4,3	4,3	McElhinny,M.W., Embleton,B.J.J., Wellman,P.	1974
Browns Creek Formation	35	39	65,5	292,5	2,5	2,5	Idnurm,M.	1994
Morney Profile, Eromanga Basin	35	65	58,8	298	3,8	3,8	Idnurm,M., Senior,B.R.	1978
Barrington Volcano, Nerriga Province, Older Volcanics comb.	40	60	68,5	310,9	5,2	5,2	McElhinny,M.W., Embleton,B.J.J., Wellman,P.	1974
Woy Woy South Basalt	46	48	54	273	6	6	Embleton,B.J.J., Schmidt,P.W., Hamilton,L.H., Riley,G.H.	1985
Peat's Ridge Basalt	48	50	66	314	8,5	9,8	Dickson,G.O.	1963

ROCKUNIT	MAG AGE RANGE		PLAT	PLONG	DP	DM	AUTHORS	YEAR
Peat's Ridge Basalt	48	50	70	314	9	10	Manwaring,E.A.	1963
Peat's Ridge Basalt	48	50	66	278	2,6	3,3	Robertson,W.A.	1979
Weathered profile	50	70	59,2	297,2	9,1	9,9	Schmidt,P.W., Ollier,C.D.	1988
Kulnura Sill	50	80	63	271	3,5	4,5	Robertson,W.A.	1979
Mogo Hill Basalt	56	59	40,6	310,2	8,6	8,6	Schmidt,P.W., Embleton,B.J.J.	1981
North Rankin 1 Drillcore	58	62	61,7	298,4	3,3	8	Idnurm,M.	1985
St.Mary's Breccia	65	100	51	324	6,1	6,4	Robertson,W.A.	1979
Bauine Granodiorite	65	97	55	220			Manwaring,E.A.	1974
North Bondi Volcanic Neck	80	100	55	325	10	10	Embleton,B.J.J., Schmidt,P.W., Hamilton,L.H., Riley,G.H.	1985
Hornsby Breccia	80	100	59,1	319,4	4,2	4,2	Schmidt,P.W., Embleton,B.J.J.	1981
Munmorah Conglomerate, Patonga Claystone	80	100	57,3	323,4	3,6	3,6	Embleton,B.J.J., McDonnell,K.L.	1980
Luddenham dyke	80	100	40	340	10	10	Embleton,B.J.J., Schmidt,P.W., Hamilton,L.H., Riley,G.H.	1985
Marsden Park Breccia pipe	80	100	48,1	307,2	6,2	6,2	Schmidt,P.W.	1982
Dundas Breccia pipe	80	100	57,7	342,1	35,6	35,6	Schmidt,P.W.	1982

ROCKUNIT	MAG AGE RANGE		PLAT	PLONG	DP	DM	AUTHORS	YEAR
St.Mary's Breccia pipe	80	100	45,9	330,1	7,6	7,6	Schmidt,P.W.	1982
Prospect dolerite	90	110	60,7	322,4	13,4	13,4	Schmidt,P.W.	1982
Mt. Dromedary Intrusive Complex	90	100	56	318	9	9	Robertson,W.A.	1963
Bunbury Basalt	90	105	49	341	10	10	Schmidt,P.W.	1976
Milton Monzonite	90	110	55,9	338	11,7	12,3	Dunlop,D.J., Schmidt,P.W., Ozdemir,O., Clark,D.A.	1997
Erskine Park Sill	100	160	23	331	9,3	9,4	Robertson,W.A.	1979
Cygnet Alkaline Complex	100	110	50	338	10	10	Robertson,W.A., Hastie,L.	1962
Otway Group	110	115	48,9	328,7	3,6	3,6	Idnurm,M.	1985
Hornsby Breccia	125	155	28,7	345,8	7	7	Schmidt,P.W., Embleton,B.J.J.	1981
Dundas Breccia pipe	130	150	30,7	14,8	15,7	15,7	Schmidt,P.W.	1982
Noosa Heads Intrusions	140	145	36	312	24	25	Robertson,W.A.	1963
North Bondi Volcanic Neck	148	154	55	0	7	7	Embleton,B.J.J., Schmidt,P.W., Hamilton,L.H., Riley,G.H.	1985
Bendigo Dykes	149	158	47	315	39	39	Schmidt,P.W.	1976
Luddenham dyke	150	195	39	1	4	4	Embleton,B.J.J., Schmidt,P.W., Hamilton,L.H., Riley,G.H.	1985

ROCKUNIT	MAG AGE RANGE		PLAT	PLONG	DP	DM	AUTHORS	YEAR
Prospect dolerite	163	173	53	359,6	6,4	6,4	Schmidt,P.W.	1982
Kangaroo Island Basalt	166	178	39	3	11	11	Schmidt,P.W.	1976
Tasmanian Dolerite	166	182	47,7	303,5	9,5	9,5	Schmidt,P.W., McDougall,I.	1977
Tasmanian Dolerite	166	182	50,7	354,5	5,2	5,2	Schmidt,P.W., McDougall,I.	1977
Sydney Basin Dykes	170	190	52,3	358,3	5,1	5,1	Robertson,W.A.	1979
Glenrowan Intrusives	176	186	45,2	20			Schmidt,P.W.	1976
Garrawilla Volcanics and Moonbi Extrusives	187	207	46,1	355,2	10	10	Schmidt,P.W.	1976
Western Victoria Basalt Belt	189	199	47	358	18	18	Schmidt,P.W.	1976
Kiama Dykes	190	210	55	350,6	14	14	Schmidt,P.W.	1990
Brisbane Tuff	208	235	39	323			Irving,E., Green,R.	1958
Brown Clays	208	235	32,3	349,9	23,8	23,8	Schmidt,P.W., Currey,D.J., Ollier,C.D.	1976
Knapp Head Dyke	208	245	39,4	339,1	7,7	8,8	Harris,L.B., Li,Z.X.	1995
Werrikimbe Volcanics	208	235	31,6	5,3	26,6	26,6	Schmidt,P.W., Aubourg,C., Lennox,P.G., Roberts,J.	1994
Milton Monzonite	220	230	15,8	351,8	8,4	9,2	Dunlop,D.J., Schmidt,P.W., Ozdemir,O., Clark,D.A.	1997

ROCKUNIT	MAG AGE RANGE		PLAT	PLONG	DP	DM	AUTHORS	YEAR
Basalt dyke H13 and baked contacts	235	290	12,1	305,9	12,7	14,3	Irving,E.	1966
Brisbane Tuff	235	241	57	323	10	11	Robertson,W.A.	1963
Munmorah Conglomerate, Patonga Claystone	241	245	30,4	326,9	7,8	7,8	Embleton,B.J.J., McDonnell,K.L.	1980
Narrabeen Chocolate Shales	241	245	49	340	14	14	Irving,E.	1963
Illawarra Coal Measures and Narrabeen Group	241	256	36	327,6	33,1	33,2	Facer,R.A.	1981
Dundee Ignimbrite	242	252	36,9	334,8	6,5	6,5	Lackie,M.A.	1988
Dundee Rhyodacite	242	252	25,8	316,3	12,4	12,7	Lackie,M.A.	1988
Moonbi and Walcha Road Adamellite thermal aureole	244	253	36,8	338	11,2	11,3	Sunata,W.	1993
Moonbi Lamprophyre	244	253	35	308	20	20	Irving,E.	1966
Gerringong Volcanics	245	290	27	349	21	21	Irving,E., Green,R.	1958
Werrie Basalt	245	256	57,2	350,3	20,2	20,2	Lackie,M.A., Schmidt,P.W.	1993
Yonkie Dome and Bismark Granodiorite	245	363	10,3	219	15,3	27,6	Manwaring,E.A.	1974
Gerringong Volcanics	249	257	44	312	11	11	Irving,E., Parry,L.G.	1963
Werrie Basalt	256	290	37,3	0,6	32,1	34,6	Schmidt,P.W.	1988

ROCKUNIT	MAG AGE RANGE		PLAT	PLONG	DP	DM	AUTHORS	YEAR
Stirling Range Drive Dyke	256	323	49,4	254	37,4	43,2	Harris,L.B., Li,Z.X.	1995
Long Point Dyke	256	323	21,5	284,2	23,1	24	Harris,L.B., Li,Z.X.	1995
Lower Marine Basalt	256	290	46	302	6,8	7,4	Irving,E., Parry,L.G.	1963
Alum Rocks	269	282	5,3	301,7	16	18,6	Auborg,C., Klootwijk,C.T., Korsch,R.J.	1994
Featherbed Volcanics	280	305	43	311,7	8,5	9,3	Klootwijk,C., Giddings,J.W., Percival,P.	1993
Mount Leyshon Intrusive Complex	280	292	43,2	317,3	6	6,4	Clark,D.A.	1996
Newcastle Range Volcanics	283	330	65,7	307,1	5,3	7	Anderson,K.	2000
Tuckers Igneous Complex	284	291	47,5	323	6	6,6	Clark,D.A.	1996
Percy Creek Volcanics	290	323	23,3	317,2	36,4	36,4	Chamalaun,F.H.	1968
Upper Kuttung sediments combined	290	323	50	320	9	9	Irving,E.	1966

Appendix 5 - Palaeodirectional data from studied Australian intrusions

Palaeodirectional results from Moss Vale Intrusions.

Gingenbullen Dolerite (GB) Thermal demagnetisation. A cores.					
HBT Components					
Sample	Temp fron	Temp to	Dec	Inc	MAD
GB0101A	500	560	15	56.3	5.4
GB0102A	500	560	124.8	76.2	3.4
GB0103A	500	560	119.7	81.9	2.2
GB0104A	500	560	177.7	54.8	12.4
GB0105A	500	560	166.9	82.1	0.8
GB0106A	500	560	99.5	40.1	9
GB0107A	300	580	93.9	62.2	5.2
GB0108A					
mean			107.2	73.5	
			A95=20.2	K=9.9	
GB0201A	450	560	156.1	76.6	2.7
GB0202A	450	560	145.6	75	2.6
GB0203A	450	560	100.3	71	2.6
GB0204A	450	530	83.5	73.8	3.4
GB0205A	400	560	135	81.9	3.8
GB0206A	400	530	169	77.8	3.8
MEAN			127.8	78	
			A95=7.2	K=86.6	
GB0301A	450	580	143.2	80.5	2.2
GB0302A	500	560	123.9	79.7	2.6
GB0303A	500	580	138.6	79.4	1.9
GB0304A	?????				
MEAN			101.9	84.9	
			A95=17	K=53.7	
GB0401A	400	560	305	72	3.2
GB0402A	450	580	355.8	77.3	7.7
GB0403A	400	530	322.7	70.9	9.2
GB0404A	450	560	198.9	73.7	8.6
GB0405A	400	560	178.5	72.1	7.8
MEAN			278.7	83.4	
			A95=16.8	K=21.6	

Sample	Temp from	Temp to	Dec	Inc	MAD
GB0501A	400	580	167.5	81.6	6
GB0502A	530	580	194.1	53.1	9.8
GB0503A	500	560	270.7	78.4	10.8
GB0504A	400	560	340.6	64.9	9.7
GB0505A	400	530	141	79.2	8.3
GB0506A	500	580	202.2	79.4	4.3
			191.8	81.4	
			A95=16.8	K=16.9	
GB0601A	500	580	284	64.8	11.3
GB0602A	400	530	189.4	52.2	1.1
GB0603A	500	580	213.7	69.7	9.3
GB0604A	400	560	197.8	58.6	6
GB0605A	400	560	204.7	54.1	6.7
GB0606A	450	560	214.7	49.9	9.8
GB0607A	500	580	195.9	34.5	5.7
MEAN			208.5	57.6	
			A95=14.6	K=18	
GB0701A	530	580	183.8	55.6	8.3
GB0702A	530	580	153.7	74.8	12.7
GB0704A	350	600	201.9	80.5	2
GB0705A	400	600	229	85	3.1
GB0707A	?????				
MEAN			182.8	75	
			A95=16.6	K=31.8	
OVERALL MEAN			174.2	80.8	
			A95=10.8	K=32.2	
VGP	LAT	-52.4		dp	17.3
	LONG	153.2		dm	18

Gingen Bullen Dolerate Thermal demagnetisation. A cores.					
LBT Components					
Sample	Temp from	Temp to	Dec	Inc	MAD
GB0101A	150	300	25.1	-41.1	4.2
GB0102A	150	350	43	-71.6	2.6
GB0103A	150	450	356.6	-74.3	9.1
GB0104A	150	450	38.8	-80.4	1.8
GB0105A	150	450	354	-82.9	6.3
GB0106A	Possible lightning strike				
GB0107A	Possible lightning strike				
GB0108A	150	450	334.1	-85.7	3.6
MEAN			45.2	-68.1	
			A95=27.7	K=5.7	
GB0201A	0	300	10.3	-71.8	5.4
GB0202A	150	400	52.9	-69.4	11.7
GB0203A	150	400	20.8	-69	12.1
GB0204A	150	350 X300	354.7	-79.8	9.4
GB0205A	300	400	329.6	-83.2	8.1
GB0206A	300	400	43.9	-61.2	1.9
MEAN			26	-73.8	
			A95=9.2	K=53.9	
GB0301A	0	450	10.5	-59.3	5.4
GB0302A	250	400	280.7	-73.8	3.2
GB0303A	300	400	1.2	-75.4	6
GB0304A	0	450	331.9	-74.5	2.8
MEAN			343.8	-73.9	
			A95=16.6	K=31.6	
GB0401A	150	450	90.1	-84	9
GB0402A	200	350	251.6	-52.6	6.2
GB0403A	100	300	193.8	-69.6	5.2
GB0404A	0	250	16.1	-72.2	6.1
GB0405A	0	300	51.8	-72.8	5.6
MEAN			257.2	-87	
			A95=24	K=11.1	

Sample	Temp from	Temp to	Dec	Inc	MAD
GB0501A	200	300	24	-75.6	1.6
GB0502A	200	300	4.7	-76.1	3.2
GB0503A	150	300	227.6	-71.1	7.2
GB0504A	0	250	185.3	-69.2	4.5
GB0505A	0	300	341.7	-76.8	4.3
GB0506A	300	400	35.7	-74.8	4.8
MEAN			349.3	-86.7	
			A95=14.6	K=21.9	
GB0601A	300	400	47.5	-60.2	4.9
GB0602A	150	350	359	-65.9	5.1
GB0603A	250	400	120	-70.4	7.1
GB0604A	0	250	354.6	-69.6	4.1
GB0605A	0	350	18.6	-65.5	3.5
GB0606A	0	400	2.9	-67.9	6.2
GB0607A	0	400	24.7	-57.4	5.4
MEAN			24.5	-69.3	
			A95=11.8	K=26.9	
GB0701A	0	350	197.9	-69.7	3.6
GB0702A	300	400	111.7	-81	6.7
GB0704A	150	350	9.3	-64.5	3.3
GB0705A	0	350	27.9	-74.7	8.4
GB0707A	0	400	219.8	-80.4	7.2
MEAN			41.4	-81.7	
			A95=18.3	K=18.4	
OVERALL MEAN			21.3	-78.7	
			A95=7.7	K=62.2	
VGP	LAT	53.1	DP	12.4	
	LONG	323.3	DM	12.9	

Gibralter Microsyenite (GS) Thermal demagnetisation				
Sample	Temp range	Decl	incl	M.A.D.
GS0101A	250-450	82.7	-9.4	3.8
GS0102A	150-500	120.2	7.4	5.7
GS0103A	200-500	106.3	40.5	5
GS0104A	150-630	137.3	-65.4	2.2
GS0105A	300-630	138.1	6.8	3.8
GS0107A	450-630	156	-19	0.8
Very high intensities, random directions - Lightning strik				
GS0201B	150-300	243.9	86.2	6.3
GS0202A	100-350	206.4	71.1	2.3
GS0203A	100-450	188.9	68.7	3.2
GS0204A	250-400	184.6	72.7	13.1
MEAN		196.2	75.2	
		A95=10.3	K=80.1	
GS0301B	150-300	195.5	69	1.9
GS0302B	150-400	190.3	67.5	1.6
GS0303B	250-450	194.3	70.8	6.8
GS0304B	100-300	186.9	64.9	2.8
GS0305B	150-250	186.2	71.5	1.9
GS0306B	150-400	189.1	72.4	4.1
GS0307A	150-300	194.5	70.9	4.2
MEAN		190.9	69.6	
		A95=2.2	k=756.6	
GS0403B	150-530	157.1	67.8	6.6
GS0404B	200-500	34.7	55.5	4.6
MEAN		75.9	74.5	K=5.4
Site 2 and 3 Mean				
Dec	inc	k	a95	
193.1	72.4	387.9	12.7	
plat	plong	dp	dm	S
65.2	133.5	7.9	8.9	6.3

Palaeodirectional results from Kiama dyke (KD) swarm.

Barrack Point Site 1		BP01		
Sample	Temp-range	Dec	Inc	MAD
BP0101A				
BP0102A	100-400	57	-46	5.5
BP0103A	100-350	310	-52	7.5
BP0104A	100-400	30	-53	7.5
BP0105A	100-500	308	-73	7.7
BP0106A	100-500	445	-87	6.5
BP0107A	100-350	334	-82	7.9
BP0108A				
Mean	Dec	Inc	k	a95
	6	-73	10	22
VGP	latp	longp	dp	dm
	66	323	35	39.2
BP0103A	500-560	8	44	5.4
BP0104A	500-580	338	71	6
BP0105A	530-580	278	73	Circular plc
BP0107A	530-580	259	66	13.4
Mean	Dec	Inc	k	a95
	324	71	10	22
VGP	latp	longp	dp	dm
	-5	131	33.3	38.3

Sample	Temps	Dec	Inc	MAD
CR0101A	100-500	27	-60	3.5
CR0102A	100-530	5	-64	4.5
CR0103A				0
CR0104A	200-350	15	-75	2.2
CR0105A	150-610	1	-71	2.9
CR0106A	100-400	23	-54	7.6
CR0107A	100-610	48	-43	6
Mean	Dec	Inc	k	a95
	24	-62	31.6	12
VGP	latp	longp	dp	dm
	70	273	14	19
HBT component				
CR0104A	400-500	24	-66	1
VGP	latp	longp		
	-68	106		

CATH ROCKS SITE 2		CR02		
Sample	Temp range	Dec	Inc	MAD
CR0201A				
CR0202A	100-560	337	-78	5.4
CR0203A	350-580	324	-76	2.4
CR0205A	100-610	321	-78	4.5
Mean	Dec	Inc	A95	K
	327	-77	3	1411
VGP	latp	longp	dp	dm
	54	354	5	6

CATH ROCKS SITE 3		CR03		
Sample	Temp range	Dec	Inc	MAD
CR0301A				
CR0302A	200-560	321	-72	4.3
CR0303A				
CR0304A	100-400	330	-61	7
CR0305A	100-500	6	-57	10
CR0306A	250-500	0	-74	8.3
CR0307A	100-200	45	-61	7.7
Mean	Dec	Inc	a95	k
	359	-68	15	28
VGP	latp	longp	dp	dm
	74	333	21	25

CATH ROCKS 4		CR04		
Sample	Temp range	Dec	Inc	MAD
CR0401A	250-530	208	-78	3.9
CR0402A	150-530	202	-78	5.7
CR0403A	100-580	172	-76	3.6
CR0404A	0-300	311	-67	6.9
CR0405A	250-350	327	-63	2.5
CR0406A	100-560 X250	337	-75	3.4
CR0407A	0-500	322	-79	4.9
CR0408A	100-300	27	-68	7.7
Mean	Dm	Im	k	a95
	315	-82	22	11
VGP	latp	longp	dp	dm
	41	160	23	24
HBT component				
CR0404A	450-560	20	-65	7.2
CR0405A	350-560	6	-73	9.4
CR0408A	300-530	352	-78	6.9
Mean	Dm	Im	k	$\alpha 95$
	9	-72	109	8
VGP	latp	longp	dp	dm
	67	318	12	14

CATH ROCKS 5			CR05	
Same dyke as CR02				
Sample	Temps	Dec	Inc	MAD
CR0501A	100-530	318	-79	3.7
CR0502A	0-530	326	-80	3.2
CR0503A	100-530	310	-84	4.1
Mean	Dec	Inc	a95	k
	319	-81	4	787
VGP	latp	longp	dp	dm
	47	348	7	8

CATH ROCKS 6		CR06		
Sample	Temp range	Dec	Inc	MAD
CR0601A	400-530	18	-55	1.8
CR0603A	350-500	18	-65	2.6
CR0605A	350-450	46	-68	1.9
CR0606A	400-580	265	-72	5.5
Mean	Dm	Im	k	a95
	13	-71	15.1	18
VGP	latp	longp	dp	dm
	67	212	27	31

CATH ROCKS 7		CR07		
Sample	Temps	Dec	Inc	MAD
CR0701A	0-450	309	-84	5.2
CR0702A	100-350	325	-81	4.3
CR0703A	100-450	332	-72	5.7
CR0705A	100-500	16	-76	7.5
CR0706A	100-400	320	-87	6.7
CR0707A	100-580	15	-81	5.3
CR0708A	150-500	160	-74	5
Mean	Dec	Inc	A95	k
	347	-85	9	51
VGP	latp	longp	dp	dm
	44	334	18	18

CATH ROCKS 8		CR08		
Xenolith site in cr01 dyke				
LBT component				
Sample	Temp range	Dec	Inc	MAD
CR0801A	0-400	357	-75	2.6
CR0803A	100-300	354	-68	3.3
CR0804A	100-400	352	-62	5.7
Mean	Dec	Inc	A95	K
	354	-68	10	153
VGP	latp	longp	dp	dm
	73	344	14	16.7
HBT component				
CR0801A	450-530	173	71	7.5
CR0803A	400-500	166	69	4.2
CR0804A	400-500	165	68	5.2
Mean	Dec	Inc	k	a95
	168	69	1425.2	2
VGP	latp	longp	dp	dm
	-70	173	2.8	3.3

MINNEMURRA SITE 1		MM01		
Sample	Temp range	Dec	Inc	MAD
MM0101A	150-560	12	-85	2.7
MM0102A	200-530	355	-78	2.9
MM0103A	100-560	349	-69	4.5
MM0104A	250-560	8	-84	1.7
Mean	Dec	Inc	a95	k
	356	-79	9	114
VGP	latp	longp	dp	dm
	56	333	16	17

MINNIMURA 2		MM02		
Sample	Temps	Dec	Inc	MAD
MM0201A	100-500	3	-74	4.2
MM0202A	350-500	349	-80	3.7
MM0203A	100-530	11	-81	9.3
MM0204A	200-530	11	-72	2.9
Mean	Dec	Inc	A95	K
	4	-77	6	271
VGP	latp	longp	dp	dm
	59	328	10	11

RED POINT SITE 1		RP01		
Sample	Temp range	Dec	Inc	MAD
RP0101A	100-450	22	-69	6.6
RP0102A	530-580	354	-57	4.8
RP0103A	250-580	100	-66	10.8
RP0104A	0-580	335	-73	10.5
Mean	Dec	Inc	k	a95
	18	-73	16	18
VGP	latp	longp	dp	dm
	63	310	29	32
HBT component				
RP0101A	500-580	12	86	5.2
VGP	latp	longp	dp	dm
	27	333	35	36

RED POINT 2		RP02		
Sample	Temp range	Dec	Inc	MAD
RP0201A	100-250	320	-59	3.3
RP0202A	500-560	332	-63	2.6
Mean	Dec	Inc	A95	K
	326	-61	15	265
VGP	latp	longp	dp	dm
	63	35	17.5	22.9

Palaeodirectional results from Newcastle dyke (ND) swarm.

Catherine Hill Bay site 1		CH01			
	Jnrm				
	10^-6Am^2/kg	Temp range	Dec	Inc	MAD
CH0101A	16.9	250-450	274	69	Circular plot
CH0103A	60.6	350-560	110	83	13.4
CH0104E	4.9				
CH0106A	49.4	450-560	262	13	9.6
CH0107A	33.2	400-560	106	84	9.8
CH0110A	32.9	450-560	321	73	9.3
Mean (except CH0106A)		Dm	Im	k	α95
		299	84	28.5	17
VGP		latp	longp	dp	dm
		-28	141	33	34

Catherine Hill Bay		CH02			
	Jnrm				
	10^-6Am^2/kg	Temp range	Dec	Inc	MAD
CH0201A	70.5	250-560	253	82	5.1
CH0202A	66.2	150-560	333	83	10
CH0203B	85	100-560	110	88	6.9
CH0204A	45.8	100-560	210	75	7.9
CH0205A	37.8	250-560	167	86	6.8
mean		dec	inc	a95	k
		229	86	8	96.7
VGP		latp	longp	dp	dm
		-38.2	144	15.3	15.4

Little Red Head		LR01			
		LBT component			
Sample	Jnrm	Temp range	Dec	Inc	MAD
LR0101A	102	150-450	35	-74	
LR0103A	92.2	150-450	0	-76	8.6
LR0104A	88.8	0-450	328	-77	8.1
LR0105A	60.8	150-450	49	-77	8.2
LR0106A	102.1	100-500	3	-65	6.5
LR0107A	55.8	200-400	349	-67	13.1
LR0108D	83.7	350-450	331	-65	9.5
Mean		D_m	I_m	k	α_{95}
		359	-73	k=62.5	a95=7.7
VGP		PLAT	PLONG	DP	DM
		-65	153	12.2	13.7
		HBT component			
Sample	Jnrm	Temp range	Dec	Inc	MAD
LR0104A		530-600	314	50	10.8
LR0106A		560-600	161	72	7.4
LR0107A		560-600	252	53	4.9
LR0108D		530-600	98	66	circular plot
Mean		Dm	Im	k	α95
		260.57108	81.07351	5.674572	29.3853907
VGP		latp	longp	dp	dm
		-34.2	130.4	78	81

Newcastle Dyke		NE01			
Sample	Jnrm	Temp range	Dec	Inc	MAD
NE0102A	108.2	100-500	9	-67	4.1
NE0103A	105.3	350-400	321	-86	0.5
NE0104A	63.9	350-500	30	-79	13.1
NE0105A	78.6	250-450	279	-75	12.1
NE0106A	73.1	0-500	39	-66	12.3
NE0107A	59.6	0-350	47	-52	14.1
NE0109A	78.9	100-500	267	-67	11.5
Mean		Dm	Im	k	a95
		7.243549	-78.0563	16.27078	13.11822
VGP		latp	longp	dp	dm
		55.5	327.8	23	24.4

	Jnrm	Temp range	Dec	Inc	MAD
NH0101A	54.8	500-640	213	60	14.3
NH0103A	52.5	500-580	332	76	14.8
NH0104A	63.9	360-560	34	-75	11.9
NH0105A	40.1	500-580	335	64	6.4
NH0107A	27.7	Too noisy			
NH0108A	34.8	400-530	267	50	circ
NH0109A	563	500-600	176	69	12
NH0110A	177	450-580	17	65	11.8
Mean		Dm	Im	k	a95
		270	79	10	20
VGP		latp	longp	dp	dm
		-30.8	126.6	36	38

Palaeodirectional results from Bawley Point Gabbro (BPG).

BPG site BA01 LBT				
Sample	Temp range	Dec	Inc	MAD
BA0101A	100-300	47.4	-77.1	6.3
BA0102A	100-200	356.5	-66.5	0.8
BA0103A	0-300	10.9	-76.8	
BA0104A				
BA0105A	0-300	9.4	-67.4	13.9
BA0106A				
BA0107A	100-200	348.3	-60.4	8.7
	Dec	Inc	k	a95
Mean	5.0912243	-70.5752	66	10
	latp	longp	dp	dm
VGP	70.3	321.6	15	17.3
BPG site BA01 HBT				
Sample	Temp range	Dec	Inc	MAD
BA0101A	530-580	203	63	CIRC
BA0102A	530-610	197	69	CIRC
BA0105A	530-610	225	69	CIRC
BA0106A	450-610	224	72	CIRC
	Dec	Inc	k	a95
Mean	211	69	159	7
	latp	longp	dp	dm
VGP	-62	108	10	12

BPG site BB01 LBT component				
Sample	Temp range	Dec	Inc	MAD
BB0104A	0-150	63.2	-78.7	2.3
BB0102A	0-200	209	-56.1	15
BB0107A	0-150	72.4	-41.6	9.8
	Dec	Inc	k	a95
Mean	106	-75	5	38
	latp	longp	dp	dm
VPG	24	301	64	70
BPG site BB01 HBTcomponent				
Sample	Temp range	Dec	Inc	MAD
BB0101	400-610	143	57	7.2
BB0102	200-530	83	52	Circular
BB0103	250-500	115	54	Circular
	Dec	Inc	k	a95
Mean	112	57	22	17
	latp	longp	dp	dm
VPG	-37	217	18	25

BPG site BR01 LBT component				
Sample	Temp range	Dec	Inc	MAD
BR0102A	100-300	347	-76	9.5
BR0103A	100-300	242	-69	9.2
BR0104A	0-300	347	-80	13.9
BR0105A	100-250	333	-69	3.5
	Dec	Inc	k	a95
Mean	314	-78	31	13
	latp	longp	dp	dm
VPG	49	355	23	24
BPG site BR01 HBTcomponent				
Sample	Temp range	Dec	Inc	MAD
BR0101A	300-530	212	53	Circ
BR0104A	530-580	222	52	5.3
BR0105A	300-610	220	68	7.5
	Dec	Inc	k	a95
Mean	218	58	74	9
	latp	longp	dp	dm
VPG	-60	77	10	13

BPG site GB01 LBT				
Sample	Temp range	Dec	Inc	MAD
GB0104	0-200	210	-68	10.4
GB0105	0-150	235	-64	5.2
	Dec	Inc	k	a95
Mean	223	-67	112	9
	latp	longp	dp	dm
VGP	3	357	12	15
BPG site GB01 HBT				
Sample	Temp range	Dec	Inc	MAD
GB0102A	500-560	330	58	Circ
GB0103A	450-610	347	51	Circ
GB0104A	500-610	348	49	Circ
GB0106A	500-580	313	63	Circ
	Dec	Inc	k	a95
Mean	336.616	56.02086	54.01735	9.524264
	latp	longp	dp	dm
VGP	14.7	131.1	10.3	14.3

BPG site JH01 LBT component				
Sample	Temp range	Dec	Inc	MAD
JH0101A	100-200	298	-72	4.1
JH0105A	0-450	243	-55	8.6
JH0106A	0-450	256	-48	7.8
	Dec	Inc	k	a95
Mean	259	-60	21	17
	latp	longp	dp	dm
VPG	15	21	19	26
BPG site JH01 HBTcomponent				
Sample	Temp range	Dec	Inc	MAD
JH0103A	300-450	101	85	
JH0104A	450-560	62	83	11
JH0105A	450-530	41	83	10.8
	Dec	Inc	k	a95
Mean	64	84	607	3
	latp	longp	dp	dm
VPG	-30	162	6	6

BPG site MB01 LBT component				
Sample	Temp range	Dec	Inc	MAD
MB0101A	200-300	359	-65	2.3
MB0103A	100-350	352	-70	4.6
MB0104A	0-300	340	-61	5.7
MB0105A	100-300	3	-70	5.3
MB0106A	100-450	6	-74	5.1
	Dec	Inc	k	a95
Mean	355	-68	158	5
	latp	longp	dp	dm
VPG	73.5	342.4	7	8.4
BPG site JH01 HBTcomponent				
Sample	Temp range	Dec	Inc	MAD
MB0103A	450-580	264	75	Circ
MB0104A	450-560	326	82	Circ
MB0105A	400-560	300	83	Circ
MB0106A	450-560	5	83	Circ
	Dec	Inc	k	a95
Mean	302	83	115	7
	latp	longp	dp	dm
VPG	-27	137	13	14

Palaeodirectional results from Bundarra (BD) granodiorite

Bundarra (BD) granodiorite Site 1			LBT component		
Sample	Jnrm	Temp range	Dec	Inc	MAD
BD0101A	1.19	0-530	265	-74	1.5
BD0102A	2.16	0-450	280	-78	8.8
BD0104A	5.6	0-450	IRM overprint		
BD0105A	0.31	0-500	IRM overprint		
	Dec	Inc	k	a95	
Mean	271	-76	455	12	
	latp	longp	dp	dm	
VGP	20.2	356.6	20.4	22.1	
Bundarra (BD) granodiorite Site 1			HBT component		
Sample	Jnrm	Temp range	Dec	Inc	MAD
BD0101A	1.19	530-590	140	69	6.4
BD0102A	2.16	530-590	117	80	1.5
BD0104A	5.6	500-590	130	74	3.1
BD0105A	0.31	530-590	97	65	4.1
	Dec	Inc	k	a95	
Mean	120	73	81	10	
	latp	longp	dp	dm	
VGP	-34.2	181.9	15.8	17.8	

Bundarra (BD) granodiorite Site 2			LBT component		
Sample	Jnrm	Temp range	Dec	Inc	MAD
BD0201A	83.66	complete IRM overprint			
BD0202A	27.67	complete IRM overprint			
BD0203A	1.36	0-150	317	-16	2.8
BD0206A	2.31	100-250	322	-57	8.7
BD0207A	1.93	0-530	338	-78	3.8
	Dec	Inc	k	a95	
Mean	321	-51	7	52	
	latp	longp	dp	dm	
VGP	54.1	35	47.3	70.2	
Bundarra (BD) granodiorite Site 1			LBT component		
Sample	Jnrm	Temp range	Dec	Inc	MAD
BD0203A	1.36	200-530	74	78	1.9
	latp	longp			
VGP	-14.2	171.3			

Bundarra (BD) granodiorite Site3					
Sample	Jnrm	Temp range	Dec	Inc	MAD
BD0301A	30.77	0-590	252	-76	10.6
BD0302A	3.13	Too Noisy			
BD0303A	571.76	complete IRM overprint			
BD0304A	193.99	complete IRM overprint			
	latp	longp			
VGP	11.9	354.2			

Bundarra (BD) granodiorite Site 4			LBT component		
Sample	Jnrm	Temp range	Dec	Inc	MAD
BD0401A	17.75	0-250	302	-52	13.8
BD0402A	115.09	0-250	134	-80	7
BD0403A	42.55	0-300	275	-49	5.7
	Dec	Inc	k	a95	
Mean	284	-67	8	47	
	latp	longp	dp	dm	
VGP	25.5	13	64.1	77.6	
Bundarra (BD) granodiorite Site 4			HBT component		
Sample	Jnrm	Temp range	Dec	Inc	MAD
BD0401A	17.75	250-590	95	-10	8.8
BD0402A	115.09	250-590	143	-36	8.1
BD0403A	Too noisy				
	Dec	Inc	k		
Mean	117	-25	5		
	latp	longp			
VGP	-18.6	261.6			

Palaeodirectional results from Eungella granodiorites (EG)

Exmoor Creek (EC) granodiorite Site 1				
Sample	Jnrm	Temp range	Dec	Inc
EC0101B	0.02	CRM development		
EC0102A	44	CRM development		
EC0103B	55.4	590-650	304	68
EC0104A	475.2	IRM overprint		
EC0105A	73.2	CRM development		
EC0106A	35.6	590-650	58	63
	Dec	Inc	k	a95
Mean	9	76	8	
	latp	longp	dp	dm
VGP	5.4	152	81.5	88.4

Sample	Jnrm	Temp range	Dec	Inc	MAD
EP0104A	345.3	IRM overprint			
EP0105A	40.4	0-560	0	-44	2.3
	latp	longp			
VGP	85.8	148			

Exe Vale (EV) granodiorite Site 1					
Sample	Jnrm	Temp range	Dec	Inc	MAD
EV0101A	63.5	IRM overprint			
EV0102A	44.9	IRM overprint			
EV0103A	1.6	350-500	9	-83	3
EV0105A	1.5	300-500	11	-76	1.7
	Dec	Inc	k	a95	
Mean	10	-80	267	15	
	latp	longp	dp	dm	
VGP	41	324	27	29	

Mt Barker (MB) granodiorite Site 1					
Sample	Jnrm	Temp range	Dec	Inc	MAD
MB0101A	16.5	590-680	356	-78	1.1
MB0102A	21.1	590-680	356	-77	1.1
MB0104A	19.8	590-680	340	-83	1
MB0105A	16.8	560-680	339	-80	0.4
MB0106A	32.3	560-580	5	-81	0.6
MB0107A	35.9	560-580	4	-82	0.6
	Dec	Inc	k	a95	
Mean	354	-80	759	2	
	latp	longp	dp	dm	
VGP	40	331	4	4	

Pipeline (PL) granodiorite Site 1				
Sample	Jnrm	Temp range	Dec	Inc
PL0101A	10.8	620-680	201	47
PL0102A	15.7	620-680	180	61
PL0103A	2.7	620-680	161	61
PL0104A	8.6	620-680	44	63
PL0105A	92.7	620-680	184	68
PL0106A	1.4	620-680	159	68
	Dec	Inc	k	a95
Mean	170	69	12	20
	latp	longp	dp	dm
VGP	-58	160	21.6	25.4
Pipeline (PL) granodiorite Site 2				
Sample	Jnrm	Temp range	Dec	Inc
PL0201A	8.4	560-650	125	69
PL0202A	9.9	Too noisy		
PL0203A	4.5	590-650	101	35
PL0204A	3	590-650	197	74
	Dec	Inc	k	a95
Mean	122	64	8	48
	latp	longp	dp	dm
VGP	-37	196	61.1	76.6

Palaeodirectional results from Yeppoon Highway gabbro

Yeppon Highway (YH) gabbro			LBT component		
sample	Jnrm	Temp range	Dec	Inc	MAD
YH0101A	1.3	100-320	332	-76	11.6
YH0102A	1.1	100-270	265	-48	3.3
YH0102B	1.2	100-270	240	-62	12.5
YH0104B	1.8	100-270	232	-64	4.4
YH0105A	0.5	100-320	242	-56	2.7
YH0105B	0.3	100-360	262	-51	9.1
YH0106A	0.4	0-360	263	-55	11.6
YH0106B	0.4	100-270	255	-42	5.8
YH0106C	0.2	100-270	257	-33	4.9
	Dec	Inc	k	a95	
Mean	256	-56	23	11	
	latp	longp	dp	dm	
VGP	3	22	11	16	

Yeppon Highway (YH) gabbro			HBT component		
sample	Jnrm	Temp range	Dec	Inc	MAD
YH0101A*	1.3	400-510	39	-80	5.2
YH0102A*	1.1	400-480	254	-77	1.8
YH0102B*	1.2	400-480	31	-79	3.9
YH0103B	3.7	360-480	293	-4	9.7
YH0103C*	1.1	400-480	318	-70	5.2
YH0104A	1.6	360-480	271	-15	14.8
YH0105A*	0.5	400-480	315	-81	3.7
YH0105B*	0.3	400-480	101	-75	3.8
	Dec	Inc	k	a95	
Mean(*)	350	-85	36	11	
	latp	longp	dp	dm	
VGP	34	333	22	22	

Appendix 6: pTRM check anomalies observed during the experimental analysis of the Thellier method

CR0107A: Maximum χ_{RT} anomaly is + 30.0% after 601 stage

Temperature (°C)	pTRM check (%)	NRM check (%)
100	1.6	-2.1
200	-1.3	-1.0
300	-5.0	-0.2
400	6.2	-0.3
500	-7.3	5.0
600		0.2
mean	-1.1	0.3
total	-5.7	1.5

CR0502A: Maximum χ_{RT} anomaly is + 129.3% after 601 stage

Temperature (°C)	pTRM check (%)	NRM check (%)
100	0.7	-2.1
200	-0.4	-0.7
300	-6.2	0.5
400	-3.1	1.4
500	-1.1	4.6
600		0.1
mean	-2.0	0.6
total	-10.0	3.7

CR0503A: Maximum χ_{RT} anomaly is + 76.4% after 601 stage

Temperature (°C)	pTRM check (%)	NRM check (%)
100	0.8	-1.5
200	1.6	-0.7
300	-4.6	-0.7
400	-0.3	-1.1
500	13.3	-1.4
600		-0.1
mean	2.2	-0.9
total	10.9	-5.5

CR0703A: Maximum χ_{RT} anomaly is + 9.0% after 403 stage

Temperature (°C)	pTRM check (%)	NRM check (%)
100	0.4	-4.0
200	-0.4	-0.1
300	-0.8	0.9
400	1.8	-0.5
500	5.4	-3.5
600		0.0
mean	1.3	-1.2
total	6.4	-7.3

GB0107C: Maximum χ_{RT} anomaly is - 2.6% after 601 stage

Temperature (°C)	pTRM check (%)	NRM check (%)
100	1.7	-2.9
200	3.5	-2.8
300	1.4	0.0
400	5.0	-1.5
500	2.3	-0.5
600		0.1
mean	2.8	-1.3
total	14.0	-7.5

GB0606B: Maximum χ_{RT} anomaly is + 9.6% after 601 stage

Temperature (°C)	pTRM check (%)	NRM check (%)
100	0.6	-0.7
200	1.9	-1.3
300	5.5	-2.3
400	9.9	-3.7
500	-5.2	0.3
600		-0.1
mean	2.5	-1.3
total	12.7	-7.8

GB0703B: Maximum χ_{RT} anomaly is + 2.9% after 500 stage

Temperature (°C)	pTRM check (%)	NRM check (%)
100	-2.2	-1.0
200	2.2	-1.7
300	2.2	-0.2
400	4.1	-1.1
500	-0.4	0.7
600		-0.1
mean	1.2	-0.6
total	5.9	-3.4

GS0205B: Maximum χ_{RT} anomaly is - 2.3% after 601 stage

Temperature (°C)	pTRM check (%)	NRM check (%)
100	0.58	-2.14
200	0.41	-0.02
300	1.06	-0.57
400	3.34	-1.86
500	8.79	-3.77
600		0.06
mean	2.8	-1.4
total	14.2	-8.3

GS0206B: Maximum χ_{RT} anomaly is - 2.4% after 601 stage

Temperature (°C)	pTRM check (%)	NRM check (%)
100	1.3	-0.5
200	0.6	-0.3
300	0.7	-0.4
400	2.9	-1.5
500	7.9	-1.9
600		-0.1
mean	2.7	-0.8
total	13.5	-4.6

GS0301C: Maximum χ_{RT} anomaly is - 2.3% after 601 stage

Temperature (°C)	pTRM check (%)	NRM check (%)
100	0.5	-1.9
200	0.2	0.1
300	0.2	-0.1
400	4.1	-1.3
500	11.7	-4.9
600		-0.2
mean	3.4	-1.4
total	16.8	-8.5

GS0302A: Maximum χ_{RT} anomaly is + 1.5% after 503 stage

Temperature (°C)	pTRM check (%)	NRM check (%)
100	0.8	-0.4
200	1.1	-0.1
300	0.6	-0.1
400	2.5	-1.4
500	12.2	-1.5
600		0.1
mean	3.4	-0.6
total	17.2	-3.5

LR0109B: Maximum χ_{RT} anomaly is + 17.1% after 601 stage

Temperature (°C)	pTRM check (%)	NRM check (%)
100	2.1	-5.2
200	0.9	-1.8
300	0.9	-1.3
400	4.7	-0.5
500	7.3	0.1
600		0.0
mean	3.2	-1.4
total	15.9	-8.6

NE0101C: Maximum χ_{RT} anomaly is + 18.1% after403 stage

Temperature (°C)	pTRM check (%)	NRM check (%)
100	0.8	-0.9
200	1.0	-0.7
300	0.3	-1.4
400	6.9	-2.8
500	7.3	-0.6
600		-0.1
mean	3.2	-1.1
total	16.2	-6.5

NE0105B: Maximum χ_{RT} anomaly is + 21.3% after 403 stage

Temperature (°C)	pTRM check (%)	NRM check (%)
100	0.2	-2.1
200	0.0	-0.3
300	-0.5	-0.3
400	7.0	-3.2
500	18.5	-2.4
600		-0.1
mean	5.0	-1.4
total	25.1	-8.5

Appendix 7: All RS data

suite no.	Average Age (Ma)	Average VDM/VADM (10^{22} Am^2)	N	σ (10^{22} Am^2)
1	10.0	9.1	8	4.7
2	10.2	7.1	1	
3	10.3	5.4	1	
4	10.3	2.7	1	
5	10.3	1.5	1	
6	11.3	5.7	1	
7	11.5	2.0	1	
8	11.7	9.7	6	3.8
9	12.0	2.1	6	0.8
10	12.0	6.5	1	
11	12.4	9.2	25	4.8
12	13.0	13.0	1	
13	13.5	4.7	1	
14	13.8	7.7	1	
15	13.8	2.8	1	
16	14.0	4.8	1	
17	14.5	6.3	1	
18	14.8	13.3	1	
19	14.8	8.2	1	
20	14.9	3.8	1	
21	15.0	9.0	1	
22	15.0	10.9	1	
23	15.5	4.3	4	0.8
24	15.5	7.2	19	3.2
25	15.7	7.4	1	
26	16.6	9.2	2	1.2
27	17.9	2.6	1	
28	20.0	2.7	1	
29	22.0	4.6	1	
30	23.0	1.9	1	
31	27.6	5.5	7	3.0
32	30.0	5.7	8	2.4
33	30.0	11.5	2	0.2
34	31.0	4.5	1	
35	31.0	2.9	1	
36	32.0	1.9	1	
37	32.9	3.0	3	0.8
38	33.3	1.8	1	
39	34.0	3.9	1	
40	34.0	7.0	1	
41	34.0	1.9		
42	35.2	4.0	1	
43	35.7	4.1	1	
44	38.9	4.6	1	
45	42.0	9.6	1	
46	43.5	5.1	1	
47	49.0	4.0	1	
48	52.0	1.9	1	
49	55.2	21.5	2	2.7

suite no.	Average Age (Ma)	Average VDM/VADM (10^{22} Am^2)	N	σ (10^{22} Am^2)
50	56.2	10.2	3	8.3
51	64.7	12.0	7	10.0
52	64.7	5.8	38	3.5
53	65.0	8.4	7	2.0
54	67.1	4.2	47	2.3
55	72.0	13.6	1	
56	72.0	1.7	1	
57	72.0	9.7	1	
58	77.6	4.2	1	
59	78.3	7.4	1	
60	84.0	1.9	1	
61	85.9	4.8	27	1.4
62	88.0	4.9	1	
63	92.0	7.9	1	
64	92.0	7.8	1	
65	94.8	3.8	4	1.3
66	97.0	6.9	1	
67	111.0	2.6	1	
68	114.6	4.4	1	
69	117.0	5.3	22	1.6
70	117.5	5.1	14	2.4
71	122.4	4.7	1	
72	123.0	3.2	5	1.1
73	125.0	3.2	2	0.5
74	126.0	2.3	5	0.9
75	126.0	3.9	1	
76	133.0	5.3	6	2.0
77	138.0	1.8	1	
78	143.5	3.2	15	0.8
79	150.0	2.7	9	0.7
80	155.7	3.1	1	
81	156.5	3.2	1	
82	165.5	2.3	24	0.3
83	166.8	0.8	1	
84	180.0	4.6	10	2.0
85	182.5	10.4	2	1.3
86	187.5	4.5	28	1.0
87	193.5	3.6	4	0.2
88	201.0	3.1	2	0.2
89	201.0	3.9	4	0.4
90	225.0	10.6	1	
91	244.6	4.3	34	1.3
92	253.0	4.0	5	1.6
93	273.0	12.9	1	
94	276.5	7.7	61	3.3
95	279.0	6.1	21	2.6
96	280.0	6.7	8	0.5
97	285.0	6.8	1	
98	290.0	4.2	4	1.7

suite no.	Average Age (Ma)	Average VDM/VADM (10^{22} Am^2)	N	σ (10^{22} Am^2)
99	300.0	12.0	1	
100	301.0	4.1	15	1.6
101	310.6	9.2	32	0.8
102	325.0	10.3	57	0.9
103	347.0	2.3	13	2.4
104	366.0	1.9	1	
105	377.5	3.8	1	
106	381.9	4.3	4	0.3
107	384.0	2.5	4	1.1
108	384.0	1.5	5	0.5
109	397.5	4.3	16	0.9